frontiers | Research Topics

Complement: Latest developments regarding structure, mechanism, and connections to other proteolytic pathways

Edited by
József Dobó, Péter Gál and Brian V. Geisbrecht

Published in
Frontiers in Immunology

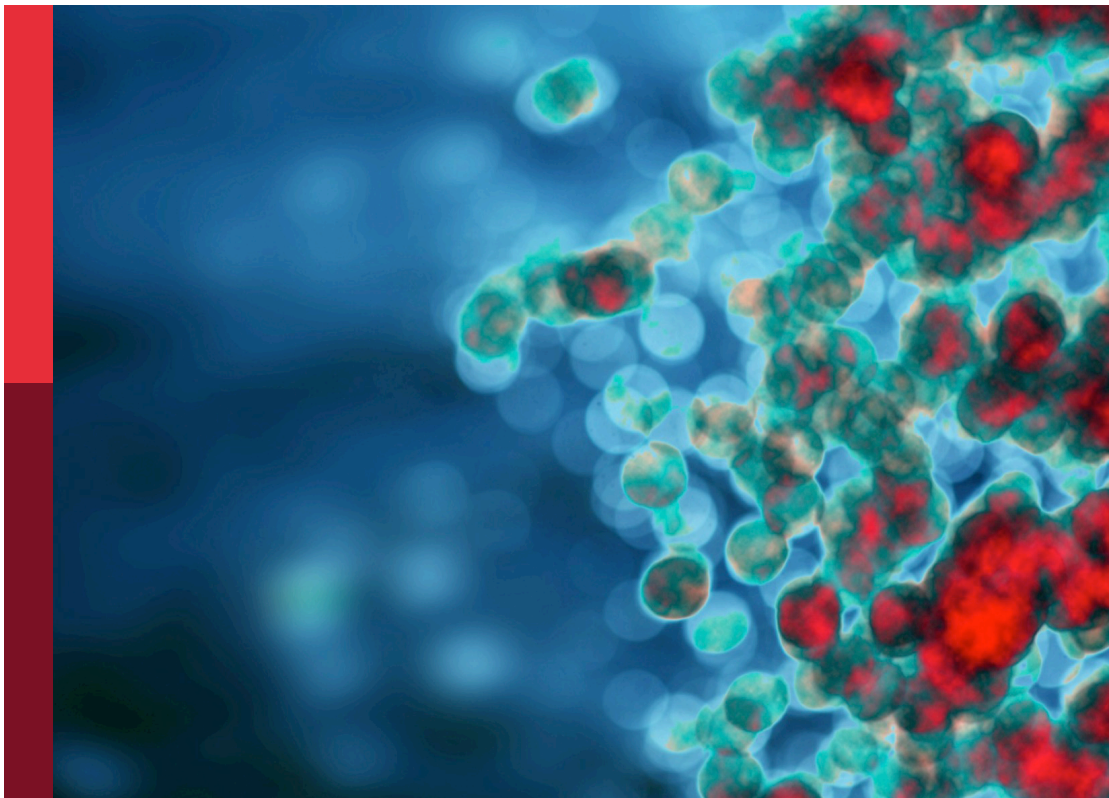

ISSN 1664-8714
ISBN 978-2-83251-623-2
DOI 10.3389/978-2-83251-623-2

About Frontiers

Frontiers is more than just an open access publisher of scholarly articles: it is a pioneering approach to the world of academia, radically improving the way scholarly research is managed. The grand vision of Frontiers is a world where all people have an equal opportunity to seek, share and generate knowledge. Frontiers provides immediate and permanent online open access to all its publications, but this alone is not enough to realize our grand goals.

Frontiers journal series

The Frontiers journal series is a multi-tier and interdisciplinary set of open-access, online journals, promising a paradigm shift from the current review, selection and dissemination processes in academic publishing. All Frontiers journals are driven by researchers for researchers; therefore, they constitute a service to the scholarly community. At the same time, the *Frontiers journal series* operates on a revolutionary invention, the tiered publishing system, initially addressing specific communities of scholars, and gradually climbing up to broader public understanding, thus serving the interests of the lay society, too.

Dedication to quality

Each Frontiers article is a landmark of the highest quality, thanks to genuinely collaborative interactions between authors and review editors, who include some of the world's best academicians. Research must be certified by peers before entering a stream of knowledge that may eventually reach the public - and shape society; therefore, Frontiers only applies the most rigorous and unbiased reviews. Frontiers revolutionizes research publishing by freely delivering the most outstanding research, evaluated with no bias from both the academic and social point of view. By applying the most advanced information technologies, Frontiers is catapulting scholarly publishing into a new generation.

What are Frontiers Research Topics?

Frontiers Research Topics are very popular trademarks of the *Frontiers journals series*: they are collections of at least ten articles, all centered on a particular subject. With their unique mix of varied contributions from Original Research to Review Articles, Frontiers Research Topics unify the most influential researchers, the latest key findings and historical advances in a hot research area.

Find out more on how to host your own Frontiers Research Topic or contribute to one as an author by contacting the Frontiers editorial office: frontiersin.org/about/contact

Complement: Latest developments regarding structure, mechanism, and connections to other proteolytic pathways

Topic editors

József Dobó — Institute of Enzymology, Research Centre for Natural Sciences, Hungarian Academy of Sciences (MTA), Hungary

Péter Gál — Institute of Enzymology, Research Centre for Natural Sciences, Hungary

Brian V. Geisbrecht — Kansas State University, United States

Citation

Dobó, J., Gál, P., Geisbrecht, B. V., eds. (2023). *Complement: Latest developments regarding structure, mechanism, and connections to other proteolytic pathways*. Lausanne: Frontiers Media SA. doi: 10.3389/978-2-83251-623-2

Table of contents

frontiers | Frontiers in Immunology

TYPE Editorial
PUBLISHED 24 January 2023
DOI 10.3389/fimmu.2023.1144038

OPEN ACCESS

EDITED AND REVIEWED BY
Francesca Granucci,
University of Milano-Bicocca, Italy

*CORRESPONDENCE
Brian V. Geisbrecht
GeisbrechtB@ksu.edu

SPECIALTY SECTION
This article was submitted to Molecular Innate Immunity, a section of the journal Frontiers in Immunology

RECEIVED 13 January 2023
ACCEPTED 17 January 2023
PUBLISHED 24 January 2023

CITATION
Dobó J, Gál P and Geisbrecht BV (2023) Editorial: Complement: Latest developments regarding structure, mechanism, and connections to other proteolytic pathways.
Front. Immunol. 14:1144038.
doi: 10.3389/fimmu.2023.1144038

Editorial: Complement: Latest developments regarding structure, mechanism, and connections to other proteolytic pathways

József Dobó[1], Péter Gál[1] and Brian V. Geisbrecht[2]*

[1]Institute of Enzymology, Research Centre for Natural Sciences, Budapest, Hungary, [2]Department of Biochemistry & Molecular Biophysics, Kansas State University, Manhattan, KS, United States

KEYWORDS

proprotein convertases, MASP-3, age-related macular degeneration (AMD), C2, heme, Borrelia, gC1qR, coagulation

Editorial on the Research Topic
Complement: Latest developments regarding structure, mechanism, and connections to other proteolytic pathways

It is with great pleasure that we introduce you to the Research Topic entitled "Complement: Latest Developments Regarding Structure, Mechanism, and Connections to Other Proteolytic Pathways". Consisting of two focused review articles, seven original research articles, and one brief report, we think that this collection makes for an attractive cross-section of current basic research endeavors in the topic area. Furthermore, as these contributions arise from a range of approaches including *in vivo* animal studies, single-cell transcriptomics, interaction analysis, structural biology, and assays of immune function, we believe this collection provides an excellent showcase of the diversity of experimentation and thought within the field. With that in mind, the following paragraphs provide brief synopses of the individual manuscripts and the scientific context from which they were written.

As proteins destined for the extracellular environment, the biogenesis of various complement components is necessarily complex. This is even more the case for the numerous complement components that must undergo processing from their respective proproteins to their mature forms. In this review, Dobó et al. discuss the role of proprotein convertases on the intracellular and extracellular processing complement proteins and their overall contributions to complement function. With new roles for complement being reported regularly, this review provides a useful resource for understanding the basic events necessary for generating fully active complement components. These considerations are especially relevant in light of the continually emerging role of the intracellular complement system.

Of course, another layer of regulation must be considered when complement components assemble into multipartite functional units, such as the initiating complexes of the classical (CP) or lectin (LP) pathways. Although MASP-3 has been shown to circulate in the blood in its active form, how this is influenced by its interaction with LP pattern recognition molecules remains unknown. In their manuscript, Kusakari et al. use a series of

recombinant forms of MASP-3 to investigate its activation, assembly, and clearance in experimental mice. These authors showed that while MASP-3 binding to pattern recognition molecules is not required for MASP-3 activation, it does appear to influence the kinetics of MASP-3 retention in the blood. Since MASP-3 has been shown previously to activate pro-factor D, these observations may inform future efforts aimed at developing inhibitors of the complement alternative pathway (AP).

When mentioning therapeutic development, the complement system has received considerable attention recently due to the approval of the C3 inhibitor, pegcetacoplan, for treatment of paroxysmal nocturnal hemoglobinuria (PNH). This same compound is currently undergoing evaluation for treatment of age-related macular degeneration (AMD), which is characterized by excessive C3 activation in the retina and surrounding tissues. However, mixed results for other complement inhibitors in AMD trials led Zauhar et al. to investigate complement homeostasis in the eye at single-cell resolution. These authors found temporal and spatial differences in local complement component production between healthy and diseased eyes. Together, their observations provide a more nuanced understanding of complement's roles in maintaining function of the retina and surrounding tissues, and how it might be inhibited to therapeutic benefit.

Whereas changes in local complement component production in the eye have only recently been discovered, the genetic risk factors linked to development of AMD have been known for some time. Unfortunately, the functional consequences of many rare variants in Factor H (FH) and Factor I (FI) remain unknown. To address this issue systematically, Hallam et al. devised a method for generating recombinant FI and thereafter developed a real-time assay for assessing formation of the ternary complex between C3b, FH, and FI. Interestingly, these authors showed that certain rare variants in FI appear to have dominant negative effects by competing with wild-type FI for binding to the complex of C3b and FH. The work described in this manuscript should permit design of more effective interventions for AMD that account for individuals' genotypes.

Although FH has been known as the primary regulator of the AP for decades, the functions of a family of FH-related proteins (FHRs) have become apparent more recently. As with FH, coding variants in FHR1 have been linked to the development of atypical hemolytic uremic syndrome (aHUS), which is a rare thrombotic microangiopathy that can lead to end-stage renal disease. To better understand the mechanism through which FHR1 variants may contribute to disease, Xu et al. examined the effects of two isoforms known as FHR1*A and FHR1*B on regulation of the AP. These authors uncovered several functional differences for FHR1*B, including an increased affinity for C3b and a greater ability to impede FH regulatory activities. Together, these observations enhance understanding of FHR function and provide new insights into the molecular events that may underlie aHUS development in certain patients.

As with aHUS patients, those with the rare kidney diseases known as C3 glomerulopathies display evidence of unregulated complement activity. While many such individuals have gain-of-function coding variants in components of the AP, such as Factor B, newer studies have identified patients that harbor mutations in complement component C2. In this brief report, Kuźniewska et al. investigated the functional consequences of patient-derived mutations in the von Willebrand factor A (vWA) domain of complement C2. Their work further establishes the functional analogies between Factor B and C2 and reveals that mutations in the vWA domain of these paralogs may have unpredictable consequences on complement activity.

The synopses above illustrate examples of genetic variations leading to changes in complement component function. However, the possibility that endogenous small molecules might also affect complement components remains relatively unexplored. Since free heme has been described as an activator of the AP, Gerogianni et al. sought to define the mechanism behind its action. These authors showed that heme binds directly to FI and inhibits its ability to degrade soluble and surface-bound C3b in the presence of either FH or soluble complement receptor-1 as a cofactor. Interestingly, they also found that the heme-scavenging protein, hemopexin, elicited a protective function toward FI, so long as it was present prior to exposure to free heme. These observations have important implications for regulation of the AP in hemolytic disorders.

When discussing mechanisms of complement regulation, it is almost impossible to ignore the many lessons learned from studying pathogen-derived immune evasion proteins. In this manuscript, Booth et al. continue their recent line of investigation into the BBK32 family of CP inhibitors produced by *Borrelia* spp. Using biochemical, structural, and functional studies, these authors found that FbpA and FbpB share the ability of *B. burgdorferi* BBK32 to bind C1r and inhibit its activity. Interestingly, they also found that while FbpA binds to both zymogen and activated C1r, FbpB is selective for activated C1r alone. These results not only further understanding of complement evasion by an emerging human pathogen, they provide new information on a family of inhibitors selective for the activation state of complement component C1r.

Given the title of this collection, we think investigating connections between complement and other proteolytic pathways is a promising area of research. Indeed, one of the best understood of these connections is the interaction between gC1qR (a potent initiator of the CP), coagulation factor FXII, high-molecular weight kininogen (HMWK), and prekallikrein (PK) that occurs on the surface of endothelial cells in response to inflammatory stimuli. In this manuscript, Zhang et al. use a structure/function approach to further define the gC1qR/FXII interaction and explore how it is perturbed by a panel of monoclonal antibodies. Since the gC1qR/FXII/HMWK/PK complex triggers excessive generation of the vasodilator bradykinin in angioedema, these results provide new insights into how assembly of this complex might be inhibited as a potential treatment.

The current emphasis on therapeutic discovery is likely to continue for the foreseeable future, yet is best positioned when it seeks to manipulate events whose functional consequences are well established. Clearly, much remains to be discovered. To that end, Pryzdial et al. conclude this collection with a review article that examines the many biochemical and cellular connections between complement and coagulation. By changing our focus from one that looks at individual pathways to a more wholistic view that treats these two proteolytic systems as coresident in the same physiological compartment, the authors seek to remove many of the distinctions made for convenience at the expense of understanding. In doing so, they set the stage for identifying new points of crosstalk between complement, coagulation, and still other proteolytic pathways.

We hope you find this collection timely, informative, and thought-provoking for new lines of investigation into the complement system and other proteolytic pathways.

Author contributions

BG drafted the editorial manuscript. JD and PG corrected the manuscript. All authors approved its final version.

Acknowledgments

We would like to thank all authors for their contributions to this Research Topic. We are also grateful to all reviewers for their effort in evaluating the submitted manuscripts.

Conflict of interest

The authors declare that the research was conducted in the absence of any commercial or financial relationships that could be construed as a potential conflict of interest.

Publisher's note

frontiers in Immunology

ORIGINAL RESEARCH
published: 21 January 2022
doi: 10.3389/fimmu.2022.755694

Atypical Hemolytic Uremic Syndrome-Associated FHR1 Isoform FHR1*B Enhances Complement Activation and Inflammation

Boyang Xu[1†], Yuqi Kang[1†], Yujing Du[2], Weiyi Guo[1], Li Zhu[1] and Hong Zhang[1]*

[1] Renal Division, Department of Medicine, Peking University First Hospital, Peking University Institute of Nephrology, Key Laboratory of Renal Disease (Peking University), National Health Commission, Key Laboratory of Chronic Kidney Disease Prevention and Treatment, Ministry of Education, Beijing, China, [2] Department of Nuclear Medicine, Peking University First Hospital, Beijing, China

OPEN ACCESS

Edited by:
József Dobó, Hungarian Academy of Sciences (MTA), Hungary

Reviewed by:
Mihály Józsi, Eötvös Loránd University, Hungary
Eleni Gavriilaki, G. Papanikolaou General Hospital, Greece

***Correspondence:**
Li Zhu
funnyzhuli@bjmu.edu.cn

[†]These authors have contributed equally to this work and share first authorship

Specialty section:
This article was submitted to Molecular Innate Immunity, a section of the journal Frontiers in Immunology

Received: *09 August 2021*
Accepted: *03 January 2022*
Published: *21 January 2022*

Citation:
*Xu B, Kang Y, Du Y, Guo W, Zhu L and Zhang H (2022) Atypical Hemolytic Uremic Syndrome-Associated FHR1 Isoform FHR1*B Enhances Complement Activation and Inflammation. Front. Immunol. 13:755694. doi: 10.3389/fimmu.2022.755694*

Atypical hemolytic uremic syndrome (aHUS) is a rare but severe type of thrombotic microangiopathy that is triggered by the abnormal activation of the alternative complement pathway. Previous studies have reported that three completely linked coding variants of *CFHR1* form two haplotypes, namely, *CFHR1**A (c.469C, c.475C, c.523G) and *CFHR1**B (c.469T, c.475G, c.523C). *CFHR1**B is associated with susceptibility to aHUS. To explore the genetic mechanism by which *CFHR1* isoforms contribute to aHUS, we compared the structures of FHR1*A and FHR1*B by homology modeling and found differences in the angles between SCR3 and SCR4-SCR5, as FHR1*B had a larger angle than FHR1*A. Then, we expressed FHR1*A and FHR1*B recombinant proteins and compared their functions in complement system regulation and inflammation. We found that FHR1*B presented a significantly higher capacity for binding C3b and necrotic cells than FHR1*A. In a cofactor assay, the FHR-1*B showed stronger influence on FH mediated cofactor function than the FHR-1*A, resulted in fewer C3b cleavage products. In the C3 convertase assays, FHR1*B showed more powerful effect compared with FHR1*A regarding to de-regulate FH function of inhibition the assembling of C3bBb. Additionally, we also found that FHR1*B triggered monocytes to secrete higher levels of IL-1β and IL-6 than FHR1*A. In the present study, we showed that variants of *CFHR1* might differently affect complement activation and sterile inflammation. Our findings provide a possible mechanism underlying the predisposition to aHUS caused by *CFHR1* isoform *CFHR1**B.

Keywords: complement, FHR1, complement activation, aHUS, inflammation

INTRODUCTION

Atypical hemolytic uremic syndrome (aHUS) is a rare but severe type of thrombotic microangiopathy that mainly presents as a triad of microangiopathic hemolytic anemia (negative Coombs' test results), thrombocytopenia, and acute renal failure (1); aHUS has a mortality rate of 25%, and half of the patients with aHUS progress to end-stage renal disease (2). In contrast to

typical hemolytic uremic syndrome, which is caused by infection with Shiga toxin-producing *Escherichia coli (*3), aHUS is mainly caused by abnormalities in the alternative complement pathway that trigger complement system overactivation and further cause endothelial cell damage and thrombosis (4, 5). Among all aHUS patients, approximately 60% have genetic abnormalities in complement pathway proteins (6, 7), and 20-30% of these genetic abnormalities are located in Complement factor H (FH) (2, 8).

FH is an important negative complement regulatory protein of the alternative pathway that can accelerate the decay of C3 convertase and C5 convertase and facilitate the cleavage of C3b by factor I (FI). In addition, humans have 5 genes (*CFHRs*) located downstream of the *CFH* gene that encode 5 complement FH-related proteins (FHR1, FHR2, FHR3, FHR4, and FHR5), which show high sequence similarity to FH (9, 10). Some complement FH-related proteins, including FHR1, FHR2 and FHR5, can compete with FH and dysregulate complement activation (11–14). Moreover, FHR1 was reported to bind to monomeric C-reactive protein and enhance complement activation (15). FHR-1 bound to late apoptotic and necrotic cells to enhance complement activation alone and in collaboration with monomeric CRP and pentraxin 3 (16). FHR1 was reported to modulate neutrophil functions independent of complement activation (17). More recently, Irmscher et al. reported the function of FHR1, namely, the induction of monocytic inflammation independent of complement (18, 19). Currently, the function of FHRs is still incompletely understood.

A variety of genetic abnormalities in *CFH* and *CFHRs*, including deletions, variants and hybrid genes (7), have been reported as predisposing factors of aHUS. Moreover, some common variants of *CFH* and *CFHRs* have been associated with susceptibility to aHUS. Recently, Abarrategui-Garrido et al. (20) reported three completely linked coding variants of *CFHR1* exon 4 (c.469 C>T, c.475 C>G, and c.523 G>C), which changed three amino acids in the SCR3 domain of FHR1 to form two FHR1 isotypes, namely, FHR1*B (p.157Tyr, p.159Val, p.175Gln; basic isoform) and FHR1*A (p.157His, p.159Leu, p.175Glu; acidic isoform). Furthermore, these authors also observed that *CFHR1*B* predisposed patients to susceptibility to aHUS (20). In addition, Anne Kopp, et al. found aHUS-associated FHR1*B variant showed reduced binding to PTX3 in comparison with FHR1*A (21).

Based on the genetic evidence about the role of *CFHR1* in aHUS, in this study, we investigated the structures and functions of the FHR1*A and FHR1*B proteins to explore the mechanism underlying the roles of these *CFHR1* isotypes in aHUS.

METHODS

Homology Modeling of FHR1*A and FHR1*B

There was no complete crystal structure of the FHR1 protein in the protein data bank (PDB) database. We performed homology modeling of SCR3-5 of FHR1*A and FHR1*B by using the ModBase database (22) to predict the effects of coding variants of FHR1 on the structure of its encoded protein. The C-terminal region (SCR18-20) of FH (PDB accession code: 3SW0), which showed a high sequence identity with the C-terminal region of FHR1, was defined as the template structure, and the models of FHR1*A and FHR1*B were analyzed *via* PyMOL software version 1.7.0.0. The homology modeling results were further evaluated with the given quality criteria (23).

Protein Expression and Purification of FHR1

The codon-optimized (*Homo sapiens*) DNA sequences for *CFHR1*A* and *CFHR1*B* (fused to a hexa-histidine tag at the C-terminus), which had been synthesized and ligated into the pTT5 vector, were customized and provided by Genescript. The expression vectors were then transiently transfected into 293F cells using polyethyleneimine according to the manufacturer's instructions (PEI, Polysciences Inc.). Then, the 293F cells were cultured in serum-free HEK293 cell complete medium (Sino Biological Inc.) in an incubator with 5% CO_2 at 37°C for four days. After centrifugation and filtering, the harvested cell supernatant was then applied to a Ni Sepharose column (GE Healthcare) to obtain the His-tagged FHR1 proteins. The purified FHR1*A and FHR1*B proteins were finally concentrated in PBS by using an Amicon Ultra Centrifugal Filter (Merck). After purification and concentration, FHR-1 proteins were stored in PBS in -80°C.

Identification of the Expressed FHR1 Proteins

The recombinant FHR1*A and FHR1*B proteins were analyzed by Coomassie blue staining and Western blotting. Briefly, the FHR1 proteins were separated by SDS-polyacrylamide gel electrophoresis (SDS-PAGE), and then, the gels were stained with Coomassie blue staining solution. For Western blotting, after SDS-PAGE, the FHR1 proteins were transferred to polyvinylidene fluoride membranes (PVDF membranes, Millipore). After blocking, the membranes were immunoblotted with mouse anti-His tag (Origene) or mouse anti-human FHR1 antibody (R&D, cross-reacts with FH), followed by anti-mouse IgG-HRP antibodies (Santa Cruz). Finally, the membranes were developed with a chemiluminescent HRP substrate (Millipore) according to the manufacturer's instructions.

Binding of FHR1 to C3b

To assess the capacities of FHR1*A and FHR1*B to bind C3b, we conducted solid-phase C3b binding assays. Serial dilutions of the recombinant FHR1*A and FHR1*B proteins (2.5 μg/ml-0.078 μg/ml in PBS) were coated onto plates (Thermo Fisher Scientific) and incubated at 4°C for more than 16 hours. After washing with 0.1% PBST and blocking with 1%BSA/PBST at 37°C for 1 hour, C3b (2 μg/ml) was added and incubated at 37°C for 1 hour. Then, FHR1-bound C3b was detected using a C3c polyclonal antibody (Dako), followed by the addition of an anti-rabbit IgG-alkaline phosphatase antibody (Santa Cruz). In the reverse setting,

100nM C3b (Complement Tech) dissolved in TBS (140mM NaCl, 2mM $CaCl_2$, 1mM $MgCl_2$ and 10mM Tris, pH 7.4) were immobilized in the microtiter plates at 4°C overnight. After blocking with 3% milk in 0.02%TBST for 2 hours at 25°C, serially diluted FHR1-A and FHR1-B proteins (10μg/ml-1.25μg/ml) were added and incubated for 30min at 37°C. And mouse anti-human FHR1 antibody (R&D, cross-reacts with FH) was added as primary antibody, followed by adding AP-conjugated goat anti-mouse IgG antibody (Sigma-Aldrich). Finally, the plates were developed with alkaline phosphatase chromogenic substrate (Sigma-Aldrich), and the optical density was read at 405 nm.

Binding of Surface-Bound C3b

Binding of FHR1 with surface-bound C3b was detected as previously reported (24). In brief, Saccharomyces cerevisiae strain (Mingzhoubio B47202) cells were resuspended in TBS and added in the microtiter plates 200μl per well for about 45min RT for deposition. After washing away the extra cells with 0.02% TBST and blocking with 3% milk in 0.02%TBST for 2 hours at 25°C, 100nM C3b or TBS were added and incubated for 1 hour at 37°C. And after incubation with serial dilution of FHR1*A and FHR1*B (5μg/ml-1.25μg/ml), mouse anti-human FHR1 antibody (R&D, cross-reacts with FH), and AP-conjugated goat anti-mouse IgG antibody (Sigma-Aldrich) were added for incubation in succession. In the last, alkaline phosphatase chromogenic substrate were added and the optical density was read at 405 nm.

Binding of FHR1 to Necrotic Cells

The capacities of FHR1*A and FHR1*B to bind to necrotic cells were examined by flow cytometry using human umbilical vein endothelial cells (HUVECs) as previously reported (18, 25). HUVECs were purchased from ScienCell Corporation (ScienCell, Carlsbad, CA) and cultured according to the manufacturer's protocols. Briefly, 10^6 HUVECs/ml were incubated at 90°C for 10 min in 1%BSA/PBS and after blocking with 1%BSA/PBS, cells were then incubated with serial dilutions of the recombinant FHR1 proteins (FHR1*A or FHR1*B; 0.313 μg/ml-0.078 μg/ml in 1%BSA/PBS) at 37°C for 30 min. After washing with PBS, the HUVECs were stained with a mouse anti-human FHR1 antibody (JHD10, Hycult Biotech, cross-reacts with FHR2 and FHR5) or mouse IgG1 [CT6] isotype control (Abcam) followed by incubation with an Alexa Fluor® 647-conjugated anti-mouse IgG antibody (Cell Signaling Technology) as the secondary antibody. The necrosis induction was measured by propidium iodide and Annexin V staining (BD556547). Double positive for both Annexin V and PI cells were determined as necrotic cells. Cell acquisition was performed by a FACScan flow cytometer (BD), 10,000 cells were measured for each sample and data were analyzed by FlowJo (v10).

Competition ELISA Assay for FHR1 and FH for C3b

To compare the capacity of FHR1*A and FHR1*B to compete with FH to bind C3b, FH (9 μg/ml) was immobilized on the surface of a microtiter plate (Thermo Fisher Scientific) at 4°C overnight. After blocking with 1% BSA/PBST at 37°C for 1 hour, serial dilutions of the recombinant FHR1*A or FHR1*B proteins (2.5 μg/ml-0.039 μg/ml) as well as C3b (0.25 μg/ml) were added to the plates. After shaking for 30 sec, the plates were incubated at 37°C for 1 hour. After washing with 0.1%PBST, FH-bound C3b was detected with a C3c polyclonal antibody (Dako), followed by incubation with an alkaline phosphatase-conjugated anti-rabbit IgG antibody as the secondary antibody (Sigma-Aldrich). The plates were then developed with alkaline phosphatase chromogenic substrate (Sigma-Aldrich), and the optical density was read at 405 nm.

Cofactor Assay

To investigate the effect of FHR1 on the cofactor activity of FH, the generation of C3b cleavage products by complement factor I (CFI) was assessed by SDS-PAGE and Western blotting. Two serially diluted isoforms of FHR1 (125 μg/ml-62.5 μg/ml), alone or in combination with FH (15.64 ng), were mixed with C3b (1.1 μg) and CFI (100 ng) and then incubated at 37°C for 30 min. After SDS-PAGE and Western blotting, the C3b degradation product (α' 43 kDa) was detected with a C3c polyclonal antibody (Dako), followed by an HRP-conjugated anti-rabbit IgG antibody (Jackson ImmunoResearch Labs). The membranes were developed with a chemiluminescent HRP substrate (Millipore), and the signals of the C3b degradation product (α' 43 kDa) were analyzed by ImageJ.

Convertase Assay

To evaluate the potential effect of FHR1 on the FH-mediated regulation of the C3bBb, C3 convertase assay was performed as previously described (24). In brief, at first 5μg/ml C3b (Complement Tech) were immobilized in the microtiter plates. After blocking with 3% milk in 0.02%TBST for 2 hours at 25°C, 4μg/ml factor B (Millipore), 8μg/ml properdin (Millipore), 0.2μg/ml factor D (Millipore), 20μg/ml BSA (Sigma-Aldrich), altogether with 100nM factor H (Complement Tech) and serially diluted FHR1*A or FHR1*B (300nM-500nM) were added. After incubation, anti-factor B goat polyclonal antibody (Sigma-Aldrich) was added for incubation, followed by adding AP-conjugated rabbit anti-goat IgG antibody (Sigma-Aldrich). Finally, after incubated with alkaline phosphatase chromogenic substrate, the optical density was read at 405 nm.

Stimulation of Inflammatory Cytokine Production of Monocytes by FHR-1

As previously reported (18), we evaluated the effect of FHR1 as a driver of monocytic inflammation. Briefly, peripheral blood mononuclear cells (PBMCs) were freshly isolated from the whole blood of three independent healthy donors by the density gradient centrifugation method using Ficoll Pague Plus (GE Healthcare Life Science). Then, the monocytes were indirectly magnetically labeled and isolated from the PBMCs using the Classic Monocyte Isolation Kit (Miltenyi Biotec). Then, 96-well microtiter plates (Thermo Fisher Scientific) were coated with recombinant-FHR1*A, FHR1*B, and BSA for 1 hour at 37°C. Then, $1x10^5$ monocytes were incubated in the plates with immobilized FHR1 in complete medium with 10% normal human serum (NHS) for 20 hours at 37°C in an incubator

with 5% CO_2. Finally, the levels of the inflammatory factors IL-1β and IL-6 in the supernatants after 20 hours of incubation were measured by enzyme-linked immunosorbent assay (ELISA) using IL-1β (R&D) and IL-6 (R&D) ELISA kits according to the manufacturers' protocols.

Statistical Analyses

Continuous variables with normal distribution are expressed as mean ± standard deviation and independent *t*-test or One way-ANOVA is used for comparison between groups. For non-normally distributed variables, the median and interquartile range (IQR) are used for description, while the Kruskal-Wallis test or Mann-Whitney U test is used for comparison. Statistics were performed using SPSS25.0 software and graphing were performed by GraphPad Prism 7.0 software. A two-tailed P value less than 0.05 was considered statistically significant.

RESULTS

Modeling Evaluation and Analysis

The structural models of FHR1*A and FHR1*B were successfully established *via* Modbase, and we selected the most reliable models for further analysis according to the quality criteria provided by the database (**Figures 1A, B**). After aligning the models of FHR1*A and FHR1*B (**Figure 1C**), we discovered that the overall spatial structures were similar. Although the secondary structure of the β-fold in SCR3 was not altered by the amino acid changes at p.139 and p.157, the conformations of FHR1*A and FHR1*B were still slightly different due to the three different amino acids, and SCR3 of FHR1*B was more prone to SCR4-5 than that of FHR1*A. To better analyze the conformation, we set p.189Lys as the vertex and p.189Lys-p.194Pro as the edge to measure the angles formed by different amino acids in SCR3 (**Table 1**). The angles in FHR1*B are generally smaller than those in FHR1*A, ranging from 6.3° to 8.9° (**Figures 1D, E**).

Western Blotting Analysis of the Recombinant FHR1 Proteins

We expressed recombinant FHR1*A and FHR1*B proteins with His-tag in eukaryotic expression system and purified by Ni Sepharose affinity chromatography. On SDS-PAGE gels, the recombinant FHR1*A and FHR1*B proteins showed two clear bands at approximately 40 kDa, which were detected with the His-tag antibody and FHR1 monoclonal antibody; these results were consistent with two previously reported glycosylated forms

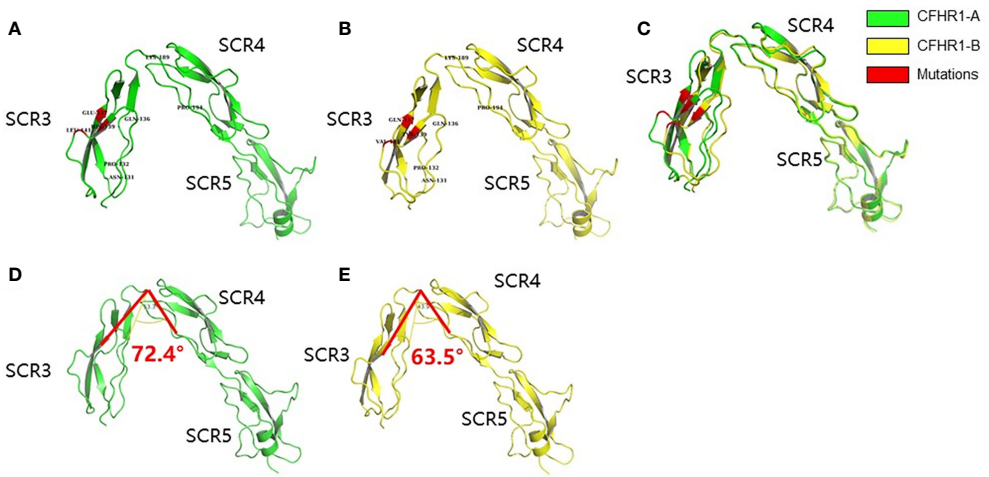

FIGURE 1 | Schematic diagram of the homologous modeling structure of FHR1*A and FHR1*B. The SCR3-SCR5 of FHR1*A **(A)** and FHR1*B **(B)** are shown in green and yellow, respectively. The mutant amino acids are shown in red. The aligned view of SCR3-SCR5 of FHR1*A and FHR1*B showed some differences **(C)**. The structures of SCR4-SCR5 are identical between FHR1*A and FHR1*B, while SCR3 of FHR1*B is more prone to SCR4-5 than that of FHR1*A. The representative angle (∠p.139-p.189-p.194) of *CFHR1**B **(E)** is smaller than that of *CFHR1**A **(D)**, with a maximum angle difference of 8.9°.

TABLE 1 | The included angles of SCR3 to SCR4-5 in FHR1*A and FHR1*B.

Amino acids	FHR1*A	FHR1*B	Differences
p.139His (FHR1*A)/Tyr (FHR1*B)	72.4	63.5	8.9
p.141Leu (FHR1*A)/Val (FHR1*B)	80.6	73.3	7.3
p.157Glu (FHR1*A)/Gln (FHR1*B)	81.7	75.4	6.3

*p.189Lys was set as the vertex and p.189Lys- p.194Pro was set as the edge to measure the angles formed by different amino acids in SCR3. The differences in the included angles in FHR1*A and FHR1*B range from 6.3° to 8.9°.*

of FHR1 (42 kDa and 37 kDa, **Supplemental Figure 1**) (26). Thereafter, the recombinant FHR1*A and FHR1*B proteins were used in the following experiments.

FHR1*B Exhibited Increased Binding to C3b Compared With FHR1*A

Since the C-terminus of FHR1 showed 98% sequence identity with that of FH and the C-terminus of FH contained a C3b binding site, we explored the capacity of the two isoforms of FHR1 to bind to C3b. In the binding assay, both isoforms, namely, FHR1*A and FHR1*B, bound C3b in a dose-dependent manner. Moreover, at the same concentrations (either 1.25 μg/ml or 2.5 μg/ml), FHR1*B exhibited significantly higher C3b binding capacity than FHR1*A (FHR1*B vs. FHR1*A: at 1.25 μg/ml concentration, P=0.021; at 2.5 μg/ml concentration, P=0.003, **Figure 2A**). In the reverse setting, dose-dependent binding of the FHR-1 isoforms to immobilized C3b was measured, and FHR1*B also showed higher capacity of binding to C3b than FHR1*A (FHR1*B vs. FHR1*A: at 1.25μg/ml concentration, P=0.002; at 2.5μg/ml concentration, P=0.001; at 5μg/ml concentration, P=0.002; at 10μg/ml concentration, P<0.001, **Figure 2B**).

FHR1*B Exhibited Increased Binding to Surface-Bound C3b Compared With FHR1*A

In surface-bound C3b binding assay, in which C3b was bound to Saccharomyces cerevisiae strain, we found that the FHR1*B isotype also has a stronger binding ability than FHR1*A to surface-bound C3b. (FHR1*B vs. FHR1*A: at 1.25μg/ml concentration, P=0.006; at 2.5μg/ml concentration, P<0.001; at 5μg/ml concentration, P=0.001, **Figures 2C, D**).

FHR1*B Exhibited Increased Binding to Necrotic HUVECs Compared With FHR1*A

FHR1 was previously reported to bind to necrotic cells (13); therefore, we compared the capacity of the FHR1 isoforms to bind to necrotic HUVECs. We observed that both FHR1 isoforms bound to necrotic HUVECs (**Figure 3**) in a dose-dependent manner. In addition, at the same concentrations (0.313 μg/ml-0.078 μg/ml), FHR1*B showed significantly increased capacity to bind to necrotic HUVECs compared with FHR1*A (FHR1*B vs. FHR1*A: at 0.313 μg/ml concentration, P=0.001; at 0.156 μg/ml concentration, P<0.001; at 0.078 μg/ml concentration, P=0.001).

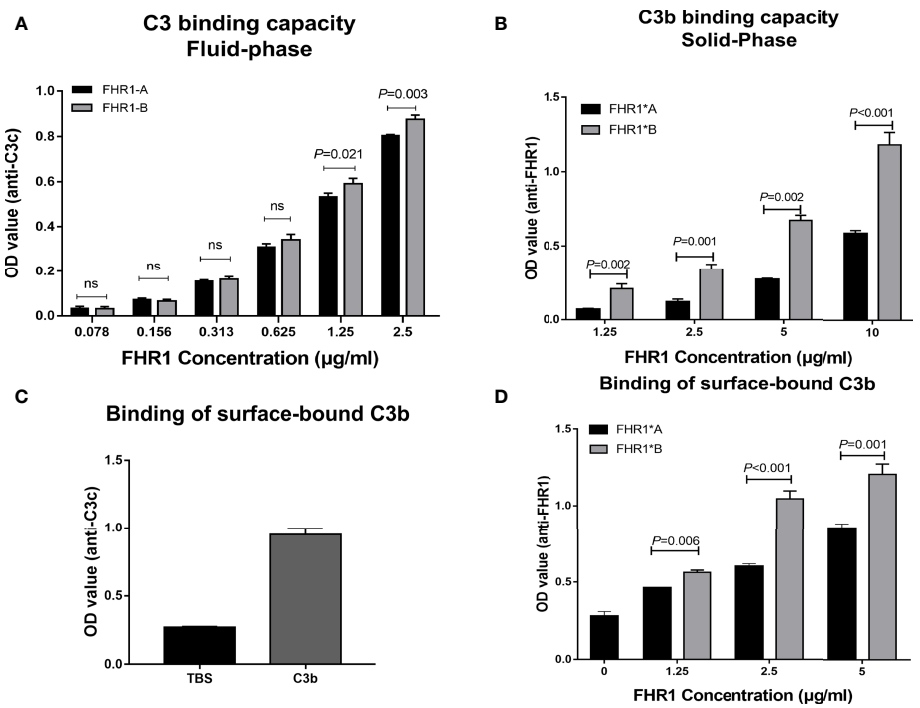

FIGURE 2 | Interaction of the two FHR1 isoforms with C3b. Equal concentrations of two immobilized isoforms of FHR1 (0.078 μg/ml-2.5 μg/ml) bound C3b (2 μg/ml) in a dose-dependent manner. The binding-C3b was finally detected. FHR1*B showed a higher capacity to bind C3b at a concentration of 1.25 μg/ml **(A)**. In a reverse setting, equal concentrations of two isoforms of FHR1 (1.25 μg/ml-10 μg/ml) bound immobilized C3b (100nM) in a dose-dependent manner. The bound FHR1 was detected at last. FHR1*B also showed higher binding capacity to C3b **(B)**. Moreover, the 100nM C3b were added onto the microplates, overspread with the *Saccharomyces cerevisiae*, and equal concentrations of two isoforms of FHR1 (1.25 μg/ml-5 μg/ml) was added. The surface-bound C3b was detected by anti-C3c antibody **(C)**, and the binding of FHR1 to surface-bound C3b was detected with anti-FHR1 antibody **(D)**. The representative figures from three independent experiments are shown. The results are representative of three independent experiments. The data are presented as the means ± SDs. The symbol ns indicates nonsignificance.

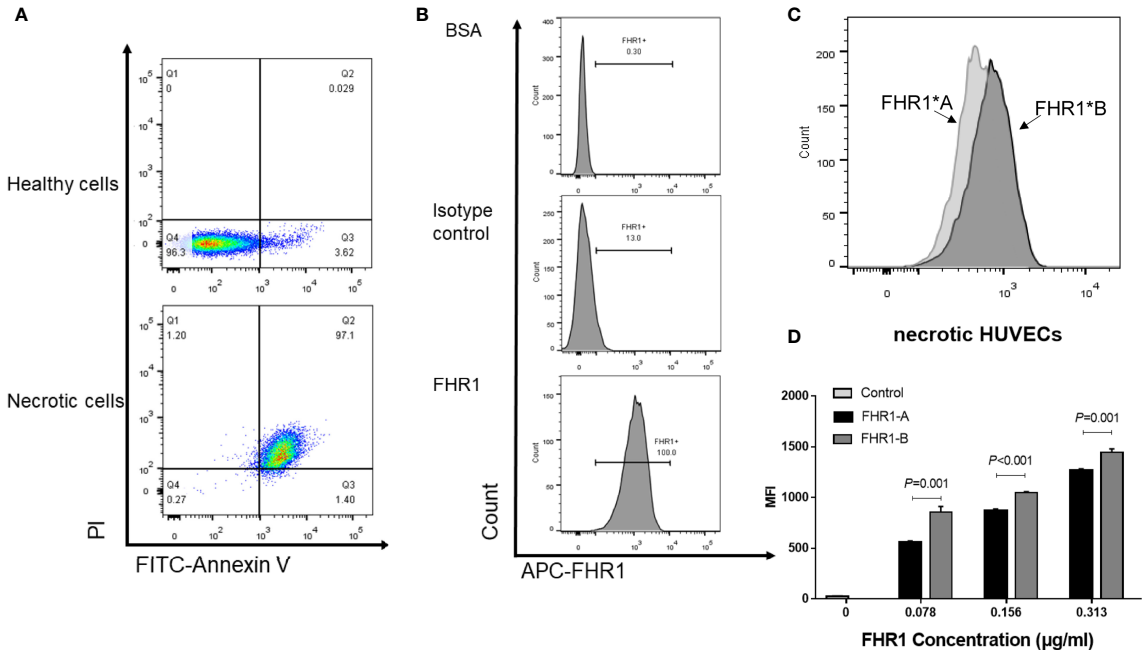

FIGURE 3 | Binding of the FHR1 isoforms to necrotic cells. Necrosis cells was evaluated by PI and Annexin V staining. Double positive for both Annexin V and PI cells were considered as necrotic cells **(A)**. The representative figures for blank control, isotype control and sample incubated with FHR1 protein were showed **(B)**. FHR1 proteins (0.078 μg/ml-0.313 μg/ml) bound to necrotic HUVECs in a dose-dependent manner. The representative figures for samples incubated with both FHR1*A and FHR1*B protein were showed **(C)**. In addition, compared to FHR1*A, FHR1*B presented significantly increased capacity to bind to necrotic HUVECs at concentrations between 0.078 μg/ml and 0.313 μg/ml **(D)**. The results are representative of three independent experiments. The data are presented as the means ± SDs. MFI, Mean fluorescence intensity.

FHR1*B Exhibited Increased Competition With FH for C3b Compared With FHR1*A

Since FHR1 was found to function as a competitive antagonist of FH to modulate activation of the complement cascade (27), we next explored whether FHR1*A and FHR1*B showed different levels of competition with FH. First, we evaluated the competition of FHR1*A and FHR1*B with FH for binding C3b. We found that FHR1*A and FHR1*B competed with FH for binding C3b in a dose-dependent manner, which was similar to previously reported observations of FHR1 (27). Moreover, within the concentration range of 0.078 μg/ml to 2.5 μg/ml, FHR1*B exhibited stronger competition with FH for binding C3b than FHR1*A, as FHR1*B decreased the binding by 10.49% (0.078 μg/ml FHR-1) and 30.52% (2.5 μg/ml FHR-1), while FHR1*A decreased the binding by only 1.11% and 10.73% (**Figure 4A**).

Next, we performed a cofactor assay to assess the deregulation of FHR1 by FH in terms of its CFI cofactor activity. As previously reported, unlike FH, FHR1 showed no intrinsic cofactor activity for CFI (**Figures 5A, B**). Here, we observed that FHR1 competed with FH in a dose-dependent manner, which led to a reduction in the CFI cofactor activity of FH. At the same concentrations (either 125 μg/ml or 62.5 μg/ml), FHR1*B showed a higher capacity for de-regulating FH-mediated CFI cofactor activity than FHR1*A (FHR1*B vs. FHR1*A: at 62.5 μg/ml concentration, $P<0.001$; at 125 μg/ml concentration, $P<0.001$; **Figures 5C, D**).

FHR1*B Exhibited Higher Deregulation Effect on FH Mediated Regulation of the Solid-Phase C3 Convertase

Given the negative regulation of FH on C3 convertase formation into consideration, we investigated the potential different effect of FHR1*B and FHR1*A on FH mediated regulation of the solid-phase C3 convertase. We found that FH inhibited the C3bBb assembling, while both isoforms of FHR1 competed with FH and reversed the inhibition. Moreover, FHR1*B showed more powerful deregulation effect on FH than FHR1*A, regarding the FH mediated regulation of the solid-phase C3 convertase. (FH vs. TBS, $P<0.001$. FHR1*B vs. FHR1*A: at 300nM concentration, $P=0.009$; at 400nM concentration, $P=0.005$; at 500nM concentration, $P=0.007$, **Figure 4B**).

FHR1*B Induced Elevated Secretion of Higher IL-1β and IL-6 Than FHR1*A

Recently, FHR1 was reported to play a proinflammatory role. We therefore compared the effects of FHR1*A and FHR1*B on monocytes. We found that monocytes incubated with FHR1*B secreted higher levels of IL-1β and IL-6 than monocytes incubated with FHR1*A. (FHR1*B vs. FHR1*A: IL-1β, $P<0.001$; IL-6, $P<0.001$; **Figure 6**).

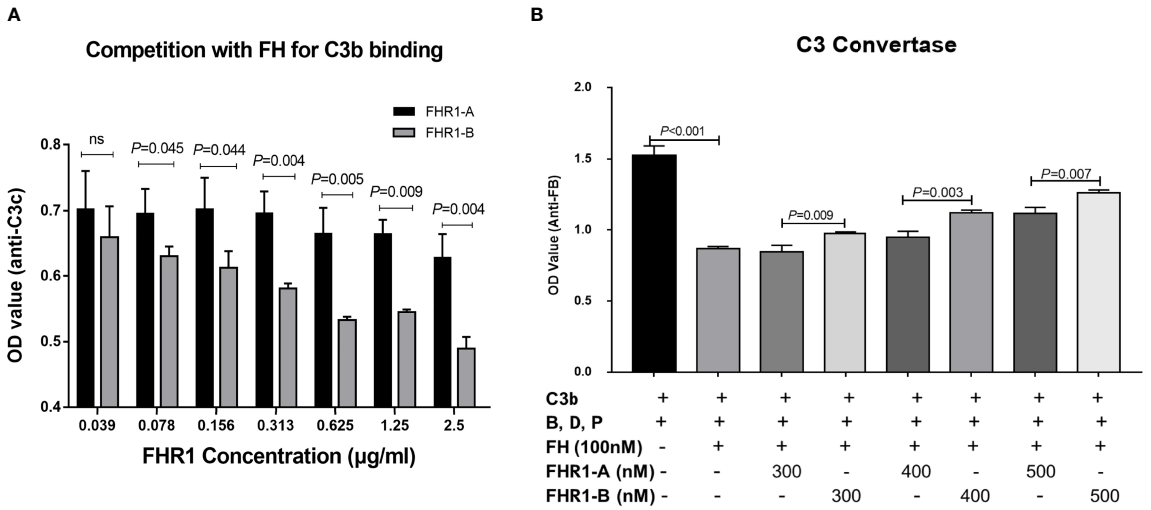

FIGURE 4 | Competition assays of FHR1 with FH to C3b and C3b convertase assays. FHR1*A and FHR1*B compete with FH for binding C3b in a dose-dependent manner, and FHR1*B binds more C3b than FHR1*A at concentrations of 0.078 μg/ml-2.5 μg/ml **(A)**. FH inhibited the C3bBb assembling, while both isoforms of FHR1 competed with FH and reverse the inhibition to some extent. Moreover, FHR1*B showed a more powerful deregulation effect on FH mediated regulation of the solid-phase C3 convertase **(B)**. The results are representative of three independent experiments. The data are presented as the means ± SDs.

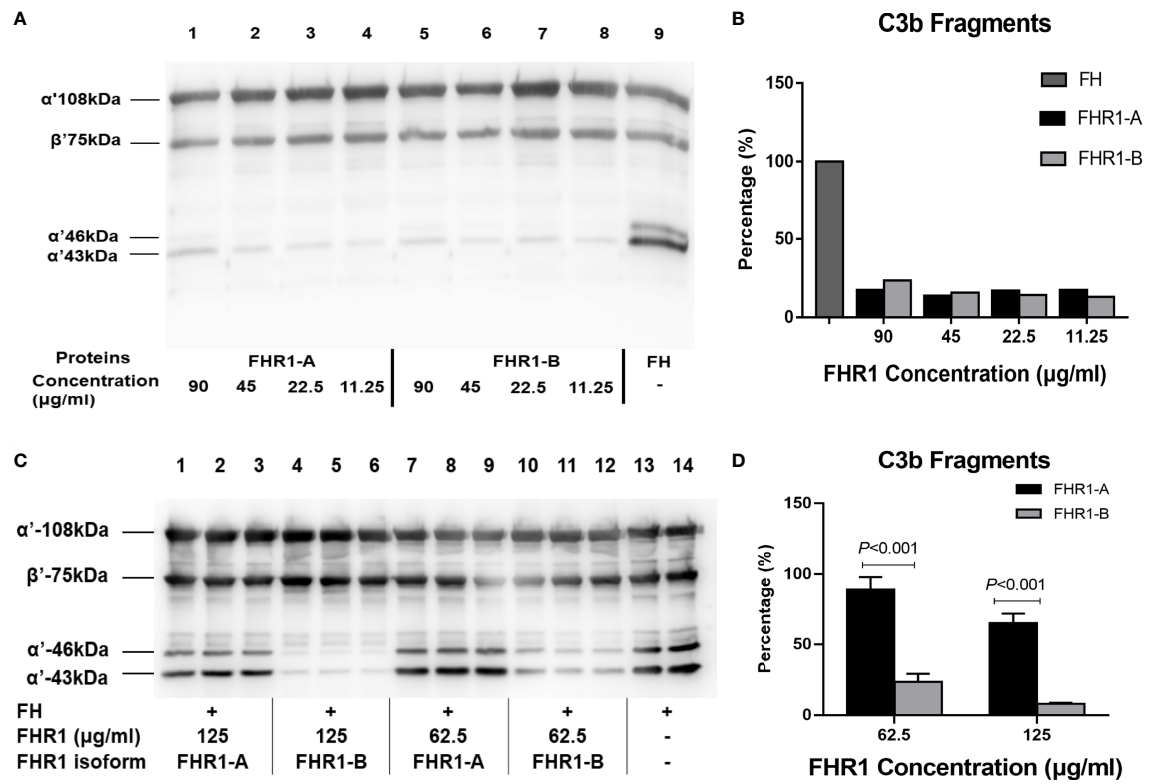

FIGURE 5 | Effect of the FHR1 isoforms on the cofactor activity of FH. Compared to FH (positive control, lane 9), both FHR1*A (lanes 1-3) and FHR1*B (lanes 4-6) at concentrations of 90-11.25 ug/ml showed no or little FI cofactor activity **(A)**. When incubated with C3b, FI and FH together, the FHR1 groups (lanes 1-3, 4-6, 7-9, 10-12 were technical replicates, respectively; **(C)** generated fewer C3b cleavage products than the group without FHR1 (no-FHR1 control, lanes 13-14, technical replicates; **(C)**. Furthermore, the FHR1*B groups generated more C3b cleavage products than the FHR1*A groups at the same concentrations **(C, D)**. The data are presented as the means ± SDs.

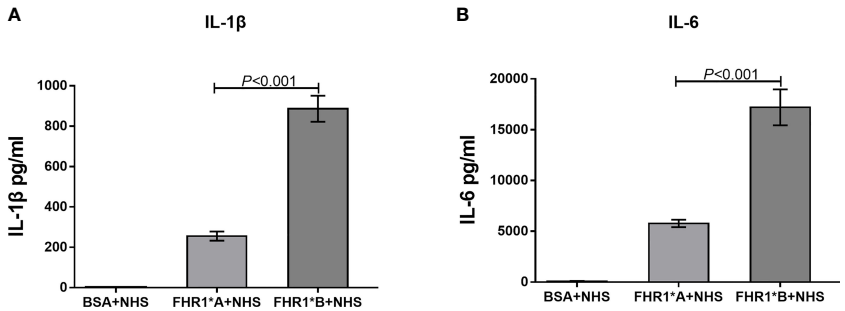

FIGURE 6 | FHR1 induces monocytes to secrete inflammatory cytokines. Compared to BSA, both FHR1*A and FHR1*B significantly increased IL-1β **(A)** and IL-6 **(B)** secretion by monocytes. In addition, FHR1*B induced the secretion of higher levels of IL-1β **(A)** and IL-6 **(B)** by monocytes than FHR1*A. The data are presented as the means ± SDs. The results are representative of three independent experiments. The data are presented as the means ± SDs.

DISCUSSION

aHUS is a rare variant of thrombotic microangiopathy that is triggered by abnormal alternative complement pathway activation, which leads to complement deposition on endothelial cells and causes endothelial cell swelling and detachment (28). In the present study, we showed that the *CFHR1* isoform *CFHR1*B*, which increases susceptibility to aHUS, has higher capacity for binding to C3b and could induce more inflammation than *CFHR1*A*, which suggested the involvement of *CFHR1* in aHUS.

CFHR1 is a member of the *CFH* gene family, and its encoded product FHR1 is composed of 5 SCR domains. Three C-terminal SCRs (SCR3-5) of FHR1 show high sequence similarity with SCR18-20 of FH. The crystal structure of FH SCR18-20 was determined to be a "J"-shape, in which SCR18 folds back toward SCR19. This structural characteristic of FH SCR18-20 suggested the presence of conformational mobility between SCR18 and SCR19 and little flexibility between SCR19 and SCR20 (29). FHR1*A and FHR1*B have three different amino acids in the SCR3 regions. To determine whether these three coding variants affected the protein structure of FHR1, we compared FHR1*A and FHR1*B by homology modeling and determine the differences in the angles between SCR3 and SCR4-SCR5. Therefore, we hypothesized that these angle differences might affect the protein flexibility of FHR1 and indirectly affect the function of FHR1 SCR4-SCR5.

Although only a few studies have focused on FHR1 SCR4-SCR5, its homologous motif in FH, SCR19-SCR20, has been widely investigated. Increasing evidence shows that FH SCR19 and SCR20 contain binding sites for C3b, glycosaminoglycans, and endothelial cells (30–32). Moreover, the majority of aHUS-associated FH mutations cluster within SCR19-SCR20 (7), supporting its interaction with endothelial cells. Similarly, FHR1 also has the ability to bind C3b and the surface of necrotic HUVECs (13, 18). To verify our hypothesis that the changes in the FHR1 structure induced by coding variants might indirectly influence the function of FHR1 SCR4-SCR5, we compared the capacities of FHR1*A and FHR1*B to bind C3b (including surface-bound C3b) as well as to necrotic HUVECs. Our results indicated that FHR1*B showed significantly higher capacity to bind to not only C3b (including surface-bound C3b) but also necrotic HUVECs. Our findings indicated that the coding variants of SCR3 may affect the function of FHR1, such as its binding C3b and necrotic cells.

In addition, FHR1 was reported to function as a competitive antagonist of FH (27). FH is a vital regulatory protein of complement in plasma that inhibits complement activation in two ways: interfering with the assembly and facilitating the decay of C3/C5 convertases by binding to C3b and acting as a cofactor to facilitate the cleavage of C3b by CFI (33). Therefore, we next evaluated the function of FHR1*A and FHR1*B in the de-regulation of FH. We found that both FHR1*A and FHR1*B could compete with FH to influence C3b binding, decrease the CFI-mediated cleavage and inactivation of C3b, and regulate C3 convertase formation in a dose-dependent manner, and these results are consistent with the FH competitor function of FHR1 (12, 13, 27). Compared to FHR1*A, FHR1*B presented an increased capacity to compete with FH, as shown by the generation of fewer FI-mediated cleavage products of C3b and more formation of C3 convertase, which would enhance complement activation. Our results indicated a stronger effect of FHR1*B than FHR1*A in the deregulation of FH.

Moreover, Irmscher et al. recently reported that FHR1 bound to necrotic-type cells and activated monocytic inflammasomes, and proved the FHR1 induced inflammation was independent of complement (15). In the present study, we also observed that FHR1*B has more powerful effects on triggering inflammation *via* monocytes, indicating that FHR1*B may cause damage in patients with aHUS through enhancement of both complement activation and inflammation.

However, our study had some limitations. Firstly, FHR-1 can form homodimers and heterodimers in circulation. However, lack of complete crystal structure of the FHR1 protein hindered us to further investigate the structural difference of FHR1*A and FHR1*B on dimers. Secondly, we didn't evaluate the differences regarding complement activation and inflammation in aHUS patients with homozygous FHR1*A and FHR1*B in the present study. Future studies focused on genotype-phenotype correlation in large aHUS cohort will be needed. Thirdly, in the cofactor assay, the concentration of FHR1 to show effective competition for FH regarding the cofactor function is higher than physiologic concentration in circulation. Although local concentration of

FHR3 and FHR4 in AMD patients were reported as much higher than in circulation (34), we are still lack of similar information about local FHR1 concentration.

In summary, our study showed that coding variants of *CFHR1* (c. C469T, c. C475G, c. G523C) might change the protein structure of FHR1, thereby influencing the FH de-regulation and proinflammatory functions of FHR1 and therefore influencing complement activation and inflammation. Our findings provide a possible genetic mechanism underlying the predisposition to aHUS caused by the *CFHR1* isoform *CFHR1*B*.

DATA AVAILABILITY STATEMENT

The raw data supporting the conclusions of this article will be made available by the authors, without undue reservation.

ETHICS STATEMENT

The studies involving human participants were reviewed and approved by the ethics committee of Peking University First Hospital. The patients/participants provided their written informed consent to participate in this study.

AUTHOR CONTRIBUTIONS

LZ and HZ conceived and designed the study. BX, YK, and WG carried out the experiments and analyzed the data. BX, YK, and LZ wrote the manuscript. All authors have read and approved the manuscript.

FUNDING

This project was supported by grants from the National Science Foundation of China (81922013, 81970598, 82070733), National Science Foundation of Beijing (7192209, 7202206), National Key Research and Development Program of China (2020YFC2005003), Beijing Science and Technology Plan Project of China (D181100000118003, Z161100000516005) and Chinese Academy of Medical Sciences Research Unit-Peking University (No. 2019RU023).

ACKNOWLEDGMENTS

We would like to thank Prof. Junyu Xiao and Dr. Yaxin Li for their help in recombinant FHR1 protein expression.

SUPPLEMENTARY MATERIAL

The Supplementary Material for this article can be found online at: https://www.frontiersin.org/articles/10.3389/fimmu.2022.755694/full#supplementary-material

REFERENCES

1. Venables JP, Strain L, Routledge D, Bourn D, Powell HM, Warwicker P, et al. Atypical Haemolytic Uraemic Syndrome Associated With a Hybrid Complement Gene. *PloS Med* (2006) 3:e431. doi: 10.1371/journal.pmed.0030431
2. Noris M, Remuzzi G. Atypical Hemolytic-Uremic Syndrome. *N Engl J Med* (2009) 361:1676–87. doi: 10.1056/NEJMra0902814
3. Fakhouri F, Zuber J, Frémeaux-Bacchi V, Loirat C. Haemolytic Uraemic Syndrome. *Lancet (London England)* (2017) 390:681–96. doi: 10.1016/S0140-6736(17)30062-4
4. Goodship TH, Cook HT, Fakhouri F, Fervenza FC, Frémeaux-Bacchi V, Kavanagh D, et al. Atypical Hemolytic Uremic Syndrome and C3 Glomerulopathy: Conclusions From a "Kidney Disease: Improving Global Outcomes" (Kdigo) Controversies Conference. *Kidney Int* (2017) 91:539–51. doi: 10.1016/j.kint.2016.10.005
5. Raina R, Krishnappa V, Blaha T, Kann T, Hein W, Burke L, et al. Atypical Hemolytic-Uremic Syndrome: An Update on Pathophysiology, Diagnosis, and Treatment. *Ther Apheresis Dialysis* (2019) 23:4–21. doi: 10.1111/1744-9987.12763
6. Fremeaux-Bacchi V, Fakhouri F, Garnier A, Bienaimé F, Dragon-Durey MA, Ngo S, et al. Genetics and Outcome of Atypical Hemolytic Uremic Syndrome: A Nationwide French Series Comparing Children and Adults. *Clin J Am Soc Nephrol: CJASN* (2013) 8:554–62. doi: 10.2215/CJN.04760512
7. Nester CM, Barbour T, de Cordoba SR, Dragon-Durey MA, Fremeaux-Bacchi V, Goodship TH, et al. Atypical Ahus: State of the Art. *Mol Immunol* (2015) 67:31–42. doi: 10.1016/j.molimm.2015.03.246
8. Maga TK, Nishimura CJ, Weaver AE, Frees KL, Smith RJ. Mutations in Alternative Pathway Complement Proteins in American Patients With Atypical Hemolytic Uremic Syndrome. *Hum Mutat* (2010) 31:E1445–60. doi: 10.1002/humu.21256
9. Díaz-Guillén MA, Rodríguez de Córdoba S, Heine-Suñer D. A Radiation Hybrid Map of Complement Factor H and Factor H-Related Genes. *Immunogenetics* (1999) 49:549–52. doi: 10.1007/s002510050534
10. Pérez-Caballero D, González-Rubio C, Gallardo ME, Vera M, López-Trascasa M, Rodríguez de Córdoba S, et al. Clustering of Missense Mutations in the C-Terminal Region of Factor H in Atypical Hemolytic Uremic Syndrome. *Am J Hum Genet* (2001) 68:478–84. doi: 10.1086/318201
11. Józsi M, Zipfel PF. Factor H Family Proteins and Human Diseases. *Trends Immunol* (2008) 29:380–7. doi: 10.1016/j.it.2008.04.008
12. Fritsche LG, Lauer N, Hartmann A, Stippa S, Keilhauer CN, Oppermann M, et al. An Imbalance of Human Complement Regulatory Proteins CFHR1, CFHR3 and Factor H Influences Risk for Age-Related Macular Degeneration (AMD). *Hum Mol Genet* (2010) 19:4694–704. doi: 10.1093/hmg/ddq399
13. Heinen S, Hartmann A, Lauer N, Wiehl U, Dahse HM, Schirmer S, et al. Factor H-Related Protein 1 (CFHR-1) Inhibits Complement C5 Convertase Activity and Terminal Complex Formation. *Blood* (2009) 114:2439–47. doi: 10.1182/blood-2009-02-205641
14. Tortajada A, Yébenes H, Abarrategui-Garrido C, Anter J, García-Fernández JM, Martínez-Barricarte R, et al. C3 Glomerulopathy-Associated CFHR1 Mutation Alters FHR Oligomerization and Complement Regulation. *J Clin Invest* (2013) 123:2434–46. doi: 10.1172/JCI68280
15. Csincsi Á I, Szabó Z, Bánlaki Z, Uzonyi B, Cserhalmi M, Kárpáti É, et al. FHR-1 Binds to C-Reactive Protein and Enhances Rather Than Inhibits Complement Activation. *J Immunol* (2017) 199:292–303. doi: 10.4049/jimmunol.1600483
16. Kárpáti É, Papp A, Schneider AE, Hajnal D, Cserhalmi M, Csincsi Á I, et al. Interaction of the Factor H Family Proteins FHR-1 and FHR-5 With DNA and Dead Cells: Implications for the Regulation of Complement Activation

and Opsonization. *Front Immunol* (2020) 11:1297. doi: 10.3389/fimmu.2020.01297
17. Losse J, Zipfel PF, Józsi M, Factor H. And Factor H-Related Protein 1 Bind to Human Neutrophils *via* Complement Receptor 3, Mediate Attachment to Candida Albicans, and Enhance Neutrophil Antimicrobial Activity. *J Immunol* (2010) 184:912–21. doi: 10.4049/jimmunol.0901702
18. Irmscher S, Brix SR, Zipfel SLH, Halder LD, Mutlutürk S, Wulf S, et al. Serum FHR1 Binding to Necrotic-Type Cells Activates Monocytic Inflammasome and Marks Necrotic Sites in Vasculopathies. *Nat Commun* (2019) 10:2961. doi: 10.1038/s41467-019-10766-0
19. Skerka C, Pradel G, Halder LD, Zipfel PF, Zipfel SLH, Strauß O. Factor H-Related Protein 1: A Complement Regulatory Protein and Guardian of Necrotic-Type Surfaces. *Br J Pharmacol* (2020) 178(14):2823–31. doi: 10.1111/bph.15290
20. Abarrategui-Garrido C, Martínez-Barricarte R, López-Trascasa M, de Córdoba SR, Sánchez-Corral P. Characterization of Complement Factor H-Related (CFHR) Proteins in Plasma Reveals Novel Genetic Variations of CFHR1 Associated With Atypical Hemolytic Uremic Syndrome. *Blood* (2009) 114:4261–71. doi: 10.1182/blood-2009-05-223834
21. Kopp A, Strobel S, Tortajada A, Rodríguez de Córdoba S, Sánchez-Corral P, Prohászka Z, et al. Atypical Hemolytic Uremic Syndrome-Associated Variants and Autoantibodies Impair Binding of Factor H and Factor H-Related Protein 1 to Pentraxin 3. *J Immunol* (2012) 189:1858–67. doi: 10.4049/jimmunol.1200357
22. Pieper U, Webb BM, Dong GQ, Schneidman-Duhovny D, Fan H, Kim SJ, et al. Modbase, a Database of Annotated Comparative Protein Structure Models and Associated Resources. *Nucleic Acids Res* (2014) 42:D336–46. doi: 10.1093/nar/gkt1144
23. Eramian D, Eswar N, Shen MY, Sali A. How Well can the Accuracy of Comparative Protein Structure Models be Predicted? *Protein Sci* (2008) 17:1881–93. doi: 10.1110/ps.036061.108
24. Hebecker M, Józsi M. Factor H-Related Protein 4 Activates Complement by Serving as a Platform for the Assembly of Alternative Pathway C3 Convertase *via* its Interaction With C3b Protein. *J Biol Chem* (2012) 287:19528–36. doi: 10.1074/jbc.M112.364471
25. Manuelian T, Hellwage J, Meri S, Caprioli J, Noris M, Heinen S, et al. Mutations in Factor H Reduce Binding Affinity to C3b and Heparin and Surface Attachment to Endothelial Cells in Hemolytic Uremic Syndrome. *J Clin Invest* (2003) 111:1181–90. doi: 10.1172/JCI16651
26. Timmann C, Leippe M, Horstmann RD. Two Major Serum Components Antigenically Related to Complement Factor H Are Different Glycosylation Forms of a Single Protein With No Factor H-Like Complement Regulatory Functions. *J Immunol* (1991) 146:1265–70.
27. Goicoechea de Jorge E, Caesar JJ, Malik TH, Patel M, Colledge M, Johnson S, et al. Dimerization of Complement Factor H-Related Proteins Modulates Complement Activation In Vivo. *Proc Natl Acad Sci USA* (2013) 110:4685–90. doi: 10.1073/pnas.1219260110
28. Stühlinger W, Kourilsky O, Kanfer A, Sraer JD. Letter: Haemolytic-Uraemic Syndrome: Evidence for Intravascular C3 Activation. *Lancet (London England)* (1974) 2:788–9. doi: 10.1016/S0140-6736(74)90991-X
29. Morgan HP, Mertens HD, Guariento M, Schmidt CQ, Soares DC, Svergun DI, et al. Structural Analysis of the C-Terminal Region (Modules 18-20) of Complement Regulator Factor H (FH). *PloS One* (2012) 7:e32187. doi: 10.1371/journal.pone.0032187
30. Jokiranta TS, Cheng ZZ, Seeberger H, Jòzsi M, Heinen S, Noris M, et al. Binding of Complement Factor H to Endothelial Cells is Mediated by the Carboxy-Terminal Glycosaminoglycan Binding Site. *Am J Pathol* (2005) 167:1173–81. doi: 10.1016/S0002-9440(10)61205-9
31. Jokiranta TS, Hellwage J, Koistinen V, Zipfel PF, Meri S. Each of the Three Binding Sites on Complement Factor H Interacts With a Distinct Site on C3b. *J Biol Chem* (2000) 275:27657–62. doi: 10.1074/jbc.M002903200
32. Ferreira VP, Herbert AP, Hocking HG, Barlow PN, Pangburn MK. Critical Role of the C-Terminal Domains of Factor H in Regulating Complement Activation at Cell Surfaces. *J Immunol* (2006) 177:6308–16. doi: 10.4049/jimmunol.177.9.6308
33. Ferreira VP, Pangburn MK, Cortés C. Complement Control Protein Factor H: The Good, the Bad, and the Inadequate. *Mol Immunol* (2010) 47:2187–97. doi: 10.1016/j.molimm.2010.05.007
34. Schäfer N, Grosche A, Reinders J, Hauck SM, Pouw RB, Kuijpers TW, et al. Complement Regulator FHR-3 is Elevated Either Locally or Systemically in a Selection of Autoimmune Diseases. *Front Immunol* (2016) 7:542. doi: 10.3389/fimmu.2016.00542

Conflict of Interest: The authors declare that the research was conducted in the absence of any commercial or financial relationships that could be construed as a potential conflict of interest.

Publisher's Note: All claims expressed in this article are solely those of the authors and do not necessarily represent those of their affiliated organizations, or those of the publisher, the editors and the reviewers. Any product that may be evaluated in this article, or claim that may be made by its manufacturer, is not guaranteed or endorsed by the publisher.

frontiers | Frontiers in Immunology

ORIGINAL RESEARCH
published: 27 May 2022
doi: 10.3389/fimmu.2022.886733

Borrelia miyamotoi FbpA and FbpB Are Immunomodulatory Outer Surface Lipoproteins With Distinct Structures and Functions

Charles E. Booth Jr[1†], *Alexandra D. Powell-Pierce*[2†], *Jon T. Skare*[2*] *and Brandon L. Garcia*[1*]

[1] Department of Microbiology and Immunology, Brody School of Medicine, East Carolina University, Greenville, NC, United States, [2] Department of Microbial Pathogenesis and Immunology, College of Medicine, Texas A&M University, Bryan, TX, United States

Pathogens that traffic in the blood of their hosts must employ mechanisms to evade the host innate immune system, including the complement cascade. The Lyme disease spirochete, *Borreliella burgdorferi*, has evolved numerous outer membrane lipoproteins that interact directly with host proteins. Compared to Lyme disease-associated spirochetes, relatively little is known about how an emerging tick-borne spirochetal pathogen, *Borrelia miyamotoi*, utilizes surface lipoproteins to interact with a human host. *B. burgdorferi* expresses the multifunctional lipoprotein, BBK32, that inhibits the classical pathway of complement through interaction with the initiating protease C1r, and also interacts with fibronectin using a separate intrinsically disordered domain. *B. miyamotoi* encodes two separate *bbk32* orthologs denoted *fbpA* and *fbpB*; however, the activities of these proteins are unknown. Here, we show that *B. miyamotoi* FbpA binds human fibronectin in a manner similar to *B. burgdorferi* BBK32, whereas FbpB does not. FbpA and FbpB both bind human complement C1r and protect a serum-sensitive *B. burgdorferi* strain from complement-mediated killing, but surprisingly, differ in their ability to recognize activated C1r versus zymogen states of C1r. To better understand the observed differences in C1r recognition and inhibition properties, high-resolution X-ray crystallography structures were solved of the C1r-binding regions of *B. miyamotoi* FbpA and FbpB at 1.9Å and 2.1Å, respectively. Collectively, these data suggest that FbpA and FbpB have partially overlapping functions but are functionally and structurally distinct. The data presented herein enhances our overall understanding of how bloodborne pathogens interact with fibronectin and modulate the complement system.

Keywords: complement C1r, classical pathway of complement, *Borrelia miyamotoi*, complement evasion, spirochete, BBK32

OPEN ACCESS

Edited by:
Péter Gál, Research Centre for Natural Sciences, Hungary

Reviewed by:
Christine Gaboriaud, UMR5075 Institut de Biologie Structurale (IBS), France
Cláudia Vilhena, Leibniz Institute for Natural Product Research and Infection Biology, Germany

***Correspondence:**
Brandon L. Garcia
garciabr18@ecu.edu
Jon T. Skare
jskare@tamu.edu

[†]*These authors have contributed equally to this work*

Specialty section:
This article was submitted to Molecular Innate Immunity, a section of the journal Frontiers in Immunology

Received: *28 February 2022*
Accepted: *19 April 2022*
Published: *27 May 2022*

Citation:
Booth CE Jr, Powell-Pierce AD, Skare JT and Garcia BL (2022) Borrelia miyamotoi FbpA and FbpB Are Immunomodulatory Outer Surface Lipoproteins With Distinct Structures and Functions. Front. Immunol. 13:886733. doi: 10.3389/fimmu.2022.886733

INTRODUCTION

In the United States, tick-borne relapsing fever (TBRF) is caused by the spirochetes *Borrelia hermsii* and *Borrelia turicatae*. Whereas these spirochetes are vectored by the soft tick of the *Ornithodoros* genus, a related TBRF pathogen, *Borrelia miyamotoi*, is transmitted by ixodid ticks that also vector the agent of Lyme disease (LD), *Borreliella burgdorferi* (1–6). A recent study suggests that *B. miyamotoi* is more widespread in some areas of the U.S. than previously recognized (7). Human infection by *B. miyamotoi* results in overlapping but differing pathology from TBRF, and is known as *B. miyamotoi* disease (BMD) (4, 6). In immunocompetent hosts, BMD presents as a recurrent influenza-like illness that is treatable with doxycycline, ceftriaxone, azithromycin, and potentially amoxicillin (8, 9). Although BMD-, TBRF-, and LD-causing spirochetes are tick-transmitted, their lifestyles within vertebrate hosts differ (10, 11). In the context of vertebrate infection, LD *Borreliella* are thought to survive within the skin and briefly in the bloodstream as a means to disseminate to deeper distal tissues (12–14), while TBRF and BMD *Borrelia* predominantly exist in host blood, indicating a heightened need to evade both soluble and cellular blood-borne immune components (1, 15).

To survive in immunocompetent hosts, TBRF and BMD spirochetes exhibit a robust antigenic variation mechanism *via* a surface-exposed lipoprotein termed variable major protein (Vmp), which allows them to evade clearance from the adaptive immune response (4, 16–18). Each Vmp-associated serotype leads to high bacteremia until a targeted antibody response lowers the relapsing fever *Borrelia* load, after which a new serotype arises, resulting in a "relapse" (19, 20). TBRF symptoms are correlated with the presence of blood-borne spirochetes and the gene conversion event that produces unique Vmp proteins is associated with relapses for TBRF, though less prevalent in BMD (1, 4). In addition to their Vmp-associated immune evasive strategy, *B. miyamotoi* uses other surface lipoproteins to target innate immune mechanisms, including the complement system (21–25). The complement system serves as a first line of defense against invading pathogens. It is initiated through three pathways known as the alternative (AP), lectin (LP), and classical pathway (CP). The CP plays a critical role in elimination of foreign cells and is initiated by antibody-antigen complexes bound by the circulating complement component, C1 (26, 27). Upon activation of C1, proteolytic cleavage of downstream complement components leads to a self-amplifying cascade, resulting in opsonization and phagocytosis of the target cell, modulation of adaptive immunity, neutrophil synergy, and bactericidal activity through formation of the terminal complement complex (TCC), also known as the membrane attack complex (MAC) (27). To avoid destruction of healthy self-cells, host regulators bind complement components, preventing their activation in circulation, such as C1 esterase inhibitor (C1-INH), or on the surface of cells, such as Factor H (FH) (27, 28). A number of bacterial complement inhibitors have been characterized, from inhibitors of complement activation in Gram-positive pathogens, to inhibitors of the MAC in susceptible Gram-negative pathogens, as well as factors that reduce opsonization and phagocytosis by host immune cells (29, 30).

While the complement/complement-evasion axis is better understood for Lyme disease-associated spirochetes (31), recent reports highlight the likely importance of complement evasion by *B. miyamotoi*. CbiA, a surface-exposed FH, C3, C3b, C4b, and C5-binding lipoprotein, inhibits both the CP and AP (21). BOM1093 is a *B. miyamotoi* vitronectin-binding protein that inhibits complement *via* vitronectin's endogenous TCC-inhibitory activity (25). Additionally, Vlp15/16 and Vlp18 were shown to inhibit the AP, though the mechanism of this activity has not yet been determined (22). The identification of a range of complement inhibitors, despite the relative nascent research into *B. miyamotoi* pathogenesis, is consistent with its blood-borne lifecycle in the vertebrate host.

We have previously shown that the *B. burgdorferi* BBK32 surface-exposed lipoprotein inhibits the CP by directly binding and inhibiting C1r, a serine protease required for activation of the CP (31–34). Separately, we demonstrated that BBK32 provides resistance to a serum-sensitive strain of *B. burgdorferi*, indicating a biologically relevant role for BBK32 in complement resistance (32–34). In addition, BBK32 is multifunctional, also acting as an adhesin to fibronectin and glycosaminoglycans (GAGs) (35–40). Additional work showed that BBK32 is required for optimal *B. burgdorferi* infection (35, 40). Phylogenetic analyses revealed orthologous protein families to BBK32 in both BMD and TBRF spirochetes, designated FbpA, FbpB, and FbpC (41). Both BMD and TBRF spirochetes harbor different sets of Fbp genes, with *Borrelia miyamotoi* encoding only *fbpA* and *fbpB*. In the TBRF pathogen *B. hermsii*, FbpC has been shown to bind fibronectin, however whether *B. miyamotoi* Fbp proteins retain functional similarity to BBK32 has not previously been explored (41, 42). In this study, we characterized the ability of *B. miyamotoi* FbpA and FbpB to bind human fibronectin and the complement protease C1r. Our detailed structure-function investigation reveals that these proteins exhibit differential interactions with both fibronectin and C1r, differences in the three-dimensional structures of their complement inhibitory domains, and demonstrates their ability to protect a serum-sensitive strain of *B. burgdorferi* from serum-mediated killing. Collectively, our data show that Fbp proteins from *B. miyamotoi* harbor partially overlapping, but distinct functions from one another. The novel finding that FbpB specifically recognizes active C1r may inform future efforts to develop therapeutics that are specific for the classical pathway of complement. The need for such complement-directed drugs is highlighted by the association of dysregulated or overactivated complement in important human pathologies (43–45).

MATERIALS AND METHODS

Growth of Bacterial Strains

Borreliella burgdorferi B31 strain B314 (46) (**Table 1**) was grown to mid-log phase in BSK-II and 6% normal rabbit serum (Pel-Freez Biologicals, Rogers, AR) under conventional conditions (1% CO_2, 32°C, pH 7.6). Genetically transformed *B. burgdorferi* strains were grown with kanamycin at 300 μg/mL. *Borrelia miyamotoi* strain FR64b was grown in MKP-F media (24)

TABLE 1 | Bacterial Strains and Plasmid Constructs used in this study.

***E. coli* strains**	**Description**	**Reference**
NEB 5α	*fhuA2* (*argF-lacZ*)U169 *phoA glnV44* ϕ80(*lacZ*)ΔM15 *gyrA96 recA1 relA1 endA1 thi-1 hsdR17*	New England Biolabs
BL21(DE3)	F^-*ompT hsd*S_B (r_B^-, m_B^-) *gal dcm* (DE3)	ThermoFisher Scientific
***Borreliella burgdorferi* strains**	**Description**	**Reference**
B314	Serum-sensitive, non-infectious *B. burgdorferi* B31 derivative strain lacking all linear plasmids	(46)
B314 pBBE22*luc*	B314 with shuttle vector encoding *bbe22* and *B. burgdorferi* codon optimized *luc* gene under the control of a strong borrelial promoter (P_{flaB}-*luc*); kan^R.	(40)
B314 pCD100	B314 with wildtype *bbk32* under control of its native promoter in pBBE22*luc*; kan^R.	(32)
B314 pAP8	B314 with *B. miyamotoi fbpA* under control of the *B. burgdorferi bbk32* promoter in pBBE22*luc*; kan^R.	This study
B314 pAP13	B314 with *B. miyamotoi fbpA-R264A-K343A* (*fbpA* DA) under control of the *B. burgdorferi bbk32* promoter in pBBE22*luc*; kan^R.	This study
B314 pAP11	B314 with *B. miyamotoi fbpB* under control of the *B. burgdorferi bbk32* promoter in pBBE22*luc*; kan^R.	This study
Borrelia miyamotoi	**Description**	**Reference**
FR64b	*Borrelia miyamotoi* isolate originally discovered in Japan and subsequently found in the U.S.	(47)
Plasmids		
pBBE22*luc*	Borrelial shuttle vector containing *bbe22* and *B. burgdorferi* codon-optimized *luc* gene under the control of a strong borrelial promoter (P_{flaB}-*luc*)	(40)
pCD100	Knock in construct of wild-type *bbk32* with its native promoter in pBBE22*luc*.	(32)
pAP8	Knock in construct encoding *B. miyamotoi fbpA* under the control of the *B. burgdorferi bbk32* promoter in pBBE22*luc*.	This study
pAP13	Knock in construct encoding *B. miyamotoi fbpA-R264A-K343A* (*fbpA* DA) under the control of the *B. burgdorferi bbk32* promoter in pBBE22*luc*.	This study
pAP11	Knock in construct encoding *B. miyamotoi fbpB* under the control of the *B. burgdorferi bbk32* promoter in pBBE22*luc*.	This study
pT7HMT-BBK32-C	Construct used for overexpression of recombinant BBK32-C.	(32)
pT7HMT-C1r-CCP2-SP	Construct used for overexpression of recombinant C1r-CCP2-SP.	(33)
pT7HMT-FbpA-C	Construct used for overexpression of recombinant FbpA-C.	This study
pT7HMT-FbpB-C	Construct used for overexpression of recombinant FbpB-C.	This study
pT7HMT-FbpB-Δ5C	Construct used for overexpression of recombinant FbpBΔ5-C.	This study
pT7HMT-FbpA DA-C	Construct used for overexpression of recombinant FbpA DA-C (R264A-K343A).	This study
pT7HMT-MBP-FbpA-N	Construct used for overexpression of recombinant MBP fusion protein FbpA-N	This study
pT7HMT-MBP-FbpB-N	Construct used for overexpression of recombinant MBP fusion protein FbpB-N	This study

under the same conditions listed above for *B. burgdorferi*. *Escherichia coli* strain NEB-5α (New England Biolabs) was grown in Luria broth media under aerobic conditions at 37°C and, as appropriate, with kanamycin at 50 μg/mL. *E. coli* strain BL21 (DE3) (Thermo Fisher) was grown in Terrific Broth (Fisher Bioreagents) with kanamycin (50 μg/mL) at 37°C until an OD_{600} between 0.6-0.8 was achieved, then moved to 16°C overnight for production of recombinant Fbp proteins.

Plasmid Constructs

The following constructs for *B. miyamotoi* FR64b *fbpA* (UNIPROT#: AHH06014.1) and *fbpB* (UNIPROT#: AHH05635.1) were subcloned into pT7HMT or a modification of pT7HMT encoding maltose binding protein (MBP) (48). All plasmid constructs are listed in **Table 1**. *E. coli* codon-optimized DNA fragments were purchased from IDT Technologies gBlock Gene Fragment Service or produced using PCR amplification templated from previously cloned constructs using methodology and constructs previously described (32–34, 48): FbpA-C residues 222-371; FbpA-C-R264A-K343A; FbpB-C residues 264-432; FbpB-Δ5C residues 264-427; FbpA-N residues 152-201; and FbpB-N residues 207-248. Oligonucleotides used are listed in **Table 2**. Residue numbering were based on UNIPROT numbering. The expression constructs for *B. burgdorferi* BBK32-C and C1r-CCP2-SP originated from previous studies (32, 33).

Expression constructs for *B. miyamotoi fbpA* and *fbpB* were assembled using the NEBBuilderHiFi DNA Assembly Cloning Kit as described in (34). The *B. miyamotoi fbpA* and *fbpB* genes were transcriptionally linked with the *bbk32* promoter from *B. burgdorferi* to promote equal expression in B314 relative to *bbk32*. The R264A and K343A mutations in *fbpA* were constructed sequentially by synthesizing a 194 bp fragment of *fbpA* from nucleotide 918 to 1112 containing the R264A mutation, and then once the R264A construct was obtained, with a 254 bp fragment from nucleotide 1112 to 1366 containing the K343A mutation. Both DNA fragments were synthesized by IDT gBlocks using the native *B. miyamotoi* strain FR64b *fbpA* sequences. The fragments were each assembled into the *fbpA* gene using primers that added overhangs complementing the *fbpA* gene adjacent to the synthesized fragments. These fragments were then assembled into the *fbpA*-expressing vector using NEBuilderHiFi DNA Assembly Cloning Kit. All plasmids were sequenced to ensure the desired mutations were obtained and that no additional mutations were introduced during the assembly process.

Transformation of *B. burgdorferi*

Transformation of strain B314 with the plasmid constructs pAP8, pAP11, and pAP13 was done as previously described (33, 49).

TABLE 2 | Oligonucleotides used in this report.

Oligonucleotides	5' to 3' sequence	Description	Reference
pncAF *lucF*	TATTGGAATTAATAGGCGGTGATG GAGGGGTTGTATTTGTTGACG	Oligonucleotide pair used to confirm *bbk32*, *fbpA*, and *fbpB* knock-in constructs	(32)
BmAUSF BmADSR	CTTTAAAGGAGAGAAAGCATGATAGTTAAAAGTAAATAT TGCATGCCTGCAGGTCGACCTAATACCAAGGACCATCTC	Oligonucleotide pair used to amplify *B. miyamotoi fbpA* for assembly with the *bbk32* promoter and pBBE22*luc*; used to assemble pAP8	This study
K32PBmABmBFusionF K32PBmAFusionR	GAGGTACCCGGGGATCCGTACTTTGTTCACCCTCTTG ATATTTACTTTTAACTATCATGCTTTCTCTCCTTTAAAG	Oligonucleotide pair used to amplify the *bbk32* promoter for assembly with *fbpA* and pBBE22*luc*; used to assemble pAP8	This study
BmBUSF BmBDSR	CTTTAAAGGAGAGAAAGCATGATTTTTAAAAATA GCATGCCTGCAGGTCGACTTATCTTGCAACAATACCTG	Oligonucleotide pair used to amplify *B. miyamotoi fbpB* for assembly with the *bbk32* promoter and pBBE22*luc* used to assemble pAP11	This study
K32PBmABmBFusionF K32PBmBFusionR	GAGGTACCCGGGGATCCGTACTTTGTTCACCCTCTTG TATTTTTAAAAATCATGCTTTCTCTCCTTTAAAG	Oligonucleotide pair used to amplify the *bbk32* promoter for assembly with *fbpB* and pBBE22*luc* used to assemble pAP11	This study
BmAR264AF BmAR264AR	GGAAATAAGGCTAGACAATCGATACAAGTCTTATCTGG TTTAATAGCTCCTTAAGATCTTTCTCAAGTTCTTCTTTTG	Oligonucleotide pair used to amplify the R264A fragment to generate a precursor of pAP13	This study
BmAK343AF BmAK343AR	CAAAAGAAGAACTTGAGAAAGATCTTAAGGAGCTATTAAA TGCATGCCTGCAGGTCGACCTAATACCAAGGACCATCTC	Oligonucleotide pair used to amplify the K343A fragment of *fbpA* for site directed mutagenesis of *fbpA* K343 used to assemble pAP13	This study
BmB_D5C_Fwd_BAM BmB_D5C_Rev_Not	GATGATGGATCCGACAACCAGTACAAATTCAAACT GATGATGCGGCCGCTTAGGTACGGGTCA	Oligonucelotide pair used to amplify the FbpB-Δ5C fragment using the pT7HMT-FbpB-C construct template	This study

Protein Expression and Purification

Recombinant proteins were expressed and purified as in (32, 33). Briefly, after elution of the Ni column using the Elution buffer (20 mM Tris (pH 8.0), 500 mM NaCl, 500 mM Imidazole), the proteins were exchanged into 20 mM Tris (pH 8.0), 500 mM NaCl, 10 mM Imidazole using a Desalting 26/10 column (GE Healthcare). The His-tag was then removed by incubation with the tobacco etch virus (TEV) protease and 5 mM β-mercaptoethanol overnight at room temperature. The TEV digested proteins were separated from the His-tag by passing over a 5 mL HisTrap-FF column on the FPLC with the captured flowthrough further purified using a HiLoad Superdex 75 PG gel filtration column (GE Healthcare). The single peak after gel filtration was examined using SDS-PAGE analysis, then pooled and exchanged into HBS buffer (10 mM HEPES [pH 7.3], 140 mM NaCl). The C1r-CCP2-SP construct was purified according to previously published protocols with an added final gel filtration chromatography step using a HiLoad Superdex 75 PG column (GE Healthcare) and exchanged into HBS buffer (33, 34, 50, 51). Purified full-length complement proteins of both the zymogen and enzymatically active forms of C1r were obtained from Complement Technology, Inc. (Tyler, TX). Purified full-length human fibronectin was purchased from Millipore Sigma. Sequence alignments of the proteins were generated using Clustal alignment server from EMBL-EBI.

Surface Plasmon Resonance

Surface plasmon resonance (SPR) was performed on a Biacore T200 instrument set to 25°C with a flowrate of 30 µL/min. The running buffer was HBS-T (10 mM HEPES (pH 7.3), 140 mM NaCl, and 0.005% Tween 20) or HBS-T containing 5 mM $CaCl_2$. Proteins of interest were immobilized on CMD200 sensor chips (Xantec Bioanalytics) *via* standard amine coupling as before (32–34). Immobilization quantities were as follows: human plasma fibronectin over MBP-FbpA-C (1015.3 RU), MBP-FbpB-C (1074.1 RU); C1r-CCP2-SP over FbpA-C (1061.2 RU), FbpB-C (877.7 RU), FbpA-C-R264A-K343A (FbpA DA-C) (1591.8 RU); C1r zymogen or active C1r over FbpA-C (852.4 RU), FbpB-C (1116.6 RU). C1r-CCP2-SP over Fbps was performed in multi-cycle using a twofold dilution series of the C1r-CCP2-SP ranging from 0-100 nM. Data was obtained in triplicate with each cycle having an association time of 2 min, a dissociation time of 3 min, and three 1 min injections of regeneration buffer (0.1 M Glycine [pH 2.0], 2.5 M NaCl). Equilibrium dissociation constants (K_D) were obtained from the resulting kinetic fits generated by the Biacore T200 Evaluation Software (GE Healthcare). Zymogen or active C1r binding data for FbpA-C and FbpB-C was obtained in single cycle using a fivefold dilution series of either C1r zymogen or active C1r ranging from 0-100 nM. Data was obtained in triplicate with each cycle having an association time of 5 min, a final dissociation time of 1 hour, and two 1 min regeneration injections with regeneration buffer (0.1 M Glycine [pH 2.0], 2.5 M NaCl). Equilibrium dissociation constants (K_D) were obtained from the resulting kinetic fits generated by the Biacore T200 Evaluation Software (GE Healthcare). Human plasma fibronectin was buffer exchanged into HBS-T and then injected over MBP-FbpA-N or MBP-FbpB-N. Data was obtained in multicycle using a twofold dilution series ranging from 0-500 nM. Data was obtained in triplicate with each cycle having an association time of 2 min, a dissociation time of 3 min, and two 1 min injections of regeneration buffer (10 mM CAPS [pH 10.0]). Steady-state affinity fits were performed using Biacore T200 Evaluation Software.

Surface Plasmon Resonance Competition Experiments

SPR was performed using conditions described for the direct binding experiments. FbpA-C (935.4 RU), FbpB-C (1082.9 RU),

and FbpB-Δ5C (1115.4 RU) were immobilized on a new CMD200 sensor chip (Xantec Bioanalytics) *via* standard amine coupling as before (32–34). 25 nM C1r-CCP2-SP alone, or with 25 nM FbpA-C, FbpB-B, FbpA DA-C, or FbpB-Δ5C were injected over the Fbp biosensors. Injections were performed in triplicate with each cycle having an association time of 2 min, a dissociation time of 3 min, and two 1 min injections of regeneration buffer (0.1 M Glycine [pH 2.0], 2.5 M NaCl). The binding response just prior to injection stop was used to determine differences for the ability of the soluble Fbp proteins to compete with immobilized Fbps for C1r-CCP2-SP binding.

Generation of Polylonal Antibodies Against FbpA and FbpB

Polyclonal antibodies reactive with FbpA and FbpB were generated by separately immunizing female C57BL/6 mice intradermally with 25 μg either FbpA-C or FbpB-C in an equal volume of PBS and TiterMax® Gold Adjuvant (Sigma Aldrich) as outlined (52). Two weeks after the initial immunization, mice were boosted with 25 μg of the same protein. Two weeks after boosting, mice were euthanized and blood was immediately isolated by exsangunation, allowed to clot, and serum removed after low speed centrifugation. Reactivity and specificity of each serum sample to *B. miyamotoi* FbpA and FbpB was evaluated by Western Blot using purified recombinant protein. All animal work was reviewed and approved by the Texas A&M University Institutional Animal Care and Use Committee (protocol number 2019-0422).

Far Western Overlay Analysis With Full-Length *B. miyamotoi* Proteins

Far Western overlays were carried out as described in (32, 35). Briefly, *B. burgdorferi* strain B314 derivatives were cultured in BSKII media supplemented with 300 μg/mL kanamycin. Cultures were harvested and *B. burgdorferi* whole-cell lysates were generated for B314 strains producing FbpA, FbpB, FbpA DA, or from the pBBE22*luc* vector-only control. 2.5 x10^7 whole cell equivalents were resolved by SDS-PAGE with 0.625 μg of recombinant Fbp-C and MBP-Fbp-N proteins used as controls for C1r and fibronectin, respectively. The SDS-PAGE resolved proteins were transferred to a PVDF membrane and then blocked overnight in 5% non-fat milk. The blots were washed and incubated with 20 μg of zymogen or active C1r for 1 hour. PVDF membranes were probed for C1r binding using a goat antibody to human C1r (R&D Systems) at a 1:3,000 dilution followed by a rabbit anti-goat antibody conjugated to HRP (Invitrogen) at a 1:5,000 dilution. Similar experimentation was done after incubation with 20 μg of human fibronectin with subsequent binding determined using a mouse monoclonal antibody specific for human fibronectin conjugated to HRP (Santa Cruz Biotechnology) at a 1:1,000 dilution. All blots were then visualized using the SuperSignal™ West Pico Plus chemiluminescent kit (Thermo Scientific). Control Western blots were performed as above with 2.5 x10^7 whole cell equivalents to monitor Fbp expression and to serve as loading controls. To probe for FbpA and FbpB expression, mouse antibodies against FbpA or FbpB were used at a 1:5,000 dilution, respectively. To examine the flagellar protein FlaB, a mouse monoclonal antibody specific for FlaB (US Biologicals, Inc.) was used at a 1:20,000 dilution. Detection of membrane bound immune complexes was facilitated with a goat anti-mouse immunoglobulin HRP conjugate diluted 1:10,000 (Invitrogen). Visualization was the same as above. All Far Western blots were performed in duplicate.

Crystallization, Structure Determination, Refinement, and Analysis

FbpA-C was concentrated to 12.8 mg/mL total protein in a buffer of (10 mM HEPES [pH 7.3], 50 mM NaCl). Crystals were obtained by vapor diffusion of sitting drops at 20°C by mixing 1 μL of protein with 1 μL of precipitant solution (0.1 M Tris [pH 8.5], 2 M ammonium sulfate). Large crystal plate clusters generally appeared after 9-10 d. Sequential rounds of micro-seeding produced samples of sufficient size and quality for harvesting. Samples were cryopreserved in precipitant solution supplemented with an additional 20% glycerol.

Crystallization trials using FbpB-C failed to produce diffraction quality crystals. Constructs removing residues from the N-terminus and C-terminus were screened resulting in identification of crystallization conditions for a construct of FbpB where five residues were removed from the C-terminus (*i.e.*, FbpB-Δ5C). FbpB-Δ5C was concentrated to 19.1 mg/mL and 8.69 mg/mL in 10 mM Tris (pH 8.0), 50 mM NaCl buffer. Crystals of FbpB-Δ5C were obtained by vapor diffusion of sitting drops at 4°C for both concentrations. Initial crystals grew in a condition containing 0.2M $MgCl_2$, 0.1M Tris (pH 8.5), 30% PEG 4,000 and an optimized condition was identified by additive screening 4 mg/mL in 0.2 M $MgCl_2$, 0.1 M Tris (pH 8.5), 26.25% PEG 4,000, 35 mM spermidine followed by microseeding. Crystals were harvested and cryoprotected by supplementing the crystallization buffer with 10% glycerol.

Monochromatic X-ray diffraction data were collected at 0.975Å (FbpA-C) or 1.00Å (FbpB-Δ5C) wavelength using beamline 22-ID of the Advanced Photon Source (Argonne National Laboratory). Diffraction data were integrated, scaled, and reduced using the HKL2000 software suite (53) and assessed for data quality (54) (**Table 3**). FbpA-C crystals grew in the space group P21 and contained two copies in the asymmetric unit which were related by twofold non-crystallographic symmetry. FbpB-Δ5C crystals grew in space group C2 and contained a single copy of FbpB-Δ5C in the asymmetric unit. Initial phases for FbpA-C were obtained by molecular replacement using a single copy of a poly-alanine model of BBK32-C (PBD:6N1L) generated with the program CHAINSAW *via* the CCP4 software package (55). Initial phases for FbpB-Δ5C were obtained by molecular replacement using a FbpA-C polyalanine model that was created using CHAINSAW from CCP4 (55). Following an initial round of refinement, models for FbpA-C and FbpB-Δ5C were completed by a combination of automated chain tracing using PHENIX.AUTOBUILD (56–58) and manual building into electron density maps using COOT (59). The final model was completed upon iterative cycles of manual rebuilding and refinement using PHENIX.REFINE (56–58). The N-terminal

TABLE 3 | Refinement data for the solved FbpA and FbpB crystal structures.

Data collection and refinement		
Data collection	FbpA $_{(222–371)}$	FbpB $_{(267-427)}$
Space group	P 1 21 1	C 1 2 1
Cell dimensions		
a, b, c, Å	58.43, 40.32, 74.09	62.77, 46.21, 59.56
α, β, γ, °	90.00, 105.41, 90.00	90.00, 102.94, 90.00
Resolution, Å	50.0-1.90 (1.97-1.90)	50-2.09 (2.17-2.09)
R_{meas}	0.166 (0.654)	0.115 (0.424)
R_{pim}	0.068 (0.276)	0.054 (0.209)
$CC_{1/2}$	0.988 (0.834)	0.995 (0.910)
I/σI	13.2 (2.13)	20.2 (2.42)
Completeness, %	97.3 (97.7)	96.5 (93.5)
Redundancy	5.8 (5.3)	4.4 (3.5)
Refinement		
Resolution, Å	35.71-1.90	33.21-2.09
No. reflections	25,840	9,513
R_{work}/R_{free}	0.206, 0.232	0.225, 0.258
No. non-hydrogen atoms	2,694	1,288
Protein	2,492	1,252
Water	202	36
B-factors		
Protein	27.6	44.2
Water	33.5	45.5
Rmsd		
Bond lengths, Å	0.014	0.010
Bond angles, °	1.39	1.27

Values in parantheses refer to the highest-resolution shell.

cloning artifact sequence for FbpA-C (Residues G-S-T-G-S) and FbpB-Δ5C, and residues 264-268, 355, 401-403, and 427 of FbpB-Δ5C were not modeled in the final refined structure due to poor electron density. Refined coordinates and structure factors have been deposited in the Protein Data Bank, Research Collaboratory for Structural Bioinformatics, Rutgers University (www.rcsb.org/) under PDB ID codes 7RPR for FbpA-C and 7RPS for FbpB-Δ5C. A description of crystal cell constants, diffraction data quality, and properties of the final models for FbpA-C and FbpB-Δ5C can be found in **Table 3**. Representations of the protein structures and electron density maps were generated by PyMol (www.pymol.org/).

Circular Dichroism

Far-UV spectra were collected to assess the secondary structure for FbpA-C, FbpB-C, FbpA DA-C, and FbpB-Δ5C. Samples were diluted to 10 μM in 10 mM Na_3PO_4 based on previous protocols (60). Spectra for a buffer control were used to subtract background noise. Spectra were collected across a wavelength range of 180-300 nm, at 120 nm min^{-1}, using 1 nm step, 0.5 sec response, and 1 nm bandwidth. Data was collected using a Chirascan V100 instrument with a square small volume quartz cuvette with a path length of 0.05 cm (Applied Photophysics, UK).

Analytical Gel Filtration Chromatography

Analytical gel filtration was performed as before (34). 100 μg of FbpB-C and FbpB-Δ5C in a total volume of 500 μL were injected onto a Superdex 75 10/300 GL column (GE Healthcare) at a flowrate of 0.5 mL/min. The running buffer used was 10 mM HEPES (pH 7.3), 140 mM NaCl.

C1r-CCP2-SP Enzyme Inhibition Assay

A colorimetric assay was used to monitor dose-dependent inhibition of C1r-CCP2-SP enzyme activity based off (33, 34). 1 μM Fbps-C were incubated with 15 nM C1r-CCP2-SP enzyme and 300 μM of the serine protease substrate Z-Gly-Arg-thiobenzyl (MP Biomedical) in HBS buffer (10 mM HEPES [pH 7.3] and 140 mM NaCl). Enzyme cleavage of Z-Gly-Arg-thiobenzyl was determined by incubating the reaction with 100 μM DTNB (5,5'-Dithiobis-[2-nitrobenzoic acid], Ellman's reagent). The EnSight Multimode Plate Reader (PerkinElmer) was used to read the absorbance values for the reaction at 412 nm. Data were obtained in triplicate and normalized with 15 nM C1r-CCP2-SP lacking inhibitor as a positive control that represented the 100% amount of Z-Gly-Arg-thiobenzyl cleaved by C1r-CCP2-SP in 30 min at 25°C. Using a DTNB and Z-Gly-Arg-thiobenzyl only negative control allowed for subtraction of any non-specific colorimetric change.

ELISA-Based Complement Inhibition Assay

An ELISA-based assay that utilizes IgM as a specific activator of the classical pathway as described (32–34, 50, 61), was used to determine the pathway's downstream effect while in the presence of the Fbps. Data were obtained in triplicate and normalized using no inhibitor with 2% normal human serum (Innovative Research) as a positive control that represented the 100% amount of C4b deposition in 1 hour at 37°C. Non-specific interactions were subtracted out using a negative control with no serum. An EnSight Multimode Plate Reader (PerkinElmer) was used to read the absorbance values at 450 nm for the reaction.

Hemolysis Assay

A hemolysis assay that uses antibody-opsonized sheep red blood cells to specifically activate the classical pathway was performed as previously described (32, 33, 62) to determine if *B. miyamotoi* Fbp-C proteins protected erythrocytes from complement-mediated hemolysis. A serial dilution series of Fbp-C proteins was incubated with buffer-exchanged pre-sensitized sheep erythrocytes (Complement Technology) and 2% normal human serum (Innovative Research). After a 1 hour incubation at 37°C the reaction was clarified *via* centrifugation at 500 x g and the absorbance read using an EnSight Multimode Plate Reader (PerkinElmer) at 412 nm. Data were obtained in triplicate normalized using a no inhibitor with serum positive control that represented the 100% cell lysis at 37°C in 1 hour. Background hemolysis was subtracted out using a negative control with only buffer and red blood cells.

Quantitative ELISA to Assess *B. miyamotoi* Lipoproteins Binding to Serum C1r

The interaction of *B. miyamotoi* Fbp proteins with C1r in human serum was measured using an ELISA-type binding assay based on (63). Fbp proteins were immobilized overnight onto high-binding 96-well plates (Greiner Bio-One) at 0.2 mg/mL in 100 mM $NaCO_3$ (pH 9.6). A twofold serial dilution of normal human serum (Innovative Research) ranging from 0.0012-10% serum in CP Assay buffer (10 mM HEPES [pH 7.3], 140 mM NaCl, 2 mM $CaCl_2$, 0.5 mM $MgCl_2$, 0.1% gelatin) was incubated with immobilized Fbp-C proteins at 37°C for 1 hour. The amount of serum C1r bound to immobilized Fbps was found using a goat antibody to human C1r (R&D Systems) diluted 1:2,000 and immune complexes detected with rabbit anti-goat Ig conjugated to HRP (Invitrogen) at a 1:3,000 dilution. Data were obtained in at least duplicate and read at 450 nm using the EnSight Multimode Plate Reader (PerkinElmer) with non-specific interactions subtracted out using a negative control with no serum.

Proteinase K Accessibility Assays

B. burgdorferi strain B314 was grown to mid-log phase and harvested by centrifugation at 4,500 x g for 10 minutes at 4°C, and washed once with PBS. The cell pellet was resuspended in 0.8 mL of either PBS alone, or PBS with proteinase K to a final concentration of 200 μg/mL, and incubated at 20°C for 40 min. Reactions were terminated by the addition of phenylmethylsulfonyl fluoride (PMSF) to a final concentration of 1 mM. Cells were centrifuged (4,500 x g for 10 min at 4°C), washed twice with PBS, and resuspended in sample buffer. Samples corresponding to $5x10^7$ whole cell equivalents were run on SDS-PAGE gel, transferred to PVDF membranes and immunoblotted with mouse polyclonal antibodies to FbpA and FbpB or monoclonal antibodies directed against BBK32 or borrelial FlaB (US Biologicals Inc.) and imaged with chemiluminescence as previously described (33).

Serum Complement Sensitivity Assay

Assays were performed as in (33, 34). Briefly, *B. burgdorferi* strain B314 producing BBK32 (pCD100), *B. miyamotoi* FbpA (pAP8) or FbpA-DA (pAP13), and *B. miyamotoi* FbpB (pAP11) (see **Table 1**), as well as the vector-only control B314 pBBE22*luc*, were grown at 32°C in 1% CO_2 to early- to mid-log phase and diluted in complete BSK-II media to a final cell density of $1x10^6$ cells/mL. *B. burgdorferi* cells were then incubated in 15% normal human serum (Complement Technology) or heat inactivated serum (55°C for 30 min.), with thermal inactivation of complement proteins as a positive control for survival, for 1.5 hours at 37°C under gentle agitation. Cell survival was assessed by dark field microscopy based on cell motility and overt membrane damage or lysis.

Soluble Protein Inhibition Rescue Assay

The ability of exogenous *B. miyamotoi* FbpA-C, FbpA DA-C, and FbpB-C to rescue serum-sensitive *B. burgdorferi* B314 pBBE22*luc* was measured similarly to the serum sensitivity assay. Exogenous complement inhibitory proteins were added at a final concentration of 48 nM, 240 nM, and 1.2 μM, approximately five-fold less than, equal to, and five-fold greater than the concentration of C1r in the human serum sample used. Survival was compared to that of B314 pBBE22*luc* with no exogenous protein addition, and of B314 pCD100, which produces BBK32, as described for the serum sensitivity assays.

Statistics

Data is shown as the average of the replicates with 95% confidence intervals. Half-maximal inhibitory concentrations (IC_{50}) values for the CP inhibitory ELISA and CP hemolysis assays were determined using a non-linear variable slope regression fit. The half-maximal effective concentration (EC_{50}) for the serum C1r binding ELISA was determined using a non-linear one-site total regression fit. One-way ANOVA was used for the C1r enzyme and competition SPR experiments to determine differences among the means, followed by a *post-hoc* Tukey analysis for pairwise comparison of each Fbp protein. For serum sensitivity and B314 "rescue" assays, two-way ANOVA with a Šidák correction for multiple comparisons was used. All statistical analysis was performed using GraphPad Prism version 9.3.

RESULTS

B. miyamotoi Encodes Two Orthologous Proteins to *B. burgdorferi* BBK32

B. burgdorferi BBK32 interacts with multiple host proteins through non-overlapping protein domains. The N-terminus of BBK32 (BBK32-N) binds to fibronectin (35–37, 40, 64–70), while the C-terminal domain (BBK32-C) interacts with complement serine protease C1r (32, 33). Relapsing fever spirochetes encode a combination of up to three separate BBK32 orthologs termed fibronectin binding proteins (Fbps) (41) (**Figure 1A**). Fbp genes organize into three protein families denoted FbpA, FbpB, and FbpC and vary in their sequence identity to BBK32 between 56-62% (FbpAs), 25-30% (FbpBs), and 22-27% (FbpCs) (**Figure S1A**). A BLASTp search of the *B. miyamotoi* strain FR64b genomic

sequence, using *B. burgdorferi* strain B31 BBK32 as a query, identified only two orthologous sequences; one belonging to the FbpA family and one to the FbpB family (**Figure 1A**). Unlike *B. miyamotoi* FbpA, FbpB lacks significant amino acid sequence homology for a key motif that is important for BBK32's interaction with fibronectin (**Figure 1B**) (i.e., gelatin-binding domain sequence [GBD]) (69). Similarly, while a critical residue involved in the BBK32/C1r interaction is conserved in both FbpA and FbpB (i.e. BBK32-R248/FbpA-R264/FbpB-R309), another important 'hot-spot' lysine residue is conserved only in FbpA (BBK32-K327/FbpA-K343) (**Figure 1B**) (34).

Differential Interactions of *B. miyamotoi* Fbps With Human Fibronectin

We hypothesized that the sequence variation in predicted functional sites of FbpB, and to a lesser degree FbpA, may result in altered function of *B. miyamotoi* Fbps relative to BBK32. To test this, we first began by evaluating the direct interaction of each protein with human fibronectin. We expressed and purified recombinant maltose-binding protein (MBP) fusion proteins that encoded the predicted fibronectin-binding site based on alignment to BBK32 (termed MBP-FbpA-N and MBP-FbpB-N) (**Figure 1B**, green box). Surface plasmon resonance (SPR) experiments were carried out by immobilizing each fusion protein on the surface of an SPR sensorchip and evaluating purified human fibronectin as an analyte in a dose-dependent manner. MBP-FbpA-N bound dose-dependently to soluble human fibronectin (K_D = 170 nM) (**Figures 2A, C**), whereas MBP-FbpB-N exhibited no detectable interaction with fibronectin at concentrations up to 500 nM (**Figures 2B, D**).

To exclude the possibility that FbpB may utilize a site outside of the predicted fibronectin-binding region to engage fibronectin, and to evaluate the interaction in the context of a full-length lipoprotein, we expressed intact *fbpA* and *fbpB* ectopically in *B. burgdorferi* strain B314. *B. burgdorferi* B314 is a serum-sensitive, high-passaged strain that has lost all linear plasmids including the 36 kilobase linear plasmid (lp36) that encodes *bbk32* (46). Equivalent protein lysates from *B. burgdorferi* strain B314 derivatives were tested for their ability to produce native *B. miyamotoi* FbpA, a double alanine mutant of FbpA at residues 264 and 343—R264A and K343A—denoted FbpA-DA (discussed below), and FbpB, by SDS-PAGE and Western immunoblot analysis (**Figures S2A, B**). Whereas the antibody to FbpA recognized only the FbpA protein, antisera to FbpB recognized both FbpB and, to a lesser extent, FbpA (**Figure S2A**). We then tested these same samples using a Far Western approach with human fibronectin as the probe. Both FbpA and FbpA-DA in B314 bound human fibronectin whereas samples containing FbpB or the pBBE22*luc* shuttle vector control spirochetes exhibited no detectable binding (**Figure 2E**). Consistent with the SPR experiments (**Figures 2A–D**), recombinant MBP-FbpA-N fusion protein bound human fibronectin in this assay format, whereas the MBP-FbpB-N protein did not (**Figure 2E**). Analysis of total lysate samples by SDS-PAGE (**Figure S2B**) and FlaB protein by Western blot (**Figure 2E**) demonstrated equivalent protein levels were used for comparison. These results show that while *B. miyamotoi* FbpA retains BBK32-like fibronectin-binding activity, FbpB does not.

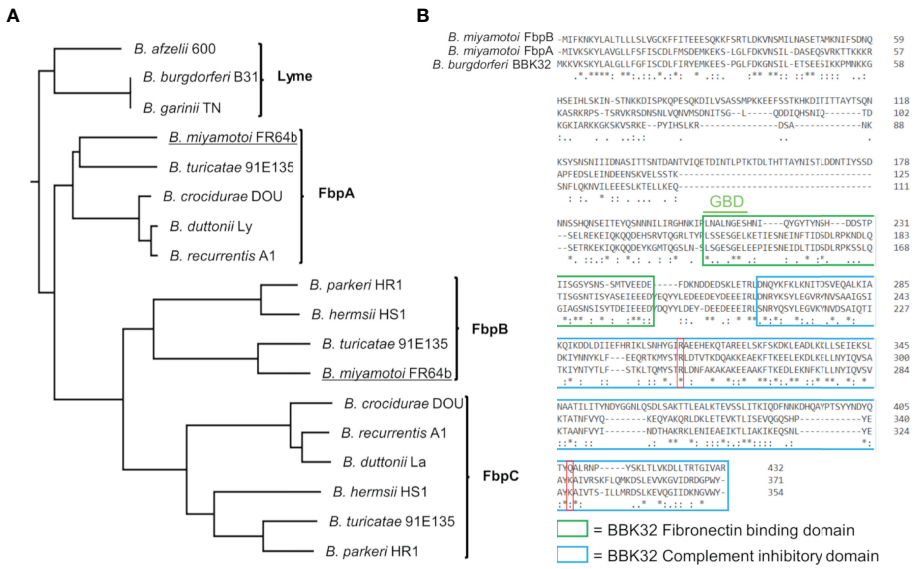

FIGURE 1 | *B. miyamotoi* encodes two orthologous genes to *B. burgdorferi* BBK32. **(A)** BBK32 orthologs are found in relapsing fever (RF)-associated and *B. miyamotoi* spirochetes and are denoted FbpA, FbpB, and FbpC (41). *B. miyamotoi* FR64b FbpA and FbpB are underlined. **(B)** An alignment of *B. miyamotoi* strain FR64b FbpA and FbpB to *B. burgdorferi* strain B31 BBK32 shows differences of the amino acid sequences within the fibronectin binding (green box) and complement inhibitory domains (blue box). The gelatin-binding domain (GBD) of BBK32 is denoted. The key residues R248 and K327 of BBK32 involved in complement C1r binding are indicated by a red box. * conserved, : strongly similar, . weakly similar.

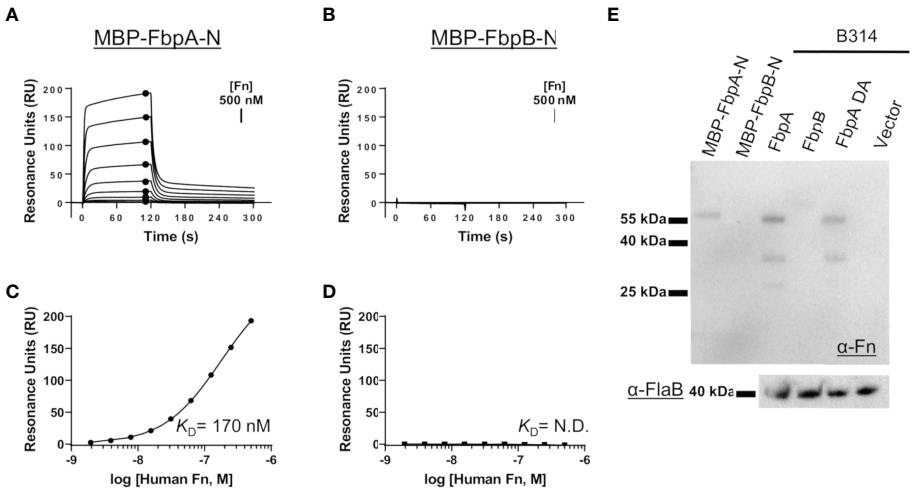

FIGURE 2 | Assessing the interaction of human fibronectin with *B. miyamotoi* FbpA and FbpB. **(A, B)** SPR was used to quantitatively measure the interaction between FbpA-N **(A)** and FbpB-N **(B)** with human fibronectin. MBP-Fbp-N fusion proteins (Fbp sequences denoted by green box in **Figure 1B**) were immobilized on a sensorchip using amine coupling, then a twofold dilution series of purified human fibronectin ranging from 1.95-500 nM was injected. A representative sensorgram from the three replicates for each biosensor surface is shown. **(C, D)** Equilibrium dissociation constants (K_D) were determined using steady state fits and are shown as the mean +/- standard deviation of three replicates in **Table 4** for FbpA **(C)** and FbpB **(D)**. Closed circles in **(A)** correspond to the steady-state response used for calculation of the steady state fits in **(C)**, respectively. A K_D value for the fibronectin interactions with MBP-FbpB-N was not determined (N.D.). **(E)** To assess if full-length Fbp proteins were capable of binding fibronectin, a Far Western approach was implemented by probing full-length Fbps from *B. burgdorferi* strain B314 "knock-in" lysates with fibronectin. Full-length FbpB fails to interact with fibronectin, whereas FbpA and FbpA DA do. A spirochete transformed with shuttle vector only (pBBE22*luc*) and recombinant MBP-FbpA-N/MBP-FbpB-N were used as controls. A Western blot against the flagellar protein FlaB (α-FlaB) was used as a loading control.

B. miyamotoi FbpA and FbpB Bind to Activated C1r in a BBK32-Like Manner

Next, we examined if *B. miyamotoi* FbpA and FbpB bound human C1r in a manner similar to *B. burgdorferi* BBK32 (32–34). BBK32 binds C1r *via* a C-terminal domain where residues R248 and K327 are critical in mediating the interaction with the S1 site of the C1r serine protease (SP) domain and the B-loop of C1r, respectively (34). Each of these key residues are conserved in FbpA (i.e., R264 and K343), whereas in FbpB, only the arginine is conserved (i.e., R309) (**Figure 1B**). We expressed and purified recombinant C-terminal truncation constructs of *B. miyamotoi* FbpA (FbpA-C), a site-directed double alanine mutant of FbpA-C (FbpA-R264A-K343A, denoted FbpA DA-C) (**Figure S2C**), and FbpB (FbpB-C), and assessed their direct interaction with a recombinant activated C1r construct encompassing the complement control protein 2 and serine protease domains (C1r-CCP2-SP). SPR binding assays showed that FbpA-C and FbpB-C bound with high affinity to C1r-CCP2-SP with K_D = 0.90 nM and 1.4 nM, respectively (**Figures 3A, B** and **Table 4**), whereas FbpA DA-C exhibited no detectable C1r-CCP2-SP binding (**Figure 3C**).

Next, we determined if FbpA-C and FbpB-C could compete with one another for binding to C1r-CCP2-SP. Equimolar mixtures of C1r-CCP2-SP with soluble FbpA-C, FbpA DA-C or FbpB-C were injected over immobilized FbpA-C and FbpB-C. Significantly reduced binding signals were observed when soluble FbpA-C or FbpB-C was used, but not for FbpA DA-C, indicating that active FbpA and FbpB proteins are capable of competing with one another for binding to activated C1r (**Figures 3D–F**). These results suggest that both FbpA and FbpB bind to activated C1r in a manner similar to what has been reported for BBK32 and underscores the importance of the conserved R248 and K327 residues (BBK32 numbering) in the FbpA/C1r interaction (34). Interestingly, although BBK32-K327 is not conserved in FbpB (**Figure 1B**), this did not preclude high-affinity interaction with activated C1r-CCP2-SP.

Differential Inhibition of Human Classical Pathway Complement Activation by *B. miyamotoi* FbpA and FbpB

B. miyamotoi FbpA-C and FbpB-C were next assessed for the ability to inhibit the classical complement cascade due ostensibly to the inhibition of C1r. A classical pathway-specific ELISA-based assay was implemented with Fbp-based inhibitors and normal human serum (32–34). As expected, in light of the C1r-CCP2-SP binding data (**Figure 3**), FbpA-C demonstrated potent inhibition of classical pathway-mediated complement activation (IC_{50} = 23 nM), whereas the FbpA DA-C mutant lost all inhibitory activity (**Figure 4A** and **Table 4**). FbpB-C blocked complement activation but, surprisingly, was ~80-fold less potent than FbpA (IC_{50} = 1,900 nM) despite having similar high affinity for activated C1r-CCP2-SP. To confirm these activities, each protein was serially diluted and incubated with opsonized sheep erythrocytes and normal human serum. Consistent with the ELISA-based assay, FbpA, but not FbpA DA prevented hemolysis (**Figure 4B**). In this assay format,

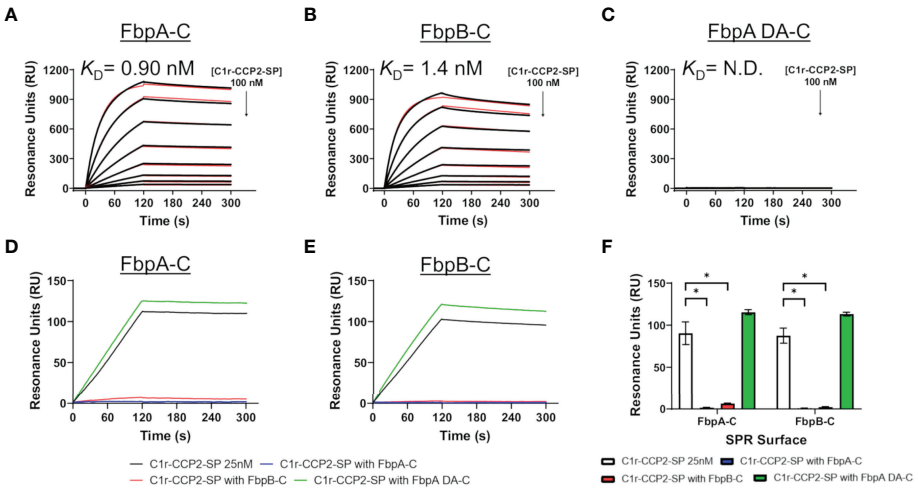

FIGURE 3 | Assessing the interaction of human C1r with *B. miyamotoi* FbpA and FbpB. SPR was used to assess protein-protein interactions between the C-terminal regions of each Fbp protein and activated C1r-CCP2-SP. Immobilized **(A)** FbpA-C, **(B)** FbpB-C, and **(C)** FbpA-C-R264A-K343A (referred to as FbpA DA-C throughout) were subjected to an injection series of serially diluted C1r-CCP2-SP (0.78 - 100 nM). A representative sensorgram from the three replicates for each Fbp is shown with the black curve being the sensorgram and the red curve the associated kinetic fit. K_D values were determined using kinetic fits and are shown as the mean +/- standard deviation of three replicates in **Table 4**. A K_D value for C1r-CCP2-SP interactions with FbpA DA-C was not determined (N.D.). **(D, E)** Competition experiments were carried out using 25 nM C1r-CCP2-SP alone or mixed with 25 nM soluble Fbp proteins injected over FbpA-C **(D)** or FbpB-C **(E)**. **(F)** Comparisons of statistical significance were performed for data shown in panels **(D, E)** using a one-way ANOVA followed by a multiple comparison Tukey test (* = $p < 0.05$).

TABLE 4 | SPR and complement assay results.

	MBP-FbpA-N	MBP-FbpB-N
SPR (Affinity Fit): Human Fibronectin (K_D)	170 ± 5.4 nM	N.D.
	FbpA-C	**FbpB-C**
SPR (Kinetic Fit):C1r-CCP2-SP (K_D)	0.90 ± 0.0017 nM	1.4 ± 0.024 nM
SPR (Kinetic Fit):C1r-CCP2-SP (k_a)	$3.3x10^5$ ± $3.6x10^3$ 1/Ms	$3.9x10^5$ ± $5.3x10^2$ 1/Ms
SPR (Kinetic Fit):C1r-CCP2-SP (k_d)	$3.1x10^{-4}$ ± $2.0x10^{-5}$ 1/s	$5.5x10^{-4}$ ± $8.8x10^{-6}$ 1/s
Complement ELISA (IC_{50})	23 (18 to 30) nM	1,900 (1,600 to 2,300) nM
Erythrocyte Hemolysis (IC_{50})	220 (170 to 280) nM	N.D.
SPR (Kinetic Fit): C1r Zymogen (K_D)	0.85 ± 0.036 nM	N.D.
SPR (Kinetic Fit): C1r Zymogen (k_a)	$2.2x10^4$ ± $2.3x10^3$ 1/Ms	N.D.
SPR (Kinetic Fit): C1r Zymogen (k_d)	$1.9x10^{-5}$ ± $1.2x10^{-6}$ 1/s	N.D.
SPR (Kinetic Fit): Active C1r (K_D)	0.39 ± 0.049 nM	1.1 ± 0.042 nM
SPR (Kinetic Fit): Active C1r (k_a)	$6.8x10^4$ ± $1.0x10^3$ 1/Ms	$6.8x10^4$ ± $8.0x10^2$ 1/Ms
SPR (Kinetic Fit): Active C1r (k_d)	$2.7x10^{-5}$ ± $2.3x10^{-6}$ 1/s	$7.6x10^{-5}$ ± $3.6x10^{-6}$ 1/s
Serum C1r Binding (EC_{50})	0.27 (0.23 to 0.32) %	N.D.

95% Confidence interval = (), Standard deviation (S.D.)= ± S.D., N. D., Not Determined.

FbpB-C had even lower activity, showing no inhibition at concentrations up to 4μM.

Structural Differences Between *B. miyamotoi* FbpA-C and FbpB-C

While differences in the ability of *B. miyamotoi* FbpA and FbpB to bind fibronectin are likely attributed to low sequence conservation of critical fibronectin-binding motifs in FbpB (**Figure 1B**) (36, 37, 66, 69, 70), the basis for differences in the complement inhibitory activities of FbpA-C and FbpB-C were less clear. To determine if FbpA and FbpB have altered structures in their C1r-binding C-terminal regions, we solved the crystal structures of each protein. FbpA-C crystals diffracted to a limiting resolution of 1.9Å ($R_{free\ (\%)}/R_{work\ (\%)}$ = 20.6/23.2) (PDB: 7RPR) (**Figure 5A**, **Figures S3A, B** and **Table 3**). FbpB-C was recalcitrant to crystallization; however, an active FbpB-C construct lacking five C-terminal residues (**Figure S4**, referred to as FbpB-Δ5C hereafter), was crystallized and the structure resolved to a limiting resolution of 2.1Å ($R_{free\ (\%)}/R_{work\ (\%)}$ = 22.5/25.8) (PDB: 7RPS) (**Figure 5B**, **Figures S3C, D** and **Table 3**).

A structural overlay with BBK32-C (PDB: 6N1L) and *B. miyamotoi* FbpA-C and FbpB-Δ5C reveals that all three

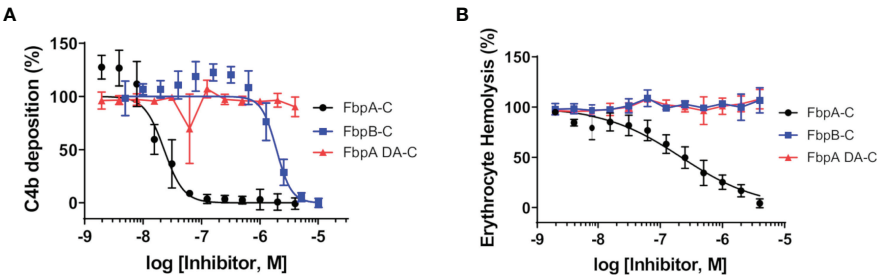

FIGURE 4 | Assessing the complement inhibitory properties of *B. miyamotoi* FbpA and FbpB *in vitro*. **(A)** An ELISA-based assay specific for CP complement activation was used to determine if FbpA-C and FbpB-C were able to inhibit human CP progression. FbpA-C, FbpA DA-C, and FbpB-C, were serially diluted two-fold then incubated with normal human serum, followed by detection of deposited C4b. IC_{50} values were determined using normalized non-linear regression analysis and reported in **Table 4** along with 95% confidence intervals. **(B)** A CP hemolysis assay was carried out using a two-fold serial dilution of Fbp proteins incubated with pre-sensitized sheep erythrocytes and 2% normal human serum. MAC formation and progression of the CP was measured by detecting MAC-mediated erythrocyte hemolysis. IC_{50} values were determined using normalized non-linear regression analysis and reported in **Table 4** along with 95% confidence intervals.

proteins have similar folds involving a core four-helix bundle (helices 1, 3, 4, and 5) with alpha helix 2 extending away from the core (**Figure 5C**). BBK32-C was previously shown to interact with activated C1r using two primary binding sites: i) the active site of C1r involving several BBK32 residues, including R248, and ii) the B-loop of C1r involving residues on the fifth alpha helix, including K327 (34). A structural overlay of FbpA-C, FbpB-Δ5C, and BBK32-C shows that the three proteins retain an overall similar structure around the conserved R248 residue (BBK32 numbering) (**Figure 5D**). However, we noted that the area near BBK32-K327 involves a minor structural alteration in FbpA-C and a more major alteration in FbpB-Δ5C (**Figure 5E**). In FbpA-C, the kinked portion of alpha helix 5 extends one turn longer than in BBK32, resulting in FbpA-C containing an additional surface-exposed residue on this helix (**Figure 5E**). More strikingly, the structure of FbpB-Δ5C has a significantly altered secondary structure in this region when compared to both FbpA-C and BBK32-C (**Figure 5E**). Specifically, FbpB-Δ5C shows a loss of secondary structure within alpha helix 5 that accommodates a loop insertion sequence (i.e., residues Q394-Q405), which are not conserved in both BBK32-C or FbpA-C. Furthermore, a proline residue (P397) in this sequence interrupts the alpha helical secondary structure in FbpB-Δ5C. A portion of this unique loop structure in FbpB has apparent increased disorder in the crystal structure, indicated by weak electron density surrounding residues 401-403 in this region of the protein. Collectively, these data show that FbpA and FbpB are structurally divergent from BBK32 at a functionally critical region of the protein on the fifth alpha helix (**Figures 5C–E**).

B. miyamotoi FbpA and FbpB Differentially Recognize C1r Activation States

C1r is a serine protease subcomponent of the C1 complex which circulates in blood as an inactive zymogen, and is converted to an activated enzyme by autocatalysis when C1 binds to an activating ligand (71–75). This transition involves a conformational change in the SP domain of C1r resulting in a rearrangement of several loop structures, including the C1r B-loop (75) (**Figure S5**). We have previously shown that BBK32 binds to both active and zymogen forms of C1r in a manner that relies on R248 and K327 (34). Given the involvement of B-loop residues in the BBK32-K327 binding site, the observed structural differences at this site in the Fbp crystal structures (**Figure 5**), and the potential for different conformations of this loop between zymogen and active states of C1r (**Figure S5**) (75), we hypothesized that FbpA and FbpB may have altered recognition properties for zymogen C1r.

To assess this, *B. miyamotoi* FbpA-C and FbpB-C were immobilized on an SPR chip and a five-fold dilution series of either zymogen or active forms of full-length purified C1r were injected over each surface. Interestingly, while FbpA-C was able to bind to both zymogen and active forms of C1r readily (C1r zymogen K_D = 0.85 ± 0.036 nM, active C1r K_D = 0.39 ± 0.049 nM), FbpB selectively interacted with active C1r only (active C1r K_D= 1.1 ± 0.042 nM) (**Figure 6A**). We next confirmed that the selective nature of FbpB was observed with full-length proteins expressed in *B. burgdorferi* B314 strains in an approach identical to that presented for fibronectin in **Figure 2E**. Whereas FbpA could recognize both zymogen and activated forms of purified C1r, FbpB preferentially bound activated C1r. The negative controls, FbpA DA and vector-only lysates, did not bind either form of C1r as expected (**Figure 6B**), although we note that FbpA DA retained fibronectin binding (**Figure 2E**).

We considered whether the apparent zymogen/active C1r selectivity differences between FbpA and FbpB could be observed in serum where C1r is in a zymogen form (71–74). To test this, we implemented a serum-based ELISA-type binding assay. *B. miyamotoi* FbpA-C, FbpB-C, and FbpA DA-C were immobilized onto an ELISA plate and incubated with a dilution series of normal human serum followed by detection of C1r binding using a C1r antibody. FbpA-C readily bound serum C1r (half-maximal effective concentration (EC_{50}) = 0.27% (v/v) serum concentration), while FbpB-C and FbpA DA-C did not (**Figure 6C**). However, consistent with the ability of FbpB-C to bind tightly to previously activated forms of C1r (**Figures 3**, **6A**), FbpB-C inhibited the enzymatic activity of pre-activated C1r-CCP2-SP enzyme similar to FbpA-C (**Figure 6D**). Collectively, these results show that, like BBK32,

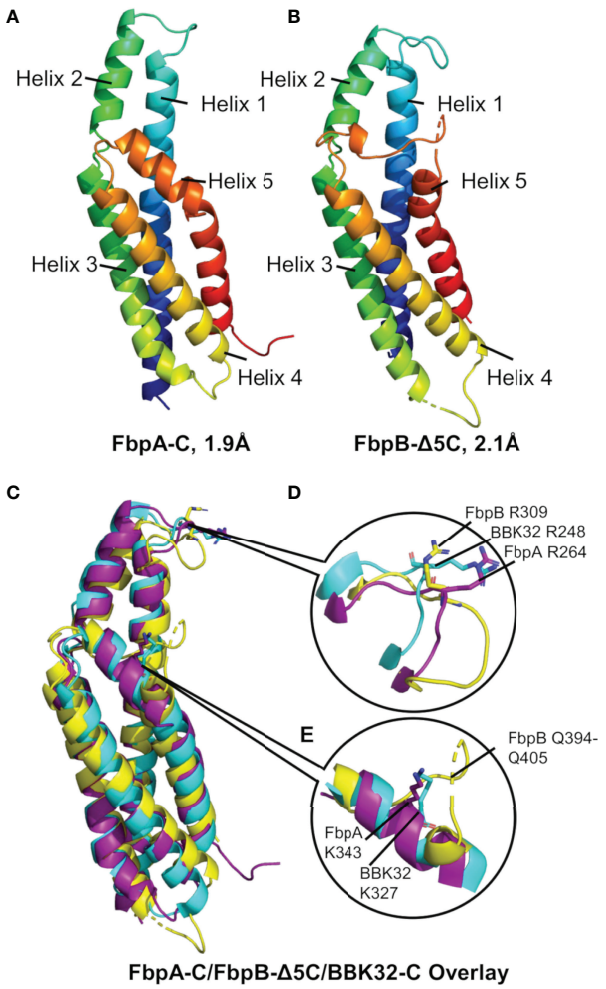

FIGURE 5 | The crystal structures of *B. miyamotoi* FbpA-C and FbpB-Δ5C. Crystal structures of **(A)** FbpA-C (PDB Code: 7RPR) and **(B)** FbpB-Δ5C (PDB Code: 7RPS) were solved to a limiting resolution of 1.9Å and 2.1Å, respectively. Both FbpA-C and FbpB-Δ5C are shown as a color spectrum where blue represents the N-terminus and red represents the C-terminus. **(C)** A structural alignment of FbpA-C (purple), FbpB-Δ5C (yellow), and *B) burgdorferi* BBK32-C (cyan, PDB Code: 6N1L). **(D)** Each protein is structurally similar near the functionally critical BBK32-R248 residue (i.e., FbpA-R264 and FbpB-R309). **(E)** Differences between BBK32-C, FbpA-C, and FbpB-C are found at the functionally critical BBK32-K327 residue (K343 in *B miyamotoi* FbpA). FbpB-Δ5C shows an altered secondary structure with an extended loop structure corresponding to residues Q394-Q405 that aligns to the alpha helical structures found in both FbpA-C and BBK32-C.

B. miyamotoi FbpA can bind and inhibit both the zymogen and active forms of C1r, whereas *B. miyamotoi* FbpB selectively interacts with and inhibits only the active form of the C1r protease.

B. miyamotoi Fbp Proteins Protect a Serum-Sensitive Strain of *B. burgdorferi* From Complement-Mediated Killing

Next, we assessed the protection *B. miyamotoi* FbpA and FbpB conferred to *B. burgdorferi* B314 when ectopically expressed on the cell surface. Since *B. miyamotoi* has not yet been genetically manipulated, we modeled these proteins' surface expression and activity in B314 relative to a pBBE22*luc* vector-only control and cells producing BBK32, given that BBK32 confers serum resistance to strain B314 (32–34). As a prelude to the serum sensitivity assay, we first tested whether *B. miyamotoi* FbpA, FbpA DA or FbpB were surface exposed in *B. burgdorferi* strain B314 relative to a B314 BBK32 control, as well as expressed on the surface of *B. miyamotoi* strain FR64b, using the well-established proteinase K accessibility assay (32, 76). The results clearly show that FbpA, FbpA DA, FbpB, and BBK32 were all produced and are all protease-sensitive, indicating surface exposure in strain B314. However, only FbpA is detected on the surface of *B. miyamotoi* strain FR64b, potentially due to the *in vitro* growth conditions not being conducive for expression of *fbpB* (**Figure 7A**). Importantly, the subsurface endoflagellar protein, FlaB, was unaffected by the treatment in both *B. miyamotoi* strain FR64b and *B. burgdorferi* B314, indicating the preserved structural integrity of the borrelial cells tested (**Figure 7A**). As observed in **Figure S2A**, antibody to *B. miyamotoi* FbpB also recognized FbpA and FbpA DA, albeit to a lesser extent (**Figure 7A**).

We then exposed each B314 knock-in strain to normal human serum and assessed the viability of the cells. *B. miyamotoi* FbpA conferred levels of resistance comparable to BBK32, while the FbpA DA strain was as sensitive to serum killing as the vector-only control (**Figure 7B**). In contrast to the lower apparent inhibitory activity of recombinant FbpB-C (**Figure 4**), *B. burgdorferi* strain B314 producing FbpB on the surface also conferred significant protection against human serum (**Figure 7B**). In order to more fully address differences in the resistance observed for FbpB in the prior assays, we incubated serum sensitive B314 pBBE22*luc* with differential levels of *B. miyamotoi* FbpA-C, FbpB-C, FbpA DA-C, and *B. burgdorferi* BBK32-C to ask whether these soluble components could provide resistance to complement-dependent killing with normal human serum and thus "rescue" this sensitive *B. burgdorferi* strain. Exogenous addition of the C-terminus of the *B. miyamotoi* Fbps and *B. burgdorferi* BBK32-C resulted in dose-dependent rescue for BBK32-C, FbpA-C, and FbpB-C (**Figure 7C**). However, the inhibitory effect was weaker for FbpB-C, with significant inhibition observed only at the 1.2 μM treatment, which is comparable to the IC_{50} value observed for FbpB-C in the ELISA-based inhibition assay (**Figure 4**). Consistent with its inability to inhibit complement, addition of FbpA DA-C was unable to rescue serum-based killing of B314 pBBE22*luc* cells at any of the protein concentrations used (**Figure 7C**). Collectively, these data demonstrate that ectopically-produced *B. miyamotoi* FbpA and FbpB confer resistance to human serum.

DISCUSSION

Like other tick-borne microbial agents, *B. miyamotoi* spirochetes must survive host immune defenses, including complement, beginning at the tick bloodmeal stage and throughout host infection. *B. miyamotoi* has been reported to evade the

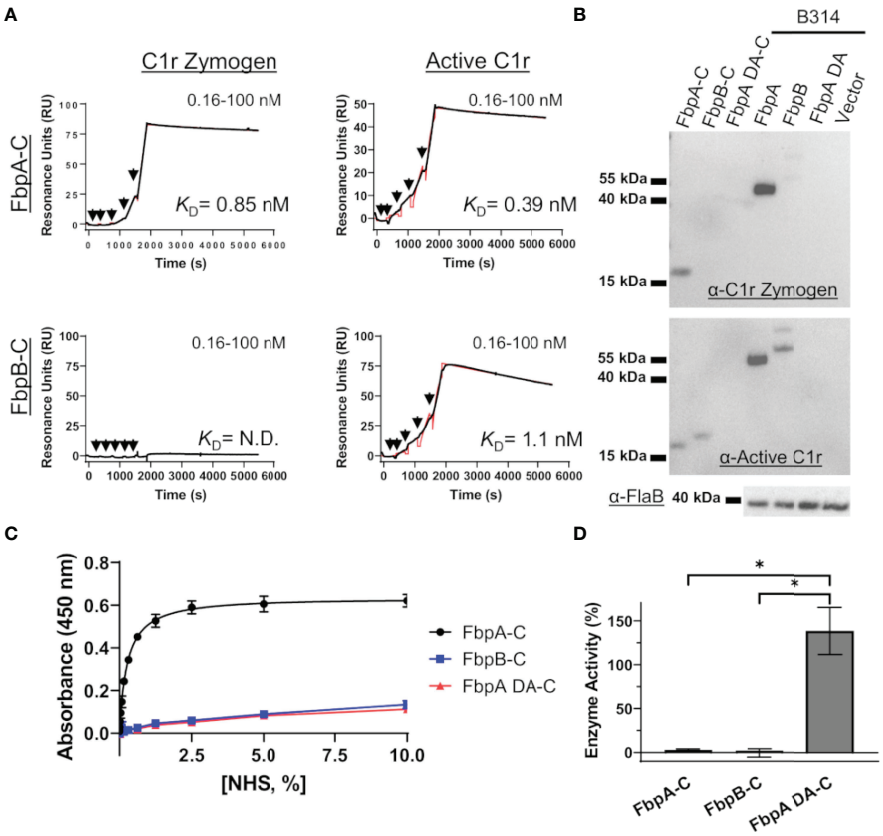

FIGURE 6 | FbpA-C and FbpB-C interact differentially with zymogen and activated forms of human C1r. **(A)** Single cycle SPR was used to determine binding affinities of C1r zymogen or active C1r ranging from 0.16 - 100 nM injected over immobilized Fbps. A representative sensorgram from a three-injection series for each Fbp-C and C1r active state is shown with the black curve being the sensorgram and the red curve the associated kinetic fit. K_D's were determined using kinetic fits and are shown as the average and standard deviation of three replicates in **Table 4**. **(B)** Far Western overlays using *B. burgdorferi* B314 lysates probed with zymogen or enzymatic forms of purified full-length C1r, followed by an antibody to C1r. **(C)** An ELISA-type binding assay was used to determine the ability of FbpA-C, FbpA DA-C and FbpB-C to interact with C1r in human serum. FbpA-C (black), FbpB-C (blue), and FbpA DA-C (red) were immobilized on an ELISA plate then incubated with a two-fold dilution series of normal human serum ranging from 0.0012-10%. Corresponding EC_{50} values for FbpA-C, FbpB-C, and FbpA DA-C are reported in **Table 4**. **(D)** Fbp-mediated inhibition of purified active C1r-CCP2-SP enzymatic activity was assessed by incubating 15 nM C1r-CCP2-SP with a 1 μM of FbpA-C (white), FbpB-C (striped), and FbpA DA-C (grey). C1r-CCP2-SP enzymatic activity was determined by incubation with a C1r substrate (Z-Gly-Arg-sBzl) that, once cleaved, reacts with DTNB resulting in a colorimetric change. No statistical difference was found between FbpA-C and FbpB-C inhibitory activity, whereas FbpA DA-C exhibited significant loss in inhibitory activity. Statistical analysis was performed using a one-way ANOVA followed by a multiple comparison Tukey test (*=p<0.05).

alternative pathway (AP) of complement through recruitment of endogenous complement regulators or plasmin, and produces lipoproteins that directly bind to and inhibit complement proteins, like CbiA, to protect the spirochete from complement-mediated killing (21, 22, 77). However, little is known about how *B. miyamotoi* defends against the classical pathway (CP), which may be particularly important during later stages of infection when an adaptive immune response has been developed. Interestingly, the Lyme disease spirochete *B. burgdorferi* has evolved at least two mechanistically distinct inhibitors of the classical complement pathway, i) BBK32 (32–34) and ii) ElpB/ElpQ (78). As *elp* genes with CP inhibitory activity have yet to be identified in *B. miyamotoi* genomes, we hypothesized that *B. miyamotoi* may use orthologs of BBK32 to neutralize the classical complement cascade and/or exert BBK32-like fibronectin-binding activity (32–34).

B. miyamotoi strain FR64b encodes two BBK32 orthologs, FbpA and FbpB, that share 56% and 25% amino acid sequence identity to *B. burgdorferi* strain B31 BBK32, respectively (**Figures 1B**, **S1**). *B. miyamotoi* strain LB-2001, a North American strain of *B. miyamotoi* (24), also encodes FbpA and FbpB proteins with 85% and 81% identity to FR64b FbpA and FbpB, respectively. We found that *B. miyamotoi* strain FR64b FbpA exhibits similar activity to BBK32 for both fibronectin-binding and C1r-binding/inhibition. The results presented herein highlight that FbpA and BBK32 are multifunctional proteins capable of interacting with more than one host protein *via* separate domains (32–37, 40, 64–68). Similar to what has been proposed for *B. burgdorferi* BBK32, the anti-C1r activity found here for FbpA may selectively protect *B. miyamotoi* from CP-mediated complement killing. This is supported by the ability of FbpA to protect previously serum-

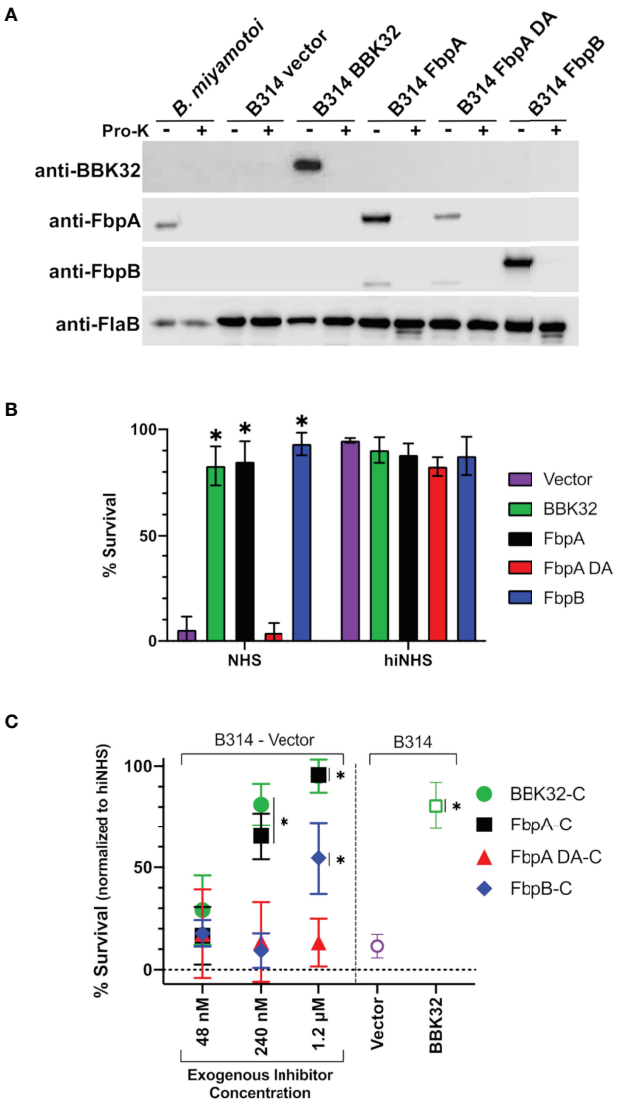

FIGURE 7 | Determining the ability of surface-expressed *B. miyamotoi* FbpA and FbpB to protect a serum-sensitive strain of *B. burgdorferi*. **(A)** Western blots of lysates from *B. miyamotoi* strain FR64b and *B burgdorferi* B314 isolates expressing *fbpA*, *fbpA-DA*, *fbpB*, and *bbk32* were probed with antibodies to FbpA (anti-FbpA), FbpB (anti-FbpB), BBK32 (anti-BBK32) and FlaB (anti-FlaB), the latter as a loading control and a control for a subsurface target. Vector refers to the plasmid-only backbone sample (B314/pBBE22*luc*). Samples from each population were subjected to proteinase K accessibility treatments to determine the surface expression of the proteins. Due to its periplasmic location, the flagellar protein, FlaB, is unaffected by proteinase K in intact cells and depicts structural integrity in the treated *B. miyamotoi* and B314 derivatives listed. **(B)** *B. miyamotoi* Fbp proteins were tested for their ability to confer resistance to normal human serum (NHS) sensitive *B. burgdorferi* strain B314 relative to vector-only and BBK32-expressing controls (negative and positive controls, respectively). Asterisks depict a significant increase in survival relative to FbpA DA and the vector control (*=p<0.0001). All strains exposed to heat inactivated NHS (hiNHS), rendering complement proteins inactive, were largely unaffected. **(C)** Rescue assays were used to determine if soluble exogenous recombinant proteins could promote survival of serum-sensitive vector-containing *B. burgdorferi* B314. Increasing five-fold concentrations of BBK32-C, FbpA-C, FbpA DA-C, and FbpB-C were added in serum sensitivity assays. The middle samples (i.e., 240 nM) have added recombinant protein that is roughly equivalent to the concentration of C1r in the assay conditions employed. Cells were assessed *via* darkfield microscopy. Included as controls are a vector-only strain of B314 with no exogenous protein addition, as well as a BBK32-producing B314 isolate (right side). Asterisks depict a significant increase in survival relative to the vector control (*=p<0.015). Significance for serum sensitivity and rescue assays was determined using two-way ANOVA with a Šidák correction for multiple comparisons.

sensitive spirochetes from complement-mediated bacteriolysis (**Figure 7B**). The functional consequence of the fibronectin-binding activity of *B. miyamotoi* FbpA interacting with fibronectin may be related to extravasation as has been shown for BBK32 (35–37, 40, 64–68), and/or it may serve other functions including acting as an adhesin to the vascular endothelium or binding to plasma fibronectin, another activity reported for BBK32 (38, 65, 79).

The functional consequence of *B. miyamotoi* FbpA and FbpB production within a host will need to be investigated *in vivo*. A

current limitation is the lack of an immunocompetent mouse model for *B. miyamotoi* to determine the temporal expression of *fbpA* and *fbpB* during mammalian infection. The culturing of *B. miyamotoi* is possible (24), but challenging, and allows for only limited experimentation. Additionally, genetic manipulation of *B. miyamotoi* has not yet been reported. To overcome these challenges, we used an established human serum sensitivity assay in which serum resistance can be quantitatively measured and correlated with protein production of *B. miyamotoi* FbpA and FbpB on the surface of the serum-sensitive *B. burgdorferi* strain B314, e.g., as a "knock-in" construct (**Figure 7B**) (32–34). Alternatively, we tested whether the addition of exogenous FbpA-C, FbpA DA-C, or FbpB-C could "rescue" normal human serum-dependent killing of a sensitive B314 derivative (**Figure 7C**). The "knock-in" system is a minimalist approach that measures the complement inhibitory activity of surface-exposed proteins due to the absence of all linear plasmid-encoded lipoproteins and the concomitant absence of redundant immune evasion mechanisms. Proteinase K accessibility assays confirmed the surface localization of *B. miyamotoi* FbpA, FbpA DA, and FbpB in the surrogate *B. burgdorferi* B314 knock-in background (**Figure 7A**). Interestingly, only FbpA was produced following *in vitro* cultivation of *B. miyamotoi* strain FR64b and surface-expression was also confirmed; no FbpB was detectable by Western immunoblotting (**Figure 7A**). Limited cultivation conditions were tested here for *B. miyamotoi* and additional experimentation using mammalian-like growth conditions may also induce FbpB production comparable to that observed for pathogenesis-associated proteins in *B. burgdorferi* (80).

In contrast to *B. miyamotoi* FbpA, we found that FbpB fails to interact with human fibronectin in a BBK32-like manner and lacks a key motif that is known to be important for BBK32 recognition of fibronectin (37, 66) (**Figure 2**). The C1r-binding activity for FbpB proved to be more complex. Unlike BBK32/FbpA, FbpB fails to interact with zymogen forms of human C1r but instead selectively binds and inhibits the activated form (**Figures 3**, **6A, B, D**). The crystal structures presented here of FbpA-C and FbpB-C show that a defining feature of the C1r-binding domains for BBK32 and *B. miyamotoi* Fbps is a four-helix core with an extended second alpha helix that presents a functional arginine residue on a small surface-loop (**Figures 5C, D**). However, the crystal structure of FbpB revealed structural differences in the fifth alpha helix relative to FbpA and BBK32. FbpB has a divergent loop structure in this region and therefore lacks the same secondary structure seen in both FbpA and BBK32 (**Figure 5E**). We have previously shown that residues on the fifth alpha helix of BBK32 interact with a non-active site loop on C1r known as the B-loop (34). Despite these structural differences, FbpB-C was still capable of saturable inhibition of human complement activation, although at several orders of magnitude weaker potency in the ELISA-based assay (**Figure 4A**). Recombinant FbpB-C also protected serum sensitive spirochetes from complement-mediated killing, but was significantly weaker in its ability to do so relative to FbpA-C (**Figure 7C**). Initially, these results pointed to FbpA being the more relevant classical pathway complement inhibitor in *B. miyamotoi* and suggested that targeting of the zymogen form of human C1r is an important functional feature of this class of inhibitors. However, in our serum sensitivity assays, where *B. miyamotoi* FbpA and FbpB were produced ectopically on the surface of *B. burgdorferi*, both proteins conferred significantly greater protection to B314 than FbpA DA or the vector-only control (**Figure 7B**). These data suggest that within the physiological context of complement activation on the spirochete surface, FbpB's inhibition of activated C1r is sufficient to prevent downstream complement activation. Thus, the selective recognition of activated C1r by FbpB implies that it functions at a different temporal or spatial level than FbpA. Combined with the differences in relative fibronectin-binding activities of FbpA and FbpB, our data suggest that Fbp proteins have evolved to have partially overlapping, but non-identical functions compared to the Lyme disease-associated BBK32 orthologs.

Nonetheless, *B. miyamotoi* FbpB's conferred resistance in the human serum sensitivity assays was initially surprising based on *in vitro* biochemical data showing very limited inhibition of serum-based complement activation (**Figure 4B**). The lack of consensus between FbpB activity in the human serum sensitivity assay relative to FbpB-C likely reflects differences in the truncated soluble form of the recombinant protein relative to the full-length lipoprotein-tethered surface-exposed configuration (**Figure 7B**). Given that soluble FbpB-C significantly protected serum-sensitive spirochetes at high concentrations (**Figure 7C**), one explanation may be that differences observed in the B314 background are related to sufficient protein concentrations of surface-exposed FbpB that can confer complement resistance to these borrelial cells (**Figure 7B**). Another possibility is suggested by the observation that soluble FbpB-C does not interact with zymogen C1r in serum (**Figure 6C**), but rather interacts and inhibits C1r only once activated (**Figure 6**). Thus soluble forms of FbpA, but not FbpB, are capable of binding to C1r prior to surface activation. This difference likely makes the inhibitory activity of FbpB more dependent on surface localization compared to FbpA, which binds tightly to zymogen C1r in solution (**Figure 6C**).

In summary, we have characterized the structure and function of two *bbk32* orthologs within the emerging pathogen *B. miyamotoi*, termed FbpA and FbpB. Our investigation showed that FbpA and FbpB share some activities with one another and with *B. burgdorferi* BBK32. However, important differences – both structurally and at the functional level – were found to influence their relative ability to interact with both human fibronectin and complement C1r. Surprisingly, our data suggest that *B. burgdorferi* BBK32 and *B. miyamotoi* Fbp proteins have evolved distinct molecular mechanisms across the family of inhibitors. These observations have significance for understanding how *B. miyamotoi* modulates the host immune response and provides novel insight into the diverse structure-function relationships of this multifunctional class of borrelial lipoproteins.

DATA AVAILABILITY STATEMENT

The datasets presented in this study can be found in online repositories. The names of the repository/repositories and accession number(s) can be found below: http://www.wwpdb.org/, 7RPR, http://www.wwpdb.org/, 7RPS.

ETHICS STATEMENT

The animal work described herein was reviewed and approved by Texas A&M IACUC.

AUTHOR CONTRIBUTIONS

CB and AP-P are equal contributors. JS and BG are co-corresponding authors. JS and BG designed research. CB and AP-P conducted research. AP-P, JS, BG CB analyzed data. CB, AP-P, JS, and BG wrote the paper.

FUNDING

Support was provided by Public Health Service Grant R01-AI146930 from the National Institute of Allergy and Infectious Diseases (to JS and BG). X-ray diffraction data were collected at Southeast Regional Collaborative Access Team 22-ID beamline at the Advanced Photon Source, Argonne National Laboratory. Supporting institutions may be found at www.ser-cat.org/members.html.

SUPPLEMENTARY MATERIAL

The Supplementary Material for this article can be found online at: https://www.frontiersin.org/articles/10.3389/fimmu.2022.886733/full#supplementary-material

REFERENCES

1. Lopez J, Hovius JW, Bergström S. Pathogenesis of Relapsing Fever *Curr Issues Mol Biol* (2021) 42:519–50. doi: 10.21775/cimb.042.519.
2. Lopez JE, Krishnavahjala A, Garcia MN, Bermudez S. Tick-Borne Relapsing Fever Spirochetes in the Americas. *Vet Sci* (2016) 3:1–18. doi: 10.3390/vetsci3030016
3. Wagemakers A, Staarink PJ, Sprong H, Hovius JWR. *Borrelia miyamotoi*: A Widespread Tick-Borne Relapsing Fever Spirochete. *Trends Parasitol* (2015) 31:260–9. doi: 10.1016/j.pt.2015.03.008
4. Cutler S, Vayssier-Taussat M, Estrada-Peña A, Potkonjak A, Mihalca AD, Zeller H. A New *Borrelia* on the Block: *Borrelia miyamotoi* - a Human Health Risk? *Euro Surveill* (2019) 24:1–14. doi: 10.2807/1560-7917.ES.2019.24.18.1800170
5. Telford SR, Goethert HK, Molloy PJ, Berardi VP, Chowdri HR, Gugliotta JL, et al. *Borrelia miyamotoi* Disease: Neither Lyme Disease Nor Relapsing Fever. *Clin Lab Med* (2015) 35:867–82. doi: 10.1016/j.cll.2015.08.002
6. Talagrand-Reboul E, Boyer PH, Bergström S, Vial L, Boulanger N. Relapsing Fevers: Neglected Tick-Borne Diseases. *Front Cell Infect Microbiol* (2018) 8:98. doi: 10.3389/fcimb.2018.00098
7. Johnston D, Kelly JR, Ledizet M, Lavoie N, Smith RP, Parsonnet J, et al. Frequency and Geographic Distribution of *Borrelia miyamotoi*, *Borrelia burgdorferi*, and *Babesia microti* Infections in New England Residents. *Clin Infect Dis* (2022), 1–6. doi: 10.1093/cid/ciac107
8. Krause PJ, Narasimhan S, Wormser GP, Rollend L, Fikrig E, Lepore T, et al. Human *Borrelia miyamotoi* Infection in the United States. *N Engl J Med* (2013) 368:291–3. doi: 10.1056/nejmc1215469
9. Koetsveld J, Draga ROP, Wagemakers A, Manger A, Oei A, Visser CE, et al. *In Vitro* Susceptibility of the Relapsing-Fever Spirochete *Borrelia miyamotoi* to Antimicrobial Agents. *Antimicrob Agents Chemother* (2017) 61:1–9. doi: 10.1128/AAC.00535-17
10. Lynn GE, Breuner NE, Eisen L, Hojgaard A, Replogle AJ, Eisen RJ. An Immunocompromised Mouse Model to Infect *Ixodes scapularis* Ticks With the Relapsing Fever Spirochete, *Borrelia miyamotoi*. *Ticks Tick Borne Dis* (2019) 10:352–9. doi: 10.1016/j.ttbdis.2018.11.017
11. Barbour AG, Bunikis J, Travinsky B, Hoen AG, Diuk-Wasser MA, Fish D, et al. Niche Partitioning of *Borrelia burgdorferi* and *Borrelia miyamotoi* in the Same Tick Vector and Mammalian Reservoir Species. *Am J Trop Med Hyg* (2009) 81:1120–31. doi: 10.4269/ajtmh.2009.09-0208
12. Kullberg BJ, Vrijmoeth HD, van de Schoor F, Hovius JW. Lyme Borreliosis: Diagnosis and Management. *BMJ* (2020) 369:1–20. doi: 10.1136/bmj.m1041
13. Steere AC, Strle F, Wormser GP, Hu LT, Branda JA, Hovius JWR, et al. Lyme Borreliosis. *Nat Rev Dis Primers* (2016) 2:1–19. doi: 10.1038/nrdp.2016.90
14. Radolf JD, Strle K, Lemieux JE, Strle F. Lyme Disease in Humans *Curr. Issues Mol Biol* (2021) 42:333–84. doi: 10.21775/cimb.042.333
15. Dworkin MS, Schwan TG, Anderson DE, Borchardt SM. Tick-Borne Relapsing Fever. *Infect Dis Clin North Am* (2008) 22:449–68. doi: 10.1016/j.idc.2008.03.006
16. Hamase A, Takahashi Y, Nohgi K, Fukunaga M. Homology of Variable Major Protein Genes Between *Borrelia hermsii* and *Borrelia miyamotoi*. *FEMS Microbiol Lett* (1996) 140:131–7. doi: 10.1016/0378-1097(96)00168-1
17. Barbour AG, Dai Q, Restrepo BI, Stoenner HG, Frank SA. Pathogen Escape From Host Immunity by a Genome Program for Antigenic Variation. *Proc Natl Acad Sci USA* (2006) 103:18290–5. doi: 10.1073/pnas.0605302103
18. Barbour AG. Multiple and Diverse Vsp and Vlp Sequences in *Borrelia miyamotoi*, a Hard Tick-Borne Zoonotic Pathogen. *PloS One* (2016) 11:1–16. doi: 10.1371/journal.pone.0146283
19. Barbour AG. Antigenic Variation of Surface Proteins of *Borrelia* Species. *Rev Infect Dis* (1988) 10:399–402. doi: 10.1093/cid/10.Supplement_2.S399
20. Wagemakers A, Koetsveld J, Narasimhan S, Wickel M, Deponte K, Bleijlevens B, et al. Variable Major Proteins as Targets for Specific Antibodies Against *Borrelia miyamotoi*. *J Immunol* (2016) 196:4185–95. doi: 10.4049/jimmunol.1600014
21. Röttgerding F, Wagemakers A, Koetsveld J, Fingerle V, Kirschfink M, Hovius JW, et al. Immune Evasion of *Borrelia miyamotoi*: CbiA, a Novel Outer Surface Protein Exhibiting Complement Binding and Inactivating Properties. *Sci Rep* (2017) 7:1–15. doi: 10.1038/s41598-017-00412-4
22. Schmidt FL, Sürth V, Berg TK, Lin Y-P, Hovius JW, Kraiczy P. Interaction Between *Borrelia miyamotoi* Variable Major Proteins Vlp15/16 and Vlp18 With Plasminogen and Complement. *Sci Rep* (2021) 11:1–13. doi: 10.1038/s41598-021-84533-x
23. Teegler A, Herzberger P, Margos G, Fingerle V, Kraiczy P. The Relapsing Fever Spirochete *Borrelia miyamotoi* Resists Complement-Mediated Killing by Human Serum. *Ticks Tick Borne Dis* (2014) 5:898–901. doi: 10.1016/j.ttbdis.2014.07.011
24. Wagemakers A, Oei A, Fikrig MM, Miellet WR, Hovius JW. The Relapsing Fever Spirochete *Borrelia miyamotoi* Is Cultivable in a Modified Kelly-Pettenkofer Medium, and is Resistant to Human Complement. *Parasites Vectors* (2014) 7:1–6. doi: 10.1186/1756-3305-7-418
25. Sato K, Kumagai Y, Sekizuka T, Kuroda M, Hayashi T, Takano A, et al. Vitronectin Binding Protein, BOM1093, Confers Serum Resistance on *Borrelia miyamotoi*. *Sci Rep* (2021) 11:1–13. doi: 10.1038/s41598-021-85069-w
26. Varela JC, Tomlinson S. Complement: An Overview for the Clinician. *Hematol/Oncol Clin North Am* (2015) 29:409–27. doi: 10.1016/j.hoc.2015.02.001

27. Merle NS, Church SE, Fremeaux-Bacchi V, Roumenina LT. Complement System Part I - Molecular Mechanisms of Activation and Regulation. *Front Immunol* (2015) 6:262. doi: 10.3389/fimmu.2015.00262
28. Bjanes E, Nizet V. More Than a Pore: Nonlytic Antimicrobial Functions of Complement and Bacterial Strategies for Evasion. *Microbiol Mol Biol Rev* (2021) 85:1–27. doi: 10.1128/mmbr.00177-20
29. Frank MM. Annihilating Host Defense. *Nat Med* (2001) 7:1285–6. doi: 10.1038/nm1201-1285
30. Lambris JD, Ricklin D. Geisbrecht B V. Complement Evasion by Human Pathogens. *Nat Rev Microbiol* (2008) 6:132–42. doi: 10.1038/nrmicro1824
31. Skare JT, Garcia BL. Complement Evasion by Lyme Disease Spirochetes. *Trends Microbiol* (2020) 28:1–11. doi: 10.1016/j.tim.2020.05.004
32. Garcia BL, Zhi H, Wager B, Höök M, Skare JT. *Borrelia burgdorferi* BBK32 Inhibits the Classical Pathway by Blocking Activation of the C1 Complement Complex. *PloS Pathog* (2016) 12:1–28. doi: 10.1371/journal.ppat.1005404
33. Xie J, Zhi H, Garrigues RJ, Keightley A, Garcia BL, Skare JT. Structural Determination of the Complement Inhibitory Domain of *Borrelia burgdorferi* BBK32 Provides Insight Into Classical Pathway Complement Evasion by Lyme Disease Spirochetes. *PloS Pathog* (2019) 15:1–29. doi: 10.1371/journal.ppat.1007659
34. Garrigues RJ, Powell-Pierce AD, Hammel M, Skare JT, Garcia BL. A Structural Basis for Inhibition of the Complement Initiator Protease C1r by Lyme Disease Spirochetes. *J Immunol* (2021) 207:2856–67. doi: 10.4049/JIMMUNOL.2100815
35. Seshu J, Esteve-Gassent MD, Labandeira-Rey M, Kim JH, Trzeciakowski JP, Höök M, et al. Inactivation of the Fibronectin-Binding Adhesin Gene *bbk32* Significantly Attenuates the Infectivity Potential of *Borrelia burgdorferi*. *Mol Microbiol* (2006) 59:1591–601. doi: 10.1111/j.1365-2958.2005.05042.x
36. Probert WS, Kim JH, Höök M, Johnson BJB. Mapping the Ligand-Binding Region of *Borrelia burgdorferi* Fibronectin-Binding Protein BBK32. *Infect Immun* (2001) 69:4129–33. doi: 10.1128/IAI.69.6.4129-4133.2001
37. Harris G, Ma W, Maurer LM, Potts JR, Mosher DF. *Borrelia burgdorferi* Protein BBK32 Binds to Soluble Fibronectin *Via* the N-terminal 70-kDa Region, Causing Fibronectin to Undergo Conformational Extension. *J Biol Chem* (2014) 289:22490–9. doi: 10.1074/jbc.M114.578419
38. Kim JH, Singvall J, Schwarz-Linek U, Johnson BJB, Potts JR, Höök M. BBK32, a Fibronectin Binding MSCRAMM From *Borrelia burgdorferi*, Contains a Disordered Region That Undergoes a Conformational Change on Ligand Binding. *J Biol Chem* (2004) 279:41706–14. doi: 10.1074/jbc.M401691200
39. Lin YP, Chen Q, Ritchie JA, Dufour NP, Fischer JR, Coburn J, et al. Glycosaminoglycan Binding by *Borrelia burgdorferi* Adhesin BBK32 Specifically and Uniquely Promotes Joint Colonization. *Cell Microbiol* (2015) 17:860–75. doi: 10.1111/cmi.12407
40. Hyde JA, Weening EH, Chang M, Trzeciakowski JP, Höök M, Cirillo JD, et al. Bioluminescent Imaging of *Borrelia burgdorferi In Vivo* Demonstrates That the Fibronectin-Binding Protein BBK32 Is Required for Optimal Infectivity. *Mol Microbiol* (2011) 82:99–113. doi: 10.1111/j.1365-2958.2011.07801.x
41. Lewis ERG, Marcsisin RA, Campeau Miller SA, Hue F, Phillips A, AuCoin DP, et al. Fibronectin-Binding Protein of *Borrelia hermsii* Expressed in the Blood of Mice With Relapsing Fever. *Infect Immun* (2014) 82:2520–31. doi: 10.1128/IAI.01582-14
42. Brenner C, Bomans K, Habicht J, Simon MM, Wallich R. Mapping the Ligand-Binding Region of *Borrelia hermsii* Fibronectin-Binding Protein. *PloS One* (2013) 8:26–8. doi: 10.1371/journal.pone.0063437
43. Ricklin D, Mastellos DC, Reis ES, Lambris JD. The Renaissance of Complement Therapeutics. *Nat Rev Nephrol* (2017) 14:26–47. doi: 10.1038/nrneph.2017.156
44. Ricklin D, Lambris JD. Complement in Immune and Inflammatory Disorders: Pathophysiological Mechanisms. *J Immunol* (2013) 190:3831–8. doi: 10.4049/jimmunol.1203487
45. Mastellos DC, Ricklin D, Lambris JD. Clinical Promise of Next-Generation Complement Therapeutics. *Nat Rev Drug Discov* (2019) 18:707–29. doi: 10.1038/s41573-019-0031-6
46. Sadziene A, Wilske B, Ferdows MS, Barbour AG. The Cryptic *ospC* Gene of *Borrelia burgdorferi* B31 Is Located on a Circular Plasmid. *Infect Immun* (1993) 61:2192–5. doi: 10.1128/iai.61.5.2192-2195.1993
47. Fukunaga M, Takahashi Y, Tsuruta Y, Matsushita O, Ralph D, McClelland M, et al. Genetic and Phenotypic Analysis of *Borrelia miyamotoi* Sp. Nov., Isolated From the Ixodid Tick *Ixodes persulcatus*, the Vector for Lyme Disease in Japan. *Int J Syst Bacteriol* (1995) 45:804–10. doi: 10.1099/00207713-45-4-804
48. Geisbrecht BV, Bouyain S, Pop M. An Optimized System for Expression and Purification of Secreted Bacterial Proteins. *Protein Expr Purif* (2006) 46:23–32. doi: 10.1016/j.pep.2005.09.003
49. Samuels DS, Drecktrah D, Hall LS. Genetic Transformation and Complementation. *Methods Mol Biol* (2018) 1690:183–200. doi: 10.1007/978-1-4939-7383-5_15
50. Rushing BR, Rohlik DL, Roy S, Skaff DA, Garcia BL. Targeting the Initiator Protease of the Classical Pathway of Complement Using Fragment-Based Drug Discovery. *Molecules* (2020) 25:1–20. doi: 10.3390/molecules25174016
51. Kardos J, Gál P, Szilágyi L, Thielens NM, Szilágyi K, Lõrincz Z, et al. The Role of the Individual Domains in the Structure and Function of the Catalytic Region of a Modular Serine Protease, C1r. *J Immunol* (2001) 167:5202–8. doi: 10.4049/jimmunol.167.9.5202
52. Harlow E, Lane D. *"Antibodies: A Laboratory Manual", 2nd ed*. Cold Spring Harbor, New York: Cold Spring Harbor (1998). pp. 103–19.
53. Otwinowski Z, Minor W. Processing of X-ray Diffraction Data Collected in Oscillation Mode. *Methods Enzymol* (1997) 276:307–26. doi: 10.1016/S0076-6879(97)76066-X
54. Karplus PA, Diederichs K. Linking Crystallographic Model and Data Quality. *Science* (2012) 336:1030–3. doi: 10.1126/science.1218231
55. Winn MD, Ballard CC, Cowtan KD, Dodson EJ, Emsley P, Evans PR, et al. Overview of the CCP4 Suite and Current Developments. *Acta Crystallogr* (2011) 67:235–42. doi: 10.1107/S0907444910045749
56. Zwart PH, Afonine PV, Grosse-Kunstleve RW, Hung LW, Ioerger TR, McCoy AJ, et al. Automated Structure Solution With the PHENIX Suite. *Methods Mol Biol* (2008) 426:419–35. doi: 10.1007/978-1-60327-058-8_28
57. Adams PD, Grosse-Kunstleve RW, Hung LW, Ioerger TR, McCoy AJ, Moriarty NW, et al. Phenix: Building New Software for Automated Crystallographic Structure Determination. *Acta Crystallogr* (2002) 58:1948–54. doi: 10.1107/S0907444902016657
58. Adams PD, Afonine PV, Bunkóczi G, Chen VB, Davis IW, Echols N, et al. Phenix: A Comprehensive Python-based System for Macromolecular Structure Solution. *Acta Crystallogr* (2010) 66:213–21. doi: 10.1107/S0907444909052925
59. Emsley P, Lohkamp B, Scott WG, Cowtan K. Features and Development of COOT. *Acta Crystallogr* (2010) 66:486–501. doi: 10.1107/S0907444910007493
60. Summers BJ, Garcia BL, Woehl JL, Ramyar KX, Yao X. Geisbrecht B V. Identification of Peptidic Inhibitors of the Alternative Complement Pathway Based on *Staphylococcus aureus* SCIN Proteins. *Mol Immunol* (2015) 67:193–205. doi: 10.1016/j.molimm.2015.05.012
61. Roos A, Bouwman LH, Munoz J, Zuiverloon T, Faber-Krol MC, Fallaux-van den Houten FC, et al. Functional Characterization of the Lectin Pathway of Complement in Human Serum. *Mol Immunol* (2003) 39:655–68. doi: 10.1016/S0161-5890(02)00254-7
62. Nilsson UR, Nilsson B. Simplified Assays of Hemolytic Activity of the Classical and Alternative Complement Pathways. *J Immunol Methods* (1984) 72:49–59. doi: 10.1016/0022-1759(84)90432-0
63. Grosskinsky S, Schott M, Brenner C, Cutler SJ, Kraiczy P, Zipfel PF, et al. *Borrelia recurrentis* Employs a Novel Multifunctional Surface Protein With Anti-Complement, Anti-Opsonic and Invasive Potential to Escape Innate Immunity. *PloS One* (2009) 4:1–12. doi: 10.1371/journal.pone.0004858
64. Ebady R, Niddam AF, Boczula AE, Kim YR, Gupta N, Tang TT, et al. Biomechanics of *Borrelia burgdorferi* Vascular Interactions. *Cell Rep* (2016) 16:2593–604. doi: 10.1016/j.celrep.2016.08.013
65. Moriarty TJ, Shi M, Lin YP, Ebady R, Zhou H, Odisho T, et al. Vascular Binding of a Pathogen Under Shear Force Through Mechanistically Distinct Sequential Interactions With Host Macromolecules. *Mol Microbiol* (2012) 86:1116–31. doi: 10.1111/mmi.12045
66. Probert WS, Johnson BJB. Identification of a 47 kDa Fibronectin-Binding Protein Expressed by *Borrelia burgdorferi* Isolate B31. *Mol Microbiol* (1998) 30:1003–15. doi: 10.1046/j.1365-2958.1998.01127.x
67. Liang X, Garcia BL, Visai L, Prabhakaran S, Meenan NAG, Potts JR, et al. Allosteric Regulation of Fibronectin/α5β1 Interaction by Fibronectin-Binding MSCRAMMS. *PloS One* (2016) 11:1–17. doi: 10.1371/journal.pone.0159118
68. Niddam AF, Ebady R, Bansal A, Koehler A, Hinz B, Moriarty TJ. Plasma Fibronectin Stabilizes *Borrelia burgdorferi*-Endothelial Interactions Under

Vascular Shear Stress by a Catch-Bond Mechanism. *Proc Natl Acad Sci USA* (2017) 114:3490–8. doi: 10.1073/pnas.1615007114
69. Raibaud S, Schwarz-Linek U, Kim JH, Jenkins HT, Baines ER, Gurasiddappa S, et al. *Borrelia burgdorferi* Binds Fibronectin Through a Tandem β-Zipper, a Common Mechanism of Fibronectin Binding in Staphylococci, Streptococci, and Spirochetes. *J Biol Chem* (2005) 280:18803–9. doi: 10.1074/jbc.M501731200
70. Prabhakaran S, Liang X, Skare JT, Potts JR, Höök M. A Novel Fibronectin Binding Motif in MSCRAMMs Targets F3 Modules. *PloS One* (2009) 4:e5412. doi: 10.1371/journal.pone.0005412
71. Lepow IH, Ratnoff OD, Levy LR. Studies on the Activation of a Proesterase Associated With Partially Purified First Component of Human Complement. *J Exp Med* (1958) 107:451–74. doi: 10.1084/jem.107.3.451
72. Ziccardi RJ, Cooper NR. Activation of C1r by Proteolytic Cleavage. *J Immunol* (1976) 116:504–9.
73. Ziccardi RJ. The First Component of Human Complement (C1): Activation and Control. *Springer Semin Immunopathol* (1983) 6:213–30. doi: 10.1007/BF00205874
74. Ziccardi RJ. Spontaneous Activation of the First Component of Human Complement (C1) by an Intramolecular Autocatalytic Mechanism. *J Immunol* (1982) 128:1–5.
75. Budayova-Spano M, Grabarse W, Thielens NM, Hillen H, Lacroix M, Schmidt M, et al. Monomeric Structures of the Zymogen and Active Catalytic Domain of Complement Protease C1r: Further Insights Into the C1 Activation Mechanism. *Structure* (2002) 10:1509–19. doi: 10.1016/S0969-2126(02)00881-X
76. Probert WS, Allsup KM, LeFebvre RB. Identification and Characterization of a Surface-Exposed, 66-Kilodalton Protein From *Borrelia burgdorferi*. *Infect Immun* (1995) 63:1933–9. doi: 10.1128/iai.63.5.1933-1939.1995
77. Nguyen NTT, Röttgerding F, Devraj G, Lin YP, Koenigs A, Kraiczy P. The Complement Binding and Inhibitory Protein CbiA of *Borrelia miyamotoi* Degrades Extracellular Matrix Components by Interacting With Plasmin (Ogen). *Front Cell Infect Microbiol* (2018) 8:23. doi: 10.3389/fcimb.2018.00023
78. Pereira MJ, Wager B, Garrigues RJ, Gerlach E, Quinn JD, Osburne MS, et al. Lipoproteome Screening of the Lyme Disease Agent Identifies Inhibitors of Antibody-Mediated Complement Killing. *Proc Nat Acad Sci USA* (2022) 119 (13):e2117770119. doi: 10.1073/pnas.2117770119
79. Moriarty TJ, Norman MU, Colarusso P, Bankhead T, Kubes P, Chaconas G. Real-Time High Resolution 3D Imaging of the Lyme Disease Spirochete Adhering to and Escaping From the Vasculature of a Living Host. *PloS Pathog* (2008) 4:17–9. doi: 10.1371/journal.ppat.1000090
80. Coburn J, Garcia B, Hu LT, Jewett MW, Kraiczy P, Norris SJ, et al. Lyme Disease Pathogenesis. *Curr Issues Mo. Biol* (2021) 42:473–518. doi: 10.21775/cimb.042.473

Conflict of Interest: The authors declare that the research was conducted in the absence of any commercial or financial relationships that could be construed as a potential conflict of interest.

Publisher's Note: All claims expressed in this article are solely those of the authors and do not necessarily represent those of their affiliated organizations, or those of the publisher, the editors and the reviewers. Any product that may be evaluated in this article, or claim that may be made by its manufacturer, is not guaranteed or endorsed by the publisher.

frontiers | Frontiers in Immunology

ORIGINAL RESEARCH
published: 15 June 2022
doi: 10.3389/fimmu.2022.895519

As in Real Estate, Location Matters: Cellular Expression of Complement Varies Between Macular and Peripheral Regions of the Retina and Supporting Tissues

Randy Zauhar[1†], Josef Biber[2†], Yassin Jabri[3†], Mijin Kim[4], Jian Hu[5], Lew Kaplan[2], Anna M. Pfaller[2], Nicole Schäfer[3,6], Volker Enzmann[7,8], Ursula Schlötzer-Schrehardt[9], Tobias Straub[10], Stefanie M. Hauck[11], Paul D. Gamlin[12], Michael B. McFerrin[13], Jeffrey Messinger[12], Christianne E. Strang[13], Christine A. Curcio[12], Nicholas Dana[4], Diana Pauly[3,14‡], Antje Grosche[2‡], Mingyao Li[5‡] and Dwight Stambolian[4‡]*

[1] Department of Chemistry and Biochemistry, The University of the Sciences in Philadelphia, Philadelphia, PA, United States, [2] Department of Physiological Genomics, Ludwig-Maximilians-Universität München, Planegg-Martinsried, Germany, [3] Department of Ophthalmology, University Hospital Regensburg, Regensburg, Germany, [4] Department of Ophthalmology, Perelman School of Medicine, University of Pennsylvania, Philadelphia, PA, United States, [5] Department of Biostatistics, Epidemiology and Informatics, University of Pennsylvania Perelman School of Medicine, Philadelphia, PA, United States, [6] Department of Orthopaedic Surgery, Experimental Orthopaedics, Centre for Medical Biotechnology (ZMB), University of Regensburg, Regensburg, Germany, [7] Department of Ophthalmology, Inselspital, Bern University Hospital, University of Bern, Bern, Switzerland, [8] Department of BioMedical Research, University of Bern, Bern, Switzerland, [9] Department of Ophthalmology, Friedrich-Alexander-Universität Erlangen-Nürnberg, Erlangen, Germany, [10] Bioinformatics Unit, Biomedical Center, Ludwig-Maximilians-University Munich, Planegg-Martinsried, Germany, [11] Metabolomics and Proteomics Core and Research Unit Protein Science, Helmholtz-Zentrum München, Neuherberg, Germany, [12] Department of Ophthalmology and Visual Sciences, University of Alabama at Birmingham, Birmingham, AL, United States, [13] Department of Psychology, University of Alabama at Birmingham, Birmingham, AL, United States, [14] Experimental Ophthalmology, University of Marburg, Marburg, Germany*

The cellular events that dictate the initiation of the complement pathway in ocular degeneration, such as age-related macular degeneration (AMD), is poorly understood. Using gene expression analysis (single cell and bulk), mass spectrometry, and immunohistochemistry, we dissected the role of multiple retinal and choroidal cell types in determining the complement homeostasis. Our scRNA-seq data show that the cellular response to early AMD is more robust in the choroid, particularly in fibroblasts, pericytes and endothelial cells. In late AMD, complement changes were more prominent in the retina especially with the expression of the classical pathway initiators. Notably, we found a spatial preference for these differences. Overall, this study provides insights into the heterogeneity of cellular responses for complement expression and the cooperation of neighboring cells to complete the pathway in healthy and AMD eyes. Further, our findings provide new cellular targets for therapies directed at complement.

Keywords: single cell, complement, age-related macular degeneration, retina, RPE/choroid

OPEN ACCESS

Edited by:
József Dobó,
Hungarian Academy of Sciences (MTA), Hungary

Reviewed by:
Carsten Faber,
University of Copenhagen, Denmark
Chen Yu,
Duke University, United States
Dorottya Csuka,
Semmelweis University, Hungary

***Correspondence:**
Dwight Stambolian
stamboli@pennmedicine.upenn.edu

[†]These authors have contributed equally to this work

[‡]These authors share senior authorship

Specialty section:
This article was submitted to Molecular Innate Immunity, a section of the journal Frontiers in Immunology

Received: *13 March 2022*
Accepted: *11 May 2022*
Published: *15 June 2022*

Citation:
Zauhar R, Biber J, Jabri Y, Kim M, Hu J, Kaplan L, Pfaller AM, Schäfer N, Enzmann V, Schlötzer-Schrehardt U, Straub T, Hauck SM, Gamlin PD, McFerrin MB, Messinger J, Strang CE, Curcio CA, Dana N, Pauly D, Grosche A, Li M and Stambolian D (2022) As in Real Estate, Location Matters: Cellular Expression of Complement Varies Between Macular and Peripheral Regions of the Retina and Supporting Tissues. Front. Immunol. 13:895519. doi: 10.3389/fimmu.2022.895519

INTRODUCTION

Complement, a part of innate immunity serves as the first line of defense against foreign pathogens and altered cells. Depending on context, it is initiated by three distinct pathways: classical (CP), lectin (LP) and alternative pathway (AP). There are 40 - 60 complement proteins with various functions such as chemoattraction of immune cells, activation of leukocytes, opsonization of invading pathogens, lysis of susceptible pathogens, and synaptic pruning (1–4). The effector functions of the complement system are controlled through proteolytic generation of activation fragments that either bind to cell receptors or covalently attach to cell surfaces adjacent to sites of complement activation. It is the job of membrane bound regulatory molecules to modulate complement pathway activation proportionally to limit damage to host tissues (5, 6). The primary site of biosynthesis for the majority of the fluid-phase complement proteins is the hepatocyte and more than 90% of plasma complement is derived from the liver. Extrahepatic cells such as macrophages, endothelial cells and neurons can also produce complement constitutively and when induced (7).

CP activation is dependent on the binding of the recognition molecule C1q to patterns like IgM and IgG immune complexes, RNA, DNA, phosphatidylserine, CRP and others while the LP is activated when mannose binding lectin (MBL) or ficolins (FCN) bind to carbohydrate structures. Following activation, the CP and LP lead to successive cleavage of C4 and C2 and formation of the C3 convertase [C4bC2bC3b]. The AP is activated by spontaneous hydrolysis of C3 to C3(H_2O) that subsequently binds complement factor B (FB). Cleavage of FB to Bb and Ba by complement factor D (FD) leads to formation of the AP C3 convertase [C3b(H_2O)Bb]. Of note, the AP includes an amplification loop for the CP and LP through the action of C3 (H_2O)Bb on C3 to generate C3b which forms C3bBb and additional cleaving of C3. Finally, generation of C3b by any of the three pathways will lead to the generation of the C5 convertase and the common terminal pathway (1–4).

Structures such as the brain and eye have their own local complement expression due to the inability of bloodborne complement proteins to pass through the blood-brain and blood-retinal barriers (8–12). The retina is a specialized light-sensitive multilayered tissue composed of neurons, glia, and vasculature. The retinal pigment epithelium (RPE) is a monolayer of pigmented cells that metabolically supports outer retina and participates in the renewal of photoreceptor outer segments (13, 14). The underlying choroid is a specialized component of the systemic circulation, with pericytes/smooth muscle cells, fibroblasts, melanocytes, neurons, and immune cells (15). Understandably, it is important to determine the complement expression of the distinct cell types in the human retina, RPE and choroid. The idea of a local complement biosynthesis in the retina, RPE and choroid has been supported by earlier studies (16, 17). Importantly, several eye diseases such as glaucoma, diabetic retinopathy, autoimmune uveitis and age-related macular degeneration (AMD), have reported genetic associations with complement (18–20). A large effort of AMD research has been complement based due to strong evidence for complement dysregulation and the identification of complement protein in extracellular deposits called drusen (21, 22). C3, complement receptor 1 (CR1), and terminal complement proteins C5b-9 (membrane attack complex, MAC) have been identified within drusen (23–25). In addition, genome wide association studies (GWAS) have reported significant associations of *complement factor H (CFH)*, *C3*, *complement factor I (CFI)*, *complement factor 9 (C9)*, and *complement factor B (CFB)* with AMD, further evidence that complement is involved in AMD (26).

AMD is a major cause of visual impairment in patients over the age of 65 (27). Currently it affects about 200 million worldwide and is predicted to increase to 300 million by 2040 (28). For reasons still being learned, AMD primarily affects the macula region (29), a specialized region in the retina of humans and non-human primates. In its advanced stages, there are two forms of AMD, geographic atrophy (GA; dry AMD) and choroidal neovascularization (CNV; wet AMD) (30). Both forms are associated with degeneration of photoreceptors, RPE and choroid. Although the current treatment for the wet form of AMD are intraocular injections of antibodies directed at vascular endothelial growth factor (VEGF) many of these treated patients go on to develop atrophy and further vision loss (31–33). Currently, there is no effective treatment for dry AMD. Biochemical, histological, and genetic studies have implicated several pathways involved in AMD, including oxidative damage, chronic inflammation, complement system malfunction and dysregulation of lipids as well as extracellular matrix (34, 35).

Recent clinical trials have utilized drugs to delay AMD progression through alteration of the complement pathway (reviewed in [36–38)]. C3 inhibitors have received the most attention due to the dominant role of C3 as a control point for all three complement pathways. POT-4, a compstatin derivative and C3 inhibitor was used in clinical trials but had to be terminated due to lack of efficacy (39, 40). A second derivative of POT-4, APL-2 (Pegcetacoplan), recently completed phase 3 trials and showed a decrease in GA growth by 25% but was complicated by new onset choroidal neovascularization (CNV) (41). Clinical trials aiming to inhibit C5 have been met with modest success. Avacincaptad Pegol, a C5 inhibitor, was effective at reducing geographic atrophy (GA) growth by 28% but also suffered from a higher onset of CNV in the treated group (41, 42). Monoclonal antibodies directed at C5, Eculizumab and LFG316, have been used to treat GA but were unsuccessful in reducing GA progression (43). Other clinical trials directed at complement factors FD, properdin and FB did not show clinical efficacy (43, 44). Recent reports have raised concerns about treating GA with complement inhibitors (44). Reasons for these failures or modest successes with complications might include route of administration, inappropriate target cells for modulation, failure to select patients most likely to benefit, insensitive trial endpoints, and limited understanding of both complement expression in healthy retina, RPE and choroid and the role of complement in AMD pathophysiology.

This urgent need to assess the complement gene expression in single cells, resolve cell types, characterize the signature of complement expression across cells, and identify differences in

health and disease can now be met implementing recent technological breakthroughs in single cell RNA-sequencing (scRNA-seq) (45–47). To the best of our knowledge, this is the first comprehensive study that describes the single cell RNA and protein expression of complement in the human retina, RPE and choroid. Protein expression was determined for many of the complement expressing genes either by mass spectrometry or western blotting. We also compared our human complement expression to our previously published mouse complement single cell retina data to report differences that should be considered before testing drugs targeted for humans in preclinical mouse studies (48). Finally, we identified local complement expression changes in retina and choroid from post-mortem eyes affected with early AMD. Our results underscore the power of single cell technologies to gain deeper insight into complement homeostasis and assist in our understanding of the complement dysregulation occurring in AMD. Our results increase the knowledge base that exists for ocular complement and will provide investigators with essential additional information to design novel therapies.

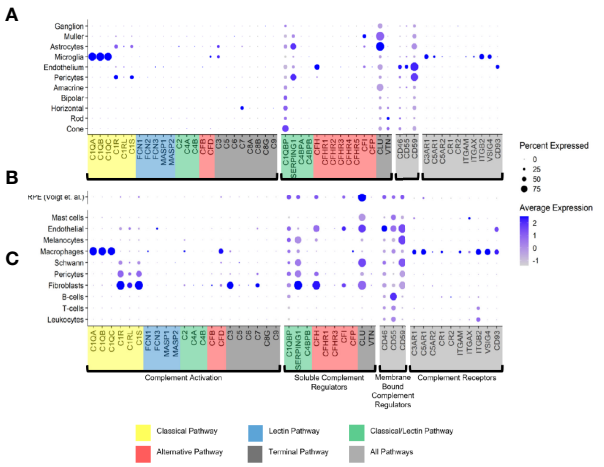

FIGURE 1 | Cell type specific complement expression in the combined macula and peripheral human retina, choroid and RPE. **(A)** Dot plot showing expression pattern of genes of the complement pathways across cell types identified in the combined macula and peripheral retina. The dot plot was generated using Dotplot in the R Seurat package. The size of the dots represents the percentage of cells that expressed gene markers while color shows average expression levels of gene markers. **(B)** Reprocessed combined macula and peripheral RPE data from Voigt et al. (51). **(C)** Dot plot showing expression pattern of known gene markers across cell types identified in the combined macula and peripheral choroid.

RESULTS

Atlas of Complement Expression in the Human Retina, RPE and Choroid Identified by scRNA-seq

Aiming to better understand the contribution of locally produced complement components to immune homeostasis in the posterior part of the human eye, we generated complement expression profiles for all cell types of the human retina, RPE and choroid *via* scRNA-seq (**Table S1**). Cell clusters were annotated using known gene markers for retina and choroidal cell types and clusters sharing the same markers were combined into 11 cell types for the retina and 10 cell types for the choroid (49–51). To analyze the RPE for complement expression we re-processed the scRNA-seq data from Voigt et al (51).

Only a few complement activators were expressed in the retina and included *C1QA-C*, *C1R*, *C1RL*, *C1S*, *CFB*, *CFD*, *C3* and *C7* (**Figure 1A**). Activators for the LP, *FCN1/3* and *MASP1/3*, had minimal expression. By *in situ* hybridization, *CFD* and *C3* transcripts were confirmed in microglia (**Figure 2A**). Moreover, the *C7* expression that surprisingly was confined to horizontal cells was verified as well (**Figure 2A**). Of the cells expressing secreted complement components, microglia had the highest transcription especially for *C1QA-C*. Surprisingly, the RPE had negligible expression of complement activators (**Figure 1B**), while all the activators for the CP were expressed in the choroid, albeit not in every cell type (**Figure 1C**). In the choroid, macrophages had the highest expression of *C1QA-C* while fibroblasts demonstrated robust expression signals for *C1R, C1RL* and *C1S*. Of note, *C3* the central component of the complement pathway was robustly transcribed in fibroblasts (**Figure 1C**).

The soluble complement regulators *component 1q subcomponent binding protein* (*C1QBP*) and *clusterin* (*CLU*) were transcribed by all the retinal cell types, while *CFH* transcription was mostly confined to the endothelium (**Figures 1A**, **2B**). A modest *CFI* expression signal was present in Müller glia and endothelium (**Figures 1A**, **2B**). SERPING1, a regulator dissociating the C1 complex by binding C1r and C1s, showed robust expression in both pericytes and astrocytes. In the RPE, we found moderate expression of regulators *C1QBP*, *SERPING1*, *CFH*, *CFI* and robust expression of *CLU* (**Figure 1B**). Finally, most of the regulators were expressed in various cell types of the choroid (**Figure 1C**). Choroidal fibroblasts had robust signals for *SERPING1*, *CFH* and *CLU*. It should be noted that *CFHR2* and *CFHR5* had no detectable expression in the retina and RPE/choroid. *CFHR1*, *CFHR3* and *CFHR4* expression was weak and limited to specific cell types in the retina and RPE/choroid.

The membrane bound complement regulators *CD46*, *CD55* and *CD59*, demonstrated robust expression in retinal vascular endothelium (**Figure 1A**). Surprisingly, *CD55* transcripts were also found by *in situ* hybridization to co-localize with the microglia marker *AIF1* (**Figure 2B**). CD59, which blocks membrane perforation of C5b-9, is expressed on all retinal cell types to varying degrees. Positive expression of *CD59* across all retinal cell types would make the retina resistant to MAC damage unless the regulators became overwhelmed. A similar conclusion would apply for the RPE and choroid due to moderate to robust expression of all three membrane bound regulators in most cell types. Noteworthy is the absence of *CD59* from choroidal B and T cells.

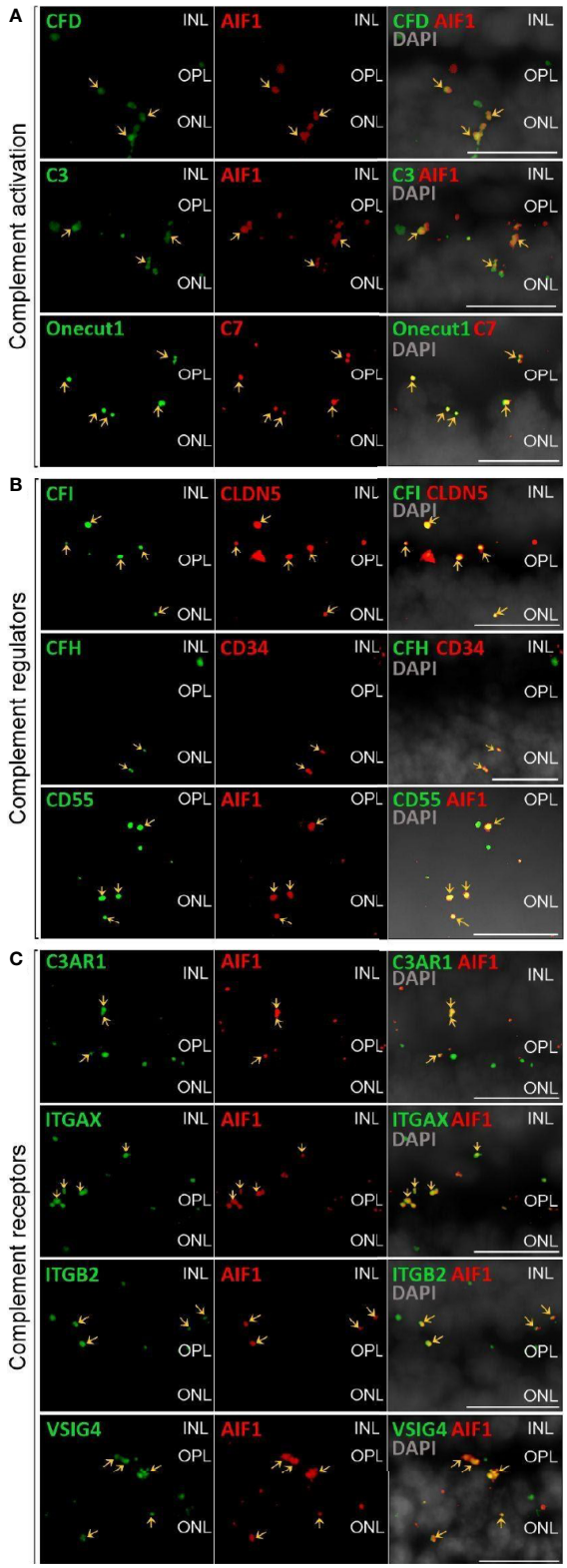

FIGURE 2 | Continued

FIGURE 2 | Validation of scRNA-seq for retinal complement component expression by *in situ* hybridization. **(A)** Factors driving complement activation were chosen for detection by *in situ* hybridization. *CFD* expression from microglia was detected in the inner nuclear layer (INL), outer plexiform layer (OPL) and outer nuclear layer (ONL), but was mostly associated with microglia expressing *AIF1* (alias *IBA1*) in the OPL. *C3* expression was mostly limited to microglia located in OPL. *C7* transcripts were detected in the OPL with overlap of signal with the horizontal marker Onecut1 in the OPL. **(B)** Soluble (*CFH, CFI*) and membrane-bound (*CD55*) complement regulators primarily colocalized with vascular cells and microglia. Signals of *CFH* transcript were strongest from INL and OPL and overlapped with the endothelial marker *CD34*. *CFI* expression associated with the endothelial marker *CLDN5* was strongest in the INL and OPL. *CD55* was robustly expressed in microglia expressing *AIF*. **(C)** Complement receptor *C3AR1* transcripts were detected at low levels in the INL and OPL and co-localized with the microglia marker *AIF1*. *ITGAX* was robustly expressed in the OPL and co-localized with the microglia marker *AIF1* in the OPL. *ITGB2* transcripts were less abundantand co-localized with *AIF1* in the OPL. Also *VSIG4* was strongly expressed in OPL and ONL co-localizing with the microglia marker *AIF1*. **(A–C)** Arrows indicate co-localization of the gene of interest with respective cell marker. Scale bars, 20 µm.

Finally, we identified the cell types expressing complement receptors which would make these cells most responsive to changes in local complement homeostasis. The integrin family receptors, *ITGAM*, *ITGB2G* and *ITGAX*, bind iC3b facilitating immune clearance and phagocytosis (1). Retinal microglia expressed all three receptors (**Figures 1A**, **2C**). *VSIG4*, an immunoglobulin superfamily receptor, is also highly expressed in retinal microglia and is responsible for phagocytosis of C3b and iC3b (1). *CD93*, involved in clearance of apoptotic cells, is expressed in retinal endothelial cells. *C3AR* and *C5AR*, receptors for C3a and C5a, are modestly expressed in microglia cells. This microglia-specific expression pattern could also be confirmed by *in situ* hybridization for *C3AR*, *ITGAX*, *ITGB2* and *VSIG4* (**Figure 2C**). Interestingly, except for *C5AR1*, none of the complement receptors were detectable by scRNA-seq in the RPE. Choroidal macrophages demonstrated a similar expression profile to retinal microglia (**Figure 1**). In addition, choroidal T cells and leukocytes expressed *ITGB2*.

Differential Expression Between Normal Macula and Peripheral Retina and Choroid

Significant differences in complement expression were detected in healthy retinal cells from the macula and peripheral retina (**Data File S1**). We found transcript reduction in the macula for *CFI* in astrocytes, *CLU* in bipolar, horizontal and ganglion cells as well as *VTN* in rods. In contrast, *VTN* in cones, *CD46* in endothelial cells and *CD59* in pericytes were increased in the macula compared to the periphery.

Similarly, a number of choroidal genes showed significant expression differences between cells located in sub-macula and peripheral regions (**Data File S1**). These differences included decreased *CLU* in Schwann cells, *C3* in macrophages, *CFI* and *C1R* in endothelial cells, *CFH* in pericytes, *C1R*, *C1S*, *CLU*, *CFD*, *C3*, *CD55* and *SERPING* in fibroblasts, and *CFH* and *SERPING* in melanocytes. We found increased expression in the sub-macula region compared to the periphery in macrophages for *C1Q*, *C2* and *VSIG4*.

Complement Transcriptome of Human Retinal Cell Types, RPE and Choroid Partially Translated Into Protein Expression

It is known that transcript expression does not necessarily correlate with protein levels (52, 53). This has also been confirmed at the single cell level under very well-controlled conditions and underscores the necessity of measuring proteins as well as RNA (54). Accordingly, we validated select transcripts at the protein level (**Figures 3–6**). Purified retinal cells were obtained by sequential magnetic-activated cell sorting (MACS) of ITGAM-positive microglia, CD31-positive vascular cells (endothelium, pericytes), and CD29-positive Müller glia, while the remaining cell population consisted of photoreceptors and other neuronal types (**Figure S1**) (48). The cell populations with high yield in terms of cell numbers recovered after MACS (Müller glia, neurons, RPE/choroid) were subjected to LC-MS/MS mass spectrometry (**Figure 3**). The level of cell enrichment was determined by marker gene expression and marker protein abundance (**Figure S1**).

Remarkably, consistent with scRNA-seq, the soluble complement regulators CLU and C1QBP as well as the membrane bound regulator CD59 were detected at protein level (via LC-MS/MS mass spectrometry) in all cells of the inner and outer retina and in most cell types of the RPE/choroid, albeit at varying levels and rates (**Figure 3**). Western blot analysis of some selected candidates confirmed that their identified RNAs were translated (**Figures 4–6**). C1s is an esterase cleaving C2/C4, thereby facilitating the formation of the CP C3-convertase. C1s peptides were not detected by LC-MS/MS mass spectrometry possibly because this method is less sensitive to proteins of low abundance (**Figure 3**). Western blot did detect C1s heavy chain in the Müller cell population, which includes astrocytes, and also in the CD31-positive vascular cell population (**Figure 4B**). Thus, the findings of *C1S* transcripts in astrocytes, Müller cells, and pericytes (**Figure 1A**) by scRNA-seq were confirmed. To a lesser extent, C1s protein was also found in microglia, RPE/choroid and retinal neurons (**Figure 4A**).

C3, the central protein of the complement system, is under tight regulation to prevent inadvertent complement activation. *C3* transcript detection using scRNA-seq was mainly restricted to microglia and astrocytes in the retina and to fibroblasts in RPE/choroid (**Figure 1**). Its protein was also detected in or on purified retinal neurons *via* LC-MS/MS mass spectrometry (**Figure 3**) and western blot (**Figure 5**). Also, C3 cleavage product, C3d, was detected in or on all purified retinal cell types (**Figure 5A**).

Also, VTN and components of the terminal pathway (C5, C6, C8A, C8B, C8G, C9) proteins were detected in RPE/choroid samples (**Figure 3**). However, protein analysis sometimes provided contradictory results. This challenge of detecting secreted proteins is clearly reflected in our data. LC-MS/MS mass spectrometry is an unbiased screening method that can miss complement components already secreted and not tightly attached to cell surfaces. As a result, lower levels of intracellular proteins might be under the detection limit. The same is true for western blot analyses of enriched retinal cell populations,

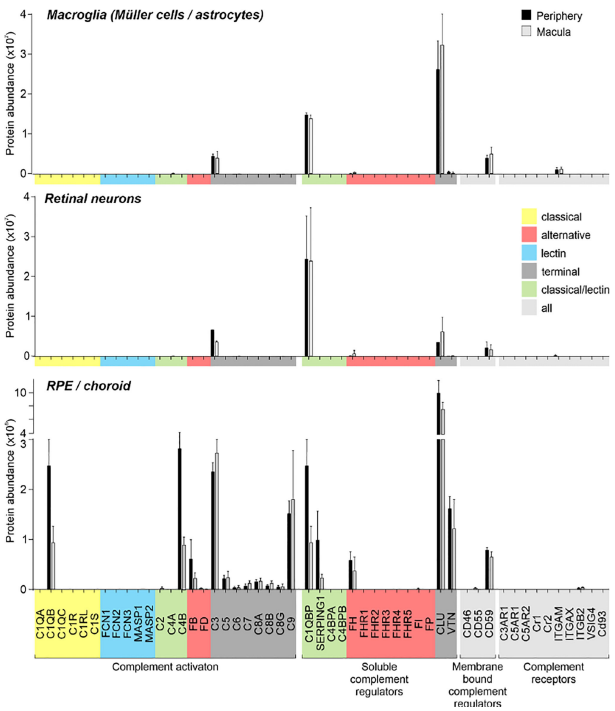

FIGURE 3 | Complement proteome of macroglia (Müller cell, astrocytes), retinal neurons and RPE/choroid in the macular and peripheral human eye. Müller cells and retinal neurons were purified from peripheral and macular retinal tissue punches (6 mm in diameter) from 5 donor retinae (**Table S1**) by magnetic-activated cell sorting (MACS) and were submitted to quantitative LC MS/MS mass spectrometry. Contamination with astrocytes is likely, because no surface marker yet separates them clearly from Müller cells. Müller cells definitely outnumber astrocytes. Macroglia and neurons were depleted from ITGAM (alias CD11B)-positive microglia/macrophages and CD31-positive vascular cells. RPE/choroid was collected after the removal of retinal tissue and comprised a mixture of RPE and choroidal cell types including pericytes, endothelial cells, fibroblast and immune cells. Given the intense perfusion of choroidal tissues, these samples do not allow unequivocal discrimination of the source especially of soluble complement components as they could be expressed by local cell types or by liver cells and enter the choroid *via* the circulation.

although they are more sensitive than LC-MS/MS mass spectrometry. To achieve the most complete picture of protein localization in the tissue, we added immunostaining to detect protein accumulation of select complement components at protein level, irrespective of the actual, expressing source in the tissue. C1s localized to the ganglion cell layer (GCL) and at spots all over the retina possibly reflecting its secretion into the interstitial space (**Figures 4C–E**). C3 was specifically detected on cones of the macular retina (**Figure 5E**), and also Müller cells (**Figure 5D**) – the latter being in line with transcript data.

Similarly, protein expression was determined for additional complement factors. C7 stood out from the list of terminal complement components, since scRNA-seq indicated a very specific expression by horizontal cells (**Figure 1**). However, LC-MS/MS mass spectrometry detected C7 in RPE/choroid samples only (**Figure 3**), while western blot detected whole C7 in neuroretina as well as RPE/choroid and C7 cleavage products

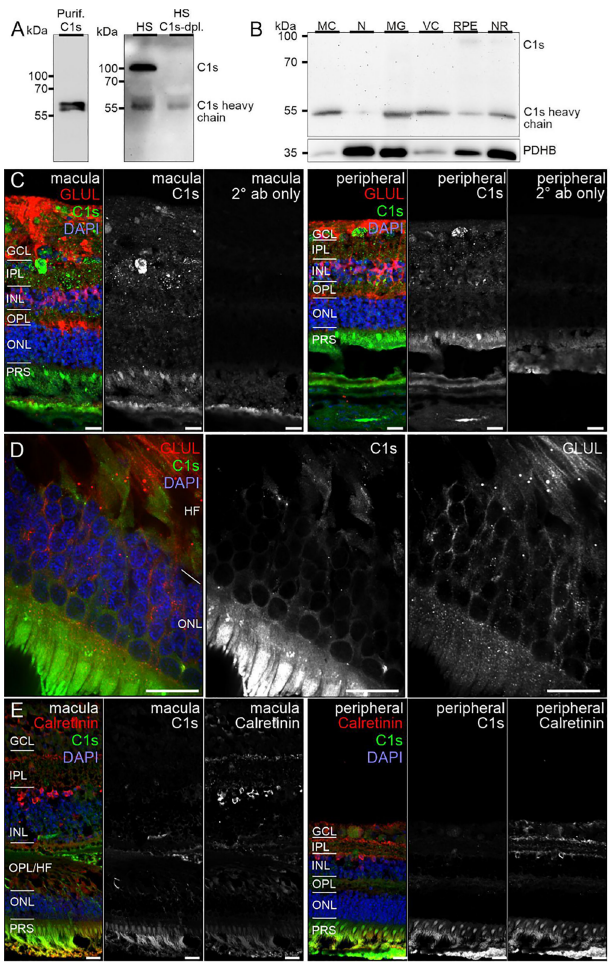

FIGURE 4 | C1s protein expression in the human retina. **(A)** Full C1s (~75 kDa) and the C1s heavy chain (~47 kDa) were reliably detected by Western blot using purified C1s protein and human serum (HS). C1s-depleted HS still contained remaining C1s heavy chain, while full length C1s was absent. **(B)** Western blot analysis of C1s on purified retinal cell types from peripheral human retina and RPE/choroid. The total protein extracted per cell population was loaded. PDHB (pyruvate dehydrogenase beta subunit) served as housekeeper that has been shown to be expressed at equal levels in all investigated cell types. In contrast to HS, primarily the heavy chain of C1s was detected in retinal samples. C1s levels were highest in Müller cells (MC) and vascular cells (VC). MG, microglia; NR, whole neuroretina. RPE, retinal pigment epithelium including choroid. **(C)** Representative micrographs of C1s-stainings from macular (*left*) and peripheral (*right*) retinae. Photoreceptors and cells of the ganglion cell layer (GCL) as well as punctate structures in the inner plexiform layer (IPL) displayed highest labeling intensities. Sections were co-stained for the Müller cell marker glutamine synthetase (GLUL). **(D)** Higher magnification of the outer nuclear layer (ONL) and Henle fiber layer (HL) in the macular retina showed a partial overlap of C1s and GLUL. **(E)** Co-staining of C1s with calretinin, a marker of inner retinal neurons such as ganglion and amacrine cells, yielded no considerable overlap. **(C-E)** INL, inner nuclear layer; OPL, outer plexiform layer; PRS, photoreceptor inner and outer segments. Scale bars, 20 µm.

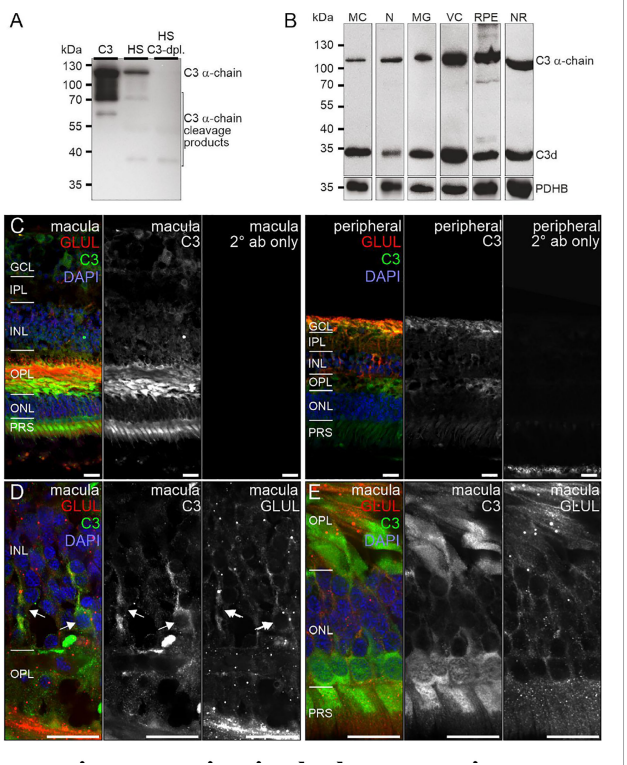

FIGURE 5 | C3 protein expression in the human retina. **(A)** The C3 α-chain (~120 kDa) and its cleavage products were robustly detected by Western blot if purified C3 or human serum (HS) was loaded. No characteristic bands were detected in C3-depleted HS. **(B)** Western blot analysis of C3 on purified retinal cell types from peripheral human retina and RPE/choroid. The total protein extracted per cell population was loaded. PDHB served as housekeeper since not the exact same amount of protein could be loaded given the low protein yield from the microglial (MG) and vascular cell (VC) populations. The C3 α-chain and its cleavage product C3d were detected in every retinal cell population at comparable levels. MC, Müller cells; N, retinal neurons; NR, whole neuroretina; RPE, RPE/choroid mixed samples. **(C)** Representative micrographs of C3-stainings from macular (*left*) and peripheral (*right*) retinae. Photoreceptors, photoreceptor terminals and Müller cell processes were positively labeled. Co-staining for the Müller cell marker glutamine synthetase (GLUL) demonstrated an overlap primarily in cells from the peripheral retina. **(D)** Higher magnification of the inner nuclear layer (INL) highlighting the co-localization of C3 and GLUL (arrows). **(E)** Co-staining of C3 and GLUL did not result in an overlap in the outer retina. C3 stained cone photoreceptors (asterisk) which form a single row excluding rod photoreceptors from that layer in the central retina. **(C–E)** GCL, ganglion cell layer; IPL, inner plexiform layer; OPL, outer plexiform layer; ONL, outer nuclear layer; PRS, photoreceptor inner and outer segments. Scale bars, 20 µm.

in all retinal cell populations (**Figure 6B**). In support of this finding, C7 immunoreactivity was detected across the whole retinal section (**Figures 6C, D**).

Acting together with FH, FI inactivates C3b through sequential cleavage to iC3b, C3c, C3dg and finally C3d. Western blotting identified FI in/on microglia, Müller cells and CD31-positive vascular cells, but very little association with neurons or RPE/choroid (**Figure 6F**). The location of FI in microglia was confirmed by immunostaining (**Figure 6G**). FH, an additional regulator of complement activation, inactivates C3b in the presence of FI. LC-MS/MS mass spectrometry and western blots identified FH in RPE/choroid (**Figure 3**; **Figure 6J**). Since contamination of the RPE/choroid samples

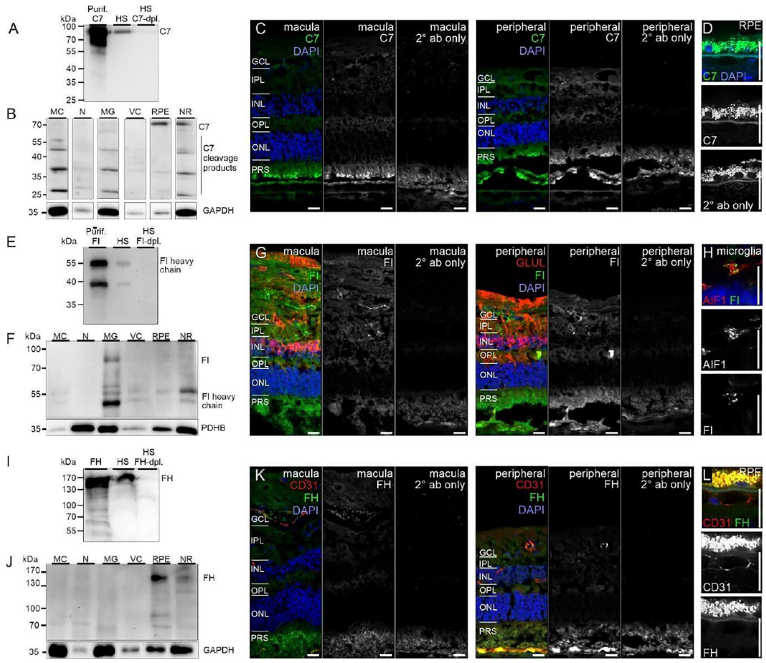

FIGURE 6 | CFI, CFH and C7 protein expression in the human retina. **(A)** Loading purified C7 or human serum (HS), full length C7 was detected as a single band (~90 kDa) and cleavage products <90 kDa. **(B)** Full-length C7 was detected at low levels in purified cell types, but robustly in RPE/choroid. Cleavage products were detected in all cell populations. C7 immunoreactivity was similar in macular and peripheral retinal sections. **(D)** Higher magnification of the C7 staining in RPE. **(E)** Loading purified CFI or HS, only the CFI heavy chain (~50 kDa) was unequivocally detected by Western blot. **(F)** CFI was present in Müller cells (MC), microglia (MG), vascular cells (VC) and RPE/choroid, but not in neurons. **(G)** Comparable CFI-labeling of structures of the macular and peripheral retina. CFI-immunoreactivity partially overlapped with that of the Müller cell marker glutamine synthetase (GLUL). **(H)** Higher magnification of the inner plexiform layer (IPL) demonstrating co-localization of CFI with IBA1-positive microglia. **(I)** Detection of CFH (~150 kDa) by Western blot using purified CFH and HS. **(J)** CFH was only detected in RPE/choroid. A contamination with CFH from the system circulation cannot be excluded. **(K)** CFH immunoreactivity was confined to vessel lumens. **(L)** Minor CFH immunoreactivity at the RPE – Bruch's membrane interface at higher magnification. **(B, F, J)** PDHB or GAPDH (Glyceraldehyde-3-phosphate dehydrogenase) served as housekeepers. N, neurons; NR, whole neuroretina. **(C, D, G, H, K, L)** GCL, ganglion cell layer; OPL, outer plexiform layer; ONL, outer nuclear layer; PRS, photoreceptor segments. Scale bars, 20 µm.

with systemic FH protein is likely, these results have to be interpreted with caution. Immunostaining located FH on the luminal side of retinal and choroidal vessels (**Figures 6K, L**), consistent with our scRNA-seq result of the endothelial cell's robust expression of *CFH* (**Figure 1**).

Human and Murine Retinal Cells Showed Species-Specific Complement Transcriptomes

Experimental approaches to investigate human diseases and underlying complement action involved studies in mouse models (48, 55–57). To facilitate the transfer of murine complement results to the human system, we compared the scRNA-seq expression of different complement components in the normal human peripheral (rod-dominated) retina and our own published study on rod-rich mouse retina (**Figure 7**) (48). Several differences in complement expression were observed between both species. For the CP, elevated expression levels were found in human compared to mouse retina: *C1Q*, the molecular recognition component for activation of the CP, is exclusively expressed by microglia in mice and humans, with high expression of all three components of this complex (*C1QA*, *C1QB* and *C1QC*) in both human and mouse (**Figure 7**). The remaining components of the C1 complex, *C1R* and *C1S*, which activate C4 and C2 upon recognition of antigen-antibody complexes, show significant overlapping expression in pericytes. Human pericytes and astrocyte/Müller cell fractions express both *C1R* and *C1S* at similar levels. Mouse pericytes and endothelial cells also express these transcripts, whereby *C1S* is detected at higher levels than *C1R* in the mouse. LP proteins were almost not detectable in both mouse and human, suggesting this pathway has a negligible role in maintaining cellular homeostasis in the normal eye. With respect to the AP activators, *CFD* is expressed in human microglia and not detectable in scRNA-seq, but with qPCR, in the mouse retina. *C3*, involved in both CP and AP, is especially detected in human microglia (**Figure 7**). Murine microglia showed much lower expression levels (48).

The soluble regulators of the CP demonstrated differences between human and mouse (**Figure 7**). *C1QBP* expression was more robust across all human cell types compared to mouse. *SERPING1* also showed higher expression in human than in murine endothelial cells, microglia, Müller cells and pericytes.

The soluble regulators of the AP, *CFH* and *CFI*, showed very large differences. *CFH* was strongly expressed in human endothelial cells, while its expression in mouse was highest in microglia and pericytes. Interestingly, FI which acts in concert with FH, showed high expression in human endothelium and Müller glia but was almost undetectable in the mouse retina (**Figure 7**) (48). *VTN* and *CLU*, both soluble negative regulators of all complement pathways, are differentially expressed across all cell types, with expression of *CLU* higher in human than mouse in all cell types except cones. *VTN* is expressed at higher levels in mouse compared to human in all cell types except horizontal cells.

Overall, we found higher levels for the terminal soluble and membrane bound complement regulators in the human retina compared to the mouse retina (**Figure 7**). *CD46* was expressed in most human retinal cell types, but had no expression in mouse retina. Similarly, *CD55* was only expressed in human, specifically in microglia, endothelial and ganglion cells. Finally, *CD59* is expressed broadly, but differentially, across cell types, with expression generally being higher in human than in mouse in all cell types except cones. *CD59* expression is absent in mouse microglia and pericytes.

Notably, we found more agreement of complement receptors for microglia in mouse and human. While mouse microglia express all three anaphylatoxin receptors, human microglia express only *C3AR1* and *C5AR1*. The expression of the integrins *ITGAM*, *ITGAX* and *ITGB2* are also exclusive to microglia. *ITGAX* and *ITGB2* show significant expression in human microglia, *ITGAM* and *ITGB2* in mouse microglia. The complexes of these integrins, ITGAM/ITGB2 and ITGAX/ITGB2, termed CR3 and CR4 respectively, recognize inactivated complement C3 (iC3b) on cell surfaces (58–60).

We also found interesting species-specific differences with respect to proteins. C3 protein was detected *via* western blot in all purified human retinal cell types (**Figure 4B**), while it could only be identified in samples from murine RPE and neurons (48). Moreover, the complement inhibitor FH was present in samples from all mouse retinal cell types except for vascular cells (48), but on the other hand FH protein was only detectable in human RPE (**Figure 6J**).

In summary, there are distinct complement expression differences between the mouse and human retina which should be considered when using the mouse as a model for developing therapeutics intended for humans.

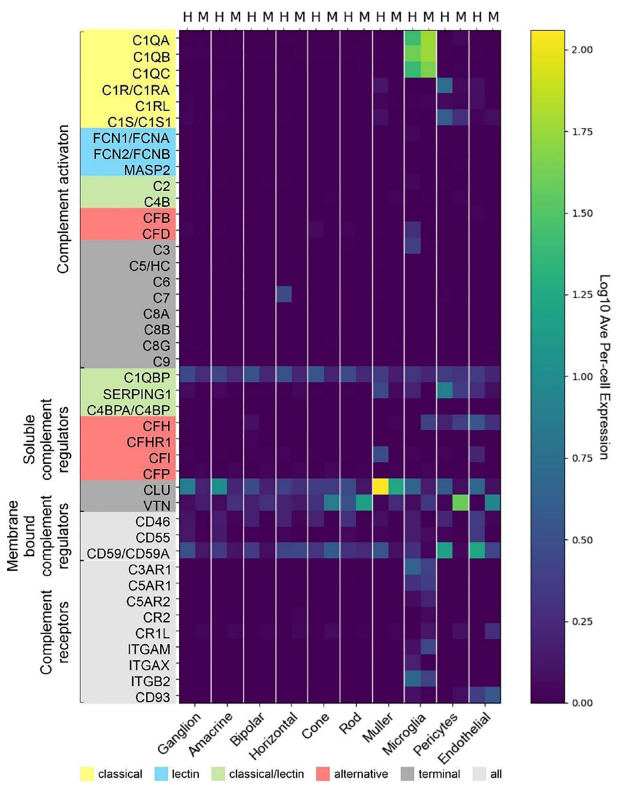

FIGURE 7 | Comparison of cell type-specific complement expression between peripheral human (H) and mouse (M) retina. Expression of complement components was determined by scRNA-seq. For cross-species comparison data from the present study on human retina was compared to recently published data from mouse retina (48). Expression is measured in units of FPKM (Fragments Per Kilobase of transcript per Million mapped reads) and color-coded on a logarithmic scale.

AMD-Associated Changes of the Complement Transcriptome by Single-Cell RNA-seq in Human Retina and Choroid

The species-related differences in complement necessitate a focus on human donor tissue to fully understand the role of complement in AMD pathology. To achieve this, we applied scRNA-seq to samples from early AMD cases and healthy donors. We clustered human retinal cells collected from human retina from donor eyes (**Table S1**) and performed analyses of complement gene expression, comparing early AMD macula vs normal macula and macula vs periphery in early AMD samples. For the comparison of early AMD vs. normal macula retina we identified several complement genes with significant differential expression for the retina ($p \leq 0.05$); most fold changes are small in magnitude (**Figure 8A** and **Data File S1**). The largest fold changes (FC) were found for *C1Q* which is down-regulated in microglia, *C3* which is up-regulated in astrocytes, and *C7* which is upregulated in horizontal cells. In microglia the anaphylatoxin receptor *C5AR1* and *CFD* was up-regulated and *ITGB2* was down-regulated. Membrane-bound complement inactivator *CD46* was upregulated in endothelium, pericytes and in bipolar cells. *CFI* was up-regulated in astrocytes and potential gliotic Müller cells, but down-regulated in homeostatic Müller cells. The inhibitor of MAC formation *CD59* was up-regulated in astrocytes and Müller cells and down-regulated in pericytes. The complement regulator *CLU* was up-regulated in astrocytes and bipolar cells and down-regulated in microglia and in Müller cells. Complement regulator *C1QBP* was down-regulated in both astrocytes and pericytes. In pericytes, *C1S*, which is required for *C1* activation, was up-regulated 1.6-fold.

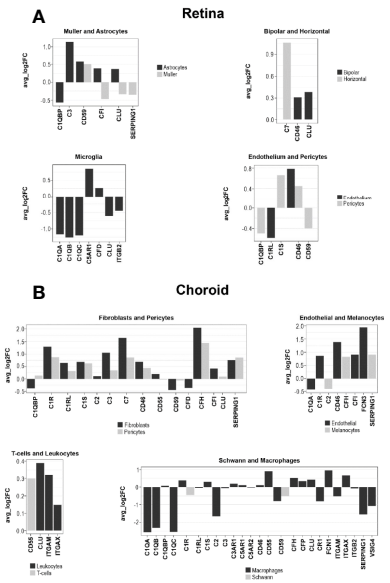

FIGURE 8 | Log fold change (FC) of complement gene transcription within retina and choroidal cells from donors diagnosed with early AMD. **(A)** LogFC of Differentially expressed (DE) retinal genes between early AMD macula and normal macula were defined as a gene showing expression in at least 10% of cells within a cell type and a $P \leq 0.05$. **(B)** LogFC of DE choroidal genes between early AMD macula and normal macula were defined as in A.

To find regional expression differences for retina complement in AMD, we also compared early AMD macula vs. early AMD periphery (**Data File S1**). The largest differential expression between macula and periphery was found in astrocytes, where *C3* and *CFI* show about 2-fold lower expression in macula compared to periphery. *C3* showed higher expression in microglia in the macula. Other complement genes show fold change smaller than 1.5-fold.

Cells from the choroid were collected from the same donor eyes for single-cell complement analyses similar to retinal cells. In contrast to our results for retina, the choroid showed larger changes to 5-fold (**Figure 8B** and **Data File S1**). All the cell types in the choroid manifested transcriptional differences in one or more complement genes when comparing early AMD and normal macula sub-macular choroid (**Figure 8B** and **Data File S1**). Melanocytes had increased *SERPING1* and *CFH* expression. Macrophages showed a decline in *C1Q* (5-fold) and *SERPING1* (3.3-fold) and *CD59*. Increases in C*FH* expression were seen in early AMD sub-macular regions. In AMD donors, choroidal endothelial cells from the sub-macular region showed an increase in *CD46* and *FCN3* (3.8-fold). Pericytes showed increased expression of *C1R*, *C1S*, *CD46*, C*FH*, *C7*, *C3* and *SERPING1*. Choroidal fibroblasts from the sub-macular region had higher *C3*, C*FH*, *SERPING1* and C*FI* expression in early AMD. and a decrease of C*FD* (1.2-fold) in early AMD. Fibroblasts also expressed *C7* at higher levels than pericytes. Leukocytes, T and B cells had minimal differentially expressed (DE) complement transcripts.

Choroidal sub-macula and peripheral cells from early AMD donors were compared for potential clues to explain why the macula is the preferred site of AMD pathology. The largest differences between sub-macula and periphery (**Data File S1**) of the choroid in early AMD were present in Schwann cells, melanocytes, macrophages, endothelial, and fibroblasts. Schwann cells had less *CLU* and C*FD* expression in the sub-macular region. Macrophages from the sub-macula showed decreased *C1QB*, *CR1*, *C3* and increased C*FD*, *CD55*, and *FCN1*. Choroidal endothelial cells from the sub-macular region had a 2.8-fold increase of *FCN3*. Choroidal fibroblasts from the sub-macular region showed decreases in *CLU*, *SERPING1*, *C1R*, *C1S*, *C3*, *CD55* and increased C*FD* expression.

Early and Late AMD-Associated Changes of the Complement Transcriptome by Bulk RNA-seq in Human Retina and RPE/Choroid

We next determined the difference in complement expression using bulk RNA-seq data obtained from retina and RPE/choroid/sclera tissue samples from normal and patients diagnosed with AMD. Because this dataset includes results from early- and late-stage AMD cases, it also allowed us to answer the question of whether trends in complement changes in early AMD are confirmed or even amplified with disease progression. In macular retina (MR), the majority of complement genes are up-regulated in late AMD (**Data File S2** and **Figure 9**). The largest FC are for all components of the C1 complex (*C1QA, C1QB, C1QC, C1R, C1S*) that recognizes antibody-antigen interactions and initiates the CP of complement activation. FC (late AMD versus normal) for these genes range from 67-fold for *C1Q* to 32-fold for *C1R*. Activators of the AP, *CFB* (8-fold) and *CFD* (16-fold) were also strongly upregulated. *FCN1*, an activator of the LP, was 17-fold upregulated in the MR of late AMD. Interestingly, the gamma subunit of C8 is expressed in our samples at very low levels and with little variation with respect to location or disease state while C9 is completely absent in our data (**Figure 9**). The next-highest fold changes in MR are the soluble negative regulators of complement activation, *CFH* up-regulated 63-fold and *SERPING1* up-regulated 37-fold in late AMD. This trend was slightly visible already in early AMD retinae and is in line with *CFH* upregulation in pericytes determined by scRNA-seq as well. Of the membrane-bound inhibitors of complement activation, only *CD59* is significantly up-regulated (5-fold in late AMD). *CLU*, which inhibits formation of the terminal C5b-9 complex, is expressed at a high level irrespective of disease stage or location (**Figure 9**). *VTN*, another antagonist of C5b-9 complex formation, is expressed at low levels and is the only inhibitor down-regulated (3-fold) in MR of late AMD patients. Also, *CFP* is up-regulated 4-fold suggesting a more active amplification loop of C3 convertase formation in AMD. Other genes with significant up-regulation in MR in late AMD include the anaphylatoxin receptors, *C3AR1*, *C5AR1* and *C5AR2* (15-24-fold), the integrins *ITGAM*, *ITGAX*, *ITGB2* (3-20-fold), and the adhesion molecule *CD93* (20-fold). In peripheral retina (PR),

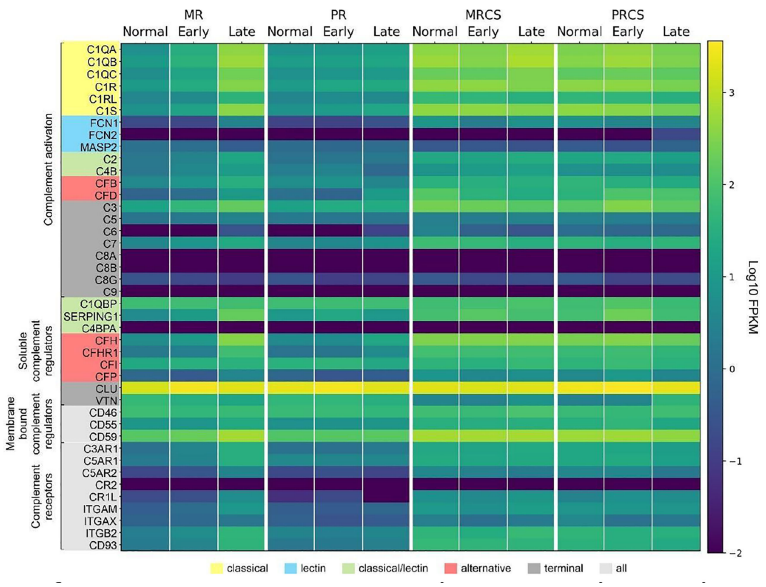

FIGURE 9 | Heat map of complement gene expression determined using bulk RNA-seq for macular retina (MR), peripheral retina (PR), macular RPE/choroid/sclera (MRCS) and peripheral RPE/choroid/sclera (PRCS) from normal, early AMD and advanced AMD donors. Expression is measured in units of FPKM and color-coded on a logarithmic scale.

some up-regulation is observed in late AMD, but with much smaller fold-changes (**Data File S2** and **Figure 9**).

In macular RPE/choroid/sclera (MRCS) and peripheral RPE/choroid/sclera (PRCS) bulk data, patterns of expression for most complement genes do not depend strongly on disease state. For some of the deviations the interpretation is not clear. For example, *CFD* shows modest down-regulation with AMD in MRCS and up-regulation in PRCS. Because these samples contain RPE cells and, most importantly, a large proportion of scleral cells in addition to choroidal cells, no cross-comparison was performed with the data from our scRNA-seq approach to avoid over- or misinterpretation of the data.

These observations thus partially confirm our findings from the scRNA-seq approach and, importantly, suggest a robust perturbation of complement homeostasis in the MR in advanced AMD which is not present in the retina periphery, choroid MRCS and PRCS.

DISCUSSION

Understanding how the local complement homeostasis in the retina and supporting tissues is changing in the course of diseases like AMD is key to identify appropriate targets and optimal timing for a successful therapeutic intervention. Anderson et al. published a comprehensive analysis of complement expression in human RPE, choroid and retina (17). Their analysis was done on tissue layer lysates as opposed to the current study which focused on single cells from these layers. They characterized the choroid as the predominant source of soluble regulators, SERPING1 and C4BP. The membrane regulators, CD55 and CD46, were also higher expressed in the choroid than in RPE or retina. C3 and the terminal pathway genes, C5 and C7, expression was localized within the choroid as well. While the regulators CLU and VTN were expressed in all three layers. LP expression was very low in all three layers. Tissue lysates from several donors with AMD were also assayed by quantitative PCR but no significant differences were detected between normal and AMD eyes (17). Their overall results concluded that the choroid was the predominant source of CP and AP components, rather than the RPE or retina. Our study extends the Anderson et al. study to single cell expression of the complement genes in normal retina, RPE and choroid as well as early AMD retina and choroid (17).

A Refined Map of Complement Expression in Retina, RPE and Choroid

C1q is the recognition protein for the CP and it must complex with both C1r and C1s to activate the CP (1). The retina showed distributed transcription of *C1Q*, *C1R* and *C1S* with *C1Q* expressed in microglia and *C1R*/ *C1S* expressed in both astrocytes and pericytes (**Figure 1A**). Of note, *C1Q* was expressed by almost all sequenced microglia. Astrocytes and pericytes expressed also most of the soluble complement regulator *SERPING1*, a dissociator of the C1 complex (**Figure 1A**). Thus astrocytes/pericytes appear to have opposing roles as activators and inhibitors of the CP. Interestingly, *SERPING1* is significantly downregulated in astrocytes in macula vs periphery in early AMD (**Data File S1**).

In the normal choroid, *C1Q* is solely expressed in macrophages which is in line with findings for retinal

microglia (**Figures 1A, C**). Choroidal pericytes and fibroblasts express both *C1R* and *C1S* (**Figure 1C**). Multiple cell types in the choroid including fibroblasts, pericytes, Schwann cells and melanocytes show robust *SERPING1* expression. According to scRNA-seq results, the RPE has minimal transcription of CP activators (**Figure 1B**).

The initiators of the LP pathway, FCN1-3 and MASP1, showed no expression in the normal retina, choroid and RPE suggesting the LP pathway is inactive in all healthy layers.

The C3 convertase is short-lived with a half-life of about 90 seconds requiring stabilization to assure efficient host defense (1). Properdin (gene ID: CFP) stabilizes the alternative C3 convertase and is solely expressed in macrophages of the choroid but is not expressed in RPE and retina (**Figure 1**). While an antagonistic inactivator of C3, FI, was primarily contributed by Müller glia, an important macroglial cell type in the retina (**Figure 1A**).

The late-acting complement components of the terminal pathway, including C7, assemble into the terminal complement complex to form either a cell membrane pore that induces cell lysis or a soluble sC5b-9 complex with multiple functions. Except for C7, the other components of the terminal pathway were not detected in healthy cells. *C7* transcripts were expressed in both normal retina and choroid, albeit confined to the horizontal cells in the retina and fibroblasts in the choroid. *C7* transcripts translate into a 91 kDa protein that we demonstrated to be present in the healthy neuroretina and RPE by western blotting (**Figure 7B**). C7 has a prominent cathepsin D cleavage sites leading to lysosomal protein degradation fragments, which were additionally detected in all retinal cell types (61). The functional relevance of C7 cleavage products however is still unknown. Immunostaining showed a uniform distribution of C7 in the macular and peripheral human retina. This study, thus, provides new insights into the retinal localization of C7 as the only late complement protein expressed in the neuroretina (**Figure 2**). Additionally, *C7* is upregulated in both astrocytes and horizontal cells in early AMD.

Terminal complement components, namely the C5b-9 complex, have previously been detected only in the Bruch's membrane/choroid complex in aged healthy controls (17, 62). Pore formation is triggered *via* the conversion of C5 to C5b by surface-bound C5 convertases and subsequent local formation of C5b6. The next step, binding of C5b6 with C7 must occur rapidly to prevent release of C5b6 from the membrane surface. If C7 concentrations near the site of complement activation are limiting, the stable bimolecular C5b6 complex dissociates from the C5 activating complex and accumulates in solution (63). If this C5b6 complex subsequently encounters C7, fluid-phase C5b-7 is formed, and this complex can lyse normal cells at a different location from the initial site by 'reactive lysis' (64). Therefore, it is advantageous to have local retinal horizontal and choroidal fibroblasts expressing C7 so that its presence can prevent diffusion of C5b6 from the cell membrane.

The soluble inhibitors for the C5b-9 terminal complex, CLU and VTN, had different cellular expression patterns. In the retina, all cells expressed *CLU* but in the choroid its expression was limited to mast, endothelial, melanocytes, Schwann, pericytes and fibroblasts. RPE also had robust *CLU* expression activity. *VTN* was expressed in rods, cones and horizontal cells. Very low *VTN* expression was detected in both choroid and RPE. The robust expression of *VTN* and *CLU* in healthy cells is important to decrease the deposition of C5b-9 onto their surface. Importantly, *CLU* was upregulated in both ganglion and horizontal cells in the macula of early AMD.

Implications of Cell Type-Specific Protein Signatures for Selected Complement Components

To infer functional implications of a particular complement component in retinal immune homeostasis, one must ask where the respective protein accumulates in the tissue, especially if, as it is the case with most complement components, the protein of interest is secreted. Our protein expression data of selected complement components in the healthy adult human retina showed for the first time (i) an intraretinal localization of C1s and C7, (ii) spatial differences for C3 detection in the macula and periphery, and (iii) a FI colocalization with microglial cells, indicating a physiological function of the complement system in the human retina.

C1s, is one of the first proteolytically active components of the CP. The assembly of the classical C3 convertase (C4bC2a) requires the activity of C1s. We detected the heavy chain of C1s mainly in Müller and vascular cells purified from healthy retinal tissue (**Figure 4B**). Human retinal immunostaining showed associated C1s deposition in the macular and peripheral areas in the inner plexiform, ganglion cell, and compartments of the photoreceptor layers (**Figures 4C, D**). The punctate C1s-positive structures did not overlap with the tested Müller cell, amacrine or ganglion cell markers or nuclei, but seemed to be allocated to cell surfaces or the intercellular space. According to the human cell atlas, C1s is mainly localized in the nucleoplasm and additionally in the cytoplasm (65). In line with present findings, we recently detected C1s heavy chain in the photoreceptor and ganglion cell layer of healthy, photodamaged and post-ischemic murine retinas (48, 66).

C3 is the central complement protein and all complement pathways converge at the level of C3 activation. It is expressed differently in the RPE, retina and choroid. *C3* mRNA was modestly expressed in retinal microglia and astrocytes, robustly expressed in choroidal fibroblasts and minimally expressed in RPE cells (**Figure 1**). We detected C3 protein deposition in healthy retinas (**Figures 6C–F**). In the retinal periphery, C3 protein colocalized with Müller cells, endothelium and with cells in the ganglion cell layer (**Figure 5D**). In the macular region, C3 protein was detected in the outer plexiform layer and on cone photoreceptors (**Figure 5C**). Previous work also reported C3 immunoreactivity for a subset of cone photoreceptors approximately 1.5 mm peripheral to geographic atrophy lesions but not in healthy retinas (67). The outer plexiform layer and photoreceptor-associated C3 deposition in healthy tissue was largely restricted to the macular region in our study (**Figure 5C**). Comparison of our results with other studies is

difficult as in most cases it is not clearly specified which retinal regions were used for staining in healthy controls and the ganglion cell layer was never imaged (17, 67, 68). Our C3 protein results for the healthy retina add to the current knowledge on C3 immunoreactivity in Bruch's membrane/choroid.

While the liver is the predominant source of circulating C3 (69), it has been shown to be synthesized by immune and nonimmune cells such as lymphocytes, neutrophils, epithelial, and endothelial cells (9, 70, 71). In some cases, the accumulation of intracellular C3 can aggravate tissue damage, while in others it can be protective against cytokine induced death (72–75). There is good evidence that intracellular complement provides tissue specific protection against distinct stimuli such as injury and in some cases functions in cell metabolism (76–78). Kulkarni et al. published elegant work on C3 biosynthesis in human airway epithelial cells that is augmented during times of stress and acts as a cytoprotectant (71). The same study found increased intracellular C3 in airway epithelial cells in end-stage lung disease due to cystic fibrosis or chronic obstructive pulmonary disease. In our study choroidal fibroblasts demonstrated an increase of C3 expression in early AMD, potentially for a protective effect. It is unknown how intracellular C3 stores in the choroid and retina are modulated and whether altering these stores is deleterious or protective.

Complement responses are tightly regulated. The damaging C3 cleavage product, C3b, is inhibited by FH and FI in the fluid phase and on membrane surfaces by the receptors CD55 and CD46. Retinal endothelial cells express *CFH* and *CFI*, while Müller glia express *CFI*. Also, the choroid had robust expression of *CFH* and *CFI* from endothelial cells and fibroblasts. Western blots associated FI mainly with the retinal microglial cell population (**Figure 6F**) and to a lesser extent to RPE/choroid. This corresponded with FI immunostaining in the plexiform layers in the adult healthy retina, and with overlapping microglial staining in the inner plexiform layer (**Figures 6G, H**) (79). In addition, partial overlap of FI staining with the Müller cell marker glutamine synthetase was observed, which is consistent with their single-cell mRNA profile (**Figures 2**, **6G**). In line with these findings, previous publications localized FI immunoreactivity mainly to the inner retina (17).

FH is the major complement inhibitor of the AP. Consistent with previous reports (17, 80), we detected FH protein in the RPE/choroid and at vessels in the healthy human retina. We could not identify spatial differences between macular and peripheral retinal tissue. This suggests a role in maintaining retinal immune privilege at the inner and outer retinal blood barrier rather than intraretinal activity.

Almost half the retinal cell types expressed *CD55* or *CD46* which inactivates C3b and C4b in the presence of FI. Not detectable expression of *CD55* and *CD46* in ganglion cells, astrocytes, microglia, rods, cones and Müller glia makes these cell types more susceptible to damage from C3b and C4b binding. In addition, every choroidal cell type expressed either *CD46* or *CD55*, providing broad protection from C3b and C4b. RPE expressed *CFH* and *CFI* and modestly expressed the receptors *CD46* and *CD55* that provide a reasonable barrier against complement damage. Our finding of less *CD46* and *CD55* expression on normal rods and cones might be the reason C3 is able to accumulate on photoreceptor surfaces in AMD.

ScRNA-seq Refines Our Understanding on the Cellular Contribution to Complement Changes in AMD

While only very moderate changes in complement expression were observed in early AMD for retinal cell types, our choroidal scRNA-seq findings demonstrated increased expression of the secreted complement components *CFI, C1R, FCN3, CFH, C3, C7* and *SERPING1*. *C3* was increased in fibroblasts (2-fold) and pericytes (1.3-fold) and *C7* was increased 3-fold in fibroblasts and 1.8-fold in pericytes. *FCN3* had minimal expression in normal endothelial cells but increased 3.8-fold in early AMD. Ficolins serve as recognition molecules for the LP and activate the MBL-associated serine protease family, MASPs. Importantly, *FCN3* is a primate specific gene and only exists as a pseudogene in mice (81). It has been reported to bind to apoptotic Jurkat cells promoting C3 and C4 activation (82). The membrane regulator CD46 was ubiquitously expressed in normal choroid and showed higher expression in most of the same cell types in early AMD (fold change ranging from 1.1-2.6). The rise in *CD46* expression could be a compensatory response to the enhanced secreted complement component expression. In early AMD, *CFH* also showed large increases in early AMD in macrophages, pericytes, and fibroblasts - most likely to offset increased C3b.

Our comparison of the sub-macula vs peripheral choroid in early AMD identified significant increases in *FCN3* expression in endothelial cells of the sub-macula (3-fold) than in peripheral choroid. Interestingly, FCN3 was reported to be elevated in the vitreous of eyes with proliferative diabetic retinopathy along with increased VEGF suggesting a collaboration between FCN3 and VEGF to stimulate inflammation and angiogenesis (83). Other differences in choroidal macular complement expression from early AMD eyes included a 3-fold decrease of *CFD* and 1.5-1.6-fold decrease of *CLU* in Schwann cells and fibroblasts as well as a 1.4-fold *FCN1* and 1.3-fold C*FD* increase in macrophages compared to their cellular counterparts from peripheral AMD choroid.

Currently, there are two competing theories of the tissue layer responsible for the initiation of AMD. One theory implicates RPE cell dysregulation as the starting location because drusen and RPE pigmentary changes often precede advanced AMD stages (84). Alternatively, more recent evidence cites the choriocapillaris as the initiating site due to capillary dropout, a hallmark of early AMD (85). In line with this, Lutty et al. reported attenuation of the vascular supply in the submacular region with overlying normal RPE in early AMD (86). The vascular diminution was confined to the macula and absent in the periphery providing strong evidence that the choroid, not the RPE, could be the initiation site of AMD (81). Our complement results in the macula of early AMD provide further evidence (i) that there are choroidal expression differences confined to the macula region and (ii) that the retinal cell complement

expression signature is not as dramatically changed as observed in the choroid which implies that (iii) the disruption of the local complement homeostasis in early AMD is driven by the choroid rather than retinal cell types. Since our analysis did not include RPE, we cannot determine its contribution to the pathology.

Bulk RNAseq Confirms Early Changes of Complement Expression That Are Accelerated With AMD Progression

While bulk RNA-seq data are relatively insensitive to gene expression changes limited to specific cell types (which might provide important clues to mechanisms of disease initiation), this approach does provide a global picture of large-scale changes in expression at the tissue level. In particular our data for macular and peripheral retina reveal that AMD progression is associated with increasing up-regulation of a number of complement genes associated with the CP and AP and therewith validate findings from our scRNA-seq approach, and that these changes are largely restricted to the macular retina (**Figure 8** and **Data File S2**).

In moving from normal through early and into late-stage AMD there is progressive up-regulation in the macula retina of complement genes associated with the CP, including all components *C1Q*, the *C1Q*-associated activators *C1R* and *C1S*, *C2* and *C3*, and the initial members of the membrane attack complex *C5*, *C6* and *C7*. The soluble complement inhibitors *CFH* and *SERPING1* are also up-regulated, as well as the membrane-bound regulator of the C5b-9, *CD59*, perhaps reflecting regulatory feedback accompanying complement activation. The up-regulation of anaphylatoxin receptors (*C3AR1*, *C5AR1*, *C5AR2*) is most pronounced in late AMD, as is the expression of *ITGAM* and *ITGB2*, implying the activation of phagocytosis related to complement-coated particles in late AMD. This pattern of progressive up-regulation of complement genes is only weakly observed in the peripheral retina.

In contrast, the expression levels of complement genes in the macular and peripheral RPE/choroid/sclera (RCS) are similar to the highest levels observed in the macular retina, and are relatively uniform with respect to disease stages, with a small number of differentially-expressed complement genes (**Data File S2**). Interestingly all the DE genes in macula RCS show down-regulation in late AMD, while genes in the periphery RCS are mainly up-regulated. In particular, expression of *CFD* is down-regulated in late AMD in MRCS, and up-regulated in PRCS. We note that the expression of the terminal C5b-9 components *C8* and *C9* are largely absent in all of our RNA-seq data, but are observed at the protein level which may reflect proteins transported from the choroid blood supply.

A recent study of nine complement genes in normal eyes and eyes with early, intermediate and advanced AMD partially recapitulates our results (87). Their results for macula retina showed a complex pattern of regulation for most of the nine complement genes examined when moving from early to intermediate AMD and partially agree with our results. However, their results are almost in complete accord with our findings for late-stage AMD, showing up-regulation of *C1QA*, *C3*, *C4B*, *CFB*, *CFD*, *CFH* and *MASP1* in late AMD with respect to control. In contrast, we did not reproduce their finding of significant up-regulation of *CFI* and down-regulation of *CFP*. Our results for RCS similarly showed higher average expression for most complement genes compared to macula retina. Additionally, both studies showed down-regulation of *CFD* in the RPE/choroid. Both studies found no expression for terminal MAC component *C9*.

Our bulk data results suggest that even though the initiation of AMD may not depend strongly on changes in retinal cells, the macula retina is still the principal site of complement activation as the disease progresses.

Species Differences in Retinal Complement Expression Complicate the use of Animal Models in AMD Research

A thorough comparison of the cellular landscape of complement expression in the retina across species is important to assess the usability of animal and specifically mouse models to investigate pathological mechanisms of AMD for the development of human therapies. For that reason, we compared results from the present study on human retina with previous results collected from its mouse counterpart and, indeed, found considerable differences (48). These low levels in mouse retina (but significant detection in the human retina) should be considered when investigating the mouse AP. Finally, there is the striking difference regarding membrane bound complement regulator expression. Absence of CD46 and CD55 in mouse retina would suggest a different pathway for inactivating both C3b and C4b at the cell membrane surface. Of course, these expression differences exist under a normal physiological state and could change in the setting of disease.

Our results provide strong evidence of complement synthesis in the healthy retina, RPE and choroid. The body of evidence suggests that local complement expression impacts all cell types and that complement's functions in the tissue environment could go beyond its role in the innate system (88). Accordingly, there is an urgent need to further investigate alternative complement functions in the human eye. Multiple publications provide evidence for complement orchestrating normal cell and organ development even in the immune privileged central nervous system (89, 90). These include direct tissue repair and regulation of basic processes of the cell, particularly in metabolism (77). A receptor for C1q has been identified on mitochondria which in the presence of intracellular C1q mediates mitochondrial ROS production (91). A direct link between C3a and downregulation of proteasome activity was reported in human RPE cells from older individuals, suggesting a link with intracellular protein longevity (92). Our data identified multiple complement genes expressed under normal physiological conditions that must have biological functions that maintain integrity of the retina, RPE and choroid. Further studies are necessary to investigate complement function for its role in homeostasis to provide a foundation for AMD clinical trials evaluating treatment with complement inhibitors [reviewed in (36–38)].

Limitations of our study include a focus on European American donors and a limited number of disease donors for single cell analysis.

MATERIALS AND METHODS

Human Donor Eyes

Tissues were obtained from human eye donors at different institutions, as indicated below. The Institutional Review Boards of each institution approved the respective use of human tissues.

Study Subjects and scRNA-seq

Samples were taken from macular and peripheral regions of the retina from two normal donor eyes (**Table S1**, samples 18-1077-W, 18-1132-P) at UAB and used in scRNA-seq studies at UPenn as described in (93). Briefly, raw counts were converted to log-normalized expression values with a scale factor of 10,000 UMIs per cell, the 2,000 most variable genes across all cells were identified, and the cells were clustered using the DESC algorithm (94). Eleven major retinal cell types were identified using this data, providing cell-type-specific expression profiles for complement genes.

Additional samples were obtained from three donor eyes (**Table S1**, samples 20-1166-W, 20-1438-W, 20-1484-W) at UAB and used in scRNA studies at UPenn. All donor eyes were collected within 6 hours postmortem and characterized for presence of AMD and other pathology by author C.A.C. Following removal of the anterior chamber and vitreous, the eyecup was immersed in oxygenated Ames media. Relief cuts were made in the posterior eyecup to expose the tissue and 8mm punches were obtained from macular retina and temporal (peripheral) retina and carefully isolated from the retinal pigment epithelium. The choroidal layer was isolated similarly. The isolated tissue layers were dissociated with activated papain (Worthington Biochemical Corp.) as previously optimized to obtain a high percentage of viable cells. After dissociation, magnetic bead-based removal of dead cells (Miltenyi Biotec) was used to reach the optimum target for viability of 85-95% per sample. Viability was determined by FACS sort or by staining an aliquot of the dissociated cells with trypan blue, 0.4% (Sigma-Aldrich). Single cell transcriptome libraries were prepared by using 10xGenomics Single Cell 3' biased v2 kit according to the company's manual. The constructed single cell libraries were sequenced by HiSeq 2000 sequencer (Illumina, Inc., San Diego, CA, USA) with total reads per cell targeted for a minimum of 50,000. Raw base call (BCL) files were aligned to human genome reference GRCh38-2020-A and processed with 10x Genomics Cell Ranger 3.1.0 to produce gene count matrices for each sample. For each sample replicate, we performed initial quality control using Cell Ranger (Version 3.1.0). Then, we further filtered the data using Seurat (version 3.0). A cell was retained in downstream analyses if it meets the following criteria (1): More than 200 genes are detected (2); Total number of UMIs is between 1,000 and 25,000. Retina and choroid cells were separated into two datasets and analyzed separately from each other. Each dataset was processed using Seurat 3.0, a statistical framework to combine cell gene expression profiles measured by scRNA-seq (95). Expression data was normalized by dividing the counts for each feature of a cell by the total counts for that cell and multiplying the result by a scale factor of 10,000; this was then transformed to a natural-log scale. Gene expression levels were normalized using the 2,000 most variable features in the datasets as identified by Seurat's *FindVariableFeatures* function. Cell clustering was completed using Seurat's shared nearest neighbor (SNN) modularity optimization-based clustering algorithm. This clustering was performed and evaluated using a range of resolution values, with a resolution of 1.5 being selected for the choroid cells and 0.2 for the retina cells. Differentially expressed genes for the generated clusters were compared to known choroid and retina cell type markers to identify and label cell-types, and cell-type-specific expression profiles for complement genes were determined. Eleven major retinal and ten major choroidal cell types were identified in this analysis. Since no RPE cells were recovered in this study, sc-RNA-seq data from Voigt et al. was reanalyzed and used to supplement our data with complement gene expression levels for that single cell type (51).

Bulk Tissue Processing and Data Generation

Eye Collection and AMD Assessment

This study utilized 14 pairs of eyes from non-diabetic Caucasian donors 69-95 yr of age (84.73 yr ± 5.53 yr; 7 males and 7 females) at a death-to-preservation interval of < 6 hr. Ocular health histories were not available. Eyes were opened by eye bank recovery personnel using an 18 mm diameter corneal trephine, followed by a snip to the iris to facilitate penetration of preservatives into the fundus. The left eye was preserved in RNAlater (Qiagen) at 4°C. Left eyes were shipped on wet ice *via* overnight courier to University of Pennsylvania where they were processed for bulk RNA sequencing upon arrival.The right eye was preserved in 2% glutaraldehyde and 1% paraformaldehyde in 0.1M phosphate buffer at 4°C. It was assessed for maculopathy at UAB by internal inspection using a dissecting scope (Nikon SMZ-U) with oblique trans- and epi-illumination in consultation with an MD medical retina specialist, ex vivo multimodal imaging of excised 8 mm diameter macular punches using digital color photography and spectral domain optical coherence tomography volume scans (SD-OCT; Spectralis, Heidelberg Engineering) with a custom tissue holder (co-author JDM), and high-resolution epoxy-resin histology, as described. The definition of AMD used in this study was the presence of one large druse (>125 μm in diameter) in the macula or severe RPE changes in the setting of at least one druse or continuous basal linear deposit, with or without the presence of neovascularization and its sequelae. Eyes with geographic atrophy had at least one region 250 μm in diameter lacking a continuous RPE layer (but possibly containing 'dissociated' RPE). Unremarkable eyes were those lacking characteristics of AMD or other chorioretinal disease as

discernible in either histology or ex vivo imaging; these served as comparison eyes.

Sequencing and Analysis of Bulk Data

RNA for the eye tissues was extracted using the AllPrep DNA/RNA Mini Kit (Qiagen). Extracted RNA samples underwent quality control assessment using R6K ScreenTape on a 2200 Tapestation (Agilent, Santa Clara, CA, USA) and were quantified using Qubit 2.0 Fluorometer from Life Technologies (Grand Island, NY). All RNA samples selected for sequencing had an RNA integrity number of ≥8. The Strand-specific RNA library was prepared from 100 ng total RNA using the Encore Complete RNA-seq library kit (Nugen Technologies, Inc., San Carlos, CA, USA) according to the manufacturer's protocol. RNA-sequencing was performed at the Center for Applied Genomics at the Children's Hospital of Philadelphia per standard protocols. The prepared libraries were clustered and then sequenced using HiSeq 2000 sequencer (Illumina, Inc., San Diego, CA, USA) with four RNA-seq libraries per lane (2 × 101-bp paired-end reads). The RNA-seq data were aligned to the hg38 reference genome using GSNAP (version 2016-06-30) with known splice sites (SNP file build 147) taken into account. In order to eliminate mapping errors and reduce potential mapping ambiguity owing to homologous sequences, several filtering steps were applied. Specifically, we required the mapping quality score of ≥30 for each read, reads from the same pair were mapped to the same chromosome with expected orientations and the mapping distance between members of the read pair was 200,000 bp. Quality control analysis of the aligned data was performed using program RNA-SeQC. All subsequent analyses were based on filtered alignment files. Per-gene counts were generated from the GSNAP alignments using the HTSeq-count program (version 0.6.0) using default 'union' mode and the HG38 reference genome.

In Situ Hybridization

Human Retina Tissue Preparation

Within 6 hours of death, posterior poles were fixed in freshly made 4% paraformaldehyde/0.1M phosphate-buffered (PB, pH 7.4, Thomas Scientific, LLC, Swedesboro, NJ, USA) overnight, then washed and stored in 1% paraformaldehyde/0.1 M PB at 4°C. Eyes were shipped on wet ice *via* overnight courier to University of Pennsylvania. This study conformed to Institutional Review Board regulations for use of human tissues at University of Alabama at Birmingham (UAB) and at University of Pennsylvania. Dissection of retina/choroid/sclera was performed as described (96). Retina tissues were cryoprotected in increasing concentration of sucrose as described (97) followed by embedding in OCT (Tissue Tek, Sakura Finetek USA, Torrance, CA, USA) and immediately snap-frozen in ice-cold 2-methylbutane. The frozen tissue was sliced at 10 μm in the cryostat and stored at -80°C.

RNA-FISH Protocol

Single molecule RNA *in situ* hybridization (RNA-FISH) was carried out with the RNAscope® Multiplex Fluorescent Reagent Kit v2 (Advanced Cell Diagnostics, INC, Newark, CA, USA). Probes were used for this study are: Hs-AIF1-C3 (#433121-C3), Hs-ONECUT1 (#490081), Hs-CD34-C2 (#560821-C2), Hs-CFH (#428731), Hs-CFI (#421921), Hs-CLDN5-C2 (#517141-C2), Hs-RLBP1-C2 (#414221-C2), Hs-FOS (#319901), Hs-JUN (#470541), Hs-C3AR (#461101), Hs-ITGAX (#419151), Hs-ITGB2 (#480281), Hs-VSIG4 (#446361), Hs-C3 (#430701), Hs-C7-C3 (#534791-C3), Hs-CD46 (#430151), Hs-CD55 (#426551), Hs-CFD (#420831). Positive control RNAscope® 3-plex probe (#320861) and RNAscope® 3-plex negative control probe (#320871) were used (data not shown) for each experiment. In addition, probe diluent (#300041) was used for negative control.

Proteomic Profiling of MACS Enriched Retinal Cell Types

Tissue Collection

Samples for proteome profiling were isolated from a set of five donor eyes. The Institutional Review Board at University of Regensburg approved the use of human tissues for this purpose. One eye per donor from five non-diabetic Caucasian donors 59-89 yrs of age (4 males and 1 female) at a death-to-experimentation interval of < 30 hr were included in this analysis (**Table S1**). Ocular health histories were not available. Eyes were opened by eye bank recovery personnel using an 18 mm diameter corneal trephine and stored on ice for transfer to the laboratory for further processing.

Cell Purification From Human Donor Retina

Retinal cell types were enriched as described previously using magnetic-activated cell sorting (MACS) (98). Briefly, retinal punches (6 mm in diameter, centered over the fovea and for comparison, the peripheral punch was performed at 1 mm from the macular punch and inferiorly in relation to it) were treated with papain (0.2 mg/ml; Roche Molecular Biochemicals) for 30 minutes at 37 °C in the dark in Ca^{2+}- and Mg^{2+}-free extracellular solution (140 mM NaCl, 3 mM KCl, 10 mM HEPES, 11 mM glucose, pH 7.4). After several washes and 4 minutes of incubation with DNase I (200 U/ml), retinae were triturated in extracellular solution (now with 1 mM $MgCl_2$ and 2 mM $CaCl_2$). To purify microglial and vascular cells, the retinal cell suspension was subsequently incubated with anti-mouse/human ITGAM (alias CD11B) and anti-human CD31 microbeads according to the manufacturer's protocol (Miltenyi Biotec, Bergisch Gladbach, Germany). The respective binding cells were depleted from the retinal suspension using large cell (LS)-columns, prior to Müller cell enrichment. To purify Müller glia, the cell suspension was incubated in extracellular solution containing biotinylated anti-human CD29 (0.1 mg/ml, Miltenyi Biotec) for 15 minutes at 4°C. Cells were washed in an extracellular solution, spun down, resuspended in the presence of anti-biotin ultra-pure MicroBeads (1:5; Miltenyi Biotec,) and incubated for 10 minutes at 4°C. After washing, CD29+ Müller cells were separated using LS columns according to the manufacturer's instructions (Miltenyi Biotec). Cells in the flow through of the last sorting step - depleted of microglia, vascular cells and Müller glia - were considered as the neuronal population. RPE was obtained by scraping from the sclera of the punched-out piece of tissue after the retina had been removed, so those samples inevitably contained cells of the underlying choroid. Therefore,

those samples are referred to as RPE/choroid throughout the manuscript.

LC-MS/MS Mass Spectrometry Analysis

LC-MS/MS analysis was performed as described previously on a Q-Exactive HF mass spectrometer (Thermo Fisher Scientific Inc., Waltham, MA, U.S.A.) coupled to an Ultimate 3000 RSLC nano-HPLC (Dionex, Sunnyvale, CA) (99, 100). Briefly, 0.5 µg sample was automatically loaded onto a nano trap column (300 µm inner diameter × 5 mm, packed with Acclaim PepMap100 C18. 5 µm, 100 Å; LC Packings, Sunnyvale, CA) before separation by reversed phase chromatography (HSS-T3 M-class column, 25 cm, Waters) in an 80 minutes non-linear gradient from 3 to 40% acetonitrile (ACN) in 0.1% formic acid (FA) at a flow rate of 250 nl/min. Eluted peptides were analysed by the Q-Exactive HF mass spectrometer equipped with a nano-flex ionization source. Full scan MS spectra (from m/z 300 to 1500) and MS/MS fragment spectra were acquired in the Orbitrap with a resolution of 60,000 or 15000 respectively, with maximum injection times of 50 ms each. Up to ten most intense ions were selected for HCD fragmentation depending on signal intensity (TOP10 method). Target peptides already selected for MS/MS were dynamically excluded for 30 seconds. Spectra were analyzed using the Progenesis QI software for proteomics (Version 3.0, Nonlinear Dynamics, Waters, Newcastle upon Tyne, U.K.) for label-free quantification, as previously described (98). All features were exported as a Mascot generic file (mgf) and used for peptide identification with Mascot (version 2.4) in the UniProtKB/Swiss-Prot taxonomy mouse database (Release 2017.02, 16871 sequences). Search parameters used were: 10 ppm peptide mass tolerance, 20 mmu fragment mass tolerance, one missed cleavage allowed, carbamidomethylation set as fixed modification, and methionine oxidation, asparagine or glutamine deamidation were allowed as variable modifications. A Mascot-integrated decoy database search calculated an average false discovery rate (FDR) of < 1%.

Western Blot

Cell pellets of enriched cell populations from retinal punches were dissolved in reducing Laemmli sample buffer, denatured and sonicated. Neuronal protein extraction reagent (Thermo Fisher Scientific, Braunschweig, Germany) was added to the neuron populations. Samples were separated on a 12% SDS-PAGE. The immunoblot was performed as previously described (101). Detection was performed with primary and secondary antibodies diluted in blocking solution (**Table S2**). Blots were developed with WesternSure PREMIUM Chemiluminescent Substrate (LI-COR, Bad Homburg, Germany). To validate specificity of the antibodies, all of them were tested on human serum and purified proteins as positive control and human serum depleted for the respective complement factor as negative control (**Table S3**).

Immunofluorescence Labeling

To stain for complement components in the macular and peripheral retina, human eyes (postmortem time < 8 hours) were cryosectioned. The research complies with the human research act (HRA) stating that small quantities of bodily substances removed in the course of transplantation may be anonymized for research purposes without consent (HRA chapter 5, paragraph 38, Switzerland). Before sectioning, the eyes were immersion-fixated with 4% paraformaldehyde (PFA) for 48 hours. Thereafter, the central part of the eye cup containing the optic nerve head and the macula including the underlying RPE, choroid and sclera was dissected. The tissue was submitted to cryoprotection, embedded in OCT and cut into 20 µm thick sections. Retinal detachment from the RPE is an artifact commonly observed in cryosections

Retinal sections were permeabilized (0.3% Triton X-100 plus 1.0% DMSO in PBS) and blocked (5% normal donkey serum with 0.3% Triton X-100 and 1.0% DMSO in PBS) for 2 h at room temperature. Primary antibodies were incubated overnight at 4°C. Sections were washed (1% bovine serum albumin in PBS) and incubated with secondary antibodies (2 h at room temperature). Cell nuclei were labeled with DAPI (1:1000; Life Technologies). Control experiments without primary antibodies showed no nonspecific labeling. Images were taken with a custom-made VisiScope CSU-X1 confocal system (Visitron Systems, Puchheim, Germany) equipped with high-resolution sCMOS camera (PCO AG, Kehlheim, Germany).

Quantification and Statistical Analysis

Statistical analyses were performed using Prism (Graphpad Software, San Diego, CA, USA). In most of the experiments in the present study results from 4 to 5 biological replicates were collected. Since this low number of input values does not allow an appropriate estimation about a normal Gaussian distribution, significance levels were determined by the non-parametric Mann-Whitney U test unless stated otherwise. All data are expressed as mean ± standard error (SEM) unless stated otherwise. Detailed information about specific n-values, implemented statistical tests and coding of significance levels are provided in the respective Figure legends.

DATA AVAILABILITY STATEMENT

The datasets presented in this study can be found in online repositories. The names of the repository/repositories and accession number(s) can be found below: GEO, accession IDs: GSE188280, GSE155154, GSE155288.

AUTHOR CONTRIBUTIONS

Conceptualization: DP, AG, ML, DS. Methodology: RZ, JB, DS, YJ, MK, JH, LK, AP, NS, VE, US-S, TS, SH, PG, MM, JM, CS. Investigation: RZ, JB, YJ, DS, MK, LK, AP. Visualization: RZ, JB, YJ, MK, LK, AP. Supervision: DP, AG, ML, DS. Writing—original draft: RZ, JB, YJ, DP, AG, ML, DS. Writing—review & editing: RZ, JB, YJ, LK, SH, CC, DP, AG, ML, DS. All authors contributed to the article and approved the submitted version.

FUNDING

This project was supported by Deutsche Forschungsgemeinschaft DFG-GR 4403/5-1 (AG), ProRetina Foundation Germany Pro-Re/Seed/Kaplan-Grosche.8-2019 (AG, LK), Deutsche Forschungsgemeinschaft DFG-PA 1844/3-1 (DP), Deutsche Forschungsgemeinschaft DFG-HA 6014/5-1 (SH), Support Sight Foundation (TSSF) (DS), and National Institutes of Health grant R21EY031877 (ML), P30 EY003039 (UAB), R01EY030192 (ML), R01EY031209 (DS, CC, ML). Collection of human donor eyes for bulk RNA-sequencing studies was funded by the Arnold and Mabel Beckman Initiative for Macular Research (DS, CC).

ACKNOWLEDGMENTS

We thank Gabriele Jäger, Dirkje Felder, Renate Foeckler, Andrea Danullis and Elfriede Eckert for excellent technical support of cell preparation, immune detection and molecular biology.

SUPPLEMENTARY MATERIAL

The Supplementary Material for this article can be found online at: https://www.frontiersin.org/articles/10.3389/fimmu.2022.895519/full#supplementary-material

REFERENCES

1. Merle NS, Church SE, Fremeaux-Bacchi V, Roumenina LT. Complement System Part I - Molecular Mechanisms of Activation and Regulation. *Front Immunol* (2015) 6:262. doi: 10.3389/fimmu.2015.00262
2. Merle NS, Noe R, Halbwachs-Mecarelli L, Fremeaux-Bacchi V, Roumenina LT. Complement System Part II: Role in Immunity. *Front Immunol* (2015) 6:257. doi: 10.3389/fimmu.2015.00257
3. Stephan AH, Barres BA, Stevens B. The Complement System: An Unexpected Role in Synaptic Pruning During Development and Disease. *Annu Rev Neurosci* (2012) 35:369–89. doi: 10.1146/annurev-neuro-061010-113810
4. Presumey J, Bialas AR, Carroll MC. Complement System in Neural Synapse Elimination in Development and Disease. *Adv Immunol* (2017) 135:53–79. doi: 10.1016/bs.ai.2017.06.004
5. Schatz-Jakobsen JA, Pedersen DV, Andersen GR. Structural Insight Into Proteolytic Activation and Regulation of the Complement System. *Immunol Rev* (2016) 274:59–73. doi: 10.1111/imr.12465
6. Cserhalmi M, Papp A, Brandus B, Uzonyi B, Józsi M. Regulation of Regulators: Role of the Complement Factor H-Related Proteins. *Semin Immunol* (2019) 45:101341. doi: 10.1016/j.smim.2019.101341
7. Barnum SR. Complement: A Primer for the Coming Therapeutic Revolution. *Pharmacol Ther* (2017) 172:63–72. doi: 10.1016/j.pharmthera.2016.11.014
8. Barnum SR. Complement in Central Nervous System Inflammation. *Immunol Res* (2002) 26:7–13. doi: 10.1385/IR:26:1-3:007
9. Morgan BP, Gasque P. Extrahepatic Complement Biosynthesis: Where, When and Why? *Clin Exp Immunol* (1997) 107:1–7. doi: 10.1046/j.1365-2249.1997.d01-890.x
10. Nataf S, Stahel PF, Davoust N, Barnum SR. Complement Anaphylatoxin Receptors on Neurons: New Tricks for Old Receptors? *Trends Neurosci* (1999) 22:397–402. doi: 10.1016/S0166-2236(98)01390-3
11. Cunha-Vaz JG. The Blood-Retinal Barriers System. Basic Concepts and Clinical Evaluation. *Exp Eye Res* (2004) 78:715–21. doi: 10.1016/S0014-4835(03)00213-6
12. Cunha-Vaz J, Bernardes R, Lobo C. Blood-Retinal Barrier. *Eur J Ophthalmol* (2011) 21 Suppl 6:S3–9. doi: 10.5301/EJO.2010.6049
13. Kolb H. Simple Anatomy of the Retina. In: H Kolb, E Fernandez and R Nelson, editors. *Webvision: The Organization of the Retina and Visual System*. Salt Lake City UT: University of Utah Health Sciences Center (2005).
14. Strauss O. "The Retinal Pigment Epithelium". In: H Kolb, E Fernandez and R Nelson, editors. *Webvision: The Organization of the Retina and Visual System*. Salt Lake City, UT: University of Utah Health Sciences Center (2011).
15. Nickla DL, Wallman J. The Multifunctional Choroid. *Prog Retin Eye Res* (2010) 29:144–68. doi: 10.1016/j.preteyeres.2009.12.002
16. Bora NS, Gobleman CL, Atkinson JP, Pepose JS, Kaplan HJ. Differential Expression of the Complement Regulatory Proteins in the Human Eye. *Invest Ophthalmol Vis Sci* (1993) 34:3579–84.
17. Anderson DH, Radeke MJ, Gallo NB, Chapin EA, Johnson PT, Curletti CR, et al. The Pivotal Role of the Complement System in Aging and Age-Related Macular Degeneration: Hypothesis Re-Visited. *Prog Retin Eye Res* (2010) 29:95–112. doi: 10.1016/j.preteyeres.2009.11.003
18. Zhang J, Gerhardinger C, Lorenzi M. Early Complement Activation and Decreased Levels of Glycosylphosphatidylinositol-Anchored Complement Inhibitors in Human and Experimental Diabetic Retinopathy. *Diabetes* (2002) 51:3499–504. doi: 10.2337/diabetes.51.12.3499
19. Jha P, Sohn J-H, Xu Q, Nishihori H, Wang Y, Nishihori S, et al. The Complement System Plays a Critical Role in the Development of Experimental Autoimmune Anterior Uveitis. *Invest Ophthalmol Vis Sci* (2006) 47:1030–8. doi: 10.1167/iovs.05-1062
20. Mullins RF, Russell SR, Anderson DH, Hageman GS. Drusen Associated With Aging and Age-Related Macular Degeneration Contain Proteins Common to Extracellular Deposits Associated With Atherosclerosis, Elastosis, Amyloidosis, and Dense Deposit Disease. *FASEB J* (2000) 14:835–46. doi: 10.1096/fasebj.14.7.835
21. Zarbin MA. Age-Related Macular Degeneration: Review of Pathogenesis. *Eur J Ophthalmol* (1998) 8:199–206. doi: 10.1177/112067219800800401
22. Curcio CA. Soft Drusen in Age-Related Macular Degeneration: Biology and Targeting *Via* the Oil Spill Strategies. *Invest Ophthalmol Vis Sci* (2018) 59:AMD160–81. doi: 10.1167/iovs.18-24882
23. Johnson LV, Leitner WP, Staples MK, Anderson DH. Complement Activation and Inflammatory Processes in Drusen Formation and Age Related Macular Degeneration. *Exp Eye Res* (2001) 73:887–96. doi: 10.1006/exer.2001.1094
24. Anderson DH, Talaga KC, Rivest AJ, Barron E, Hageman GS, Johnson LV. Characterization of Beta Amyloid Assemblies in Drusen: The Deposits Associated With Aging and Age-Related Macular Degeneration. *Exp Eye Res* (2004) 78:243–56. doi: 10.1016/j.exer.2003.10.011
25. Crabb JW, Miyagi M, Gu X, Shadrach K, West KA, Sakaguchi H, et al. Drusen Proteome Analysis: An Approach to the Etiology of Age-Related Macular Degeneration. *Proc Natl Acad Sci USA* (2002) 99:14682–7. doi: 10.1073/pnas.222551899
26. Fritsche LG, Igl W, Bailey JNC, Grassmann F, Sengupta S, Bragg-Gresham JL, et al. A Large Genome-Wide Association Study of Age-Related Macular Degeneration Highlights Contributions of Rare and Common Variants. *Nat Genet* (2016) 48:134–43. doi: 10.1038/ng.3448
27. Ferris FL3rd. Senile Macular Degeneration: Review of Epidemiologic Features. *Am J Epidemiol* (1983) 118:132–51. doi: 10.1093/oxfordjournals.aje.a113624
28. Mitchell P, Liew G, Gopinath B, Wong TY. Age-Related Macular Degeneration. *Lancet* (2018) 392:1147–59. doi: 10.1016/S0140-6736(18)31550-2
29. Quinn N, Csincsik L, Flynn E, Curcio CA, Kiss S, Sadda SR, et al. The Clinical Relevance of Visualising the Peripheral Retina. *Prog Retin Eye Res* (2019) 68:83–109. doi: 10.1016/j.preteyeres.2018.10.001
30. Ambati J, Fowler BJ. Mechanisms of Age-Related Macular Degeneration. *Neuron* (2012) 75:26–39. doi: 10.1016/j.neuron.2012.06.018
31. Kuehlewein L, Dustin L, Sagong M, Hariri A, Mendes TS, Rofagha S, et al. Predictors of Macular Atrophy Detected by Fundus Autofluorescence in Patients With Neovascular Age-Related Macular Degeneration After Long-Term Ranibizumab Treatment. *Ophthalmic Surg Lasers Imaging Retina* (2016) 47:224–31. doi: 10.3928/23258160-20160229-04

32. Bhisitkul RB, Mendes TS, Rofagha S, Enanoria W, Boyer DS, Sadda SR, et al. Macular Atrophy Progression and 7-Year Vision Outcomes in Subjects From the ANCHOR, MARINA, and HORIZON Studies: The SEVEN-UP Study. *Am J Ophthalmol* (2015) 159:915–24.e2. doi: 10.1016/j.ajo.2015.01.032
33. Comparison of Age-related Macular Degeneration Treatments Trials (CATT) Research Group, Maguire MG, Martin DF, Ying G-S, Jaffe GJ, Daniel E, et al. Five-Year Outcomes With Anti-Vascular Endothelial Growth Factor Treatment of Neovascular Age-Related Macular Degeneration: The Comparison of Age-Related Macular Degeneration Treatments Trials. *Ophthalmology* (2016) 123:1751–61. doi: 10.1016/j.ophtha.2016.03.045
34. Holz FG, Strauss EC, Schmitz-Valckenberg S, van Lookeren Campagne M. Geographic Atrophy: Clinical Features and Potential Therapeutic Approaches. *Ophthalmology* (2014) 121:1079–91. doi: 10.1016/j.ophtha.2013.11.023
35. Fleckenstein M, Keenan TDL, Guymer RH, Chakravarthy U, Schmitz-Valckenberg S, Klaver CC, et al. Age-Related Macular Degeneration. *Nat Rev Dis Primers* (2021) 7:31. doi: 10.1038/s41572-021-00265-2
36. Desai D, Dugel PU. Complement Cascade Inhibition in Geographic Atrophy: A Review. *Eye* (2022) 36:294–302. doi: 10.1038/s41433-021-01765-x
37. Park YG, Park YS, Kim I-B. Complement System and Potential Therapeutics in Age-Related Macular Degeneration. *Int J Mol Sci* (2021) 22. doi: 10.3390/ijms22136851
38. Qin S, Dong N, Yang M, Wang J, Feng X, Wang Y. Complement Inhibitors in Age-Related Macular Degeneration: A Potential Therapeutic Option. *J Immunol Res* (2021) 2021:9945725. doi: 10.1155/2021/9945725
39. Chi Z-L, Yoshida T, Lambris JD, Iwata T. Suppression of Drusen Formation by Compstatin, a Peptide Inhibitor of Complement C3 Activation, on Cynomolgus Monkey With Early-Onset Macular Degeneration. *Adv Exp Med Biol* (2010) 703:127–35. doi: 10.1007/978-1-4419-5635-4_9
40. Park DH, Connor KM, Lambris JD. The Challenges and Promise of Complement Therapeutics for Ocular Diseases. *Front Immunol* (2019) 10:1007. doi: 10.3389/fimmu.2019.01007
41. Liao DS, Grossi FV, El Mehdi D, Gerber MR, Brown DM, Heier JS, et al. Complement C3 Inhibitor Pegcetacoplan for Geographic Atrophy Secondary to Age-Related Macular Degeneration: A Randomized Phase 2 Trial. *Ophthalmology* (2020) 127:186–95. doi: 10.1016/j.ophtha.2019.07.011
42. *Apellis Announces Detailed Results From Phase 3 DERBY and OAKS Studies Presented at Retina Society Annual Meeting*. Available at: https://investors.apellis.com/news-releases/news-release-details/apellis-announces-detailed-results-phase-3-derby-and-oaks (Accessed October 18, 2021).
43. Wu J, Sun X. Complement System and Age-Related Macular Degeneration: Drugs and Challenges. *Drug Des Devel Ther* (2019) 13:2413–25. doi: 10.2147/DDDT.S206355
44. Holz FG, Sadda SR, Busbee B, Chew EY, Mitchell P, Tufail A, et al. Efficacy and Safety of Lampalizumab for Geographic Atrophy Due to Age-Related Macular Degeneration: Chroma and Spectri Phase 3 Randomized Clinical Trials. *JAMA Ophthalmol* (2018) 136:666–77. doi: 10.1001/jamaophthalmol.2018.1544
45. Park J, Shrestha R, Qiu C, Kondo A, Huang S, Werth M, et al. Single-Cell Transcriptomics of the Mouse Kidney Reveals Potential Cellular Targets of Kidney Disease. *Science* (2018) 360:758–63. doi: 10.1126/science.aar2131
46. McKenna A, Gagnon JA. Recording Development With Single Cell Dynamic Lineage Tracing. *Development* (2019) 146. doi: 10.1242/dev.169730
47. Satija R, Farrell JA, Gennert D, Schier AF, Regev A. Spatial Reconstruction of Single-Cell Gene Expression Data. *Nat Biotechnol* (2015) 33:495–502. doi: 10.1038/nbt.3192
48. Pauly D, Agarwal D, Dana N, Schäfer N, Biber J, Wunderlich KA, et al. Cell-Type-Specific Complement Expression in the Healthy and Diseased Retina. *Cell Rep* (2019) 29:2835–48.e4. doi: 10.1016/j.celrep.2019.10.084
49. Macosko EZ, Basu A, Satija R, Nemesh J, Shekhar K, Goldman M, et al. Highly Parallel Genome-Wide Expression Profiling of Individual Cells Using Nanoliter Droplets. *Cell* (2015) 161:1202–14. doi: 10.1016/j.cell.2015.05.002
50. Shekhar K, Lapan SW, Whitney IE, Tran NM, Macosko EZ, Kowalczyk M, et al. Comprehensive Classification of Retinal Bipolar Neurons by Single-Cell Transcriptomics. *Cell* (2016) 166:1308–23.e30. doi: 10.1016/j.cell.2016.07.054
51. Voigt AP, Mulfaul K, Mullin NK, Flamme-Wiese MJ, Giacalone JC, Stone EM, et al. Single-Cell Transcriptomics of the Human Retinal Pigment Epithelium and Choroid in Health and Macular Degeneration. *Proc Natl Acad Sci USA* (2019) 116:24100–7. doi: 10.1073/pnas.1914143116
52. Liu Y, Beyer A, Aebersold R. On the Dependency of Cellular Protein Levels on mRNA Abundance. *Cell* (2016) 165:535–50. doi: 10.1016/j.cell.2016.03.014
53. Kjell J, Fischer-Sternjak J, Thompson AJ, Friess C, Sticco MJ, Salinas F, et al. Defining the Adult Neural Stem Cell Niche Proteome Identifies Key Regulators of Adult Neurogenesis. *Cell Stem Cell* (2020) 26:277–93.e8. doi: 10.1016/j.stem.2020.01.002
54. Brunner A-D, Thielert M, Vasilopoulou CG, Ammar C, Coscia F, Mund A, et al. Ultra-High Sensitivity Mass Spectrometry Quantifies Single-Cell Proteome Changes Upon Perturbation. *Mol Syst Biol* (2021) 18(3):e10798. doi: 10.1101/2020.12.22.423933
55. Radu RA, Hu J, Yuan Q, Welch DL, Makshanoff J, Lloyd M, et al. Complement System Dysregulation and Inflammation in the Retinal Pigment Epithelium of a Mouse Model for Stargardt Macular Degeneration. *J Biol Chem* (2011) 286:18593–601. doi: 10.1074/jbc.M110.191866
56. Lenis TL, Sarfare S, Jiang Z, Lloyd MB, Bok D, Radu RA. Complement Modulation in the Retinal Pigment Epithelium Rescues Photoreceptor Degeneration in a Mouse Model of Stargardt Disease. *Proc Natl Acad Sci USA* (2017) 114:3987–92. doi: 10.1073/pnas.1620299114
57. Jabri Y, Biber J, Diaz-Lezama N, Grosche A, Pauly D. Cell-Type-Specific Complement Profiling in the ABCA4 Mouse Model of Stargardt Disease. *Int J Mol Sci* (2020) 21. doi: 10.3390/ijms21228468
58. Bajic G, Yatime L, Sim RB, Vorup-Jensen T, Andersen GR. Structural Insight on the Recognition of Surface-Bound Opsonins by the Integrin I Domain of Complement Receptor 3. *Proc Natl Acad Sci USA* (2013) 110:16426–31. doi: 10.1073/pnas.1311261110
59. Xu S, Wang J, Wang J-H, Springer TA. Distinct Recognition of Complement Ic3b by Integrins αβ and αβ. *Proc Natl Acad Sci USA* (2017) 114:3403–8. doi: 10.1073/pnas.1620881114
60. Jensen RK, Bajic G, Sen M, Springer TA, Vorup-Jensen T, Andersen GR. Complement Receptor 3 Forms a Compact High Affinity Complex With Ic3b. *J Immunol* (2020) 206(12):3032–42. doi: 10.1101/2020.04.15.043133
61. Li F, Leier A, Liu Q, Wang Y, Xiang D, Akutsu T, et al. Procleave: Predicting Protease-Specific Substrate Cleavage Sites by Combining Sequence and Structural Information. *Genomics Proteomics Bioinf* (2020) 18:52–64. doi: 10.1016/j.gpb.2019.08.002
62. Mullins RF, Schoo DP, Sohn EH, Flamme-Wiese MJ, Workamelahu G, Johnston RM, et al. The Membrane Attack Complex in Aging Human Choriocapillaris: Relationship to Macular Degeneration and Choroidal Thinning. *Am J Pathol* (2014) 184:3142–53. doi: 10.1016/j.ajpath.2014.07.017
63. Doorduijn DJ, Bardoel BW, Heesterbeek DAC, Ruyken M, Benn G, Parsons ES, et al. Bacterial Killing by Complement Requires Direct Anchoring of Membrane Attack Complex Precursor C5b-7. *PloS Pathog* (2020) 16:e1008606. doi: 10.1371/journal.ppat.1008606
64. Thompson RA, Lachmann PJ. Reactive Lysis: The Complement-Mediated Lysis of Unsensitized Cells. I. The Characterization of the Indicator Factor and its Identification as C7. *J Exp Med* (1970) 131:629–41. doi: 10.1084/jem.131.4.629
65. *Cell Atlas - C1S - The Human Protein Atlas*. Available at: https://www.proteinatlas.org/ENSG00000182326-C1S/cell (Accessed August 27, 2021).
66. Schäfer N, Grosche A, Schmitt SI, Braunger BM, Pauly D. Complement Components Showed a Time-Dependent Local Expression Pattern in Constant and Acute White Light-Induced Photoreceptor Damage. *Front Mol Neurosci* (2017) 10:197. doi: 10.3389/fnmol.2017.00197
67. Katschke KJJr, Xi H, Cox C, Truong T, Malato Y, Lee WP, et al. Classical and Alternative Complement Activation on Photoreceptor Outer Segments Drives Monocyte-Dependent Retinal Atrophy. *Sci Rep* (2018) 8:7348. doi: 10.1038/s41598-018-25557-8
68. Loyet KM, Deforge LE, Katschke KJJr, Diehl L, Graham RR, Pao L, et al. Activation of the Alternative Complement Pathway in Vitreous Is Controlled by Genetics in Age-Related Macular Degeneration. *Invest Ophthalmol Vis Sci* (2012) 53:6628–37. doi: 10.1167/iovs.12-9587
69. Circolo A, Garnier G, Fukuda W, Wang X, Hidvegi T, Szalai AJ, et al. Genetic Disruption of the Murine Complement C3 Promoter Region Generates Deficient Mice With Extrahepatic Expression of C3 mRNA. *Immunopharmacology* (1999) 42:135–49. doi: 10.1016/S0162-3109(99)00021-1

70. Vandermeer J, Sha Q, Lane AP, Schleimer RP. Innate Immunity of the Sinonasal Cavity: Expression of Messenger RNA for Complement Cascade Components and Toll-Like Receptors. *Arch Otolaryngol Head Neck Surg* (2004) 130:1374–80. doi: 10.1001/archotol.130.12.1374
71. Kulkarni HS, Elvington ML, Perng Y-C, Liszewski MK, Byers DE, Farkouh C, et al. Intracellular C3 Protects Human Airway Epithelial Cells From Stress-Associated Cell Death. *Am J Respir Cell Mol Biol* (2019) 60:144–57. doi: 10.1165/rcmb.2017-0405OC
72. Satyam A, Kannan L, Matsumoto N, Geha M, Lapchak PH, Bosse R, et al. Intracellular Activation of Complement 3 Is Responsible for Intestinal Tissue Damage During Mesenteric Ischemia. *J Immunol* (2017) 198:788–97. doi: 10.4049/jimmunol.1502287
73. Sünderhauf A, Skibbe K, Preisker S, Ebbert K, Verschoor A, Karsten CM, et al. Regulation of Epithelial Cell Expressed C3 in the Intestine - Relevance for the Pathophysiology of Inflammatory Bowel Disease? *Mol Immunol* (2017) 90:227–38. doi: 10.1016/j.molimm.2017.08.003
74. Atanes P, Ruz-Maldonado I, Pingitore A, Hawkes R, Liu B, Zhao M, et al. C3aR and C5aR1 Act as Key Regulators of Human and Mouse β-Cell Function. *Cell Mol Life Sci* (2018) 75:715–26. doi: 10.1007/s00018-017-2655-1
75. Dos Santos RS, Marroqui L, Grieco FA, Marselli L, Suleiman M, Henz SR, et al. Protective Role of Complement C3 Against Cytokine-Mediated β-Cell Apoptosis. *Endocrinology* (2017) 158:2503–21. doi: 10.1210/en.2017-00104
76. Arbore G, Kemper C, Kolev M. Intracellular Complement - the Complosome - In Immune Cell Regulation. *Mol Immunol* (2017) 89:2–9. doi: 10.1016/j.molimm.2017.05.012
77. Hess C, Kemper C. Complement-Mediated Regulation of Metabolism and Basic Cellular Processes. *Immunity* (2016) 45:240–54. doi: 10.1016/j.immuni.2016.08.003
78. Liszewski MK, Elvington M, Kulkarni HS, Atkinson JP. Complement's Hidden Arsenal: New Insights and Novel Functions Inside the Cell. *Mol Immunol* (2017) 84:2–9. doi: 10.1016/j.molimm.2017.01.004
79. Karlstetter M, Scholz R, Rutar M, Wong WT, Provis JM, Langmann T. Retinal Microglia: Just Bystander or Target for Therapy? *Prog Retin Eye Res* (2015) 45:30–57. doi: 10.1016/j.preteyeres.2014.11.004
80. Wyatt MK, Tsai J-Y, Mishra S, Campos M, Jaworski C, Fariss RN, et al. Interaction of Complement Factor H and Fibulin3 in Age-Related Macular Degeneration. *PloS One* (2013) 8:e68088. doi: 10.1371/journal.pone.0068088
81. Endo Y, Matsushita M, Fujita T. The Role of Ficolins in the Lectin Pathway of Innate Immunity. *Int J Biochem Cell Biol* (2011) 43:705–12. doi: 10.1016/j.biocel.2011.02.003
82. Kuraya M, Ming Z, Liu X, Matsushita M, Fujita T. Specific Binding of L-Ficolin and H-Ficolin to Apoptotic Cells Leads to Complement Activation. *Immunobiology* (2005) 209:689–97. doi: 10.1016/j.imbio.2004.11.001
83. Zheng B, Li T, Chen H, Xu X, Zheng Z. Correlation Between Ficolin-3 and Vascular Endothelial Growth Factor-To-Pigment Epithelium-Derived Factor Ratio in the Vitreous of Eyes With Proliferative Diabetic Retinopathy. *Am J Ophthalmol* (2011) 152:1039–43. doi: 10.1016/j.ajo.2011.05.022
84. Bhutto I, Lutty G. Understanding Age-Related Macular Degeneration (AMD): Relationships Between the Photoreceptor/Retinal Pigment Epithelium/Bruch's Membrane/Choriocapillaris Complex. *Mol Aspects Med* (2012) 33:295–317. doi: 10.1016/j.mam.2012.04.005
85. Whitmore SS, Sohn EH, Chirco KR, Drack AV, Stone EM, Tucker BA, et al. Complement Activation and Choriocapillaris Loss in Early AMD: Implications for Pathophysiology and Therapy. *Prog Retin Eye Res* (2015) 45:1–29. doi: 10.1016/j.preteyeres.2014.11.005
86. Lutty GA, McLeod DS, Bhutto IA, Edwards MM, Seddon JM. Choriocapillaris Dropout in Early Age-Related Macular Degeneration. *Exp Eye Res* (2020) 192:107939. doi: 10.1016/j.exer.2020.107939
87. Demirs JT, Yang J, Crowley MA, Twarog M, Delgado O, Qiu Y, et al. Differential and Altered Spatial Distribution of Complement Expression in Age-Related Macular Degeneration. *Invest Ophthalmol Vis Sci* (2021) 62:26. doi: 10.1167/iovs.62.7.26
88. Kolev M, Kemper C. Keeping It All Going-Complement Meets Metabolism. *Front Immunol* (2017) 8:1. doi: 10.3389/fimmu.2017.00001
89. Schafer DP, Lehrman EK, Kautzman AG, Koyama R, Mardinly AR, Yamasaki R, et al. Microglia Sculpt Postnatal Neural Circuits in an Activity and Complement-Dependent Manner. *Neuron* (2012) 74:691–705. doi: 10.1016/j.neuron.2012.03.026
90. Orsini F, De Blasio D, Zangari R, Zanier ER, De Simoni M-G. Versatility of the Complement System in Neuroinflammation, Neurodegeneration and Brain Homeostasis. *Front Cell Neurosci* (2014) 8:380. doi: 10.3389/fncel.2014.00380
91. Ten VS, Yao J, Ratner V, Sosunov S, Fraser DA, Botto M, et al. Complement Component C1q Mediates Mitochondria-Driven Oxidative Stress in Neonatal Hypoxic-Ischemic Brain Injury. *J Neurosci* (2010) 30:2077–87. doi: 10.1523/JNEUROSCI.5249-09.2010
92. Ramos de Carvalho JE, Klaassen I, Vogels IMC, Schipper-Krom S, van Noorden CJF, Reits E, et al. Complement Factor C3a Alters Proteasome Function in Human RPE Cells and in an Animal Model of Age-Related RPE Degeneration. *Invest Ophthalmol Vis Sci* (2013) 54:6489–501. doi: 10.1167/iovs.13-12374
93. Lyu Y, Zauhar R, Dana N, Strang CE, Hu J, Wang K, et al. Implication of Specific Retinal Cell-Type Involvement and Gene Expression Changes in AMD Progression Using Integrative Analysis of Single-Cell and Bulk RNA-Seq Profiling. *Sci Rep* (2021) 11:15612. doi: 10.1038/s41598-021-95122-3
94. Li X, Wang K, Lyu Y, Pan H, Zhang J, Stambolian D, et al. Deep Learning Enables Accurate Clustering With Batch Effect Removal in Single-Cell RNA-Seq Analysis. *Nat Commun* (2020) 11:2338. doi: 10.1038/s41467-020-15851-3
95. Stuart T, Butler A, Hoffman P, Hafemeister C, Papalexi E, Mauck WM3rd, et al. Comprehensive Integration of Single-Cell Data. *Cell* (2019) 177:1888–1902.e21. doi: 10.1016/j.cell.2019.05.031
96. Curcio CA, Sloan KR, Meyers D. Computer Methods for Sampling, Reconstruction, Display and Analysis of Retinal Whole Mounts. *Vision Res* (1989) 29:529–40. doi: 10.1016/0042-6989(89)90039-4
97. Guidry C, Medeiros NE, Curcio CA. Phenotypic Variation of Retinal Pigment Epithelium in Age-Related Macular Degeneration. *Invest Ophthalmol Vis Sci* (2002) 43:267–73.
98. Grosche A, Hauser A, Lepper MF, Mayo R, von Toerne C, Merl-Pham J, et al. The Proteome of Native Adult Müller Glial Cells From Murine Retina. *Mol Cell Proteomics* (2016) 15:462–80. doi: 10.1074/mcp.M115.052183
99. Frik J, Merl-Pham J, Plesnila N, Mattugini N, Kjell J, Kraska J, et al. Cross-Talk Between Monocyte Invasion and Astrocyte Proliferation Regulates Scarring in Brain Injury. *EMBO Rep* (2018) 19. doi: 10.15252/embr.201745294
100. Lepper MF, Ohmayer U, von Toerne C, Maison N, Ziegler A-G, Hauck SM. Proteomic Landscape of Patient-Derived CD4+ T Cells in Recent-Onset Type 1 Diabetes. *J Proteome Res* (2018) 17:618–34. doi: 10.1021/acs.jproteome.7b00712
101. Schäfer N, Grosche A, Reinders J, Hauck SM, Pouw RB, Kuijpers TW, et al. Complement Regulator FHR-3 Is Elevated Either Locally or Systemically in a Selection of Autoimmune Diseases. *Front Immunol* (2016) 7:542. doi: 10.3389/fimmu.2016.00542

Conflict of Interest: CC is a consultant for Apellis.

The remaining authors declare that the research was conducted in the absence of any commercial or financial relationships that could be constructed as a potential conflict of interest.

Publisher's Note: All claims expressed in this article are solely those of the authors and do not necessarily represent those of their affiliated organizations, or those of the publisher, the editors and the reviewers. Any product that may be evaluated in this article, or claim that may be made by its manufacturer, is not guaranteed or endorsed by the publisher.

frontiers | Frontiers in Immunology

ORIGINAL RESEARCH
published: 05 July 2022
doi: 10.3389/fimmu.2022.887742

gC1qR/C1qBP/HABP-1: Structural Analysis of the Trimeric Core Region, Interactions With a Novel Panel of Monoclonal Antibodies, and Their Influence on Binding to FXII

Ying Zhang[1], *Alexander J. Vontz*[1†], *Ethan M. Kallenberger*[1†], *Xin Xu*[1†], *Nicoleta T. Ploscariu*[1†‡], *Kasra X. Ramyar*[1†], *Brandon L. Garcia*[1‡], *Berhane Ghebrehiwet*[2*] *and Brian V. Geisbrecht*[1*]

[1] Department of Biochemistry & Molecular Biophysics, Kansas State University, Manhattan, KS, United States, [2] Department of Medicine, Stony Brook University, Stony Brook, NY, United States

The protein gC1qR/C1qBP/HABP-1 plays an essential role in mitochondrial biogenesis, but becomes localized at the cellular surface in numerous pathophysiological states. When this occurs on endothelial cells, surface-exposed gC1qR activates the classical pathway of complement. It also promotes assembly of a multi-protein complex comprised of coagulation factor XII (FXII), pre-kallikrein (PK), and high-molecular weight kininogen (HMWK) that activates the contact system and the kinin-generating system. Since surface-exposed gC1qR triggers intravascular inflammatory pathways, there is interest in identifying molecules that block gC1qR function. Here we further that objective by reporting the outcome of a structure/function investigation of gC1qR, its interactions with FXII, and the impact of a panel of monoclonal anti-gC1qR antibodies on FXII binding to gC1qR. Although deletion mutants have been used extensively to assess gC1qR function, none of these proteins have been characterized structurally. To that end, we determined a 2.2 Å resolution crystal structure of a gC1qR mutant lacking both of its acidic loops, but which retained nanomolar-affinity binding to FXII and FXIIa. This structure revealed that the trimeric gC1qR assembly was maintained despite loss of roughly thirty residues. Characterization of a novel panel of anti-gC1qR monoclonal antibodies identified several with biochemical properties distinct from previously described antibodies, as well as one which bound to the first acidic loop of gC1qR. Intriguingly, we found that each of these antibodies could partly inhibit binding of FXII and FXIIa to gC1qR. Based on these results and previously published studies, we offer new perspectives for developing gC1qR inhibitors.

Keywords: gC1qR/C1qBP/HABP-1, FXII, protein-protein interactions, monoclonal antibodies, inhibitors

Edited by:
Jean van den Elsen,
University of Bath, United Kingdom

Reviewed by:
Daniel Ricklin,
University of Basel, Switzerland
Alex Macpherson,
UCB Pharma, United Kingdom

***Correspondence:**
Berhane Ghebrehiwet
Berhane.Ghebrehiwet@sbumed.org
Brian V. Geisbrecht
GeisbrechtB@ksu.edu

†*These authors have contributed equally to this work*

‡***Present addresses:***
Nicoleta T. Ploscariu, Bijvoet Centre for Biomolecular Research, Utrecht University, Utrecht, Netherlands
Brandon L. Garcia, Department of Microbiology & Immunology, East Carolina University, Greenville, NC United States

Specialty section:
This article was submitted to Molecular Innate Immunity, a section of the journal Frontiers in Immunology

Received: *01 March 2022*
Accepted: *06 June 2022*
Published: *05 July 2022*

Citation:
Zhang Y, Vontz AJ, Kallenberger EM, Xu X, Ploscariu NT, Ramyar KX, Garcia BL, Ghebrehiwet B and Geisbrecht BV (2022) gC1qR/C1qBP/HABP-1: Structural Analysis of the Trimeric Core Region, Interactions With a Novel Panel of Monoclonal Antibodies, and Their Influence on Binding to FXII. Front. Immunol. 13:887742. doi: 10.3389/fimmu.2022.887742

INTRODUCTION

gC1qR/C1qBP/HABP-1 is a multicompartmental and multifunctional protein that undergoes spatiotemporal changes in its distribution in response to various cellular and systemic stimuli (1). Although it normally functions within the cell and plays an essential role in mitochondrial biogenesis by virtue of its mRNA binding activity (2), gC1qR exposed at the cellular surface serves as a route to gain cellular entry for numerous pathogens as well as acting as an inflammatory trigger in a number of other diseases including vascular disorders and various cancers [Reviewed in (1)]. Because of its multicompartmental distribution and lack of a transmembrane domain, gC1qR does not meet the criteria of a classical receptor. Instead, it is considered as a prototype of a 'danger associated' or 'damage associated' molecular pattern by virtue of its enhanced surface expression during infection or inflammatory processes. Consequently, its recognition by components of the innate immune system can initiate potent inflammatory reactions that promote disease, including the complement system, the contact pathway, and the kinin-generating system (1).

Histological studies have shown that gC1qR is expressed on epithelial tumors of diverse origins (3) and elevated levels of gC1qR have likewise been correlated with poor clinical outcomes in breast cancer patients (4, 5). Although these relationships have not been defined as causal, a more contemporary study has shown that anti-gC1qR therapy slows tumor growth in an animal model of breast cancer (6). This emerging proof-of-concept evidence suggests that therapeutic targeting of cell surface-exposed gC1qR may be beneficial in certain cancers. Naturally, it raises questions of whether an analogous approach could be applicable to other diseases as well. A recent report suggests that anti-gC1qR therapy merits further investigation for treatment of specific types of angioedema (7), although this line of inquiry would be strengthened by additional studies using animal models of disease. Nevertheless, these observations have collectively rekindled interest in understanding how gC1qR interacts with various ligands to promote extracellular inflammatory reactions, and how these are influenced by the structure of gC1qR.

The gC1qR transcript encodes a pre-pro protein of 282 amino acids from which an N-terminal segment (i.e. residues 1-73) is removed by site-specific cleavage (8). The mature form of the gC1qR polypeptide therefore consists of residues 74-282 (1) and its crystal structure has been solved to 2.25 Å resolution (9). This structure showed an unusual fold comprised of two prominent N- and C-terminal α-helices positioned more or less anti-parallel to one another, with a relatively large, seven-stranded anti-parallel β-sheet at its core. In addition to this, a number of other key structural features of the gC1qR protein were also revealed. Chief among these is oligomerization of the gC1qR monomer into a toroidal, ring-like trimer (9). The gC1qR ring has an outer diameter of approximately 75 Å, an inner diameter of roughly 20 Å, and is approximately 30 Å thick throughout its circumference (9). Although the biological implications of gC1qR oligomerization remain unclear, the abundance of acidic residues in its sequence, combined with its unusual fold, imparts an asymmetric charge distribution to the gC1qR trimer. Whereas one aspect of the gC1qR trimer has an overall neutral charge, the opposite face of the trimer is rich in negative charge character (9). This noteworthy feature has influenced subsequent predictions regarding gC1qR interactions with its various ligands (1, 10). The contributions of two loops, comprised of residues 139-163 and 190-201 and which connect strands β3-β4 and β5-β6, respectively, have also been the source of some speculation (10). Although these loops are disordered in the gC1qR crystal structure (9), they themselves are rich in acidic residues and project outward from the negatively charged face of the gC1qR trimer. This has raised questions about the role these two loops play in ligand binding, such as whether they function independently or if they cooperate with residues/sites derived from the core of the gC1qR trimer.

Although many endogenous and exogenous ligands for gC1qR have been described (1), there remains little structural information on how these molecules bind to gC1qR. A significant development in this area occurred recently when Kaira et al. reported a crystal structure of gC1qR bound to the ~10 kDa type-II fibronectin domain that is found near the N-terminus of human FXII (hereafter FXII-FNII) (11). This study identified the second acidic loop of gC1qR as a major binding determinant for FXII-FNII, and provided new insights into assembly of the multiprotein complex between gC1qR, FXII, HMWK, and kallikrein that leads to activation of the contact system as well as the kinin-generating system (11). However, the fragment used in that study represents only a small portion of full-length FXII, suggesting that other important features of the FXII/gC1qR interaction may remain to be discovered. We undertook the current study to investigate that possibility, as well as to further define the structural features of gC1qR that mediate its interactions with FXII and other ligands relevant to initiating the contact pathway. We also describe identification of a new panel of anti-gC1qR monoclonal antibodies and show that these antibodies can partly inhibit FXII binding to gC1qR even though they recognize distinct epitopes on the gC1qR protein. Together, these results further our understanding of gC1qR structure/function and lay the foundation for future development of gC1qR-targeted inhibitors.

MATERIALS & METHODS

gC1qR Proteins

Samples of wild-type gC1qR were overexpressed and purified from recombinant strains of *E. coli.* Briefly, a designer gene fragment encoding residues 74-282 of human gC1qR was subcloned into the prokaryotic expression vector pT7HMT (12) and the resulting sequence-confirmed plasmid was used to transform competent cells of *E. coli* strain BL21(DE3). Cells were cultured in 1 L of terrific broth using standard procedures, and protein expression was induced overnight at 18°C by addition of IPTG (1 mM final concentration). Unless otherwise indicated, all purification steps were carried out at room temperature. Following cell harvest, the induced cell pellet was resuspended and processed for NiNTA affinity chromatography under native conditions as previously described (13). The polyhistidine tag was removed from the recombinant protein by digestion with TEV protease using a

100:1 mass ratio of target protein to protease and incubating overnight at room temperature (12); following removal of imidazole by buffer exchange, the digested sample was reapplied to an NiNTA affinity column and the unbound fraction was collected. The protein sample was further purified by gel-filtration chromatography using a Superdex S200 26/60 column (Cytiva Life Sciences) that had been previously equilibrated in PBS (pH 7.4). Fractions were analyzed by SDS-PAGE and those containing purified, trimeric gC1qR were pooled, concentrated, quantitated, and stored at either 4 or -80ºC for later use.

Gene fragments encoding the gC1qR mutants gC1qR-D1, gC1qR-D2, and gC1qR-DD (**Figure 1A**) were prepared using gene synthesis (GenScript USA). Following sequence confirmation, each fragment was cloned into pT7HMT and used to transform competent cells of *E. coli* strain BL21(DE3). Each mutant protein was overexpressed and purified using a procedure identical to that used for wild-type gC1qR. Gene fragments encoding either gC1qR or gC1qR-DD with a C-terminal avi-tag sequence (i.e. GLNDIFEAQKIEWHE) prior to the stop codon were likewise prepared using gene synthesis, cloned into pT7HMT, and used to transform *E. coli* strain BL21 (DE3) cells. As above, expression and purification of gC1qR-avi or gC1qR-DD-avi was accomplished through procedures identical to those used for the wild-type gC1qR protein.

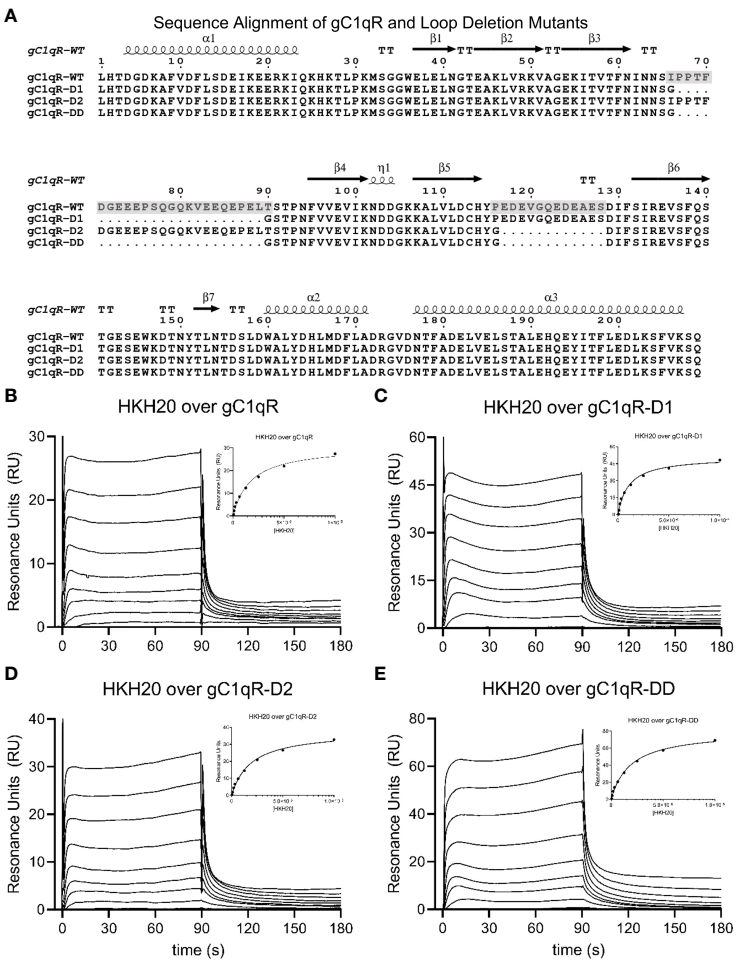

FIGURE 1 | Generation and Characterization of a Panel of Loop-deletion Mutants in gC1qR. **(A)** Sequence/structure alignment of the mature form of wild-type gC1qR and three deletion mutants wherein either one or both negatively charged loops have been replaced by a short glycine linker. The locations of secondary structure elements, as seen in the crystal structure of wild-type gC1qR (9), are shown above the alignment. Transparent grey boxes highlight the locations of the first and second acidic loops in the wild-type gC1qR sequence. Please note that the first residue in this alignment corresponds to Leu 74 in the human gC1qR sequence. **(B)** Surface plasmon resonance characterization of the interaction between wild-type gC1qR and peptide HKH-20 derived from human high-molecular weight kininogen. Reference-corrected sensorgrams for a two-fold dilution series of HKH-20 peptide (10 mM highest concentration) injected over a surface of immobilized gC1qR. A plot where SPR response immediately prior to injection stop is shown as a function of HKH-20 concentration is inset. Data shown in this panel were modified from Ghebrehiwet et al. (1) **(C)** Surface plasmon resonance characterization of the interaction between mutant gC1qR-D1 and peptide HKH-20. **(D)** Surface plasmon resonance characterization of the interaction between mutant gC1qR-D2 and peptide HKH-20. **(E)** Surface plasmon resonance characterization of the interaction between mutant gC1qR-DD and peptide HKH-20.

Both chemical and enzymatic protein biotinylation strategies were used in the course of this study. Modification of wild-type gC1qR or gC1qR-DD *via* their surface-exposed amine groups was accomplished using the EZ-link NHS-PEG4-Biotin reagent according to manufacturer's suggestions (ThermoFisher). Reactions were carried out to yield sub-stoichiometric labeling to avoid modification of all surface-exposed amines. gC1qR-avi and gC1qR-DD-avi were biotinylated *in vitro* using recombinant BirA enzyme and the general strategy reported in a previous publication (14). The biotinylation reaction was carried out in a buffer of 20 mM HEPES (pH 7.4), 140 mM NaCl, 5 mM $MgCl_2$ and contained 200 μM target protein, 4 mM ATP, 300 μM biotin, and 2 μM of a BirA fusion protein (14). Successful biotinylation of all proteins was confirmed by blotting and detection with an HRP-streptavidin conjugate according to manufacturer's suggestions (Thermo Scientific #21130).

Other Proteins and Peptides

Samples of native (HMWK) and activated High Molecular Weight Kininogen (HMWKa) were obtained from Enzyme Research Laboratories. Peptide HKH-20, which corresponds to the gC1qR-binding motif from human HMWK (sequence HKHGHGHGKHKNKGKKNGKH), was synthesized and purified by GenScript. Samples of native (FXII) and activated Factor XIIa (FXIIa) were also obtained from Enzyme Research Laboratories. A recombinant form of the type-II fibronectin domain of human Factor XII/XIIa (FXII-FNII) was expressed and purified from *E. coli*. A synthetic gene fragment encoding human FXII-FNII was first subcloned into the prokaryotic expression vector pT7HMT (12), and the sequence-confirmed plasmid was used to transform competent cells of *E. coli* strain BL21(DE3). Cells were cultured in 1 L of terrific broth using standard procedures and protein expression was induced overnight at 37°C by addition of IPTG (1 mM final concentration). Unless otherwise indicated, all purification steps were carried out at room temperature. The induced cell pellet was extracted with denaturant, clarified by high-speed centrifugation, and the his-tagged FXII-FNII was purified by NiNTA affinity chromatography according to previously published methods (12). Following elution, the purified protein was reduced with TCEP (1 mM final concentration) at 37°C for 30 min, placed in SpectraPor 3500 dialysis tubing, and dialyzed overnight at room temperature against a buffer of 0.1 M Tris-HCl (pH 8.3), 2.5 M urea, 20 mM glycine, 0.5 mM EDTA, and 2 mM L-cysteine. The next day the sample was dialyzed overnight against 4 L of PBS (pH 7.4). The refolded protein was separated from soluble aggregates by gel-filtration chromatography using a Superdex S75 26/60 column (Cytiva Life Sciences) that had been equilibrated in PBS (pH 7.4). Fractions were analyzed by SDS-PAGE and those containing purified, monomeric FXII-FNII were pooled, concentrated, quantitated, and stored at either 4 or -80°C for later use.

Crystallization, X-ray Diffraction, Structure Solution, and Refinement

Single crystals of gC1qR-DD were grown by vapor diffusion of hanging drops at 20°C. Briefly, 1 μl of a gC1qR-DD sample (10 mg/ml protein in ddH_2O) was mixed with an equal volume of a precipitant solution consisting of 0.1 M BisTris-HCl (pH 6.5), 0.1 M sodium chloride, and 1.5 M ammonium sulfate and equilibrated over 500 μl of the same precipitant solution. Plate shaped crystals formed within 2-3 days. Prior to X-ray diffraction analysis, single crystals were cryopreserved by dragging individual samples through a small volume of Santovac Cryo Oil (Hampton Research) and flash cooling in a bath of liquid nitrogen. X-ray diffraction data were collected at 1.000 Å wavelength using beamline 22-BM of the Advanced Photon Source at Argonne National Laboratory. Individual reflections were indexed, integrated, merged, and scaled in the space group $P6_322$ using the HKL2000 software package (15).

The structure of gC1qR-DD was solved by molecular replacement using PHASER (16) as implemented in the PHENIX software suite (17) and a monomer of wild-type gC1qR [PDB entry 1P32 (9)] as a search model. Initial electron density maps were calculated at 2.2 Å limiting resolution following placement of a single copy of the gC1qR search model. The structure was then improved by a combination of manual rebuilding using Coot (18) and reciprocal space positional, B-factor, and TLS refinement using PHENIX.REFINE (17). The final polypeptide model consisted of gC1qR residues 76-247, with chain breaks from residues 98-100 and 138-141 due to weak electron density in those areas. In addition, 40 ordered solved molecules were also included in the final model. The refined coordinates and structure factors have been deposited in the PDB using the accession code 7TE3. All representations of protein structures were generated and rendered by PyMol (www.pymol.org/).

Generation, Purification, and Characterization of anti-gC1qR Monoclonal Antibodies

A sample of wild-type gC1qR was used for the generation of mouse monoclonal antibodies in conjunction with ProMab Biotechnologies. Immunization of experimental mice and preparation of hybridoma lines were carried out according to the proprietary protocols of the vendor. Selection of hybridoma lines for further analysis was based initial quantitation of the anti-gC1qR immunoreactivity present in clonal culture supernatants following direct ELISA against immobilized wild-type gC1qR using standard methods. Generation of ascites fluid in experimental mice and purification of anti-gC1qR mAb IgG using Protein G affinity chromatography was likewise performed using standard procedures by ProMab Biotechnologies. Following purification, the mAbs were buffer exchanged into PBS (pH 7.4), quantitated, aliquoted, and stored at either 4 or -80°C for later use.

Western blotting was used to further characterize anti-gC1qR antibodies. 100 ng of wild-type gC1qR, gC1qR-D1, gC1qR-D2, and gC1qR-DD were separated by Tris-Tricine SDS-PAGE and transferred to a PVDF blotting membrane. Following blocking with a solution of 10% (w/v) non-fat dry milk dissolved in TBS-T (20 mM tris-HCl (pH 8.0), 150 mM NaCl, 0.01% (v/v) Tween-20) for 10 min, each membrane was probed with 1 μg/ml of mAb in blocking solution for 60 min. After a series of washes, each membrane was probed with a 1:10,000 dilution of anti-mouse IgG/

IgM HRP conjugate (ThermoFisher #31446) in blocking solution for 30 min. Following further washing, peroxidase activity was detected using SuperSignal West Pico PLUS reagent (ThermoFisher #34580) according to manufacturer's suggestions.

Surface Plasmon Resonance Binding Studies

Interactions of various ligands with immobilized forms of gC1qR were investigated by surface plasmon resonance (SPR). All experiments were performed at 25°C on a Biacore T-200 instrument (Cytiva Life Sciences) using a running buffer of HBS-T (20 mM HEPES (pH 7.4), 140 mM NaCl, and 0.005% (v/v) Tween-20) and a flowrate of 30 µl/min. Binding of peptide HKH-20 to wild-type gC1qR and the three gC1qR deletion mutants was initially assessed (1, 19). Samples of various gC1qR proteins were prepared at final concentrations of 10-50 µg/ml in 10 mM acetate buffer (pH 3.5) and coupled to individual flow cells of a CMD200M sensor chip (Xantec Bioanalytics GmbH) using standard amine coupling chemistry. The final immobilization densities achieved were as follows: gC1qR, 361 RU; gC1qR-D1, 487 RU; gC1qR-D2, 360 RU; and gC1qR-DD, 874 RU. A reference surface was also prepared by activation followed by quenching with 1 M ethanolamine (pH 9.5). Solutions of HKH-20 were injected over the biosensor surface in reference subtraction mode using a two-fold series of increasing concentrations ranging from 46.9 nM to 10 µM. Each experimental cycle consisted of an association phase of 1.5 min followed by a dissociation phase of 2 min. Regeneration of the biosensor surface was achieved by an injection of 2 M NaCl for 30 s. Sensorgram series were analyzed using Biacore T-200 Evaluation software v3.2 (Cytiva Life Sciences) by fitting globally to a simple affinity (dose/response) model to derive an apparent K_D.

Binding of FXII and FXIIa to biotinylated gC1qR and gC1qR-DD was measured next. The general parameters for these experiments were the same to those described above, with the exception that the running buffer contained 50 µM $ZnCl_2$ to allow for high-affinity binding of FXII-derived analytes to gC1qR. To begin, gC1qR-avi and gC1qR-DD-avi that had been enzymatically biotinylated were captured to a final level of 100 RU on one and two experimental flow cells of an SA sensor chip, respectively, while a reference surface was prepared by capturing biotin alone. This was followed by injection of a two-fold series of increasing concentrations of FXII and FXIIa ranging from 1.6 to 800 nM across all four flow cells in reference subtraction mode. Each cycle consisted of a 2 min association and 3 min dissociation phase. Regeneration of the biosensor surface was achieved by two sequential injections of 3 mM EDTA for 30 s, which was sufficient to completely dissociate the FXII-derived analytes from captured gC1qR. Sensorgram series were analyzed using Biacore T-200 Evaluation software v3.2 (Cytiva Life Sciences) by fitting globally to a ligand heterogeneity model that accounts for two independent analyte binding sites each described by a set of association and dissociation rate constants.

Binding of monoclonal antibodies to gC1qR was likewise measured by SPR. Wild-type gC1qR that had been chemically biotinylated was captured on experimental flow cells of an SA sensor chip (Cytiva Life Sciences) while a reference flow cell was prepared by capturing biotin alone. Solutions of various mAbs were injected over the biosensor surface in reference subtraction mode using a five-fold series of increasing concentrations ranging from 1.6 to 1000 nM at 30 µl/min. Each experimental cycle consisted of a 2 min association phase at a given mAb concentration, a brief dissociation phase, followed by injection of the next mAb concentration. Once each mAb sample had been injected, a final dissociation phase of 60 min was monitored. Regeneration of the biosensor surface was achieved by three consecutive injections of 0.1 M glycine (pH 2.2), 2 M NaCl for 30 s. Sensorgram series were analyzed using Biacore T-200 Evaluation software v3.2 (Cytiva Life Sciences) by fitting to a bivalent analyte kinetic model to derive the respective association and dissociation rate constants.

Finally, SPR was also used to assess selectivity of mAb-1 for various forms of gC1qR. In this experiment, a solution of mAb-1 was prepared at a final concentration of 10 µg/ml in 10 mM acetate buffer (pH 4.5) and covalently coupled to individual flow cells of a CMD200M sensor chip. An ethanolamine-quenched reference surface was also prepared. Solutions of various gC1qR proteins were injected over the biosensor surface in reference subtraction mode using a five-fold series of increasing concentrations ranging from 0.8 to 500 nM (expressed as gC1qR monomer). Parameters for each experimental cycle, regeneration of the surface, and data analysis were identical to those described in the preceding paragraph.

Alpha Screen Bead Binding Assays

AlphaScreen bead-based competition binding assays (Perkin Elmer) were used to evaluate the interactions between various anti-gC1qR mAbs and chemically biotinylated wild-type gC1qR. All reaction mixtures consisted of a fixed concentration of anti-gC1qR mAb, a fixed concentration of biotinylated gC1qR (described above), 20 µg/ml anti-mouse AlphaScreen Acceptor beads, 20 µg/ml streptavidin AlphaScreen Donor beads, and a putative competitor molecule. Each reaction was carried out in a final volume of 25 µl using a buffer of 20 mM HEPES (pH 7.4), 140 mM NaCl, 0.1% (w/v) bovine serum albumin, and 0.05% (v/v) Tween-20. The final concentrations for each mAb and biotinylated gC1qR combination were optimized in pair-wise fashion to maximize the dynamic range of the assay according to manufacturer's suggestions. Step-wise additions of all reagents, incubation times, and data analyses were carried out as previously described (20–22).

Competition Binding Studies Using Surface Plasmon Resonance

Competition binding studies between various anti-gC1qR mAbs and FXII, FXIIa, and FXII-FNII were carried out by SPR. All parameters for these experiments were the same as those described above where these proteins were used as analytes. To begin, gC1qR-avi that had been biotinylated enzymatically was captured to a final level of either ~100 RU (101 ± 4.4 RU, for n=15 experimental flow cells used in this study) or ~1000 RU (1063 ± 59 RU, for n=15 experimental flow cells used in this

study) on all three experimental flow cells of an SA sensor chip, while a reference surface was prepared by capturing biotin alone. Next, to ensure the bioactivity of the captured gC1qR-avi, the second flow cell on each sensor chip was used to perform a single-cycle kinetic study in reference subtraction mode by injecting a five-fold series of increasing mAb concentrations ranging from 1.6 to 1000 nM. Thereafter, a competition study was carried out by presaturating the second flow cell on each sensorchip with 100 nM mAb, followed by injection of a two-fold series of increasing concentrations of FXII-derived analytes across all four flow cells in reference subtraction mode as described above. Each cycle consisted of a 1 min presaturation injection across the second flow cell (carried out at 10 µl/min) prior to a 2 min association and 3 min dissociation phase for each analyte across all four flow cells at 30 µl/min; regeneration of the biosensor surface was achieved by two sequential injections of 3 mM EDTA for 30 s. Sensorgram series were analyzed using Biacore T-200 Evaluation software v3.2 (Cytiva Life Sciences) by fitting globally to a ligand heterogeneity model that accounts for two independent analyte binding sites each described by a set of association and dissociation rate constants. Assessments of precision were obtained by averaging the fitting parameters for the sensorgrams obtained from the third and fourth flow cells of each experiment across five independent biosensor chips at both low and high capture densities. These aggregate values were used as basis for comparison with those obtained following mAb presaturation, which were carried out only a single time for each mAb at low and high capture densities to minimize materials consumption.

RESULTS

Generation and Structure/Function Analysis of Loop-Deletion Mutants in gC1qR

Previous structural analyses of the mature form of gC1qR (i.e. residues 74-282) revealed that there are two prominently disordered regions in each gC1qR polypeptide (9). These presumed loop regions connect strands β3-β4 and β5-β6 (9), and are hereafter referred to as "Loop 1" and "Loop 2", respectively. Both Loop 1 and Loop 2 are rich in acidic amino acids and have been proposed to contribute to the asymmetric charge distribution of the gC1qR trimer (**Figure 1A**). Although the roles of these and other loop regions that connect canonical secondary structure elements in gC1qR have been previously investigated using deletion mutagenesis (23), there exists little detailed information on the structural status of loop-deleted forms of gC1qR. Furthermore, the consequences of deleting these acidic loops simultaneously and/or eliminating their function through loop-targeting monoclonal antibodies remain unexplored.

To address these limitations, we used the existing crystal structure of mature gC1qR to design individual deletion mutants of Loop 1 (i.e. gC1qR-D1) and Loop 2 (i.e. gC1qR-D2) wherein the entire acidic loop was replaced with either two or one glycine residue(s), respectively (**Figure 1A** and **Figure S1**). In addition to this, we designed a double deletion mutant that simultaneously removed both Loop 1 and Loop 2 (i.e. gC1qR-DD) using the same strategy described above (**Figure 1A**). We expressed each form of gC1qR in *E. coli* and purified the mutant proteins for subsequent structure/function analyses (**Figure S1**). Significantly, we found that all three forms of gC1qR were highly soluble and behaved as trimers in solution similarly to wild-type gC1qR (**Figure S1**). To characterize these new mutants in gC1qR, we used a surface plasmon resonance-based approach where forms of gC1qR were covalently coupled through their surface-accessible primary amines to a biosensor flow cell and soluble ligands were injected over each flow cell in reference-correction mode. Although numerous ligands for g1qR have been described (1), we opted to use the human high-molecular weight kininogen (HMWK)-derived peptide, HKH-20 (1, 19), in this initial study since this interaction pair does not require exposure to stringent chemical conditions to regenerate the biosensor surface. As reported previously [**Figure 1B** and (1)], we found that wild-type gC1qR bound HKH-20 with an apparent K_D value of 8.7 µM; this corresponded well to the apparent equilibrium dissociation constant we reported for HKH-20 binding to the same protein using an isothermal titration calorimetry approach (6.3 µM) (1). Consistent with the results reported for wild-type gC1qR, we found that both gC1qR-D1 (**Figure 1C**) and gC1qR-D2 (**Figure 1D**) bound to HKH-20 with affinities of ~10 µM. Intriguingly, we also observed a similar affinity for gC1qR-DD binding to HKH-20 (**Figure 1E**). Although this result was somewhat surprising as the HKH-20 peptide is highly positively charged and both loops in gC1qR are rich in negatively charged residues (**Figure 1A**), we interpreted these data to mean that neither acidic loop is directly involved in binding to HKH-20 (1).

To gain further insight into the physical properties of these loop-deleted gC1qR mutants, we crystallized the gC1qR-DD protein. We collected X-ray diffraction data to 2.2 Å limiting resolution and solved the structure of gC1qR-DD by molecular replacement using the published structure of the wild-type gC1qR monomer as a search model (9). Following several rounds of manual rebuilding, our model of gC1qR-DD had R_{work} and R_{free} values of 23.3% and 28.8%, respectively (**Table 1**). The asymmetric unit of the crystal contained a single copy of the gC1qR-DD polypeptide from residues 76-247, aside from two discontinuities in regions connecting α1-β1 (i.e. residues 98-100) and β3-β4 (i.e. residues 138-141) due to weak electron density in those areas. Although the final model contained only a single copy of the gC1qR-DD polypeptide (**Figure 2A**), the structure of the gC1qR-DD trimer that exists in solution could be reconstructed by applying crystallographic symmetry (**Figure 2B**). The structure of the gC1qR-DD trimer superimposes well upon on that of wild-type gC1qR, as 140 of the 165 Cα positions align with a root mean square deviation of 0.544 Å (**Figure 2C**). As expected, the primary areas of structural divergence are found in the areas corresponding to the loop deletions. This feature is particularly striking in a superposition of gC1qR-DD with the structure of gC1qR bound FXII-FNII (**Figure 2D**), wherein Loop 2 adopts a well-ordered conformation that constitutes a major binding determinant for FXII-FNII, and presumably for Factor XII and FXIIa as well (11).

Although the FXII-FNII/gC1qR structure highlighted the importance of gC1qR Loop 2 in this interaction (11), both

TABLE 1 | X-ray Diffraction Data Collection and Refinement Statistics.

	gC1qR-DD (7TE3)
Data Collection	
Space group	$P\,6_3\,2\,2$
Cell dimensions	
a, *b*, *c* (Å)	80.53 80.53 114.55
Resolution (Å)	50.00-2.20 (2.28-2.20)[a]
Wilson B-Factor (Å^2)	45.4
Completeness (%)	99.9 (99.6)
I / σI	22.0 (1.2)
R_{pim}	0.032 (0.499)
$CC_{1/2}$	0.996 (0.544)
Redundancy	20.3 (13.8)
Refinement	
Resolution (Å)	37.99-2.20
No. reflections	11,768
R_{work} / R_{free} (%)	23.3 / 28.8
No. atoms	1,367
Protein	1,327
Water	40
Ramachandran Plot	
Favored / Allowed (%)	93.7 / 4.4
B-Factors	
Range & Mean (Å^2)	29.86-108.12 (55.11)
R.M.S. Deviations	
Bond lengths (Å)	0.007
Bond angles (°)	0.88

[a]*Values in parentheses are for the highest-resolution shell.*

FXII and its activated counterpart, FXIIa, are significantly larger molecules than FXII-FNII (c.f. ~80 kDa to ~10 kDa). Therefore, we wondered whether additional binding sites for FXII and FXIIa might be contributed by the trimeric gC1qR core represented by gC1qR-DD. To examine this possibility, we designed an SPR assay where both wild-type gC1qR and gC1qR-DD that had been biotinylated at a single site *via* a C-terminal avi-tag were captured on separate flow-cells of a streptavidin sensor chip followed by injection of increasing concentrations of FXII or FXIIa. We determined that the interactions between both forms of gC1qR and both forms of FXII required a mechanism incorporating two independent sets of rate constants to adequately describe the experimental data (**Figure S2** and **Table 2**). This feature did not appear to arise from polydispersity in the proteins employed in this study (**Figure S1**). Thus, it likely represented a *bona fide* feature of these interactions that could have been due to the trimeric nature of the gC1qR-avi ligand, conformational changes accompanying FXII binding such as those observed in the FXII-FNII/gC1qR crystal structure described by Kaira et al. (11), or some combination of these factors. In the case of wild-type gC1qR binding to FXII, the first binding site ($K_{D\text{-}1}$ = 4.85 ± 1.58 nM) was characterized by a fast on-rate (6.76 ± 1.40x10^5 $M^{-1}s^{-1}$) and slow off-rate (31.6 ± 3.94x10^{-4} s^{-1}), while the second binding site ($K_{D\text{-}2}$ = 97.6 ± 9.1 nM) had a slower on-rate (2.37 ± 0.24x10^4 $M^{-1}s^{-1}$) but comparable off-rate (2.30 ± 0.02x10^{-3} s^{-1}) to the first (**Table 2**). We used a similar strategy to analyze the FXIIa/gC1qR-avi sensorgrams (**Figure S2** and **Table 2**). However, in this case the first binding site was of such high apparent affinity ($K_{D\text{-}1}$ = 0.27 ± 0.37 nM) that it approached the limits measurable using the instrumentation available, while the second binding site was somewhat weaker ($K_{D\text{-}2}$ = 134 ± 36 nM) than that of FXII. The comparatively large error associated with the first site was due to difficulty in accurately measuring its dissociation rate constant through this approach (**Table 2**). We attempted to address this issue by conducting single-cycle kinetic studies, but the results failed to resolve this problem.

Intriguingly, we found that surface-captured gC1qR-DD bound with low-nanomolar apparent affinity to both FXII (**Figure 2E**) and FXIIa (**Figure 2F**). For gC1qR-DD binding to FXII, the first FXII binding site was of slightly higher affinity ($K_{D\text{-}1}$ = 1.69 ± 0.05 nM) when compared to wild-type gC1qR (**Table 2**). Similarly, the second FXII binding site was also of higher apparent affinity ($K_{D\text{-}2}$ = 26.4 ± 4.8 nM) than that of wild-type gC1qR (**Table 2**). Although the first FXIIa binding site of gC1qR-DD followed this trend ($K_{D\text{-}1}$ = 0.12 ± 0.13 nM), the second FXIIa binding site was slightly diminished ($K_{D\text{-}2}$ = 178 ± 35 nM) when compared to wild-type gC1qR (**Table 2**). In both cases, loss of the acidic loops had a greater influence on the overall saturation levels of the second FXII and FXIIa binding sites of the gC1qR proteins (**Table 2**). This suggested that any contributions of these loops are associated with this lower-affinity FXII/FXIIa binding site. Indeed, we also noticed that loss of the acidic loops resulted in subtle changes to both the shape and the overall response observed throughout all concentrations of FXII and FXIIa injected, even though the global structure/function features of the gC1qR-DD mutant remained intact (**Figures 2E, F**, and **Figure S2**). Thus, while gC1qR-DD clearly bound tighly to both FXII and FXIIa, comparison of this mutant to wild-type gC1qR strongly suggested that interactions of these ligands with gC1qR are mechanistically complex and likely to involve multiple contact sites from each binding partner.

Generation and Identification of a Loop-Specific Monoclonal Antibody Against gC1qR

Previous reports have described two monoclonal antibodies known as mAb-60.11 and mAb-74.5.2 that are powerful probes of gC1qR structure and function [Reviewed in (1)]. Specifically, whereas mAb-60.11 binds to gC1qR in a manner that interferes with recognition by complement component C1q (10), mAb-74.5.2 binds to gC1qR at site that disrupts its interaction with HMWK (24). Although the epitopes for both mAb-60.11 and mAb-74.5.2 have been mapped at peptide-level resolution on the gC1qR protein (1), neither of these mAbs recognizes residues within or in the vicinity of either of the acidic loop regions in gC1qR. Since these loops appear to play some role in gC1qR binding to certain ligands, notably FXII-FNII [**Figure 2D** and (11)], we sought to develop a novel monoclonal antibody that recognized a loop region within gC1qR and to ascertain its potential as an inhibitor of gC1qR interactions and function.

Following immunization of five mice with wild-type gC1qR and generation of B-cell hybridoma cell lines using standard approaches, we screened approximately thirty different lines for those that grew quickly, those that produced relatively high levels of antibody, and those that reacted with gC1qR immobilized on

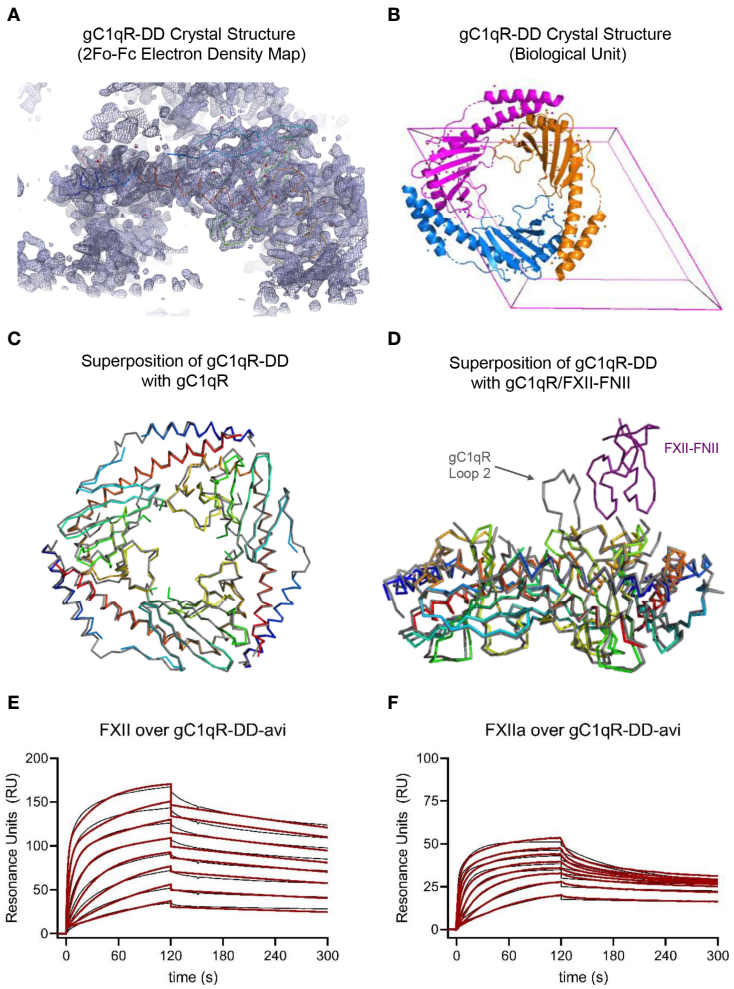

FIGURE 2 | Crystal Structure and Functional Studies of the gC1qR-DD Mutant. **(A)** Correlation of the 2Fo-Fc electron density map contoured at 1.3σ (grey mesh) with the Cα position of the final model (rainbow wire, with N-terminus in blue and C-terminus in red) for the structure of gC1qR-DD determined at 2.2 Å resolution. The U-shaped void at the bottom of this image represents the hole formed upon trimerization of gC1qR-DD monomers. **(B)** Visualization of the gC1qR-DD trimer constructed by applying the crystallographic symmetry operators of the $P6_322$ unit cell (pink box). Individual polypeptides are shown as ribbon diagrams using distinct colors. **(C)** Structural superposition of the gC1qR-DD trimer (rainbow wires) with that of wild-type gC1qR (grey wire). Structures are represented by their Cα positions only for clarity. Coordinates for wild-type gC1qR were obtained from PDB entry 1P32 (9). **(D)** Structural superposition of the gC1qR-DD trimer (rainbow wires) with that of wild-type gC1qR (grey wire) bound to the FNII domain of FXII (purple wire). Structures are represented by their Cα positions only for clarity. Coordinates for wild-type gC1qR bound to FXII-FNII were obtained from PDB entry 6SZW (11). Note that acidic loop 2 contributes a major binding determinant for FXII-FNII (11). **(E)** gC1qR-DD was enzymatically biotinylated through a C-terminal avi-tag and captured to a density of ~100 RU on two experimental flow cells of a streptavidin-derivatized sensor chip. Dose-response sensorgrams for injection of a two-fold dilution series of FXII (800 nM highest concentration) over gC1qR-DD-avi. The black trace represents the experimental data, while the red line represents the outcome of fitting to a ligand heterogeneity kinetic model. **(F)** An identical experiment to that shown in panel **(E)**, with the exception that solutions of FXIIa were used as the analytes (800 nM highest concentration).

microtiter plates in an ELISA (*Data Not Shown*). We next selected six clones for production of ascites fluid to generate large quantities of antibody and purified the anti-gC1qR IgG using Protein G affinity chromatography. We then characterized each antibody using a series of biochemical assays. Although each antibody selected bound immobilized gC1qR in an ELISA, we first examined the ability of each to bind to immobilized gC1qR in a surface plasmon resonance experiment. Since gC1qR is characterized by an asymmetric charge distribution (9), we again opted against direct coupling of the protein to the biosensor surface; instead, we used a streptavidin surface to capture gC1qR that had been chemically derivatized by a modified biotin group that included a polyethylene glycol-based spacer arm. Using single-cycle kinetic analysis, we determined that each new monoclonal antibody bound with low-nanomolar apparent affinity (<10 nM) to biotinylated gC1qR (**Figure 3**). Examination of experimental data revealed that these antibodies could be clustered into three different groups based upon their sensorgram shapes. mAb-12 and mAb-13 were characterized by the lowest overall signals but

TABLE 2 | Interaction Parameters for FXII and FXIIa with Surface Captured gC1qR and gC1qR-DD[a].

Interaction	k_{a-1} ($M^{-1}s^{-1}$)	k_{d-1} (10^{-4} s^{-1})	K_{D-1} (nM)	R_{max-1} (RU)	k_{a-2} ($M^{-1}s^{-1}$)	k_{d-2} (10^{-3} s^{-1})	K_{D-2} (nM)	R_{max-2} (RU)	χ^2 (RU^2)
FXII/ gC1qR-avi[b]	6.76±1.40x10^5	31.6±3.94	4.85±1.58	47±6	2.37±0.24x10^4	2.3±0.02	97.6±9.1	104±10	5.5±2.5
FXII/ gC1qR-DD-avi[c]	6.74±0.21x10^5	11.4±0.43	1.69±0.05	63±12	3.48±0.18x10^4	0.91±0.13	26.4±4.8	64±9	3.8±1.4
FXIIa/ gC1qR-avi[b]	4.08±0.99x10^5	0.90±1.2[d]	0.27±0.37[d]	21±1	4.82±0.91x10^4	6.30±0.51	134±36	48±2	1.4±0.2
FXIIa/ gC1qR-DD-avi[c]	11.3±1.3x10^5	1.47±1.61[d]	0.12±0.13[d]	24±4	6.37±0.84x10^4	11.2±2.0	178±35	22±3	0.7±0.2

[a]*Model accounts for two analyte binding sites on the ligand each described by a set of association and dissociation rate constants.*
[b]*Values are presented as their mean ± standard deviation obtained from two injections in total for this experiment (one flow cell from two biosensor chips, one replicate). Representative sensorgrams are shown in* ***Figure S2****.*
[c]*Values are presented as their mean ± standard deviation obtained from four injections in total (two flow cells from two biosensor chips, one replicate). Representative sensorgrams are shown in* ***Figure 2****.*
[d]*The large standard deviations associated with these values arise from fitting the dissociation rate constant of the first binding site, which lies near the limit measurable by the instrument.*

clearly had the slowest dissociation rates under these conditions; in addition, these sensorgrams were well-described by Langmuir binding models (*Data Not Shown*), suggesting that only one of the two antigen-binding regions from these intact IgG could interact with its epitope on the captured gC1qR trimer. mAb-3, mAb-5, and mAb-18 had significantly higher overall response levels, but also had faster off-rates under these conditions than either mAb-12 or mAb-13. Finally, mAb-1 had the fastest on-rate and also gave the highest overall response level, suggesting that its epitope was most accessible on the captured gC1qR trimer. Among this collection of antibodies, mAb-1 appeared unique in these properties.

The ability of mAb-74.5.2 to compete with HMWK for binding to gC1qR has been documented in both biochemical and functional studies (1, 24). Thus, we next wondered whether any of these newly generated monoclonal antibodies might exhibit similar properties to mAb-74.5.2 and inhibit binding of HMWK to gC1qR. To address this question, we established luminescent bead-based binding assays between each mAb and the chemically biotinylated gC1qR used above (*please see Materials & Methods*) and tested whether this signal could be inhibited by the presence of HMWK itself or defined regions thereof. As expected, we found that the interaction between mAb-74.5.2 and biotinylated gC1qR could be blocked by unlabeled gC1qR (a positive control), as well as purified human HMWK or the HKH-20 peptide [**Figure 4A** and (1)]. We also found that a fusion protein of *E. coli* maltose-binding protein (MBP) and HKH-20 (designed to more accurately mimic the size of HMWK than the HKH-20 peptide alone) inhibited the interaction, whereas MBP itself did not (**Figure 4A**). Interestingly, we found that the signal generated by mAb-1 and biotinylated gC1qR was only diminished by approximately one-half using any of the HMWK ligands described above (**Figure 4B**). mAb-3 exhibited properties that were largely indistinguishable from mAb-74.5.2 (**Figure 4C**), as did mAb-5, with the distinction being that the latter was not as sensitive to the presence of saturating levels of HKH-20 peptide (**Figure 4D**). mAb-12 also behaved somewhat similarly to mAb-74.5.2, with the caveat that its interaction could be fully competed by the HKH-20 peptide but not the HMWK protein (**Figure 4E**); although we did not test it directly, we presume that the same may be true for mAb-13, since its interaction with gC1qR was almost identical to mAb-12 in our previous SPR experiment (**Figures 3D, E**). Finally, we found that mAb-18 binding to biotinylated gC1qR was not effectively competed by HMWK or the HKH-20 peptide (**Figure 4F**). This result was somewhat surprising, as our initial binding studies suggested that mAb-18 might display properties similar to mAb-3 and mAb-5 (**Figures 3B, C, F**). Considering these results, we concluded that several of these monoclonal antibodies recognized epitopes distinct from each other and from that of mAb-74.5.2.

As final means of characterizing these newly generated monoclonal antibodies, we used our panel of deletion mutants in gC1qR to examine whether any antibody bound to one of the acidic loops. We separated identical quantities of wild-type gC1qR, gC1qR-D1, gC1q-D2, and gC1qR-DD by SDS-PAGE, transferred the samples to a blotting membrane, and processed each membrane for western blotting. Whereas mAb-3, mAb-5, mAb-12, and mAb-18 all reacted equivalently with each form of gC1qR, we found that mAb-1 lost reactivity for both gC1qR-D1 and gC1qR-DD (**Figure 5A**). This result indicated that the epitope recognized by mAb-1 was within the first acidic loop of gC1qR. To investigate this result through an alternative approach, we covalently coupled mAb-1 to a biosensor flow cell and used SPR to measure its ability to bind various forms of gC1qR (**Figures 5B-E**). Consistent with the results obtained by western blotting, we found that wild-type gC1qR (**Figure 5B**) and gC1qR-D2 (**Figure 5D**) bound well to the mAb-1 surface, but neither gC1qR-D1 (**Figure 5C**) nor gC1qR-DD (**Figure 5E**) did so. Interestingly, we noted that gC1qR-D2 appeared to bind more tightly than wild-type gC1qR to mAb-1. This suggested that removal of the second acidic loop may have made the gC1qR epitope recognized by mAb-1 more accessible for interactions. Together, these results identified mAb-1 as a novel monoclonal antibody that recognizes an epitope within the first acidic loop of gC1qR, and provided characterization of several additional anti-gC1qR monoclonal antibodies that could be used for future structure/function studies.

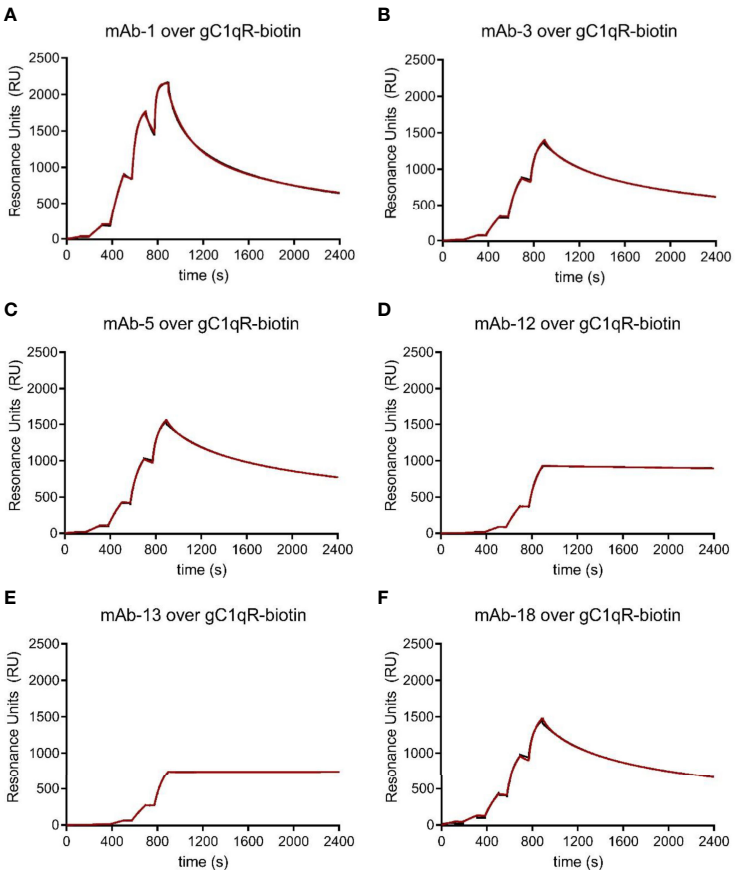

FIGURE 3 | Characterization of a Novel Panel of anti-gC1qR Monoclonal Antibodies. Purified anti-gC1qR monoclonal antibodies were prepared from ascites fluid and their interactions with chemically biotinylated gC1qR were assessed by surface plasmon resonance. **(A)** Reference-corrected sensorgram from a single cycle kinetic study where a five-fold dilution series of mAb-1 (1 μM highest concentration) was injected over a surface of biotinylated gC1qR. The black trace represents the experimental data, while the red line represents the outcome of fitting to a bivalent analyte kinetic model. **(B)** Identical to panel **(A)**, except for mAb-3 served as the analyte. **(C)** Identical to panel **(A)**, except for mAb-5 served as the analyte. **(D)** Identical to panel **(A)**, except for mAb-12 served as the analyte. **(E)** Identical to panel **(A)**, except for mAb-13 served as the analyte. **(F)** Identical to panel **(A)**, except for mAb-18 served as the analyte.

Multiple Anti-gC1qR Antibodies Interfere With Binding of FXII to gC1qR

When exposed on the endothelial cell surface, gC1qR serves as a scaffold for assembly of a multi-protein complex that leads to activation of the contact system and generation of bradykinin. A component of this complex is FXII and its enzymatically active counterpart, FXIIa. The crystal structure of gC1qR bound to FXII-FNII (11) not only revealed that FXII-FNII binds asymmetrically to the second acidic loop in the gC1qR trimer (**Figure 2D**), it also showed that this loop becomes ordered and forms a zipper motif with a β-strand derived from FXII-FNII (11). Although the acidic loops of gC1qR appear to be intrinsically disordered in the absence of binding partners (9), examination of the unbound gC1qR structure shows that these regions must extend from the same surface of the trimer; this suggests that these loops may be in relatively close physical proximity to one another and, furthermore, that loop specific ligands like mAb-1 might interfere with FXII binding to gC1qR. To test this hypothesis, we designed a competition SPR study. We initially captured gC1qR that had been biotinylated *via* a C-terminal avi-tag on the experimental flow cells of a streptavidin-modified sensorchip. We then compared binding of FXII and FXIIa to a single flow cell that was presaturated with an anti-gC1qR antibody prior to each injection series with two control flow cells that were not (**Figure S3**).

We utilized five independent sensorchips in this study at a low gC1qR capture density and five at a high gC1qR capture density. We were able to reproducibly capture ~100 RU of gC1qR-avi on each experimental flow cell of the first cohort and ~1000 RU on each experimental flow cell of the second (*please see Materials & Methods*). Consequently, we obtained multiple independent measurements of FXII and FXIIa binding to gC1qR-avi (n=10) at each density, which allowed a detailed assessment of data reproducibility across this entire set of experiments (**Figure S3** and **Table S1**). Although both FXII and FXIIa bound strongly to the gC1qR-avi surface as before, we again found the sensorgrams fit poorly to a Langmuir binding model. However, by again invoking a mechanism with a second

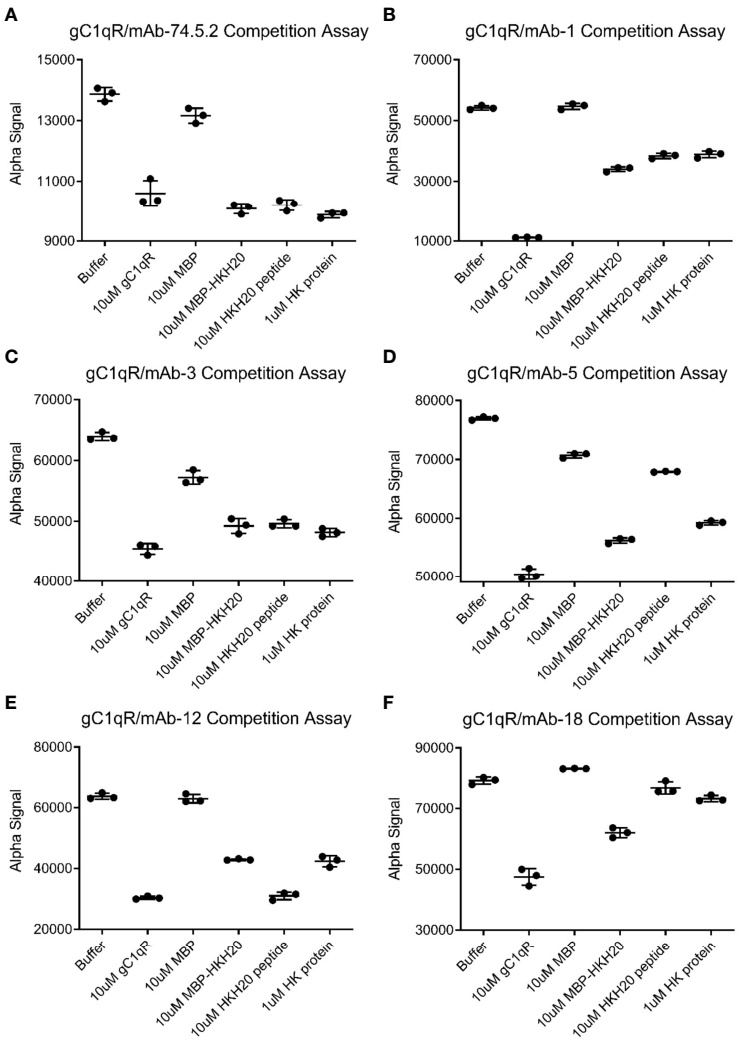

FIGURE 4 | Competitive Behavior of Novel Monoclonal Antibodies on the Interaction of gC1qR with High-Molecular Weight Kininogen (HMWK) Derived Ligands. Various anti-gC1qR monoclonal antibodies were incubated with chemically biotinylated gC1qR and used to generate a luminescent signal using a bead-based AlphaAssay approach. The abilities of a single concentration of HMWK-derived ligands, or various controls, to compete the luminescent signal were measured in triplicate. **(A)** Data for competition of binding between biotinylated gC1qR and mAb-74.5.2, which is known to block binding of HMWK to gC1qR (1, 24). Data shown in this panel were modified from Ghebrehiwet et al. (1). **(B)** Data for competition of binding between biotinylated gC1qR and mAb-1. **(C)** Data for competition of binding between biotinylated gC1qR and mAb-3. **(D)** Data for competition of binding between biotinylated gC1qR and mAb-5. **(E)** Data for competition of binding between biotinylated gC1qR and mAb-12. **(F)** Data for competition of binding between biotinylated gC1qR and mAb-18. Note that the wider black line represents the mean of the three measurements, while the thinner lines are values plus and minus one standard deviation.

set of rate constants, we found that the FXII/gC1qR-avi interaction was well-described by two independent binding sites (**Figure 6A** and **Table S1** c.f. **Table 2**).

We then compared the parameters for FXII and FXIIa binding to captured gC1qR-avi to gC1qR-avi that had been presaturated with various monoclonal antibodies (**Figure 6**, **Figures S3**, **S4**, and **Table S1**). As we hypothesized from examination of the FXII-FNII/gC1qR structure (11) and the epitope mapping study described above (**Figure 5**), we found that presaturation with mAb-1 diminished the signal from injecting either FXII (**Figure 6B**) or FXIIa (**Figure 6H**) by roughly 40% across all concentrations when compared to controls. Inspection of the fitting parameters suggested that perturbation of both binding sites was responsible for this effect, as the overall saturation level (i.e. $R_{max\text{-}1}$ and $R_{max\text{-}2}$) dropped to a comparable extent when compared to the control values (**Table S1**). We also found that mAb-1 partially inhibited FXII and FXIIa binding to gC1qR-avi at higher gC1qR capture densities (**Figure S4** and **Table S1**). Interestingly, we found that mAb-3 was a poor inhibitor of FXII (**Figure 6C**) and FXIIa (**Figure 6I**) binding at low gC1qR-avi capture densities, but comparable to mAb-1 at higher gC1qR-avi capture densities (**Figure S4**). Surprisingly, when we presaturated the gC1qR-avi surface with either mAb-5 (**Figure 6D**), mAb-12 (**Figure 6E**), or

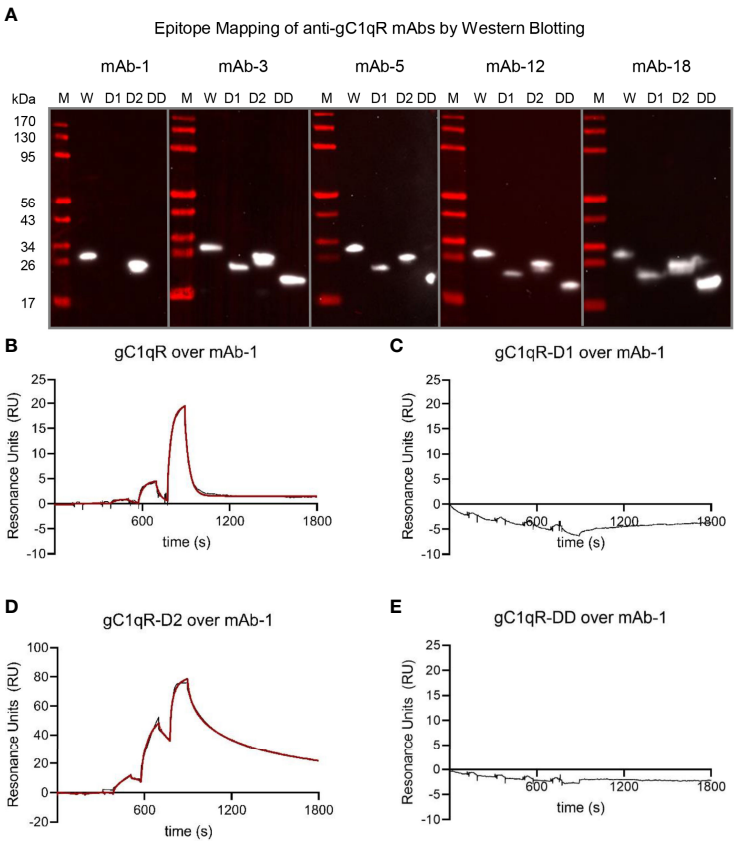

FIGURE 5 | The Epitope of mAb-1 Lies in the First Acidic Loop of gC1qR. The locations of the epitopes for novel anti-gC1qR monoclonal antibodies were mapped using a combination of Western blotting and surface plasmon resonance. **(A)** Epitope mapping by Western blotting. Samples of wild-type gC1qR, gC1qR-D1, gC1qR-D2, and gC1qR-DD were separated by SDS-PAGE, transferred to membranes, and probed with various monoclonal antibodies prior to detection using a chemiluminescent approach. Images representing individual experiments are separated by grey lines, while the values for molecular weight standards are shown at the left of the panel. Note that only mAb-1 showed differential reactivity to forms of gC1qR missing the acidic loops. **(B)** Reference-corrected sensorgram from a single-cycle kinetic study where a five-fold dilution series of wild-type gC1qR (1 μM highest concentration) was injected over a surface of immobilized mAb-1. The black trace represents the experimental data, while the red line represents the outcome of fitting to a kinetic model. **(C)** Identical to panel **(B)**, except that gC1qR-D1 served as the analyte. **(D)** Identical to panel **(B)**, except that gC1qR-D2 served as the analyte. **(E)** Identical to panel **(B)**, except that gC1qR-DD served as the analyte. Note that panels **(C, E)** do not show the outcome of a fit, since there was no appreciable binding of mAb-1 to those analytes.

mAb-18 (**Figure 6F**), we observed generally similar inhibition of FXII binding as we found for mAb-1 (**Figure 6A**), and the same was also true for binding of FXIIa (**Figures 6J–L**). Moreover, we observed a similar effect on FXII and FXIIa binding at higher gC1qR capture densities following presaturation with mAb-1, mAb-5, mAb-12, and mAb-18 (**Figure S4**).

Examination of the fitting parameters from experiments on both FXII and FXIIa failed to identify any single antibody or group of antibodies that were more potent inhibitors than the others (**Figure S3** and **Table S1**), even though these antibodies have diverse biochemical properties and appear to recognize distinct epitopes on gC1qR (**Figures 3**–**5**). Furthermore, while select antibodies (i.e. mAb-3) manifest increased potency as a function of gC1qR capture densities (**Figures 6** and **S4**), the resulting inhibitory effect never exceeded that displayed by any of the others. As a group, the most obvious effect these antibodies had on gC1qR binding to FXII and FXIIa was partial lowering of both apparent R_{max} values when compared to uninhibited controls (**Figure S3** and **Table S1**). Although multiple anti-gC1qR antibodies interfere with binding of FXII and FXIIa to gC1qR to an extent, no antibody in this collection was entirely effective in blocking these interactions completely.

DISCUSSION

gC1qR at the surface of endothelial cells can bind to C1q, whereby it triggers the classical pathway of complement, as well as FXII, HMWK, and PK, whereby it initiates both the contact system of coagulation and the kinin-generating system (1). Despite the fact that they are conceptually distinct, these pathways appear to participate in extensive crosstalk with one another in a variety of physiological and pathophysiological settings (25, 26). While further defining these interrelationships is a topic of active

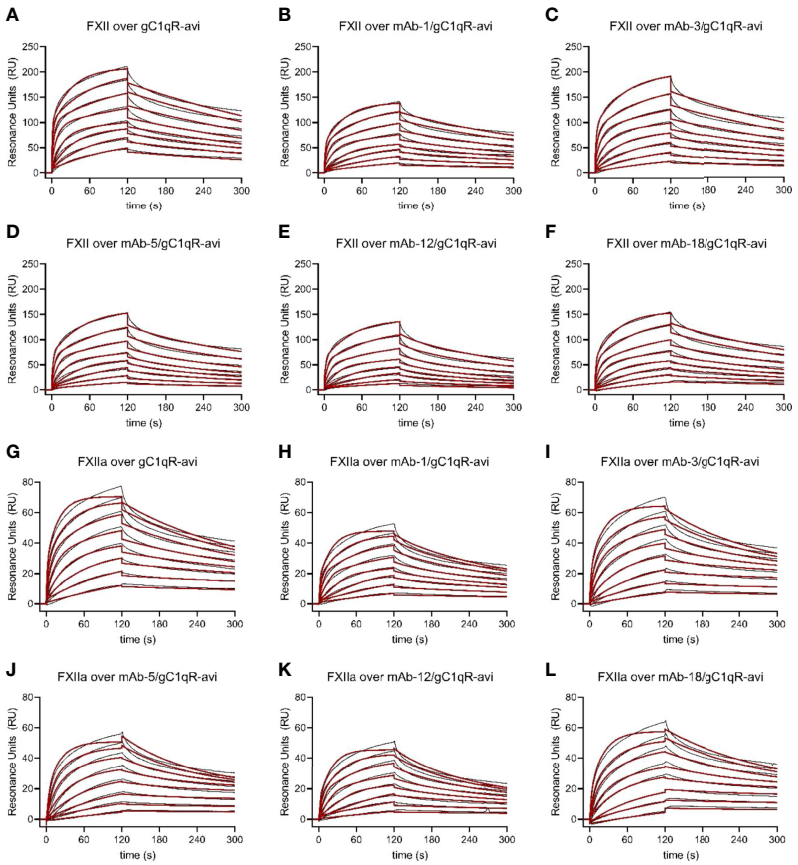

FIGURE 6 | Multiple anti-gC1qR Antibodies Interfere with Binding of Factor XII and Factor XIIa to gC1qR. Wild-type gC1qR was enzymatically biotinylated through a C-terminal avi-tag and captured to a density of ~100 RU on the experimental flow cells of a streptavidin-derivatized sensor chip. After confirmation of mAb binding to the captured gC1qR-avi using a single-cycle kinetic experiment (*Data Not Shown*), the impact of that mAb on FXII and FXIIa binding to gC1qR was assessed by pre-loading a single flow cell with saturating levels of the mAb followed by injecting various concentrations of FXII and FXIIa over all three experimental flow cells. **(A)** Dose-response sensorgram series (black traces) and fits (red traces) for injection of FXII over a gC1qR-avi surface. **(B)** Analogous to panel **(A)**, except with presaturation of mAb-1. **(C)** Analogous to panel **(A)**, except with presaturation of mAb-3. **(D)** Analogous to panel **(A)**, except with presaturation of mAb-5. **(E)** Analogous to panel (A), except with presaturation of mAb-12. **(F)** Analogous to panel **(A)**, except with presaturation of mAb-18. **(G)** Dose-response sensorgram series (black traces) and fits (red traces) for injection of FXIIa over a gC1qR-avi surface. **(H)** Analogous to panel **(G)**, except with presaturation of mAb-1. **(I)** Analogous to panel **(G)**, except with presaturation of mAb-3. **(J)** Analogous to panel **(G)**, except with presaturation of mAb-5. **(K)** Analogous to panel **(G)**, except with presaturation of mAb-12. **(L)** Analogous to panel **(G)**, except with presaturation of mAb-18.

investigation, the large number of gC1qR ligands (1) and the paucity of detailed structural and biochemical information on how these interactions form remains a significant obstacle to therapeutic development. A major breakthrough in this area was made recently when Kaira et al. reported the structure of the FXII-FNII bound to gC1qR (11). Although FXII-FNII represents only a small fragment (~10 kDa) of the much larger FXII protein (~80 kDa including glycosylation), this structure revealed important details about FXII/gC1qR interactions. Among these were the identification of the second acidic loop of gC1qR (i.e. residues 190-201) as a key binding determinant for asymmetric assembly of the gC1qR/FXII and gC1qR/FXII/HMWK complexes (11). Whereas the binding site for FXII-FNII is present in each gC1qR polypeptide, only one site appears to be occupied in the context of the gC1qR trimer. Steric occlusion of the otherwise equivalent binding sites has been suggested to be responsible for preventing additional FXII-FNII from binding to gC1qR (11). Presumably, this effect would be exacerbated in the case of full-length FXII, or in the presence of other large ligands such as HMWK.

Since both acidic loops project from the same face of the gC1qR trimer (9), we hypothesized that large molecules, including antibodies, that bind to either of the acidic loops of gC1qR might inhibit FXII binding. In this study, we identified a new monoclonal antibody (mAb-1) that bound specifically to an epitope within the first acidic loop of gC1qR (i.e. residues 139-163) (**Figure 5**); although these residues do not represent the FXII-FNII binding site *per se*, the apparent physical proximity of the acidic loops to one another in the gC1qR structure (9) suggested that this antibody might still interfere with FXII binding. Indeed, we found that presaturation with mAb-1

reduced the number of available binding sites, as judged by its effects on the R_{max} associated with both binding sites on gC1qR for FXII (**Figures 6**, **S4** and **Table S1**). Although we observed a similar effect for mAb-1 on binding of FXIIa (**Figures 6**, **S4**, and **Table S1**), we found that inhibition of FXII-FNII binding appeared to be slightly more modest (**Figure S5**). We suspect that the presence of the ~150 kDa antibody bound to acidic loop 1 could not fully block access of the much smaller FXII-FNII (~10 kDa) to its binding site on acidic loop 2. Curiously, though, we found that several other monoclonal antibodies which recognize distinct gC1qR epitopes from mAb-1 (**Figures 3**–**5**) also seemed to inhibit FXII binding to a similar extent (**Figures 6**, **S3**, **S4**, and **Table S1**). We interpret this to mean that the presence of almost any exogenous gC1qR ligand the size of a ~150 kDa antibody might inhibit binding of the ~80 kDa FXII to gC1qR to some degree. We believe this concept might be generally relevant to this system, since all the monoclonal antibodies examined here except mAb-18 also perturbed binding of the ~110 kDa HMWK to gC1qR (**Figure 4**). While we only investigated their effects on binary gC1qR complexes, the ability of our monoclonal antibodies to interfere with the higher-order gC1qR/FXII/HMWK assemblies identified by Kaira et al. (11) seems likely.

Although they recognize distinct epitopes on gC1qR (**Figures 3**–**5**), we found that each of the monoclonal antibodies described here binds gC1qR with a relatively high apparent affinity (**Figure 3**). This raises questions as to why each these monoclonal antibodies appear to block FXII binding partly, but not completely (**Figures 6**, **S3**, **S4**, and **Table S1**). Paradoxically, we believe that size is an important consideration in this respect as well. Examination of the gC1qR structure shows that its ring-like assembly is approximately 75 Å in diameter (9). Examination of the structure for an intact IgG-class antibody however reveals that the distal ends of its two antigen-binding F(ab) motifs are separated by greater than 140 Å through space (27). While the hinge regions of antibodies clearly provide for some flexibility, it seems unlikely that both antigen-binding sites of an intact monoclonal antibody could bind their cognate epitopes in a single gC1qR trimer. Consistent with this idea, we noted that the sensorgrams obtained by injecting either mAb-12 or mAb-13 over gC1qR were well-described by Langmuir binding models (*Data Not Shown*). In light of these considerations, we believe the trimeric assembly of gC1qR presents a unique quandary for inhibitor design such that intact monoclonal antibodies may not be the best route forward. Although intact antibodies may be able to bridge adjacent gC1qR trimers such as those proposed by Kaira et al. (11), smaller fragments of high affinity monoclonal antibodies, such as F(ab) or scFv, or alternatives such as camelid-derived nanobodies (i.e. VHH), may provide high-affinity binders in a smaller overall size that could more effectively occupy each of the potential binding sites in a single gC1qR trimer. Such molecules might also provide the advantage of not activating downstream immune effector functions against endothelia, including the classical complement pathway and/or antibody-dependent cytotoxicity *via* FcγR-bearing immune cells, as this might have undesirable consequences in diseases like hereditary angioedema. Clearly, additional work will be needed to identify inhibitors with these properties and to fully evaluate them in appropriate models of disease.

Whereas the acidic loop regions of gC1qR have received considerable attention in our work here and elsewhere (9–11), the most prominent structural feature of the gC1qR trimer is its ring-like assembly (9, 10). In the present report, we provided additional information on this aspect of gC1qR by determining a 2.2 Å resolution crystal structure of a gC1qR double loop deletion mutant (i.e. gC1qR-DD). We found that gC1qR-DD behaved as a trimer in solution and this arrangement was likewise visible in its crystal structure (**Figure 2**). We also found that gC1qR-DD bound tightly to both FXII and FXIIa with apparent affinity in the low nanomolar range (**Figure 2** and **Table 2**). This latter result was particularly intriguing considering the FXII-FNII/gC1qR crystal structure (11), which could be interpreted as arguing that the second acidic loop is the only determinant of gC1qR binding to FXII and FXIIa. Yet considering the FXII-FNII/gC1qR structure (11) alongside the information presented here (**Figure 2** and **Table 2**), we suspect that the interaction between FXII/FXIIa and gC1qR most likely involves sites derived from the second acidic loop of gC1qR as well as its trimeric core and, equally importantly, additional regions of FXII besides its N-terminal FNII domain. Indeed, such a model is easiest to reconcile with the extensive binding studies we present here (**Figures 2**, **6**, **Table 2**, **Figures S2**, **S4**, and **Table S1**). Although additional structural information would be invaluable in deciphering how gC1qR binds FXII/FXIIa, obtaining it is likely to be challenging since this interaction is not adequately described by reductionist biochemical models (e.g. domain fragments) even though these are often more tractable for structural studies.

There remain some inconsistencies in the literature regarding how gC1qR interacts with HMWK. However, both our group (1) and others (11) have shown previously that peptides derived from HMWK residues 493-516 bind gC1qR with affinities in the 1-10 μM range independently of metal-ion cofactor. Here we expanded on this observation by showing that none of our loop deletion mutants in gC1qR lost their ability to bind the HMWK-derived peptide HKH-20 in an SPR study (**Figure 1**). Again, these results were consistent with that those of Kaira et al., who used a combination of deletion mutagenesis and isothermal titration calorimetry to show that a region encompassing residues 214-224 of gC1qR is a critical determinant for HMWK binding (11). It is interesting to note that these residues lie at the bottom of the central cavity formed upon gC1qR trimerization (9) and that this area is not perturbed in the gC1qR-DD crystal structure (**Figures 2C, D**). Still, this raises questions about not only these residues' accessibility for HMWK binding, but whether any structural rearrangements need to occur in gC1qR prior to binding HMWK. We believe continued dissection of these questions from a structurally-oriented perspective will be required not only to understand how gC1qR, HMWK, and FXII interact with one another, but to

determine how best to block these interactions for therapeutic purposes.

DATA AVAILABILITY STATEMENT

The datasets presented in this study can be found in online repositories. The names of the repository/repositories and accession number(s) can be found below: PDB, accession code: 7TE3.

AUTHOR CONTRIBUTIONS

YZ: designed and performed protein-protein interaction experiments and analyzed data. AV: assisted with characterization of monoclonal antibodies and binding studies. EK: assisted with characterization of monoclonal antibodies and binding studies. XX: assisted with characterization of monoclonal antibodies and binding studies. NP: assisted with characterization of monoclonal antibodies and binding studies. KR: assisted with characterization of monoclonal antibodies, binding studies, and X-ray crystallography. BGa: assisted with characterization of monoclonal antibodies, binding studies, and analyzed data BGh: designed of the overall scope of the study and wrote the manuscript. BGe: designed of the overall scope of the study, analyzed data, and wrote the manuscript. All authors contributed to the article and approved the submitted version.

FUNDING

This research was supported by U.S. National Institutes of Health grant R35GM140852 to BGe and grant R56AI122376 to BGh. We also acknowledge the Terry C. Johnson Center of Kansas State University for its generous support of the initial stages of this work and for support of AV and EK as Cancer Research Awardees.

ACKNOWLEDGMENTS

X-ray diffraction data were collected at Southeast Regional Collaborative Access Team (SER-CAT) 22-BM beamline at the Advanced Photon Source, Argonne National Laboratory. A list of supporting institutions may be found on the SER-CAT website. Use of the Advanced Photon Source was supported by the U.S. Department of Energy, Office of Science, Office of Basic Energy Sciences, under Contract No. W-31-109-Eng-38.

SUPPLEMENTARY MATERIAL

The Supplementary Material for this article can be found online at: https://www.frontiersin.org/articles/10.3389/fimmu.2022.887742/full#supplementary-material

REFERENCES

1. Ghebrehiwet B, Geisbrecht BV, Xu X, Savitt AG, Peerschke EIB. The C1q Receptors: Focus on Gc1qr/P33 (C1qbp, P32, Habp-1). *Semin Immunol* (2019) 45:101338. doi: 10.1016/j.smim.2019.101338
2. Yagi M, Uchiumi T, Takazaki S, Okuno B, Nomura M, Yoshida S-I, et al. P32/Gc1qr Is Indispensable for Fetal Development and Mitochondrial Translation: Importance of Its Rna-Binding Ability. *Nucleic Acids Res* (2012) 40:9717–37. doi: 10.1093/nar/gks774
3. Dembitzer FR, Kinoshita Y, Burstein D, Phelps RG, Beasley MB, Garcia R, et al. Gc1qr Expression in Normal and Pathologic Human Tissues: Differential Expression in Tissues of Epithelial and Mesenchymal Origin. *J Histochem Cytochem* (2012) 60:467–74. doi: 10.1369/0022155412440882
4. Chen Y-B, Jiang C-T, Zhang G-Q, Wang J-S, Pang D. Increased Expression of Hyaluronic Acid Binding Protein 1 Is Correlated with Poor Prognosis in Patients with Breast Cancer. *J Surg Oncol* (2009) 100:382–6. doi: 10.1002/jso.21329
5. Niu M, Sun S, Zhang G, Zhao Y, Pang D, Chen Y. Elevated Expression of Habp1 Is Correlated with Metastasis and Poor Survival in Breast Cancer Patients. *Am J Cancer Res* (2015) 5:1190–8.
6. Peerschke EI, de Stanchina E, Chang Q, Manova-Todorova K, Barlas A, Savitt AG, et al. Anti Gc1qr/P32/Habp1 Antibody Therapy Decreases Tumor Growth in an Orthotopic Murine Xenotransplant Model of Triple Negative Breast Cancer. *Antibodies* (2020) 9:51. doi: 10.3390/antib9040051
7. Fandaros M, Joseph K, Kaplan AP, Rubenstein DA, Ghebrehiwet B, Yin W. Gc1qr Antibody Can Modulate Endothelial Cell Permeability in Angioedema. *Inflammation* (2022) 45:116–28. doi: 10.1007/s10753-021-01532-w
8. Ghebrehiwet B, Lim BL, Peerschke EI, Willis AC, Reid KB. Isolation, Cdna Cloning, and Overexpression of a 33-Kd Cell Surface Glycoprotein That Binds to the Globular "Heads" of C1q. *J Exp Med* (1994) 179:1809–21. doi: 10.1084/jem.179.6.1809
9. Jiang J, Zhang Y, Krainer AR, Xu RM. Crystal Structure of Human P32, a Doughnut-Shaped Acidic Mitochondrial Matrix Protein. *Proc Natl Acad Sci USA* (1999) 96:3572–7. doi: 10.1073/pnas.96.7.3572
10. Ghebrehiwet B, Jesty J, Peerschke EIB. Gc1q-R/P33: Structure-Function Predictions from the Crystal Structure. *Immunobiology* (2002) 205:421–32. doi: 10.1078/0171-2985-00143
11. Kaira BG, Slater A, McCrae KR, Dreveny I, Sumya U, Mutch NJ, et al. Factor Xii and Kininogen Asymmetric Assembly with Gc1qr/C1qbp/P32 Is Goverened by Allostery. *Blood* (2020) 136:1685–97. doi: 10.1182/blood.2020004818
12. Geisbrecht BV, Bouyain S, Pop M. An Optimized System for the Expression and Purification of Secreted Bacterial Proteins. *Prot Expr Purif* (2006) 46:23–32. doi: 10.1016/j.pep.2005.09.003
13. Barta ML, Skaff DA, McWhorter WJ, Herdendorf TJ, Miziorko HM, Geisbrecht BV. Crystal Structures of Staphylococcus Epidermidis Mevalonate Diphosphate Decarboxylase Bound to Inhibitory Analogs Reveal New Insight into Substrate Binding and Catalysis. *J Biol Chem* (2011) 286:23900–10. doi: 10.1074/jbc.M111.242016
14. Fairhead M, Howarth M. Site-Specific Biotinylation of Purified Proteins Using Bira. *Methods Mol Biol* (2015) 1266:171–84. doi: 10.1007/978-1-4939-2272-7_12
15. Otwinowski Z, Minor W. Processing of X-Ray Diffraction Data Collected in Oscillation Mode. *Methods Enzymol* (1997) 276:307–26. doi: 10.1016/S0076-6879(97)76066-X
16. McCoy AJ, Grosse-Kunstleve RW, Adams PD, Winn MD, Storoni LC, Read RJ. Phaser Crystallographic Software. *J Appl Cryst* (2007) 40:658–74. doi: 10.1107/S0021889807021206
17. Adams PD, Afonine PV, Bunkoczi G, Chen VB, Davis IW, Echols N, et al. Phenix: A Comprehensive Python-Based System for Macromolecular Structure Solution. *Acta Cryst D Biol Crystallogr* (2010) 66:213–21. doi: 10.1107/S0907444909052925
18. Emsley P, Lohkamp B, Scott WG, Cowtan K. Features and Development of Coot. *Acta Cryst D Biol Crystallogr* (2010) 66:486–501. doi: 10.1107/S0907444910007493
19. Nakazawa Y, Joseph K, Kaplan AP. Inhibition of Contact Activation by a Kininogen Peptide (Hkh20) Derived from Domain 5. *Int Immunopharm* (2002) 2:1875–85. doi: 10.1016/S1567-5769(02)00182-0
20. Garcia BL, Summers BJ, Ramyar KX, Tzekou A, Lin Z, Ricklin D, et al. A Structurally Dynamic N-Terminal Helix Is a Key Functional Determinant in

Staphylococcal Complement Inhibitor (Scin) Proteins. *J Biol Chem* (2013) 288:2870–81. doi: 10.1074/jbc.M112.426858
21. Garcia BL, Summers BJ, Zhuoer L, Ramyar KX, Ricklin D, Fu Z-Q, et al. Diversity in the C3b Contact Residues and Tertiary Structures of the Staphylococcal Complement Inhibitor (Scin) Protein Family. *J Biol Chem* (2012) 287:628–40. doi: 10.1074/jbc.M111.298984
22. Garcia BL, Skaff DA, Chatterjee A, Hanning A, Walker JK, Wyckoff GJ, et al. Identification of C3b-Binding Small-Molecule Complement Inhibitors Using Cheminformatics. *J Immunol* (2017) 198:3705–18. doi: 10.4049/jimmunol.1601932
23. Ghebrehiwet B, Jesty J, Xu S, Vinayagasundaram R, Vinayagasundaram U, Ji Y, et al. Structure-Function Studies Using Deletion Mutants Identify Domains of Gc1qr/P33 as Potential Therapeutic Targets for Vascular Permeability and Inflammation. *Front Immunol* (2011) 2:58. doi: 10.3389/fimmu.2011.00058
24. Joseph K, Ghebrehiwet B, Peerschke EI, Reid KB, Kaplan AP. Identification of the Zinc-Dependent Endothelial Cell Binding Protein for High Molecular Weight Kininogen and Factor Xii: Identity with the Receptor That Binds to the Globular "Heads" of C1q (Gc1q-R). *Proc Natl Acad Sci USA* (1996) 93:8552–7. doi: 10.1073/pnas.93.16.8552
25. Markiewski MM, Nilsson B, Ekdahl KN, Mollnes TE, Lambris JD. Complement and Coagulation: Strangers or Partners in Crime? *Trends Immunol* (2007) 28:184–92. doi: 10.1016/j.it.2007.02.006
26. Oikonomopoulou K, Ricklin D, Ward PA, Lambris JD. Interactions between Coagulation and Complement - Their Role in Inflammation. *Semin Immunopathol* (2012) 34:151–65. doi: 10.1007/s00281-011-0280-x
27. Harris LJ, Skaletsky E, McPherson A. Crystallographic Structure of an Intact Igg1 Monoclonal Antibody. *J Mol Biol* (1998) 275:861–72. doi: 10.1006/jmbi.1997.1508

Conflict of Interest: The authors declare that the research was conducted in the absence of any commercial or financial relationships that could be construed as a potential conflict of interest.

Publisher's Note: All claims expressed in this article are solely those of the authors and do not necessarily represent those of their affiliated organizations, or those of the publisher, the editors and the reviewers. Any product that may be evaluated in this article, or claim that may be made by its manufacturer, is not guaranteed or endorsed by the publisher.

frontiers | Frontiers in Immunology

REVIEW
published: 06 July 2022
doi: 10.3389/fimmu.2022.958121

Proprotein Convertases and the Complement System

*József Dobó**, *Andrea Kocsis*, *Ráhel Dani* and *Péter Gál**

Institute of Enzymology, Research Centre for Natural Sciences, Budapest, Hungary

Proteins destined for secretion - after removal of the signal sequence - often undergo further proteolytic processing by proprotein convertases (PCs). Prohormones are typically processed in the regulated secretory pathway, while most plasma proteins travel though the constitutive pathway. The complement system is a major proteolytic cascade in the blood, serving as a first line of defense against microbes and also contributing to the immune homeostasis. Several complement components, namely C3, C4, C5 and factor I (FI), are multi-chain proteins that are apparently processed by PCs intracellularly. Cleavage occurs at consecutive basic residues and probably also involves the action of carboxypeptidases. The most likely candidate for the intracellular processing of complement proteins is furin, however, because of the overlapping specificities of basic amino acid residue-specific proprotein convertases, other PCs might be involved. To our surprise, we have recently discovered that processing of another complement protein, mannan-binding lectin-associated serine protease-3 (MASP-3) occurs in the blood by PCSK6 (PACE4). A similar mechanism had been described for the membrane protease corin, which is also activated extracellularly by PCSK6. In this review we intend to point out that the proper functioning of the complement system intimately depends on the action of proprotein convertases. In addition to the non-enzymatic components (C3, C4, C5), two constitutively active complement proteases are directly activated by PCs either intracellularly (FI), or extracellularly (MASP-3), moreover indirectly, through the constitutive activation of pro-factor D by MASP-3, the activity of the alternative pathway also depends on a PC present in the blood.

Keywords: complement system, proprotein convertase, lectin pathway, alternative pathway, classical pathway, protein secretion and processing, MASP-3

OPEN ACCESS

Edited by:
Simon John Clark,
University of Tübingen, Germany

Reviewed by:
Angela Armento,
University of Tübingen, Germany
Kenneth Reid,
University of Oxford, United Kingdom

****Correspondence:***
József Dobó
dobo.jozsef@ttk.hu
Péter Gál
gal.peter@ttk.hu

Specialty section:
This article was submitted to Molecular Innate Immunity, a section of the journal Frontiers in Immunology

Received: *31 May 2022*
Accepted: *13 June 2022*
Published: *06 July 2022*

Citation:
Dobó J, Kocsis A, Dani R and Gál P (2022) Proprotein Convertases and the Complement System. Front. Immunol. 13:958121. doi: 10.3389/fimmu.2022.958121

SYNOPSIS OF THE COMPLEMENT SYSTEM

The complement system (**Figure 1A**) is an integral part of the immune system. It is the most powerful molecular effector arm of the innate immune system, but it is also connected to the adaptive immunity in many ways [for reviews see (1–4)]. The most important components of the complement system are serine proteases (**Figure 1B**), which form a proteolytic cascade system (5). Other components include pattern recognition molecules (C1q, MBL, ficolins), the thioester-containing molecules (C3, C4), the components of the membrane attack complex (C5, C6, C7, C8, C9), membrane-bound receptors and

regulators, and fluid-phase regulators. These proteins act in synergy to monitor surfaces, and to label and eliminate invading pathogen microbes or damaged or altered self-cells. Because of the cascade-like manner of complement activation the initial activation signal is amplified tremendously and results in a highly efficient cytotoxic effect and in releasing potent inflammation-promoting proteolytic fragments (e.g. anaphylatoxins). The activity of the complement system is regulated in many ways to avoid self-tissue damage and to focus the complement-mediated damage to the pathogens. Uncontrolled, excessive activation of the complement system could result in or contribute to the development of many serious diseases [for reviews see (6–8)].

Depending on the activation-surface the complement cascade can be activated through three different pathways: the classical, the lectin, and the alternative pathways (**Figure 1A**). Immune complexes are the most powerful activators of the classical pathway. C1q binds to the IgG or IgM components of the immune complexes which results in the activation of the C1r and C1s serine proteases (9, 10). One C1q molecule with two C1r and two C1s molecules form the C1 complex (11). C1s is the executive protease of the C1 complex. It cleaves the subsequent components of the classical pathway: C4 and C2. The bigger proteolytic fragment of C4, C4b binds to the surface through an ester or amid bound and captures C2, the serine protease component of the classical pathway C3-convertase enzyme complex. C4b-bound C2 is cleaved and activated by C1s, yielding the C4bC2a complex.

Abbreviations: ↓, indicates a cleavage site; 3MC, Malpuech-Michels-Mingarelli-Carnevale (syndrome) aka, also known as; BAR-PC, basic amino acid residue-specific proprotein convertase; C1…C9, complement component 1-9; C1q, C1r, C1s, subcomponents of C1; C4BP, C4b-binding protein; CHO, Chinese hamster ovary (cells); CHRD, cysteine- and histidine-rich domain; CR1, complement receptor 1 (aka C3b/C4b receptor); CRD, cysteine-rich domain; dec-RVKR-cmk, decanoyl-Arg-Val-Lys-Arg-chloromethylketone; ER, endoplasmic reticulum; FB, factor B; FD, factor D; FH, factor H; FI, factor I; FIMAC, factor I membrane attack complex (domain); Gdf11, growth/differentiation factor 11; IGF-II, insulin-like grow factor-II; IGFBP-5, insulin-like growth factor-binding protein 5; HEK, human embryonic kidney (cells); Hep3B, a human hepatoma cell line; HepG2, a human hepatoma cell line; HDL, high-density lipoprotein; HSPG, heparan sulfate proteoglycans; HUVEC, human umbilical vein endothelial cells; L1, neural adhesion molecule L1; LDL, low-density lipoprotein; LDLRA, low-density lipoprotein receptor type A (domain); LDLR, low-density lipoprotein receptor; MASP, mannan-binding lectin-associated serine protease; MAp44, mannan-binding lectin-associated protein 44 (kDa); MBL, mannan-binding lectin; MBTPS1, membrane-bound transcription factor protease, site-1 (aka SKI-1); MCP, membrane cofactor protein; MMP, matrix metalloprotease; NARC-1, neural apoptosis regulated convertase 1; NEC, neuroendocrine convertase; NPLC-KC, a human hepatoma cell line; PACE, paired basic amino acid-cleaving enzyme (aka furin, PCSK3); PACE4, paired basic amino acid-cleaving enzyme 4 (aka PCSK6); PC, proprotein convertase; PCSK, proprotein convertase subtilisin/kexin; PCSK1-9, proprotein convertase subtilisin/kexin type 1-9; PC5A, secreted, short isoform of PCSK5 (aka PC6A); PC5B, membrane-bound, long isoform of PCSK5 (aka PC6B); PDGF, platelet-derived growth factor; RGD, tripeptide motif of Arg-Gly-Asp; RPTPμ, receptor protein tyrosine phosphatase μ; S1P, site-1 protease; SKI-1, subtilisin/kexin-isozyme 1 (aka MBTPS1); SP, serine protease (domain); SPC4, subtilisin-like proprotein convertase 4 (aka PCSK6); TGN, trans-Golgi network; TGF-β, transforming growth factor-β; TIMP, tissue inhibitors of metalloproteases; VSMC, vascular smooth muscle cells.

The activation of the lectin pathway generates the same C3 convertase complex as the classical pathway. In the lectin pathway there are various pattern recognition molecules (MBL, ficolins, collectins) that are associated with the serine protease components MASPs (12). Upon the pattern recognition molecules bind to the carbohydrate pattern on the surface of the bacteria, MASP-1 autoactivates and activates MASP-2 (13). MASP-2 cleaves C4, while C2 is cleaved by both MASP-1 and MASP-2 generating the C4b2a convertase complex. Regardless of the activation route, C3 is cleaved by the C3 convertase complexes into two pieces. The bigger fragment, C3b binds to the activation surface like C4b, while the smaller fragment, the anaphylatoxin C3a is released to the circulation.

The alternative pathway initiates when C3b appears on the activation surface (14). C3b captures FB and the C3b-bound FB is cleaved by FD. FD is continuously cleaved by MASP-3 in the blood, even before the advent of any activation signal. C3bBb is the alternative pathway C3 convertase, which cleaves more C3b resulting in generation of more C3 convertase complexes. This positive feed-back mechanism ensures the amplification of the complement activation initiated by either the classical or the alternative pathway (15). The alternative pathway can also be initiated on its own through the so-called "tick-over" mechanism (16). C3 slowly hydrolyses in the circulation and the resulting C3 (H_2O) resembles to C3b. C3(H_2O) binds FB, which is cleaved by FD. C3(H_2O)Bb is a fluid phase C3 convertase which can generate C3b near any surface. The surfaces of the self-cells are protected by different complement inhibitors against complement-mediated damage. On the unprotected surfaces (e.g. bacterial surface), however, the deposited C3b initiates the amplification loop of the alternative pathway leading to full-scale complement activation.

When the density of the deposited C3b reaches a certain point the specificity of the C3 convertase complexes switches to C5 (17, 18), which are traditionally regarded as the C5 convertases ($C4b2aC3b_n$, $C3bBbC3b_n$). From this point the three activation pathways continue in a common terminal pathway. The smaller proteolytic fragment of C5, C5a is an extremely potent anaphylatoxin. The larger proteolytic fragment, C5b, binds C6 and C7. The C5b-7 complex associates with the membrane of the invaded cells and captures C8 and multiple C9 molecules (19). After conformational changes the C5b-9 complex forms a pore on the cell membrane resulting in the lysis and destruction of the target cell.

Since the complement system is potentially dangerous to the host, there are various mechanisms to control complement activity. The activity of the serine proteases of the complement system is regulated by two ways. The first way is zymogen activation. Most of the serine proteases of the complement system are synthetized and secreted as inactive zymogens (5). Activation during the cascade reaction occurs through limited proteolysis. The one-chain zymogen molecule is cleaved at the activation peptide, and the resulting two-chain molecule has the full proteolytic activity. The logic behind the amplification power of the proteolytic cascade systems lies in that each active serine protease cleaves and activates multiple zymogen

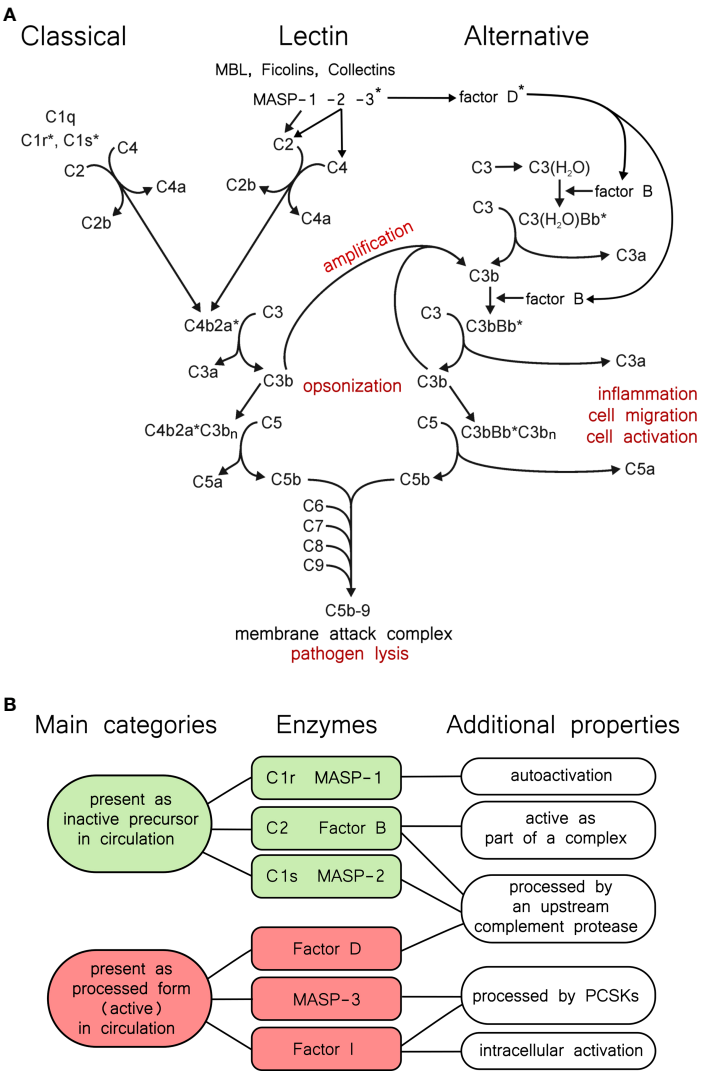

FIGURE 1 | The complement system and properties of its proteases. **(A)** Overview of the complement system. The three activation routes, the amplification loop, and the terminal pathway are described in the text, and this panel is intended to aid the reader as a guide. Asterisks indicate active proteases. **(B)** Categories of complement proteases by activation status. Green and red shading indicates the two main categories. Typical serine proteases are synthesized in the proenzyme form, and remain proenzymic until a they are cleaved into the active form following a trigger. In the complement system C1r, C1s, MASP-1, and MASP-2 fall into this category. Among these, C1r and MASP-1 can efficiently autoactivate. MASP-3, FD, and FI, are present predominantly (or completely) in the active form in the blood, however they have very narrow substrate specificities. C2 and FB are special cases, because they gain a transient activity following cleavage as parts of the C4bC2a, or the C3bBb complex.

molecules downstream the cascade. In this way an exponential amplification scheme ensures the efficient answer against the initial stimulus. The other proteolytic cascade systems in the blood (e.g. blood coagulation, fibrinolysis) work on the same principle (20). These cascade systems are evolutionary and functionally closely related and there are many cross-talks between them. Probably the most interesting step in the cascade reaction is the first proteolytic step, which is an autoactivation in the case of the classical and the lectin pathway. In this case the "inactive" zymogen molecule has some low proteolytic activity, that is enough to activate another zymogen molecule. The resulting active protease then activates more zymogen molecules with high efficiency. C1r in the classical pathway and MASP-1 in the lectin pathway have pronounced autoactivation capacity (**Figure 1B**). MASP-2 also can autoactivate, however, it takes place only in high concentration and after prolonged incubation (21). This is not the physiological case; in order to get a quick and efficient lectin pathway activation MASP-1 autoactivates and cleaves zymogen MASP-2 (13). Interestingly, active MASP-2 cleaves zymogen MASP-1 more efficiently, than zymogen MASP-2 (22). Zymogen C1s has no autoactivation ability, it is cleaved exclusively by C1r. The serine proteases of the C3/C5 convertase complexes, C2 and FB, also cannot autoactivate. C2

TABLE 1 | Human (mammalian) proprotein convertase genes and major protein variants.

gene	protein name PCSK nomenclature	other common protein name(s)	intracellular lumenal (L), membrane-bound (M), or secreted (S)	cleaves after basic (B), or non-basic (N) residues	notes
PCSK1/ NEC1	PCSK1	PC1, PC3, PC1/3, NEC1	L	B	confined to the neuroendocrine system, involved in the processing of proinsulin and other hormones
PCSK2/ NEC2	PCSK2	PC2, NEC2	L	B	
PCSK3/ FURIN	PCSK3	furin, PACE	M	B	ubiquitous, highly expressed in the liver
PCSK4	PCSK4	PC4	L	B	restricted to testicular and ovarian germ cells
PCSK5	PCSK5 short	PC5A, PC6A	S	B	ubiquitous
	PCSK5 long	PC5B, PC6B	M	B	ubiquitous, may have a redundant role with furin
PCSK6	PCSK6	PACE4, SPC4	S	B	ubiquitous
PCSK7	PCSK7	PC7, PC8	M	B	ubiquitous, may have a redundant role with other PCs
PCSK8/ MBTPS1/ SKI1	PCSK8 (rarely used)	MBTPS1, SKI-1	M	N	ubiquitous, involved in the processing of transcription factors
PCSK9	PCSK9	PC9, NARC-1	S	N	cleaves only itself, regulates cholesterol level

is activated by C1s, MASP-1, or MASP-2, while FB is activated by FD. Surprisingly, there are three serine proteases of the complement system which are present in cleaved, processed form in the circulation: MASP-3, FI and FD (**Figure 1B**). As we will see in the following sections these proteases are processed quite differently. MASP-3 and FD are present predominantly in cleaved form in the blood, however zymogen molecules were also detected in low concentrations (23, 24). FI is fully converted. In the case of these proteases proteolytic processing alone does not ensure proteolytic activity. In the case of the FD and FI the cleaved molecules do not have the conformation necessary for proteolytic activity (25, 26). They are present in a distorted conformation, and the fully active conformation is induced by the substrate. These proteases have very narrow substrate specificity. FD cleaves only C3b-bound FB. The proconvertase complex, C3bB, binds FD and induces the conformational change in the molecule to get full proteolytic activity (27). FI can cleave C3b and C4b but only in the presence of cofactors (FH for C3b, C4BP for C4b, MCP or CR1 for both). FI gains the proteolytic conformation in the C3b/C4b-cofactor-FI ternary complex (28). There is no experimental 3D structure of empty activated MASP-3 protease, but we cannot rule out that its structure is distorted, like that of FD and FI. The only proven physiological substrate of MASP-3 is pro-FD. Another substrate might exist, since MASP-3 has a role in the development. Lack of MASP-3 activity results in the development of 3MC (Malpuech-Michels-Mingarelli-Carnevale) syndrome (29, 30).

Another way of regulation is mediated by inhibitors. The most important fluid-phase inhibitors of the serine proteases of the serum cascade systems are the serpins (31, 32). C1-inhibitor inhibits C1r, C1s, MASP-1 and MASP-2 (33). The serpins are "suicide-inhibitors"; they make stable covalent complex with the active serine proteases and prevents them to cleave more substrate. The serpin-serine protease complex is then removed from the circulation. Antithrombin is a major inhibitor of thrombin, but it is an efficient inhibitor of MASP-1, as well, especially in the presence of heparin (34). Intriguingly, the three "pre-cleaved" proteases, MASP-3, FD and FI, have no known physiological inhibitor. These proteases are regulated through their narrow substrate specificity and through the substrate induction. Active C2 (C2a) and FB (Bb) also lack fluid phase inhibitors. The convertases are labile complexes; C2a and Bb can easily dissociate from them. Once dissociated, C2a and Bb cannot re-associate with C4b and C3b, respectively. The dissociation is facilitated by different factors on the cell membrane (35). Interestingly there is a positive regulator of the complement activation, properdin, which stabilizes the alternative pathway C3 convertase (C3bBb), but not the classical/lectin pathway C3 convertase (C4b2a) (36, 37).

It is also important from a regulatory point of view that the activated complement proteins react very quickly before inactivation occurs. This mechanism ensures, that the complement activation takes place locally, preferably on the surface of the pathogens, and not systemically. For example, C3 and C4 contain a reactive thioester bond. After convertase-mediated cleavage, the thioester bond becomes exposed and makes an ester or amid bond on the surface of the target cell (38). If the C3b or C4b cannot reach the cell surface in time, it will react with water (hydrolysis) and cannot attach to surface any more. In this way only the target cell will be destroyed by the complement-mediated attack and the probability of the bystander lysis will be very low. The formation of the membrane attack complex is also regulated. Vitronectin is competing with the membrane binding of C5b-7 complex and prevents its insertion into the membrane (39). Clusterin is also a regulator of membrane attack complex formation (40).

Most of the complement components are synthetized in the liver. There are several exceptions: C1q and properdin are synthesized mainly by leucocytes, FD is expressed almost exclusively by adipose tissue (41). It is interesting that MASP-1 and MASP-3 are the alternative splice products of the *MASP1* gene, but their expression pattern is different. MASP-1 is produced in the liver, while MASP-3 expression was also detected in several extra-hepatic tissues, such as colon, heart and skeletal muscle (42). Local production of complement proteins can also occur in various other tissues including the

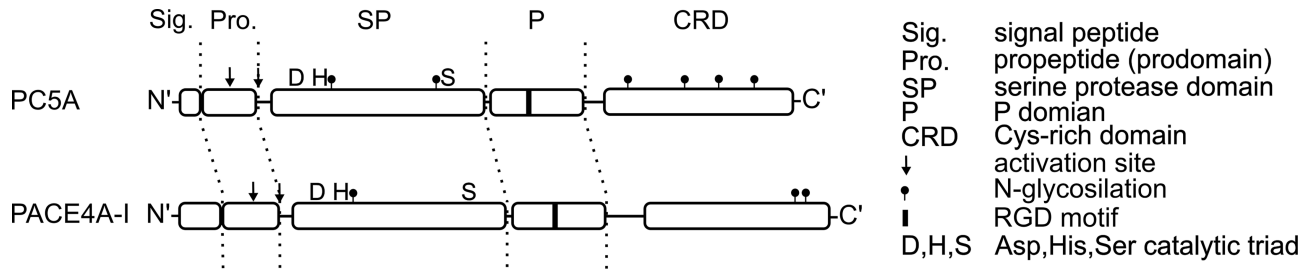

FIGURE 2 | Domain structures of PCSK5 (PC5A isoform), and PCSK6 (PACE4A-I isoform). PC5A is the shorter, secreted isoform of the two main isoforms of PCSK5. PCSK6 (PACE4) has several secreted isoforms. PACE4A-I is considered as the main (canonical) isoform. Two autocatalytic cleavages (↓) after and within the prodomain are required for activation. The second cleavage is thought to occur extracellularly.

eye and the kidney, which may contribute to complement-mediated diseases affecting these organs (43, 44).

BRIEF INTRODUCTION TO MAMMALIAN PROPROTEIN CONVERTASES

The story of proprotein convertases (PCs) goes back to the proteolytic processing of pro-insulin, and the discovery of the homology between the yeast protease kexin (KEX2) and its mammalian counterpart furin (45, 46). In this paper we do not wish to review proprotein convertases comprehensively, because there are excellent reviews published in this subject e.g (47–50).. On the other hand, we intend to provide a brief list of the human (mammalian) enzymes (**Table 1**), their function, tissue distribution, and substrate specificity, because it will aid us to categorize PCs that may be required for the processing of certain complement proteins.

It had been known that the two-chain mature insulin, held together by disulfide bridges, is synthetized as a single chain polypeptide pre-pro-insulin (45, 47, 51). After removal of the signal peptide, the first cleavage is performed by PC1 (aka PC3) and the second by PC2 in the secretory granules. The remaining polybasic residues are removed by carboxypeptidases. PC1 and PC2 are confined to neuroendocrine and endocrine cells, where they act as the major processing enzymes in the regulated secretory pathway of peptide hormones. Because of their roles in pro-hormone processing PCs were initially called prohormone convertases. On the other hand, because of their location PC1 and PC2 are unlikely to act on complement proteins *in vivo*, and this is also true for PC4 (PCSK4).

The first mammalian PC to be identified was furin, when it became evident that it is homologous to the yeast enzyme kexin. The serine protease domain of furin and kexin belongs to the subtilisin fold, giving rise to the name: proprotein convertase subtilisin/kexin (PCSK). Furin is probably the best characterized of all PCs. It preferentially cleaves after R-X-K/R-R↓ sequence (where X represents any amino acid), but often it cleaves after the less optimal R-X-X-R↓, or K/R-X-X-X-K/R-R↓ sequences (48). Trafficking of furin is also well characterized, and serves as an example for other PCs. After translocation to the endoplasmic reticulum (ER) and removal of the signal peptide it is anchored to the cell membrane through its C-terminal transmembrane segment. The first autocatalytic cleavage occurs in the ER at neutral pH between the pro-domain and the serine protease domain. The prodomain still associates with the serine protease domain inhibiting furin. The second, slower cleavage occurs within the prodomain at moderately acidic pH in the trans-Golgi network (TGN), secretory vesicles and endosomes, resulting in a fully active enzyme (48, 52). Most furin substrates are processed in these compartments during the constitutive secretory pathway. Membrane bound furin also appears on the cell surface, where it can process several substrates, e.g. viral proteins (50). Furin recycles between the cell surface and the TGN *via* early endosomes. Soluble extracellular furin has been described *via* shedding, and furin can also act in the secretory granules of the regulated secretory pathway. To sum up, furin is active in many compartments, therefore it is generally considered as the major proprotein processing enzyme.

In this review we will use the abbreviation of BAR-PC (basic amino acid residue-specific proprotein **c**onvertase), having the general recognition sequence of K/R-X_n-K/R↓ (where n=0,2,4,6), which typically, but not always contains consecutive (paired) basic amino acid residues (53). Seven genes encode for BAR-PCs and two for PCs that cleave after non-basic residues (**Table 1**). BAR-PCs recognize quite similar sequences therefore some degree of redundancy is possible between the members. In addition to the slightly different preferred sequences, their intracellular trafficking, differential expression in tissues, and the site of their activation can be the determining factors for the substrate specificity of a certain BAR-PC *in vivo*. In general, spatial segregation largely determines the unique features of PCs (54). It is important to note that PCs, like other enzymes of the subtilisin fold are strictly Ca^{2+}-dependent enzymes. This property can help differentiate their action from serine proteases of the chymotrypsin fold.

We have started work on PCs because we realized that activation of certain enzymes by PCs can occur in the blood (see later). In the next section we introduce the three known secreted PCs that are present in extracellular fluids. PCSK9 is also included, as a well-known example of a PC present at high levels in the blood, despite being in a proteolytically inactive (inhibited) state. PACE4 has been also detected in the

blood (55, 56), while so far no one reported the presence of PC5A in the blood, however it could be present in other extracellular fluids.

SECRETED PROPROTEIN CONVERTASES

PCSK6 (PACE4)

PCSK6 (proprotein convertase subtilisin/kexin type 6) gene is located close to the *FURIN* (*PCSK3*) gene on human chromosome 15, referring to the common origin of these enzymes (57). Eight different splice variants of the *PCSK6* gene have been described, although most of them were found only at mRNA level. The PACE4 (paired basic amino acid cleaving enzyme 4), SPC4 (subtilisin-like proprotein convertase 4), and the more recent PCSK6 names are used simultaneously for the protein products. PACE4 is widely expressed in human tissues. It is mainly expressed in liver, but also in the lung, gut, spleen, brain, placenta and neuroendocrine tissues (58). Three isoforms, PACE4A-I, PACE4A-II, PACE4B are probably secreted *via* the constitutive pathway (59). PACE4 efficiently cleaves substrates at R-X-K/R-R↓, R-X-X-R↓ sequences, and also recognizes short R-R↓ and K-R↓ motifs (60). PACE4A-I is the full-length enzyme (**Figure 2**), and like all PCs requires Ca^{2+} for the catalysis, and also shows marked temperature sensitivity (61). PACE4 has a multidomain structure, before the structural domains, it starts with an extremely long signal sequence (63 amino acids), which is followed by a propeptide (or prodomain), an S8-type serine protease domain, a P (or Homo B) domain, and finally a Cys-rich domain (CRD) composed of tandem furin-like repeats at the C-terminus. PACE4 is synthesized as a zymogen, and its autoactivation requires two proteolytic events after and within the prodomain. The first cleavage takes place in the endoplasmic reticulum (ER) (62), and the second occurs presumably at the cell surface after the secretion (63). In subtilisin-like enzymes, the prodomain acts as an intramolecular chaperone (64), promoting the formation of the correct fold, while its pH-dependent binding to the catalytic domain may inhibit the activity during secretion, as it has been shown for furin (65). The P domain is also essential for appropriate folding, it stabilizes the protease domain through hydrophobic interactions (66) and it carries an RGD tripeptide motif that controls the protein trafficking through the ER (67), and it can also play a role in the binding of integrins on the cell surface. Unlike many other proprotein convertases (PCs) PACE4 lacks the transmembrane region, therefore it is released into the extracellular matrix. A cationic region of the CRD can tether PACE4 to the extracellular matrix on the cell surface *via* heparan sulfate proteoglycans (HSPGs) (68), and there can inactivate the HSPG-bound endothelial lipase and lipoprotein lipase (69) modifying the high-density lipoprotein (HDL) metabolism. CRD also interacts with tissue inhibitors of metalloproteases (TIMPs) (70), and through them PACE4A-I could regulate extracellular matrix remodeling. A quarter of the *PCSK6* knock out mice embryos die prenatally showing sever cardiovascular and craniofacial malformations. Half of the embryos showed left pulmonary isomerism and abnormal, right-sided stomach, pancreas and spleen. Dysfunction of PACE4A-I results an altered left-right patterning during the embryogenesis. PACE4 is responsible for the processing of Nodal precursor protein that activates the transforming growth factor-β (TGF-β) signaling pathway (58, 71). PACE4A-I selectively cleaves the B isoform of insulin receptor at insulin-target tissues that increases the production of glucokinase and affects glucose metabolism (72). PACE4A-I also processes the insulin-like grow factor-II (IGF-II) (73). RNA silencing of PACE4 suppresses the myosin light chain expression in skeletal muscle cells. It could be restored by addition of processed IGF-II suggesting that PACE4A-I accelerates the myogenic differentiation (74). PACE4A-I seems to enhance proliferation of prostate cancer cells *in vitro* and the growth of tumor xenografts in mice (75). In the case of mice keratinocyte cultures PACE4A-I overexpression enhances the invasiveness of malignant cells and it also triggers the conversion of non-invasive cell types to malignant *via* activating matrix metalloproteases (76). In contrast to normal thyroid parenchyma, malignant thyroid nodules expresses PACE4A-I (77). These results suggest that PACE4 could be a promising diagnostic tool and therapeutic target of some cancer types. PACE4A-II isoform has a short deletion in a disordered region after the P domain. It was demonstrated *in vitro* that PACE4A-II processes pro-von Willebrand factor as well as PACE4A-I, and it activates rat complement pro-C3 more efficiently than the full-length form (78).

PCSK5 (PC5A Isoform)

A PC encoded by the *PCSK5* (proprotein convertase subtilisin/kexin type 5) gene was discovered in two laboratories at the same time (79, 80). It explains why it has two parallel names in the literature, proprotein convertase 5 and 6 (PC5, PC6), but often referred to as PC5/6 or PCSK5. The *PCSK5* gene encodes two protein isoforms PC5A and B having different tissue distribution and structural differences at the C-terminus. Both isoforms are expressed equally in the liver; PC5A is the dominant isoform in heart, lung, ovary and in neuronal tissues, whereas PC5B is the major form in kidney and in the intestinal tract (81). PC5A isoform (**Figure 2**) has a shorter CRD than that of B isoform and it lacks the transmembrane domain, therefore PC5A is soluble and it is secreted on the regulated secretory pathway (82), while PC5B localized only in the trans-Golgi vesicles (83). PC5A shares many structural and *in vitro* functional similarities with PACE4. Like PACE4, it also takes part in regulation of HDL level through inactivation of endothelial lipase and lipoprotein lipase (69). In neural tissues PC5A expression overlaps with the expression of neural adhesion molecule L1. In the hippocampus PC5A performs the first proteolytic cleavage of L1 on the neuron surface which is required for release, dimerization and activation of L1 (84). Through L1 processing PC5A plays a role in neuronal migration, growth and regeneration. Normal *PCSK5* gene function seems to be essential in embryonic development as demonstrated by knock-out studies. Lack of functional *PCSK5* leads to early embryonic death in mice model (81). KO embryos exhibited homeotic malformations, absence of tail and kidneys, development of additional ribs, and collapsed lung. Very similar phenotypes were observed in growth/

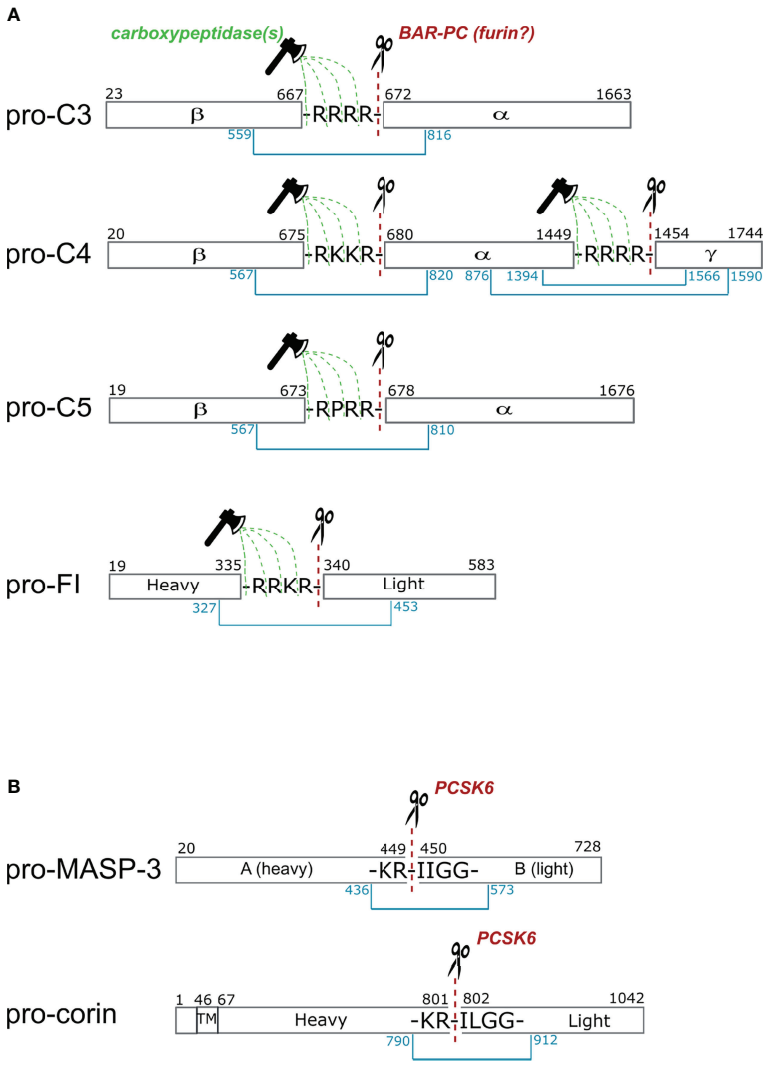

FIGURE 3 | Cleavage sites of proprotein convertases after paired basic residues in C3, C4, C5, factor I, MASP-3 and corin. **(A)** Complement proteins that are processed intracellularly by proprotein convertases. Cleavage sites of basic amino acid residue-specific proprotein convertases (BAR-PC) are indicated as red dashed lines and scissors. Residual amino acids are trimmed off by carboxypeptidases marked with green dashed lines and ax. After BAR-PC cleavage, the complement proteins disintegrate into multiple chains: α and β chains in C3 and C5, α, β and γ chains in C4 and; heavy and light chains in the case of FI. The light chain of FI represents the serine protease domain in the active enzyme. Chains are held together by disulfide bonds indicated with blue lines. Black numbers show the first and last amino acids of each chain, while blue numbers stand for cysteines that form interchain disulfide bonds. **(B)** These two proteins are processed extracellularly by proprotein convertases. The sequences are very similar near the cleavage sites in MASP-3 and corin. The cleavage sites in the propeptide segment performed by PCSK6 are illustrated with red dashed lines and scissors. The with disulfide bonds connecting the heavy and light chains are indicated with blue lines. In corin the transmembrane (TM) region is also shown, while the activation takes place in the extracellular part of the protein.

differentiation factor 11 (Gdf11) knock out mice. PC5 and Gdf11 mRNA showed an overlapped appearance in PCSK KO embryos, suggesting that Gdf11 is a potential substrate of PC5 (85). In human umbilical vein endothelial cells (HUVECs) PC5 is the major activator of receptor protein tyrosine phosphatase μ (RPTPμ) that promotes the monolayer formation of the endothelium based on inhibition of cell growth (86). Separate overexpression of different PCs in colorectal cancer cell line revealed that PC5A is the most potent proteolytic activator of αv-integrin (87). In vascular smooth muscle cells (VSMCs) PC5 activated αv-integrin promotes the cell migration and adhesion to vitronectin (88). A potent vessel remodeling factor, the platelet-derived growth factor (PDGF) upregulates *PCSK5* gene expression in VSMC culture and increases the PC5 protein level, as it was proven *ex vivo* in an atherosclerotic aorta model (89). Co-localization of vitronectin, αv-integrin and PC5 on VSMC in atherosclerotic lesions suggests that PC5 has an important role is the development of atherosclerosis. *In vitro* analyses of PC5 mutants having altered post translational modification (90) and studies of liver specific PC5 knock out mice (91) revealed that

PC5A and furin can cleave PCSK9 on hepatocyte surface to modify its fold and activity.

PCSK9

Based on the observation that subtilisin/kexin isozyme 1 (SKI-1) encoded by the *PCSK8* gene cleaves after non-basic residues, gene databases were screened to identify ortholog enzymes. This *in silico* method led to the discovery of proprotein convertase subtilisin/kexin type 9 (PCSK9), which was first described as neural apoptosis-regulated convertase (NARC-1). PCSK9 mRNA was detected in the liver, kidney, cerebellum, and small intestine. PCSK9 is a member of the proteinase K subfamily. Like other PCs, PCSK9 is synthesized as a zymogen, and the autocatalytic cleavage takes place in the ER. PCSK9 prefers hydrophobic residues at the P1, P3, P5 positions in the recognition motif (92). Compared to the above mentioned PCs, PCSK9 shows structural differences; it lacks the conserved P domain and carries a Cys- and His-rich domain (CHRD) at the C-terminus. In the absence of the P domain, the CHRD domain could stabilize folding (93). After autoactivation, the prodomain remains bound to the catalytic domain locking the substrate-binding groove, thus PCSK9 does not exhibit enzyme activity against any other substrate (94). *PCSK9* gene point mutations are found to be associated with autosomal dominant hypercholesterolemia (95) predicting a role in lipid metabolism. CRHD binds the low-density lipoprotein receptor (LDLR) on hepatocyte surface, enhances its uptake in clathrin coated vesicles and degradation in lysosomes, therefore high PCSK9 level results in increased LDL level in the circulation (96, 97). PCSK9 repression seems to be a promising therapeutic strategy in hypercholesterolemia and in associated cardiovascular diseases.

COMPLEMENT PROTEINS PROCESSES BY PROPROTEIN CONVERTASES AND THE STORY OF CORIN

C3, C4, C5 Family

The C3 family proteins, C3, C4 and C5, are structurally homologues and their effect during complement activation is based on similar molecular mechanism. Upon cleavage by the convertase complexes these molecules undergo major conformational changes which enable them to bind the next components of the complement system (C3b: FB; C4b: C2; C5b: C6, C7) and attach to the surface. These are crucial events for organizing the complement activation. C3, C4 and C5 are members of the α_2-macroglobulin family. They have evolved most likely from a common ancestral gene (98). C3 and C4, like α_2-macroglobulin, contains the internal thioester bond, which is necessary to localize the complement activation to the surface of the target cell (99). All three proteins are synthesized as single chain pre-pro molecules and undergo posttranslational modifications in the endoplasmic reticulum and in the Golgi. Probably the most important posttranslational modification is the proteolytic cleavage by proprotein convertases, which yields the mature subunit structure.

C3 is mainly synthesized in the liver. The pre-pro molecule consists of 1663 amino acids. The α and β chains are separated by a tetra-arginine sequence between Ala^{667} and Ser^{672} (**Figure 3A**). In an experiment Misumi et al. showed that co-expression of C3 and furin in COS cells resulted in correctly processed C3 (100). Without furin co-expression only about half of the pro-C3 expressed was processed by endogenous proprotein convertase activity of the cells. This experiment proved that a proprotein convertase is responsible for the correct processing of pro-C3, but we cannot claim that furin is the exclusive processing enzyme. Very likely furin is the major processing protease, however, because of the redundant substrate specificity we cannot exclude the role of other proprotein convertases. As we mentioned in the previous section PACE4 also can process pro-C3 (78).

The primary site of C4 synthesis is also the liver. The pre-pro single-chain C4 consists of 1744 amino acids. In the polypeptide chain two tetrabasic sequences that separates the β-, α-, and γ-chains, that are ideal cleavage sequences for proprotein convertases. Between the β- and α-chains there is a Arg-Lys-Lys-Arg sequence and between the α- and γ-chains there is a tetra-arginine sequence (**Figure 3A**). Based on the analogy of C3, it is very probable that pro-C4 is processed by a furin-like proprotein convertase, but there is no direct experimental evidence for this. In 1980, before the discovery of the proprotein convertases, Goldberger and Colten showed that plasmin can process pro-C4 correctly *in vitro* (101). This is possible, since other proteases having similar substrate specificity can cleave at the tetrabasic sequence. Plasmin is a trypsin-like protease that cleaves after basic amino acids (Lys or Arg). After the discovery of the proprotein convertases (in the 1990s), however, it became evident, that these enzymes are responsible for the processing of the pro-proteins along the secretory pathway (102). Interestingly, C4 is further processed after secretion in the in the blood plasma (103). A 22-residue peptide from the C-terminus of the α-chain is removed by a metalloprotease having elastase-like specificity (104).

C5 is synthetized by the liver hepatocytes. The pro-form of C5 contains 1676 amino acids (105). There is an Arg-Pro-Arg-Arg linker sequence between the β- and α-chains (**Figure 3A**). The pro-C5 processing occurs during secretion. Until now the processing enzyme has not been identified experimentally but based on the linker sequence, we can assume that a furin-like proprotein convertase is responsible for the cleavage.

It is important to note, that furin, and the other proprotein convertases cleaves after the last amino acid of the tetrabasic linker sequence. After this cleavage the tetrabasic sequence remains attached to the C-terminus of one of the chains (β-chain of C3 and C5, and β- and α-chains of C4). In the mature proteins, however, the tetrabasic sequences are completely removed. This might be important for the full biological activity. We know from the example of insulin, that after

proprotein convertase-mediated cleavage the C-terminally exposed basic residues are trimmed off by carboxypeptidases to generate fully active peptides (47, 54). One can assume, that in the case of C3, C4 and C5 a similar mechanism takes place, however the carboxypeptidase cleavage might occur in the blood plasma after secretion.

Factor I

Factor I (FI) is a major regulator of complement activation since it is able to degrade activated C3b and C4b in the presence of its cofactors and dismantle C3b convertases of all pathways. The proper functioning of FI is crucial to protect host cells from unwanted complement attack and also to produce fragments for opsonization. FI is a glycoprotein which is found in its active two-chain form of 88 kDa in human blood. As the majority of complement serine proteases, FI is synthetized as pre-proprotein primarily in hepatocytes (106). Several other cell types also express functional FI such as monocytes, myoblasts, fibroblasts, human umbilical vein embryonic cells (HUVEC) and keratinocytes (107). FI is a multidomain protein of five domains namely FIMAC (factor I membrane attack complex) domain, CD5 domain (also called SRCR domain), two LDLRA (low-density lipoprotein receptor type A) domains located on the heavy chain, and SP (serine protease) domain on the light chain (108). Compared to other complement proteases, Factor I is different in terms of activation. It is the only complement protease that is activated inside the cell during secretion. After being released from the cell it circulates as an active protease without any known inhibitor in the blood. The physiological function of FI is controlled through cofactors which modify the affinity and specificity towards its substrates. Crystal structure indicated that the SP domain in free FI is partially distorted (26). This finding explains the low catalytic activity of FI towards small peptide substrates (109). However, the SP domain showed stabilized conformation in the ternary complex of FI with its cofactor FH and its substrate C3b. Data revealed that the SP domain can reach its fully active conformation only in complex with its substrates and cofactors (28).

The single polypeptide chain synthesized intracellularly contains a signal sequence and an activation linker (R^{336}-R-K-R^{339}). The precursor undergoes posttranslational modification while migrates through the Golgi, gets three sites glycosylated on the light and also on the heavy chain and afterwards the linker region is cut out. The sequence of the linker region is a typical BAR-PC recognition site (**Figure 3A**), nonetheless the exact activator of FI is still unknown. Although the activation of complement FI is not fully understood, several experimental facts indicate involvement of proprotein convertases in the process. Early attempts to produce active two-chain enzyme were carried out in different hepatoma derived cell lines (Hep3B, NPLC-KC and HepG2) (110). The proportion of the single-chain pro-FI and the mature protein in different cell cultures vary from each other. NPLC-KC and Hep3b cells predominantly produced the two-chain form while HepG2 cells mostly secreted the single-chain form of FI. The authors also showed that other multidomain complement protein such as C3, C4 and C5 were secreted as mature proteins by the mentioned three hepatoma cell lines. The major product did not differ regardless of their source. These findings indicate that the intracellular posttranslational modification of FI may require other activator than that of C3, C4 or C5. The possibility that cleavage of proprotein takes place extracellularly was ruled out since pro-FI was not activated when incubated in human plasma.

Active FI can also be expressed by insect cells. Baculovirus expression system using *Trichopulsia ni* (High Five) cells yielded fully processed FI, although molecular weight of the protease was somewhat different compared to the serum protein due to altered glycosylation (111). In order to improve the yield of active form, FI was co-expressed in mammalian cells with a possible activator, furin (112). Monkey kidney cells (COS-1) secreted more than 90% of FI as single-chain zymogen, while Chinese hamster ovary cells (CHO-K1) expressed 50% of that. However, when cells were co-transfected with both FI and furin cDNA, the ratio of two forms significantly changed. Processing became complete, portion of the mature FI moved above 90%. Human embryonic kidney cells (HEK293) co-transfected with furin resulted in mature FI sufficient quality and quantity for crystallization (28). Furin or other intracellular proprotein convertases could cleave the linker region between Arg^{339} and Ile^{340}, however another enzymatic step is still needed. Residual basic amino acids on the new C-terminus have to be cut off otherwise FI could not reach full activity. A well-known example for this process is the maturation of insulin (54). Although not every detail of the intracellular posttranslational modifications of FI have been fully clarified yet, the evidences listed above strongly support the involvement of proprotein convertases.

Corin

Corin is an essential enzyme for maintaining normal blood pressure (113). It is a trypsin-like serine protease that cleaves pro-atrial natriuretic peptide (pro-ANP) to generate an active hormone, ANP. ANP is a cardiac hormone playing an important role in regulating salt-water balance and blood pressure. The structure and function of corin resembles that of the complement proteases in several aspects. Corin is a multidomain serine protease. It is a type II transmembrane protease having an N-terminal transmembrane domain and a C-terminal trypsin-like serine protease domain. Between the transmembrane domain and the serine protease domain there are two frizzled domains, eight low density lipoprotein receptor repeats and a scavenger receptor domain. It is highly expressed in cardiomyocytes, and it is expected to exert its function on the surface of these cells (114). Recently, however, soluble corin was detected in the human circulation, indicating that corin is shed from the cardiomyocytes (115). Corin, like most of the complement proteases, is synthetized as an inactive one-chain zymogen, and it is activated by limited proteolysis at a conserved (**Figure 3B**) site between Arg^{801} and Ile^{802} (116). The resulting two-chain molecule shows full enzymatic activity. The two polypeptide chains are held together by a disulfide bond. Failure of corin activation can result in developing hypertension and heart disease. Accordingly, naturally occurring corin gene variants

with impaired zymogen activation have been identified in patients (117). The activation sequence and the mode of activation of corin resembles to that of the plasma cascade enzymes. Corin has no autoactivation capacity therefore it must be activated by other protease. Since the trypsin-like enzymes having a common evolutionary origin form a protease network in the blood plasma and on the surface of different cells (e.g. endothelial cells, leucocytes, cardiomyocytes, etc.), it seemed obvious that the activator protease should be sought among them. It was a big surprise, however, when it was discovered, that the activator protease is a proprotein convertase, PCSK6 (aka PACE4) (55). A proprotein convertase-specific inhibitor completely blocked the activation of corin, and a similar effect was exerted by using siRNAs against PCSK6 expression. PCSK6 knockout mice have only zymogen corin in the heart and they show symptoms of hypertension. The first reason for the surprise was that the proprotein convertases represent a different evolutionary line of the serine proteases (the subtilisins) compared to the trypsin-like proteases (118). It was the first example in the blood for a cross-talk between the proprotein convertase and the trypsin-like protease network. The second reason for the surprise was that corin is secreted as a zymogen and the proprotein convertase-mediated activation takes place on the surface of the cells. The proprotein convertases usually act inside the cells, along the secretory pathway, as we have seen in the example of C3, C4, C5 and FI. In the case of corin, however, it was shown that corin and PCSK6 use different secretory pathways. Chen et al. demonstrated that a soluble corin mutant lacking the transmembrane domain was activated by PCSK6 in the conditioned medium of HEK293 cells but not intracellularly (119). Blocking PCSK6 secretion by monensin and subsequent immunostaining indicated that corin and PCSK6 were secreted *via* different intracellular pathways, which may explain the lack of corin activation inside the cell. The detection of secreted PCSK6 in the human blood indicated that PCSK6 may process other proteins in the circulation thereby modulating the effect of the proteolytic cascade systems (56).

MASP-3

MASP-3 was discovered as the third serine protease component of the lectin pathway of complement (120). Originally it had been thought to negatively regulate the lectin pathway, as it had no known natural substrate despite having a functional serine protease domain (120). MASP-3 had been implicated to cleave insulin-like growth factor-binding protein 5 (IGFBP-5), however, *in vivo* relevance of this reaction has not been established (121). More importantly, certain mutations that effect the catalytic activity of MASP-3 can cause a serious developmental disorder, the 3MC (Malpuech-Michels-Mingarelli-Carnevale) syndrome (122), which is characterized by cognitive defects, craniofacial dismorphysm, and other abnormalities. It is interesting that PCSK6 KO mice (58, 123) and 3MC (human) patients (124) show similar craniofacial deformities. The exact pathomechanism of this disease remains to be solved, however, it indicates that MASP-3 might have a role outside the regular scheme of the complement system, and both MASP-3 and PCSK6 may be involved in the same mechanistic route.

MASP-3 is expressed as a splice variant from the *MASP1* gene, which has three products that have been identified at the protein level, MASP-1, MASP-3 and MAp44 (125–127). Map44 is indeed a regulatory molecule without any catalytic activity. MASP-1 and MASP-3 are, however, functional serine proteases. The first evidence that MASP-1 and/or MASP-3 might play a role in the activation of the alternative pathway was provided by the group of Teizo Fujita (128). They generated *MASP1* knockout mice by replacing the second exon encoding a common region shared by both proteases (129). Serum derived from mice lacking both proteases had minimal alternative pathway activity, because it contained proenzymic factor D (pro-FD). Initially MASP-1 was implicated as the pro-FD activator (maturase) (128). While *in vitro*, MASP-1, and a number of other proteases, can process pro-FD in to FD (130), *in vivo* MASP-3 is the FD maturase enzyme (24, 131, 132). Under normal resting conditions, unperturbed by ongoing coagulation or complement activation, MASP-3 is already present predominantly in the activated, two-chain form (23), while MASP-1 and other implicated proteases are proenzymic. Hence, in normal human individuals MASP-3 has a homeostatic role: it is present (mostly) as an active enzyme and continuously activates pro-FD, which is, as a result, also present predominantly in the mature FD form (24, 133). It worth mentioning that human and mouse MASP-3 seems to behave very similarly in this respect therefore the FD maturase function of MASP-3 is probably conserved among mammalian species (132, 134).

As MASP-3 is mostly present in the blood as a mature, active enzyme the question immediately arises: how MASP-3 is activated? This question implies two problems, where does MASP-3 activation take place, and which protease or proteases activate MASP-3?

Notably, when MASP-3 was expressed in eukaryotic cell lines, insect or mammalian (CHO) cells, it was always secreted into the medium a one-chain zymogen (135–137). This strongly suggests that MASP-3 is not activated intracellularly. For the first time, MASP-3 was expressed in insect cells, and it was convincingly proved that MASP-3 cannot autoactivate (135). Interestingly, when isolated MASP-3 was stored at 4 °C for months, it slowly became activated by an unknown contaminating protease. The cleavage occurred even if the catalytically inactive S664A (precursor numbering) mutant MASP-3 was isolated and then stored at 4 °C. The activation did not occur at 37 °C suggesting that the activating enzyme is heat-labile. Although this insect protease has never been identified, presumably it was a BAR-PC, which seems to be also secreted like PACE4 (PCSK6).

We have recently identified PCSK6 (PACE4) as the most likely activator of MASP-3 and showed that the activation of MASP-3 takes place in the blood using human samples (138). Evidences that support this mechanism are as follows. The inactive S664A MASP-3 variant became cleaved ("activated") when added to blood samples containing Ca^{2+} (e.g. hirudin plasma, or serum). On the other hand, the reaction did not

occur in EDTA plasma. It important to note again that proprotein convertases require Ca^{2+} for their activity. Most importantly, the "activation" (cleavage) reaction of MASP-3 S664A was completely blocked in hirudin plasma by the general proprotein convertase inhibitor decanoyl-Arg-Val-Lys-Arg-chloromethylketone (dec-RVKR-cmk) specific for BAR-PCs. Hence we were looking for a proprotein convertase, which is secreted and cleaves after paired basic residues. It is remarkable that the protease, corin, which is also activated in the blood by PCSK6 (PACE4), has a very similar sequence motif around the activation site to that of MASP-3 (**Figure 3B**). Nevertheless, there is another BAR-PC, which is secreted, namely the PC5A, a major isoform of PCSK5. We have expressed both PCSK6 (PACE4) and PCSK5 (PC5A isoform) in CHO cells, and found that both could activate MASP-3 *in vitro*. We have also shown that the MASP-3 activator in hirudin plasma is also heat-labile, because the activator remained active for a longer period of time at 25 °C. It was published that PACE4 (PCSK6) is very sensitive to even moderately high temperatures such as 37 °C (61). And finally, we and others have shown that PCSK6 is present in the blood as a soluble protein (55, 56), whereas PCSK5 (PC5A) is not, or at least no one could detect it. Taken together, PCSK6 (PACE4) emerges as possibly the sole, or at least the major activator of MASP-3 in human blood. As MASP-3 is the activator pro-FD, and FD is essential for the alternative pathway of complement, we have identified PCSK6 as an essential, highest level activator of complement. It is important to note that this activation sequence occurs constantly in normal healthy individuals in a homeostatic fashion. The described mechanism is summarized on **Figure 4**.

CONCLUSION AND PERSPECTIVES

The complement system is a part of the proteolytic network of the human body. It has been known for a long time that the blood cascade systems – complement, coagulation, fibrinolysis – interact with each other; there are cross-activation steps, and there are common inhibitors. For example, MASP-1 can initiate coagulation by activating prothrombin (139); and C1-inhibitor, the major inhibitor of the classical and the lectin pathway, also inhibits the contact activation system (FXIIa and plasma kallikrein). It was also described that zymogen activation can occur between proteases of different mechanistic groups. Plasmin can initiate the activation of several metalloprotease zymogens (e.g. MMP-1/-3/-9/-13). In this way plasmin could facilitate matrix degradation during various physiological and pathological events (140). Another example of cross-class activation is when the serine protease granzymes, released by cytotoxic T cells or natural killer cells, initiate the apoptosis by activating the cysteine protease caspases in the target cells (141). The discovery that a proprotein convertase is involved in the alternative pathway activation drew attention to the cooperation between the proprotein convertases and the complement system

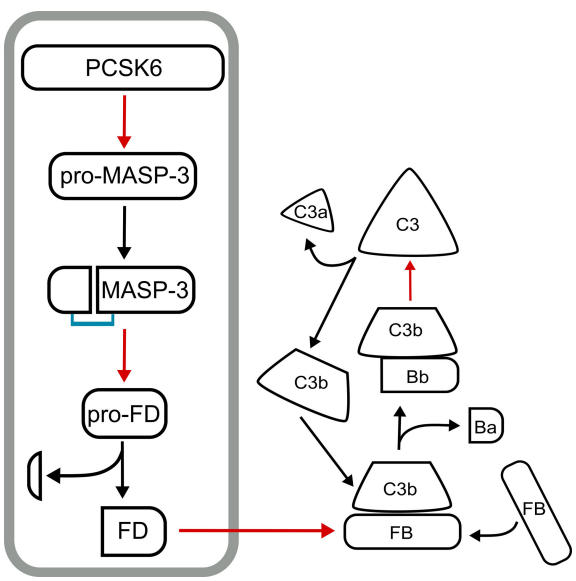

FIGURE 4 | The PCSK6-MASP-3-FD axis. The proenzyme form of MASP-3 (pro-MASP-3) is constitutively activated in the blood by PCSK6 (PACE4). Active MASP-3 cleaves pro-factor D (pro-FD) also constitutively. These two cleavage events are required to keep the alternative pathway of complement ready for action on appropriate surfaces. The PCSK6-MASP-3-FD axis is in a grey box, while subsequent events of the alternative pathway following FD activation are shown on the right. Red arrows point from a protease to its substrate, while black arrows indicate conversion.

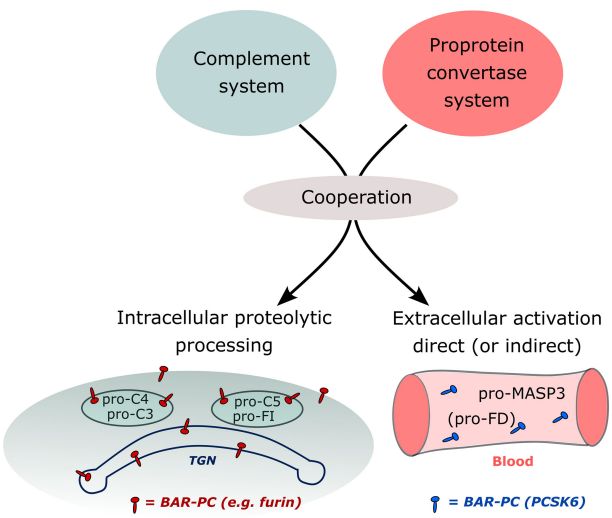

FIGURE 5 | Processing of complement proteins by proprotein convertases in different compartments of the body. Cooperation between the complement system and BAR-PCs (basic amino acid residue-specific proprotein convertases) results in proteolytic processing of complement proteins inside the cell or extracellularly in the blood. BAR-PCs such as furin localize to the membrane of the trans-Golgi network (TGN), secretory vesicles and endosomes. Processing of pro-C3, pro-C4, pro-C5, and pro-factor I probably occurs in these compartments. The direct activation of pro-MASP-3 occurs in the blood by circulating PCSK6 (PACE4). Pro-factor D is the substrate of active MASP-3 therefore it is an example of indirect activation by BAR-PCs.

(**Figure 5**). Although both the proprotein convertases and the complement proteases are serine proteases, they represent quite different evolutionary lines (i.e. trypsin-like vs. subtilisin-like proteases).

PCSK6 is the highest level initiator enzyme of the alternative pathway. In the pre-initiation phase of the alternative pathway, before any activation signal appears, PCSK6 activates MASP-3, which in turn activates FD (**Figure 4**). These reactions ensure that when C3b appears on the surface, the alternative pathway can be started immediately with high efficiency because sufficient amount of active FD is available. The proprotein convertases also play a crucial role in the intracellular processing of several complement proteins such as FI, C3, C4 and C5 (**Figure 5**). Knowing these interactions, we cannot rule out that there are other hidden connections between the proprotein convertases and the complement system.

For example, the anaphylatoxins C3a and C5a can modulate the tumor microenvironment by promoting tumorigenesis through the recruitment of myeloid-derived suppressor cells for inhibiting antitumor CD8+ T cells and through induction of neovascularization (142). Complement components are present in the tumor: they can be secreted either by the tumor cells, or by tumor-infiltrating immune cells, or they can enter the tumor through the vasculature. Cancer cell-born proteases can directly cleave C3 and C5 generating the anaphylatoxins. Nitta et al. demonstrated that cancer cells display a serine protease, which cleaves C5 and releases C5a (143). This protease is likely a proprotein convertase since its activity is completely blocked by the BAR-PC-specific inhibitor (dec-RVKR-cmk).

Also, proprotein convertases may contribute to the intracellular action of the complement proteins, since the anaphylatoxins can be released intracellularly (144, 145). Further studies are needed to reveal all the functional connections between the components of the complex protease network of the immune system including the proprotein convertases and the complement proteases.

AUTHOR CONTRIBUTIONS

All authors listed have made a substantial, direct, and intellectual contribution to the work and approved it for publication.

FUNDING

The study was supported by the Eötvös Loránd Research Network (ELKH) grant KEP-5/2021, and the National Research, Development and Innovation Office (NKFIH) grants K134711 and 2020-1.1.2-PIACI-KFI-2021-00273.

REFERENCES

1. Merle NS, Church SE, Fremeaux-Bacchi V, Roumenina LT. Complement System Part I - Molecular Mechanisms of Activation and Regulation. *Front Immunol* (2015) 6:262. doi: 10.3389/fimmu.2015.00262
2. Merle NS, Noe R, Halbwachs-Mecarelli L, Fremeaux-Bacchi V, Roumenina LT. Complement System Part II: Role in Immunity. *Front Immunol* (2015) 6:257. doi: 10.3389/fimmu.2015.00257
3. Hajishengallis G, Reis ES, Mastellos DC, Ricklin D, Lambris JD. Novel Mechanisms and Functions of Complement. *Nat Immunol* (2017) 18:1288–98. doi: 10.1038/ni.3858
4. Ricklin D, Hajishengallis G, Yang K, Lambris JD. Complement: A Key System for Immune Surveillance and Homeostasis. *Nat Immunol* (2010) 11:785–97. doi: 10.1038/ni.1923
5. Sim RB, Tsiftsoglou SA. Proteases of the Complement System. *Biochem Soc Trans* (2004) 32:21–7. doi: 10.1042/bst0320021
6. Morgan BP, Harris CL. Complement, a Target for Therapy in Inflammatory and Degenerative Diseases. *Nat Rev Drug Discovery* (2015) 14:857–77. doi: 10.1038/nrd4657
7. Mastellos DC, Ricklin D, Lambris JD. Clinical Promise of Next-Generation Complement Therapeutics. *Nat Rev Drug Discovery* (2019) 18:707–29. doi: 10.1038/s41573-019-0031-6
8. Dobó J, Kocsis A, Gál P. Be on Target: Strategies of Targeting Alternative and Lectin Pathway Components in Complement-Mediated Diseases. *Front Immunol* (2018) 9:1851. doi: 10.3389/fimmu.2018.01851
9. Diebolder CA, Beurskens FJ, de Jong RN, Koning RI, Strumane K, Lindorfer MA, et al. Complement is Activated by IgG Hexamers Assembled at the Cell Surface. *Science* (2014) 343:1260–3. doi: 10.1126/science.1248943
10. Sharp TH, Boyle AL, Diebolder CA, Kros A, Koster AJ, Gros P. Insights Into IgM-Mediated Complement Activation Based on *in Situ* Structures of IgM-C1-C4b. *Proc Natl Acad Sci U S A* (2019) 116:11900–5. doi: 10.1073/pnas.1901841116
11. Zwarthoff SA, Widmer K, Kuipers A, Strasser J, Ruyken M, Aerts PC, et al. C1q Binding to Surface-Bound IgG is Stabilized by C1r2s2 Proteases. *Proc Natl Acad Sci U S A* (2021) 118:e2102787118. doi: 10.1073/pnas.2102787118
12. Holmskov U, Thiel S, Jensenius JC. Collections and Ficolins: Humoral Lectins of the Innate Immune Defense. *Annu Rev Immunol* (2003) 21:547–78. doi: 10.1146/annurev.immunol.21.120601.140954
13. Héja D, Kocsis A, Dobó J, Szilágyi K, Szász R, Závodszky P, et al. Revised Mechanism of Complement Lectin-Pathway Activation Revealing the Role of Serine Protease MASP-1 as the Exclusive Activator of MASP-2. *Proc Natl Acad Sci U S A* (2012) 109:10498–503. doi: 10.1073/pnas.1202588109
14. Lachmann PJ. Looking Back on the Alternative Complement Pathway. *Immunobiology* (2018) 223:519–23. doi: 10.1016/j.imbio.2018.02.001
15. Harboe M, Ulvund G, Vien L, Fung M, Mollnes TE. The Quantitative Role of Alternative Pathway Amplification in Classical Pathway Induced Terminal Complement Activation. *Clin Exp Immunol* (2004) 138:439–46. doi: 10.1111/j.1365-2249.2004.02627.x
16. Pangburn MK, Schreiber RD, Müller-Eberhard HJ. Formation of the Initial C3 Convertase of the Alternative Complement Pathway. Acquisition of C3b-Like Activities by Spontaneous Hydrolysis of the Putative Thioester in Native C3. *J Exp Med* (1981) 154:856–67. doi: 10.1084/jem.154.3.856
17. Mannes M, Dopler A, Zolk O, Lang SJ, Halbgebauer R, Höchsmann B, et al. Complement Inhibition at the Level of C3 or C5: Mechanistic Reasons for Ongoing Terminal Pathway Activity. *Blood* (2021) 137:443–55. doi: 10.1182/blood.2020005959
18. Roumenina LT. Terminal Complement Without C5 Convertase? *Blood* (2021) 137:431–2. doi: 10.1182/blood.2020010133
19. Tegla CA, Cudrici C, Patel S, Trippe R, Rus V, Niculescu F, et al. Membrane Attack by Complement: The Assembly and Biology of Terminal Complement Complexes. *Immunol Res* (2011) 51:45–60. doi: 10.1007/s12026-011-8239-5
20. Krem MM, Di Cera E. Evolution of Enzyme Cascades From Embryonic Development to Blood Coagulation. *Trends Biochem Sci* (2002) 27:67–74. doi: 10.1016/s0968-0004(01)02007-2

21. Gál P, Harmat V, Kocsis A, Bián T, Barna L, Ambrus G, et al. A True Autoactivating Enzyme. Structural Insight Into Mannose-Binding Lectin-Associated Serine Protease-2 Activations. *J Biol Chem* (2005) 280:33435–44. doi: 10.1074/jbc.M506051200
22. Megyeri M, Harmat V, Major B, Végh Á, Balczer J, Héja D, et al. Quantitative Characterization of the Activation Steps of Mannan-Binding Lectin (MBL)-Associated Serine Proteases (MASPs) Points to the Central Role of MASP-1 in the Initiation of the Complement Lectin Pathway. *J Biol Chem* (2013) 288:8922–34. doi: 10.1074/jbc.M112.446500
23. Oroszlán G, Dani R, Szilágyi A, Závodszky P, Thiel S, Gál P, et al. Extensive Basal Level Activation of Complement Mannose-Binding Lectin-Associated Serine Protease-3: Kinetic Modeling of Lectin Pathway Activation Provides Possible Mechanism. *Front Immunol* (2017) 8:1821. doi: 10.3389/fimmu.2017.01821
24. Pihl R, Jensen L, Hansen AG, Thøgersen IB, Andres S, Dagnæs-Hansen F, et al. Analysis of Factor D Isoforms in Malpuech-Michels-Mingarelli-Carnevale Patients Highlights the Role of MASP-3 as a Maturase in the Alternative Pathway of Complement. *J Immunol Baltim Md 1950* (2017), 199:2158-2170 ji1700518. doi: 10.4049/jimmunol.1700518
25. Jing H, Macon KJ, Moore D, DeLucas LJ, Volanakis JE, Narayana SV. Structural Basis of Profactor D Activation: From a Highly Flexible Zymogen to a Novel Self-Inhibited Serine Protease, Complement Factor D. *EMBO J* (1999) 18:804–14. doi: 10.1093/emboj/18.4.804
26. Roversi P, Johnson S, Caesar JJE, McLean F, Leath KJ, Tsiftsoglou SA, et al. Structural Basis for Complement Factor I Control and its Disease-Associated Sequence Polymorphisms. *Proc Natl Acad Sci U S A* (2011) 108:12839–44. doi: 10.1073/pnas.1102167108
27. Forneris F, Ricklin D, Wu J, Tzekou A, Wallace RS, Lambris JD, et al. Structures of C3b in Complex With Factors B and D Give Insight Into Complement Convertase Formation. *Science* (2010) 330:1816–20. doi: 10.1126/science.1195821
28. Xue X, Wu J, Ricklin D, Forneris F, Di Crescenzio P, Schmidt CQ, et al. Regulator-Dependent Mechanisms of C3b Processing by Factor I Allow Differentiation of Immune Responses. *Nat Struct Mol Biol* (2017) 24:643–51. doi: 10.1038/nsmb.3427
29. Rooryck C, Diaz-Font A, Osborn DPS, Chabchoub E, Hernandez-Hernandez V, Shamseldin H, et al. Mutations in Lectin Complement Pathway Genes COLEC11 and MASP1 Cause 3MC Syndrome. *Nat Genet* (2011) 43:197–203. doi: 10.1038/ng.757
30. Yongqing T, Wilmann PG, Reeve SB, Coetzer TH, Smith AI, Whisstock JC, et al. The X-Ray Crystal Structure of Mannose-Binding Lectin-Associated Serine Proteinase-3 Reveals the Structural Basis for Enzyme Inactivity Associated With the Carnevale, Mingarelli, Malpuech, and Michels (3MC) Syndrome. *J Biol Chem* (2013) 288:22399–407. doi: 10.1074/jbc.M113.483875
31. Huntington JA. Serpin Structure, Function and Dysfunction. *J Thromb Haemost JTH* (2011) 9 Suppl 1:26–34. doi: 10.1111/j.1538-7836.2011.04360.x
32. Gettins PGW. Serpin Structure, Mechanism, and Function. *Chem Rev* (2002) 102:4751–804. doi: 10.1021/cr010170+
33. Davis AE, Lu F, Mejia P. C1 Inhibitor, a Multi-Functional Serine Protease Inhibitor. *Thromb Haemost* (2010) 104:886–93. doi: 10.1160/TH10-01-0073
34. Paréj K, Dobó J, Závodszky P, Gál P. The Control of the Complement Lectin Pathway Activation Revisited: Both C1-Inhibitor and Antithrombin are Likely Physiological Inhibitors, While α2-Macroglobulin is Not. *Mol Immunol* (2013) 54:415–22. doi: 10.1016/j.molimm.2013.01.009
35. Forneris F, Wu J, Gros P. The Modular Serine Proteases of the Complement Cascade. *Curr Opin Struct Biol* (2012) 22:333–41. doi: 10.1016/j.sbi.2012.04.001
36. van den Bos RM, Pearce NM, Granneman J, Brondijk THC, Gros P. Insights Into Enhanced Complement Activation by Structures of Properdin and Its Complex With the C-Terminal Domain of C3b. *Front Immunol* (2019) 10:2097. doi: 10.3389/fimmu.2019.02097
37. Pedersen DV, Gadeberg TAF, Thomas C, Wang Y, Joram N, Jensen RK, et al. Structural Basis for Properdin Oligomerization and Convertase Stimulation in the Human Complement System. *Front Immunol* (2019) 10:2007. doi: 10.3389/fimmu.2019.02007
38. Gadjeva M, Dodds AW, Taniguchi-Sidle A, Willis AC, Isenman DE, Law SK. The Covalent Binding Reaction of Complement Component C3. *J Immunol Baltim Md 1950* (1998) 161:985–90.
39. Sheehan M, Morris CA, Pussell BA, Charlesworth JA. Complement Inhibition by Human Vitronectin Involves non-Heparin Binding Domains. *Clin Exp Immunol* (1995) 101:136–41. doi: 10.1111/j.1365-2249.1995.tb02289.x
40. McDonald JF, Nelsestuen GL. Potent Inhibition of Terminal Complement Assembly by Clusterin: Characterization of its Impact on C9 Polymerization. *Biochemistry* (1997) 36:7464–73. doi: 10.1021/bi962895r
41. White RT, Damm D, Hancock N, Rosen BS, Lowell BB, Usher P, et al. Human Adipsin is Identical to Complement Factor D and is Expressed at High Levels in Adipose Tissue. *J Biol Chem* (1992) 267:9210–3. doi: 10.1016/S0021-9258(19)50409-4
42. Seyfarth J, Garred P, Madsen HO. Extra-Hepatic Transcription of the Human Mannose-Binding Lectin Gene (Mbl2) and the MBL-Associated Serine Protease 1-3 Genes. *Mol Immunol* (2006) 43:962–71. doi: 10.1016/j.molimm.2005.06.033
43. Armento A, Ueffing M, Clark SJ. The Complement System in Age-Related Macular Degeneration. *Cell Mol Life Sci CMLS* (2021) 78:4487–505. doi: 10.1007/s00018-021-03796-9
44. Zipfel PF, Wiech T, Gröne H-J, Skerka C. Complement Catalyzing Glomerular Diseases. *Cell Tissue Res* (2021) 385:355–70. doi: 10.1007/s00441-021-03485-w
45. Steiner DF. On the Discovery of Precursor Processing. *Methods Mol Biol Clifton NJ* (2011) 768:3–11. doi: 10.1007/978-1-61779-204-5_1
46. Seidah NG. The Proprotein Convertases, 20 Years Later. *Methods Mol Biol Clifton NJ* (2011) 768:23–57. doi: 10.1007/978-1-61779-204-5_3
47. Zhou A, Webb G, Zhu X, Steiner DF. Proteolytic Processing in the Secretory Pathway. *J Biol Chem* (1999) 274:20745–8. doi: 10.1074/jbc.274.30.20745
48. Thomas G. Furin at the Cutting Edge: From Protein Traffic to Embryogenesis and Disease. *Nat Rev Mol Cell Biol* (2002) 3:753–66. doi: 10.1038/nrm934
49. Seidah NG, Prat A. The Biology and Therapeutic Targeting of the Proprotein Convertases. *Nat Rev Drug Discovery* (2012) 11:367–83. doi: 10.1038/nrd3699
50. Garten W. Characterization of Proprotein Convertases and Their Involvement in Virus Propagation. *Act Viruses Host Proteases* (2018), 16:205–48. doi: 10.1007/978-3-319-75474-1_9
51. Steiner DF, Cunningham D, Spigelman L, Aten B. Insulin Biosynthesis: Evidence for a Precursor. *Science* (1967) 157:697–700. doi: 10.1126/science.157.3789.697
52. Molloy SS, Thomas L, VanSlyke JK, Stenberg PE, Thomas G. Intracellular Trafficking and Activation of the Furin Proprotein Convertase: Localization to the TGN and Recycling From the Cell Surface. *EMBO J* (1994) 13:18–33. doi: 10.1002/j.1460-2075.1994.tb06231.x
53. Seidah NG, Chrétien M. Proprotein and Prohormone Convertases: A Family of Subtilases Generating Diverse Bioactive Polypeptides. *Brain Res* (1999) 848:45–62. doi: 10.1016/s0006-8993(99)01909-5
54. Seidah NG, Sadr MS, Chrétien M, Mbikay M. The Multifaceted Proprotein Convertases: Their Unique, Redundant, Complementary, and Opposite Functions. *J Biol Chem* (2013) 288:21473–81. doi: 10.1074/jbc.R113.481549
55. Chen S, Cao P, Dong N, Peng J, Zhang C, Wang H, et al. PCSK6-Mediated Corin Activation is Essential for Normal Blood Pressure. *Nat Med* (2015) 21:1048–53. doi: 10.1038/nm.3920
56. Yang S-F, Chou R-H, Lin S-J, Li S-Y, Huang P-H. Serum PCSK6 and Corin Levels are Not Associated With Cardiovascular Outcomes in Patients Undergoing Coronary Angiography. *PLoS One* (2019) 14:e0226129. doi: 10.1371/journal.pone.0226129
57. Kiefer MC, Tucker JE, Joh R, Landsberg KE, Saltman D, Barr PJ. Identification of a Second Human Subtilisin-Like Protease Gene in the Fes/Fps Region of Chromosome 15. *DNA Cell Biol* (1991) 10:757–69. doi: 10.1089/dna.1991.10.757
58. Constam DB, Robertson EJ. SPC4/PACE4 Regulates a TGFbeta Signaling Network During Axis Formation. *Genes Dev* (2000) 14:1146–55. doi: 10.1101/gad.14.9.1146
59. Benjannet S, Savaria D, Laslop A, Munzer JS, Chrétien M, Marcinkiewicz M, et al. Alpha1-Antitrypsin Portland Inhibits Processing of Precursors

Mediated by Proprotein Convertases Primarily Within the Constitutive Secretory Pathway. *J Biol Chem* (1997) 272:26210–8. doi: 10.1074/jbc.272.42.26210
60. Gordon VM, Rehemtulla A, Leppla SH. A Role for PACE4 in the Proteolytic Activation of Anthrax Toxin Protective Antigen. *Infect Immun* (1997) 65:3370–5. doi: 10.1128/iai.65.8.3370-3375.1997
61. Sucic JF, Moehring JM, Inocencio NM, Luchini JW, Moehring TJ. Endoprotease PACE4 is Ca2+-Dependent and Temperature-Sensitive and can Partly Rescue the Phenotype of a Furin-Deficient Cell Strain. *Biochem J* (1999) 339(Pt 3):639–47. doi: 10.1042/bj3390639
62. Nagahama M, Taniguchi T, Hashimoto E, Imamaki A, Mori K, Tsuji A, et al. Biosynthetic Processing and Quaternary Interactions of Proprotein Convertase SPC4 (Pace4). *FEBS Lett* (1998) 434:155–9. doi: 10.1016/s0014-5793(98)00970-3
63. Mayer G, Hamelin J, Asselin M-C, Pasquato A, Marcinkiewicz E, Tang M, et al. The Regulated Cell Surface Zymogen Activation of the Proprotein Convertase PC5A Directs the Processing of its Secretory Substrates. *J Biol Chem* (2008) 283:2373–84. doi: 10.1074/jbc.M708763200
64. Shinde U, Inouye M. Propeptide-Mediated Folding in Subtilisin: The Intramolecular Chaperone Concept. *Adv Exp Med Biol* (1996) 379:147–54. doi: 10.1007/978-1-4613-0319-0_16
65. Dillon SL, Williamson DM, Elferich J, Radler D, Joshi R, Thomas G, et al. Propeptides are Sufficient to Regulate Organelle-Specific pH-Dependent Activation of Furin and Proprotein Convertase 1/3. *J Mol Biol* (2012) 423:47–62. doi: 10.1016/j.jmb.2012.06.023
66. Lipkind GM, Zhou A, Steiner DF. A Model for the Structure of the P Domains in the Subtilisin-Like Prohormone Convertases. *Proc Natl Acad Sci U S A* (1998) 95:7310–5. doi: 10.1073/pnas.95.13.7310
67. Rovère C, Luis J, Lissitzky JC, Basak A, Marvaldi J, Chrétien M, et al. The RGD Motif and the C-Terminal Segment of Proprotein Convertase 1 are Critical for its Cellular Trafficking But Not for its Intracellular Binding to Integrin Alpha5beta1. *J Biol Chem* (1999) 274:12461–7. doi: 10.1074/jbc.274.18.12461
68. Tsuji A, Sakurai K, Kiyokage E, Yamazaki T, Koide S, Toida K, et al. Secretory Proprotein Convertases PACE4 and PC6A are Heparin-Binding Proteins Which are Localized in the Extracellular Matrix. Potential Role of PACE4 in the Activation of Proproteins in the Extracellular Matrix. *Biochim Biophys Acta* (2003) 1645:95–104. doi: 10.1016/s1570-9639(02)00532-0
69. Jin W, Fuki IV, Seidah NG, Benjannet S, Glick JM, Rader DJ. Proprotein Convertases [Corrected] are Responsible for Proteolysis and Inactivation of Endothelial Lipase. *J Biol Chem* (2005) 280:36551–9. doi: 10.1074/jbc.M502264200
70. Nour N, Mayer G, Mort JS, Salvas A, Mbikay M, Morrison CJ, et al. The Cysteine-Rich Domain of the Secreted Proprotein Convertases PC5A and PACE4 Functions as a Cell Surface Anchor and Interacts With Tissue Inhibitors of Metalloproteinases. *Mol Biol Cell* (2005) 16:5215–26. doi: 10.1091/mbc.e05-06-0504
71. Beck S, Le Good JA, Guzman M, Ben Haim N, Roy K, Beermann F, et al. Extraembryonic Proteases Regulate Nodal Signalling During Gastrulation. *Nat Cell Biol* (2002) 4:981–5. doi: 10.1038/ncb890
72. Kara I, Poggi M, Bonardo B, Govers R, Landrier J-F, Tian S, et al. The Paired Basic Amino Acid-Cleaving Enzyme 4 (PACE4) is Involved in the Maturation of Insulin Receptor Isoform B: An Opportunity to Reduce the Specific Insulin Receptor-Dependent Effects of Insulin-Like Growth Factor 2 (IGF2). *J Biol Chem* (2015) 290:2812–21. doi: 10.1074/jbc.M114.592543
73. Duguay SJ, Jin Y, Stein J, Duguay AN, Gardner P, Steiner DF. Post-Translational Processing of the Insulin-Like Growth Factor-2 Precursor. Analysis of O-Glycosylation and Endoproteolysis. *J Biol Chem* (1998) 273:18443–51. doi: 10.1074/jbc.273.29.18443
74. Yuasa K, Masuda T, Yoshikawa C, Nagahama M, Matsuda Y, Tsuji A. Subtilisin-Like Proprotein Convertase PACE4 is Required for Skeletal Muscle Differentiation. *J Biochem (Tokyo)* (2009) 146:407–15. doi: 10.1093/jb/mvp090
75. Couture F, D'Anjou F, Desjardins R, Boudreau F, Day R. Role of Proprotein Convertases in Prostate Cancer Progression. *Neoplasia N Y N* (2012) 14:1032–42. doi: 10.1593/neo.121368
76. Mahloogi H, Bassi DE, Klein-Szanto AJP. Malignant Conversion of non-Tumorigenic Murine Skin Keratinocytes Overexpressing PACE4. *Carcinogenesis* (2002) 23:565–72. doi: 10.1093/carcin/23.4.565
77. Fradet L, Temmar R, Couture F, Belzile M, Fortier P-H, Day R. Evaluation of PACE4 Isoforms as Biomarkers in Thyroid Cancer. *J Otolaryngol - Head Neck Surg J Oto-Rhino-Laryngol Chir Cervico-Faciale* (2018) 47:63. doi: 10.1186/s40463-018-0311-x
78. Mori K, Kii S, Tsuji A, Nagahama M, Imamaki A, Hayashi K, et al. A Novel Human PACE4 Isoform, PACE4E is an Active Processing Protease Containing a Hydrophobic Cluster at the Carboxy Terminus. *J Biochem (Tokyo)* (1997) 121:941–8. doi: 10.1093/oxfordjournals.jbchem.a021677
79. Lusson J, Vieau D, Hamelin J, Day R, Chrétien M, Seidah NG. cDNA Structure of the Mouse and Rat Subtilisin/Kexin-Like PC5: A Candidate Proprotein Convertase Expressed in Endocrine and Nonendocrine Cells. *Proc Natl Acad Sci U S A* (1993) 90:6691–5. doi: 10.1073/pnas.90.14.6691
80. Nakagawa T, Hosaka M, Torii S, Watanabe T, Murakami K, Nakayama K. Identification and Functional Expression of a New Member of the Mammalian Kex2-Like Processing Endoprotease Family: Its Striking Structural Similarity to PACE4. *J Biochem (Tokyo)* (1993) 113:132–5. doi: 10.1093/oxfordjournals.jbchem.a124015
81. Essalmani R, Hamelin J, Marcinkiewicz J, Chamberland A, Mbikay M, Chrétien M, et al. Deletion of the Gene Encoding Proprotein Convertase 5/6 Causes Early Embryonic Lethality in the Mouse. *Mol Cell Biol* (2006) 26:354–61. doi: 10.1128/MCB.26.1.354-361.2006
82. De Bie I, Marcinkiewicz M, Malide D, Lazure C, Nakayama K, Bendayan M, et al. The Isoforms of Proprotein Convertase PC5 are Sorted to Different Subcellular Compartments. *J Cell Biol* (1996) 135:1261–75. doi: 10.1083/jcb.135.5.1261
83. Xiang Y, Molloy SS, Thomas L, Thomas G. The PC6B Cytoplasmic Domain Contains Two Acidic Clusters That Direct Sorting to Distinct Trans-Golgi Network/Endosomal Compartments. *Mol Biol Cell* (2000) 11:1257–73. doi: 10.1091/mbc.11.4.1257
84. Kalus I, Schnegelsberg B, Seidah NG, Kleene R, Schachner M. The Proprotein Convertase PC5A and a Metalloprotease are Involved in the Proteolytic Processing of the Neural Adhesion Molecule L1. *J Biol Chem* (2003) 278:10381–8. doi: 10.1074/jbc.M208351200
85. Essalmani R, Zaid A, Marcinkiewicz J, Chamberland A, Pasquato A, Seidah NG, et al. *In Vivo* Functions of the Proprotein Convertase PC5/6 During Mouse Development: Gdf11 is a Likely Substrate. *Proc Natl Acad Sci U S A* (2008) 105:5750–5. doi: 10.1073/pnas.0709428105
86. Campan M, Yoshizumi M, Seidah NG, Lee ME, Bianchi C, Haber E. Increased Proteolytic Processing of Protein Tyrosine Phosphatase Mu in Confluent Vascular Endothelial Cells: The Role of PC5, a Member of the Subtilisin Family. *Biochemistry* (1996) 35:3797–802. doi: 10.1021/bi952552d
87. Lissitzky JC, Luis J, Munzer JS, Benjannet S, Parat F, Chrétien M, et al. Endoproteolytic Processing of Integrin Pro-Alpha Subunits Involves the Redundant Function of Furin and Proprotein Convertase (PC) 5A, But Not Paired Basic Amino Acid Converting Enzyme (PACE) 4, PC5B or PC7. *Biochem J* (2000) 346 Pt 1:133–8.
88. Stawowy P, Kallisch H, Borges Pereira Stawowy N, Stibenz D, Veinot JP, Gräfe M, et al. Immunohistochemical Localization of Subtilisin/Kexin-Like Proprotein Convertases in Human Atherosclerosis. *Virchows Arch Int J Pathol* (2005) 446:351–9. doi: 10.1007/s00428-004-1198-7
89. Stawowy P, Blaschke F, Kilimnik A, Goetze S, Kallisch H, Chrétien M, et al. Proprotein Convertase PC5 Regulation by PDGF-BB Involves PI3-Kinase/P70(S6)-Kinase Activation in Vascular Smooth Muscle Cells. *Hypertens Dallas Tex 1979* (2002) 39:399–404. doi: 10.1161/hy0202.103000
90. Benjannet S, Rhainds D, Hamelin J, Nassoury N, Seidah NG. The Proprotein Convertase (PC) PCSK9 is Inactivated by Furin and/or PC5/6A: Functional Consequences of Natural Mutations and Post-Translational Modifications. *J Biol Chem* (2006) 281:30561–72. doi: 10.1074/jbc.M606495200
91. Essalmani R, Susan-Resiga D, Chamberland A, Abifadel M, Creemers JW, Boileau C, et al. *In Vivo* Evidence That Furin From Hepatocytes Inactivates PCSK9. *J Biol Chem* (2011) 286:4257–63. doi: 10.1074/jbc.M110.192104
92. Seidah NG, Benjannet S, Wickham L, Marcinkiewicz J, Jasmin SB, Stifani S, et al. The Secretory Proprotein Convertase Neural Apoptosis-Regulated Convertase 1 (NARC-1): Liver Regeneration and Neuronal Differentiation. *Proc Natl Acad Sci U S A* (2003) 100:928–33. doi: 10.1073/pnas.0335507100

93. Benjannet S, Rhainds D, Essalmani R, Mayne J, Wickham L, Jin W, et al. NARC-1/PCSK9 and its Natural Mutants: Zymogen Cleavage and Effects on the Low Density Lipoprotein (LDL) Receptor and LDL Cholesterol. *J Biol Chem* (2004) 279:48865–75. doi: 10.1074/jbc.M409699200
94. Cunningham D, Danley DE, Geoghegan KF, Griffor MC, Hawkins JL, Subashi TA, et al. Structural and Biophysical Studies of PCSK9 and its Mutants Linked to Familial Hypercholesterolemia. *Nat Struct Mol Biol* (2007) 14:413–9. doi: 10.1038/nsmb1235
95. Abifadel M, Varret M, Rabès J-P, Allard D, Ouguerram K, Devillers M, et al. Mutations in PCSK9 Cause Autosomal Dominant Hypercholesterolemia. *Nat Genet* (2003) 34:154–6. doi: 10.1038/ng1161
96. Zhang D-W, Lagace TA, Garuti R, Zhao Z, McDonald M, Horton JD, et al. Binding of Proprotein Convertase Subtilisin/Kexin Type 9 to Epidermal Growth Factor-Like Repeat A of Low Density Lipoprotein Receptor Decreases Receptor Recycling and Increases Degradation. *J Biol Chem* (2007) 282:18602–12. doi: 10.1074/jbc.M702027200
97. Ni YG, Condra JH, Orsatti L, Shen X, Di Marco S, Pandit S, et al. A Proprotein Convertase Subtilisin-Like/Kexin Type 9 (PCSK9) C-Terminal Domain Antibody Antigen-Binding Fragment Inhibits PCSK9 Internalization and Restores Low Density Lipoprotein Uptake. *J Biol Chem* (2010) 285:12882–91. doi: 10.1074/jbc.M110.113035
98. Campbell RD, Law SK, Reid KB, Sim RB. Structure, Organization, and Regulation of the Complement Genes. *Annu Rev Immunol* (1988) 6:161–95. doi: 10.1146/annurev.iy.06.040188.001113
99. Law SK, Dodds AW. The Internal Thioester and the Covalent Binding Properties of the Complement Proteins C3 and C4. *Protein Sci Publ Protein Soc* (1997) 6:263–74. doi: 10.1002/pro.5560060201
100. Misumi Y, Oda K, Fujiwara T, Takami N, Tashiro K, Ikehara Y. Functional Expression of Furin Demonstrating its Intracellular Localization and Endoprotease Activity for Processing of Proalbumin and Complement Pro-C3. *J Biol Chem* (1991) 266:16954–9. doi: 10.1016/S0021-9258(18)55396-5
101. Goldberger G, Colten HR. Precursor Complement Protein (Pro-C4) is Converted *In Vitro* to Native C4 by Plasmin. *Nature* (1980) 286:514–6. doi: 10.1038/286514a0
102. Nakayama K. Furin: A Mammalian Subtilisin/Kex2p-Like Endoprotease Involved in Processing of a Wide Variety of Precursor Proteins. *Biochem J* (1997) 327(Pt 3):625–35. doi: 10.1042/bj3270625
103. Chan AC, Mitchell KR, Munns TW, Karp DR, Atkinson JP. Identification and Partial Characterization of the Secreted Form of the Fourth Component of Human Complement: Evidence That it is Different From Major Plasma Form. *Proc Natl Acad Sci U S A* (1983) 80:268–72. doi: 10.1073/pnas.80.1.268
104. Hortin G, Chan AC, Fok KF, Strauss AW, Atkinson JP. Sequence Analysis of the COOH Terminus of the Alpha-Chain of the Fourth Component of Human Complement. Identification of the Site of its Extracellular Cleavage. *J Biol Chem* (1986) 261:9065–9. doi: 10.1016/S0021-9258(19)84488-5
105. Ooi YM, Colten HR. Biosynthesis and Post-Synthetic Modification of a Precursor (Pro-C5) of the Fifth Component of Mouse Complement (C5). *J Immunol Baltim Md 1950* (1979) 123:2494–8.
106. Nilsson SC, Sim RB, Lea SM, Fremeaux-Bacchi V, Blom AM. Complement Factor I in Health and Disease. *Mol Immunol* (2011) 48:1611–20. doi: 10.1016/j.molimm.2011.04.004
107. Timár KK, Junnikkala S, Dallos A, Jarva H, Bhuiyan ZA, Meri S, et al. Human Keratinocytes Produce the Complement Inhibitor Factor I: Synthesis is Regulated by Interferon-Gamma. *Mol Immunol* (2007) 44:2943–9. doi: 10.1016/j.molimm.2007.01.007
108. Barnum SR, Schein TN. *The Complement FactsBook*. Academic Press. (2017). London, United Kingdom 514 p.
109. Tsiftsoglou SA, Sim RB. Human Complement Factor I Does Not Require Cofactors for Cleavage of Synthetic Substrates. *J Immunol Baltim Md 1950* (2004) 173:367–75. doi: 10.4049/jimmunol.173.1.367
110. Goldberger G, Arnaout MA, Aden D, Kay R, Rits M, Colten HR. Biosynthesis and Postsynthetic Processing of Human C3b/C4b Inactivator (Factor I) in Three Hepatoma Cell Lines. *J Biol Chem* (1984) 259:6492–7. doi: 10.1016/S0021-9258(20)82168-1
111. Ullman CG, Chamberlain D, Ansari A, Emery VC, Haris PI, Sim RB, et al. Human Complement Factor I: Its Expression by Insect Cells and its Biochemical and Structural Characterisation. *Mol Immunol* (1998) 35:503–12. doi: 10.1016/s0161-5890(98)00052-2
112. Wong MJ, Goldberger G, Isenman DE, Minta JO. Processing of Human Factor I in COS-1 Cells Co-Transfected With Factor I and Paired Basic Amino Acid Cleaving Enzyme (PACE) cDNA. *Mol Immunol* (1995) 32:379–87. doi: 10.1016/0161-5890(94)00151-p
113. Zhou Y, Wu Q. Corin in Natriuretic Peptide Processing and Hypertension. *Curr Hypertens Rep* (2014) 16:415. doi: 10.1007/s11906-013-0415-7
114. Gladysheva IP, Robinson BR, Houng AK, Kováts T, King SM. Corin is Co-Expressed With Pro-ANP and Localized on the Cardiomyocyte Surface in Both Zymogen and Catalytically Active Forms. *J Mol Cell Cardiol* (2008) 44:131–42. doi: 10.1016/j.yjmcc.2007.10.002
115. Jiang J, Wu S, Wang W, Chen S, Peng J, Zhang X, et al. Ectodomain Shedding and Autocleavage of the Cardiac Membrane Protease Corin. *J Biol Chem* (2011) 286:10066–72. doi: 10.1074/jbc.M110.185082
116. Liao X, Wang W, Chen S, Wu Q. Role of Glycosylation in Corin Zymogen Activation. *J Biol Chem* (2007) 282:27728–35. doi: 10.1074/jbc.M703687200
117. Dong N, Fang C, Jiang Y, Zhou T, Liu M, Zhou J, et al. Corin Mutation R539C From Hypertensive Patients Impairs Zymogen Activation and Generates an Inactive Alternative Ectodomain Fragment. *J Biol Chem* (2013) 288:7867–74. doi: 10.1074/jbc.M112.411512
118. Gherardini PF, Wass MN, Helmer-Citterich M, Sternberg MJE. Convergent Evolution of Enzyme Active Sites is Not a Rare Phenomenon. *J Mol Biol* (2007) 372:817–45. doi: 10.1016/j.jmb.2007.06.017
119. Chen S, Wang H, Li H, Zhang Y, Wu Q. Functional Analysis of Corin Protein Domains Required for PCSK6-Mediated Activation. *Int J Biochem Cell Biol* (2018) 94:31–9. doi: 10.1016/j.biocel.2017.11.010
120. Dahl MR, Thiel S, Matsushita M, Fujita T, Willis AC, Christensen T, et al. MASP-3 and its Association With Distinct Complexes of the Mannan-Binding Lectin Complement Activation Pathway. *Immunity* (2001) 15:127–35. doi: 10.1016/s1074-7613(01)00161-3
121. Cortesio CL, Jiang W. Mannan-Binding Lectin-Associated Serine Protease 3 Cleaves Synthetic Peptides and Insulin-Like Growth Factor-Binding Protein 5. *Arch Biochem Biophys* (2006) 449:164–70. doi: 10.1016/j.abb.2006.02.006
122. Gajek G, Świerzko AS, Cedzyński M. Association of Polymorphisms of MASP1/3, COLEC10, and COLEC11 Genes With 3MC Syndrome. *Int J Mol Sci* (2020) 21:E5483. doi: 10.3390/ijms21155483
123. Malfait A-M, Seymour AB, Gao F, Tortorella MD, Le Graverand-Gastineau M-PH, Wood LS, et al. A Role for PACE4 in Osteoarthritis Pain: Evidence From Human Genetic Association and Null Mutant Phenotype. *Ann Rheum Dis* (2012) 71:1042–8. doi: 10.1136/annrheumdis-2011-200300
124. Sirmaci A, Walsh T, Akay H, Spiliopoulos M, Sakalar YB, Hasanefendioğlu-Bayrak A, et al. MASP1 Mutations in Patients With Facial, Umbilical, Coccygeal, and Auditory Findings of Carnevale, Malpuech, OSA, and Michels Syndromes. *Am J Hum Genet* (2010) 87:679–86. doi: 10.1016/j.ajhg.2010.09.018
125. Dobó J, Pál G, Cervenak L, Gál P. The Emerging Roles of Mannose-Binding Lectin-Associated Serine Proteases (MASPs) in the Lectin Pathway of Complement and Beyond. *Immunol Rev* (2016) 274:98–111. doi: 10.1111/imr.12460
126. Garred P, Genster N, Pilely K, Bayarri-Olmos R, Rosbjerg A, Ma YJ, et al. A Journey Through the Lectin Pathway of Complement-MBL and Beyond. *Immunol Rev* (2016) 274:74–97. doi: 10.1111/imr.12468
127. Gál P, Dobó J. "MASP-1.,". In: S Choi, editor. *Encyclopedia of Signaling Molecules*. Cham: Springer International Publishing (2018). p. 2965–72. doi: 10.1007/978-3-319-67199-4_101691
128. Takahashi M, Ishida Y, Iwaki D, Kanno K, Suzuki T, Endo Y, et al. Essential Role of Mannose-Binding Lectin-Associated Serine Protease-1 in Activation of the Complement Factor D. *J Exp Med* (2010) 207:29–37. doi: 10.1084/jem.20090633
129. Takahashi M, Iwaki D, Kanno K, Ishida Y, Xiong J, Matsushita M, et al. Mannose-Binding Lectin (MBL)-Associated Serine Protease (MASP)-1 Contributes to Activation of the Lectin Complement Pathway. *J Immunol Baltim Md 1950* (2008) 180:6132–8. doi: 10.4049/jimmunol.180.9.6132
130. Oroszlán G, Kortvely E, Szakács D, Kocsis A, Dammeier S, Zeck A, et al. MASP-1 and MASP-2 Do Not Activate Pro-Factor D in Resting Human Blood, Whereas MASP-3 Is a Potential Activator: Kinetic Analysis Involving

Specific MASP-1 and MASP-2 Inhibitors. *J Immunol Baltim Md 1950* (2016) 196:857–65. doi: 10.4049/jimmunol.1501717
131. Dobó J, Szakács D, Oroszlán G, Kortvely E, Kiss B, Boros E, et al. MASP-3 is the Exclusive Pro-Factor D Activator in Resting Blood: The Lectin and the Alternative Complement Pathways are Fundamentally Linked. *Sci Rep* (2016) 6:31877. doi: 10.1038/srep31877
132. Hayashi M, Machida T, Ishida Y, Ogata Y, Omori T, Takasumi M, et al. Cutting Edge: Role of MASP-3 in the Physiological Activation of Factor D of the Alternative Complement Pathway. *J Immunol Baltim Md 1950* (2019) 203:1411–6. doi: 10.4049/jimmunol.1900605
133. Lesavre PH, Müller-Eberhard HJ. Mechanism of Action of Factor D of the Alternative Complement Pathway. *J Exp Med* (1978) 148:1498–509. doi: 10.1084/jem.148.6.1498
134. Gál P, Dobó J, Pál G. Comment on "Cutting Edge: Role of MASP-3 in the Physiological Activation of Factor D of the Alternative Complement Pathway". *J Immunol Baltim Md 1950* (2019) 203:3091. doi: 10.4049/jimmunol.1901055
135. Zundel S, Cseh S, Lacroix M, Dahl MR, Matsushita M, Andrieu J-P, et al. Characterization of Recombinant Mannan-Binding Lectin-Associated Serine Protease (MASP)-3 Suggests an Activation Mechanism Different From That of MASP-1 and MASP-2. *J Immunol Baltim Md 1950* (2004) 172:4342–50. doi: 10.4049/jimmunol.172.7.4342
136. Skjoedt M-O, Hummelshoj T, Palarasah Y, Honore C, Koch C, Skjodt K, et al. A Novel Mannose-Binding Lectin/Ficolin-Associated Protein is Highly Expressed in Heart and Skeletal Muscle Tissues and Inhibits Complement Activation. *J Biol Chem* (2010) 285:8234–43. doi: 10.1074/jbc.M109.065805
137. Iwaki D, Kanno K, Takahashi M, Endo Y, Matsushita M, Fujita T. The Role of Mannose-Binding Lectin-Associated Serine Protease-3 in Activation of the Alternative Complement Pathway. *J Immunol Baltim Md 1950* (2011) 187:3751–8. doi: 10.4049/jimmunol.1100280
138. Oroszlán G, Dani R, Végh BM, Varga D, Ács AV, Pál G, et al. Proprotein Convertase Is the Highest-Level Activator of the Alternative Complement Pathway in the Blood. *J Immunol Baltim Md 1950* (2021) 206:2198–205. doi: 10.4049/jimmunol.2000636
139. Jenny L, Dobó J, Gál P, Schroeder V. MASP-1 Induced Clotting–The First Model of Prothrombin Activation by MASP-1. *PLoS One* (2015) 10: e0144633. doi: 10.1371/journal.pone.0144633
140. Ramos-DeSimone N, Hahn-Dantona E, Sipley J, Nagase H, French DL, Quigley JP. Activation of Matrix Metalloproteinase-9 (MMP-9) *via* a Converging Plasmin/Stromelysin-1 Cascade Enhances Tumor Cell Invasion. *J Biol Chem* (1999) 274:13066–76. doi: 10.1074/jbc.274.19.13066
141. Tibbs E, Cao X. Emerging Canonical and Non-Canonical Roles of Granzyme B in Health and Disease. *Cancers* (2022) 14:1436. doi: 10.3390/cancers14061436
142. Roumenina LT, Daugan MV, Petitprez F, Sautès-Fridman C, Fridman WH. Context-Dependent Roles of Complement in Cancer. *Nat Rev Cancer* (2019) 19:698–715. doi: 10.1038/s41568-019-0210-0
143. Nitta H, Murakami Y, Wada Y, Eto M, Baba H, Imamura T. Cancer Cells Release Anaphylatoxin C5a From C5 by Serine Protease to Enhance Invasiveness. *Oncol Rep* (2014) 32:1715–9. doi: 10.3892/or.2014.3341
144. West EE, Kolev M, Kemper C. Complement and the Regulation of T Cell Responses. *Annu Rev Immunol* (2018) 36:309–38. doi: 10.1146/annurev-immunol-042617-053245
145. Reis ES, Mastellos DC, Hajishengallis G, Lambris JD. New Insights Into the Immune Functions of Complement. *Nat Rev Immunol* (2019) 19:503–16. doi: 10.1038/s41577-019-0168-x

Conflict of Interest: The authors declare that the research was conducted in the absence of any commercial or financial relationships that could be construed as a potential conflict of interest.

frontiers | Frontiers in Immunology

ORIGINAL RESEARCH
published: 22 July 2022
doi: 10.3389/fimmu.2022.901876

Heme Interferes With Complement Factor I-Dependent Regulation by Enhancing Alternative Pathway Activation

*Alexandra Gerogianni[1,2], Jordan D. Dimitrov[3], Alessandra Zarantonello[3], Victoria Poillerat[3], Satheesh Chonat[4,5], Kerstin Sandholm[2], Karin E. McAdam[6], Kristina N. Ekdahl[1,2,7], Tom E. Mollnes[6,8,9], Camilla Mohlin[1,2], Lubka T. Roumenina[3] and Per H. Nilsson[1,2,6]**

[1] Linnaeus Centre for Biomaterials Chemistry, Linnaeus University, Kalmar, Sweden, [2] Department of Chemistry and Biomedicine, Linnaeus University, Kalmar, Sweden, [3] Centre de Recherche des Cordeliers, INSERM, Sorbonne Université, Université de Paris, Paris, France, [4] Aflac Cancer and Blood Disorders Center, Children's Healthcare of Atlanta, Atlanta, GA, United States, [5] Department of Pediatrics, Emory University School of Medicine, Atlanta, GA, United States, [6] Department of Immunology, Oslo University Hospital and University of Oslo, Oslo, Norway, [7] Department of Immunology, Genetics and Pathology, Rudbeck Laboratory, Uppsala University, Uppsala, Sweden, [8] Centre of Molecular Inflammation Research, and Department of Clinical and Molecular Medicine, Norwegian University of Science and Technology, Trondheim, Norway, [9] Research Laboratory, Nordland Hospital, Bodo, Norway

OPEN ACCESS

Edited by:
Dimitrios C. Mastellos, National Centre of Scientific Research Demokritos, Greece

Reviewed by:
Brian V. Geisbrecht, Kansas State University, United States
Gregory M. Vercellotti, University of Minnesota Twin Cities, United States

***Correspondence:**
Per H. Nilsson
per.h.nilsson@lnu.se

Specialty section:
This article was submitted to Molecular Innate Immunity, a section of the journal Frontiers in Immunology

Received: *22 March 2022*
Accepted: *23 June 2022*
Published: *22 July 2022*

Citation:
Gerogianni A, Dimitrov JD, Zarantonello A, Poillerat V, Chonat S, Sandholm K, McAdam KE, Ekdahl KN, Mollnes TE, Mohlin C, Roumenina LT and Nilsson PH (2022) Heme Interferes With Complement Factor I-Dependent Regulation by Enhancing Alternative Pathway Activation. Front. Immunol. 13:901876. doi: 10.3389/fimmu.2022.901876

Hemolysis, as a result of disease or exposure to biomaterials, is characterized by excess amounts of cell-free heme intravascularly and consumption of the protective heme-scavenger proteins in plasma. The liberation of heme has been linked to the activation of inflammatory systems, including the complement system, through alternative pathway activation. Here, we investigated the impact of heme on the regulatory function of the complement system. Heme dose-dependently inhibited factor I-mediated degradation of soluble and surface-bound C3b, when incubated in plasma or buffer with complement regulatory proteins. Inhibition occurred with factor H and soluble complement receptor 1 as co-factors, and the mechanism was linked to the direct heme-interaction with factor I. The heme-scavenger protein hemopexin was the main contaminant in purified factor I preparations. This led us to identify that hemopexin formed a complex with factor I in normal human plasma. These complexes were significantly reduced during acute vasoocclusive pain crisis in patients with sickle cell disease, but the complexes were normalized at their baseline outpatient clinic visit. Hemopexin exposed a protective function of factor I activity *in vitro*, but only when it was present before the addition of heme. In conclusion, we present a mechanistic explanation of how heme promotes uncontrolled complement alternative pathway amplification by interfering with the regulatory capacity of factor I. Reduced levels of hemopexin and hemopexin-factor I complexes during an acute hemolytic crisis is a risk factor for heme-mediated factor I inhibition.

Keywords: heme, complement, factor I, co-factor activity, hemopexin, hemolysis

INTRODUCTION

Intravascular hemolysis is observed in various diseases, including sickle cell disease (SCD) (1), malaria, atypical hemolytic uremic syndrome (2), and sepsis (3). Hemolysis can also be a complication after a blood transfusion or exposure to biomaterials, where mechanical forces in the cardiovascular devices can rupture erythrocytes (4–6). Upon disruption of the erythrocytes, hemoglobin is released into the plasma. Heme is an iron prosthetic group and an essential component of hemoglobin and other hemeproteins (7). Under pro-oxidative conditions, heme is oxidized into the ferric (Fe^{3+}) state and is then prone to be released from the hemoglobin (7, 8). This plasma free heme is a pro-oxidative and pro-inflammatory mediator that can trigger innate immune activation (9). Studies have linked heme to innate immune activation *via* triggering complement- and Toll-like receptor 4-activation (10, 11). Platelets, endothelial cells (12, 13), and the coagulation system (14, 15) are other vasculature components that heme can activate.

Any toxicity from hemoglobin and heme is compensated by the presence of abundant plasma scavenger molecules (16). Haptoglobin, an acute-phase protein, captures hemoglobin and prevents heme from being released. Monocytes express CD163 that clear haptoglobin-hemoglobin from plasma, and endothelial cells can induce expression of heme-oxygenases to degrade heme into less toxic byproducts. Additionally, plasma hemopexin binds plasma-free heme and neutralizes its reactivity (4, 8, 17–19). However, these systems can be saturated under massive or continuous hemolysis (20).

Activation of the complement system can occur *via* three routes: classical, lectin, and the alternative pathway (21). All three pathways lead to the formation of a convertase that cleaves C3 into C3a and C3b. Every surface-bound C3b can initiate or propagate the alternative pathway activation, thus, rapidly amplifying the response. Therefore, it is critical to immediately degrade C3b into iC3b to control this amplification course on non-pathogenic substrates and host surfaces. C3b is degraded by factor I to iC3b and C3f, and iC3b can further be degraded to C3c and C3dg fragments (22–24). Factor I is a serine protease that requires the presence of co-factors, i.e., the soluble factor H, the membrane-bound complement receptor 1 (CR1, CD35), or the membrane co-factor protein (MCP, CD46), to cleave the alpha´-chain of C3b (25).

Multiple studies have linked intravascular hemolysis and the presence of cell-free heme in plasma to alternative complement pathway activation (26–29). The mechanism is not fully understood but is related in part to the interaction of heme with C3 (2). Among the regulators of C3, factor H shows weak interaction with heme, but no data are available for factor I (2). This study aimed to investigate how heme dysregulates complement regulatory function at the level of factor I.

MATERIALS AND METHODS

Reagents

Porcine hemin [ferriprotoporphyrin IX chloride] obtained from Merck (Darmstadt, Germany) was prepared as previously described (2). Hemin refers to the oxidized Fe^{3+}-analog of heme. Human factor C3 was purified according to the method described by Hammer et al. (30). C3b was prepared by digestion of C3 with 1% (w/w) trypsin from bovine pancreas (Merck) for 5 minutes at 22°C and separated with gel filtration on Sephadex G100 (GE Healthcare, Chicago, IL), which was then equilibrated with 10 mM phosphate buffer (pH 7.4) and 0.145 M saline (PBS). Human complement factor H was purified from human serum as described by Hammer et al. (30) but modified with euglobulin precipitation, according to Nilsson et al. (31). Human complement factor I was procured from CompTech (Tyler, TX) and human plasma hemopexin from Merck. Biotinylated antibodies were prepared with the biotinylation reagent biotinamidohexanoic acid N-hydroxysuccinimide ester (Merck) (32). The compstatin analog Cp40 [yI[CV(MeW)QDW-Sar-AHRC](NMe)I-NH_2] to block C3-cleavage (33), was kindly provided by John D. Lambris. Soluble CR1 (sCR1) was obtained from T Cell Sciences Inc (Cambridge, MA).

Whole Blood Collection and Plasma Preparation

Patients with sickle cell disease were recruited at Children's Healthcare of Atlanta, Georgia, USA, under a local IRB-approved study. Ethylenediaminetetraacetic acid (EDTA)-plasma samples were collected at two time points; hospital admission for acute vasoocclusive pain crisis (VOC) and during their baseline outpatient clinic at least four weeks later. Whole blood was collected from healthy donors (n = 20) in 4.5 mL cryotubes (Cryo Tube™ Vials; Thermo Scientific, Waltham, MA) containing thrombin inhibitor, lepirudin (Refludan; Celgene, Uxbridge, UK) at a final concentration of 50 μg/mL. Whole blood was centrifuged at 3000 x g for 15 minutes to collect plasma. A human plasma pool (NHP) was created by pooling plasma from six healthy donors. All plasma samples were stored at -80°C.

Absorbance Spectroscopy

Aliquots of heme, resulting in final concentrations of 0.25 to 64 μM, were added to an optical cell containing factor I (CompTech) or PBS as control, and incubated for two minutes in the dark at room temperature. The absorbance spectra in the 350 – 700 nm wavelength range were recorded using an Agilent Cary 100 spectrophotometer (Agilent Technologies, Santa Clara, CA). The data on the difference between protein-bound heme and free heme at absorbance maxima (λ = 395 nm) in the Soret peak was used to build titration binding curves.

Measurement of Binding of Heme to Factor I by Surface Plasmon Resonance

The binding of heme to factor I was further evaluated by surface plasmon resonance (BIAcore 2000 instrument). Factor I (CompTech) was immobilized on a CM5 sensor chip using an amino-coupling kit as recommended by the manufacturer (Cytiva, Uppsala, Sweden), and a control flowcell was mock-immobilized. The experiments were performed using PBS (pH 7.4) with 0.005% (v/v) Tween 20 as a running buffer. Heme was diluted from a 10 mM stock in PBS just before injection and introduced to the

flowcells at a flow rate of 10 µl/min. Regeneration of the chip surface was achieved by brief exposure (30 s) to a solution containing 0.3 M imidazole. The binding to the surface of the control flow cell was subtracted from the binding to the factor I-coated flow cells. BIAevaluation software (version 4.1; Biacore) was used to evaluate the kinetic rate constants.

In Silico Analyses of Heme Binding to Factor I

The atomic coordinates of factor I were taken either from PDB ID 2XRC (34) or extracted from the C3b/fH1-4:19-20/FI (PDB ID 5O32) and used for the molecular docking (35). HexServer (http://hexserver.loria.fr/) with default parameters was used to accommodate the heme molecule to FI (36), as described previously for C1q and C3 (2, 37). Criteria for final factor I-heme complex selection were based on the total energy of binding. Visualization of the top ten complexes was done by PyMol (www.pymol.org). To evaluate for potential functional relevance, we visualized the predicted top ten heme-binding positions at the structure of FI alone or at the C3b/fH1-4:19-20/FI complex structure.

Evaluation of Degradation of Soluble C3b

A complement co-factor assay was employed to determine C3b-degradation. C3b (10 µg) was incubated with factor I (0.1 µg) and the co-factors (0.1 µg) factor H or sCR1 in PBS for up to 60 minutes. Heme was included in the incubations in concentrations between 8 and 64 µM. Incubations that contained C3b, factor I, and factor H or sCR1 served as positive controls. Incubations that contained C3b, factor H, and sCR1, without factor I, served as negative controls. Hemopexin (40 µg/ml) was included during the incubation in separate experiments. In these setups, all samples contained heme at 32 µM. Four different 30-minute incubations were included for each of the two co-factors, i) all components (C3b, factor I, heme, hemopexin, and co-factor) were added simultaneously, ii) factor I was pre-incubated with heme for 15 minutes before addition of C3b, co-factor, and hemopexin, iii) all components but hemopexin were pre-incubated for 15 minutes before addition of hemopexin, iv) factor I was preincubated with hemopexin for 15 minutes before C3b, co-factor and heme were later added. The 30-minute incubation time started after adding all the components mentioned above. All incubations were carried out in 1.8 mL Nunc-cryotubes (Nunc, Roskilde, Denmark) at 37°C. Reduced (5x) SDS-PAGE sample buffer (Biorad, Hercules, CA) was added at the end of each incubation, and the samples were moved to a heating block and incubated for another 10 minutes at 95°C. Finally, the samples were loaded on 4 – 15% Tris-glycine gels and applied to SDS-PAGE electrophoresis. The gels were stained with Coomassie Brilliant Blue G-250 dye (Biorad).

Quantification of Degradation of Surface-Bound C3b

According to the manufacturer's protocol, Bio-Plex Pro™ magnetic COOH beads were immobilized with 6 µg cystamine sulfate hydrate (Merck) using the amine coupling kit (Biorad). Dithiothreitol (DTT; Roche Diagnostics, Rotkreuz, Switzerland) 6 mM was used for the reduction of the internal disulfide bond of cystamine (38). The beads were incubated with DTT at 22°C for 20 minutes, followed by thorough washing with PBS. To conjugate C3b to the free sulfhydryl of the immobilized cystamine, 20 µg of purified C3 and 1.6% (w/v) of trypsin were incubated with the beads for 20 minutes at 37°C. The reaction was later stopped by washing with PBS. The C3b-beads were then incubated in black flat-bottom 96-well plates together with factor I (0.15 µg) and factor H or sCR1 (1.3 µg), with increasing heme concentrations in three-fold serial dilutions (up to 32.4 µM). Trypsin (140 µg/mL) incubated with C3b-beads was used as a positive control. After incubation for one hour at 37°C on agitation, C3b-fragments were detected using two different antibodies, either biotinylated polyclonal rabbit anti-human C3c antibody (Dako, 4 µg/mL) or biotinylated monoclonal anti-human-iC3b-neo (Quidel, A209, 4 µg/mL). Both antibodies were followed by streptavidin-phycoerythrin (PE; Biorad), diluted at 1:100. Incubations with the antibody and streptavidin took place for 30 minutes at 22°C on agitation in the dark. All dilutions were done in PBS with 0.1% (v/v) Tween 20 and 0.05% (w/v) bovine serum albumin (BSA) (Merck). The beads were washed three times with PBS 0.05% (v/v) Tween 20 between every incubation step. Mean fluorescent intensity (MFI) was detected by Bio-Plex MAGPIX Multiplex Reader (Biorad).

Likewise, we repeated this process with lepirudin-anticoagulant plasma instead of purified components. The plasma was then centrifuged for 10 minutes at 9400 x g and diluted 1:5 with PBS containing Cp40 (8 µM). Next, heme was added to the plasma in concentrations of up to 32.4 µM, and C3b-beads were added and incubated for up to 60 minutes at 37°C.

Factor I Purification

Normal human citrate-plasma (235 mL) was supplemented with EDTA to 5 mM final concentration. Polyethyleneglycol (4 kDa) was added to the plasma at 8% (w/v) concentration, incubated for 30 minutes at 4°C on rotation, and then centrifuged at 13000 x g for 30 minutes at 4°C. The supernatant was isolated and diluted at 1:2 with 5 mM EDTA, and the pH was adjusted to 6.0 with hydrochloric acid (HCl). The supernatant was loaded on a 50 mL SP-Sepharose Fast Flow 26/10 50 mL column equilibrated with a 20 mM phosphate buffer (pH 6.0) with 50 mM sodium chloride (NaCl), 5 mM EDTA, and 0.02% (w/v) NaN_3, with a flow rate of 5 mL per minute. The column was washed with 10 volume fractions of equilibration buffer and eluted with a 250 mL NaCl gradient (50 mM – 400 mM). One hundred 2.5 mL fractions were collected.

Factor I was detected in eluted fractions using direct ELISA. The fractions were coated in wells of a microtiter plate, 50 µl per well, and incubated overnight at 4°C. The wells were blocked with 1% (w/v) bovine serum albumin diluted in a 10 mM phosphate buffer containing 145 mM NaCl. Factor I was detected using sheep anti-human factor I (The Binding Site, Birmingham, UK), followed by a rabbit anti-sheep IgG with

horseradish peroxidase (HRP) by Dako (Glostrup, Denmark). The fractions containing factor I (in total 130 mL) were pooled and dialyzed three times against 1 liter 10 mM Tris-HCl (pH 8.5), 200 mM NaCl, 0.02% NaN_3. The dialysate was loaded, at 1 mL per minute flowrate, on a 15-mL Wheat Germ Agglutinin Sepharose column equilibrated with a 10 mM Tris-HCl, 200 mM NaCl, 0.02% NaN_3 pH 8.5. The same buffer was used for washing the column, five column volumes. Factor I was eluted with 10% (w/v) N-acetyl-D-glucosamine supplemented to the washing buffer in 90 fractions, 0.5 mL each. As detected with the direct ELISA, the fractions containing factor I (34 fractions) were pooled and dialyzed two times against 1 L 10 mM Tris-HCl (pH 8.5) with 0.02% NaN_3. The dialysate was applied, with a flow rate of 2.5 mL per minute, on an 8-mL Mono Q column, equilibrated with the 10 mM Tris-HCl (pH 8.5) 0.02% NaN_3, and washed with 24 column fractions of the equilibration buffer. The column was eluted with a 0-220 mM NaCl-linear gradient supplemented with the equilibration buffer for 60 minutes, followed by 10 minutes with the 220 mM-NaCl buffer. The factions were evaluated for factor I and hemopexin.

As for factor I, hemopexin was detected in a direct ELISA with fractions diluted at 1:250 in PBS. Hemopexin was detected using a rabbit anti-human hemopexin (Dako) followed by a polyclonal anti-rabbit IgG-HRP (Dako). Depending on when factor I was eluted in the chromatogram, fractions were pooled in one early pool, labeled as pool 1, and one late pool, referred to as pool 2. The presence of hemopexin and factor I in pool 1 and pool 2 were assessed by Western blot. The samples (10 µg) included two commercial factor I preparations from CompTech and Quidel for comparison, and two hemopexin preparations, one commercial (R&D Systems, Abingdon, UK) and one purified in-house (27). The samples were mixed with reduced and non-reduced Laemmli loading buffer (Biorad) and heated for 10 minutes at 94°C. The proteins were separated on a 4%-15% SDS-PAGE and transferred to a polyvinylidene difluoride (PVDF) membrane (Biorad). Hemopexin was detected by a biotinylated rabbit anti-human hemopexin antibody (Dako) followed by streptavidin-HRP (Biorad). A biotinylated sheep anti-human factor I (Abcam) followed by streptavidin-HRP (Biorad) was used to identify factor I. The bands were detected by chemiluminescence and imaged by Chemi Doc ™ MP Gel Imaging System (Biorad). Finally, a functional test was applied to evaluate the ability of the two pools to degrade C3b effectively. Purified C3b (10 µg) was incubated with all the different factor I-preparations (2 µg), as analyzed above with Western blotting, and factor H (2 µg) at 37°C for 60 minutes in PBS (pH 7.4). The samples were run on a 4%-15% SDS-PAGE under reduced conditions and were stained with Coomassie Brilliant Blue.

Hemopexin, Factor I, and Factor I/Hemopexin-Complex Immunoassays

Hemopexin was quantified in plasma by ELISA as previously described (27). Factor I and the factor I/hemopexin-complexes were quantified in immunoassays developed on the xMAP-platform. Bio-Plex Pro™ magnetic COOH beads (Biorad) were immobilized with monoclonal mouse anti-human complement factor I antibodies (Abcam, Cambridge, U.K.) using the Bio-Plex Pro™ magnetic COOH beads amine coupling kit according to the manufacturer's instructions (Biorad). For both factor I and factor I/hemopexin-complexes, beads amounting to 2500 per well in 96-well plates (Bio-Plex Pro™ black flat bottom plate; Biorad) were incubated with EDTA-plasma samples (1:500 for the factor I/hemopexin-complexes and 1:300 for factor I), for 30 minutes at RT on agitation. Biotinylated rabbit anti-human hemopexin antibody (Dako), diluted at 1:50, followed by streptavidin-PE (Biorad), diluted at 1:100, was used to detect the complexes. Biotinylated sheep anti-human factor I (Abcam) diluted at 1:300, followed by streptavidin-PE (Biorad), diluted at 1:100, was used to detect factor I. Pool 1, co-purified with hemopexin, was used as the standard for measuring factor I/hemopexin complexes. The international complement standard #1 (39) was used as the standard for factor I. We followed the same incubation conditions for the C3b quantification protocol as described above. MFI was detected by Bio-Plex MAGPIX Multiplex Reader (Biorad).

Statistical Analysis

The SDS-PAGE data was analyzed by Image J (US National Institutes of Health, https://imagej.nih.gov/ij). The statistical analysis and absorbance spectroscopy calculations were performed using GraphPad Prism version 7.7 for Mac (San Diego, CA). Paired t-test was applied to compare two columns, and either ordinary/repeated measures with Dunnette's multiple comparisons or non-parametric one-way ANOVA were used to compare multiple columns.

RESULTS

Heme Interacts With Factor I

Absorbance spectroscopy and surface plasmon resonance (SPR) were used to examine the ability of heme to interact with factor I. The absorbance spectra showed that heme bound to soluble factor I in a dose-dependent manner (**Figures 1A, B**). Increasing heme concentrations, up to 64 µM, increased the absorbance at 414 nm, referring to the Soret peak of heme. The interaction was dose-dependent but the curve did not reach saturation in our experimental conditions, to allow us to correctly deduce the binding affinity (an approximation from the fit would be ~40 µM). Therefore, we confirmed the binding by SPR. Heme at 0.075 to 10 µM was let to interact with surface-immobilized factor I, and the interaction was analyzed using SPR. Heme interacted with factor I with an apparent association rate (k_a) of $1.03x10^2$ $M^{-1}s^{-1}$ and a dissociation rate (k_d) of $1.19x10^{-3}$ s^{-1} (**Figure 1C**). The apparent equilibrium dissociation constant (K_D) was calculated to $1.15x10^{-5}$ M (11.5 µM). *In silico* modeling was employed to predict the putative binding site between heme and factor I. The modelling indicated that the putative site of interaction of heme to factor I (both when taken alone (2XRC) or extracted from the C3b/fH1-4:19-20/FI (5O32)) was at the interface between the heavy and the light chain of factor I

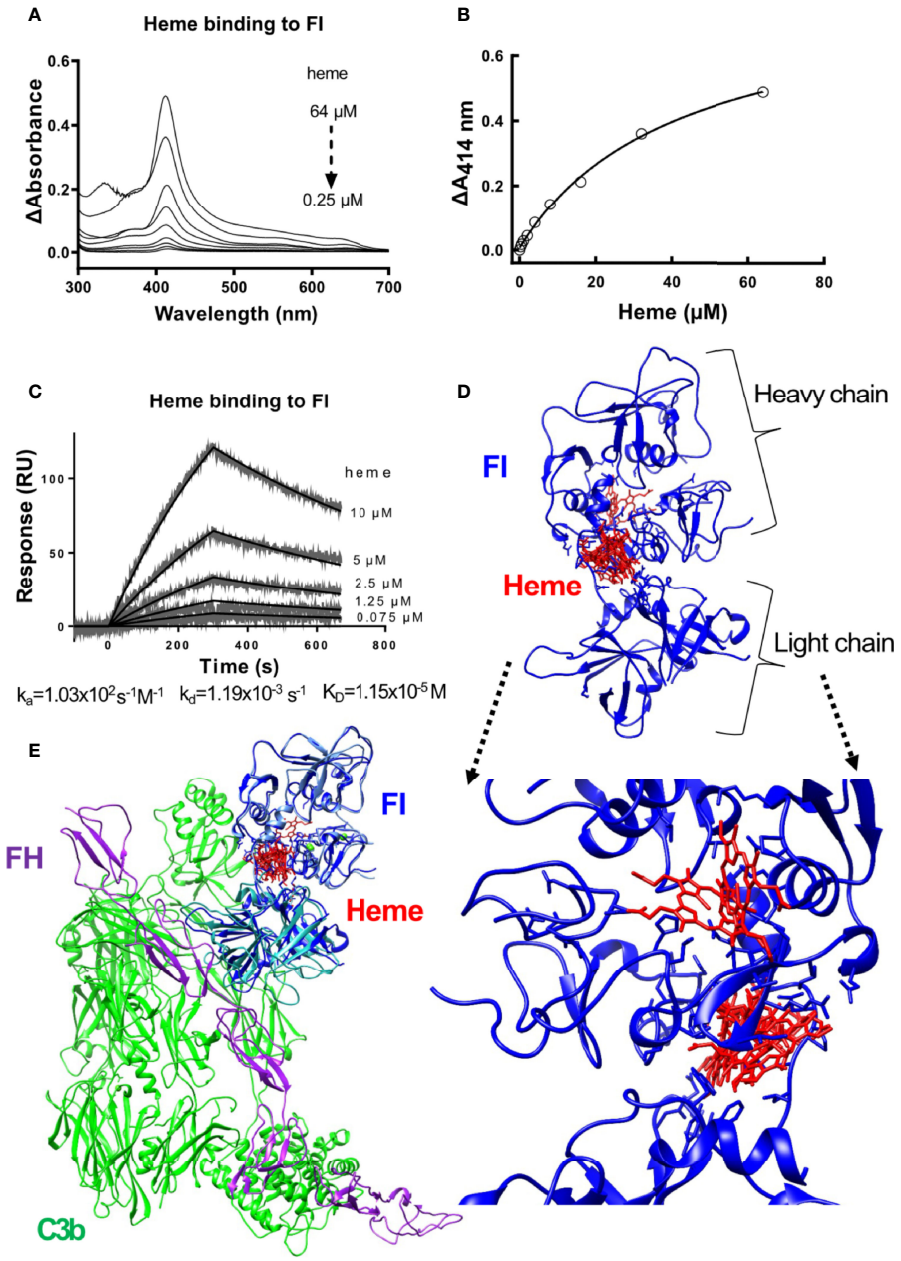

FIGURE 1 | Heme binding to factor I **(A, B)** Absorbance spectroscopy of heme (0.25-64 µM) binding to factor I (FI) from Comptech, shown as an absorbance spectrum **(A)** and at wavelength 414 nm **(B)**. **(C)** SPR analysis of the binding of different concentrations of heme to factor I (Comptech) immobilized on a Biacore sensor chip. **(D)** Molecular docking of heme (red) to factor I (blue). The top ten complexes are visualized. **(E)** Overlap of the factor I-heme complexes with the structure of the complex C3b/fH1-4:19-20/FI (5O32).

(**Supplementary Figure 1** and **Figure 1D**), and may potentially affect its enzymatic activity and the integration with the C3b/factor H and by homology, the C3b/CR1 complex (**Figure 1E**).

Heme Inhibits Factor I-Mediated Degradation of Soluble C3b

The impact of heme to factor I binding was investigated by evaluating factor I-mediated degradation of soluble C3b in the presence of heme. Purified C3b was incubated together with factor I and the co-factors factor H or soluble CR1 (sCR1) in increasing heme concentrations (8-64 µM) at 37°C. C3b-degradation was analyzed on an SDS-PAGE by densitometric comparison of the factor I-sensitive alpha′-chain (101 kDa) in relation to the inert beta-chain (75 kDa). Factor I degraded C3b in the presence of both factor H (**Figures 2A, C**) and sCR1 (**Figures 2B, D**). Heme interfered with this degradation; there

was decreased cleavage of the α-chain of C3b as the heme concentration increased, both at 15- and 60-minutes incubation time. Heme at 64 μM significantly inhibited the C3b-cleavage, both with factor H and sCR1 as co-factors ($p<0.05$).

Heme Inhibits Factor I-Mediated Degradation of Surface Bound C3b

The impact of heme on factor I-activity was further evaluated by the degradation of surface-bound C3b. Magnetic beads with C3b coupled *via* the C3b-thioester were incubated with factor I and factor H (**Figures 3A, C**) or sCR1 (**Figures 3B, D**) at 37°C for 60 minutes. Heme was included from 32.4 μM and in threefold dilutions to 1.1 μM. The degradation of C3b was evaluated as reduction of C3c-fragment-detection (**Figures 3A, B**) or increased detection of iC3b on the beads (**Figures 3C, D**). Factor I, together with factor H or sCR1, was able to degrade C3b on the beads' surface, as shown by decreased amounts of C3c on the bead's surface (**Figures 3A, B**) and increased detection of iC3b (**Figures 3C, D**). The loss of C3c was more profound when sCR1 was used as a co-factor, and increase in iC3b was more profound for factor H. Heme interfered with this degradation in a dose-dependent manner, as more binding of the C3c-fragments was detected when heme was included in the incubations. Heme at 32.4 μM significantly ($p < 0.01$) reduced the loss of C3c-fragments from the beads compared to the conditions without heme. In separate experiments, the ability of heme to interfere with C3b-degradation in 20% lepirudin-plasma, containing only endogenous factor I and soluble co-factors; factor H and sCR1, was evaluated by incubating C3b-coated beads with increasing concentration of heme (up to 32.4 μM) for up to 60 minutes (**Figure 3E**). Incubation of the beads in plasma showed a time-dependent reduction of C3c-containing fragments on the bead surface. The addition of heme to plasma inhibited the C3b-degradation in a dose-dependent manner, and the effect was more pronounced with higher heme-concentrations. All tested heme-concentrations (1.1 – 32.4 μM) significantly ($p < 0.05$) reduced the liberation of C3c from the beads.

Factor I in Plasma Is Encountered in Complex With Hemopexin

Factor I was purified from normal human citrate-plasma by sequential chromatography on a Sepharose FF column (**Figure 4A**), lectin agarose column (**Figure 4B**), and a Mono Q ion-exchange column (**Figures 4C, D**). From the latter, factor I was eluted in two peaks (**Figure 4C**). These peaks were pooled separately and referred to as pool 1 and pool 2 representing the early and late eluted peaks of factor I. By an enzyme-linked immunosorbent assay (ELISA) (**Figure 4C**) and Western blot (**Figures 4E, F**), hemopexin was identified as the main contaminant present in both pools. In comparison to pool 2,

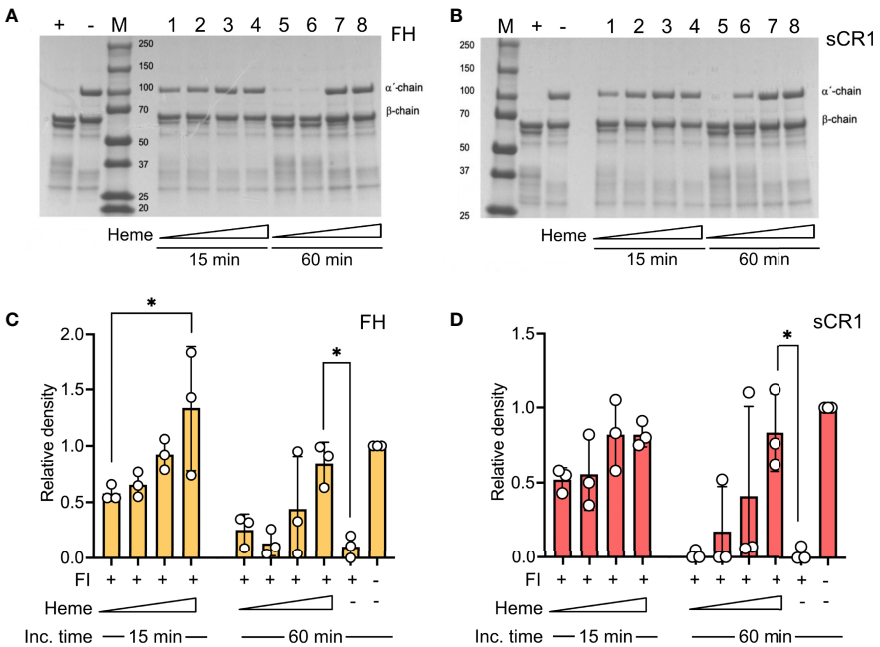

FIGURE 2 | Effect of heme on factor I-mediated degradation of soluble C3b. C3b (10 μg) was incubated in the presence of factor I (FI, 0.1 μg) and **(A, C)** factor H (FH, 0.1 μg) or **(B, D)** soluble complement receptor 1 (sCR1, 0.1 μg) at 37°C for 15 and 60 minutes, in phosphate buffered saline (PBS) pH 7.4. The samples were run on a 4-15% SDS-PAGE under reduced conditions and stained with Coomassie Brilliant Blue. The gels shown **(A, B)** are each a representative gel from three independent experiments. **(A, B)** The samples are displayed as follows: positive control (+); negative control, which lacks FI (-); molecular weight marker (M). For samples 1-8, heme was included in increasing concentrations (lane 1, 5: 8 μM; lane 2, 6: 16 μM, lane 3, 7: 32 μM, lane 4, 8: 64 μM) for 15 minutes (1-4) or 60 minutes (5-8), as indicated in the figure. **(C, D)** C3b-degradation was evaluated by densitometric measurement and displayed as the relative density of the C3b intact α´-chain at 101 kDa in relation to the β-chain at 75 kDa. The values are shown as mean +/- standard deviation of n=3. *$p < 0.05$.

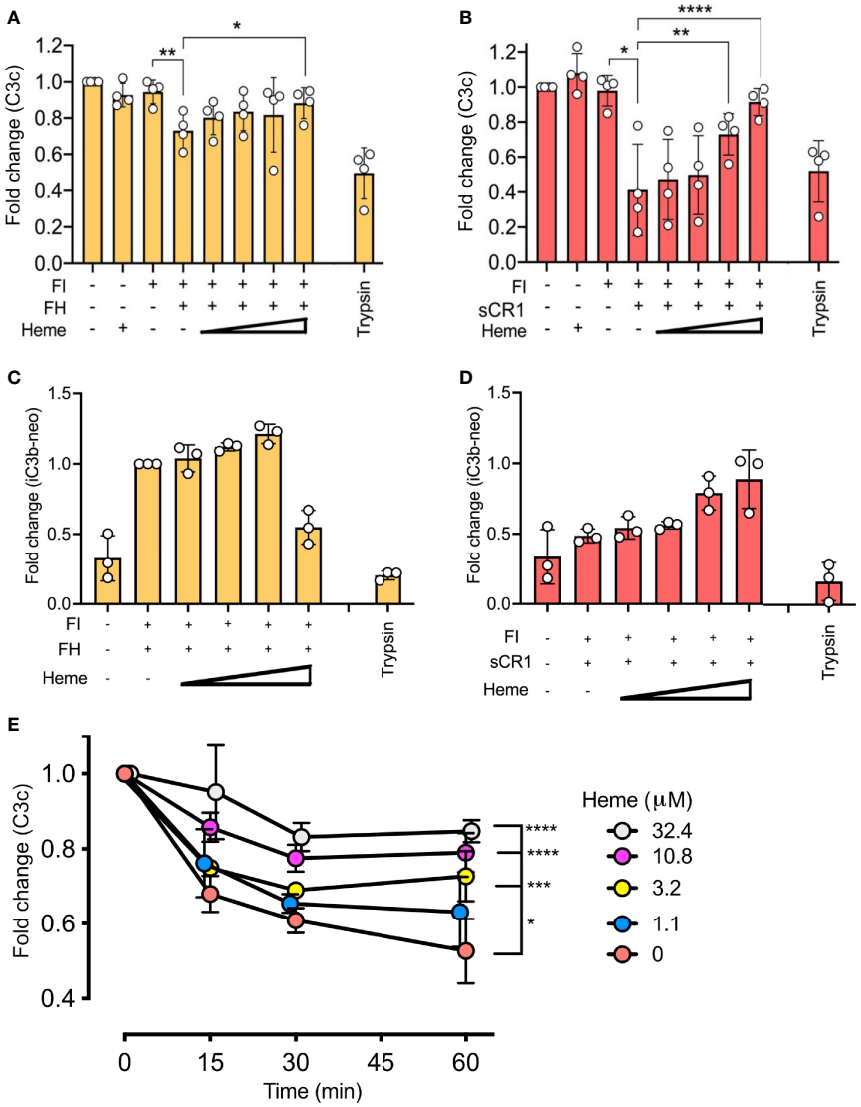

FIGURE 3 | Effect of heme on factor I (FI)-mediated degradation of surface-bound C3b. C3b, covalently connected bound to magnetic beads, were analyzed for factor I (FI-mediated degradation by **(A–D)** purified components in phosphate buffered saline (PBS) and **(E)** lepirudin plasma at 37°C. Degradation of C3b was analyzed by a polyclonal anti-C3c antibody **(A, B, E)**, and a monoclonal iC3b antibody **(C, D)**. **(A–D)** Factor I (FI, 0.1 μg) and **(A, C)** factor H (FH, 0.1 μg) or **(B, D)** soluble complement receptor 1 (sCR1, 0.1 μg) were incubated with C3b-beads at 37° C for 60 minutes in PBS pH 7.4. Heme was supplemented in increasing amounts (1.1, 3.2, 10.8, 32.4 μM). Trypsin was included as a positive control. Values are shown as the mean of three independent experiments +/- standard deviation. Paired t-tests were used to compare C3b-beads and FI with and without co-factor. **(E)** One-way ANOVA non-parametric test was used for the comparison between C3b-beads with FI and co-factor with various concentrations of heme. **(E)** C3b-beads were incubated in lepirudin-plasma supplemented with compstatin Cp40 (8 μM) and heme in concentrations from 0–32.4 μM for 15, 30, or 60 minutes at 37°C. The graph shows mean +/- standard deviation from three independent experiments, all normalized to the mean fluorescent intensity (MFI) of beads at the start of incubation. One-way ANOVA non-parametric test was used for the comparison between C3b-beads with heme versus C3b-beads with various concentrations of heme. *$p < 0.05$, **$p < 0.01$, ***$p < 0.001$, ****$p < 0.0001$.

Pool 1 contained a lower amount of factor I (**Figure 4E**) but a higher amount of hemopexin (**Figure 4F**). Interestingly, factor I was present in low amounts in a hemopexin-preparation purified from normal human serum. No hemopexin was detected in the factor I-preparations bought from CompTech or Quidel (**Figure 4F**). Hemopexin-factor I complex formation was evaluated by sandwich-ELISAs where pool 1 was incubated in microtiter-wells coated with antibodies directed against factor I and detected with anti-hemopexin and vice versa (**Figure 4G**). Both assays showed that the eluate contained complexes consisting of both factor I and hemopexin. An effort to remove hemopexin from factor I in pool 1 by applying it to a heme-agarose column caused a complete loss of factor I (data not shown). Both pools were evaluated for their ability to degrade fluid phase C3b in the presence of co-factors. Only factor I in pool 1, and the commercial preparations were found to have

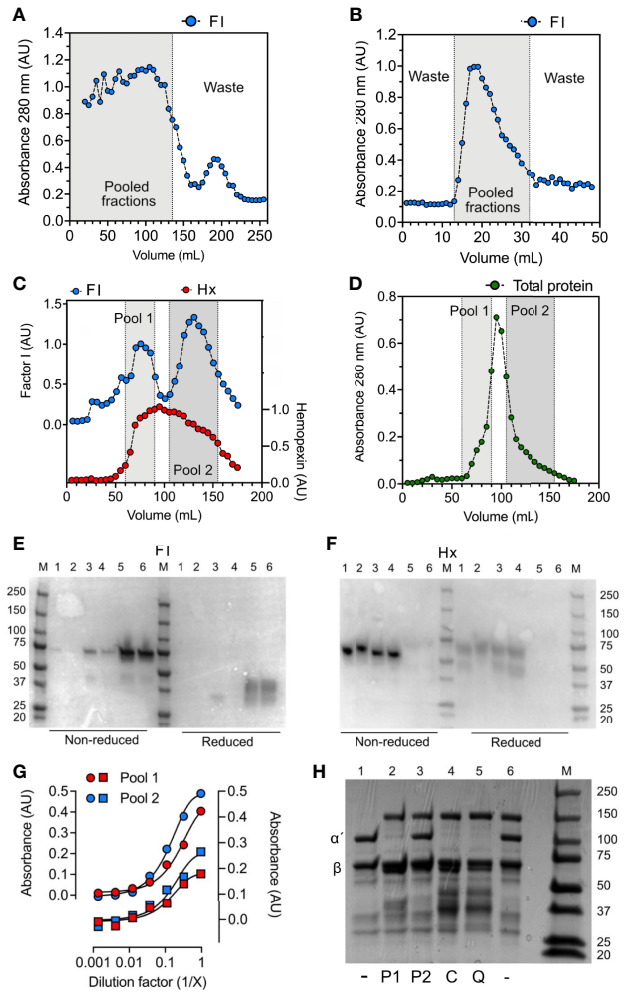

FIGURE 4 | Hemopexin co-purifies with factor I. For the purification of factor I (FI), human plasma was, after PEG precipitation, centrifuged at 13 000 x g for 30 minutes, and the supernatant was applied for sequential chromatography. **(A–D)** Chromatograms for **(A)** Sepharose FF, **(B)** lectin agarose, and **(C, D)** Mono Q columns. **(A–C)** Fractions were analyzed by direct ELISA by coating fractions in microtiter plate wells and analyzing for factor I (FI, blue) and hemopexin (only the Mono Q column) (Hx, red) content using specific polyclonal antibodies. **(D)** Total protein in fractions from the Mono Q column was evaluated by absorbance measurements at 280 nm (absorbance units, AU). **(A, B)** Fractions within the gray area were pooled and applied for the next column. **(C, D)** The elution fractions from the Mono Q column **(C, D)** were pooled in two different pools: 1 (light grey) and 2 (dark grey) according to the two elution peaks for factor I **(E, F)** Western blot for factor I **(E)** and hemopexin **(F)** under non-reduced and reduced conditions. The following samples (10 μg) were analyzed: hemopexin purified from human serum (1), recombinant hemopexin (2), factor I "pool 2" (3), factor I "pool 1" (4), purified factor I bought from Quidel (5), purified factor I bought from CompTech (6). M corresponds to molecular weight marker. **(G)** Sandwich ELISA with pool 1 (red) and pool 2 (blue) incubated in threefold dilutions on microtiter plates coated with anti-FI (circles) and anti-hemopexin (squares) and detected with anti-hemopexin (circles) and anti-FI (squares). **(H)** SDS-PAGE for the degradation of C3b with different factor I-preparations (as indicated below the gel), incubated for 60 minutes at 37°C. All samples contain C3b, samples 2-6 contains factor H, and samples 2-5 contain factor I: pool 1 (P1) (2), pool 2 (P2) (3), CompTech factor I (C) (4), and Quidel factor I (Q) (5). The intact alpha´- and beta chain of C3b are indicated by α´ and β, respectively.

catalytic activity, whereas no activity was found for factor I in pool 2 (**Figure 4H**).

Patients With SCD Demonstrate Decreased Levels of Hemopexin and Factor I/Hemopexin Complexes

The observation that hemopexin and factor I co-purified by two separate protocols (i.e., the factor I- and hemopexin purification protocol) led us to hypothesize that hemopexin might form a complex with factor I already in human plasma. Factor I, hemopexin, and factor I-hemopexin complexes were evaluated in normal human plasma, and patients with SCD (n = 18) collected during admission to the hospital during VOC and later during a baseline follow-up visit. Hemopexin levels were significantly lower ($p < 0.0001$) in the patients with SCD both during 'acute' and 'baseline' when compared to healthy controls (n=50) (**Figure 5A**). The mean hemopexin concentration (+/- SD) in this patient population increased from 0.80 +/- 0.59 mg/

mL during an acute crisis to 0.86 mg/mL +/-0.69 during their baseline visits, although not statistically significant. The mean concentration of factor I was lower in patients with SCD in comparison to a pool of plasma samples from healthy donors (**Figure 5B**). The mean concentration (+/- SD) increased from 19.6 +/- 5.1 µg/mL to 21.3 +/- 4.8 µg/mL from admission to heathy visit, which was not statistically significant. Factor I-hemopexin complexes were found in the plasma pool from healthy donors, and in SCD patients (**Figure 5C**). Interestingly, these complex levels increased by 39% from 'acute' to 'baseline' visits ($p < 0.01$).

Hemopexin Rescues Factor I-Activity

To evaluate the physiological role of hemopexin in the context of heme and factor I-mediated degradation of C3b, heme at 32 µM was incubated for 15 minutes at 37°C with C3b, factor I, and either factor H or sCR1, and with hemopexin added at different stages of the incubations (**Figure 6**). Pre-incubation of factor I with heme for 15 minutes before adding C3b, co-factor, and hemopexin led to heme-mediated inhibition of the C3b-degradation, despite the scavenger-property of hemopexin (**Figure 6**). In contrast, pre-incubation of factor I with hemopexin for 15 minutes and then adding heme rescued

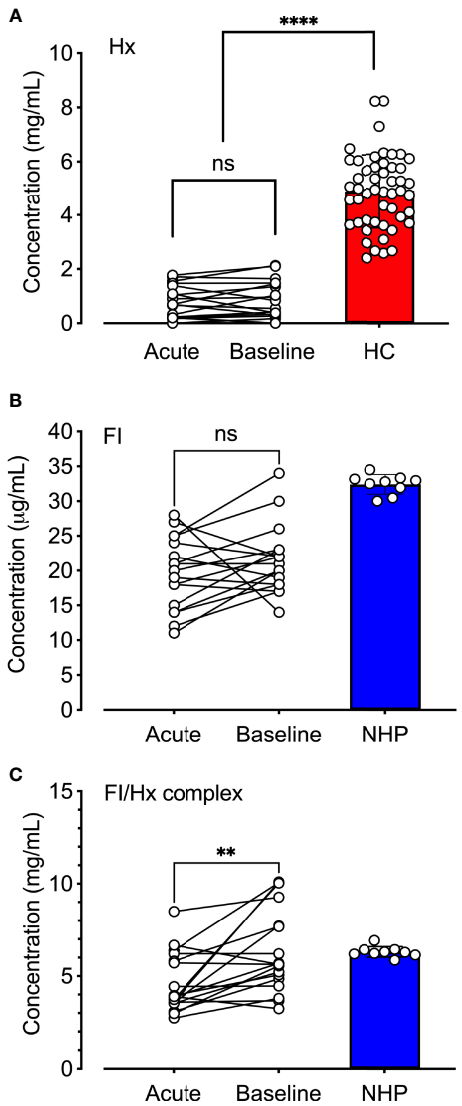

FIGURE 5 | Quantification of hemopexin, factor I, and factor I-hemopexin-complexes in patients with sickle cell disease. **(A)** Hemopexin (Hx), **(B)** factor I (FI), and **(C)** factor I/hemopexin-complexes (FI-Hx complex) were quantified in EDTA-plasma samples from patients with SCD (n = 18) obtained during acute vasoocclusive pain crisis (acute), and a follow-up sample was collected at their baseline healthy visit at least four weeks after the acute episode (baseline). Normal human EDTA-plasma from 52 healthy individuals was used as controls for the hemopexin measurements (healthy controls; HC, red), and a pool of NHP (blue) sampled from six healthy donors was used as a control for the FI and the FI-Hx complex measurements. Individual values are shown together with mean and standard deviation. Paired t-test was performed in order to statistically compare the differences between the patients' admission to the hospital and the healthy visit. One-way ANOVA was used for the comparison of patients at admission and baseline versus healthy donors. ns, non-significant, **$p < 0.01$, ****$p < 0.0001$.

some factor I-activity, which resulted in partial degradation of C3b, indicating that hemopexin was able to protect factor I. This difference in C3b alpha´-chain degradation was seen for both co-factors and was statistically significant for sCR1 ($p < 0.01$) (**Figure 6**). When all the components were added simultaneously, heme inhibited C3b cleavage effectively even in the presence of hemopexin indicating that hemopexin could protect factor I from heme, but only if hemopexin was allowed to incubate with factor I before heme was introduced.

DISCUSSION

We found heme to interact with factor I, which interfered with the factor I-mediated degradation of C3b. Heme administered to either purified factor I and co-factors in buffer or lepirudin-anticoagulated plasma in concentrations corresponding to levels found in severe hemolytic conditions (2, 20, 40), impaired C3b-degradation of both soluble and surface-bound C3b. Our findings support a novel mechanism of how heme-dependent activation of the complement system depends on an impaired factor I-mediated degradation of C3b, leading to a dysregulation of the complement system, which promotes excessive C3-convertase formation and C3-cleavage.

Cell-free heme is a pro-inflammatory molecule recognized as a danger signal implicated in innate immune activation (14). Due to heme´s physicochemical properties, i.e., small hydrophobic and prooxidative (19, 41), heme can interact with several plasma proteins causing conformational changes and act as both an inhibitor (42) or inducer of inflammation (43). Several studies have investigated the role of complement activation in hemolysis and the liberation of heme. For example, in SCD, heme-induced

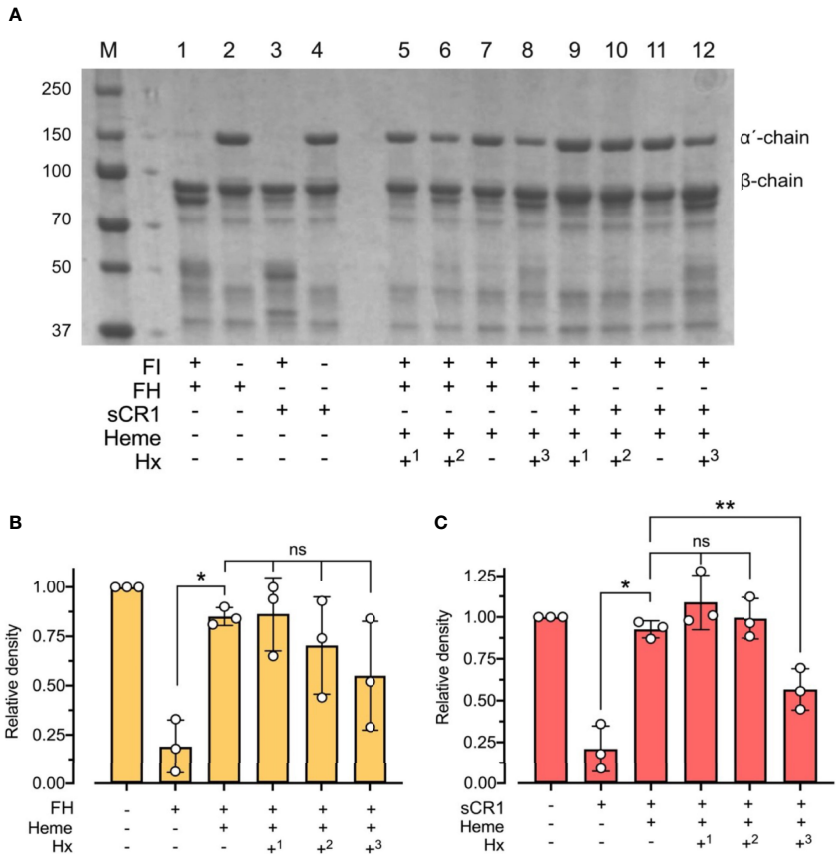

FIGURE 6 | Effect of hemopexin in heme-dependent inhibition of factor I-activity. **(A)** C3b (10 μg) was incubated with factor I (FI 0.1 μg), factor H (FH 0.1 μg) or soluble complement receptor 1 (sCR1 0.1 μg), heme (32 μM), and hemopexin (Hx) added at different time points for 60 minutes at 37°C. The samples were run on a 4 - 15% SDS-PAGE under reduced conditions and stained with Coomassie Brilliant Blue, shown as a representative gel from three independent experiments. Sample 1 - 4 represent controls without heme or hemopexin. Sample 5 - 12 include heme and hemopexin (40 μg/ml) added at different time points. In samples 5 and 9, FI was preincubated with heme for 15 minutes before adding C3b, co-factor, and Hx ($+^1$). In samples 6 - 7 and 10 - 11, all components were added simultaneously, but samples 7 and 10 lack Hx ($+^2$/-). In samples 8 and 12, FI and Hx were preincubated for 15 minutes before adding C3b, heme, and FH or sCR1 ($+^3$). **(B, C)** C3b-degradation was evaluated by densitometric measurement and displayed as the relative density of the C3b intact α´-chain at 101 kDa in relation to the β-chain at 75 kDa using factor H **(B)** and sCR1 **(C)** as the co-factors. The values are shown as mean +/- standard deviation of n = 3. Ordinary or repeated-measures one-way ANOVA with Dunnett's multiple-comparison and paired t-tests for the comparison of two columns were used for the statistical analysis. ns, nonsignificant, *$p < 0.05$, **$p < 0.01$.

complement activation has exclusively been attributed to alternative pathway activation (26–28, 44). Heme serves additionally as an inhibitor of the classical pathway by interacting with the C1q globular heads (37). However, the detailed mechanistic understanding for the strong heme-induced alternative pathway activation has been elusive.

In silico modeling showed that heme could interact directly with the native C3 close to the thioester domain, potentially mediating C3-hydrolysis (2). Hydrolysed C3, i.e., C3(H_2O), serves as an initiator for complement activation by forming the fluid phase C3 (H_2O)Bb-convertase. The C3(H_2O)Bb-convertase is, compared to the surface-bound C3bBb, a low-rate C3-convertase and cannot solely explain the strong activation seen from cell-free heme in plasma (45). However, C3(H_2O)Bb may serve as an initiator of activation by generating the initial C3b molecules. Factor H serves as co-factor for the degradation of C3b to iC3b, and CR1 as co-factor for C3b to iC3b and further to C3c and C3dg. Nevertheless, factor H does not bind heme, and it is unlikely that heme will interfere directly with the factor H function (2).

Nevertheless, the interaction of heme with the C3b degrading enzyme factor I have not been previously investigated. Here we show that heme binds directly to factor I by spectroscopy and SPR, likely between the heavy and the light chain. Based on molecular modeling, we hypothesized that heme might impact the capacity of factor I to degrade C3b. To test this hypothesis, the degradation of soluble C3b was evaluated by loss of the intact 101 kDa a´-chain of C3b in SDS-PAGE and surface-bound C3b by increased expression of iC3b, as evaluated by a neoepitope specific antibody, and reduced binding of an anti-C3c antibody. We found that both co-factors could assist in the factor I-mediated degradation of both soluble and surface-bound C3b. There was a greater increase in iC3b-expression with factor H as the cofactor, and more significant reduction in C3c-detection on the beads by using sCR1 as the co-factor. This is most certainly explained by the sCR1-catalyzed cleavage of C3b all the way to C3dg with release of C3c-fragment into the fluid phase, whereas factor H can only catalyze cleavage of C3b to iC3b, which retains the C3c-fragment still on the beads (22). Heme-dependent inhibition of factor I catalytic activity was evident in the presence of either co-factor in the incubations. It occurred in plasma, where only endogenous soluble complement components were present. Heme as low as 1.1 μM, when added to plasma diluted 1:5, inhibited degradation of surface-bound C3b. This amount of heme can be readily observed in hemolytic diseases. All of these experiments were performed in the presence of the C3-inhibitor compstatin Cp40 to prevent additional C3b-deposition.

Hemopexin is the main scavenger molecule for the clearance of cell-free heme in plasma (14, 18). By coincidence, we found hemopexin to form a complex with factor I in plasma. Hemopexin was found to be the major contaminant when purifying factor I from human plasma whereas it was not found in the commercial factor I preparations. Factor I was eluted from the Mono Q column in two peaks, and hemopexin was present in both of these. Incubation with heme-agarose in order to remove hemopexin also completely depleted factor I from the solution. Correspondingly, factor I was identified in a hemopexin-preparation. To the best of our knowledge, this is the first time hemopexin and factor I are reported to circulate in complex. Surprisingly, we did not detect a direct interaction between FI and hemopexin when was analyzed by SPR. Heme did bind to FI and hemopexin but did not promote the interaction between the two proteins. It is possible that the conformation or orientation of the partners is altered upon the covalent binding to the chip, which could have obstruct potential direct interaction, or that complex formation requires a third component, other than heme. To further evaluate our findings, we tested our hypothesis using samples collected from patients with SCD during acute VOC, and later at their own baseline. The factor I-hemopexin-complexes were also present in low concentrations in the samples of these patients during VOC but increased to levels similar to normal plasma a few weeks after VOC, in contrast to the individual components, which remained low.

Administration of plasma-derived hemopexin before or during VOC in the Townes SCD mouse model, triggered either by heme or hypoxia-reoxygenation, have shown that administration of hemopexin can prevent or reduce VOC, but also, have antioxidant and anti-inflammatory effects (46, 47). Therefore, an objective became to investigate hemopexin's role in the interplay between factor I and heme. When factor I was pre-incubated with heme, and hemopexin was added together with C3b, hemopexin could not rescue factor I activity. On the contrary, when hemopexin was pre-incubated with factor I, before exposure to heme, hemopexin to some extent rescued factor I's activity, allowing more cleavage of C3b since we could partly observe the degradation of the alpha´-chain.

Patients with SCD have a significant decrease in life expectancy compared to age-matched cohorts. If we consider their pain-adjusted quality of life, patients with SCD nearly have half the number of years compared to their counterparts. Those with more than four VOCs/year tend to have a shorter life expectancy (48, 49). Additionally, VOC has been recently associated with complement activation (50), and C5a infusion was shown to induce VOC in murine SCD models, an effect that could be blocked by targeting either C5a or C5aR (51). These results further highlight the importance of understanding the molecular mechanisms of action of hemolysis-derived heme in the pathophysiology of hemolytic diseases.

In conclusion, we propose a novel mechanism explaining how elevated levels of cell-free heme in the circulation interfere with the factor I-regulatory capacity of the complement system, mediating the inability to cleave C3b. These data have implications for all hemolytic diseases, where continuous or acute destruction of erythrocytes mediates initiation of complement activation. On the other hand, hemopexin seems to be a crucial antagonist of heme in preventing heme's deleterious impact on factor I. In conclusion, the study offers new insight into the role of heme in the inflammatory process and may contribute to developing alternative therapeutic approaches for intravascular hemolysis.

DATA AVAILABILITY STATEMENT

The original contributions presented in the study are included in the article/**Supplementary Material**. Further inquiries can be directed to the corresponding author.

ETHICS STATEMENT

The study was designed and performed according to the ethical guidelines from the declaration of Helsinki. Patients with sickle cell disease were recruited at Children's Healthcare of Atlanta, Georgia, USA under a local IRB-approved study. Sampling of human whole blood from healthy individuals for preparation of plasma was approved by the ethical committee of the Norwegian Regional Health Authority, ethical permit REK#S-04114, 2010/934. Informed written consent was obtained from all blood donors. Written informed consent to participate in this study was provided by the participants' legal guardian/next of kin.

AUTHOR CONTRIBUTIONS

AG designed and performed experiments and wrote the paper. JD, AZ, VP, VK, and KM performed or/and designed experiments. SC provided study material and edited the manuscript. KE, TM, and CM provided critical discussions and edited the manuscript. LR and PN designed and supervised the project, wrote the paper. All authors approved the final version of the manuscript.

FUNDING

This work was supported by the Norwegian Research Council (Project 274332), the Swedish Research Council (Project 2018-04087 and 2016-04519), and the Crafoord Foundation (Project 20210961 and 20190890).

SUPPLEMENTARY MATERIAL

The Supplementary Material for this article can be found online at: https://www.frontiersin.org/articles/10.3389/fimmu.2022.901876/full#supplementary-material

REFERENCES

1. Kato GJ, Steinberg MH, Gladwin MT. Intravascular Hemolysis and the Pathophysiology of Sickle Cell Disease. *J Clin Invest* (2017) 127(3):750–60. doi: 10.1172/JCI89741
2. Frimat M, Tabarin F, Dimitrov JD, Poitou C, Halbwachs-Mecarelli L, Fremeaux-Bacchi V, et al. Complement Activation by Heme as a Secondary Hit for Atypical Hemolytic Uremic Syndrome. *Blood* (2013) 122(2):282–92. doi: 10.1182/blood-2013-03-489245
3. Gaggar A, Patel RP. There Is Blood in the Water: Hemolysis, Hemoglobin, and Heme in Acute Lung Injury. *Am J Physiol Lung Cell Mol Physiol* (2016) 311(4):L714–L8. doi: 10.1152/ajplung.00312.2016
4. Schaer DJ, Buehler PW, Alayash AI, Belcher JD, Vercellotti GM. Hemolysis and Free Hemoglobin Revisited: Exploring Hemoglobin and Hemin Scavengers as a Novel Class of Therapeutic Proteins. *Blood* (2013) 121 (8):1276–84. doi: 10.1182/blood-2012-11-451229
5. Ravichandran AK, Parker J, Novak E, Joseph SM, Schilling JD, Ewald GA, et al. Hemolysis in Left Ventricular Assist Device: A Retrospective Analysis of Outcomes. *J Heart Lung Transplant* (2014) 33(1):44–50. doi: 10.1016/j.healun.2013.08.019
6. Shapira Y, Vaturi M, Sagie A. Hemolysis Associated With Prosthetic Heart Valves: A Review. *Cardiol Rev* (2009) 17(3):121–4. doi: 10.1097/CRD.0b013e31819f1a83
7. Soares MP, Bozza MT. Red Alert: Labile Heme Is an Alarmin. *Curr Opin Immunol* (2016) 38:94–100. doi: 10.1016/j.coi.2015.11.006
8. Alayash AI, Andersen CB, Moestrup SK, Bulow L. Haptoglobin: The Hemoglobin Detoxifier in Plasma. *Trends Biotechnol* (2013) 31(1):2–3. doi: 10.1016/j.tibtech.2012.10.003
9. Nyakundi BB, Toth A, Balogh E, Nagy B, Erdei J, Ryffel B, et al. Oxidized Hemoglobin Forms Contribute to Nlrp3 Inflammasome-Driven Il-1beta Production Upon Intravascular Hemolysis. *Biochim Biophys Acta Mol Basis Dis* (2019) 1865(2):464–75. doi: 10.1016/j.bbadis.2018.10.030
10. Belcher JD, Chen C, Nguyen J, Milbauer L, Abdulla F, Alayash AI, et al. Heme Triggers Tlr4 Signaling Leading to Endothelial Cell Activation and Vaso-Occlusion in Murine Sickle Cell Disease. *Blood* (2014) 123(3):377–90. doi: 10.1182/blood-2013-04-495887
11. Merle NS, Paule R, Leon J, Daugan M, Robe-Rybkine T, Poillerat V, et al. P-Selectin Drives Complement Attack on Endothelium During Intravascular Hemolysis in Tlr-4/Heme-Dependent Manner. *Proc Natl Acad Sci U.S.A.* (2019) 116(13):6280–5. doi: 10.1073/pnas.1814797116
12. Frimat M, Boudhabhay I, Roumenina LT. Hemolysis Derived Products Toxicity and Endothelium: Model of the Second Hit. *Toxins (Basel)* (2019) 11(11):1–34. doi: 10.3390/toxins11110660
13. Setty BN, BEtal SG, Zhang J, Stuart MJ. Heme Induces Endothelial Tissue Factor Expression: Potential Role in Hemostatic Activation in Patients With Hemolytic Anemia. *J Thromb Haemost* (2008) 6(12):2202–9. doi: 10.1111/j.1538-7836.2008.03177.x
14. Roumenina LT, Rayes J, Lacroix-Desmazes S, Dimitrov JD. Heme: Modulator of Plasma Systems in Hemolytic Diseases. *Trends Mol Med* (2016) 22(3):200–13. doi: 10.1016/j.molmed.2016.01.004
15. Green D, Furby FH, Berndt MC. The Interaction of the Factor Viii/Von Willebrand Factor Complex With Hematin. *Thromb Haemost* (1986) 56 (3):277–82. doi: 10.1055/s-0038-1661666
16. Nielsen MJ, Moestrup SK. Receptor Targeting of Hemoglobin Mediated by the Haptoglobins: Roles Beyond Heme Scavenging. *Blood* (2009) 114(4):764–71. doi: 10.1182/blood-2009-01-198309
17. Andersen CB, Torvund-Jensen M, Nielsen MJ, de Oliveira CL, Hersleth HP, Andersen NH, et al. Structure of the Haptoglobin-Haemoglobin Complex. *Nature* (2012) 489(7416):456–9. doi: 10.1038/nature11369
18. Ascenzi P, Bocedi A, Visca P, Altruda F, Tolosano E, Beringhelli T, et al. Hemoglobin and Heme Scavenging. *IUBMB Life* (2005) 57(11):749–59. doi: 10.1080/15216540500380871
19. Kuhl T, Imhof D. Regulatory Fe(Ii/Iii) Heme: The Reconstruction of a Molecule's Biography. *Chembiochem* (2014) 15(14):2024–35. doi: 10.1002/cbic.201402218
20. Reiter CD, Wang X, Tanus-Santos JE, Hogg N, Cannon RO3rd, Schechter AN, et al. Cell-Free Hemoglobin Limits Nitric Oxide Bioavailability in Sickle-Cell Disease. *Nat Med* (2002) 8(12):1383–9. doi: 10.1038/nm1202-799
21. Merle NS, Church SE, Fremeaux-Bacchi V, Roumenina LT. Complement System Part I - Molecular Mechanisms of Activation and Regulation. *Front Immunol* (2015) 6:262. doi: 10.3389/fimmu.2015.00262
22. Lachmann PJ, The story of complement factor I. *Immunobiology* (2019) 224 (4):511–7. doi: 10.1016/j.imbio.2019.05.003
23. Harboe M, Ulvund G, Vien L, Fung M, Mollnes TE. The Quantitative Role of Alternative Pathway Amplification in Classical Pathway Induced Terminal Complement Activation. *Clin Exp Immunol* (2004) 138(3):439–46. doi: 10.1111/j.1365-2249.2004.02627.x
24. Rodriguez E, Nan R, Li K, Gor J, Perkins SJ. A Revised Mechanism for the Activation of Complement C3 to C3b: A Molecular Explanation of a Disease-Associated Polymorphism. *J Biol Chem* (2015) 290(4):2334–50. doi: 10.1074/jbc.M114.605691
25. Nilsson SC, Nita I, Mansson L, Groeneveld TW, Trouw LA, Villoutreix BO, et al. Analysis of Binding Sites on Complement Factor I That Are Required for Its Activity. *J Biol Chem* (2010) 285(9):6235–45. doi: 10.1074/jbc.M109.097212

26. Merle NS, Grunenwald A, Rajaratnam H, Gnemmi V, Frimat M, Figueres ML, et al. Intravascular Hemolysis Activates Complement *Via* Cell-Free Heme and Heme-Loaded Microvesicles. *JCI Insight* (2018) 3(12):1–17. doi: 10.1172/jci.insight.96910
27. Thomas AM, Gerogianni A, McAdam MB, Floisand Y, Lau C, Espevik T, et al. Complement Component C5 and Tlr Molecule Cd14 Mediate Heme-Induced Thromboinflammation in Human Blood. *J Immunol* (2019) 203(6):1571–8. doi: 10.4049/jimmunol.1900047
28. Mold C, Tamerius JD, Phillips GJr. Complement Activation During Painful Crisis in Sickle Cell Anemia. *Clin Immunol Immunopathol* (1995) 76(3 Pt 1):314–20. doi: 10.1006/clin.1995.1131
29. Silver KL, Higgins SJ, McDonald CR, Kain KC. Complement Driven Innate Immune Response to Malaria: Fuelling Severe Malarial Diseases. *Cell Microbiol* (2010) 12(8):1036–45. doi: 10.1111/j.1462-5822.2010.01492.x
30. Hammer CH, Wirtz GH, Renfer L, Gresham HD, Tack BF. Large Scale Isolation of Functionally Active Components of the Human Complement System. *J Biol Chem* (1981) 256(8):3995–4006. doi: 10.1016/S0021-9258(19)69557-8
31. Nilsson UR, Mueller-Eberhard HJ. Isolation of Beta If-Globulin From Human Serum and Its Characterization as the Fifth Component of Complement. *J Exp Med* (1965) 122:277–98. doi: 10.1084/jem.122.2.277
32. Alan Johnstone RT. *Immunochemistry in Practice*. Oxford: Cambridge Mass, Blackwell Science (1996).
33. Ricklin D, Lambris JD. Compstatin: A Complement Inhibitor on Its Way to Clinical Application. *Adv Exp Med Biol* (2008) 632:273–92. doi: 10.1007/978-0-387-78952-1_20
34. Roversi P, Johnson S, Caesar JJ, McLean F, Leath KJ, Tsiftsoglou SA, et al. Structural Basis for Complement Factor I Control and Its Disease-Associated Sequence Polymorphisms. *Proc Natl Acad Sci U.S.A.* (2011) 108(31):12839–44. doi: 10.1073/pnas.1102167108
35. Xue X, Wu J, Ricklin D, Forneris F, Di Crescenzio P, Schmidt CQ, et al. Regulator-Dependent Mechanisms of C3b Processing by Factor I Allow Differentiation of Immune Responses. *Nat Struct Mol Biol* (2017) 24 (8):643–51. doi: 10.1038/nsmb.3427
36. Ghoorah AW, Devignes MD, Smail-Tabbone M, Ritchie DW. Protein Docking Using Case-Based Reasoning. *Proteins* (2013) 81(12):2150–8. doi: 10.1002/prot.24433
37. Roumenina LT, Radanova M, Atanasov BP, Popov KT, Kaveri SV, Lacroix-Desmazes S, et al. Heme Interacts With C1q and Inhibits the Classical Complement Pathway. *J Biol Chem* (2011) 286(18):16459–69. doi: 10.1074/jbc.M110.206136
38. Lin CM, Mihal KA, Krueger RJ. Introduction of Sulfhydryl Groups Into Proteins at Carboxyl Sites. *Biochim Biophys Acta* (1990) 1038(3):382–5. doi: 10.1016/0167-4838(90)90252-b
39. Bergseth G, Ludviksen JK, Kirschfink M, Giclas PC, Nilsson B, Mollnes TE. An International Serum Standard for Application in Assays to Detect Human Complement Activation Products. *Mol Immunol* (2013) 56(3):232–9. doi: 10.1016/j.molimm.2013.05.221
40. Immenschuh S, Vijayan V, Janciauskiene S, Gueler F. Heme as a Target for Therapeutic Interventions. *Front Pharmacol* (2017) 8:146. doi: 10.3389/fphar.2017.00146
41. Smith LJ, Kahraman A, Thornton JM. Heme Proteins–Diversity in Structural Characteristics, Function, and Folding. *Proteins* (2010) 78(10):2349–68. doi: 10.1002/prot.22747
42. Wissbrock A, Goradia NB, Kumar A, Paul George AA, Kuhl T, Bellstedt P, et al. Structural Insights Into Heme Binding to Il-36alpha Proinflammatory Cytokine. *Sci Rep* (2019) 9(1):16893. doi: 10.1038/s41598-019-53231-0
43. Dutra FF, Bozza MT. Heme on Innate Immunity and Inflammation. *Front Pharmacol* (2014) 5:115. doi: 10.3389/fphar.2014.00115
44. Pawluczkowycz AW, Lindorfer MA, Waitumbi JN, Taylor RP. Hematin Promotes Complement Alternative Pathway-Mediated Deposition of C3 Activation Fragments on Human Erythrocytes: Potential Implications for the Pathogenesis of Anemia in Malaria. *J Immunol* (2007) 179(8):5543–52. doi: 10.4049/jimmunol.179.8.5543
45. Fromell K, Adler A, Aman A, Manivel VA, Huang S, Duhrkop C, et al. Assessment of the Role of C3(H2o) in the Alternative Pathway. *Front Immunol* (2020) 11:530. doi: 10.3389/fimmu.2020.00530
46. Gentinetta T, Belcher JD, Brugger-Verdon V, Adam J, Ruthsatz T, Bain J, et al. Plasma-Derived Hemopexin as a Candidate Therapeutic Agent for Acute Vaso-Occlusion in Sickle Cell Disease: Preclinical Evidence. *J Clin Med* (2022) 11(3):1–15. doi: 10.3390/jcm11030630
47. Belcher JD, Chen C, Nguyen J, Abdulla F, Zhang P, Nguyen H, et al. Haptoglobin and Hemopexin Inhibit Vaso-Occlusion and Inflammation in Murine Sickle Cell Disease: Role of Heme Oxygenase-1 Induction. *PLoS One* (2018) 13(4):e0196455. doi: 10.1371/journal.pone.0196455
48. Elmariah H, Garrett ME, De Castro LM, Jonassaint JC, Ataga KI, Eckman JR, et al. Factors Associated With Survival in a Contemporary Adult Sickle Cell Disease Cohort. *Am J Hematol* (2014) 89(5):530–5. doi: 10.1002/ajh.23683
49. Lubeck D, Agodoa I, Bhakta N, Danese M, Pappu K, Howard R, et al. Estimated Life Expectancy and Income of Patients With Sickle Cell Disease Compared With Those Without Sickle Cell Disease. *JAMA Netw Open* (2019) 2(11):e1915374. doi: 10.1001/jamanetworkopen.2019.15374
50. Yoo JJ, Graciaa SH, Jones JA, Zuo Z, Arthur CM, Leong T, et al. Complement Activation During Vaso-Occlusive Pain Crisis in Pediatric Sickle Cell Disease. *Blood* (2021) 138:858. doi: 10.1182/blood-2021-154132
51. Vercellotti GM, Dalmasso AP, Schaid TRJr., Nguyen J, Chen C, Ericson ME, et al. Critical Role of C5a in Sickle Cell Disease. *Am J Hematol* (2019) 94 (3):327–37. doi: 10.1002/ajh.25384

Conflict of Interest: The authors declare that the research was conducted in the absence of any commercial or financial relationships that could be construed as a potential conflict of interest.

frontiers | Frontiers in Immunology

TYPE Review
PUBLISHED 09 August 2022
DOI 10.3389/fimmu.2022.918775

OPEN ACCESS

EDITED BY
Brian V. Geisbrecht,
Kansas State University, United States

REVIEWED BY
Bo Nilsson,
Uppsala University, Sweden
Kristina N Ekdahl,
Uppsala University, Sweden
Christian Drouet,
INSERM U1016 Institut Cochin, France

*CORRESPONDENCE
Edward L. G. Pryzdial
ed.pryzdial@blood.ca
Edward M. Conway
ed.conway@ubc.ca

SPECIALTY SECTION
This article was submitted to Molecular Innate Immunity, a section of the journal Frontiers in Immunology

RECEIVED 12 April 2022
ACCEPTED 06 July 2022
PUBLISHED 09 August 2022

CITATION
Pryzdial ELG, Leatherdale A and Conway EM (2022) Coagulation and complement: Key innate defense participants in a seamless web. *Front. Immunol.* 13:918775. doi: 10.3389/fimmu.2022.918775

Coagulation and complement: Key innate defense participants in a seamless web

Edward L. G. Pryzdial[1,2,3]*, Alexander Leatherdale[1,4] and Edward M. Conway[1,2,3,4]*

[1]Centre for Blood Research, Life Sciences Institute, University of British Columbia, Vancouver, BC, Canada, [2]Department of Pathology and Laboratory Medicine, University of British Columbia, Vancouver, BC, Canada, [3]Canadian Blood Services, Medical Affairs and Innovation, Vancouver, BC, Canada, [4]Division of Hematology, Department of Medicine, University of British Columbia, Vancouver, BC, Canada

In 1969, Dr. Oscar Ratnoff, a pioneer in delineating the mechanisms by which coagulation is activated and complement is regulated, wrote, "In the study of biological processes, the accumulation of information is often accelerated by a narrow point of view. The fastest way to investigate the body's defenses against injury is to look individually at such isolated questions as how the blood clots or how complement works. We must constantly remind ourselves that such distinctions are man-made. In life, as in the legal cliché, the devices through which the body protects itself form a seamless web, unwrinkled by our artificialities." Our aim in this review, is to highlight the critical molecular and cellular interactions between coagulation and complement, and how these two major component proteolytic pathways contribute to the seamless web of innate mechanisms that the body uses to protect itself from injury, invading pathogens and foreign surfaces.

KEYWORDS

complement, coagulation, proteolysis, innate immunity, NETs, contact system

Introduction

Historical perspectives

While early sages, including Hippocrates and Aristotle recognized that blood clots rapidly after it leaves the body, it was not until at least the 16th and 17th centuries that scientists determined that clots formed in blood vessels following injury (1). William Hewson showed in the 1770s that blood coagulated and that the so-formed clot was not

derived from the cells, but rather from the liquid portion of blood, i.e., the "coagulable lymph" or serum. Studies of the chemical basis for clotting were triggered in the 1870s with the discovery and purification of fibrinogen by the Swedish scientist Olof Hammarsten, and descriptions of prothrombin, "thrombokinase" and calcium as key participants. In 1905, a landmark "classic theory of coagulation" was described by the German physician Paul Morawitz (2), in which coagulation was proposed to occur in two stages, with thrombin generation and fibrinogen coagulation. Thus, the foundation for today's much more intricate step-wise paradigm was established.

In parallel to this blood clotting system work, in 1888, the American-British bacteriologist, George Nuttall reported that sheep blood was bacteridical for *anthrax bacilli*. This effect was later shown to be negated by preheating the blood to 55°C (3). Thereafter, the German bacteriologist, Hans Buchner named this bactericidal factor "alexine" from the Greek, loosely translated as "protective stuff" (4). Further study by the Belgian scientist, Jules Bordet, determined that the *in vivo* activity of this serum-based, heat-labile alexine was partly dependent on the presence of other heat stable factors. These findings aligned with those of German physician-scientist Nobel laureate, Paul Ehrlich, who had introduced the concept of humoral immunity, and proposed that alexine was indeed complementary to the action of antibodies. And so, in 1899, the term "complement" was coined, relegating alexine to its ancient Greek origins (5).

During the first 30-40 years of the 20th century, there was frenzied activity in both coagulation and complement, with scientists studying these complex systems distinctly, with the goal of establishing mechanistic clarity. Interestingly, in the 1920s and 1930s, Jules Bordet and others published papers claiming that complement and coagulation were related, and indeed, that prothrombin was the "midpiece of complement" (6). This notion was discarded by most, including in 1935 by the famed American chemist, Armand Quick, who made numerous contributions to coagulation, including the prothrombin time test (1).

By the 1930s, a "classical pathway" of the sequential activation of four serum complement fractions C1-C4-C2-C3, had been characterized, triggered by infection-specific immune reactants. This remained the only recognized complement activation pathway until the late 1950s (7), when Louis Pillemer, at Western Reserve University, introduced the notion of an "alternative pathway" with his discovery of properdin (8, 9). The relevance of this alternative pathway is now acknowledged for its central importance in health and disease.

Similarly rapid advances in understanding coagulation and clot dissolution (i.e., fibrinolysis) were made in the mid-1900s, as the conversion of prothrombin to thrombin had been characterized, and factor (F) V to FXIII, to varying extents, were identified, often discovered by analysis of patients with inherited deficiencies and consequent bleeding disorders (1). With the introduction in the 1960s of more powerful protein purification and analytical technologies, and the ability to generate specific polyclonal antibodies, many more components and fragments of the coagulation and complement systems were characterized (10). Interestingly, many of these discoveries in complement and coagulation occurred simultaneously - not infrequently in adjacent laboratories. Indeed, Louis Pillemer and Oscar Ratnoff were colleagues at Western Reserve University and famously collaborated on multiple works that bridged these disciplines (11) and led to the wisdom that our "body protects itself [by] a seamless web, unwrinkled by our artificialities" (12).

Over the past several decades, it has become widely accepted that complement and coagulation must be viewed as inextricably intertwined. The biochemical pathways intersect and impact the other's endpoints. The cells and molecular pathways with which each communicates are shared. The finely tune balance of initiating factors, and the site and timing of activation, amplification and resolution of coagulation and complement are most often overlapping, and most certainly coordinated *via* complex feedback mechanisms. Most notably, genetic studies in conjunction with sensitive biochemical assays and an improved understanding of the interplay between these pathways and their common cellular and molecular partners, have revealed mutations in complement regulatory factors. These cause excess complement activation, resulting in feedback-mediated hyper-coagulation and hyper-inflammation, leading to tissue damage and organ failure. Thus, introduction of remarkably effective anti-complement drugs for paroxysmal nocturnal hemoglobinuria (PNH; see Table 1 for a list of abbreviations) and atypical hemolytic uremic syndrome (aHUS) (13, 14), two devastating complement-mediated thrombotic disorders, underlines the value of bringing these two biochemical proteolytic pathways together in the clinic.

In spite of the tremendous increase in our understanding of the molecular mechanisms by which coagulation and complement pathways intersect, there is much more to be learned. In this report, we review some of the more recent and prominent discoveries of how these complex, primarily blood-borne proteolytic cascades, interact and indeed, how they interface with other critical pathways involved in innate defense. We begin with brief descriptions of each of the pathways (the reader is referred to other publications for in-depth reviews), and then highlight some of the key, potentially relevant cellular and molecular links that tie them into a cohesive, albeit complex unit. Throughout this discussion, we are reminded of Dr. Ratnoff's caution (12), that the distinction of these pathways is man-made, based partly on the limitations of *in vitro* test-tube analyses; and in reality, complement and coagulation are just two of several interacting participants in a seamless web of innate pathways, designed to effectively and efficiently protect the host.

TABLE 1 Table of Abbreviations.

ADAMTS13	a disintegrin and metalloproteinase with a thrombospondin type 1 motif, member 13
aHUS	atypical hemolytic uremic syndrome
AP	alternative pathway
APAS	antiphospholipid antibody syndrome
aPL	anionic phospholipid (e.g., phosphatidyl serine)
AT	anti-thrombin
BK	bradykinin
C1-INH	C1 inhibitor
C3aR, C5aR, C5aL2	receptors for C3a and C5a
CP	classical pathway
CPB2	carboxypeptidase B2
CS	contact system
CsA	chondroitin sulfate A
DAMP	damage/danger associated molecular pattern
FB	factor B
FD	factor D
FH	factor H
HITT	heparin induced thrombocytopenia and thrombosis
HK	high molecular weight kininogen
LP	lectin pathway
MAC	membrane attack complex (C5b-9)
MASP	MBL-associated serine protease
MBL	mannose binding lectin
MMP	matrix metalloprotease
NETs	neutrophil extracellular traps
PAI-1	plasminogen activator inhibitor-1
PAMP	pathogen associated molecular pattern
PAR	protease activated receptor
PC, APC	protein C, activated PC
PF4	platelet factor 4
Pg	plasminogen
PGI	prostacyclin
PK, PKa	plasma prekallikrein, plasma kallikrein
PNH	paroxysmal nocturnal hemoglobinuria
PRM	pathogen recognition molecule
prothrombinase	Factor Va/Factor Xa (FVa/FXa) enzymatic complex
PSGL-1	P-selectin glycoprotein 1
SUSD4	sushi domain-containing protein 4
TAFI	thrombin activatable fibrinolysis inhibitor, activated TAFI
tenase	TF/Factor VIIa (TF/FVIIa) enzymatic complex
TF	tissue factor
TFPI	tissue factor pathway inhibitor
tPA	tissue type plasminogen activator
ULIC	ultra large immune complexes
VWF, ULVWF	von Willebrand Factor, ultra large multimeric VWF

The coagulation system

Coagulation overview

Cardio-cerebrovascular diseases and thromboembolic disorders have been the leading causes of death globally for >100 years (15). The blood coagulation system has thus long been at the forefront of scientific study [for reviews (16–19)]. The system features a series of reactions in which a specific injury or stimulus triggers a cascade of limited proteolysis, whereby inactive proteins (zymogens) are converted sequentially to their respective proteases, amplified at each step to ultimately generate a fibrin clot (1, 20). Coagulation-related protease systems are tightly regulated and delicately balanced to maintain vascular homeostasis under a wide range of pathophysiologic stimuli (21). Thus, while the system is continuously active, sequential proteolysis of zymogen to active protease, and protease activity on respective substrates are held in check at each step under healthy conditions, by an array of natural anticoagulant mechanisms (22), disruption of which results in a thrombotic diathesis. These coagulation protease components and regulators not only modulate the hemostatic-thrombotic response, but also participate in other fundamental biologic processes including innate and adaptive immunity, inflammation, cell proliferation, wound healing, and cancer. It follows that dysregulation of the coagulation system may have far-reaching effects.

Coagulation initiation: Platelets, anionic phospholipid and tissue factor

Blood coagulation is initiated at sites where the vascular endothelial cell monolayer is damaged. This exposes the subendothelial stratum which contains molecules, such as collagen and von Willebrand Factor (VWF), to plasma and circulating platelets which adhere, activate and aggregate (23), thereby forming the primary vascular seal. Clot formation stabilizes the platelet plug, which alone is insufficient to withstand the shear forces of blood flow. The platelet response to vascular damage, features regulated flipping of anionic phospholipids (aPL: e.g. phosphatidylserine) from the inner to the outer cell membrane bilayer leaflet (19, 24) and the release of granule contents (25), both of which are relevant to the initiation and amplification of coagulation. Platelets release important hemostatic constituents into the circulation from α- and dense-granules (26), including, for example, platelet activating factor, platelet factor 4 (PF4), P-selectin, adenosine diphosphate and polyphosphate. These elicit local cell stimulatory effects, recruit and activate neutrophils and monocytes, and may promote further accessibility of aPL, an essential cofactor for assembly of all coagulation cofactor/enzyme protein complexes.

The essential physiologic trigger of coagulation is the transbilayer receptor, tissue factor (TF). Normally present throughout the vasculature in a subendothelial pool, TF becomes available, i.e., it is decrypted and activated, upon vascular damage (27, 28) (Figure 1). Binding of the zymogen, factor (F)VII to TF, drives a conformational transition that enables autoproteolytic activation to FVIIa (29). TF then accelerates FVIIa-mediated activation of FX by ~100,000-fold (30, 31) to form the first FXa molecules. TF/FVIIa constitutes the extrinsic tenase, which can also initiate activation of FIX (32) and FVIII (33). FIXa and FVIIIa are the protease and cofactor within the intrinsic tenase, respectively. Like all coagulation protease complexes, tenase assembly and function are Ca^{2+}- and aPL-dependent. Thus, together, TF and aPL are integral for initiation and localization of the procoagulant response to vascular damage. Particularly relevant to our discussion, TF is also located on endothelial cells and activated leukocytes, thereby well-positioned for mediating critical roles not only within, but also beyond coagulation.

Feedback amplification by thrombin

Upon generation of sufficient FXa to overcome endogenous circulating anticoagulants, such as tissue factor pathway inhibitor (TFPI) (34) or antithrombin (AT) (35), FXa then activates its cofactor, FV to FVa (36) (Figure 1). Assembly of the Ca^{2+}-dependent FVa/FXa prothrombinase complex on an aPL-containing membrane results in cleavage of prothrombin to generate the potent serine protease thrombin (37) which in turn

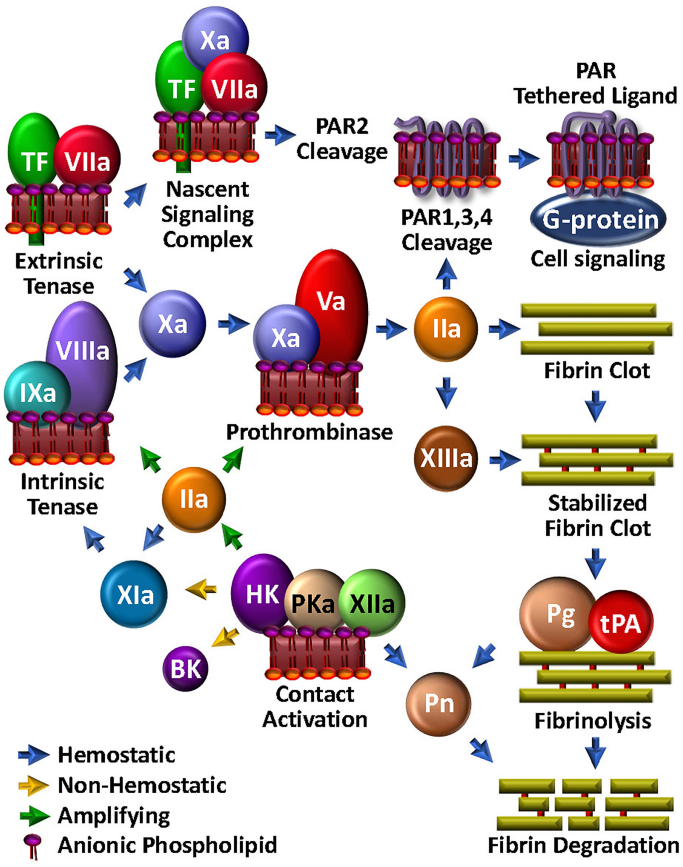

FIGURE 1
Coagulation Unwebbed. Upon vascular damage, hemostatic coagulation is initiated by exposure of TF and assembly of the extrinsic tenase, leading to prothrombinase and ultimate thrombin (IIa) production, which is responsible for direct fibrin clot formation and feedback amplification involving the intrinsic tenase. The nascent TF/FVIIa/FXa complex and thrombin facilitate PAR-mediated cell modulation. FXIIIa crosslink-stabilizes the clot. Initiation and amplification of coagulation may be facilitated by the so-called intrinsic coagulation/contact pathway. Clot degradation and solubilization is facilitated by the fibrinolysis pathway through tPA-mediated plasminogen (Pg) activation to plasmin (Pn), which can be enabled by kallikrein (PKa).

triggers polymerization of soluble fibrinogen by proteolytic conversion to fibrin cross-linked by thrombin-activated FXIII to yield a stable clot.

Thrombin recognizes several protein substrates that contribute to its own generation and explosive feedback amplification (16). Thus, it activates FV and FVIII, and converts FXI to FXIa, the latter which contributes to generating the intrinsic tenase activity by further activating FIX. Combined with the newly available FVa, up-regulated FVIIIa/FIXa tenase activity tremendously augments downstream prothrombinase assembly and the ensuing production of thrombin.

Small amounts of TF-triggered coagulation proteases, including thrombin and FXa, also elicit a wide range of thromboinflammatory effects on neighbouring platelets, neutrophils and endothelial cells *via* direct activation of cell surface expressed PARs (38) (Figure 1). These are a group of four homologous receptors (PAR1-4) that are expressed on numerous cell types (39). PAR1 is the high affinity receptor for thrombin (40, 41), but may be cleaved by several proteases. PAR2 is expressed on leukocytes and endothelial cells, and rather than thrombin, is activated by FXa, particularly in the context of the TF/FVIIa/FXa complex. Through its direct cell agonist effects on PAR2 and indirect effects on PAR1 *via* thrombin generation, TF is therefore well integrated in the thromboinflammation web, with key roles in bridging coagulation, complement and inflammation (42).

Fibrinolysis: Plasmin-mediated clot dissolution and cell modulation

Once the fibrin/platelet clot has sealed the damaged vasculature, fibrinolysis is initiated to restore normal blood flow and effect healing by assembly of the protease/substrate tissue-type plasminogen activator (tPA)/plasminogen (Pg) complex, directly on the remaining fibrin (Figure 1). Fibrin serves to localize and orient the enzyme/substrate complex for efficient proteolysis of the zymogen Pg, to its respective serine protease, plasmin. With generation and activity of plasmin tightly regulated by plasminogen activator inhibitor (PAI)-1 and alpha-2-antiplasmin, plasmin can effectively solubilize the clot and trigger cellular events that facilitate healing. Indeed, the substrate specificity of plasmin is broad (43). For example, like thrombin, plasmin cleaves PAR1, and thus participates in platelet activation (44), macrophage release of proinflammatory cytokines (45) and expression of TF (46) on monocytes. Plasmin can also activate PAR2, thereby modulating endothelial function (47). Finally, plasmin activates several matrix metalloproteases (48–50), which in turn, may impact on inflammation, hemostasis and tissue remodeling (51). Not surprisingly, plasmin has direct effects on complement activation, which will be further discussed below.

The complement system

Complement overview

A major blood-based proteolytic system, complement is orchestrated to innately respond as a first-line protector of the host from invading pathogens and damaged cells (52, 53). Like coagulation, the complement system is delicately balanced, tightly regulated and highly versatile, integrated with other innate and adaptive response systems, and linked to physiologic systems that prevent bleeding, and effect cell proliferation, tissue regeneration and healing (54). Mechanisms of generation and regulation of key proteolytic enzymes in complement versus coagulation, while similarly dependent on key ions and surface interactions, are distinct. Under healthy conditions, the complement system functions in a low activity-level surveillance mode. Like coagulation, it rapidly escalates to address the insult, in a highly localized and temporal manner. Thus, when danger signals to the host have been sufficiently averted, complement system activity defervesces, leaving biologically active proteolytic by-products that participate in recruiting inflammatory cells and adaptive immune responses, to ensure healing and a return to homeostasis.

Converging three complement initiating pathways

Complement initiation is traditionally viewed as proceeding *via* three pathways – classical (CP), lectin (LP) and alternative (AP) - all converging with the formation of C3 convertases that proteolyse C3 into cofactor, C3b, with release of the anaphylatoxin, C3a (Figure 2). Initiation of complement *via* the CP and the LP requires that complement components participate as pathogen recognition molecules (PRM) by direct or antibody-facilitated detection of a wide range of pathogen and damage/danger associated molecular patterns (PAMPs and DAMPs) perceived as being foreign. These include, for example, DNA, RNA, modified lipids, oligosaccharides, histones, heat shock proteins, formyl peptides, plasma membrane constituents, and/or extracellular matrix proteins (55), any of which may be exposed/released upon pathogen invasion and/or with cellular damage.

The initiator of CP activation is C1q, a multivalent PRM that continuously surveys blood in complex with a tetramer of the zymogen forms of the serine proteases C1r and C1s ($C1qr_2s_2$). With an infection or injury, C1q activity is triggered by the Fc regions of specific "complement-fixing" antibodies that are bound to neo-antigens and/or microbial surfaces (Figure 2). C1q can also recognize other targets, including C-reactive protein, modified lipids and carbohydrates. With binding of C1q to its target, the zymogen C1r undergoes a Ca^{2+}-dependent

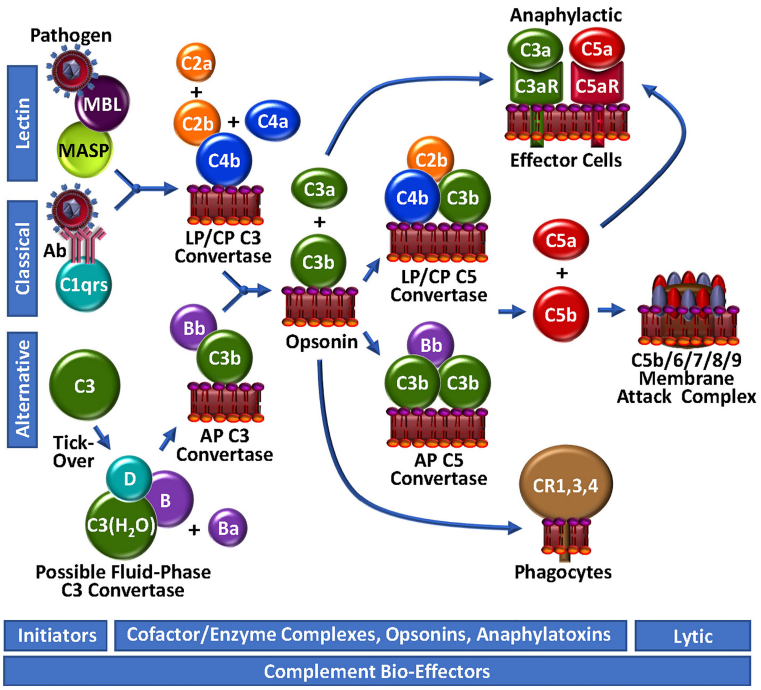

FIGURE 2
Complement Unwebbed. The LP and CP are initiated by contact with a foreign particle or damaged cells, whereupon C4b is surface-deposited in complex with C2b, forming the LP/CP C3 convertase. The AP is continuously surveying the circulation for foreign bodies by spontaneous thio-ester hydrolysis and possible formation of a highly unstable fluid-phase C3 convertase. Either the LP/CP or AP C3 convertase may result in deposition of surface C3b and generation of respective C5 convertases. C5b production triggers the assembly of the lytic membrane attack complex by the addition of C6, C7, C8 and multiple C9 molecules. Surface-bound C4b and C3b are opsonic, as are degradation fragments of C3b (not depicted), which associate with complement receptors (CR1,3,4). C3a and C5a are anaphylactic, associating with C3aR and C5aR, respectively.

conformational change to a serine protease (56), which in turn, cleaves/activates its neighbouring zymogen, C1s, to its serine protease form (57). C1s proteolyses C4 to generate two fragments: C4a is a weak anaphylatoxin, while C4b contains a reactive thioester, allowing it to covalently bind to the surfaces of nearby damaged cells/pathogens. The immobilized C4b provides a binding site for C2, which is subsequently cleaved by C1s into C2b and C2a. While C2a is liberated in a soluble form, C2b complexes with the cofactor C4b, yielding the CP C3 convertase, C4b/2b, which proteolytically catalyzes the generation of C3b and C3a from C3, thus propagating complement.

The LP follows a similar course as the CP to generate C4b/2b (58), but the triggering events are distinct. LP PRMs comprise mannose binding lectin (MBL), ficolins or collectin-11, which may individually circulate in complex with MBL-associated zymogens of serine proteases (MASP), MASP1/MASP3 and MASP2. These multi-molecular complexes specifically bind to sugars or N-acetylated groups on micro-organisms. MASP1 then autoactivates in a Ca^{2+}-dependent manner, allowing it to cleave C2 and MASP2. MASP2 also autoactivates and cleaves both C2 and C4, resulting in the formation of the C4b/2b LP C3 convertase, which is identical to the CP C3 convertase (59).

While the CP and LP apparently require an "on" signal, the AP has historically been viewed as being constitutively active (Figure 2). This is analogous to the coagulation system, which is also in a continuous "ready" state, always minimally generating low levels of FVIIa and thrombin. In the AP of complement, this is reportedly achieved *via* the so-called "tick-over" mechanism to describe spontaneous thioester hydrolysis that circulating C3 undergoes, transforming it into $C3(H_2O)$ (60). In more recent studies, this theory has been adapted/questioned with the suggestion that AP activation of C3 to $C3(H_2O)$ may require contact - or at least may be initiated and accelerated by contact - with one or more biological or artificial surfaces, such as lipids/lipid complexes, gas interfaces or biomaterials (61, 62). A continuous source of $C3(H_2O)$ in the plasma may also be activated platelets (Figure 3) which transform C3 to $C3(H_2O)$ and stabilize other AP convertases (61, 63). Regardless of the mode, once it is generated, $C3(H_2O)$ exposes a Mg^{2+}-dependent binding site for circulating zymogen factor B (FB) (64). Factor D (FD) [also known as adipsin (65)], a low abundance serine protease in serum that is secreted as a pro-enzyme by adipocytes, endothelial cells and monocytes (65, 66), may proteolyse its only known substrate, FB, in complex with $C3(H_2O)$, liberating a

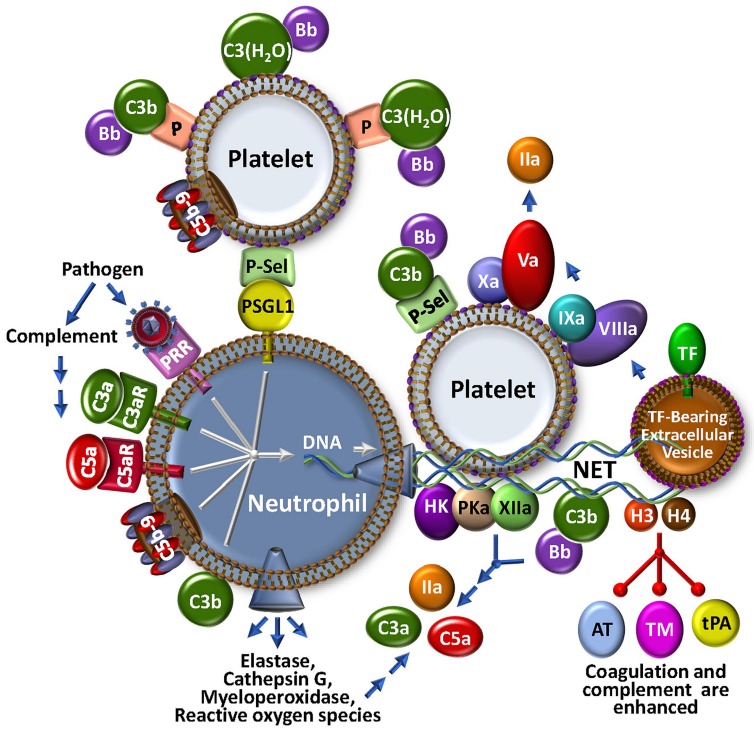

FIGURE 3
The NETosis-Coagulation-Complement Web. Neutrophils release NETs after binding of foreign particles to pathogen recognition receptors (PRR), engagement of complement anaphylatoxic or opsonic species, or association of P-selectin on activated platelets with P-selectin glycoprotein 1 (PSGL1). Stimulated neutrophils release numerous bioeffectors including neutrophil elastase, cathepsin G, myeloperoxidase and reactive oxygen species, which may affect production of coagulation and complement bioeffectors directly or indirectly through cell modulation. Release of DNA-based NETs from neutrophils, provides a complex matrix for interactions with stimulated platelets and localizes TF activity, possibly by trapping extracellular vesicles. Both coagulation and complement pathways are further propagated by direct protein factor association with NETs through the contact and alternative pathways, respectively. Multistep crosstalk between these pathways results in further generation of thrombin, C3a and C5a with potential for biological consequence. Histones, H3 and H4, are major protein constituents of NETs and enhance coagulation and complement by inhibiting the regulators, antithrombin (AT) and thrombomodulin (TM), and stabilize the clot by attenuating tPA-mediated fibrinolysis. The activated platelet surface is typically regarded as procoagulant because it provides anionic phospholipid (purple polar head groups), but platelet-bound P-selectin and properdin (P) also stabilize AP C3 convertase assembly *via* association with C3b and C3(H_2O), respectively. The platelet surface may also associate directly with C3(H_2O) toward complement activation.

soluble activation fragment Ba, and a larger Bb fragment. FD is activated by MASP1 and/or MASP3 (67–69), and interestingly, also possibly by thrombin (68, 69), thereby establishing a direct connection between the LP and the AP, as well as the coagulation system. The FD-generated Bb contains an active serine protease domain and remains bound to C3(H_2O), stabilized by properdin (70, 71), yielding C3(H_2O)/Bb, a short-lived relatively unstable fluid-phase C3 convertase, that can cleave C3 to C3a and C3b. The reactive thioester exposed by C3b allows covalent deposition onto an amine or hydroxyl group on a nearby surface. In the absence of potent negative regulators, including for example, factor H (FH), CR1 and CD55, circulating FB binds to the immobilized C3b, and following FD cleavage of FB, results in the assembly of C3b/Bb, the AP C3 convertase that can be stabilized by properdin (70), followed by subsequent downstream complement activation.

Complement amplification: C3b generation

The generation of C3b by cell-bound C4b/2b or C3b/Bb C3 convertases, converges the 3 initiating branches of complement (Figure 2). At this point, AP-mediated amplification may occur as more C3b is locally deposited, and more C3b/Bb complex is rapidly formed. This represents an unstable and transient non-covalent assembly, with ensuing rapid decay that is normally accelerated by control proteins, such as FH and CD55. However, unchecked by reduced functional expression of one or more of these negative regulators, the additional C3b molecules bind to the C3 convertases to form respectively, the CP/LP and AP C5 convertases, C4b/2b/C3b and C3b/Bb/C3b, resulting in a shift in substrate specificity favoring cleavage of C5 over C3. Further amplification is facilitated by a complex between C2b and a

covalent C4b dimer, likely produced at low-levels, but uniquely not involving the participation of C3b or C3(H_2O) in the enzymatic complex to yield C3 and C5 convertase activity (72).

The terminal pathway and the membrane attack complex

C5 convertases cleave C5 into C5b, liberating the potent biologically active anaphylatoxin, C5a (Figure 2). Generation of C5b marks the start of the terminal pathway, which spontaneously proceeds in an ion-independent manner, with rapid formation of a stable C5b,6 complex. Subsequent binding of C7 yielding the C5b-7 complex, provides first attachment of the complex to the outer leaflet of a target membrane. Addition of C8 and polymerization of ~18 C9 monomers, completes assembly of the C5b-9 pore-like, lytic membrane attack complex (MAC).

Bioactive complement activation products: 'Small but mighty' fragments

In the course of complement activation and regulation, several proteolytic by-products are generated, most of which are biologically relevant, not only for assembly of the convertases, but also in mediating further activation/amplification of complement, recruiting inflammatory cells and adaptive immunity *via* opsonization (e.g., C3- and C4-derived fragments: C3b, iC3b, C3c, C3d/g, iC4b, C4d) and triggering effects on other biological systems (e.g., anaphylatoxins C5a, C3a, C4a), including coagulation. Indeed, C3a and C5a interact with their cognate G-coupled receptors (C3aR for C3a; C5aR and C5L2 for C5a), thereby mediating diverse activities that are context-dependent, modulated by expression levels of their receptors, and local factors that control their clearance. These small but mighty fragments have profound cell modulatory effects on the immune system that, as will be discussed, spill-over into diverse responses in coagulation and beyond (73–76).

Complement and coagulation and the seamless web

Neutrophils and neutrophil extracellular traps: the web's NETs

In parallel with recruitment and adhesion of platelets and monocytes to damaged vascular endothelium at the outset of a localized infection and/or vascular inflammatory insult, neutrophils are early and key participants in thromboinflammation. Neutrophils innately respond to many stimuli, including PAMPs, DAMPs, N-formyl peptides, as well as - importantly - complement-generated anaphylatoxins C3a and C5a (Figure 3). Neutrophils are short-lived effector cells that are phagocytic, and can release multiple proteolytic enzymes (e.g., elastase, myeloperoxidase, metalloproteases, cathepsins), reactive oxygen species, cytokines and chemokines, and PF4. These may impact profoundly on thromboinflammation, for example, by further activating platelets, activating coagulation factors V, VIII and X, and complement component C5 through specific proteolysis, and inactivating natural anti-coagulant/anti-complement factors TFPI, thrombomodulin and AT (77). Stimulated neutrophils are consequently an important fulcrum for localized regulatory complement-coagulation mechanisms. It follows that major research efforts are being directed to better understand the molecules that effect neutrophil priming, activation and release. Among others, these include the C5a/C5aR axis and neutrophil chemokines such as CXCL8, neutrophil elastase and CXCR2 (78–80), some of which are being explored as therapeutic targets.

Activated neutrophils can also release neutrophil extracellular traps (NETs) (Figure 3), a process referred to as NETosis. NETs are web-like structures that are secreted during a specialized type of cell death where the cell remains intact and retains certain biological function (81, 82). NETs can also be released by activated eosinophils, basophils and monocytes. NETs trap and kill bacteria and invading pathogens, and provide a scaffold for aggregating platelets and red blood cells, contributing to thrombosis and thromboinflammation (83, 84). They are provoked by various stimuli, including bacteria and viruses, activated platelets, hypoxia, reactive oxygen species and cytokines (81, 85). Discharge of NETs by neutrophils can also be triggered by C3a and C5a *via* interactions with their receptors, C3aR and C5aR, respectively, by C5b-9 (see below), as well as following opsonization with C3b/iC3b (85–87). Interestingly, mice that are deficient in C3 or C3aR do not readily form NETs (87), emphasizing the link to complement. This is further evident in studies with COVID-19, where disease severity is tightly correlated with NETosis, reduced NET clearance, and augmented thrombin generation (88, 89). Release of TF positive NETs triggered by COVID-19 patient plasma is blocked by C5aR inhibitors (90) and pilot clinical studies with ant-C3 and anti-C5 agents suggest some protection against NETosis, inflammation and leukocytosis (91).

Since NETs comprise multiple constituents, including DNA, histones, various proteolytic enzymes, complement factors C3 and FB, lipids and other associated proteins (87, 92), they convey a myriad of properties that bridge coagulation and complement (Figure 3). The negatively charged NET components provide surfaces for activation of the contact pathway of coagulation, resulting in generation of FXIa, FXIIa and kallikrein (PKa) (93). NETs also release or expose functionally active TF and release TF positive extracellular vesicles that participate in the local amplification of thrombin generation. Histones H3 and H4 are

major NET constituents. They act as DAMPs to activate complement, and to locally concentrate neutrophil elastase, cathepsin G, and myeloperoxidase (94), which themselves may activate complement. Histones also block the function of the serpin AT, promote autoactivation of prothrombin to thrombin (95), interfere with tPA-mediated plasmin generation (96), and bind to thrombomodulin and protein C to reduce thrombin-mediated generation of activated protein C (APC) (97). While APC normally digests histones, when NET-bound (98), the histones are resistant to degradation. It follows that NET-associated thrombi are more resistant to fibrinolysis (83, 99). Neutrophil-derived proteases and reactive oxygen species also exhibit pro-inflammatory and pro-coagulant properties, suppressing the functional expression of thrombomodulin (100), and inactivating natural inhibitors of the coagulation/complement systems, including TFPI (101). Overall, NETs underline the extensive interplay between coagulation and complement - truly major components in the seamless thromboinflammatory web.

Contact activation and the kallikrein-kinin system

Triggering thrombin generation, complement activation and inflammation, the so-called intrinsic blood coagulation system and kallikrein-kinin systems, herein collectively referred to as the contact system (CS) (18). The CS represents a critical nexus within the thromboinflammatory web that is intimately connected to complement and coagulation. The major components of this system are high molecular weight kininogen (HK), plasma prekallikrein (PK) and FXII, which also assemble on negatively charged surfaces (e.g., aPL) in an auto-activating complex to produce FXIa, and thus downstream generation of thrombin (Figure 1). Based on clinical evidence that deficiency of FXII is not associated with excess bleeding, this pathway was not considered relevant in hemostasis-thrombosis. However, within the past couple of decades, the pathophysiologic relevance of this pathway in coagulation has been revealed in pre/clinical trials demonstrating that targeting FXII by various means, protects from thromboembolic disease (102–104). Its additional central role in inflammatory disorders is evident by the association of excess FXII activity with the sometimes life-threatening inflammatory disorder, hereditary angioedema (HAE) (102, 105). Indeed, anti-FXIIa treatments are holding promise as prophylaxis against angioedema due to C1-INH deficiency (106).

FXII normally circulates in the blood as a single polypeptide zymogen, that constitutively expresses a low level of activity (107), catalyzing its autoactivation, and activation of PK and FXII when in contact with a negatively charged surface, such as damaged blood vessels, invading pathogens, DNA, RNA (108), neutrophil extracellular traps (NETs) (109), anionic polysaccharides, polyphosphate, and activated endothelial cells and platelets (110, 111). FXIIa is then able to recruit HK bound to PK, leading to local cleavage of PK to generate the plasma serine protease, plasma kallikrein (PKa) (105). This in turn feeds back to generate more FXIIa and PKa. With sufficient FXIIa, FXI is activated, triggering thrombin generation and ultimately fibrin formation. Occurring at the initial site of vascular injury, FXIa is considered a supplementary source of thrombin generation. In that regard, the efficacy of FXII and FXI inhibitors, alone or in combination, to prevent thrombosis and inflammation are being explored by several groups (103, 112–114).

From within the HK/PKa/FXIIa complex, PKa proteolyses HK to form the pro-inflammatory, bradykinin (BK) (102), a nonapeptide that regulates vascular permeability and blood pressure (115). BK, tightly regulated by several peptidases (116) including, among others, carboxypeptidase B2 (CPB2) (117), also binds to G-protein coupled receptors on endothelial cells and activated leukocytes, stimulates nitric oxide and prostacyclin (PGI_2) synthesis, and release of tPA from endothelial cells (118), which dampen coagulation, platelet activation and fibrin deposition. Exogenous tPA also increases PKa activity *via* a FXII-dependent manner, a notable observation that raises the consideration of inhibiting PKa during tPA-mediated thrombolysis in stroke to reduce brain hemorrhage and edema (119).

As noted previously, FXIIa also activates complement, cleaving C1r to trigger formation of the CP C3 convertase. Whether this pathway substantially contributes to complement activation in health and disease is unknown. More likely, particularly in C1-INH deficiency, heightened release of anaphylatoxins C3a and C5a could more readily be attributed to 1) excess PKa that can cleave C3 and FB, 2) lack of neutralization of C1r, C1s and MASPs, and 3) lack of inhibition of plasmin (116, 120).

Taken together, insights gained particularly from biochemical and genetic studies of the complex role of the CS in regulating coagulation, complement and inflammation, is uncovering exciting potential therapeutic targets, including for example, FXII/FXIIa, FXI/FXIa, BK, BK receptors, HK, PK, PKa, C1-INH, and gC1qR, for a wide range of thromboinflammatory disorders.

Complement activation fragments, big and small

Terminal pathway complexes promote coagulation

Several observational studies have revealed that complement components, including C3, C4, C5a and FB are often found in thrombi (121) where they may initiate and sustain inflammation (122). C3 enhances clot stability and increases clot resistance to fibrinolysis by binding directly to fibrin, findings consistent with the prolonged bleeding time and delayed thrombosis post-injury in mice lacking C3 (123). Remarkably, few studies have further

explored the molecular mechanisms by which these complement factors alter fibrin clot structure. There has been, however, considerable focus on the pore-forming C5b-9 MAC.

With MAC assembly, the membrane integrity of the unwanted cell or microorganism can be disrupted, thereby ensuring its destruction and elimination. Not surprisingly, altering the configuration and structure of membrane components, engages other biological systems, including coagulation. Platelets, endothelial cells and leukocytes are well-positioned to participate in complement activation, and indeed to be targeted as innocent bystanders, for destruction. Indeed, these cells are particularly sensitive to sublytic concentrations of C5b-9 (sC5b-9), which induces transbilayer flipping of aPL that can readily support coagulation activation through assembly of respective cofactor/enzyme complexes, and the ultimate generation of thrombin (124, 125). This occurs in concert with augmented secretion of VWF, P-selectin and pro-inflammatory cytokines, heightened expression of leukocyte adhesion molecules (126), and the release of microvesicles that are rich in C5b-9 and P-selectin, and complement inhibitors C1-INH, clusterin, CD55 and CD59 (127), as well as functionally active TF (128). C5b-9 has also recently been shown to directly trigger NETosis, that in turn induces neutrophil release of the pro-inflammatory cytokine, IL-17 (85). Most intriguing, these latter effects of C5b-9 were dampened by exosomes derived from mesenchymal stem cells in a CD59-dependent manner (85). The clinical relevance is being tested in pilot studies, as administration of mesenchymal stem cell exosomes that naturally accumulate abundant CD59 (an inhibitor of MAC formation), appears to dampen the inflammation associated with COVID-19 (129).

When combined with thrombin, the terminal pathway components result in enhanced activation and aggregation of platelets and the release of granules (130). This is similar to the apparent co-operativity of thrombin and C5 convertase in generating a more lytic MAC ($C5b_T$-9) (131). In fact, even partial assembly to the point of C5b-7, by attaching to the outer leaflet of a target membrane, may be sufficient to trigger activation of TF on monocytic cells without inducing aPL exposure, but rather by promoting enzymatic decryption of TF *via* protein disulfide isomerase (132).

These prothrombotic, proinflammatory properties of the assembling complement terminal pathway components must be tightly regulated to prevent unwanted damage to healthy host cells. Indeed, there are several mechanisms: 1) Vitronectin binds to C5b-7, preventing it from binding to the outer membrane surface (133); 2) Clusterin interacts with C7, C8 and C9, diminishing the capacity of the C5b-9 complex to integrate into the membrane (134); 3) Polyphosphate binds to C6, destabilizing C5b,6, preventing C5b-8 and C5b-9 complexes from integrating into the membrane (135); and 4) On the cell surface, glycosylphosphatidylinositol (GPI)-linked CD59 binds to C8 and C9 and prevents C9 polymerization (136). Thus, MAC-triggered thrombo-inflammatory effects are coordinately dampened by shared regulatory pathways.

Anaphylatoxins delicately modulate coagulation

Activation of the complement system is accompanied by the liberation of potent anaphylatoxins, C3a and C5a (see Table 2 for a summary of C5a biological effects). These relatively small peptides do more than just recruit inflammatory cells to sites of injury and infection. *Via* their widely expressed cognate receptors, C3aR for C3a, and C5aR1 and C5L2 for C5a, they exhibit multiple biological functions, including the promotion of coagulation and inflammation (137, 138).

Circulating quiescent platelets can become sensitized to stimulation by either C3a or C5a by minimal pre-activation, such as by adhesion to the subendothelium following vascular damage (139). By engaging their receptors, C3a and C5a induce platelet activation and aggregation (73, 140), triggering the release of C1q, C3, C4 and C5b-9 (141), surface exposure of chondroitin sulfate A, and α-granule release and surface exposure of P-selectin and the globular head receptor for C1q (gC1q-R). P-selectin is a receptor for C3b, and thus provides a means for assembly of the AP C3 convertases, while C1q binding to gC1q-R triggers the CP. Engagement of C1q with gC1q-R also induces conformational changes in the integrin GpIIbIIIa that supports platelet adhesion and aggregation (142) and promotes further P-selectin release with recruitment of leukocytes *via* interactions with P-selectin glycoprotein-1 (PSGL-1) (143). C3 that is hydrolyzed to C3(H2O) can also bind to the surface of activated platelets in the presence of leukocyte derived properdin, thereby facilitating formation of a platelet surface-localized AP $C3(H_2O)Bb$ convertase (63, 139). This platelet bound $C3(H_2O)$ may also serve as a ligand for leukocyte cell surface receptor CD11b/CD18, promoting platelet-leukocyte interactions and recruitment of activated TF-bearing, prothrombotic monocytes.

The LP has also been implicated in platelet-facilitated hemostatic mechanisms (144), as ficolins, MASP-1 and MASP-2 are found on the surface of activated platelets. This may be attenuated by the release from activated platelets of the thiol isomerase ERp57, which interferes with ficolin recognition *via* disruption of its multimerization (145). Indeed, there are several negative regulatory mechanisms that limit complement activation on the platelet surface, presumably to prevent the early demise of these important cells. Thus, the cell surface-expressed chondroitin sulfate A (CsA) can bind to C1q, C4b binding protein and FH, the latter two which dampen the immune response and limit further complement activation (146). Furthermore, platelet α-granules can release C1-INH, FH, CD55, CD59, CD46 and clusterin, while polyphosphate is released from dense granules. When secreted onto the surface of activated platelets, these can dampen MAC generation at different stages within the complement system. Although

TABLE 2 Activities of complement factor C5a that modulate thromboinflammation.

Cellular target	Cellular response
Platelets	triggers α-granule release of constituents (e.g., P-selectin, PF4, CD40L, PAF, integrin αIIbβ3, FV, FVIII, FXI, VWF, fibrinogen, HK, TFPI, PAI-1, Pg, MMPs, C1-INH, FH, CD55, CD59, CD46, clusterin, FD
	induces dense-granule release of constituents (e.g., serotonin, ADP, ATP, ionic calcium, polyphosphate)
	triggers lysosome release of constituents (e.g., hydrolases, cathepsins, elastases, glycosidases)
	induces exposure of P-selectin, a receptor for C3b and ligand for PSGL-1 to recruit neutrophils
	triggers exposure of gC1q-R, a receptor for C1q
	triggers exposure of CsA to which C1q, C4b binding protein and FH can bind
	triggers release of procoagulant microvesicles
Endothelial cells	upregulates leukocyte adhesion molecules
	increases secretion of P-selectin, VWF
	upregulates and activates cell surface TF
	suppresses expression of thrombomodulin
	damages the glycocalyx
	triggers release of procoagulant microvesicles
Neutrophils	chemoattractant
	cells are activated and induced to release proteolytic enzymes (e.g., elastase, cathepsins), ROS, chemoattractants and cytokines
	upregulates integrins to enhance migration and adhesion
	upregulates/activates TF
	augments expression of CR3 (CD11b) which facilitates adhesion, migration, phagocytosis
	triggers release of prothrombotic/proinflammatory NETs

tightly regulated, the mechanisms that trigger P-selectin expression and accumulation of C3(H_2O) on activated platelets enable C3a and C5a to sustain their own production and activate more platelets, leukocytes and endothelial cells to propagate coagulation and hemostasis.

With activation of complement *via* the CP/LP, C4a is liberated. This is believed to also have anaphylatoxic properties, but less potent than C3a and C5a. Nonetheless, C4a is interesting, as it interacts with platelets, binding to PAR1 and PAR4, thereby triggering intracellular events that promote their activation (147). A pathophysiologic contribution to hemostasis-thrombosis has not been established.

Endothelial cells also express receptors for C3a and C5a (74, 75, 148), engagement of which induces upregulation of leukocyte adhesion molecules, P-selectin, VWF and TF (149), suppression of thrombomodulin (150), and damage to the glycocalyx (151). Underlining a role for the engagement of C5aR in coagulation, in mice with a mutation in FH that causes diffuse microvascular and macrovascular thrombosis, blockade of C5aR protects against macrovascular thrombosis (152). Interestingly, lack of C3 or FD in those same FH mutant mice prevents all thrombosis (152). C5a also induces TF expression on neutrophils (153). Taken together, C3a and C5a and their receptors are pivotal, not only in recruiting circulating platelets and inflammatory leukocytes to the site of injury, but also in facilitating their participation in a thromboinflammatory response.

In addition to the likely roles of the anaphylatoxins, C3a, C5a and C4a in the function of primary hemostatic cells, platelets and endothelial cells, there is strong evidence that platelets, endothelial cells, neutrophils, and monocytes can be profoundly influenced by other "small" complement factors (154). This is exemplified by a recent report on the potential mechanisms underlying the thrombotic syndrome, heparin induced thrombocytopenia and thrombosis (HITT), a clinico-pathological arterial and venous thrombotic syndrome associated with the generation of heparin-dependent IgG anti-PF4 antibodies. These antibodies assemble into ultra-large immune complexes (ULICs) with heparin and PF4 on platelets. In a recently proposed model (155), the HITT ULICs bind to C1q and activate complement *via* the CP in the blood and on leukocytes, which leads to incorporation of C3c and C4d. These in turn engage complement receptors and Fcγ receptors on neutrophils and monocytes, upregulating TF expression and promoting coagulation and platelet activation/adhesion on endothelial cells, leading then to further thromboinflammation. Interventions that block C1 or C3 prevent leukocyte TF expression, while C5 blockade has no effect. Although yet to be confirmed *in vivo*, the model highlights the important role that each of the many proteolytic complement activation fragments may have in coagulation and the innate response to injury, and the potential therapeutic implications.

Complementary enzymatic routes of complement and coagulation activation

Thrombin, more than a hemostatic factor

While thrombin is recognized as a central regulator of hemostasis (156), its broad substrate specificity within the humoral and cellular responses to vascular damage also interconnects thrombin to the host response to pathogen invasion through direct association with the complement network (Figure 4). Several laboratories have investigated the ability of thrombin to substitute as a C5 convertase, and claimed that thrombin, particularly at high concentrations, releases a fragment from C5 that is physically consistent with the generation of the anaphylatoxin, C5a (131, 157, 158). The C5 fragmentation milieu has biological activity in cell-based models (131, 157–159) and in some, but not all animal models (157, 160). A detailed biochemical investigation revealed that when the bona fide C5-convertase and thrombin are both present and active, as likely occurs with most injuries, non-canonical C5 and C5b cleavage products are generated that lead to the assembly of a more highly lytic $C5b_T$-9 MAC (131), thereby augmenting the thromboinflammatory response to injury. This modified C5 was

able to support binding of C6 and assembly of a MAC (161), potentially providing a "bypass" pathway that could be relevant in the strategic design of therapeutics. Contrary to its effects on C5, thrombin has limited capacity to generate a C3 convertase (162). However, thrombin may be able to enhance C3 convertase assembly indirectly *via* activation of pro-FD (68, 69), a fundamental accelerator of the AP.

Several of the preceding findings, mostly *in vitro* studies using various sources of C5, are not without controversy. *In vivo*, neither thrombin nor plasmin activated complement in a baboon sepsis model (160). More pointedly, elegant *in vitro* studies revealed that conformational changes in C5 in plasma from healthy donors, renders R947 inaccessible to cleavage by thrombin (163). It is not yet known whether protease cleavage sites, such as thrombin, within C5 (and C3) might be rendered accessible in diverse pathophysiological settings in which there are plasma disturbances in, for example, pH and electrolyte balance. In such situations, one or more of these non-canonical complement activation pathways may indeed be of clinical relevance, and thus potential therapeutic targets in disease. Further study is necessary!

Thrombin may also enhance complement *via* communication with cell surface receptors. Thus, exposure of platelets to thrombin causes deposition of C3 and the MAC (130, 164). This likely occurs *via* thrombin-triggered P-selectin release to the platelet surface, the latter which associates with C3b and enables assembly of the C3-convertase with subsequent C3 deposition and MAC formation (165). In line with the often opposing biological properties of thrombin, this also induces PAR1-mediated expression of the AP membrane control protein, CD55 (166) on vascular cells, indicating that spatial-temporal factors must be considered when evaluating the effects of these multi-versed proteases. Such observations also further underline a major theme of this review that the pathways involved in the thromboinflammatory response do not exist in isolation, but rather must finally be evaluated in the context of a more physiologic "web" of interactions.

Several other serine protease enzymes, particularly those involved in inflammation, have been reported to exhibit C5 convertase properties (167). The physiological relevance of most of these have not been established, but are worthy of consideration and further study. For example, neutrophil elastase directly cleaves C5, generating C5b,6 and a C5a-like moiety. Formation of the C5b-9 complex in this case, is limited by elastase-mediated hydrolysis of C6 (168). Cathepsin D that is released following severe tissue injury, has been directly correlated with C5 activation and generation of C5a (169). Factors IXa, Xa, XIa and PKa, have also been reported to cleave C5, bypassing the *bona fide* convertases in a C3-independent manner (157–159, 161). PKa can also cleave FH and FB (170, 171).

Plasmin: clot buster and complement activator

Several lines of evidence point to crosstalk between the fibrinolytic system and complement. For example, many chronic inflammatory disorders, such as atherosclerosis, exhibit colocalized and temporally overlapping activation of Pg with the accumulation of complement degradation products (172, 173). In addition to localization to the clot surface, plasmin generation may occur at sites of injury on endothelial cells, leukocytes or platelets - cells that are crucial for thrombin amplification and clot propagation - and where several receptors

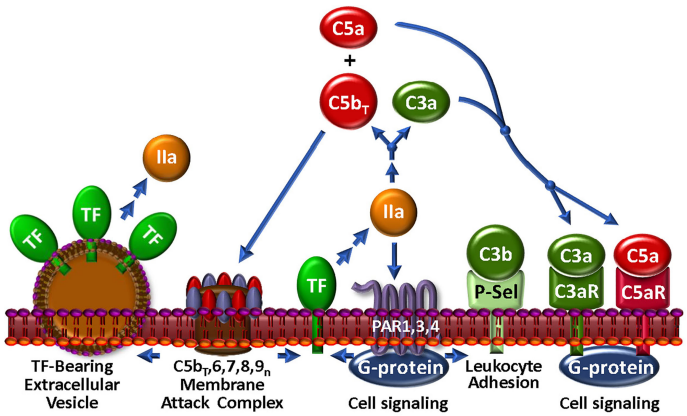

FIGURE 4
The Thrombin-Complement Web. Although the conditions under which this pathway exists *in vivo* remain to be shown, thrombin (IIa), in combination with the bona fide C5 convertase (not shown), cleaves C5 to C5b$_T$ and C5a, which promote assembly of the MAC and an anaphylactic response, respectively. The MAC may induce the generation of extracellular vesicles, a well-documented source of TF. Thrombin also cleaves C3 to generate anaphylatoxin C3a. *Via* PARs 1, 3 and 4, thrombin triggers modulation of many cell types. In particular, P-selectin (P-Sel) can associate with C3b to upregulate the AP. Stimulation through PARs also facilitates expression of TF activity to further the thrombin-mediated effects on complement.

for Pg have been identified (174), including, for example, annexin A2-S100A10 (175) and Plg-Rkt (176). Upon activation either by tPA or urokinase plasminogen activator, cell-associated plasmin is likely involved in the recruitment and activation of inflammatory and immune cells and modulators (177). This is achieved *via* direct and indirect PAR-facilitated modulation of immune and inflammatory cells (177). However, it is also believed to occur in response to direct plasmin mediated proteolytic activation of C3 and C5, with release of the potent anaphylatoxins, C3a and C5a (158, 162, 178).

Interestingly, in spite of plasmin mediating the generation of C3a and C5a, there is little evidence for the subsequent assembly of their respective C3 or C5 convertases. This may be due to plasmin-mediated degradation of the key elements required for their formation (C3b, C5b, FB). There are, however, conflicting data as to whether plasmin activation of complement can provide an alternative route to generation and deposition of C5b-9 (162, 179). It is possible that such discordant observations are a function of differences in experimental setups, as well as the spatial-temporal availability of inhibitors and negative regulators of plasmin and complement (158).

The action of plasmin and plasmin-like proteases on the complement system likely extend further. As an evolutionary adaptation, plasmin-like activity is facilitated by bacteria-encoded activators (e.g. staphylokinase) directly on a pathogen surface. In this locale, previously deposited opsonins C3b and iC3b can be removed from the pathogen surface by the acquired proteolytic activity (180). Indeed, plasmin can cleave iC3b, yielding C3d/g-like peptides that bind to complement receptors CR3/4 and CR2 on leukocytes, thereby dampening phagocytosis and enhancing macrophage secretion of IL-12, respectively (174, 181, 182). The complement-fixing fragment of IgG (i.e., Fc) is furthermore stripped from the pathogen by these plasmin-like proteases. Overall, opsonization and further deposition of C3b by the classical and alternative pathways of complement are thus prevented. These immune-evading mechanisms highlight the complex and intertwined roles of plasmin and complement in pathogen surveillance.

MASPs: Complement activator or coagulation activator?

The most abundant of the MBL-associated serine proteases in complement, MASP1, is required for activation of the LP. However, MASP1 has a promiscuous catalytic site that is more like thrombin than its CP C2-activating counterparts, C1r and C1s (183). MASP1 directly activates endothelial cells *via* PAR4 (184), thereby triggering intracellular signaling cascades that promote a pro-inflammatory response (59, 185) (Figure 5). In purified *in vitro* systems, MASP1 also activates prothrombin (186) and CPB2, cleaves fibrinogen to fibrin monomers, activates FXIII, and generates BK from HK. MASP2 is more restricted, but similarly cleaves prothrombin to thrombin (187) and activates FXII and PK (188). Once activated to FXIIa by either MASP-mediated mechanisms or the canonical contact phase mechanism, FXIIa can cleave C1r, triggering feedback amplification of complement *via* the CP (189). With the most limited substrate range of the MASPs, MASP-3 cleaves pro-factor D into factor D, thereby triggering the AP, and thus not wandering beyond complement (69).

The physiologic relevance of these apparent MASP-mediated proteolytic activities in coagulation and complement have not been confirmed. However, while MASP1 and MASP2 are >100-fold less active than the corresponding bona fide coagulation enzymes (FXa and thrombin) in cleaving prothrombin and fibrinogen, there are strong data supporting their contribution to thrombosis in various clinical situations. Mice deficient in either MASP1 or MBL are resistant to thrombosis in a carotid artery injury model (190). This is in line with clinical studies, in which patients with low MBL plasma levels had a lower risk of deep venous thrombosis (191). In light of the LP being implicated in contributing to the thromboinflammation associated with COVID-19 (183), major efforts are underway to identify agents that can block MASP2 (192). Phase 3 studies are ongoing to test the efficacy of a MASP2 inhibitor in protecting against the thrombotic microangiopathy associated with hematopoietic stem cell transplants (193). Overall, the story of MASPs in coagulation and complement and thromboinflammation is still unfolding.

Braking systems that affect complement and coagulation

As innate responders to bleeding, foreign or damaged cells, cellular by-products or invading pathogens, if unchecked, coagulation and complement activation may cause unwanted bystander damage to the host, leading to a proinflammatory and prothrombotic state with organ dysfunction and failure. Thus, tight regulation of these systems in a coordinated manner is essential. There are, indeed, multiple regulatory mechanisms at several steps - many of which are shared or overlap - these being achieved *via* membrane anchored and fluid-phase regulators.

Regulation of complement and coagulation proteases by serpins and non-serpins

Once activated, the proteases of complement, coagulation, fibrinolysis and the CS are under constant surveillance by multiple inhibitory mechanisms. Intrinsic to plasma are members of the serine protease inhibitor (serpin) homology family. Serpins deceive a protease by presenting a central reactive loop that resembles the target substrate. Upon cleavage, a gross conformational change traps the protease in an irreversible complex and is subsequently cleared (194). Serpins typically neutralize more than one type of protease. Perhaps the most important of these in coagulation is antithrombin (AT), which is the primary inhibitor of thrombin, FXa and FIXa (195, 196).

Functional deficiencies in AT substantially increase the risk of thrombosis (197). Notably, AT also inhibits MASP1 and MASP2 in the LP (198), although its pathophysiologic importance in complement activation is not known.

Clearly demonstrating a complement-coagulation overlap, C1 inhibitor (C1-INH) is a broad-specificity serpin with special significance for regulating both the contact phase branch of coagulation (199) and the CP of complement. C1-INH regulates the CS by controlling PK activation, and neutralizing the activities of PKa and FXIIa, likely better for the former than the latter (200). It also inhibits plasmin (12). In so doing, C1-INH reduces generation of the potent pro-inflammatory BK (102, 115), and within the hemostatic network, contributes to downstream inactivation of FXIa (201) and plasmin (202), thus affecting functional protease regulation in several pathways, and cell signaling *via* the PARs.

Within complement, C1-INH blocks several proteases, including C1r and C1s of the CP (203), and MASP1 and MASP2 of the LP (204), dampening generation of the CP/LP C3 convertases. In the complement system, and the coagulation system, C1-INH function is potentiated by polyanions, including heparan sulfate and polyphosphate (205–207), the latter which is a major procoagulant at several steps, including a key trigger for the CS (208–210). Independent of its function as a serpin, C1-INH also directly interacts with C3b, preventing binding of FB, and thus the formation of the AP C3 convertase (211). Based on the genetic association of C1-INH deficiency with hereditary angioedema, C1-INH should most prominently be viewed as a strategic piece for controlling BK formation (212). Notably however, its physiologic contribution to regulating coagulation has recently been revealed, with evidence - contrary to previous claims - that C1-INH deficiency is in fact, associated with an increased risk of thrombosis (213).

Non-serpin protease inhibitors are also important for the regulation of coagulation and complement. The only endogenous inhibitor of the extrinsic tenase is tissue factor pathway inhibitor (TFPI) (34, 214, 215), which may be GPI-linked and therefore a proportion is cell surface-associated. TFPI forms a high affinity quaternary complex with TF/FVIIa/FXa. Microvascular endothelial cells, monocytes, platelets and smooth muscle cells constitutively express TFPI (216) and the non-GPI-modified isoform is identified in plasma. In addition to

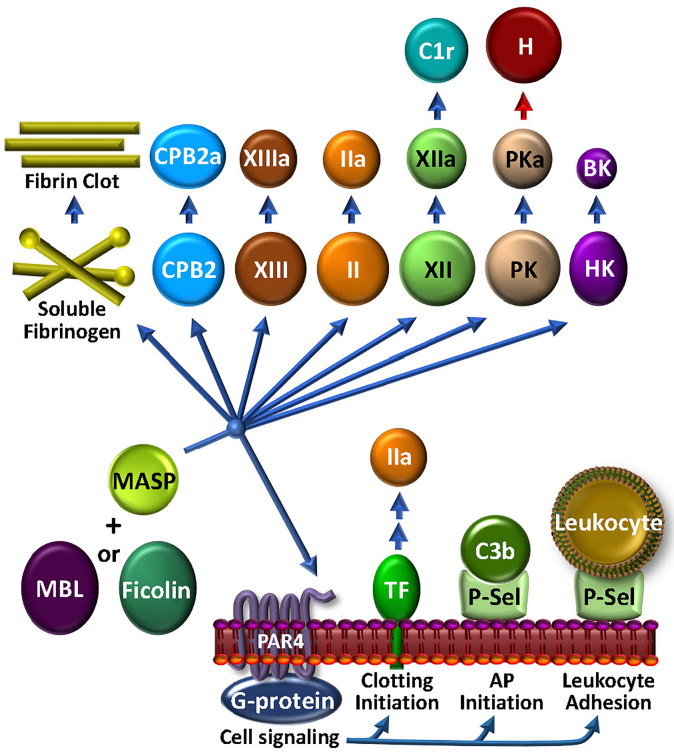

FIGURE 5
The MASP-Coagulation Web: MASPs may be either solution phase or surface bound, possibly associated with MBL, ficolin or collectin. Once triggered by engagement with an appropriate foreign lectin or other ligand, the activated MASP may stimulate cells *via* PAR4, leading to the availability of procoagulant TF or cell adhesive P-selectin activity. The latter may also participate to enhance AP C3 convertase assembly and function. MASPs have a wide array of circulating coagulation factor substrates, which may lead to bradykinin (BK) and kallikrein (PKa) that can inactivate factor H (H) and consequently up-regulate the AP, FXIIa that can activate C1r, thrombin (IIa), FXIIIa, carboxypeptidase 2 (CPB2), and fibrin production.

its role in coagulation, TFPI inhibits the LP by interfering with MASP2 cleavage of C4 and C2 (217). Interestingly, the acquired clonal hematologic disorder PNH, that is associated with excess complement activation and thrombosis, is caused by a mutation in the phosphatidylinositol glycan class A gene that encodes the protein necessary for GPI anchoring of several proteins, including in particular the complement negative regulators CD55 andCD59, but also TFPI. Thus, TFPI would predictably be absent in affected hematopoietic cells in PNH, a situation that might partially explain the heightened risk of thrombosis in these patients.

MAP-1 (aka Map44) and sMAP are alternative, non-enzymatic splice forms of MASP1/3 and MASP2, respectively. These compete for MASP binding to MBL, ficolins and collectins, thereby interfering with formation of the LP PRM (218). The relevance of these interactions, not only in complement activation and regulation, but also in coagulation, remain unclear.

Sushi domain-containing protein 4 (SUSD4) is a complement control protein that, due to alternative splicing, may be expressed as an integral membrane protein or a soluble protein. Although the mechanisms and physiologic relevance are incompletely understood, both forms inhibit formation of the C3 convertase, the soluble form targeting the CP and LP, and the membrane form, targeting the CP and AP (219). A potential direct role for SUS4 in coagulation has not been studied.

Convertases, FH and the AP

Although the convertases themselves are self-regulated by inherent instability, with half-lives in the range of minutes (220, 221), additional factors are essential to facilitate disruption of the integrity of the convertases, thereby preventing bystander injury to healthy host cells. Factor H (FH) is arguably the most potent and versatile AP negative regulator (222, 223) that targets C3 convertase, utilizing 3 distinct mechanisms to dampen complement activation. FH binds both to C3b and to host cells *via* defined molecular structures (224), whereupon it, 1) competes with FB binding to C3b, thereby preventing convertase assembly; 2) enhances serine protease factor I (FI)-mediated proteolysis of surface-bound C3b and C4b to iC3b/C3dg and iC4b/C4d, respectively, rendering them incapable of assembling a functional C3 convertase; and 3) accelerates decay of the C3b/Bb convertase. This latter decay accelerating mechanism is also used by CR1, CD55, FH-like protein-1 and the transmembrane glycoprotein receptor CD46. All of these, except CD55, also promote specific FI-mediated proteolysis of C3b and C4b (225). The liberated fragments, while incapable of assembling into a convertase, act as opsonins and trigger phagocytosis and adaptive immune responses. Interestingly, in the setting of inflammation or sepsis, C3b may be modified by a platelet-released kinase (226) such that it is resistant to the properties of FH (227). Whether this affects the function of the other cofactors for FI, is not known.

Recent *in vitro* studies have uncovered a potential co-regulatory complement-hemostasis relationship between FH and FXIa (228). FXIa cleaves FH at a site involved in enhancing the risk of age-related macular degeneration (229), reducing FH binding to endothelial cells, its cofactor activity in FI-mediated inactivation of C3b, and its C3b/Bb decay function. The FXa proteolytic activity was increased in the presence of polyphosphate, a prothrombotic polyanion that also binds to FH and exhibits anti-complement activity (135, 206). FH inhibits FXI activation by thrombin or FXIIa. Interestingly, FH has recently been found in plasma, complexed with FXIIa (230). Whether these interconnected regulatory mechanisms are relevant in health and thromboinflammatory disease is not yet known.

That FH and its protein binding-partners in the AP provide a bridge between coagulation and complement, is evident from extensive studies of patients with the thrombotic microangiopathy, atypical hemolytic uremic syndrome (aHUS). Patients with functional mutations in FH are at increased risk of developing aHUS (231–233); and indeed, loss-of-function or gain-of-function mutations in AP components that result in excess complement activation account for 60-70% of all cases of aHUS (234, 235). Interestingly, consistent with a potential role of Pg as a cofactor for FI-mediated inactivation of C3b (179), Pg-deficient variants have also been linked to aHUS (236). Most notably, and indicative of the role of complement hyperactivation triggering the thrombosis, is the protection afforded to almost all aHUS patients, with the anti-C5 antibody, eculizumab (13).

FH and thrombomodulin: Cooperative regulation of coagulation and complement

Thrombomodulin (TM) is a multidomain, transmembrane glycoprotein expressed on the surface of all vascular endothelial cells. It is a critical cofactor for thrombin-mediated activation of protein C (PC) to generate APC, catalyzing the reaction by ~1000-fold (237). Deficiency of PC augments the risk of deep vein thrombosis and thromboembolism (238) and the response to inflammatory stimuli. In a similar manner as for PC, TM also augments thrombin-mediated generation of the antifibrinolytic CPB2 (239), which also functions to inactivate pro-inflammatory mediators, BK, osteopontin, and the critical anaphylatoxins, C3a and C5a (117). The anaphylatoxins may also be proteolytically inactivated by MMP-12, activation of which is enhanced by CPB2-mediated prolongation of plasmin generation, which further produces complement opsonic fragments (240). TM reaches even further into the complement network by enhancing FI-mediated inactivation of C3b in the presence of FH (241–243). Overall, by sequestering thrombin from its myriad prothrombotic, pro-inflammatory and complement-activating effects, and by inactivating C3a, C5a and BK, and by augmenting the properties of FH, TM provides a critical and clinically relevant

bridge between coagulation and complement that additionally integrates into the thromboinflammatory web *via* its diverse properties in cell proliferation, leukocyte trafficking, and endothelial function [reviewed (244)].

FH and VWF interconnect complement and coagulation

VWF plays key roles in hemostasis and complement activation. Synthesized by megakaryocytes and endothelial cells in an ultra large multimeric form (ULVWF), it is secreted by endothelial cells following stress or injury, whereupon it is normally cleaved into smaller units by the enzyme ADAMTS13. However, with insufficient cleavage, the ULVWF multimers accumulate and promote excess platelet adhesion and aggregation and the formation of microvascular thrombi. This is manifest as the thrombotic microangiopathy, thrombotic thrombocytopenia purpura (245). ULVWF multimers provide a binding site for C3b and thus assembly of the AP C3 convertase (246), with potential subsequent activation of complement and bystander injury to neighboring cells. FH has been shown to colocalize with VWF in endothelial cell Weibel-Palade bodies, strongly suggesting a functional relationship. Although controversial, evidence indicates that FH may facilitate ADAMTS13-mediated proteolysis of the ULVWF into monomers and dimers (247–250), in addition to its established role as an AP regulator. Not only are these smaller VWF forms less amenable to C3b binding, but they may also act as a cofactor for C3b inactivation by FI (251). Thus, VWF is reciprocally indicated as a negative regulator of complement.

Concluding remarks

The preceding review highlights some of the complex interactions between complement and coagulation and how these interface with the apparently seamless web that comprise other critical pathways that are involved in the thromboinflammatory response to injury and infection. The value in deciphering the intricacies of this web of molecular and cellular relationships on disease outcome, is underlined by the overwhelming success of the terminal pathway anti-C5 antibodies, eculizumab and ravulizumab, in preventing the devastating thrombotic manifestations of aHUS and PNH (13, 14, 193). It is also evident by exciting new advances in our understanding of these interactive pathways, as several newer agents that target, for example, MASP2, FB, FD, C3, the C5a-C5aR axis, BK, BR, FXII/FXIIa, FXI/FXIa, polyanions, platelets, neutrophils and NETs, are being evaluated in clinical studies that are at various stages of development, and in many cases with promising results (reviewed in (193, 252, 253). And more are on the horizon. Varying responses indicate that tailored and personalized interventional strategies will undoubtedly be required to optimally prevent unwanted thromboinflammatory responses where coagulation and complement participate. This will necessarily entail continued research efforts to tease apart the intricacies of the web - examining pathways in isolation and in more complex environments - to uncover novel techniques and therapies, diagnostic tools and biomarkers for a wide range of disorders that reside within and extend beyond those traditionally viewed as coagulation or complement.

Author contributions

EP, AL and EC researched and wrote the manuscript. All authors contributed to the article and approved the submitted version.

Funding

EC is supported by the Canadian Institutes of Health Research (CIHR), the Natural Sciences and Engineering Research Council of Canada (NSERC), the Canada Foundations for Innovation (CFI), CanVECTOR and the Canada Research Chairs Program. He is an Adjunct Scientist with the Canadian Blood Services. EP is supported by the Canadian Blood Services and is supported by the Heart and Stroke Foundation of Canada and the CIHR. AL is supported by a MITACs Accelerate Postdoctoral Fellowship IT26813.

Conflict of interest

The authors declare that the research was conducted in the absence of any commercial or financial relationships that could be construed as a potential conflict of interest.

Publisher's note

References

1. Owen C. *A history of blood coagulation*. Rochester, Minnesota: Mayo Foundation (2001).

2. Beck EA. The chemistry of blood coagulation: a summary by Paul morawitz (1905). *Thromb haemostasis* (1977) 37:376–9. doi: 10.1055/s-0038-1649245

3. Graham-Smith GS. George Henry Falkiner Nuttall: (5 July 1862-16 December 1937). *J Hyg (Lond)* 38(1938):129–i4. doi: 10.1017/S0022172400010986

4. Buchner H. [Brief overview of the development of bacteriology since naegeli's involvement in it]. *Münchener Medizinische Wochenschriftlrm;* (1891) 38:435–7.

5. Bardhan M, Kaushik R. *Physiology, complement cascade*. Treasure Island (FL: StatPearls (2022).

6. Wising P. The identity of prothrombin as the midpiece of complement. *Acta Med Scand* (1938) 94:506–9. doi: 10.1111/j.0954-6820.1938.tb09508.x

7. Ratnoff OD, Lepow IH. Some properties of an esterase derived from preparations of the first component of complement. *J Exp Med* (1957) 106:327–43. doi: 10.1084/jem.106.2.327

8. Wedgwood RJ, Pillemer L. The nature and interactions of the properdin system. *Acta Haematol* (1958) 20:253–9. doi: 10.1159/000205491

9. Cooper NR. Complement: a nostalgic journey the Hans j. Muller-eberhard memorial lecture, Honolulu, June 14, 2004. *Mol Immunol* (2006) 43:487–95. doi: 10.1016/j.molimm.2005.04.018

10. Davie EW, Ratnoff OD. Waterfall sequence for intrinsic blood clotting. *Science* (1964) 145:1310–2. doi: 10.1126/science.145.3638.1310

11. Pillemer L, Ratnoff OD, Blum L, Lepow IH. The inactivation of complement and its components by plasmin. *J Exp Med* (1953) 97:573–89. doi: 10.1084/jem.97.4.573

12. Ratnoff OD. Some relationships among hemostasis, fibrinolytic phenomena, immunity, and the inflammatory response. *Adv Immunol* (1969) 10:145–227. doi: 10.1016/S0065-2776(08)60417-4

13. Gruppo RA, Rother RP. Eculizumab for congenital atypical hemolytic-uremic syndrome. *New Engl J Med* (2009) 360:544–6. doi: 10.1056/NEJMc0809959

14. Hillmen P, Young NS, Schubert J, Brodsky RA, Socie G, Muus P, et al. The complement inhibitor eculizumab in paroxysmal nocturnal hemoglobinuria. *New Engl J Med* (2006) 355:1233–43. doi: 10.1056/NEJMoa061648

15. W.H. Organization. *Global atlas on cardiovascular disease prevention and control*. Geneva: WHO (2011).

16. Pryzdial ELG, Lee FMH, Lin BH, Carter RLR, Tegegn TZ, Belletrutti MJ. Blood coagulation dissected. *Transfus. Apher. Sci* (2018) 57:449–57. doi: 10.1016/j.transci.2018.07.003

17. Versteeg HH, Heemskerk JW, Levi M, Reitsma PH. New fundamentals in hemostasis. *Physiol Rev* (2013) 93:327–58. doi: 10.1152/physrev.00016.2011

18. Schmaier AH. The contact activation and Kallikrein/Kinin systems: Pathophysiologic and physiologic activities. *J Thromb Haemost* (2016) 14:28–39. doi: 10.1111/jth.13194

19. Protty MB, Jenkins PV, Collins PW, O'Donnell VB. The role of procoagulant phospholipids on the surface of circulating blood cells in thrombosis and haemostasis. *Open Biol* (2022) 12:210318. doi: 10.1098/rsob.210318

20. Macfarlane RG. An enzyme cascade in the blood clotting mechanism, and its function as a biochemical amplifier. *Nature* (1964) 202:498–9. doi: 10.1038/202498a0

21. d'Alessandro E, Becker C, Bergmeier W, Bode C, Bourne JH, Brown H, et al. Thrombo-inflammation in cardiovascular disease: An expert consensus document from the third maastricht consensus conference on thrombosis. *Thromb haemostasis* (2020) 120:538–64. doi: 10.1055/s-0040-1708035

22. Rosenberg RD, Rosenberg JS. Natural anticoagulant mechanisms. *J Clin Invest* (1984) 74:1–6. doi: 10.1172/JCI111389

23. Clemetson KJ. Platelets and primary haemostasis. *Thromb Res* (2012) 129:220–4. doi: 10.1016/j.thromres.2011.11.036

24. Lenoir G, D'Ambrosio JM, Dieudonne T, Copic A. Transport pathways that contribute to the cellular distribution of phosphatidylserine. *Front Cell Dev Biol* (2021) 9:737907. doi: 10.3389/fcell.2021.737907

25. Heijnen H, van der Sluijs P. Platelet secretory behaviour: as diverse as the granules ... or not? *J Thromb Haemost* (2015) 13:2141–51. doi: 10.1111/jth.13147

26. Flaumenhaft R, Sharda A. Platelet secretion. In: AE Michelson, M Cattaneo, AL Frelinger and PJ Newman, editors. *Platelets*. (Amsterdam:Elsevier) (2019). p. 349–70.

27. Bach RR. Tissue factor encryption. *Arteriosclerosis thrombosis Vasc Biol* (2006) 26:456–61. doi: 10.1161/01.ATV.0000202656.53964.04

28. Ansari SA, Pendurthi UR, Rao LVM. Role of cell surface lipids and thiol-disulphide exchange pathways in regulating the encryption and decryption of tissue factor. *Thromb haemostasis* (2019) 119:860–70. doi: 10.1055/s-0039-1681102

29. Rao LV, Rapaport SI. Activation of factor VII bound to tissue factor: a key early step in the tissue factor pathway of blood coagulation. *Proc Natl Acad Sci U. S. A* (1988) 85:6687–91.

30. Krishnaswamy S. The interaction of human factor VIIa with tissue factor. *J Biol Chem* (1992) 267:23696–706. doi: 10.1016/S0021-9258(18)35894-0

31. Pryzdial ELG. Maestro tissue factor reaches new hEIGHT. *Blood* (2017) 130:1604–5. doi: 10.1182/blood-2017-08-798520

32. Krishnaswamy S, Field KA, Morrissey JH, Edgington TS, Mann KG. Activation of factor X by the extrinsic pathway. *Thromb Haemostasis* (1991) 65:296.

33. Kamikubo Y, Mendolicchio GL, Zampolli A, Marchese P, Rothmeier AS, Orje JN, et al. Selective factor VIII activation by the tissue factor-factor VIIa-factor xa complex. *Blood* (2017) 130:1661–70. doi: 10.1182/blood-2017-02-767079

34. Mast AE, Ruf W. Regulation of coagulation by tissue factor pathway inhibitor: Implications for hemophilia therapy. *J Thromb Haemost* (2022) 20:1290–300. doi: 10.1111/jth.15697

35. Olson ST, Richard B, Izaguirre G, Schedin-Weiss S, Gettins PG. Molecular mechanisms of antithrombin-heparin regulation of blood clotting proteinases. a paradigm for understanding proteinase regulation by serpin family protein proteinase inhibitors. *Biochimie* (2010) 92:1587–96. doi: 10.1016/j.biochi.2010.05.011

36. Schuijt TJ, Bakhtiari K, Daffre S, Deponte K, Wielders SJ, Marquart JA, et al. Factor xa activation of factor V is of paramount importance in initiating the coagulation system: lessons from a tick salivary protein. *Circulation* (2013) 128:254–66. doi: 10.1161/CIRCULATIONAHA.113.003191

37. Krishnaswamy S, Nesheim ME, Pryzdial ELG, Mann KG. Assembly of the prothrombinase complex. *Methods enzymol* (1994) 222:260–80. doi: 10.1016/0076-6879(93)22018-B

38. Hoffman M, Monroe 3DM. A cell-based model of hemostasis. *Thromb haemostasis* (2001) 85:958–65. doi: 10.1055/s-0037-1615947

39. Macfarlane SR, Seatter MJ, Kanke T, Hunter GD, Plevin R. Proteinase-activated receptors. *Pharmacol Rev* (2001) 53:245–82.

40. Vu T-KH, Hung DT, Wheaton VI, Coughlin SR. Molecular cloning of a functional thrombin receptor reveals a novel proteolytic mechanism of receptor activation. *Cell* (1991) 64:1057–68. doi: 10.1016/0092-8674(91)90261-V

41. Coughlin SR. Protease-activated receptors in hemostasis, thrombosis and vascular biology. *J Thromb Haemostasis* (2005) 3:1800–14. doi: 10.1111/j.1538-7836.2005.01377.x

42. Zelaya H, Rothmeier A, Ruf W. Tissue factor at the crossroad of coagulation and cell signaling. *J Thromb Haemost* (2018) 26:1941–52. doi: 10.1111/jth.14246

43. Keragala CB, Medcalf RL. Plasminogen: an enigmatic zymogen. *Blood* (2021) 137:2881–9. doi: 10.1182/blood.2020008951

44. Kuliopulos A, Covic L, Seeley SK, Sheridan PJ, Helin J, Costello CE. Plasmin desensitization of the PAR1 thrombin receptor: kinetics, sites of truncation, and implications for thrombolytic therapy. *Biochemistry* (1999) 38:4572–85. doi: 10.1021/bi9824792

45. Shimazu H, Munakata S, Tashiro Y, Salama Y, Dhahri D, Eiamboonsert S, et al. Pharmacological targeting of plasmin prevents lethality in a murine model of macrophage activation syndrome. *Blood* (2017) 130:59–72. doi: 10.1182/blood-2016-09-738096

46. Syrovets T, Jendrach M, Rohwedder A, Schule A, Simmet T. Plasmin-induced expression of cytokines and tissue factor in human monocytes involves AP-1 and IKKbeta-mediated NF-kappaB activation. *Blood* (2001) 97:3941–50. doi: 10.1182/blood.V97.12.3941

47. Domotor E, Bartha K, Machovich R, Adam-Vizi V. Protease-activated receptor-2 (PAR-2) in brain microvascular endothelium and its regulation by plasmin and elastase. *J neurochem* (2002) 80:746–54. doi: 10.1046/j.0022-3042.2002.00759.x

48. Werb Z. ECM and cell surface proteolysis: regulating cellular ecology. *Cell* (1997) 91:439–42. doi: 10.1016/S0092-8674(00)80429-8

49. Carmeliet P, Moons L, Lijnen R, Baes M, Lemaitre V, Tipping P, et al. Urokinase-generated plasmin activates matrix metalloproteinases during aneurysm formation. *Nat Genet* (1997) 17:439–44. doi: 10.1038/ng1297-439

50. Heissig B, Lund LR, Akiyama H, Ohki M, Morita Y, Romer J, et al. The plasminogen fibrinolytic pathway is required for hematopoietic regeneration. *Cell Stem Cell* (2007) 1:658–70. doi: 10.1016/j.stem.2007.10.012

51. Heuberger DM, Schuepbach RA. Protease-activated receptors (PARs): mechanisms of action and potential therapeutic modulators in PAR-driven inflammatory diseases. *Thromb J* (2019) 17:4. doi: 10.1186/s12959-019-0194-8

52. Ricklin D, Lambris JD. Complement-targeted therapeutics. *Nat Biotechnol* (2007) 25:1265–75. doi: 10.1038/nbt1342

53. Pouw RB, Ricklin D. Tipping the balance: intricate roles of the complement system in disease and therapy. *Semin immunopathol* (2021) 43:757–71. doi: 10.1007/s00281-021-00892-7

54. Conway EM. Complement-coagulation connections. *Blood Coagul Fibrinolysis* (2018) 29:243–51. doi: 10.1097/MBC.0000000000000720

55. Roh JS, Sohn DH. Damage-associated molecular patterns in inflammatory diseases. *Immune Netw* (2018) 18:e27. doi: 10.4110/in.2018.18.e27

56. Kidmose RT, Laursen NS, Dobo J, Kjaer TR, Sirotkina S, Yatime L, et al. Structural basis for activation of the complement system by component C4 cleavage. *Proc Natl Acad Sci United States America* (2012) 109:15425–30. doi: 10.1073/pnas.1208031109

57. Wijeyewickrema LC, Yongqing T, Tran TP, Thompson PE, Viljoen JE, Coetzer TH, et al. Molecular determinants of the substrate specificity of the complement-initiating protease, C1r. *J Biol Chem* (2013) 288:15571–80. doi: 10.1074/jbc.M113.451757

58. Degn SE, Jensen L, Hansen AG, Duman D, Tekin M, Jensenius JC, et al. Mannan-binding lectin-associated serine protease (MASP)-1 is crucial for lectin pathway activation in human serum, whereas neither MASP-1 nor MASP-3 is required for alternative pathway function. *J Immunol* (2012) 189:3957–69. doi: 10.4049/jimmunol.1201736

59. Dobo J, Schroeder V, Jenny L, Cervenak L, Zavodszky P, Gal P. Multiple roles of complement MASP-1 at the interface of innate immune response and coagulation. *Mol Immunol* (2014) 61:69–78. doi: 10.1016/j.molimm.2014.05.013

60. Lachmann PJ, Hughes-Jones NC. Initiation of complement activation. *Springer Semin immunopathol* (1984) 7:143–62. doi: 10.1007/BF01893018

61. Nilsson B, Ekdahl KN. The tick-over theory revisited: is C3 a contact-activated protein? *Immunobiology* (2012) 217:1106–10. doi: 10.1016/j.imbio.2012.07.008

62. Bexborn F, Andersson PO, Chen H, Nilsson B, Ekdahl KN. The tick-over theory revisited: formation and regulation of the soluble alternative complement C3 convertase (C3(H2O)Bb). *Mol Immunol* (2008) 45:2370–9. doi: 10.1016/j.molimm.2007.11.003

63. Saggu G, Cortes C, Emch HN, Ramirez G, Worth RG, Ferreira VP. Identification of a novel mode of complement activation on stimulated platelets mediated by properdin and C3(H2O). *J Immunol* (2013) 190:6457–67. doi: 10.4049/jimmunol.1300610

64. Des Prez RM, Bryan CS, Hawiger J, Colley DG. Function of the classical and alternate pathways of human complement in serum treated with ethylene glycol tetraacetic acid and MgCl2-ethylene glycol tetraacetic acid. *Infection Immun* (1975) 11:1235–43. doi: 10.1128/iai.11.6.1235-1243.1975

65. White RT, Damm D, Hancock N, Rosen BS, Lowell BB, Usher P, et al. Human adipsin is identical to complement factor d and is expressed at high levels in adipose tissue. *J Biol Chem* (1992) 267:9210–3. doi: 10.1016/S0021-9258(19)50409-4

66. Beatty DW, Davis AE, Cole 3FS, Einstein LP, Colten HR. Biosynthesis of complement by human monocytes. *Clin Immunol Immunopathol* (1981) 18:334–43. doi: 10.1016/0090-1229(81)90126-4

67. Takahashi M, Ishida Y, Iwaki D, Kanno K, Suzuki T, Endo Y, et al. Essential role of mannose-binding lectin-associated serine protease-1 in activation of the complement factor d. *J Exp Med* (2010) 207:29–37. doi: 10.1084/jem.20090633

68. Oroszlan G, Kortvely E, Szakacs D, Kocsis A, Dammeier S, Zeck A, et al. MASP-1 and MASP-2 do not activate pro-factor d in resting human blood, whereas MASP-3 is a potential activator: Kinetic analysis involving specific MASP-1 and MASP-2 inhibitors. *J Immunol* (2016) 196:857–65. doi: 10.4049/jimmunol.1501717

69. Dobo J, Szakacs D, Oroszlan G, Kortvely E, Kiss B, Boros E, et al. MASP-3 is the exclusive pro-factor d activator in resting blood: the lectin and the alternative complement pathways are fundamentally linked. *Sci Rep* (2016) 6:31877. doi: 10.1038/srep31877

70. Fearon DT, Austen KF. Properdin: binding to C3b and stabilization of the C3b dependent C3 convertase. *J Exp Med* (1975) 142:856–63. doi: 10.1084/jem.142.4.856

71. Cortes C, Desler C, Mazzoli A, Chen JY, Ferreira VP. The role of properdin and factor h in disease. *Adv Immunol* (2022) 153:1–90. doi: 10.1016/bs.ai.2021.12.001

72. Masaki T, Matsumoto M, Yasuda R, Levine RP, Kitamura H, Seya T. A covalent dimer of complement C4b serves as a subunit of a novel C5 convertase that involves no C3 derivatives. *J Immunol* (1991) 147:927–32.

73. Polley MJ, Nachman RL. Human platelet activation by C3a and C3a des-arg. *J Exp Med* (1983) 158:603–15. doi: 10.1084/jem.158.2.603

74. Propson NE, Roy ER, Litvinchuk A, Kohl J, Zheng H. Endothelial C3a receptor mediates vascular inflammation and blood-brain barrier permeability during aging. *J Clin Invest* (2021) 131(1):e140966. doi: 10.1172/JCI140966

75. Shivshankar P, Li YD, Mueller-Ortiz SL, Wetsel RA. In response to complement anaphylatoxin peptides C3a and C5a, human vascular endothelial cells migrate and mediate the activation of b-cells and polarization of T-cells. *FASEB J* (2020) 34:7540–60. doi: 10.1096/fj.201902397R

76. Laumonnier Y, Karsten CM, Kohl J. Novel insights into the expression pattern of anaphylatoxin receptors in mice and men. *Mol Immunol* (2017) 89:44–58. doi: 10.1016/j.molimm.2017.05.019

77. Afzali B, Noris M, Lambrecht BN, Kemper C. The state of complement in COVID-19. *Nat Rev Immunol* (2022) 2:77–84. doi: 10.1038/s41577-021-00665-1

78. Sendo F, Yoshitake H, Araki Y. Targeting of neutrophil activation in the early phase of the disease for prevention of coronavirus disease-19 severity. *Microbiol Immunol* (2022) 66:264–76. doi: 10.1111/1348-0421.12978

79. Shi H, Zuo Y, Navaz S, Harbaugh A, Hoy CK, Gandhi AA, et al. Endothelial cell-activating antibodies in COVID-19. *Arthritis Rheumatol* (2022) 74:1132–38. doi: 10.1002/art.42094

80. Carvelli J, Demaria O, Vely F, Batista L, Chouaki Benmansour N, Fares J, et al. Association of COVID-19 inflammation with activation of the C5a-C5aR1 axis. *Nature* (2020) 588:146–50. doi: 10.1038/s41586-020-2600-6

81. Fuchs TA, Abed U, Goosmann C, Hurwitz R, Schulze I, Wahn V, et al. Novel cell death program leads to neutrophil extracellular traps. *J Cell Biol* (2007) 176:231–41. doi: 10.1083/jcb.200606027

82. Mamtimin M, Pinarci A, Han C, Braun A, Anders HJ, Gudermann T, et al. Extracellular DNA traps: Origin, function and implications for anti-cancer therapies. *Front Oncol* (2022) 12:869706. doi: 10.3389/fonc.2022.869706

83. Martinod K, Wagner DD. Thrombosis: tangled up in NETs. *Blood* (2014) 123:2768–76. doi: 10.1182/blood-2013-10-463646

84. Geddings JE, Mackman N. New players in haemostasis and thrombosis. *Thromb haemostasis* (2014) 111:570–4. doi: 10.1160/TH13-10-0812

85. Loh JT, Zhang B, Teo JKH, Lai RC, Choo ABH, Lam KP, et al. Mechanism for the attenuation of neutrophil and complement hyperactivity by MSC exosomes. *Cytotherapy* (2022) 24:711–19. doi: 10.1016/j.jcyt.2021.12.003

86. Chen Y, Li X, Lin X, Liang H, Liu X, Zhang X, et al. Complement C5a induces the generation of neutrophil extracellular traps by inhibiting mitochondrial STAT3 to promote the development of arterial thrombosis. *Thromb J* (2022) 20:24. doi: 10.1186/s12959-022-00384-0

87. de Bont CM, Boelens WC, Pruijn GJM. NETosis, complement, and coagulation: a triangular relationship. *Cell Mol Immunol* (2019) 16:19–27. doi: 10.1038/s41423-018-0024-0

88. Middleton EA, He XY, Denorme F, Campbell RA, Ng D, Salvatore SP, et al. Neutrophil extracellular traps contribute to immunothrombosis in COVID-19 acute respiratory distress syndrome. *Blood* (2020) 136:1169–79. doi: 10.1182/blood.2020007008

89. Englert H, Rangaswamy C, Deppermann C, Sperhake JP, Krisp C, Schreier D, et al. Defective NET clearance contributes to sustained FXII activation in COVID-19-associated pulmonary thrombo-inflammation. *EBioMedicine* (2021) 67:103382. doi: 10.1016/j.ebiom.2021.103382

90. Skendros P, Mitsios A, Chrysanthopoulou A, Mastellos DC, Metallidis S, Rafailidis P, et al. Complement and tissue factor-enriched neutrophil extracellular traps are key drivers in COVID-19 immunothrombosis. *J Clin Invest* (2020) 130:6151–57. doi: 10.1172/JCI141374

91. Mastellos DC, Pires BGP, Fonseca BAL, Fonseca NP, Auxiliadora-martins M, Mastaglio S, et al. Complement C3 vs C5 inhibition in severe COVID-19: early clinical findings reveal differential biological efficacy. *Clin Immunol* (2020) 220:108598–8. doi: 10.1016/j.clim.2020.108598

92. Brinkmann V, Reichard U, Goosmann C, Fauler B, Uhlemann Y, Weiss DS, et al. Neutrophil extracellular traps kill bacteria. *Science* (2004) 303:1532–5. doi: 10.1126/science.1092385

93. Shi Y, Gauer JS, Baker SR, Philippou H, Connell SD, Ariens RAS. Neutrophils can promote clotting *via* FXI and impact clot structure *via* neutrophil extracellular traps in a distinctive manner in vitro. *Sci Rep* (2021) 11:1718. doi: 10.1038/s41598-021-81268-7

94. Keragala CB, Draxler DF, McQuilten ZK, Medcalf RL. Haemostasis and innate immunity - a complementary relationship: A review of the intricate relationship between coagulation and complement pathways. *Br J haematol* (2018) 180:782–98. doi: 10.1111/bjh.15062

95. Barranco-Medina S, Pozzi N, Vogt AD, Di Cera E. Histone H4 promotes prothrombin autoactivation. *J Biol Chem* (2013) 288:35749–57. doi: 10.1074/jbc.M113.509786

96. Varju I, Longstaff C, Szabo L, Farkas AZ, Varga-Szabo VJ, Tanka-Salamon A, et al. DNA, Histones and neutrophil extracellular traps exert anti-fibrinolytic

effects in a plasma environment. *Thromb haemostasis* (2015) 113:1289–98. doi: 10.1160/TH14-08-0669

97. Ammollo CT, Semeraro F, Xu J, Esmon NL, Esmon CT. Extracellular histones increase plasma thrombin generation by impairing thrombomodulin-dependent protein c activation. *J Thromb Haemost* (2011) 9:1795–803. doi: 10.1111/j.1538-7836.2011.04422.x

98. Xu J, Zhang X, Pelayo R, Monestier M, Ammollo CT, Semeraro F, et al. Extracellular histones are major mediators of death in sepsis. *Nat Med* (2009) 15:1318–21. doi: 10.1038/nm.2053

99. Longstaff C, Varju I, Sotonyi P, Szabo L, Krumrey M, Hoell A, et al. Mechanical stability and fibrinolytic resistance of clots containing fibrin, DNA, and histones. *J Biol Chem* (2013) 288:6946–56. doi: 10.1074/jbc.M112.404301

100. Glaser C, Morser J, Clarke J, Blasko E, McLean K, Kuhn I, et al. Oxidation of a specific methionine in thrombomodulin by activated neutrophil products blocks cofactor activity. *J Clin Invest* (1992) 90:2565–73. doi: 10.1172/JCI116151

101. Higuchi DA, Wun TC, Likert KM, Broze GJ. The effect of leukocyte elastase on tissue factor pathway inhibitor. *Blood* (1992) 79:1712–9. doi: 10.1182/blood.V79.7.1712.1712

102. Maas C, Renne T. Coagulation factor XII in thrombosis and inflammation. *Blood* (2018) 131:1903–9. doi: 10.1182/blood-2017-04-569111

103. Srivastava P, Gailani D. The rebirth of the contact pathway: a new therapeutic target. *Curr Opin Hematol* (2020) 27:311–9. doi: 10.1097/MOH.0000000000000603

104. Liu J, Cooley BC, Akinc A, Butler J, Borodovsky A. Knockdown of liver-derived factor XII by GalNAc-siRNA ALN-F12 prevents thrombosis in mice without impacting hemostatic function. *Thromb Res* (2020) 196:200–5. doi: 10.1016/j.thromres.2020.08.040

105. Mailer RK, Rangaswamy C, Konrath S, Emsley J, Renne T. An update on factor XII-driven vascular inflammation. *Biochim Biophys Acta Mol Cell Res* (2022) 1869:119166. doi: 10.1016/j.bbamcr.2021.119166

106. Craig T, Magerl M, Levy DS, Reshef A, Lumry WR, Martinez-Saguer I, et al. Prophylactic use of an anti-activated factor XII monoclonal antibody, garadacimab, for patients with C1-esterase inhibitor-deficient hereditary angioedema: a randomised, double-blind, placebo-controlled, phase 2 trial. *Lancet* (2022) 399:945–55. doi: 10.1016/S0140-6736(21)02225-X

107. Shamanaev A, Emsley J, Gailani D. Proteolytic activity of contact factor zymogens. *J Thromb Haemost* (2021) 19:330–41. doi: 10.1111/jth.15149

108. Kannemeier C, Shibamiya A, Nakazawa F, Trusheim H, Ruppert C, Markart P, et al. Extracellular RNA constitutes a natural procoagulant cofactor in blood coagulation. *Proc Natl Acad Sci United States America* (2007) 104:6388–93. doi: 10.1073/pnas.0608647104

109. von Bruhl ML, Stark K, Steinhart A, Chandraratne S, Konrad I, Lorenz M, et al. Monocytes, neutrophils, and platelets cooperate to initiate and propagate venous thrombosis in mice in vivo. *J Exp Med* (2012) 209:819–35. doi: 10.1084/jem.20112322

110. Muller F, Mutch NJ, Schenk WA, Smith SA, Esterl L, Spronk HM, et al. Platelet polyphosphates are proinflammatory and procoagulant mediators in vivo. *Cell* (2009) 139:1143–56. doi: 10.1016/j.cell.2009.11.001

111. Renne T. The procoagulant and proinflammatory plasma contact system. *Semin immunopathol* (2012) 34:31–41. doi: 10.1007/s00281-011-0288-2

112. Kohs TCL, Lorentz CU, Johnson J, Puy C, Olson SR, Shatzel JJ, et al. Development of coagulation factor XII antibodies for inhibiting vascular device-related thrombosis. *Cell Mol Bioeng* (2021) 14:161–75. doi: 10.1007/s12195-020-00657-6

113. Matafonov A, Leung PY, Gailani AE, Grach SL, Puy C, Cheng Q, et al. Factor XII inhibition reduces thrombus formation in a primate thrombosis model. *Blood* (2014) 123:1739–46. doi: 10.1182/blood-2013-04-499111

114. Demoulin S, Godfroid E, Hermans C. Dual inhibition of factor XIIa and factor XIa as a therapeutic approach for safe thromboprotection. *J Thromb Haemost* (2021) 19:323–9. doi: 10.1111/jth.15130

115. Fang C, Schmaier AH. Novel anti-thrombotic mechanisms mediated by mas receptor as result of balanced activities between the kallikrein/kinin and the renin-angiotensin systems. *Pharmacol Res* (2020) 160:105096. doi: 10.1016/j.phrs.2020.105096

116. Bekassy Z, Lopatko Fagerstrom I, Bader M, Karpman D. Crosstalk between the renin-angiotensin, complement and kallikrein-kinin systems in inflammation. *Nat Rev Immunol* (2021) 22:411–28. doi: 10.1038/s41577-021-00634-8

117. Campbell WD, Lazoura E, Okada N, Okada H. Inactivation of C3a and C5a octapeptides by carboxypeptidase r and carboxypeptidase n. *Microbiol Immunol* (2002) 46:131–4. doi: 10.1111/j.1348-0421.2002.tb02669.x

118. Brown NJ, Gainer JV, Stein CM, Vaughan DE. Bradykinin stimulates tissue plasminogen activator release in human vasculature. *Hypertension* (1999) 33:1431–5. doi: 10.1161/01.HYP.33.6.1431

119. Simao F, Ustunkaya T, Clermont AC, Feener EP. Plasma kallikrein mediates brain hemorrhage and edema caused by tissue plasminogen activator therapy in mice after stroke. *Blood* (2017) 129:2280–90. doi: 10.1182/blood-2016-09-740670

120. Ratnoff OD, Pensky J, Ogston D, Naff GB. The inhibition of plasmin, plasma kallikrein, plasma permeability factor, and the C'1r subcomponent of the first component of complement by serum C'1 esterase inhibitor. *J Exp Med* (1969) 129:315–31. doi: 10.1084/jem.129.2.315

121. Howes JM, Richardson VR, Smith KA, Schroeder V, Somani R, Shore A, et al. Complement C3 is a novel plasma clot component with anti-fibrinolytic properties. *Diabetes Vasc Dis Res* (2012) 9:216–25. doi: 10.1177/1479164111432788

122. Niculescu F, Rus H. The role of complement activation in atherosclerosis. *Immunologic Res* (2004) 30:73–80. doi: 10.1385/IR:30:1:073

123. Gushiken FC, Han H, Li J, Rumbaut RE, Afshar-Kharghan V. Abnormal platelet function in C3-deficient mice. *J Thromb Haemost* (2009) 7:865–70. doi: 10.1111/j.1538-7836.2009.03334.x

124. Hamilton KK, Hattori R, Esmon CT, Sims PJ. Complement proteins C5b-9 induce vesiculation of the endothelial plasma membrane and expose catalytic surface for assembly of the prothrombinase enzyme complex. *J Biol Chem* (1990) 265:3809–14. doi: 10.1016/S0021-9258(19)39666-8

125. Wiedmer T, Esmon CT, Sims PJ. Complement proteins C5b-9 stimulate procoagulant activity through platelet prothrombinase. *Blood* (1986) 68:875–80. doi: 10.1182/blood.V68.4.875.875

126. Hattori R, Hamilton KK, McEver RP, Sims PJ. Complement proteins C5b-9 induce secretion of high molecular weight multimers of endothelial von willebrand factor and translocation of granule membrane protein GMP-140 to the cell surface. *J Biol Chem* (1989) 264:9053–60. doi: 10.1016/S0021-9258(18)81901-9

127. Peerschke EI, Yin W, Ghebrehiwet B. Complement activation on platelets: implications for vascular inflammation and thrombosis. *Mol Immunol* (2010) 47:2170–5. doi: 10.1016/j.molimm.2010.05.009

128. Hisada Y, Thalin C, Lundstrom S, Wallen H, Mackman N. Comparison of microvesicle tissue factor activity in non-cancer severely ill patients and cancer patients. *Thromb Res* (2018) 165:1–5. doi: 10.1016/j.thromres.2018.03.001

129. Mazini L, Rochette L, Malka G. Exosomes contribution in COVID-19 patients' treatment. *J Trans Med* (2021) 19:234. doi: 10.1186/s12967-021-02884-5

130. Polley MJ, Nachman RL. Human complement in thrombin-mediated platelet function: uptake of the C5b-9 complex. *J Exp Med* (1979) 150:633–45. doi: 10.1084/jem.150.3.633

131. Krisinger MJ, Goebeler V, Lu Z, Meixner SC, Myles T, Pryzdial EL, et al. Thrombin generates previously unidentified C5 products that support the terminal complement activation pathway. *Blood* (2012) 120:1717–25. doi: 10.1182/blood-2012-02-412080

132. Langer F, Spath B, Fischer C, Stolz M, Ayuk FA, Kroger N, et al. Rapid activation of monocyte tissue factor by antithymocyte globulin is dependent on complement and protein disulfide isomerase. *Blood* (2013) 121:2324–35. doi: 10.1182/blood-2012-10-460493

133. Podack ER, Kolb WP, Muller-Eberhard HJ. The SC5b-7 complex: formation, isolation, properties, and subunit composition. *J Immunol* (1977) 119:2024–9.

134. Falgarone G, Chiocchia G. Chapter 8: Clusterin: A multifacet protein at the crossroad of inflammation and autoimmunity. *Adv Cancer Res* (2009) 104:139–70. doi: 10.1016/S0065-230X(09)04008-1

135. Wat J, Foley JH, Krisinger MJ, Ocariza LM, Lei V, Wasney G, et al. Polyphosphate suppresses complement *via* the terminal pathway. *Blood* (2014) 123:768–76. doi: 10.1182/blood-2013-07-515726

136. Ninomiya H, Sims PJ. The human complement regulatory protein CD59 binds to the alpha-chain of C8 and to the "b"domain of C9. *J Biol Chem* (1992) 267:13675–80. doi: 10.1016/S0021-9258(18)42266-1

137. Wood AJT, Vassallo A, Summers C, Chilvers ER, Conway-Morris A. C5a anaphylatoxin and its role in critical illness-induced organ dysfunction. *Eur J Clin Invest* (2018) 48:e13028. doi: 10.1111/eci.13028

138. Mizuno T, Yoshioka K, Mizuno M, Shimizu M, Nagano F, Okuda T, et al. Complement component 5 promotes lethal thrombosis. *Sci Rep* (2017) 7:42714. doi: 10.1038/srep42714

139. Hamad OA, Nilsson PH, Wouters D, Lambris JD, Ekdahl KN, Nilsson B. Complement component C3 binds to activated normal platelets without preceding proteolytic activation and promotes binding to complement receptor 1. *J Immunol* (2010) 184:2686–92. doi: 10.4049/jimmunol.0902810

140. Martel C, Cointe S, Maurice P, Matar S, Ghitescu M, Theroux P, et al. Requirements for membrane attack complex formation and anaphylatoxins binding to collagen-activated platelets. *PloS One* (2011) 6:e18812. doi: 10.1371/journal.pone.0018812

141. Speth C, Rambach G, Wurzner R, Lass-Florl C, Kozarcanin H, Hamad OA, et al. Complement and platelets: Mutual interference in the immune network. *Mol Immunol* (2015) 67:108–18. doi: 10.1016/j.molimm.2015.03.244

142. Nayak A, Ferluga J, Tsolaki AG, Kishore U. The non-classical functions of the classical complement pathway recognition subcomponent C1q. *Immunol Lett* (2010) 131:139–50. doi: 10.1016/j.imlet.2010.03.012

143. Yang J, Furie BC, Furie B. The biology of p-selectin glycoprotein ligand-1: its role as a selectin counterreceptor in leukocyte-endothelial and leukocyte-platelet interaction. *Thromb Haemost* (1999) 81:1–7. doi: 10.1055/s-0037-1614407

144. Kozarcanin H, Lood C, Munthe-Fog L, Sandholm K, Hamad OA, Bengtsson AA, et al. The lectin complement pathway serine proteases (MASPs) represent a possible crossroad between the coagulation and complement systems in thromboinflammation. *J Thromb Haemost* (2016) 14:531–45. doi: 10.1111/jth.13208

145. Eriksson O, Chiu J, Hogg PJ, Atkinson JP, Liszewski MK, Flaumenhaft R, et al. Thiol isomerase ERp57 targets and modulates the lectin pathway of complement activation. *J Biol Chem* (2019) 294:4878–88. doi: 10.1074/jbc.RA118.006792

146. Hamad OA, Nilsson PH, Lasaosa M, Ricklin D, Lambris JD, Nilsson B, et al. Contribution of chondroitin sulfate a to the binding of complement proteins to activated platelets. *PloS One* (2010) 5:e12889. doi: 10.1371/journal.pone.0012889

147. Wang H, Ricklin D, Lambris JD. Complement-activation fragment C4a mediates effector functions by binding as untethered agonist to protease-activated receptors 1 and 4. *Proc Natl Acad Sci United States America* (2017) 114:10948–53. doi: 10.1073/pnas.1707364114

148. Monsinjon T, Gasque P, Chan P, Ischenko A, Brady JJ, Fontaine MC. Regulation by complement C3a and C5a anaphylatoxins of cytokine production in human umbilical vein endothelial cells. *FASEB J* (2003) 17:1003–14. doi: 10.1096/fj.02-0737com

149. Foreman KE, Vaporciyan AA, Bonish BK, Jones ML, Johnson KJ, Glovsky MM, et al. C5a-induced expression of p-selectin in endothelial cells. *J Clin Invest* (1994) 94:1147–55. doi: 10.1172/JCI117430

150. Fang W, Guo ZH, Zhang BQ, Wu XF, Li P, Lv FL, et al. [Effect of C5a on expression of thrombomodulin in endothelial cells *in vitro*]. *Zhongguo wei zhong bing ji jiu yi xue = Chin Crit Care Med = Zhongguo weizhongbing jijiuyixue* (2009) 21:168–71.

151. Bongoni AK, Lu B, McRae JL, Salvaris EJ, Toonen EJM, Vikstrom I, et al. Complement-mediated damage to the glycocalyx plays a role in renal ischemia-reperfusion injury in mice. *Transplant Direct* (2019) 5:e341. doi: 10.1097/TXD.0000000000000881

152. Ueda Y, Miwa T, Ito D, Kim H, Sato S, Gullipalli D, et al. Differential contribution of C5aR and C5b-9 pathways to renal thrombic microangiopathy and macrovascular thrombosis in mice carrying an atypical hemolytic syndrome-related factor h mutation. *Kidney Int* (2019) 96:67–79. doi: 10.1016/j.kint.2019.01.009

153. Ritis K, Doumas M, Mastellos D, Micheli A, Giaglis S, Magotti P, et al. A novel C5a receptor-tissue factor cross-talk in neutrophils links innate immunity to coagulation pathways. *J Immunol* (2006) 177:4794–802. doi: 10.4049/jimmunol.177.7.4794

154. Kim H, Conway EM. Platelets and complement cross-talk in early atherogenesis. *Front Cardiovasc Med* (2019) 6:131. doi: 10.3389/fcvm.2019.00131

155. Khandelwal S, Barnes A, Rauova L, Sarkar A, Rux AH, Yarovoi SV, et al. Complement mediates binding and procoagulant effects of ultralarge HIT immune complexes. *Blood* (2021) 138:2106–16. doi: 10.1182/blood.2020009487

156. Al-Amer OM. The role of thrombin in haemostasis. *Blood Coagul Fibrinolysis* (2022) 33:145–48. doi: 10.1097/MBC.0000000000001130

157. Huber-Lang M, Sarma JV, Zetoune FS, Rittirsch D, Neff TA, McGuire SR, et al. Generation of C5a in the absence of C3: a new complement activation pathway. *Nat Med* (2006) 12:682–7. doi: 10.1038/nm1419

158. Amara U, Flierl MA, Rittirsch D, Klos A, Chen H, Acker B, et al. Molecular intercommunication between the complement and coagulation systems. *J Immunol* (2010) 185:5628–36. doi: 10.4049/jimmunol.0903678

159. Wetsel RA, Kolb WP. Expression of C5a-like biological activities by the fifth component of human complement (C5) upon limited digestion with noncomplement enzymes without release of polypeptide fragments. *J Exp Med* (1983) 157:2029–48. doi: 10.1084/jem.157.6.2029

160. Keshari RS, Silasi R, Lupu C, Taylor FBJr., Lupu F. *In vivo*-generated thrombin and plasmin do not activate the complement system in baboons. *Blood* (2017) 130:2678–81. doi: 10.1182/blood-2017-06-788216

161. Mannes M, Dopler A, Zolk O, Lang SJ, Halbgebauer R, Hochsmann B, et al. Complement inhibition at the level of C3 or C5: mechanistic reasons for ongoing terminal pathway activity. *Blood* (2021) 137:443–55. doi: 10.1182/blood.2020005959

162. Foley JH, Walton BL, Aleman MM, O'Byrne AM, Lei V, Harrasser M, et al. Complement activation in arterial and venous thrombosis is mediated by plasmin. *EBioMedicine* (2016) 5:175–82. doi: 10.1016/j.ebiom.2016.02.011

163. Nilsson PH, Johnson C, Quach QH, Macpherson A, Durrant O, Pischke SE, et al. A conformational change of complement C5 is required for thrombin-mediated cleavage, revealed by a novel ex vivo human whole blood model preserving full thrombin activity. *J Immunol* (2021) 207:1641–51. doi: 10.4049/jimmunol.2001471

164. Polley MJ, Nachman R. The human complement system in thrombin-mediated platelet function. *J Exp Med* (1978) 147:1713–26. doi: 10.1084/jem.147.6.1713

165. Del Conde I, Cruz MA, Zhang H, Lopez JA, Afshar-Kharghan V. Platelet activation leads to activation and propagation of the complement system. *J Exp Med* (2005) 201:871–9. doi: 10.1084/jem.20041497

166. Lidington EA, Haskard DO, Mason JC. Induction of decay-accelerating factor by thrombin through a protease-activated receptor 1 and protein kinase c-dependent pathway protects vascular endothelial cells from complement-mediated injury. *Blood* (2000) 96:2784–92. doi: 10.1182/blood.V96.8.2784

167. Huber-Lang M, Ekdahl KN, Wiegner R, Fromell K, Nilsson B. Auxiliary activation of the complement system and its importance for the pathophysiology of clinical conditions. *Semin immunopathol* (2018) 40:87–102. doi: 10.1007/s00281-017-0646-9

168. Doring G. The role of neutrophil elastase in chronic inflammation. *Am J Respir Crit Care Med* (1994) 150:S114–7. doi: 10.1164/ajrccm/150.6_Pt_2.S114

169. Huber-Lang M, Denk S, Fulda S, Erler E, Kalbitz M, Weckbach S, et al. Cathepsin d is released after severe tissue trauma *in vivo* and is capable of generating C5a in vitro. *Mol Immunol* (2012) 50:60–5. doi: 10.1016/j.molimm.2011.12.005

170. DiScipio RG. The activation of the alternative pathway C3 convertase by human plasma kallikrein. *Immunology* (1982) 45:587–95.

171. Saito A. Plasma kallikrein is activated on dermatan sulfate and cleaves factor h. *Biochem Biophys Res Commun* (2008) 370:646–50. doi: 10.1016/j.bbrc.2008.04.027

172. Torzewski M, Bhakdi S. Complement and atherosclerosis-united to the point of no return? *Clin Biochem* (2013) 46:20–5. doi: 10.1016/j.clinbiochem.2012.09.012

173. Huang J, Huffman JE, Yamkauchi M, Trompet S, Asselbergs FW, Sabater-Lleal M, et al. Genome-wide association study for circulating tissue plasminogen activator levels and functional follow-up implicates endothelial STXBP5 and STX2. *Arteriosclerosis thrombosis Vasc Biol* (2014) 34:1093–101. doi: 10.1161/ATVBAHA.113.302088

174. Foley JH. Plasmin(ogen) at the nexus of fibrinolysis, inflammation, and complement. *Semin Thromb hemostasis* (2017) 43:135–42. doi: 10.1055/s-0036-1592302

175. Madureira PA, Surette AP, Pipps KD, Taboski MAS, Miller VA, Waisman DM. The role of annexin A2 heterotetramer in vascular fibrinolysis. *Blood* (2011) 118:4789–97. doi: 10.1182/blood-2011-06-334672

176. Lighvani S, Baik N, Diggs JE, Khaldoyanidi S, Parmer RJ, Miles LA. Regulation of macrophage migration by a novel plasminogen receptor plg-r $_{KT}$. *Blood* (2011) 118:5622–30. doi: 10.1182/blood-2011-03-344242

177. Heissig B, Salama Y, Takahashi S, Osada T, Hattori K. The multifaceted role of plasminogen in inflammation. *Cell signalling* (2020) 75:109761. doi: 10.1016/j.cellsig.2020.109761

178. Ward PA. A plasmin-split fragment of C'3 as a new chemotactic factor. *J Exp Med* (1967) 126:189–206. doi: 10.1084/jem.126.2.189

179. Barthel D, Schindler S, Zipfel PF. Plasminogen is a complement inhibitor. *J Biol Chem* (2012) 287:18831–42. doi: 10.1074/jbc.M111.323287

180. Rooijakkers SH, van Wamel WJ, Ruyken M, van Kessel KP, van Strijp JA. Anti-opsonic properties of staphylokinase. *Microbes Infect* (2005) 7:476–84. doi: 10.1016/j.micinf.2004.12.014

181. Gasque P. Complement: a unique innate immune sensor for danger signals. *Mol Immunol* (2004) 41:1089–98. doi: 10.1016/j.molimm.2004.06.011

182. Foley JH, Peterson EA, Lei V, Wan LW, Krisinger MJ, Conway EM. Interplay between fibrinolysis and complement: Plasmin cleavage of iC3b modulates immune responses. *J Thromb Haemost* (2015) 13:610–8. doi: 10.1111/jth.12837

183. Bumiller-Bini V, de Freitas Oliveira-Tore C, Carvalho TM, Kretzschmar GC, Goncalves LB, Alencar NM, et al. MASPs at the crossroad between the complement and the coagulation cascades - the case for COVID-19. *Genet Mol Biol* (2021) 44:e20200199. doi: 10.1590/1678-4685-gmb-2020-0199

184. Megyeri M, Jani PK, Kajdacsi E, Dobo J, Schwaner E, Major B, et al. Serum MASP-1 in complex with MBL activates endothelial cells. *Mol Immunol* (2014) 59:39–45. doi: 10.1016/j.molimm.2014.01.001

185. Jani PK, Kajdacsi E, Megyeri M, Dobo J, Doleschall Z, Futosi K, et al. MASP-1 induces a unique cytokine pattern in endothelial cells: A novel link between complement system and neutrophil granulocytes. *PloS One* (2014) 9: e87104. doi: 10.1371/journal.pone.0087104

186. Jenny L, Dobo J, Gal P, Schroeder V. MASP-1 of the complement system promotes clotting *via* prothrombin activation. *Mol Immunol* (2015) 65:398–405. doi: 10.1016/j.molimm.2015.02.014

187. Krarup A, Wallis R, Presanis JS, Gal P, Sim RB. Simultaneous activation of complement and coagulation by MBL-associated serine protease 2. *PloS One* (2007) 2:e623. doi: 10.1371/journal.pone.0000623

188. Pagowska-Klimek I, Cedzynski M. Mannan-binding lectin in cardiovascular disease. *BioMed Res Int* (2014) 2014:616817. doi: 10.1155/2014/616817

189. Ghebrehiwet B, Randazzo BP, Dunn JT, Silverberg M, Kaplan AP. Mechanisms of activation of the classical pathway of complement by hageman factor fragment. *J Clin Invest* (1983) 71:1450–6. doi: 10.1172/JCI110898

190. La Bonte LR, Pavlov VI, Tan YS, Takahashi K, Takahashi M, Banda NK, et al. Mannose-binding lectin-associated serine protease-1 is a significant contributor to coagulation in a murine model of occlusive thrombosis. *J Immunol* (2012) 188:885–91. doi: 10.4049/jimmunol.1102916

191. Liang RA, Hoiland II, T. Ueland P, Snir O, Hindberg K, Braekkan SK, et al. Plasma levels of mannose-binding lectin and future risk of venous thromboembolism. *J Thromb Haemost* (2019) 17:1661–9. doi: 10.1111/jth.14539

192. Flude BM, Nannetti G, Mitchell P, Compton N, Richards C, Heurich M, et al. Targeting the complement serine protease MASP-2 as a therapeutic strategy for coronavirus infections. *Viruses* (2021) 13(2):312. doi: 10.3390/v13020312

193. Gavriilaki E, Peffault de Latour R, Risitano AM. Advancing therapeutic complement inhibition in hematologic diseases: PNH and beyond. *Blood* (2021) 139:3571–82. doi: 10.1182/blood.2021012860

194. Huntington JA. Serpin structure, function and dysfunction. *J Thromb Haemostasis* (2011) 9:26–34. doi: 10.1111/j.1538-7836.2011.04360.x

195. Ellis V, Scully M, MacGregor I, Kakkar V. Inhibition of human factor xa by various plasma protease inhibitors. *Biochim Biophys Acta* (1982) 701:24–31. doi: 10.1016/0167-4838(82)90307-7

196. Osterud B, Miller-Andersson M, Abildgaard U, Prydz H. The effect of antithrombin III on the activity of the coagulation factors VII, IX and X. *Thromb Haemost* (1976) 35:295–304. doi: 10.1055/s-0038-1647922

197. Patnaik MM, Moll S. Inherited antithrombin deficiency: a review. *Haemophilia* (2008) 14:1229–39. doi: 10.1111/j.1365-2516.2008.01830.x

198. Parej K, Dobo J, Zavodszky P, Gal P. The control of the complement lectin pathway activation revisited: both C1-inhibitor and antithrombin are likely physiological inhibitors, while alpha2-macroglobulin is not. *Mol Immunol* (2013) 54:415–22. doi: 10.1016/j.molimm.2013.01.009

199. Zeerleder S. C1-inhibitor: more than a serine protease inhibitor. *Semin Thromb hemostasis* (2011) 37:362–74. doi: 10.1055/s-0031-1276585

200. Kerr FK, Thomas AR, Wijeyewickrema LC, Whisstock JC, Boyd SE, Kaiserman D, et al. Elucidation of the substrate specificity of the MASP-2 protease of the lectin complement pathway and identification of the enzyme as a major physiological target of the serpin, C1-inhibitor. *Mol Immunol* (2008) 45:670–7. doi: 10.1016/j.molimm.2007.07.008

201. Wuillemin WA, Minnema M, Meijers JC, Roem D, Eerenberg AJ, Nuijens JH, et al. Inactivation of factor XIa in human plasma assessed by measuring factor XIa-protease inhibitor complexes: major role for C1-inhibitor. *Blood* (1995) 85:1517–26. doi: 10.1182/blood.V85.6.1517.bloodjournal8561517

202. Levi M, Roem D, Kamp AM, de Boer JP, Hack CE, ten Cate JW. Assessment of the relative contribution of different protease inhibitors to the inhibition of plasmin in vivo. *Thromb haemostasis* (1993) 69:141–6. doi: 10.1055/s-0038-1651570

203. Ziccardi RJ. Activation of the early components of the classical complement pathway under physiologic conditions. *J Immunol* (1981) 126:1769–73.

204. Rossi V, Cseh S, Bally I, Thielens NM, Jensenius JC, Arlaud GJ. Substrate specificities of recombinant mannan-binding lectin-associated serine proteases-1 and -2. *J Biol Chem* (2001) 276:40880–7. doi: 10.1074/jbc.M105934200

205. Pike RN, Wijeyewickrema LC. The molecular switches controlling the interaction between complement proteases of the classical and lectin pathways and their substrates. *Curr Opin Struct Biol* (2013) 23:820–7. doi: 10.1016/j.sbi.2013.07.016

206. Wijeyewickrema LC, Lameignere E, Hor L, Duncan RC, Shiba T, Travers RJ, et al. Polyphosphate is a novel cofactor for regulation of complement by a serpin, C1 inhibitor. *Blood* (2016) 128:1766–76. doi: 10.1182/blood-2016-02-699561

207. Beinrohr L, Murray-Rust TA, Dyksterhuis L, Zavodszky P, Gal P, Pike RN, et al. Serpins and the complement system. *Methods enzymol* (2011) 499:55–75. doi: 10.1016/B978-0-12-386471-0.00004-3

208. Malik RA, Zhou J, Fredenburgh JC, Truong TK, Crosby JR, Revenko AS, et al. Polyphosphate-induced thrombosis in mice is factor XII dependent and is attenuated by histidine-rich glycoprotein. *Blood Adv* (2021) 5:3540–51. doi: 10.1182/bloodadvances.2021004567

209. Conway EM. Polyphosphates and complement activation. *Front Med* (2019) 6:67. doi: 10.3389/fmed.2019.00067

210. Rangaswamy C, Englert H, Deppermann C, Renne T. Polyanions in coagulation and thrombosis: Focus on polyphosphate and neutrophils extracellular traps. *Thromb haemostasis* (2021) 121:1021–30. doi: 10.1055/a-1336-0526

211. Jiang H, Wagner E, Zhang H, Frank MM. Complement 1 inhibitor is a regulator of the alternative complement pathway. *J Exp Med* (2001) 194:1609–16. doi: 10.1084/jem.194.11.1609

212. Levi M, Cohn DM, Zeerleder S. Hereditary angioedema: Linking complement regulation to the coagulation system. *Res Pract Thromb Haemost* (2019) 3:38–43. doi: 10.1002/rth2.12175

213. Sundler Bjorkman L, Persson B, Aronsson D, Skattum L, Nordenfelt P, Egesten A. Comorbidities in hereditary angioedema-a population-based cohort study. *Clin Transl Allergy* (2022) 12:e12135.

214. Mast AE. Tissue factor pathway inhibitor: Multiple anticoagulant activities for a single protein. *Arterioscler Thromb Vasc Biol* (2016) 36:9–14. doi: 10.1161/ATVBAHA.115.305996

215. Maroney SA, Ellery PE, Mast AE. Alternatively spliced isoforms of tissue factor pathway inhibitor. *Thromb Res* (2010) 125 Suppl 1:S52–6. doi: 10.1016/j.thromres.2010.01.038

216. Ellery PE, Adams MJ. Tissue factor pathway inhibitor: then and now. *Semin Thromb hemostasis* (2014) 40:881–6. doi: 10.1055/s-0034-1395153

217. Keizer MP, Pouw RB, Kamp AM, Patiwael S, Marsman G, Hart MH, et al. TFPI inhibits lectin pathway of complement activation by direct interaction with MASP-2. *Eur J Immunol* (2015) 45:544–50. doi: 10.1002/eji.201445070

218. Skjoedt MO, Hummelshoj T, Palarasah Y, Honore C, Koch C, Skjodt K, et al. A novel mannose-binding lectin/ficolin-associated protein is highly expressed in heart and skeletal muscle tissues and inhibits complement activation. *J Biol Chem* (2010) 285:8234–43. doi: 10.1074/jbc.M109.065805

219. Holmquist E, Okroj M, Nodin B, Jirstrom K, Blom AM. Sushi domain-containing protein 4 (SUSD4) inhibits complement by disrupting the formation of the classical C3 convertase. *FASEB J* (2013) 27:2355–66. doi: 10.1096/fj.12-222042

220. Rawal N, Pangburn MK. C5 convertase of the alternative pathway of complement. kinetic analysis of the free and surface-bound forms of the enzyme. *J Biol Chem* (1998) 273:16828–35. doi: 10.1074/jbc.273.27.16828

221. Rawal N, Pangburn MK. Formation of high affinity C5 convertase of the classical pathway of complement. *J Biol Chem* (2003) 278:38476–83. doi: 10.1074/jbc.M307017200

222. Pangburn MK, Muller-Eberhard HJ. The alternative pathway of complement. *Springer Semin immunopathol* (1984) 7:163–92. doi: 10.1007/BF01893019

223. Licht C, Pluthero FG, Li L, Christensen H, Habbig S, Hoppe B, et al. Platelet-associated complement factor h in healthy persons and patients with atypical HUS. *Blood* (2009) 114:4538–45. doi: 10.1182/blood-2009-03-205096

224. Clark SJ, Ridge LA, Herbert AP, Hakobyan S, Mulloy B, Lennon R, et al. Tissue-specific host recognition by complement factor h is mediated by differential activities of its glycosaminoglycan-binding regions. *J Immunol* (2013) 190:2049–57. doi: 10.4049/jimmunol.1201751

225. Kim DD, Song WC. Membrane complement regulatory proteins. *Clin Immunol* (2006) 118:127–36. doi: 10.1016/j.clim.2005.10.014

226. Ekdahl KN, Nilsson B. Phosphorylation of complement component C3 and C3 fragments by a human platelet protein kinase. inhibition of factor I-mediated cleavage of C3b. *J Immunol* (1995) 154:6502–10.

227. Nilsson-Ekdahl K, Nilsson B. Phosphorylation of C3 by a casein kinase released from activated human platelets increases opsonization of immune complexes and binding to complement receptor type 1. *Eur J Immunol* (2001) 31:1047–54. doi: 10.1002/1521-4141(200104)31:4<1047::AID-IMMU1047>3.0.CO;2-Y

228. Puy C, Pang J, Reitsma SE, Lorentz CU, Tucker EI, Gailani D, et al. Cross-talk between the complement pathway and the contact activation system of coagulation: Activated factor XI neutralizes complement factor h. *J Immunol* (2021) 206:1784–92. doi: 10.4049/jimmunol.2000398

229. Chen LJ, Liu DT, Tam PO, Chan WM, Liu K, Chong KK, et al. Association of complement factor h polymorphisms with exudative age-related macular degeneration. *Mol Vision* (2006) 12:1536–42.

230. Thangaraj SS, Christiansen SH, Graversen JH, Sidelmann JJ, Hansen SWK, Bygum A, et al. Contact activation-induced complex formation between complement factor h and coagulation factor XIIa. *J Thromb Haemost* (2020) 18:876–84. doi: 10.1111/jth.14742

231. Ferreira VP, Herbert AP, Cortes C, McKee KA, Blaum BS, Esswein ST, et al. The binding of factor h to a complex of physiological polyanions and C3b on cells is impaired in atypical hemolytic uremic syndrome. *J Immunol* (2009) 182:7009–18. doi: 10.4049/jimmunol.0804031

232. Saunders RE, Abarrategui-Garrido C, Fremeaux-Bacchi V, Goicoechea de Jorge E, Goodship TH, Lopez Trascasa M, et al. The interactive factor h-atypical hemolytic uremic syndrome mutation database and website: update and integration of membrane cofactor protein and factor I mutations with structural models. *Hum Mutat* (2007) 28:222–34. doi: 10.1002/humu.20435

233. Nester CM, Barbour T, de Cordoba SR, Dragon-Durey MA, Fremeaux-Bacchi V, Goodship TH, et al. Atypical aHUS: State of the art. *Mol Immunol* (2015) 67:31–42. doi: 10.1016/j.molimm.2015.03.246

234. Tsai HM. A mechanistic approach to the diagnosis and management of atypical hemolytic uremic syndrome. *Transfusion Med Rev* (2014) 28:187–97. doi: 10.1016/j.tmrv.2014.08.004

235. Mele C, Remuzzi G, Noris M. Hemolytic uremic syndrome. *Semin immunopathol* (2014) 36:399–420. doi: 10.1007/s00281-014-0416-x

236. Bu F, Maga T, Meyer NC, Wang K, Thomas CP, Nester CM, et al. Comprehensive genetic analysis of complement and coagulation genes in atypical hemolytic uremic syndrome. *J Am Soc Nephrol* (2014) 25:55–64. doi: 10.1681/ASN.2013050453

237. Esmon CT, Stenflo J, Suttie JW. A new vitamin K-dependent protein. a phospholipid-binding zymogen of a serine esterase. *J Biol Chem* (1976) 251:3052–6. doi: 10.1016/S0021-9258(17)33498-1

238. Griffin JH, Evatt B, Zimmerman TS, Kleiss AJ, Wideman C. Deficiency of protein c in congenital thrombotic disease. *J Clin Invest* (1981) 68:1370–3. doi: 10.1172/JCI110385

239. Bajzar L, Manuel R, Nesheim M. Purification and characterization of TAFI, a thrombin-activatable fibrinolysis inhibitor. *J Biol Chem* (1995) 270:14477–84. doi: 10.1074/jbc.270.24.14477

240. Bellac CL, Dufour A, Krisinger MJ, Loonchanta A, Starr AE, Auf dem Keller U, et al. Macrophage matrix metalloproteinase-12 dampens inflammation and neutrophil influx in arthritis. *Cell Rep* (2014) 9:618–32. doi: 10.1016/j.celrep.2014.09.006

241. Delvaeye M, Noris M, De Vriese A, Esmon CT, Esmon NL, Ferrell G, et al. Thrombomodulin mutations in atypical hemolytic-uremic syndrome. *New Engl J Med* (2009) 361:345–57. doi: 10.1056/NEJMoa0810739

242. Heurich M, Preston RJ, O'Donnell VB, Morgan BP, Collins PW. Thrombomodulin enhances complement regulation through strong affinity interactions with factor h and C3b-factor h complex. *Thromb Res* (2016) 145:84–92. doi: 10.1016/j.thromres.2016.07.017

243. Tateishi K, Imaoka M, Matsushita M. Dual modulating functions of thrombomodulin in the alternative complement pathway. *Biosci Trends* (2016) 10:231–4. doi: 10.5582/bst.2016.01052

244. Loghmani H, Conway EM. Exploring traditional and non-traditional roles for thrombomodulin. *Blood* (2018) 132:148–58. doi: 10.1182/blood-2017-12-768994

245. Zheng XL, Sadler JE. Pathogenesis of thrombotic microangiopathies. *Annu Rev Pathol* (2008) 3:249–77. doi: 10.1146/annurev.pathmechdis.3.121806.154311

246. Turner NA, Moake J. Assembly and activation of alternative complement components on endothelial cell-anchored ultra-large von willebrand factor links complement and hemostasis-thrombosis. *PloS One* (2013) 8:e59372. doi: 10.1371/journal.pone.0059372

247. Feng S, Liang X, Cruz MA, Vu H, Zhou Z, Pemmaraju N, et al. The interaction between factor h and Von willebrand factor. *PloS One* (2013) 8:e73715. doi: 10.1371/journal.pone.0073715

248. Rayes J, Roumenina LT, Dimitrov JD, Repesse Y, Ing M, Christophe O, et al. The interaction between factor h and VWF increases factor h cofactor activity and regulates VWF prothrombotic status. *Blood* (2014) 123:121–5. doi: 10.1182/blood-2013-04-495853

249. Nolasco L, Nolasco J, Feng S, Afshar-Kharghan V, Moake J. Human complement factor h is a reductase for large soluble von willebrand factor multimers–brief report. *Arteriosclerosis thrombosis Vasc Biol* (2013) 33:2524–8. doi: 10.1161/ATVBAHA.113.302280

250. Turner N, Nolasco L, Nolasco J, Sartain S, Moake J. Thrombotic microangiopathies and the linkage between von willebrand factor and the alternative complement pathway. *Semin Thromb hemostasis* (2014) 40:544–50. doi: 10.1055/s-0034-1383547

251. Feng S, Liang X, Kroll MH, Chung DW, Afshar-Kharghan V. Von willebrand factor is a cofactor in complement regulation. *Blood* (2015) 125:1034–7. doi: 10.1182/blood-2014-06-585430

252. Schmidt CQ, Schrezenmeier H, Kavanagh D. Complement and the prothrombotic state. *Blood* (2021) 139:1954–72. doi: 10.1182/blood.2020007206

253. Chamardani TM, Amiritavassoli S. Inhibition of NETosis for treatment purposes: friend or foe? *Mol Cell Biochem* (2022) 477:673–88. doi: 10.1007/s11010-021-04315-x

frontiers | Frontiers in Immunology

TYPE Original Research
PUBLISHED 16 August 2022
DOI 10.3389/fimmu.2022.907023

OPEN ACCESS

EDITED BY
József Dobó,
Hungarian Academy of Sciences (MTA), Hungary

REVIEWED BY
Soren Werner Karlskov Hansen,
University of Southern Denmark, Denmark
Anne Rosbjerg,
University of Copenhagen, Denmark

*CORRESPONDENCE
Takeshi Machida
be204093@fmu.ac.jp

†These authors have contributed equally to this work and share first authorship

SPECIALTY SECTION
This article was submitted to Molecular Innate Immunity, a section of the journal Frontiers in Immunology

RECEIVED 29 March 2022
ACCEPTED 27 July 2022
PUBLISHED 16 August 2022

CITATION
Kusakari K, Machida T, Ishida Y, Omori T, Suzuki T, Sekimata M, Wada I, Fujita T and Sekine H (2022) The complex formation of MASP-3 with pattern recognition molecules of the lectin complement pathway retains MASP-3 in the circulation. *Front. Immunol.* 13:907023. doi: 10.3389/fimmu.2022.907023

The complex formation of MASP-3 with pattern recognition molecules of the lectin complement pathway retains MASP-3 in the circulation

Kohei Kusakari[1†], Takeshi Machida[1*†], Yumi Ishida[1], Tomoko Omori[1], Toshiyuki Suzuki[2], Masayuki Sekimata[2], Ikuo Wada[3], Teizo Fujita[4] and Hideharu Sekine[1]

[1]Department of Immunology, Fukushima Medical University, Fukushima, Japan, [2]Radioisotope Research Center, Fukushima Medical University, Fukushima, Japan, [3]Department of Cell Science, Institute of Biomedical Sciences, Fukushima Medical University, Fukushima, Japan, [4]Fukushima Prefectural General Hygiene Institute, Fukushima, Japan

The complement system plays an important role in host defense and is activated *via* three different activation pathways. We have previously reported that mannose-binding lectin-associated serine protease (MASP)-3, unlike its splicing variant MASP-1, circulates in an active form and is essential for the activation of the alternative pathway (AP) *via* the activation of complement factor D (FD). On the other hand, like MASP-1 and MASP-2 of the lectin pathway (LP), MASP-3 forms a complex with the pattern recognition molecules (PRMs) of the LP (LP-PRMs). Both MASP-1 and MASP-2 can be activated efficiently when the LP-PRMs complexed with them bind to their ligands. On the other hand, it remains unclear how MASP-3 is activated, or whether complex formation of MASP-3 with LP-PRMs is involved in activation of MASP-3 or its efficiency in the circulation. To address these issues, we generated wild-type (WT) and four mutant recombinant mouse MASP-3 proteins fused with PA (human podoplanin dodecapeptide)-tag (rmMASP-3-PAs), the latter of which have single amino acid substitution for alanine in the CUB1 or CUB2 domain responsible for binding to LP-PRMs. The mutant rmMASP-3-PAs showed significantly reduced *in-vivo* complex formation with LP-PRMs when compared with WT rmMASP-3-PA. In the *in-vivo* kinetic analysis of MASP-3 activation, both WT and mutant rmMASP-3-PAs were cleaved into the active forms as early as 30 minutes in the circulation of mice, and no significant difference in the efficiency of MASP-3 cleavage was observed throughout an observation period of 48 hours after intravenous administration. All sera collected 3 hours after administration of each rmMASP-3-PA showed full restoration of the active FD and AP activity in MASP-3-deficient mouse sera at the same levels as WT mouse sera. Unexpectedly, all mutant rmMASP-3-PAs showed faster clearance from the circulation than the WT rmMASP-3-PA.

10.3389/fimmu.2022.907023

To our knowledge, the current study is the first to show *in-vivo* kinetics of MASP-3 demonstrating rapid activation and clearance in the circulation. In conclusion, our results demonstrated that the complex formation of MASP-3 with LP-PRMs is not required for *in-vivo* activation of MASP-3 or its efficiency, but may contribute to the long-term retention of MASP-3 in the circulation.

KEYWORDS

complement, MASP-3, alternative pathway, lectin pathway, pattern recognition molecules

Introduction

The complement system plays essential roles in the innate immunity (1). It is activated *via* three different activation pathways; the classical pathway (CP), lectin pathway (LP), and alternative pathway (AP) (2). Activations of the CP and LP are initiated by the bindings of pattern recognition molecules (PRMs) to their ligands, i.e., binding of C1q to antigen-antibody complexes in the CP activation and binding of mannose-binding lectin (MBL), ficolins, collectin liver 1 (CL-L1 or CL-10), collectin kidney 1 (CL-K1 or CL-11) or their heterocomplex CL-LK to carbohydrates in the LP activation. Those PRMs circulate in a complex with serine proteases, C1r and C1s in the CP, and MBL-associated serine protease (MASP)-1 and MASP-2 in the LP. At the site of PRM-binding, the primary serine proteases, C1r (3) or MASP-1 (4), complexed therewith autoactivated and in turn activate the secondary serine proteases, C1s or MASP-2 (5). Afterwards, those activated secondary serine proteases cleave complement components C4 and C2 to generate a CP/LP C3 convertase, C4b2a. Eventually, C4b2a cleaves C3 into C3a and C3b; the former serves as an anaphylatoxin, and the latter may covalently bind to proteins or carbohydrates on microbial surfaces or host tissues.

On the other hand, the AP has no PRMs, and its activation is initiated by the low-level spontaneous hydrolysis of C3 on the bacterial surfaces to generate C3(H_2O) (6). Once C3(H_2O) is generated, complement factor B (FB) binds to C3(H_2O), and is cleaved into Ba and Bb fragments by an active form of complement factor D (FD), which is already activated by MASP-3, to generate an initial AP C3 convertase, C3(H_2O)Bb, which cleaves C3 to generate C3b that is bound covalently to pathogens. In turn, FB forms a complex with C3b and is cleaved by active FD, leading to the formation of the AP C3 convertase, C3bBb. In this way, the AP enhances complement activation at the C3b-binding site *via* the amplification loop. Unlike C1r, C1s, MASP-1, and MASP-2 in the CP and LP, the serine proteases MASP-3 and FD circulate in the active forms both in humans and mice (7–9); however, the activation mechanism of MASP-3 remains unclear.

MASP-3 is a splicing variant of MASP-1, and both are transcribed from the *MASP1* gene (10). They have a common heavy chain (H-chain) consisting of five domains, in the following order: an N-terminal C1r/C1s/Uegf/bone morphogenetic protein (CUB1) domain; an epidermal growth factor (EGF)-like domain; a secondary CUB (CUB2) domain; a primary complement control protein (CCP1) domain; and a secondary CCP (CCP2) domain. Since the CUB1-EGF-CUB2 motif is responsible for complex formation with the LP-PRMs, such as MBL, ficolins, CL-L1, CL-K1 and CL-LK, both MASP-1 and MASP-3 can form a complex with LP-PRMs. Some evidence that MASP-3 forms a complex with LP-PRMs has been reported. MASP-3 was first isolated as a complex with MBL from human plasma (10). Skjoedt et al. (11) reported that the mean concentration of MASP-3 was 6.4 mg/L in human serum, and a large portion of MASP-3 circulated in a complex with ficolin-3 rather than MBL or ficolin-2. Teillet et al. (12) have reported that, using surface plasmon resonance analysis, recombinant human MASP-3 with a single amino acid substitution at the CUB1 or CUB2 domain including E49, D102, H218, and Y225 for alanine shows significantly reduced ability to associate with LP-PRMs such as human MBL, L-ficolin (ficolin-2), and H-ficolin (ficolin-3). Afterwards, Henriksen et al. (13) reported that CL-LK formed a complex with MASPs including MASP-3 and could mediate LP activation. When MASP-3 was first discovered, its role in the complex with LP-PRM was thought to be a down-regulator of LP activation by displacement and/or competition with MASP-2 (10). However, our recent studies have shown that MASP-3-deficient mouse sera have comparable LP activity to WT mouse sera (9). Therefore, our results suggest that MASP-3 in complex with LP-PRMs is not involved in the activation/regulation of the LP *in vivo*.

In contrast to the H-chains common to MASP-1 and MASP-3, their light chains (L-chains) consisting of a serine protease domain are transcribed from different exons of the *MASP1* gene, and their structure and functions are different (14–17). Indeed, we have recently reported that MASP-1 and MASP-3 play independent roles in physiological activations of the LP and AP, respectively (9). MASP-1 and MASP-2 of the LP circulate in

proenzyme forms as do C1r and C1s of the CP. When these serine proteases are activated, C1 inhibitor (serpin G1) acts as their pseudosubstrate and irreversibly inhibits their activity (18, 19). On the other hand, MASP-3, which circulates mostly in an active form, has no known physiological inhibitors, and its activation or clearance kinetics *in vivo* are largely unknown.

MASP-3 has been shown to play an important role not only in complement activation *via* activation of FD, but also in embryonic development. Loss-of-function of MASP-3 due to congenital mutations in MASP-3-specific exon of the *MASP1* gene results in human 3MC syndrome characterized by a spectrum of developmental features, including developmental delay, growth retardation, intellectual disability, and characteristic facial atypia (20). Of interest, congenital mutations in the CL-L1 or CL-K1 genes also cause 3MC syndrome (21, 22). In case of mice, we have previously reported significantly reduced body weight in the MASP-3-deficient mice compared with the WT littermates (9). Taken together, it can be inferred that MASP-3 plays an important role in embryonic development by forming a complex with CL-L1, CL-K1 or CL-LK. However, the role or functional benefits of MASP-3 forming a complex with LP-PRMs in complement activation are largely unclear.

In the current study, we hypothesized that complex formation of MASP-3 with LP-PRMs is involved in the activation of MASP-3 in the circulation, similarly to the activation of MASP-1. To clarify this hypothesis, we generated a recombinant wild-type and four mutant mouse MASP-3 proteins with E49A, D102A, H218A or Y225A mutation in the CUB1 or CUB2 domain; these mutations significantly decreased the ability of human MASP-3 to associate with MBL, L-ficolin, and H-ficolin (12). These recombinant mouse MASP-3 proteins were administered to wild-type and MASP-3-deficient mice, and their activation and clearance kinetics in the circulation were analyzed.

Materials and methods

Mice

Wild-type C57BL/6J mice (C57BL/6JJcl) were purchased from CLEA Japan, Inc. (Tokyo, Japan). MASP-3-deficient C57BL/6J mice were generated by genome editing using CRISPR/Cas9 system in our previous study (9) and bred in-house for use in the current study. The WT or MASP-3-deficient C57BL/6J mice used were aged 8–14 weeks. All animal experiments, including housing, breeding, and use of the mice, were reviewed and approved by the Animal Experiments Committee of Fukushima Medical University (approval no. 2021012) and performed in accordance with the guidelines for the care and use of laboratory animals established by the committee.

Plasmid construction

A recombinant WT mouse MASP-3 protein was generated as a fusion protein with a PA-tag, a dodecapeptide derived from human podoplanin (23), at the C-terminus, termed WT rmMASP-3-PA. A full-length coding sequence of mouse MASP-3 was amplified by PCR using primers designed based on the full-length cDNA sequence of mouse MASP-3 (GenBank accession no. AB049755). The amplified cDNA fragment was introduced into a pCAG-Bsd PA tag-C vector (Wako, Osaka, Japan) using the In-Fusion® HD Cloning Kit (Takara Bio, Kyoto, Japan) according to the manufacturer's instructions, and the construct was transformed into *Escherichia coli* DH5α to amplify the plasmid.

Four different mutant rmMASP-3s, which have single amino acid substitution for alanine at E49 (E49A), D102 (D102A), H218 (H218A) or Y225 (Y225A), as depicted in Figure 1, were generated using the pCAG-Bsd PA tag-C/WT rmMASP-3 plasmid and a PrimeSTAR Mutagenesis Basal Kit (Takara Bio) according to the manufacturer's instructions. The primers used for amplification of mutant rmMASP-3 cDNAs were: 5'- aacttgGCCtcctcctatcttt gtgaa -3' and 5'- ggaggaGGCcaagttgaagtgcatga -3' for the E49A mutant; 5'- cggtcaGCTttctccaatgaggaacg -3' and 5'- ggagaaAGC tgaccggaaagtgacag -3' for the D102A mutant; 5'- tgaagacGCTcctgag gtgccctgtcc -3' and 5'- tcaggAGCgtcttcaatgtcaaaaat -3' for the H218A mutant; and 5'- ctgtcccGCTgactacattaagattaa -3' and 5'- tagtcAGCgggacagggcacctcagg -3' for the Y225A mutant. The codon for the substituted amino acid was in capital letters. The mutant DNA products were introduced into the pCAG-Bsd PA tag-C vector and then transformed into *E. coli*, as in the case of WT rmMASP-3.

Another set of WT rmMASP-3 protein was generated as an ALFA-tagged protein (24) in its C-terminus, termed WT rmMASP-3-ALFA. A full-length coding sequence of mouse MASP-3 was amplified by PCR using primers containing nucleotides corresponding to ALFA tag and an additional proline residue between them, which acts as an insulator (-PSRLEEELRRRLTE). The amplified cDNA fragment was introduced into a pCAG-Bsd PA tag-C vector and transformed into *E. coli*. Introduction of the objective cDNA fragment was confirmed by DNA sequencing.

Protein expression and purification

Plasmids for expression of WT or mutant rmMASP-3-PAs and WT rmMASP-3-ALFA were transfected into Chinese hamster ovary (CHO) cells with the FuGene-HD transfection reagent (Roche, Indianapolis, IN, USA) according to the manufacturer's instructions. After transfection, cells that were resistant to blastcidin S (Wako) were transferred to EX-CELL® 325 PF CHO serum-free medium (Sigma-Aldrich, St Louis, MO, USA) for efficient expression of introduced genes. Culture

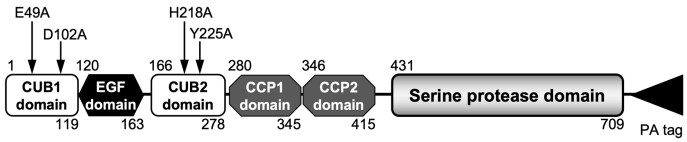

FIGURE 1
A schematic domain structure of rmMASP-3-PA. The numbers at the top and bottom represent the first and last amino acid numbers in each domain, respectively according to the information in the UniProt database (UniProt ID: P98064). The arrows indicate the four different positions of the single amino acid substitutions for alanine used in the current study.

supernatant containing expressed protein was collected and subjected to purification using anti-PA tag antibody beads (Wako) for PA-tagged proteins or ALFA Selector ST (NanoTag Biotechnologies, Göttingen, Germany) for ALFA-tagged proteins. The rmMASP-3-PAs or rmMASP-3-ALFA bound to the beads were eluted with glycine-HCl buffer (pH 2.5) followed by addition of 1/10 volume of 1 M Tris-HCl (pH 9.0) for neutralization. Expression and purification of target proteins were checked by SDS-PAGE under reducing condition followed by staining with InstantBlue staining solution (Expedeon, Heidelberg, Germany) or by Western blotting using horseradish peroxidase (HRP)-conjugated anti-mouse MASP-3 L-chain antibody (9). After the blotted membrane was treated with ECL Prime Western Blotting Detection System (GE Healthcare, Buckinghamshire, UK), objective protein bands were visualized by chemiluminescence detection using an Amersham Imager 600 (GE Healthcare). To confirm the mutation of the proteins, the purified samples were subjected to mass spectrometry according to the method reported by Takahashi et al. (16).

Assay for *in-vivo* complex formation of rmMASP-3-PA with LP-PRMs

One-hundred micrograms of each of the rmMASP-3-PAs dissolved in PBS were administered to the tail vein of the MASP-3-deficient C57BL/6J mice. The mice were bled 3 h after administration. Serum LP-PRMs that formed complexes with the administered rmMASP-3-PA were isolated by immunoprecipitation using anti-PA tag antibody beads. Briefly, 100 µL of serum samples were mixed with 50 µL of anti-PA antibody beads in a total of 200 µL with TBS supplemented with 7 mM $MgCl_2$ and 5 mM $CaCl_2$ (TBS/Mg/Ca), and then the mixture was incubated at 4°C overnight with inverted mixing. After centrifugation, the precipitated beads were washed four times with TBS/Mg/Ca and then resuspended in SDS-PAGE sample buffer with 2-mercaptoethanol in a volume equivalent to serum followed by incubation at 80°C for 10 min. Sera of mice administered with WT rmMASP-3-PA was separately subjected to immunoprecipitation using TBS supplemented with 7 mM $MgCl_2$ and 10 mM EGTA (TBS/Mg/EGTA) as a negative control in which the rmMASP-3-PA/LP-PRM complex is dissociated.

The eluates were subjected to SDS-PAGE under reducing condition followed by Western blotting. The blotted membranes were separately subjected to immunodetection using following primary antibodies; HRP-conjugated rat anti-mouse MBL-A monoclonal antibody (clone: 8G6, Hycult Biotech, Plymouth Meeting, PA, USA), HRP-conjugated rat anti-mouse MBL-C monoclonal antibody (clone: 16A8, Hycult Biotech), rabbit anti-ficolin-A polyclonal antibody (25), and rabbit anti-CL-K1 polyclonal antibody (Proteintech, Rosemont, IL, USA), followed by reaction with a HRP-conjugated secondary antibody for rabbit first antibodies. After the membranes were treated with ECL Prime Western Blotting Detection System, objective protein bands were visualized by chemiluminescence detection using the Amersham Imager 600. The band intensity detected was measured using an ImageQuant TL software (GE healthcare). For membrane stripping, the membranes were washed twice with PBS containing 0.5% Tween-20 (PBST) for 5 min and then incubated in Stripping solution (Wako) for 10 min at room temperature with shaking. After washing three times with PBST, the membranes were used for another detection. Immunodetection was also performed using HRP-conjugated anti-PA tag antibody to normalize the loading amount of rmMASP-3-PA between samples.

In-vivo activation of rmMASP-3-PA

One-hundred micrograms of each of the rmMASP-3-PAs dissolved in PBS were administered to the tail vein of the WT or MASP-3-deficient C57BL/6J mice. The mice were bled before rmMASP-3-PA administration and at 0.5, 1.5, 3, 6, 12, 24, 48 h after administration. The serum samples were collected and subjected to SDS-PAGE under reducing condition followed by Western blotting using the HRP-conjugated anti-PA tag antibody and ECL Prime Western Blotting Detection System. After photographed by the chemiluminescence mode using an

Amersham Imager 600, the band intensity detected was measured using an ImageQuant TL software.

Western blotting of FD

Mouse FD in the serum samples of MASP-3-deficient C57BL/6J mice obtained 3 h after administration of rmMASP-3-PA was immunoprecipitated with rabbit anti-mouse FD antibody, deglycosylated, and subjected to Western blotting according to the method described previously (16). Notably, mouse serum FD is detected as a smeared band by Western blotting due to various glycosylation patterns when it is not deglycosylated (data not shown). The difference in molecular mass between mouse pro-FD (26.1 kDa) and active FD (25.5 kDa) is only 0.6 kDa. In order to detect the difference by Western blotting, the immunoprecipitated serum FD was deglycosylated with N-glycosidase F (Merck, Darmstadt, Germany) and then analyzed by Western blotting.

C3 deposition assay on zymosan

The AP activity of serum samples from the MASP-3-deficient C57BL/6J mice obtained 3 h after administration of rmMASP-3-PA was measured using 10% sera diluted with TBS/Mg/EGTA and zymosan-coated microplates according to the method described previously (16). C3 deposition level on zymosan was detected with HRP-conjugated anti-PA tag antibody followed by color development with TMB substrate solution (Kirkegaard & Perry Laboratories, Gaithersburg, MD, USA). The absorbance at 450 nm was measured by a Varioskan LUX multimode microplate reader (Thermo Fisher Scientific).

Homodimer formation of MASP-3

Homodimer formation of rmMASP-3 was examined using WT/mutant rmMASP-3-PAs and WT rmMASP-3-ALFA based on the method described by Rosbjerg et al. (26). An equivalent amount (10 μg) of each rmMASP-3-PA and rmMASP-3-ALFA was mixed and dialyzed against TBS containing 10 mM EDTA (TBS/EDTA) for 24 h at 4°C. An aliquot of the dialyzed sample (4 μg of each rmMASP-3) was further dialyzed against TBS containing 5 mM $CaCl_2$ (TBS/Ca) for 24 h at 4°C and then adjusted with 20% Blocking One in TBS/Ca to 700 μL (0.14 μM of each rmMASP-3). Another aliquot was placed on ice for 24 h and then adjusted with 20% Blocking One in TBS/EDTA to 700 μL (0.14 μM of each rmMASP-3). Those samples were serially diluted with 20% Blocking One in TBS/Ca or TBS/EDTA as compatible to the buffer composition in which they dissolved, and then added to the microplate preliminarily coated with anti-PA tag antibody followed by 30-min incubation at room temperature. After washing the wells three times with PBST, rmMASP-3-ALFA that formed a homodimer with WT or mutant rmMASP-3-PAs was detected with HRP-conjugated anti-ALFA nanobody (NanoTag Biotechnologies) followed by color development with TMB substrate solution. The absorbance at 450 nm was measured using a Varioskan LUX multimode microplate reader.

Statistical analysis

Statistical analysis was performed using a GraphPad Prism 8 software for Mac OS X (GraphPad Software, San Diego, CA, USA). Multiple groups were compared using a one-way ANOVA with *post-hoc* Tukey's multiple comparison test.

Results

Generation of WT and mutant rmMASP-3-PAs

To investigate our hypothesis that forming a complex with LP-PRMs is involved in the activation of MASP-3, we generated WT and mutant rmMASP-3 proteins (Figure 1). In the present study, the WT mouse MASP-3 cDNA and four different types of mutant mouse MASP-3 cDNAs were prepared by PCR and the site-directed mutagenesis, and then introduced into the pCAG-Bsd PA tag-C vector, to be expressed as PA-tagged proteins in their C-termini. The WT and mutant rmMASP-3-PA proteins were expressed in CHO cells and purified by an affinity chromatography using anti-PA tag antibody beads. Expression and purification of the proteins were confirmed by SDS-PAGE followed by InstantBlue staining and Western blotting. As shown in Figure 2A, the InstantBlue staining showed expression and purification of approximately 110-kDa proteins for all rmMASP-3-PAs. The Western blot analysis revealed that the 110-kDa bands in the lanes for all rmMASP-3-PA samples were detected with anti-mouse MASP-3 L-chain antibody (Figure 2B). Furthermore, the objective amino acid replacements in four mutant rmMASP-3-PAs were confirmed by mass spectrometry analysis (Figure 2C). Taking all of these results together, it was confirmed that the WT and mutant rmMASP-3-PAs were generated as we had designed.

In-vivo complex formation of WT and mutant rmMASP-3-PAs with serum LP-PRMs

Teillet et al. (12) have reported that recombinant human MASP-3 with a single amino acid substitution at the positions including E49, D102, H218, and Y225 for alanine shows significantly reduced ability to associate with human ficolin-2,

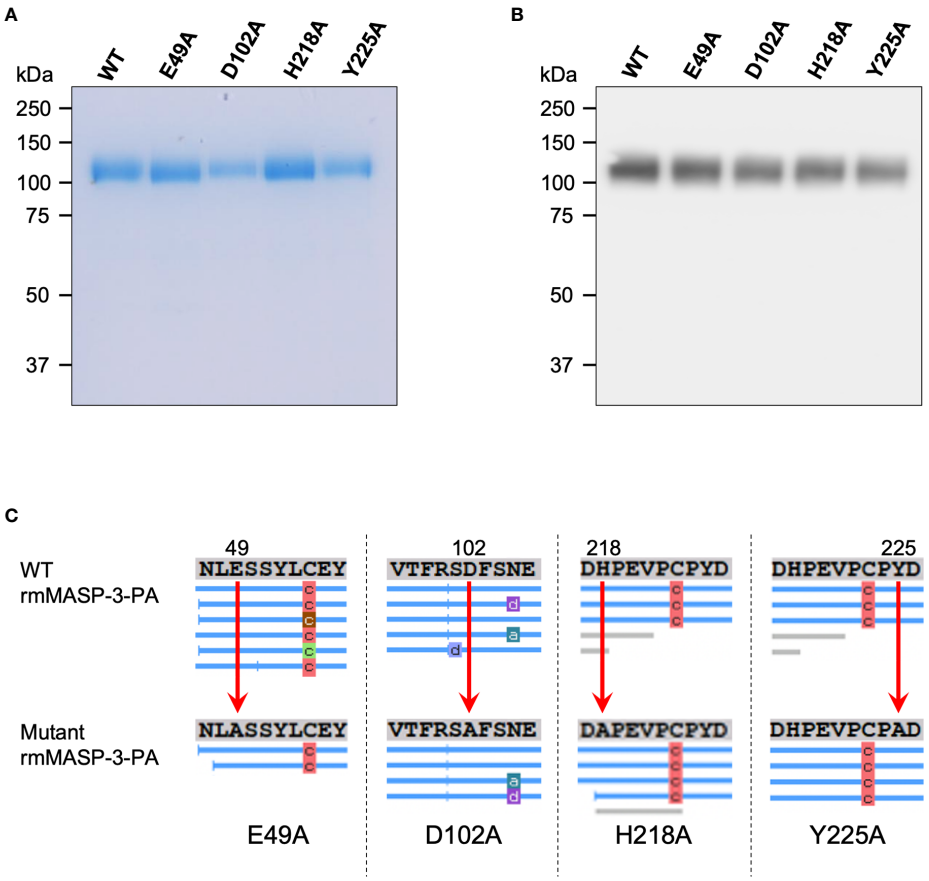

FIGURE 2
Expression and purification of WT and mutant rmMASP-3-PAs were confirmed by SDS-PAGE under reducing condition followed by InstantBlue staining **(A)** and Western blotting using anti-mouse MASP-3 L-chain antibody **(B)**. **(C)** The results on mass spectrometric analyses revealed the substitutions of target amino acids in rmMASP-3-PA (E49, D102, H218 or Y225) for alanine, as indicated by the red arrows. The blue lines below the amino acid sequences show the fragments detected by the mass spectrometry. The characters on the blue line represent as follows: "a" means ammonia-loss, "c" means carbamylation, and "d" means deamidation of the corresponding peptides in the peptide fragment, which are due to protease treatment prior to analysis with mass spectrometry.

ficolin-3 and MBL. To confirm whether mutant rmMASP-3-PAs with single amino acid mutations, E49A, D102A, H218A or Y225A, show reduced ability to form a complex with mouse LP-PRMs *in vivo*, we isolated rmMASP-3-PA/LP-PRM complexes from MASP-3-deficient mouse sera obtained 3 h after administration of each rmMASP-3-PA by immunoprecipitation experiment using anti-PA tag antibody beads. The isolated fractions were subjected to reducing SDS-PAGE followed by Western blotting using antibodies against each mouse LP-PRM.

First, we analyzed rmMASP-3-PA levels in each immunoprecipitated fraction by Western blotting using anti-PA tag antibody. As shown in Figure 3A, the detection levels of WT or mutant rmMASP-3-PAs were different between the immunoprecipitated fractions. The band intensities of proenzyme and L-chain of activated rmMASP-3-PA were measured using an imaging software, and their sum was used to normalize total rmMASP-3-PA levels between the samples.

Next, we analyzed MBL-A (Figure 3B), MBL-C (Figure 3C), ficolin-A (Figure 3D), and CL-K1 (Figure 3E) levels in each immunoprecipitated fraction by Western blotting using antibodies specific for each LP-PRM. As shown in Figures 3B–E, Western blot analysis showed apparent detection levels of each LP-PRM in the immunoprecipitated fraction obtained from sera administered with WT rmMASP-3-PA (lane 2); the detection levels of that were significantly reduced in the immunoprecipitated fraction obtained in the presence of EGTA (lane 7). In contrast, Western blot analysis showed significantly reduced detection levels of each LP-PRM in the immunoprecipitated fraction obtained from sera administered with each mutant rmMASP-3-PA (lane 3–6) compared with that administered with WT rmMASP-3-PA (lane 2).

Detection of CL-L1 or CL-LK was not performed in the current study, since there was no commercially available antibody capable of detecting mouse CL-L1 by Western

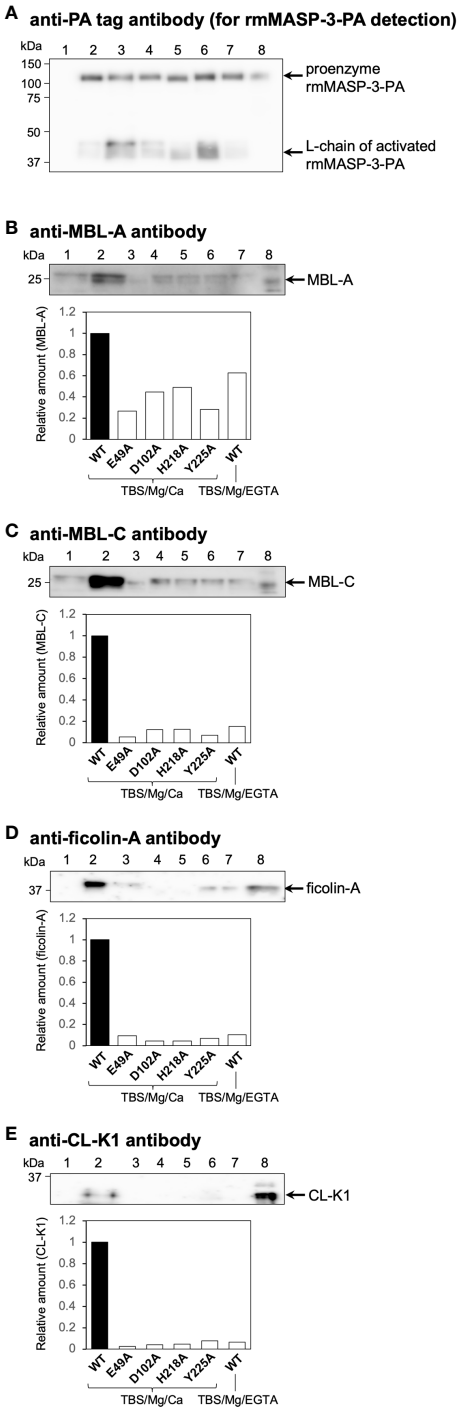

	Administered rmMASP-3-PA	IP in TBS/Mg/Ca	IP in TBS/Mg/EGTA
Lane 1	none	+	-
Lane 2	WT	+	-
Lane 3	E49A	+	-
Lane 4	D102A	+	-
Lane 5	H218A	+	-
Lane 6	Y225A	+	-
Lane 7	WT	-	+
Lane 8	WT rmMASP-3-PA directly (positive control)		

	Administered rmMASP-3-PA	IP in TBS/Mg/Ca	IP in TBS/Mg/EGTA
Lane 1	none	+	-
Lane 2	WT	+	-
Lane 3	E49A	+	-
Lane 4	D102A	+	-
Lane 5	H218A	+	-
Lane 6	Y225A	+	-
Lane 7	WT	-	+
Lane 8	WT mouse serum (positive control)		

	Administered rmMASP-3-PA	IP in TBS/Mg/Ca	IP in TBS/Mg/EGTA
Lane 1	none	+	-
Lane 2	WT	+	-
Lane 3	E49A	+	-
Lane 4	D102A	+	-
Lane 5	H218A	+	-
Lane 6	Y225A	+	-
Lane 7	WT	-	+
Lane 8	WT mouse serum (positive control)		

	Administered rmMASP-3-PA	IP in TBS/Mg/Ca	IP in TBS/Mg/EGTA
Lane 1	none	+	-
Lane 2	WT	+	-
Lane 3	E49A	+	-
Lane 4	D102A	+	-
Lane 5	H218A	+	-
Lane 6	Y225A	+	-
Lane 7	WT	-	+
Lane 8	Mouse ficolin-A (positive control)		

	Administered rmMASP-3-PA	IP in TBS/Mg/Ca	IP in TBS/Mg/EGTA
Lane 1	none	+	-
Lane 2	WT	+	-
Lane 3	E49A	+	-
Lane 4	D102A	+	-
Lane 5	H218A	+	-
Lane 6	Y225A	+	-
Lane 7	WT	-	+
Lane 8	WT mouse serum (positive control)		

FIGURE 3
In-vivo complex formation of rmMASP-3-PA with endogenous MBL-A, MBL-C, ficolin-A or CL-K1. Immunoprecipitation (IP) experiments were performed using anti-PA tag antibody beads in TBS containing 7 mM $MgCl_2$ and 5 mM $CaCl_2$ (TBS/Mg/Ca) or 10 mM EGTA (TBS/Mg/EGTA). Each band intensity of MBL-A **(B)**, MBL-C **(C)**, ficolin-A **(D)**, and CL-K1 **(E)** was calibrated with the intensity of rmMASP-3-PA **(A)** obtained from the same IP sample to normalize the loading amount of rmMASP-3-PA between the samples. Relative amounts were expressed as the ratio of each calibrated intensity against that obtained from the mouse serum administered with WT rmMASP-3-PA (lower panels in **B–E**; WT = 1).

blotting. These results indicate that mutant rmMASP-3-PAs generated in the current study have little-to-no ability to form a complex with LP-PRMs, although it remains unclear whether they could form a complex with CL-L1 or CL-LK.

In-vivo activation and clearance kinetics of WT and mutant rmMASP-3-PAs in the circulation of mice

MASP-1 forms a complex with LP-PRMs in the circulation, which can bind to carbohydrates on microbial surfaces or damaged host tissues and trigger autoactivation of MASP-1. Next, we investigated whether the complex formation of MASP-3 with LP-PRMs is involved in the activation of MASP-3 in the circulation of MASP-3-deficient mice. Each 100 μg of rmMASP-3-PA was administered intravenously to MASP-3-deficient mice. Serum samples were then collected from the mice at 0.5, 1.5, 3, 6, 12, 24 and 48 h after administration, and analyzed by Western blotting using anti-PA tag antibody. As shown in Figure 4A, L-chains of cleaved MASP-3 (i.e., activated MASP-3) were detected in all sera collected 0.5 h after administration, suggesting that proenzyme MASP-3 is converted to the active form very rapidly in the circulation. In addition, the *in-vivo* kinetics analysis showed no significant difference in the efficiency of MASP-3 activation between WT and all mutant rmMASP-3-PAs. These results indicate that the complex formation of MASP-3 with LP-PRMs was not involved in MASP-3 activation in the circulation.

Unexpectedly, we observed different *in-vivo* clearance kinetics between the WT and mutant rmMASP-3-PAs. As shown in Figures 4B, C, the proenzyme WT rmMASP-3-PA was detected even 24 h after administration, whereas the proenzyme mutant rmMASP-3-PAs were no longer detected at 12 h after administration. The half-life of each rmMASP-3-PA in the circulation from 0.5 h after administration was calculated for each mouse. The half-life values (mean ± SD, $n = 3$) were 9.6 ± 4.9 h for WT, 1.2 ± 0.2 h for E49A, 3.2 ± 1.2 h for D102A, 1.3 ± 0.3 h for H218A, and 1.5 ± 0.3 h for Y225A. Thus, WT rmMASP-3-PA had a longer half-life than all mutant rmMASP-3-PAs.

These results suggest that complex formation of MASP-3 with LP-PRMs does not contribute to the activation of MASP-3, but does contribute to the long-term retention of MASP-3 in the circulation.

Restoration of the active FD and AP activity in MASP-3-deficient mice by administration of rmMASP-3-PAs

We previously reported that sera from MASP-3-deficent mice had no or significantly reduced AP activity due to the lack of active FD in the circulation (9). We investigated whether the active FD and AP activity in MASP-3-deficient mouse could be restored by intravenous administration of rmMASP-3-PAs. First, sera collected 3 h after administration of WT or mutant rmMASP-3-PA were applied to Western blotting of FD to analyze the activation status of FD. As shown in Figure 5A, FD was detected as a 26.1 kDa protein in the sera of MASP-3-deficient mice collected prior to administration of rmMASP-3-PAs. On the other hand, FD was detected as a 25.5 kDa protein in the sera of MASP-3-deficient mice administered with each rmMASP-3-PA. These results indicate that most of the circulating proenzyme form of FD in the MASP-3-deficient mice was converted to the active form 3 h after administration of WT and mutant rmMASP-3-PAs.

Next, the sera collected above were subjected to C3 deposition assay on a zymosan-coated microplate to assess the AP activity. As shown in Figure 5B, sera from MASP-3-deficient mice administered with WT or mutant rmMASP-3-PAs showed a significant increase in C3 deposition levels compared to that prior to administration. There was no significant difference in C3 deposition levels between the sera from WT mice and those from MASP-3-deficient mice administered with each rmMASP-3-PA. These results indicate that the serum AP activity of MASP-3-deficient mice was restored to the same level as that of WT mice 3 h after administration of WT and mutant rmMASP-3-PAs.

Taken together, these results suggest that WT and the four mutant rmMASP-3-PAs can equally restore active FD and AP activity in the circulation when administered to MASP-3-deficient mice.

In-vitro dimer formation of WT and mutant rmMASP-3-PAs

MAp44 and sMAP are splicing variants of MASP-1/-3 and MASP-2 transcribed from the *MASP1* and *MASP2* genes, respectively. Both MAp44 and sMAP lack the serine protease domain (L-chain) but have CUB1-EGF-CUB2 domains. Therefore, these proteins, including MASP-1 and MASP-2, are thought to form homodimers or heterodimers with each other *via* the CUB1-EGF-CUB2 domains in their H-chains (26–28). Although dimer formation of MASP-3 has not yet been clarified, it is also considered that MASP-3 forms the homodimers or heterodimers, since MASP-3 has a H-chain common to those of MASP-1 and MAp44. We hypothesized that homodimer formation of MASP-3 is involved in the long-term retention of MASP-3 in the circulation, and faster clearance of the four mutant rmMASP-3-PAs is due to failure of homodimer formation. To clarify this hypothesis, we generated WT rmMASP-3 protein as an ALFA-tag fusion protein, designated WT rmMASP-3-ALFA, and tested whether WT rmMASP-3-ALFA forms dimers with WT or mutant rmMASP-3-PAs based on the method described by Rosbjerg et al. (26). WT rmMASP-

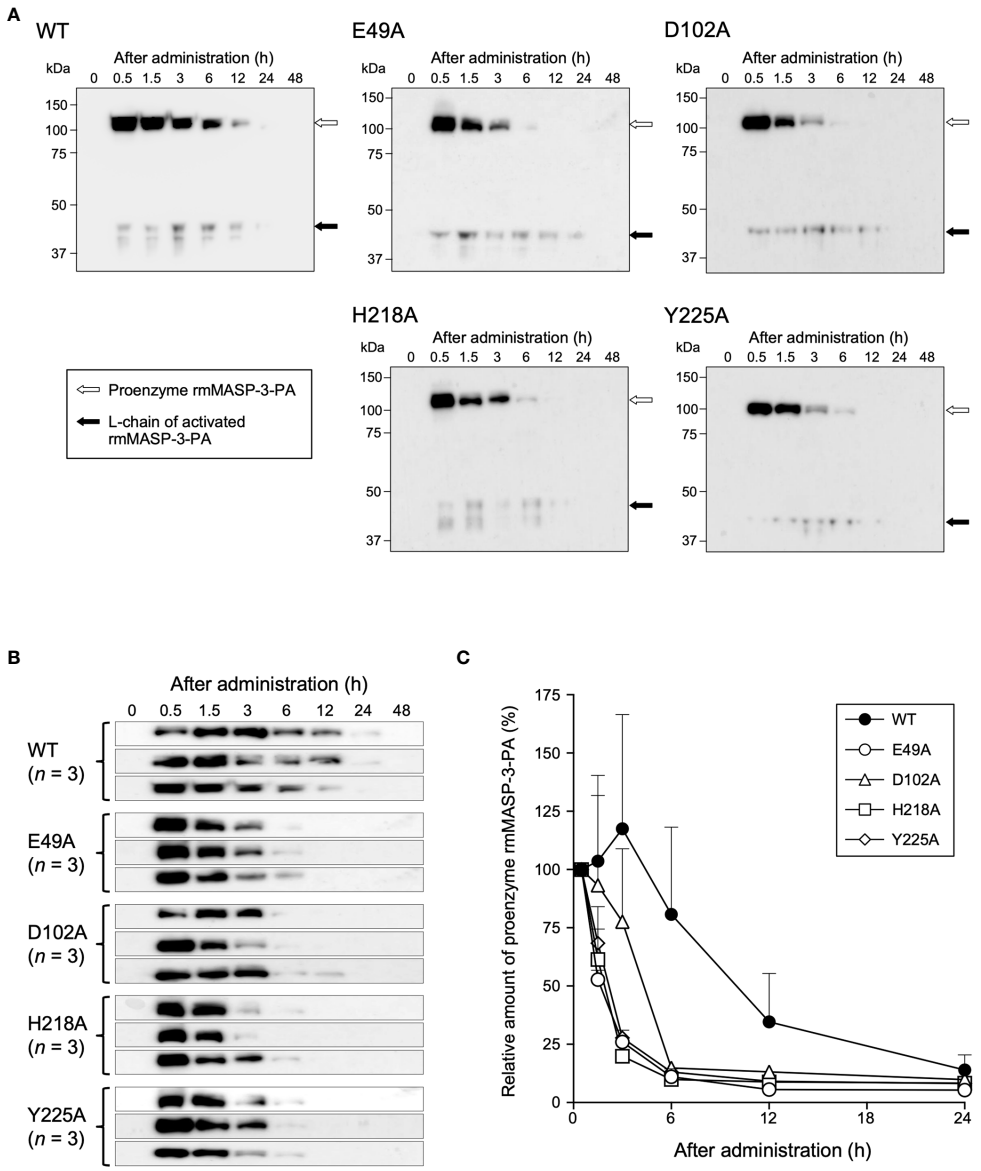

FIGURE 4
In-vivo activation and clearance kinetics of WT and mutant rmMASP-3-PAs when administered to mice. **(A)** Serum samples obtained at indicated time periods after administrations of rmMASP-3-PAs were subjected to SDS-PAGE under reducing condition followed by Western blotting using anti-PA tag antibody. The white and black arrows indicate bands for proenzyme rmMASP-3-PA and L-chain of activated rmMASP-3-PA, respectively. Similar results were obtained from three independent experiments, and representative images are shown here. **(B)** *In-vivo* clearance kinetics of proenzyme rmMASP-3-PAs when administered to mice (n = 3). **(C)** Residual amounts of the proenzyme rmMASP-3-PAs in the circulation are represented as the percentage of its band intensity against the intensity in the serum sample obtained 0.5 h after administration from the same mouse.

3-ALFA was mixed with WT, as well as each mutant rmMASP-3-PA, dialyzed against TBS/EDTA for dimer dissociation, and then dialyzed against TBS/Ca for dimer reassociation composed of rmMASP-3-ALFA and each rmMASP-3-PA. The dimers of rmMASP-3-ALFA and each rmMASP-3-PA in the dialyzed mixture were detected by sandwich ELISA using anti-PA and anti-ALFA antibodies. As shown in Figure 6, WT rmMASP-3-ALFA formed dimers with WT rmMASP-3-PA as expected. WT rmMASP-3-ALFA also formed dimers with E49A, H218A or Y225A rmMASP-3-PA at similar levels to WT rmMASP-3-PA. On the other hand, WT rmMASP-3-ALFA showed lower levels of dimer formation with D102A rmMASP-3-PA compared to that with WT or other mutant rmMASP-3-PAs. Nevertheless, there were no significant differences in MASP-3 activation and

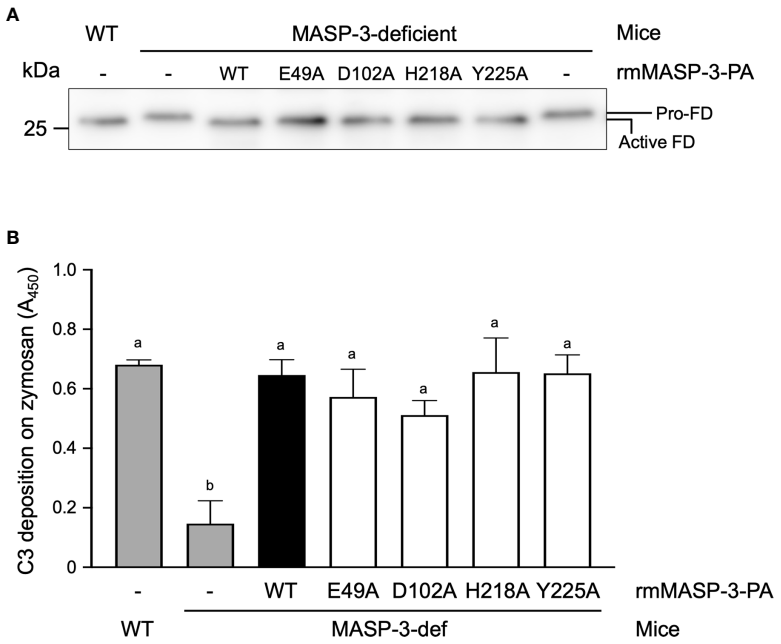

FIGURE 5
Restoration of the activation status of FD **(A)** and AP activity **(B)** in MASP-3-deficient mouse sera obtained 3 h after administrations of WT and mutant rmMASP-3-PAs. **(A)** Western blotting of FD was performed using serum samples that were preliminarily immunoprecipitated with anti-mouse FD antibody and then deglycosylated with N-glycosidase F. Pro-FD was detected at 26.1 kDa in MASP-3-deficient mouse sera (lane 2), while an active form FD was detected at a lower position (25.5 kDa; lane 1 and 3–7) than pro-FD. Similar results were obtained from three independent experiments, and a representative image is shown here. **(B)** The assay for the AP-driven serum C3 deposition activity was performed using a zymosan-coated microplate and TBS/Mg/EGTA under the Ca^{2+}-chelated conditions. Values are means + SD (n = 3) obtained by subtracting the absorbance at 450 nm of a control sample without mouse serum from the absorbance at 450 nm of each sample. Values not sharing the same letters are significantly different at $P < 0.05$, as analyzed by *post-hoc* Tukey's multiple comparisons.

long-term retention of MASP-3 in the circulation between the four mutant rmMASP-3-PAs, suggesting that homodimer formation of MASP-3 was not involved in the long-term retention of MASP-3 in the circulation. Importantly, the results of the present study suggest that mouse MASP-3 forms homodimers, and D102 in the CUB1 domain of mouse MASP-3 may play an important role in its formation.

Discussion

MASP-1 and MASP-2 can be activated under certain conditions without forming a complex with LP-PRMs (29, 30). However, the activation efficiency of MASP-1 and MASP-2 is maximized when LP-PRMs complexed with them bind to their ligands. This activation mechanism gave rise to our initial hypothesis that complex formation of MASP-3 with LP-PRMs is involved in MASP-3 activation, at least with regard to its efficiency. To verify our hypothesis, we generated WT and mutant rmMASP-3-PA proteins, the latter of which showed significantly reduced complex formation with MBL-A, MBL-C, ficolin-A, and CL-K1, although it is unclear whether the mutant rmMASP-3-PAs have ability of forming a complex with CL-L1 or CL-LK. Then, we tested their activation kinetics *via* an *in-vivo* experiment. The results presented in this report indicate that the impaired MASP-3/LP-PRM complex formation had little-to-no effect on MASP-3 activation, or its efficiency; however, the results manifest a faster clearance of mutant rmMASP-3-PAs from the circulation compared with WT rmMASP-3-PA.

Since MASP-3 is a serine protease that professionally cleaves pro-FD of the AP, it can be regarded as a complement factor of the AP. On the other hand, like MASP-1 and MASP-2, MASP-3 forms a complex with PRMs of the LP. The current study indicates that, unlike MASP-1 and MASP-2, complex formation of MASP-3 with LP-PRMs is not required for MASP-3 activation or its efficiency. There arises a question as to what the significance of complex formation of MASP-3 with LP-PRMs in the complement system is. When MASP-3 was first discovered, it was known to have a serine protease domain in the L-chain of MASP-3, but the substrate for MASP-3 was unknown (10). Regarding the role of MASP-3 in the complement system, MASP-3 was thought to be a regulator of LP activation because it competes with MASP-2 for complex formation with LP-PRMs (10). Later, MAp44 and sMAP, which form a complex with LP-PRMs but lack the serine protease domain, were found to play a regulatory role in LP activation (27, 31). In 2010, a major turning point came in the research of MASP-

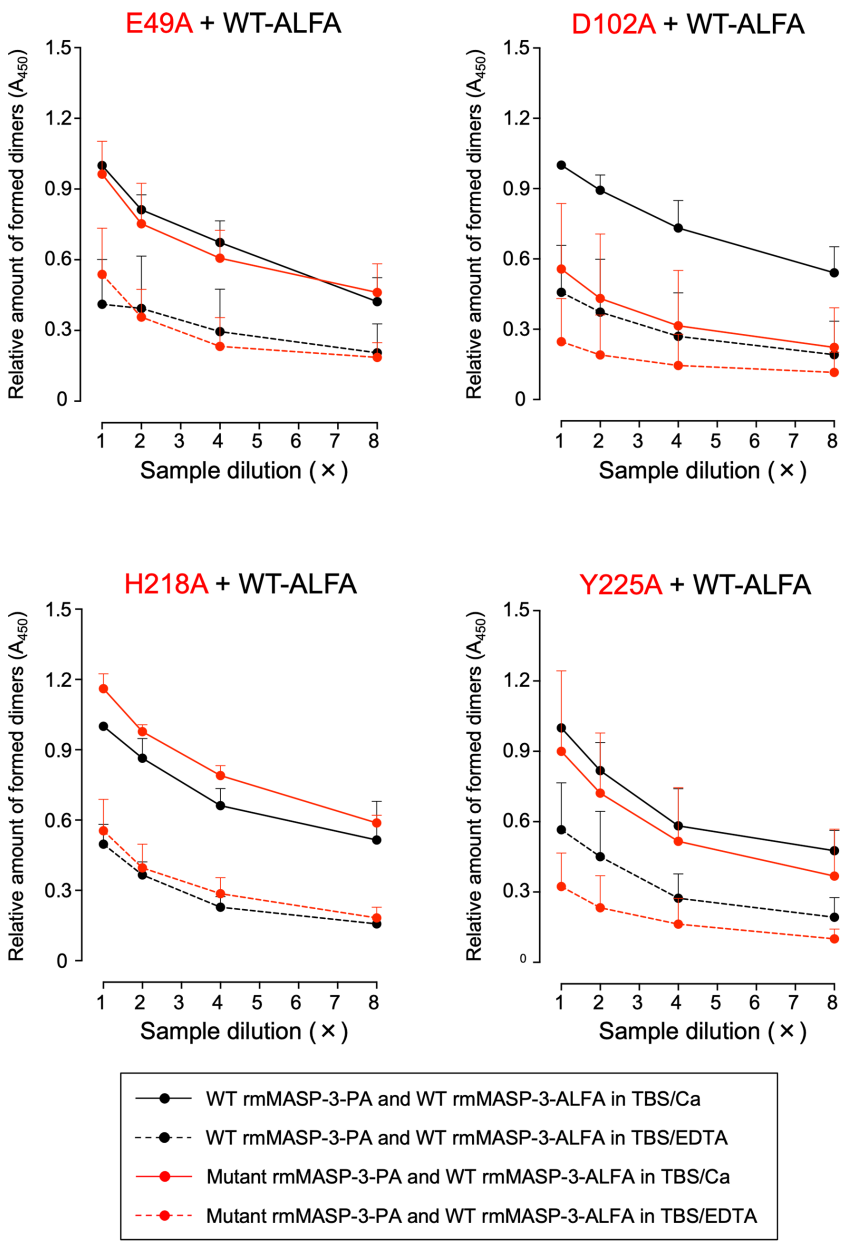

FIGURE 6
Effects of single amino acid mutations on dimer formation of rmMASP-3-PAs with WT rmMASP-3-ALFA. The black circles represent the formed dimer of WT rmMASP-3-ALFA with WT rmMASP-3-PA, and the red circles represent the formed dimer of WT rmMASP-3-ALFA with mutant rmMASP-3-PAs. The solid lines represent the results on protein mixture dialyzed in TBS/Ca for dimer formation, and the dotted lines represent the results on protein mixture dialyzed in TBS/EDTA for dimer dissociation. Values are means + SD (n = 3) of the ratio of absorbance at 450 nm of each sample against the absorbance at 450 nm of the top dilution of the "WT-PA and WT-ALFA in TBS/Ca" sample, which were measured in the same microplate. The values of each sample are obtained by subtracting the absorbance at 450 nm of a control sample without mouse serum from the absorbance at 450 nm of each sample.

3. Takahashi et al. generated *Masp1* gene-knockout mice that were deficient for both MASP-1 and MASP-3, and demonstrated that these mice lacked both LP and AP activity with a proenzyme form of FD in their circulation (16, 32). While in humans, it was reported that the sera of 3MC syndrome patients deficient for both MASP-1 and MASP-3 lacked C4 deposition activity on mannan *via* the LP but exhibited lowered hemolytic activity *via* the AP (33, 34), suggesting the existence of a backup system that activates pro-FD at least in humans. Oroszlán et al. reported that MASP-3 is present predominantly in an active form in human

resting blood, and proposed an intracomplex activation mechanism of MASP-3 *via* a proenzyme form of MASP-1 (8). These reports suggested potential crosstalk between the LP and AP *via* intracomplex activation mechanism. To clarify the individual roles of MASP-1 and MASP-3 in the LP and AP, our group generated mice that were monospecifically deficient for MASP-1 or MASP-3 and found that the MASP-1-deficient mouse sera lacked LP activity alone, whereas the MASP-3-deficient mouse sera lacked AP activity alone and had a proenzyme form of FD. In addition, MASP-3 and FD were detected predominantly as active forms in the MASP-1-deficient mouse sera. Taken together, these results indicate that MASP-1 and MASP-3 play independent roles in LP and AP activation, respectively. In other words, there is no crosstalk between the LP and AP *via* intracomplex activation mechanism of MASP-3 by MASP-1. Recently, Oroszlán *et al.* demonstrated that proprotein convertase subtilisin/kexin (PCSK) 5 and PCSK6 are able to activate MASP-3 in resting blood, and concluded that PCSK6 present in sera and plasma is likely to be a major MASP-3 activator in the circulation (35). This report provided important insights into the activation mechanism of MASP-3. However, the role and importance of MASP-3 forming a complex with LP-PRMs remained unclear. In the current study, we demonstrated that WT rmMASP-3-PA, which showed a complex formation with LP-PRMs, remained in the circulation longer than four mutant rmMASP-3-PAs, which showed an impaired complex formation with LP-PRMs. Therefore, we concluded that complex formation of MASP-3 with LP-PRMs may contribute to the long-term retention of the circulating MASP-3.

We next investigated whether the impaired complex formation of MASP-3 with LP-PRMs has an impact on the complement system. We tested restoration of the active FD and AP activity in MASP-3-deficient mice by using sera 3 h after intravenous administration of WT and mutant rmMASP-3-PAs. As a result, all MASP-3-deficient mice showed the same level of active FD and AP activity restoration as WT mice, regardless of whether the administered rmMASP-3-PA has high ability of forming a complex with LP-PRMs (Figure 5). These results indicate that the impaired complex formation of MASP-3 with LP-PRMs does not impact restoration of active FD and AP activity in MASP-3-deficient mouse sera at least 3 h after administration. These results also suggest that free MASP-3, without having formed a complex with LP-PRMs, plays predominant roles in the cleavage of the pro-FD and maintenance of AP activity, rather than MASP-3 in a complex with LP-PRMs. However, the latter MASP-3 may act as a reservoir to maintain AP activity, since the proenzyme rmMASP-3-PA, which has high ability of forming a complex with LP-PRMs, can remain longer in the circulation (Figure 4).

As described above, the current study showed that WT rmMASP-3-PA can stay longer in the circulation than mutant rmMASP-3-PAs, which have a single amino acid substitution for alanine in the CUB1-EGF-CUB2 domain at E49 (E49A), D102 (D102A), H218 (H218A) or Y225 (Y225A). We observed that the mutant rmMASP-3-PAs showed significantly reduced complex formation with LP-PRMs in the circulation. We hypothesized that these mutant rmMASP-3-PAs may be also unable to form heterodimers or homodimers, which may lead to rapid clearance of rmMASP-3-PA from the circulation. To determine this possibility, we conducted *in-vitro* experiments to test whether these mutant rmMASP-3-PAs can form homodimers with WT rmMASP-3-ALFA. We found that all mutant rmMASP-3-PAs, except mutant rmMASP-3-PA with the D102A mutation, formed homodimers with WT rmMASP-3-ALFA at the same level as homodimer formation between WT rmMASP-3-PA and WT rmMASP-3-ALFA. From these results, we concluded that homodimer formation of rmMASP-3-PA may not contribute to the long-term retention of rmMASP-3-PA in the circulation. Of note, rmMASP-3-PA with the D102A mutation showed decreased homodimer formation with WT rmMASP-3-ALFA. This finding suggests that D102 of MASP-3, a common amino acid sequence between the transcripts of the *Masp1* and *Masp2* genes (i.e., MASP-1, MASP-2, MASP-3, MAp44, and sMAP), may play an important role in the formation of homodimers and/or heterodimers.

In the current study, impaired complex formation of MASP-3 with LP-PRMs showed no significant impact on the complement system, at least in AP activity. On the other hand, lack of MASP-3 activity due to mutations in MASP-3-specific exon of the *MASP1* gene results in 3MC syndrome (20). Of interest, the genes *COLEC10* and *COLEC11*, which transcribe the LP-PRMs CL-L1 and CL-K1, respectively, are also reported to be mutated in the 3MC families (21, 22). In the process of embryonic development, it has been suggested that MASP-3 complexed with CL-K1 functions as a guidance cue for neural crest cell migration (21). Furthermore, CL-L1 and CL-K1 were found to form the heteromeric complex CL-LK, which can form a complex with MASPs including MASP-3 (13). Therefore, the main role of the MASP-3/LP-PRM complexes, especially the MASP-3/CL-LK complex, may be in embryonic development rather than in host defense.

We were unable to determine whether mutant rmMASP-3-PAs formed a complex with CL-L1 or CL-LK. However, we consider that complex formation of rmMASP-3-PA with CL-L1 or CL-LK may not significantly affect the retention of circulating rmMASP-3-PA because of the following reasons. Human serum level of CL-L1 is 0.306 μg/mL and significantly lower than those of MBL (1 μg/mL) or ficolins (ficolin-2: 3.3–5.0 μg/mL, ficolin-3: 18.4–32.6 μg/mL) (36). Furthermore, previous studies have reported that ficolin-3 is the most predominant LP-PRM forming a complex with MASP-3, compared to ficolin-2 and MBL (11). Based on these previous reports, it is likely that the MASP-3 in complex with CL-L1 or CL-LK accounts for a significantly lower proportion of the circulating MASP-3/LP-PRM complexes also in mice. Therefore, it is unlikely that the complex formation of mutant rmMASP-3-PAs with CL-L1 or CL-LK significantly affect the overall *in-vivo* clearance kinetics of MASP-3.

In conclusion, our results demonstrate that complex formation of MASP-3 with LP-PRMs is not required for

activation of MASP-3 or its efficiency. However, our results also show that the MASP-3/LP-PRM complexes may contribute to the long-term retention of MASP-3 in the circulation. Our study is the first to show *in-vivo* kinetics of MASP-3 demonstrating rapid activation and clearance in the circulation. Our study also demonstrated that free MASP-3 alone plays a sufficient role in restoring active FD and AP activity in MASP-3-deficient mice. To date, abnormal control of the AP has been shown to exacerbate the pathology of complement-related inflammatory diseases such as age-related macular degeneration (AMD) and kidney disease including atypical hemolytic-uremic syndrome (aHUS), C3 glomerulonephritis, dense-deposit disease, and lupus nephritis (37–39). In these diseases, the development of anti-complement agents that inhibit activation of the AP is eagerly awaited, and MASP-3, which is located upstream of the cascade reaction of the AP, is a promising target. Although further studies are needed, the results of the current study may provide useful information for the development of therapeutic agents targeting MASP-3.

Data availability statement

The original contributions presented in the study are included in the article/supplementary material. Further inquiries can be directed to the corresponding author.

Ethics statement

The animal study was reviewed and approved by The Animal Experiments Committee of Fukushima Medical University.

Author contributions

KK and TM are equally credited as first authors in this work. KK, TM, and HS designed the study and wrote the manuscript. KK, TM, and YI performed the experiments, analyzed the results, and made figures and tables. TO and TS assisted with the experiments. MS and IW designed and assisted with the experiments. TM, TF, and HS supervised the study. All authors contributed to the article and approved the submitted version.

Funding

This entire research was supported by JSPS KAKENHI Grant Numbers JP19K07610, JP21K07083, and JP22K07122.

Conflict of interest

The authors declare that the research was conducted in the absence of any commercial or financial relationships that could be construed as a potential conflict of interest.

Publisher's note

References

1. Ricklin D, Hajishengallis G, Yang K, Lambris JD. Complement: A key system for immune surveillance and homeostasis. *Nat Immunol* (2010) 11(9):785–97. doi: 10.1038/ni.1923

2. Garred P, Genster N, Pilely K, Bayarri-Olmos R, Rosbjerg A, Ma YJ, et al. A journey through the lectin pathway of complement–MBL and beyond. *Immunol Rev* (2016) 274(1):74–97. doi: 10.1111/imr.12468

3. Cooper NR. The classical complement pathway: Activation and regulation of the first complement component. *Adv Immunol* (1985) 37:151–216. doi: 10.1016/s0065-2776(08)60340-5

4. Matsushita M, Fujita T. Activation of the classical complement pathway by mannose-binding protein in association with a novel C1s-like serine protease. *J Exp Med* (1992) 176(6):1497–502. doi: 10.1084/jem.176.6.1497

5. Thiel S, Vorup-Jensen T, Stover CM, Schwaeble W, Laursen SB, Poulsen K, et al. A second serine protease associated with mannan-binding lectin that activated complement. *Nature* (1997) 386(6624):506–10. doi: 10.1038/386506a0

6. Janssen BJC, Christodoulidou A, McCarthy A, Lambris JD, Gros P. Structure of C3b reveals conformational changes that underlie complement activity. *Nature* (2006) 444(7116):213–6. doi: 10.1038/nature05172

7. Xu Y, Ma M, Ippolito GC, Schroeder HWJr., Carroll MC, Volanakis JE. Complement activation in factor d-deficient mice. *Proc Natl Acad Sci USA* (2001) 98(25):14577–82. doi: 10.1073/pnas.261428398

8. Oroszlán G, Dani R, Szilágyi A, Závodszky P, Thiel S, Gál P, et al. Extensive basal level activation of complement mannose-binding lectin-associated serine protease-3: Kinetic modeling of lectin pathway activation provides possible mechanism. *Front Immunol* (2017) 8:1821. doi: 10.3389/fimmu.2017.01821

9. Hayashi M, Machida T, Ishida Y, Ogata Y, Omori T, Takasumi M, et al. Cutting edge: Role of MASP-3 in the physiological activation of factor d of the alternative complement pathway. *J Immunol* (2019) 203(6):1411–6. doi: 10.4049/jimmunol.1900605

10. Dahl MR, Thiel S, Matsushita M, Fujita T, Willis AC, Christensen T, et al. MASP-3 and its association with distinct complexes of the mannan-binding lectin complement activation pathway. *Immunity* (2001) 15(1):127–35. doi: 10.1016/s1074-7613(01)00161-3

11. Skjoedt M-O, Palarasah Y, Munthe-Fog L, Ma YJ, Weiss G, Skjodt K, et al. MBL-associated serine protease-3 circulates in high serum concentrations predominantly in complex with ficolin-3 and regulates ficolin-3 mediated complement activation. *Immunobiology* (2010) 215(11):921–31. doi: 10.1016/j.imbio.2009.10.006

12. Teillet F, Gaboriaud C, Lacroix M, Martin L, Arlaud GJ, Thielens NM. Crystal structure of the CUB1-EGF-CUB2 domain of human MASP-1/3 and identification of its interaction sites with mannan-binding lectin and ficolins. *J Biol Chem* (2008) 283(37):25715–24. doi: 10.1074/jbc.M803551200

13. Henriksen ML, Brandt J, Andrieu J-P, Nielsen C, Jensen PH, Holmskov U, et al. Heteromeric complexes of native collectin kidney 1 and collectin liver 1 are found in the circulation with MASPs and activate the complement system. *J Immunol* (2013) 191(12):6117–27. doi: 10.4049/jimmunol.1302121

14. Dobó J, Harmat V, Beinrohr L, Sebestyén E, Závodszky P, Gál P. MASP-1, a promiscuous complement protease: Structure of its catalytic region reveals the basis of its broad specificity. *J Immunol* (2009) 183(2):1207–14. doi: 10.4049/jimmunol.0901141

15. Cortesio CL, Jiang W. Mannan-binding lectin-associated serine protease 3 cleaves synthetic peptides and insulin-like growth factor-binding protein 5. *Arch Biochem Biophys* (2006) 449(1–2):164–70. doi: 10.1016/j.abb.2006.02.006

16. Takahashi M, Ishida Y, Iwaki D, Kanno K, Suzuki T, Endo Y, et al. Essential role of mannose-binding lectin-associated serine protease-1 in activation of the complement factor d. *J Exp Med* (2010) 207(1):29–37. doi: 10.1084/jem.20090633

17. Iwaki D, Kanno K, Takahashi M, Endo Y, Matsushita M, Fujita T. The role of mannose-binding lectin-associated serine protease-3 in activation of the alternative complement pathway. *J Immunol* (2011) 187(7):3751–8. doi: 10.4049/jimmunol.1100280

18. Sim RB, Reboul A, Arlaud GH, Villiers CL, Colomb MG. Interaction of 125I-labelled complement subcomponents C1r and C1s with protease inhibitors in plasma. *FEBS Lett* (1979) 97(1):111–5. doi: 10.1016/0014-5793(79)80063-0

19. Matsushita M, Thiel S, Jensenius JC, Terai I, Fujita T. Proteolytic activities of two types of mannose-binding lectin-associated serine protease. *J Immunol* (2000) 165(5):2637–42. doi: 10.4049/jimmunol.165.5.2637

20. Sirmaci A, Walsh T, Akay H, Spiliopoulos M, Sakalar YB, Hasanefendioğlu-Bayrak A, et al. *MASP1* mutations in patients with facial, umbilical, coccygeal, and auditory findings of carnevale, malpuech, OSA, and michels syndromes. *Am J Hum Genet* (2010) 87(5):679–86. doi: 10.1016/j.ajhg.2010.09.018

21. Rooryck C, Diaz-Font A, Osborn DPS, Chabchoub E, Hernandez-Hernandez V, Shamseldin H, et al. Mutations in lectin complement pathway genes *COLEC11* and *MASP1* cause 3MC syndrome. *Nat Genet* (2011) 43(3):197–203. doi: 10.1038/ng.757

22. Munye MM, Diaz-Font A, Ocaka L, Henriksen ML, Lees M, Brady A, et al. *COLEC10* is mutated in 3MC patients and regulates early craniofacial development. *PloS Genet* (2017) 13(3):e1006679. doi: 10.1371/journal.pgen.1006679

23. Fujii Y, Kaneko M, Neyazaki M, Nogi T, Kato Y, Takagi J. PA tag: a versatile protein tagging system using a super high affinity antibody against a dodecapeptide derived from human podoplanin. *Protein Expr Purif* (2014) 95:240–7. doi: 10.1016/j.pep.2014.01.009

24. Götzke H, Kilisch M, Martínez-Carranza M, Sograte-Idrissi S, Rajavel A, Schlichthaerle T, et al. The ALFA-tag is a highly versatile tool for nanobody-based bioscience applications. *Nat Commun* (2019) 10(1):4403. doi: 10.1038/s41467-019-12301-7

25. Endo Y, Nakazawa N, Liu Y, Iwaki D, Takahashi M, Nakata M, et al. Carbohydrate-binding specificities of mouse ficolin a, splicing variant of ficolin a and ficolin b and their complex formation with MASP-2 and sMAP. *Immunogenet* (2005) 57(11):837–44. doi: 10.1007/s00251-005-0058-1

26. Rosbjerg A, Munthe-Fog L, Garred P, Skjoedt M. Heterocomplex formation between MBL/ficolin/CL-11-associated protein-1. *J Immunol* (2014) 192(9):4352–60. doi: 10.4049/jimmunol.1303263

27. Degn S, Jensen L, Olszowski T, Jensenius JC, Thiel S. Co-Complexes of MASP-1 and MASP-2 associated with the soluble pattern-recognition molecules drive lectin pathway activation in a manner inhibitable by MAp44. *J Immunol* (2013) 191(3):1334–45. doi: 10.4049/jimmunol.1300780

28. Paréj K, Hermann A, Donáth N, Závodszky P, Gál P, Dobó J. Dissociation and re-association studies on the interaction domains of mannan-binding lectin (MBL)-associated serine proteases, MASP-1 and MASP-2, provide evidence for heterodimer formation. *Mol Immunol* (2014) 59(1):1–9. doi: 10.1016/j.molimm.2013.12.003

29. Thielens NM, Cseh S, Thiel S, Vorup-Jensen T, Rossi V, Jensenius JC, et al. Interaction properties of human mannan-binding lectin (MBL)-associated serine proteases-1 and -2, MBL-associated protein 19, and MBL. *J Immunol* (2001) 166 (8):5068–77. doi: 10.4049/jimmunol.166.8.5068

30. Cseh S, Vera L, Matsushita M, Fujita T, Arlaud GJ, Thielens NM. Characterization of the interaction between l-ficolin/P35 and mannan-binding lectin-associated serine proteases-1 and -2. *J Immunol* (2002) 169(10):5735–43. doi: 10.4049/jimmunol.169.10.5735

31. Iwaki D, Kanno K, Takahashi M, Endo Y, Lynch NJ, Schwaeble WJ, et al. Small mannose-binding lectin-associated protein plays a regulatory role in the lectin complement pathway. *J Immunol* (2006) 177(12):8626–32. doi: 10.4049/jimmunol.177.12.8626

32. Takahashi M, Iwaki D, Kanno K, Ishida Y, Xiong J, Matsushita M, et al. Mannose-binding lectin (MBL)-associated serine protease (MASP)-1 contributes to activation of the lectin complement pathway. *J Immunol* (2008) 180(9):6132–8. doi: 10.1049/jimmunol.180.9.6132

33. Degn SE, Jensen L, Hansen AG, Duman D, Tekin M, Jensenius JC, et al. Mannan-binding lectin-associated serine protease (MASP)-1 is crucial for lectin pathway activation in human serum, whereas neither MASP-1 nor MASP-3 is required for alternative pathway activation. *J Immunol* (2012) 189(9):3957–69. doi: 10.4049/jimmunol.1201736

34. Atik T, Koparir A, Bademci G, Foster IIJ, Altunoglu U, Mutlu GY, et al. Novel *MASP1* mutations are associated with an expanded phenotype in 3MC1 syndrome. *Orphanet J Rare Dis* (2015) 10:128. doi: 10.1186/s13023-015-0345-3

35. Oroszlán G, Dani R, Végh BM, Varga D, Ács AV, Pál G, et al. Proprotein convertase is the highest-level activator of the alternative complement pathway in the blood. *J Immunol* (2021) 206(9):2198–205. doi: 10.4049/jimmunol.2000636

36. Barnum SR, Schein TN. *The complement FactsBook. second edition*. London, United Kingdom: Academic Press (2018). 514 p.

37. Thurman JM, Holer VM. The central role of the alternative complement pathway in human disease. *J Immunol* (2006) 176(3):1305–10. doi: 10.4049/jimmunol.176.3.1305

38. Barbour TD, Pickering MC, Cook HT. Dense deposit disease and C3 glomerulopathy. *Semin Nephrol* (2013) 33(6):493–507. doi: 10.1016/j.semnephrol.2013.08.002

39. Machida T, Sakamoto N, Ishida Y, Takahashi M, Fujita T, Sekine H. Essential roles for mannose-binding lectin-associated serine protease-1/3 in the development of lupus-like glomerulonephritis in MRL/lpr mice. *Front Immunol* (2018) 9:1191. doi: 10.3389/fimmu.2018.01191

frontiers | Frontiers in Immunology

TYPE Brief Research Report
PUBLISHED 15 December 2022
DOI 10.3389/fimmu.2022.1061696

OPEN ACCESS

EDITED BY
Brian V Geisbrecht,
Kansas State University, United States

REVIEWED BY
Péter Gál,
Institute of Enzymology, Research Centre for Natural Sciences, Hungary
Lambertus Petrus Van Den Heuvel,
Radboud University Medical Centre, Netherlands

*CORRESPONDENCE
Marcin Okrój
marcin.okroj@gumed.edu.pl

SPECIALTY SECTION
This article was submitted to Molecular Innate Immunity, a section of the journal Frontiers in Immunology

RECEIVED 04 October 2022
ACCEPTED 28 November 2022
PUBLISHED 15 December 2022

CITATION
Kuźniewska A, Thiel M, Kowalska D, Felberg-Miętka A, Szynkowski P, Ołdziej S, Arjona E, Jongerius I, Rodriguez de Córdoba S, Okrój M and Urban A (2022) Substitutions at position 263 within the von Willebrand factor type A domain determine the functionality of complement C2 protein. *Front. Immunol.* 13:1061696. doi: 10.3389/fimmu.2022.1061696

Substitutions at position 263 within the von Willebrand factor type A domain determine the functionality of complement C2 protein

Alicja Kuźniewska[1], Marcel Thiel[1], Daria Kowalska[1], Anna Felberg-Miętka[1], Patryk Szynkowski[1], Stanisław Ołdziej[1], Emilia Arjona[2], Ilse Jongerius[3,4], Santiago Rodriguez de Córdoba[2], Marcin Okrój[1]* and Aleksandra Urban[1,5]

[1]Department of Cell Biology and Immunology, Intercollegiate Faculty of Biotechnology of University of Gdańsk and Medical University of Gdańsk, Gdańsk, Poland, [2]Department of Molecular Biomedicine, Centro de Investigaciones Biológicas and Centro de Investigación Biomédica en Enfermedades Raras, Madrid, Spain, [3]Department of Pediatric Immunology, Rheumatology, and Infectious Diseases, Emma Children's Hospital, Amsterdam University Medical Centre, Amsterdam, Netherlands, [4]Department of Immunopathology, Sanquin Research, Landsteiner Laboratory, Amsterdam University Medical Centers (UMC), University of Amsterdam, Amsterdam, Netherlands, [5]Institute for Cancer Research, Oslo University Hospital, Oslo, Norway

The complement system is one of the first defense lines protecting from invading pathogens. However, it may turn offensive to the body's own cells and tissues when deregulated by the presence of rare genetic variants that impair physiological regulation and/or provoke abnormal activity of key enzymatic components. Factor B and complement C2 are examples of paralogs engaged in the alternative and classical/lectin complement pathway, respectively. Pathogenic mutations in the von Willebrand factor A domain (vWA) of FB have been known for years. Despite substantial homology between two proteins and the demonstration that certain substitutions in FB translated to C2 result in analogous phenotype, there was a limited number of reports on pathogenic C2 variants in patients. Recently, we studied a cohort of patients suffering from rare kidney diseases and confirmed the existence of two gain-of-function and three loss-of-function mutations within the C2 gene sequences coding for the vWA domain (amino acids 254-452) or nearly located unstructured region (243-253) of C2 protein. Herein, we report the functional consequences of amino acid substitution of glutamine at position 263. The p.Q263G variant resulted in the gain-of-function phenotype, similarly to a homologous mutation p.D279G in FB. Conversely, the p.Q263P variant found in a patient with C3 glomerulopathy resulted in the loss of C2 function. Our results confirm that the N-terminal part of the vWA domain is a hot spot crucial for the complement C2 function.

KEYWORDS

complement system, convertase, MIDAS, molecular modeling, C3 glomerulopathies

Introduction

The complement system is formed by serum proteins organized into a chain of proteolytic and conformational changes that eventually lead to the osmotic lysis of target cell (1). C2 protein is an essential component of the classical and lectin pathway convertase (C4b2a) that augments the complement system cascade. Upon activation, C2 splits into two fragments: smaller (33 kDa) C2b and a bigger fragment (66 kDa) C2a. The latter associates with the C4b fragment of the complement C4 protein and provides the enzymatic activity to the so-formed convertase complex (1). The homologous convertase complex exists in the alternative complement pathway and consists of a C3b fragment of C3 molecule and Bb fragment of factor B (FB). Factor B and C2 are paralogs that share 39% of amino acid identity, and 51% of similarity (2). Also, the structural organization of both proteins is identical: three CCP (Sushi) domains at their N terminus linked to the von Willebrand factor type A (vWA) domain and followed by serine protease (SP) domain (2). Despite similarities in the crucial components, the mode of activation of the classical/lectin and the alternative pathway is different. The first two routes need specific stimuli like antibodies fixed to the cell surface or sugar moieties characteristic for pathogens. The latter is constantly active at a low level and its further propagation depends on the lack of inhibition by endogenous regulators that define self cells and tissues (3). Therefore, any disturbances that oppose physiological regulation are potentially detrimental as may lead to auto-aggression towards the body's own structures. For this reason, more attention was brought to rare genetic variants of FB than C2. It was acknowledged that certain mutations in the vWA domain of FB resulting in the gain-of-function (GoF) phenotype are found in patients suffering from rare kidney diseases such as atypical hemolytic uremic syndrome or C3 glomerulopathies (4–8). Hyperactive FB variants can either process C3 more efficiently or escape physiological regulation by complement inhibitors. Enhanced activity of the alternative convertase leads to overproduction of C3b, which increases the chance of misguided complement attack. Conversely, loss of control on classical convertases was believed to be not sufficient for auto-aggression unless coincided with the presence of specific stimuli. Therefore, less attention was paid to hyperactive variants of C2 and only recently did the first reports on the natural GoF mutations in C2 appear (9, 10), despite the fact that translation of such substitutions between FB and C2 was demonstrated already 20 years ago (11). Most of the known and functionally-characterized GoF mutations: D279G (12), F286L (8), K323E/Q (7, 8), K350N (13, 14), S367R (4), D371G (15), Y363A (11, 16), M458I (7) localize in the vWA domain of FB. Position 279 in FB normally occupied by aspartic acid aligns with residue 263 in C2 occupied by glutamine. In the present study, we analyzed the function of the Q263P C2 variant identified in a heterozygous condition in a patient suffering from C3 glomerulonephritis (Table S1). We also produced and analyzed the Q263G variant, since the same substitution in the corresponding position was previously described as the GoF variant of FB, p.D279G.

Methods

Patient with mutation p.Q263P in C2

Patient data are retrieved from the Spanish aHUS/C3G Registry. The previous collection was described in (9), and the actual cohort is a recollection of 614 cases that have been submitted to our laboratory for complement genetic testing. Details of genetic analyses and the patient's clinical information are given in the supplementary file and Table S1.

Cell culture

The human lymphoma cell lines Raji and Ramos (American Type Culture Collection, ATCC) were cultured in RPMI 1640 medium with L-glutamine (ATCC) supplemented with 10% FBS (ATCC) at 37°C in humidified 5% CO2 atmosphere. Ramos cells with CD55 or CD46 knockout were produced by CRISPR/Cas9 technology as described in ref (17). Obtained clones of knock-out cells were sorted with sorted with FacsAria (BD) using DyLight 488-conjugated anti-CD46 monoclonal antibody and APC Mouse Anti-Human CD55 monoclonal antibody (BD).

Cloning, expression and purification of C2 variants

The wild-type C2 cDNA sequence (based on accession number NM_000063.5) was codon-optimized for expression in eukaryotic system, and six histidine codons were added at 3` terminus. The construct was synthesized and cloned into the pCEP4 vector in the framework of GeneArt Gene Synthesis service by Thermo Fisher. The Q263P and Q263G mutations were introduced using QuikChange XL Site-Directed Mutagenesis Kit (Agilent) into codon-optimized sequence of wild-type C2 cDNA. Proteins were expressed in HEK293 Freestyle cells (Thermo Fisher) transfected with the respective plasmids using Freestyle Max reagent (Thermo Fisher). Conditioned FreeStyle 293 expression medium (Thermo Fisher) was collected on the 2nd, 4th and 7th day post-transfection and stored at -80°C. Crude medium was loaded onto HisTrap FF affinity column (GE Healthcare) and eluted with linear gradient of 0-0.7 M imidazole using an Äkta Start System. The purified proteins were analyzed with SDS-PAGE electrophoresis and Western blot, as described in (9). Each

10.3389/fimmu.2022.1061696

variant of recombinant C2 protein was obtained with similar yield oscillating around 7.5 mg/L of conditioned medium.

Complement dependent cytotoxicity assay

CDC assay was performed on Raji and Ramos cell lines sensitized with rituximab (50 μg/ml) and treated with normal human serum (NHS) or C2-depleted supplemented (ΔC2, Complement Technologies) supplemented with physiological concentration (25 μg/ml) of C2 variants. The assay is described in detail in (18).

Hemolytic assay

The hemolytic assay was performed on human erythrocytes sensitized with anti-human red blood cells antibodies (Rockland, Limerick, Pa) diluted 1:50 in dextrose gelatin-veronal buffer supplemented with 1mM Ca^{2+} and Mg^{2+} (DGVB++), incubated 30 min at 37°C with shaking (300 rpm). Then erythrocytes were washed and plated on a V-shaped plate. Cells were overlaid with C2 variants (WT, Q263P, or Q263G) diluted in physiological concentration (25 μg/ml) in NHS or ΔC2 serum. Cells were pelleted and hemoglobin released to the supernatant was measured at 405 nm in a Synergy H1 microplate reader (Biotek). Cell lysis was calculated as a percentage of full lysis obtained for the supernatant of erythrocytes treated with distilled water.

Classical convertase activity assay

CP convertase assay was performed on human erythrocytes as for the hemolytic assay. Then cells were overlaid with the mixture of C2-depleted serum mixed with C2 variants (WT, Q263P, or Q263G) at physiological concentration (25 μg/ml) and compstatin (30 mM) or eculizumab (70 nM). After indicated time period, the reaction was stopped with 40 mM EDTA-GVB buffer. Cells were washed, pelleted, and overlaid with EDTA-GVB buffer containing 1:20 dilution of guinea pig serum (Harlan Laboratories). The readout of hemoglobin release was performed as described above.

Proteolysis

Purified C2 variants were incubated for 0 and 120 minutes with 4 nM C1s enzyme (Complement Technology) diluted in 5 mM veronal buffer supplemented with 1mM Ca^{2+} and Mg^{2+}. The cleavage into C2a and C2b was analyzed by Western blot and SDS-PAGE, as described in (9).

Bioinformactics and molecular modeling

For assessing amino frequency occurrence in position in MIDAS region, we used the same methods and sequences data set as it is described in reference (10). The three-dimensional models of C2a protein variants were built with SWISS-MODEL web server (swissmodel.expasy.org). The following templates and reference three-dimensional structures were used (PDB Id are provided): C2a structure (2I6Q), factor B (2OK5, 2XWB, 2WIN). For model structures visualization PyMol program was used (pymol.org).

Results

Performance of cytotoxic assays in C2-depleted serum supplemented with recombinant C2 variants aimed to dissect a phenotype of mutation whereas addition of C2 proteins to NHS that contains wild-type C2, aimed to reveal dominant or recessive character of mutation. Reconstitution of C2-depleted serum with recombinant Q263G variant significantly increases the CDC beyond the level attainable for reconstitution with wild-type C2, whereas the addition of Q263P variant resulted in cell lysis comparable to the readout of C2-depleted serum (Figure 1A). The same experiment performed in NHS revealed a dominant effect of Q263G variant, whereas the addition of Q263P variant did not affect the lysis exerted solely by NHS (Figure 1B). The same results were replicated in the model of antibody-sensitized human erythrocytes (Figure S1).

Another version of experiments on human erythrocytes enabled to dissect the C2 variants' impact on classical complement convertases. As expected, convertase activity reflected the results of CDC assay showing the LoF and GoF character of Q263P and Q263P mutations, respectively (Figure 2, Figure S2).

Afterward, the CDC level was assessed in Ramos cells with genetic knock-out of CD46 and CD55. Both molecules are membrane-bound complement inhibitors acting at the level of convertases. Results revealed that the lack of these inhibitors does not revert previously observed phenotypes of Q263G and Q263P variants, that performed significantly better or worse than the wild-type C2, respectively (Figure 3).

Proteolysis of C2 variants with activated C1s enzyme has shown no differences in cleavage efficacy between both variants and wild-type C2, indicating that these substitutions do not affect C2 cleavage and proper processing to C2a and C2b fragments is preserved (Figure S3).

Multiple sequence alignment of 151 sequences of C2 and factor B proteins as well as inspection of known three-dimensional structures reveals that the following residues (residue number for human C2 protein) are involved in metal ion binding (metal-ion-dependent adhesion site - MIDAS motif): D260, S262, S264, T337, D376. In all analyzed C2 and

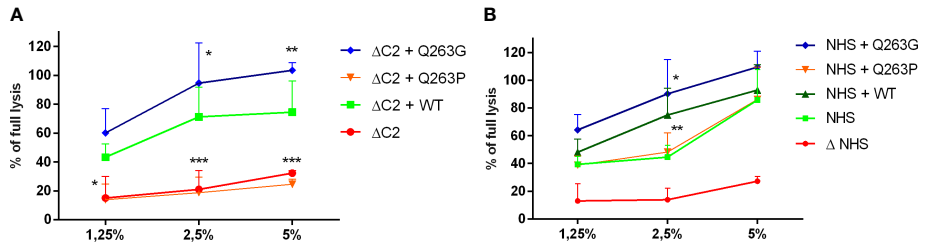

FIGURE 1
CDC of serum supplemented with C2 variants on Ramos cell. Ramos cells were loaded with calcein-AM, sensitized with rituximab and incubated with **(A)** C2-depleted serum (ΔC2) or **(B)** normal human serum (NHS) supplemented with purified, recombinant C2 variants. The fluorescence readout of released calcein was calculated as percentage of full lysis of cells achieved by incubation with 30% DMSO. Symbols *, **, and *** denote statistical significance at p levels <0.05, <0.01, and <0.001, respectively, according to Holm-Sidak's multiple comparison test.

factor B sequences, the mentioned residues are universally conserved, which shows the importance of the MIDAS motif for C2 or factor B biological activity. On the other hand, position 263 (residue in this position is not involved in metal binding) is occupied by glutamine residue or aspartic acid for C2 and factor B sequences respectively. Analysis of known protein complexes formed by C2/factor B proteins shows, that the side chain of residue 263 is not involved in any protein-protein interaction and is exposed to solvent (Figure 4A). As is shown in Figure 4B, our molecular modeling studies indicate that Q263G substitution introduces only minimal conformational changes in the MIDAS region, comparable with changes observed for identical substitution for factor B (19). Importantly, the presence of proline at the same position changes conformation of the protein backbone, which does not allow two serine residues 262 and 264 to access simultaneously to metal ion (see Figure 4C). Such conformational change is due to the conformational stiffness of pyrrolidine ring (20).

Discussion

Compared to its alternative pathway paralog, factor B, complement C2 has a much lower physiological concentration, which makes it a bottleneck of the classical complement pathway (21, 22). The same conclusion was drawn from the studies on sera collected from hematological patients treated with rituximab. Such sera showed a diminished capacity of tumor cell killing following the drug infusion, thus reflecting a systemic complement depletion, but the cytotoxic potential was restored after supplementation with C2 protein (23). Being a pathway-limiting factor explains why the addition of GoF C2 variants can markedly change the cytotoxic potential of serum, as shown in our previous publications (9, 10). In the current study, we attempted to assess the impact of amino acid substitutions in C2 at residue 263 using two different models: human lymphoma cell lines and human red blood cells. Erythrocytes, which have been used in complement assays for dozens of years, provide a

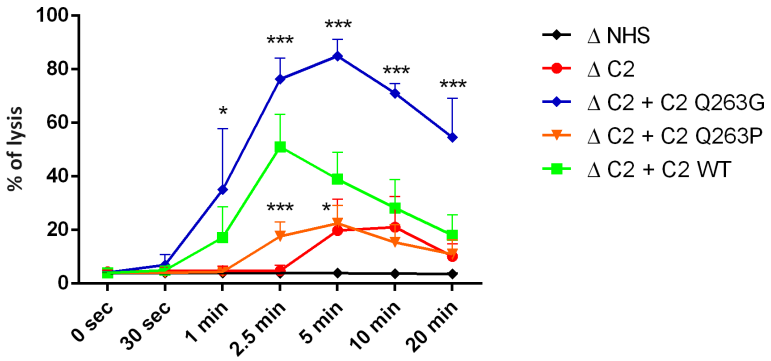

FIGURE 2
Activity of CP/LP C5 convertase formed by C2 variants. Antibody-sensitized human erythrocytes were incubated with ΔC2 serum supplemented with C2 variants and eculizumab for indicated time period to build C5 CP/LP convertases on the cell surface. Afterward, cells were washed and overlaid with guinea pig serum diluted in EDTA-buffer to form membrane attack complexes on the platform of preexisting convertases. The readout of released hemoglobin was calculated as percentage of full lysis achieved by addition of distilled water. Symbols *, and *** denote statistical significance at p levels <0.05, and <0.001, respectively, according to Holm-Sidak's multiple comparison test.

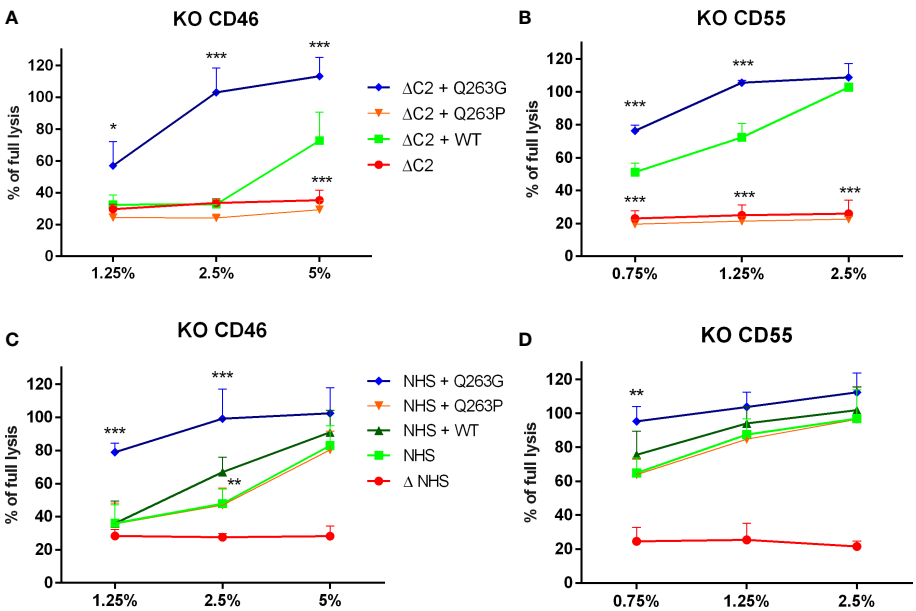

FIGURE 3
The impact of membrane-bound complement inhibitors CD46 and CD55 on CDC exerted by serum supplemented with C2 variants. CD46-knockout **(A, C)** and CD55-knockout **(B, D)** Ramos cells were loaded with calcein-AM, sensitized with rituximab and incubated with C2-depleted serum (ΔC2, graphs **(A, B)**) or normal human serum (NHS, graphs **(C, D)** supplemented with purified, recombinant C2 variants. The fluorescence readout of released calcein was calculated as percentage of full lysis of cells achieved by incubation with 30% DMSO. Symbols *, **,and *** denote statistical significance at p levels <0.05, <0.01, and <0.001, respectively, according to Holm-Sidak's multiple comparison test.

convenient readout based on the measurement of absorbance of released hemoglobin. Sheep erythrocytes sensitized with anti-sheep IgM antibodies became a gold standard in the field. However, while analyzing missense mutations in the C2 gene, we observed that functional assays performed on human but not sheep erythrocytes were appropriate to reveal the gain-of-function phenotype of certain mutants (9). This may stem from the partial incompatibility of sheep homologs of human membrane-bound inhibitors with human complement components. Therefore, in the present study, we used our recently developed assay on sensitized human erythrocytes that successfully identified the first-ever gain-of-function mutations occurring in aHUS and C3G patients (9, 10). Notably, erythrocytes do not express one of the ubiquitous membrane-bound inhibitors CD46 (MCP). Instead, they bear CD35 (CR1) inhibitor, which is not expressed by most of the

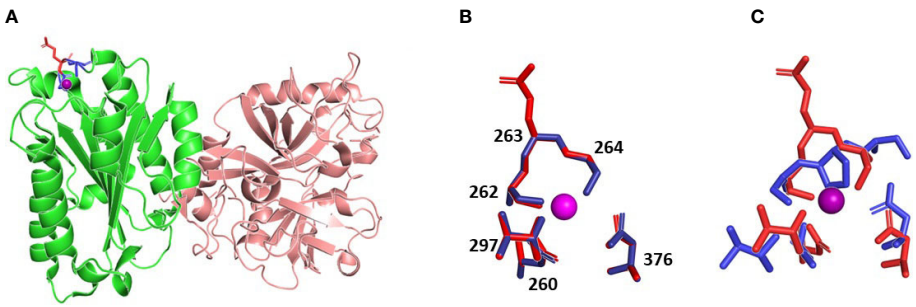

FIGURE 4
The three-dimensional models of C2 variants with Q263P and Q263G substitution. **(A)** Structure of WT C2 protein (PDB ID 2I6Q), C2a fragment indicated in green, amino acids forming MIDAS motif indicated in blue, Gln 263 indicated in red, metal ion is shown as violet sphere. **(B)** overlapping MIDAS motif residues with its numbers for WT protein (red) and model of Q263G variant (blue), metal ion is shown as violet sphere. **(C)** overlapping MIDAS motif residues for WT protein (red) and model of Q263P variant (blue), metal ion is shown as violet sphere. MIDAS motif is shown in the same orientation as on panel B.

cells of lymphoid origin. Usage of both types of human cells provides a reliable assessment of the phenotypic effect of mutations. The same results obtained in these two models firmly support our conclusion on the C2 variants' function. Similarly to previously identified GoF C2 variants, S249C and S250C (10), the Q263G variant showed its effect when mixed with the wild-type protein. LoF variant Q263P showed no cytotoxic activity alone but did not influence the activity of wild-type protein. Additionally, our conclusions were reinforced by CP/LP C3 convertase (Figure S2) and C5 convertase (Figure 2) assays that confirmed that observed readouts of CDC assays stem from different activities of convertases built up from tested C2 variants. The advantage of these assays over previously used methods is the milieu of whole serum and complement activation of real cell surface (19, 24). Such an experimental setup offers far better conditions for revealing truly physiological interactions and minimizes the odds of artefacts generated on artificial surfaces or false positive results generated in the systems using purified complement proteins only. The application of specific inhibitors of C3 (compstatin) and C5 (eculizumab) allow the complement cascade to proceed up to the levels of C3 or C5 classical convertase, respectively, but not further. The amplitude of enzymatic activity of these complexes over the time is a net result of both spontaneous or extrinsic decay/inactivation and complex formation rate. The addition of compatible guinea pig serum diluted in EDTA-containing buffer prevents *de novo* convertase formation and serve as source of terminal complement components that form membrane attack complexes on the platform of convertases formed in the previous step of the assay.

To our best knowledge, the mutation p.Q263G in C2 was not identified in patients yet. However, the pathogenic character of the corresponding mutation in factor B, p. D279G, was revealed by Roumenina et al., who identified it in an aHUS patient. The fact, that LoF mutation p.Q263P is present in a patient with C3G, a disease characterized by excessive complement activation in the fluid phase, should be considered an accidental finding not related to the pathomechanism of the disease. Partial deficiencies of C2, which would be equivalent to heterozygous non-functional C2 variants like Q263P, are common in normal populations. In this particular patient, the relevant genetic finding is the CFH A110S variant that determines a partial FH deficiency, which confers a predisposition to C3G (25). Nonetheless, our intention behind the investigation of the C2 p.Q263P variant was not a demonstration of a clinical outcome but a demonstration of the consequences of substitution at a position important for the functionality of the C2 paralog.

As revealed in other studies (26, 27) and in our molecular modeling data, residue 263 is exposed on the surface of C2 protein. According to the known structures of factor B or C2 complexes, residues 279 (factor B) and 263 (C2) are not involved in any direct protein-protein interactions. The flanking amino acid residues at positions 262 (Ser) and 264 (Ser) as well as Asp 260, Thr 337 and Asp 376 form MIDAS motif and are engaged in coordination of magnesium ion that is essential for binding to C4b and formation of proconvertase C4b2 complex (26–28). These five residues are conserved in all sequences of C2 and factor B. Modeling employed to elucidate the reason for different functionality of analyzed C2 variants does not predict any substantial changes in either protein structure or MIDAS motif upon 263 Q/P and Q/G substitutions. Our analyses seem to be in line with the results of Forneris et al., who published the crystal structure of factor B in complex with C3b fragment and suggest no major changes upon substitution of corresponding Asp 279 to Gly (29). However, substitutions may impact the capacity of metal ion binding, which is supposed to be more effective in case of the presence of small glycine residue between serines 262 and 264. Numerous motifs that bind magnesium ion present the XYX sequence, in which X residues are engaged in direct binding to the ion whereas the central position is occupied by glycine residue (30, 31). This suggests that small size of glycine provides flexibility of the motif and more effective metal binding. For instance, the presence of proline at the same position limits the number of spatial conformations. Based on molecular modeling, it is difficult to state whether Q263P variant is partially or completely devoid of metal binding capacity. This is one of the limitation of our study, as well as an unanswered question of whether Q263 variant competes with wild-type C2 for binding to C4b. This could be suggested by the stable level of CDC upon addition of the LoF C2 variant to NHS (Figure 1B and Figure S1B). Importantly, our functional assays show that neither LoF nor GoF phenotypes of C2 variants with Gln 263 substitutions depend on complement inhibition by CD46 and CD55, unlike previously characterized GoF variants R249C and S250C. These results make plausible the hypothesis that alterations of enzymatic activity of convertase formed from Q263G/P C2 variants' stem from magnesium binding capacity. Notably, the importance of substitution of residue 263 of C2 was first demonstrated over 30 years ago by Horiuchi et al., who expressed recombinant variant of C2 with glutamine 263 substituted with lysine that resulted in enhanced activity in hemolytic assay (28). The same variant was used in studies by Mortensen et al., who needed to obtain convertase complexes of extended stability for the application in structural studies (27). Similarly to our hypothesis, authors explained the feature of Q263K mutation by modifying the backbone properties of Ser 262 and Ser 264, both engaged in coordinating the Mg^{2+} ion.

Conclusions

We present the growing evidence that the von Willebrand factor type A domain and unstructured region at its N terminus contain numerous sites crucial for the enzymatic activity of classical

convertase. The corresponding gene fragment is therefore a hot spot that can accumulate mutations resulting in either LoF or GoF phenotypes. Our results speak for the necessity of identification and characterization of C2 mutations found in patients, as they potentially contribute to pathogenic conditions characterized by both diminished and excessive complement activation. We also provided an example that substitutions like the one at position 263, which triggers neither substantial structural change nor affects residues engaged in protein-protein interactions, may lead to unobvious phenotypic effects.

Data availability statement

The original contributions presented in the study are included in the article/Supplementary Material. Further inquiries can be directed to the corresponding author.

Author contributions

Conceptualization of the study: MO, SRdC, AU. Experimental work: AK, MT, DK, AF-M, PS, SO, IJ, AU. Bioinformatics and database search: EA, SRdC. Writing of the manuscript: AK, SRdC, SO, AU, MO. All authors contributed to the article and approved the submitted version.

Funding

This study was supported by National Science Centre Poland grants no. 2015/18/M/NZ6/00334 (to MO), 2018/29/N/NZ6/01413, and 2019/32/T/NZ6/00328 (both to AU), and UGrants Start 2022 no. 1220/97/2022 from the University of Gdańsk (to AK). SRdC was supported by grants from the Spanish Ministerio de Economía y Competitividad-FEDER (PID2019-104912RB-I00) and Autonomous Region of Madrid (S2017/BMD-3673, S2022/BMD-7278).

Acknowledgments

Computational resources used in this project were provided by the Informatics Center of the Metropolitan Academic Network (IC MAN-TASK) in Gdańsk, Poland.

Conflict of interest

The authors declare that the research was conducted in the absence of any commercial or financial relationships that could be construed as a potential conflict of interest.

Publisher's note

All claims expressed in this article are solely those of the authors and do not necessarily represent those of their affiliated organizations, or those of the publisher, the editors and the reviewers. Any product that may be evaluated in this article, or claim that may be made by its manufacturer, is not guaranteed or endorsed by the publisher.

Supplementary material

The Supplementary Material for this article can be found online at: https://www.frontiersin.org/articles/10.3389/fimmu.2022.1061696/full#supplementary-material

References

1. Merle NS, Church SE, Fremeaux-Bacchi V, Roumenina LT. Complement system part I - molecular mechanisms of activation and regulation. *Front Immunol* (2015) 6:262. doi: 10.3389/fimmu.2015.00262

2. Krishnan V, Xu Y, Macon K, Volanakis JE, Narayana SV. The structure of C2b, a fragment of complement component C2 produced during C3 convertase formation. *Acta Crystallogr D Biol Crystallogr* (2009) 65:266–74. doi: 10.1107/S0907444909000389

3. Ricklin D, Reis ES, Mastellos DC, Gros P, Lambris JD. Complement component C3 - the "Swiss army knife" of innate immunity and host defense. *Immunol Rev* (2016) 274:33–58. doi: 10.1111/imr.12500

4. Zhang Y, Kremsdorf RA, Sperati CJ, Henriksen KJ, Mori M, Goodfellow RX, et al. Mutation of complement factor b causing massive fluid-phase dysregulation of the alternative complement pathway can result in atypical hemolytic uremic syndrome. *Kidney Int* (2020) 98:1265–74. doi: 10.1016/j.kint.2020.05.028

5. Urban A, Borowska A, Felberg A, van den Heuvel L, Stasiłojć G, Volokhina E, et al. Gain of function mutant of complement factor b K323E mimics pathogenic C3NeF autoantibodies in convertase assays. *Autoimmunity* (2018) 51:18–24. doi: 10.1080/08916934.2017.1423286

6. Imamura H, Konomoto T, Tanaka E, Hisano S, Yoshida Y, Fujimura Y, et al. Familial C3 glomerulonephritis associated with mutations in the gene for complement factor b. *Nephrol Dial Transplant* (2015) 30:862–4. doi: 10.1093/ndt/gfv054

7. Marinozzi MC, Vergoz L, Rybkine T, Ngo S, Bettoni S, Pashov A, et al. Complement factor b mutations in atypical hemolytic uremic syndrome-disease-relevant or benign? *J Am Soc Nephrol* (2014) 25:2053–65. doi: 10.1681/ASN.2013070796

8. de Jorge EG, Harris CL, Esparza-Gordillo J, Carreras L, Arranz EA, Garrido CA, et al. Gain-of-function mutations in complement factor b are associated with atypical hemolytic uremic syndrome. *Proc Natl Acad Sci U.S.A.* (2007) 104:240–5. doi: 10.1073/pnas.0603420103

9. Urban A, Volokhina E, Felberg A, Stasiłojć G, Blom AM, Jongerius I, et al. Gain-of-function mutation in complement C2 protein identified in a patient with aHUS. *J Allergy Clin Immunol* (2020) 146:916–919 e911. doi: 10.1016/j.jaci.2020.02.014

10. Urban A, Kowalska D, Stasiłojć G, Kuźniewska A, Skrobińska A, Arjona E, et al. Gain-of-Function mutations R249C and S250C in complement C2 protein

increase C3 deposition in the presence of c-reactive protein. *Front Immunol* (2021) 12:724361. doi: 10.3389/fimmu.2021.724361

11. Kuttner-Kondo LA, Dybvig MP, Mitchell LM, Muqim N, Atkinson JP, Medof ME, et al. A corresponding tyrosine residue in the C2/factor b type a domain is a hot spot in the decay acceleration of the complement C3 convertases. *J Biol Chem* (2003) 278:52386–91. doi: 10.1074/jbc.M304620200

12. Hourcade DE, Mitchell LM, Oglesby TJ. Mutations of the type a domain of complement factor b that promote high-affinity C3b-binding. *J Immunol* (1999) 162:2906–11. doi: 10.4049/jimmunol.162.5.2906

13. Roumenina LT, Jablonski M, Hue C, Blouin J, Dimitrov JD, Dragon-Durey MA, et al. Hyperfunctional C3 convertase leads to complement deposition on endothelial cells and contributes to atypical hemolytic uremic syndrome. *Blood* (2009) 114:2837–45. doi: 10.1182/blood-2009-01-197640

14. Funato M, Uemura O, Ushijima K, Ohnishi H, Orii K, Kato Z, et al. A complement factor b mutation in a large kindred with atypical hemolytic uremic syndrome. *J Clin Immunol* (2014) 34:691–5. doi: 10.1007/s10875-014-0058-8

15. Aradottir SS, Kristoffersson AC, Roumenina LT, Bjerre A, Kashioulis P, Palsson R, et al. Factor d inhibition blocks complement activation induced by mutant factor b associated with atypical hemolytic uremic syndrome and membranoproliferative glomerulonephritis. *Front Immunol* (2021) 12:690821. doi: 10.3389/fimmu.2021.690821

16. Hourcade DE, Mitchell L, Kuttner-Kondo LA, Atkinson JP, Medof ME. Decay-accelerating factor (DAF), complement receptor 1 (CR1), and factor h dissociate the complement AP C3 convertase (C3bBb) *via* sites on the type a domain of bb. *J Biol Chem* (2002) 277:1107–12. doi: 10.1074/jbc.M109322200

17. Thielen AJ, van Baarsen IM, Jongsma ML, Zeerleder S, Spaapen RM, Wouters D. CRISPR/Cas9 generated human CD46, CD55 and CD59 knockout cell lines as a tool for complement research. *J Immunol Methods* (2018) 456:15–22. doi: 10.1016/j.jim.2018.02.004

18. Stasiłojć G, Felberg A, Urban A, Kowalska D, Ma S, Blom AM, et al. Calcein release assay as a method for monitoring serum complement activity during monoclonal antibody therapy in patients with b-cell malignancies. *J Immunol Methods* (2020) 476:112675. doi: 10.1016/j.jim.2019.112675

19. Okroj M, Holmquist E, King BC, Blom AM. Functional analyses of complement convertases using C3 and C5-depleted sera. *PloS One* (2012) 7: e47245. doi: 10.1371/journal.pone.0047245

20. Adzhubei AA, Sternberg MJ, Makarov AA. Polyproline-II helix in proteins: structure and function. *J Mol Biol* (2013) 425:2100–32. doi: 10.1016/j.jmb.2013.03.018

21. Felberg A, Taszner M, Urban A, Majeranowski A, Jaskuła K, Jurkiewicz A, et al. Monitoring of the complement system status in patients with b-cell malignancies treated with rituximab. *Front Immunol* (2020) 11:584509. doi: 10.3389/fimmu.2020.584509

22. Urban A, Majeranowski A, Stasiłojć G, Koszałka P, Felberg A, Taszner M, et al. In silico designed gain-of-Function variants of complement C2 support cytocidal activity of anticancer monoclonal antibodies. *Cancers (Basel)* (2022) 14:1270. doi: 10.3390/cancers14051270

23. Kennedy AD, Beum PV, Solga MD, DiLillo DJ, Lindorfer MA, Hess CE, et al. Rituximab infusion promotes rapid complement depletion and acute CD20 loss in chronic lymphocytic leukemia. *J Immunol* (2004) 172:3280–8. doi: 10.4049/jimmunol.172.5.3280

24. Blom AM, Volokhina EB, Fransson V, Strömberg P, Berghard L, Viktorelius M, et al. A novel method for direct measurement of complement convertases activity in human serum. *Clin Exp Immunol* (2014) 178:142–53. doi: 10.1111/cei.12388

25. Merinero HM, García SP, García-Fernández J, Arjona E, Tortajada A, de Córdoba SR. Complete functional characterization of disease-associated genetic variants in the complement factor h gene. *Kidney Int* (2018) 93:470–81. doi: 10.1016/j.kint.2017.07.015

26. Milder FJ, Raaijmakers HC, Vandeputte MD, Schouten A, Huizinga EG, Romijn RA, et al. Structure of complement component C2A: implications for convertase formation and substrate binding. *Structure* (2006) 14:1587–97. doi: 10.1016/j.str.2006.08.008

27. Mortensen S, Jensen JK, Andersen GR. Solution structures of complement C2 and its C4 complexes propose pathway-specific mechanisms for control and activation of the complement proconvertases. *J Biol Chem* (2016) 291:16494–507. doi: 10.1074/jbc.M116.722017

28. Horiuchi T, Macon KJ, Engler JA, Volanakis JE. Site-directed mutagenesis of the region around cys-241 of complement component C2. evidence for a C4b binding site. *J Immunol* (1991) 147:584–9. doi: 10.4049/jimmunol.147.2.584

29. Forneris F, Ricklin D, Wu J, Tzekou A, Wallace RS, Lambris JD, et al. Structures of C3b in complex with factors b and d give insight into complement convertase formation. *Science* (2010) 330:1816–20. doi: 10.1126/science.1195821

30. Gnatt AL, Cramer P, Fu J, Bushnell DA, Kornberg RD. Structural basis of transcription: an RNA polymerase II elongation complex at 3.3 a resolution. *Science* (2001) 292:1876–82. doi: 10.1126/science.1059495

31. Siebold C, Arnold I, Garcia-Alles LF, Baumann U, Erni B. Crystal structure of the citrobacter freundii dihydroxyacetone kinase reveals an eight-stranded alpha-helical barrel ATP-binding domain. *J Biol Chem* (2003) 278:48236–44. doi: 10.1074/jbc.M305942200

frontiers | Frontiers in Immunology

TYPE Original Research
PUBLISHED 28 December 2022
DOI 10.3389/fimmu.2022.1028760

OPEN ACCESS

EDITED BY
Brian V. Geisbrecht,
Kansas State University, United States

REVIEWED BY
József Dobó,
Hungarian Academy of Sciences (MTA), Hungary
Ronald Paul Taylor,
University of Virginia, United States

*CORRESPONDENCE
David Kavanagh
david.kavanagh@newcastle.ac.uk

†These authors share first authorship

SPECIALTY SECTION
This article was submitted to Molecular Innate Immunity, a section of the journal Frontiers in Immunology

RECEIVED 26 August 2022
ACCEPTED 14 November 2022
PUBLISHED 28 December 2022

CITATION
Hallam TM, Cox TE, Smith-Jackson K, Brocklebank V, Baral AJ, Tzoumas N, Steel DH, Wong EKS, Shuttleworth VG, Lotery AJ, Harris CL, Marchbank KJ and Kavanagh D (2022) A novel method for real-time analysis of the complement C3b:FH:FI complex reveals dominant negative *CFI* variants in age-related macular degeneration. *Front. Immunol.* 13:1028760. doi: 10.3389/fimmu.2022.1028760

A novel method for real-time analysis of the complement C3b:FH:FI complex reveals dominant negative *CFI* variants in age-related macular degeneration

Thomas M. Hallam[1,2†], Thomas E. Cox[1,2†], Kate Smith-Jackson[1,2], Vicky Brocklebank[1,2], April J. Baral[1,2], Nikolaos Tzoumas[1,2], David H. Steel[1,3,4], Edwin K. S. Wong[1,2], Victoria G. Shuttleworth[1,2], Andrew J. Lotery[5], Claire L. Harris[1,2], Kevin J. Marchbank[1,2] and David Kavanagh[1,2,6*]

[1]Translational and Clinical Research Institute, Newcastle University, Newcastle upon Tyne, United Kingdom, [2]National Renal Complement Therapeutics Centre, Royal Victoria Infirmary, Newcastle upon Tyne, United Kingdom, [3]Sunderland Eye Infirmary, Sunderland, United Kingdom, [4]Biosciences Institute, Newcastle University, International Centre for Life, Newcastle upon Tyne, United Kingdom, [5]Clinical and Experimental Sciences, Faculty of Medicine, Southampton General Hospital, University of Southampton, Southampton, United Kingdom, [6]National Institute for Health and Care Research (NIHR) Newcastle Biomedical Research Centre, Biomedical Research Building, Newcastle upon Tyne, United Kingdom

Age-related macular degeneration (AMD) is linked to 2 main disparate genetic pathways: a chromosome 10 risk locus and the alternative pathway (AP) of complement. Rare genetic variants in complement factor H (*CFH;* FH) and factor I (*CFI;* FI) are associated with AMD. FH acts as a soluble cofactor to facilitate FI's cleavage and inactivation of the central molecule of the AP, C3b. For personalised treatment, sensitive assays are required to define the functional significance of individual AP genetic variants. Generation of recombinant FI for functional analysis has thus far been constrained by incomplete processing resulting in a preparation of active and inactive protein. Using an internal ribosomal entry site (IRES)-Furin-*CFI* expression vector, fully processed FI was generated with activity equivalent to serum purified FI. By generating FI with an inactivated serine protease domain (S525A FI), a real-time surface plasmon resonance assay of C3b:FH:FI complex formation for characterising variants in *CFH* and *CFI* was developed and correlated well with standard assays. Using these methods, we further demonstrate that patient-associated rare genetic variants lacking enzymatic activity (e.g. *CFI* I340T) may competitively inhibit the wild-type FI protein. The dominant negative effect identified in inactive factor I variants could impact on

10.3389/fimmu.2022.1028760

the pharmacological replacement of FI currently being investigated for the treatment of dry AMD.

KEYWORDS

AMD (age-related macular degeneration), aHUS (atypical haemolytic uraemic syndrome), Factor I, Factor H, Complement, Surface plasmon resonance, C3G (C3 Glomerulopathy), PNH (paroxysmal nocturnal haemoglobinuria)

Introduction

Age -related macular degeneration (AMD) is the most common cause of irreversible vision loss in developed nations. The global prevalence of AMD is ~8.3% in those over 65 and it is projected to afflict 288 million by 2040 (1), representing a substantial global health and economic burden. There are two subtypes of AMD: wet and dry. Wet AMD involves angiogenesis in the choroid and/or macular neovascularisation which can rapidly progress to a disciform macular scar and legal blindness. Inhibition of vascular endothelial growth factor with monoclonal antibodies can preserve vision but many patients with wet AMD ultimately lose vision due to progressive dry AMD. Dry AMD is driven by degeneration or geographic atrophy (GA) of the retinal pigment epithelium. There is currently no treatment for GA.

In addition to behavioural and environmental factors, >30 common genetic loci have been confirmed to be associated with AMD (2). The 2 main loci identified involve: the activation of the complement system (3–9); and the age-related maculopathy susceptibility 2/high-temperature requirement A serine peptidase 1 *(ARMS2-HTRA1)* risk locus linked to overexpression of HTRA1 and accumulation of macrophages in the subretinal space with resultant inflammation (10).

The complement system is part of the innate immune response to pathogens, and it is strictly regulated to prevent collateral damage to self-tissues (11). The alternative pathway (AP) of complement is a positive amplification loop accounting for ~80-90% of all terminal pathway activation (12). It is the components [C3 (4), factor B (FB) (5)] and regulators [Factor I (FI) (3), Factor H (FH)] (6–9) of the AP that are most strongly linked to AMD. C3 is the central component of the AP and interacts with FB and Factor D (FD) to form the AP C3 convertase, C3bBb, which cleaves more C3 and results in the generation of downstream effector molecules e.g. C5a and the membrane attack complex. Regulation of the AP convertase is brought about by cleavage of C3b by the enzyme FI in association with one of its cofactors (e.g. FH) after the formation of an AP regulatory trimolecular complex (TMC) (e.g. C3b:FH:FI).

Common genetic variants in *C3*, *CFH* and *CFI* were initially associated with AMD in single nucleotide polymorphism association studies (3, 4, 6–9), however, more recently next generation sequencing studies have demonstrated an increased burden of rare genetic variants in *C3*, *CFH* and *CFI* in AMD (4, 13–18). Most of the disease-associated variants are individually rare, and a significant proportion of variants consist of missense mutations of unknown significance.

Clinical trials of FH and FI supplementation (Gemini's GEM103; ClinicalTrials.gov Identifier: NCT04684394, and Gyroscope's GT005; ClinicalTrials.gov Identifier: NCT04437368) respectively, have begun in AMD patients. While quantitative genetic defects in FI and FH are relatively straightforward to detect, and those in FI have been strongly associated with AMD, >50% of the rare genetic variants in *CFI* and *CFH* result in a protein that is secreted with unknown functional activity. With divergent pathways resulting in GA, defining the significance of rare genetic variants is critical to tailor appropriate pharmacological intervention.

Generation of recombinant FI has until now resulted in a mixture of inactive pro-I and fully processed FI. Full processing of FI requires cleavage by Furin of an RRKR linker at Arg339 followed by removal of the linker amino acids by carboxypetidases (19). So far, studies analysing FI are limited by this and require either co-transfection or downstream processing with Furin to generate a pure product. In addition, functional assays rely mainly on fluid phase C3b cleavage assays with various cofactors (20–23), although more complex zebrafish assays have also been utilised (24). These methods, however, do not enable real-time visualisation of the formation of C3b:cofactor:FI complexes.

To overcome the aforementioned difficulties, a mechanism for the generation of fully processed recombinant FI was developed. The recombinantly produced FI had equivalent activity to serum-purified wild type protein. A mutation in FI previously utilised for crystallography of the AP regulatory (25) was generated to abrogate the cleavage of C3b and probe the real-time formation of the AP regulatory TMC. The utility of the inactive variant was demonstrated through analysis of a series of rare genetic variants in *CFH* and *CFI* reported in disease (Figure 1). Furthermore, we demonstrate that the AMD-linked FI variant I340T displays a competitive inhibitory effect on WT regulatory function which has implications for pharmacological supplementation strategy.

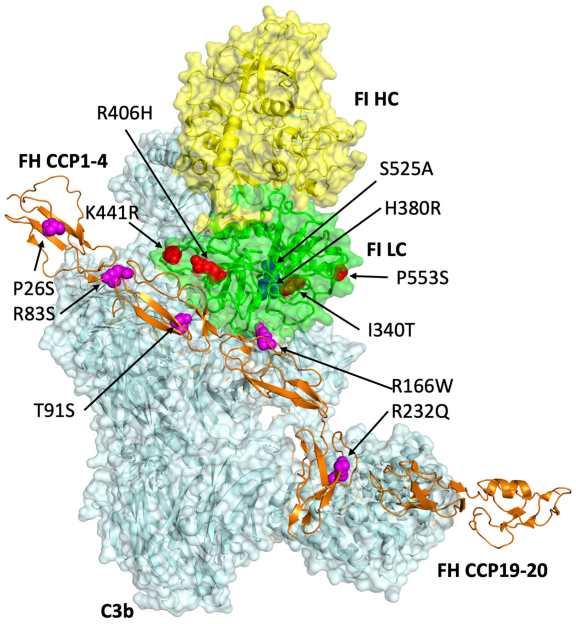

FIGURE 1
Modelling of genetic variants in *CFI* and *CFH*. Produced in Pymol V2.0 (Schrodinger LLC) using the PDB file 5o32 (Xue et al., 2017), this 3D model of FI (heavy chain: yellow; light chain: green) bound to C3b (pale cyan) and FH CCPs 1-4_19-20 (orange) displays the putative sites of amino acid residues altered by the mutations (FI: red spheres; FH: magenta spheres) identified in *CFI* and *CFH* interrogated by the present study. The FI catalytic triad including S525 is shown by blue spheres.

Methods

Protein production

Generation of FH CCP 1-4 variants in *Pichia Pastoris* (KM71H, ThermoFisher) was performed as previously described (26, 27). Primers for *CFH*1-4 mutagenesis are described in Supplemental Table 1.

FI variants were produced in HEK293T (ThermoFisher) using a polycistronic IRES vector with *Furin* and the full *CFI* cDNA sequence (NM_000204.4) designed using VectorBuilder. Full details are described at en.vectorbuilder.com/vector/VB171219-1127wqz.html. Site-directed mutagenesis was performed as described previously to introduce single (active backbone) and double (inactive backbone; given variant plus S525A) within *CFI* before transfection of HEK293T with cDNA was performed using JetPEI (Polyplus). Primers for *CFI* mutagenesis are described in Supplemental Table 2. Single clones expressing FI were selected and standard culturing of HEK in multilayer flasks resulted in the generation of supernatant for purification of FI using NHS activated HiTrap (Cytivia) affinity columns coupled with OX21 (mAb to human FI, Merck, UK) and elution with 0.1M glycine pH 2.7.

Fluid phase cofactor assays

Factor H CCP 1-4

To detect differences in efficacy of the various FH CCP 1-4 variants in acting as a fluid phase cofactor for FI in the AP regulatory TMC, each was tested in a standard C3b co-factor assay modified from Kavanagh et al. (20). In brief, 5µL of each FH1-4 protein [or full-length factor H (FLFH) as an additional control (Complement Technologies Inc. (CompTech), A137)], at 50ng/µL, was added to 1µL of C3b (A114, CompTech, 1µg/µL), and 5µL of 20ng/µL FI (A138, CompTech), made up to a total of 15µL with PBS and incubated for 30 mins at 37°C. The products were separated using a 10-20% SDS-PAGE gel under standard reducing conditions and visualised by Coomassie blue staining. Molecular weights were compared to a PageRuler™ prestained Protein ladder (10 – 250 kDa) (ThermoFisher). Breakdown of the C3b α'-chain for each test reaction was measured using densitometry performed in ImagStudio™ Lite (Licor) and normalised to the beta chain as a loading control. To control for inter-assay differences between 3 repeated measurements the normalised α' chain -remaining result was given as a ratio of the normalised C3b α' chain remaining of a negative control that was included in each assay (i.e. C3b and FI only).

Factor I

For each FI variant tested, purified FI was added to 1µL of C3b (CompTech, A114, 1µg/µL), and 2.5µL of 155ng/µL FLFH (CompTech, A137) or 200ng/µL FH1-4 (in-house, Pichia recombinant) in a 0.6mL Eppendorf. Each reaction mixture was made up to a total volume of 15µL with PBS and incubated at 37°C. The amount of FI and the incubation duration depended on the cofactor used. Thirty nanograms of FI and a 15-minute incubation was utilised for reactions with FH1-4, whereas FLFH reactions required 10ng FI and a 15-minute incubation. Density of the C3b α' -chain remaining was measured and normalised as described for FH1-4 variant cofactor assays.

Dominant negative assay

Increasing concentrations of inactive FI variants were added to WT FI in standard fluid phase CA assay tests. Twenty µg/mL S525A FI, or 40µg/mL I340T or H380R FI was serial diluted resulting in 7.5µL of (40), 20, 10, 5, 2.5 (and 1.25) µg/mL S525A (or I340T or H380R FI) being added to each standard WT test (10µg/mL), respectively, before being incubated for 60 mins at 37°C and separated by SDS-PAGE. Normalised density of the α' -chain remaining was calculated as described for FH1-4 cofactor assays.

BIAcore SPR

C3b coupling amine and thiol

Using the BIAcore S200, a Series S carboxymethyl 5 (CM5) sensor chip (both Cytivia, UK) was coupled with either 800 or

1000 RU (response units) of C3b by standard amine coupling following manufacturer's instructions (Amine Coupling Kit, Cytiva, UK). Briefly, purified C3b (CompTech, A114) was immobilised on a single flow cell of the CM5 chip by flowing 5µg/mL protein, diluted in 50mM sodium acetate at pH 4.5, whilst a second flow cell was activated and blocked for reference.

Alternatively, in order to couple C3b to the chip surface *via* nucleophilic attack on its thioester domain, after the immobilisation of a nidus of C3b by amine coupling as described previously (28) (100RU), FB and FD (CompTech, A135 and A136 at 500nM and 60nM, respectively) were injected for 60s at 10µL/min to build the AP C3 convertase on the chip-bound C3b (C3bBb). Next, C3 (A114, CompTech, at 0.1mg/mL) was injected immediately across the surface of the flow cell for 180s at 10µL/min, so that the C3 was cleaved to C3b by the chip-bound convertase. Rapid nucleophilic attack on the internal thioester resulted in covalent binding of C3b to the surface through an ester bond. Several subsequent cycles of convertase formation and C3 cleavage resulted in 800-1000RU of C3b covalently immobilised on the chip surface in a physiological orientation.

FH CCP 1-4 affinity to C3b

After size exclusion of the 5 FH1-4 variants and WT into HEPES buffered saline with surfactant Tween 20 (HBST) (10mM HEPES, 140mM NaCl, 0.05% surfactant P20) or PBS, the proteins were concentrated 10-fold using 10kDa molecular weight cut-off Vivaspin columns (Sigma-Aldrich). The 6 proteins (WT, P26S, R83S, T91S, R166W, R232Q) were flowed over both the blank flow cell (Fc) and the C3b -immobilised Fc (i.e., Fc1 to 2) at concentrations ranging from 20µM to 0.3125µM, produced by a serial 1:2 dilution in HBST or PBST (PBS with 0.05% Tween 20), for 90s at a rate of 30µL/min. Following an 120s dissociation period, the Fcs were regenerated between each variant injection using 10mM sodium acetate and 1mM NaCl for 45 seconds at 20µL/min. Data were collected at 40Hz with a 120s stabilisation period between each sample. Buffer-only controls were included at several points during the automated run and data were double-referenced to the blank Fc and blank injections. Steady state responses were plotted using the S200 BIAevaluation software (Cytiva) and utilised to calculate estimated affinity (K_D) of the variants to C3b (in µM) for each variant.

DAA Assay for FH1-4 variants

FB and FD (CompTech, A135 and A136 at 500nM and 60nM, respectively) were injected for 90s onto an 800RU C3b amine coupled CM5 chip to build a surface bound C3 convertase. The C3bBb complex was allowed to decay for 90s before 250nM FH1-4 variants were injected for 60s and decay accelerating activity of the FH1-4 proteins were compared to a negative (no FH) control. Injections were made at 20µL/min and data was collected at 40Hz. HBST supplemented with 1 mM MgCl was used as the running and dilution buffer. The flow cells were regenerated after each convertase build with an injection of pH 4 10mM sodium acetate and 1M NaCl for 40 seconds at 30µL/min.

TMC building for FH CCP 1-4 and FI variants

For FH variant testing, inactive FI (S525A) at a constant (118nM) concentration was injected with FH1-4 serially diluted 1:2 from 118nM to 14.75nM in PBST+Mg^{2+} (PBS with 0.05% Tween 20 and 1mM $MgCl_2$). Injections of FH1-4 (118-14.75nM) and FI (118nM) were made onto a C3b -coupled CM5 chip (1000RU thiol-coupled) at the given concentrations for 2 mins at 30 µl/min, with a 500 second dissociation time. These injections were all performed in PBST+Mg^{2+} buffer at 25°C. The flow cells were regenerated between each step with an injection of pH 4 10mM sodium acetate and 1M NaCl for 40 seconds at 30µL/min after the end of each test, prior to the next injection of TMC building component -containing buffer. In all experiments, FH1-4 and FI were injected independently to control for bimolecular complex responses. Data were collected at 40Hz.

For FI variant testing using the AP regulatory TMC building assay, FI variants on the inactive backbone were serially diluted 1:2 in PBST+Mg^{2+} buffer from 125nM to 15.625nM, whilst FH1-4 was kept at a constant concentration of 125nM for each test injection and TMC build.

To test AP regulatory TMC formation with active FI at 25°C, 118nM of FH1-4 and 118nM WT (active) FI were injected simultaneously.

To test AP regulatory TMC formation with I340T or H380R FI, 125nM of FH1-4 and 125nM I340T/H380R FI were injected separately and simultaneously.

All TMC building tests were repeated at least twice, with variants compared a minimum of once on thioester-coupled (shown in main text Figures) and once on amine-coupled (shown in Supplemental Data) CM5 chip surfaces.

Dominant Negative SPR experiment

Inactive WT (S525A) FI (125nM) was injected with WT FH1-4 (125nM) to form a WT TMC as standard as described earlier. To determine the dominant negative effect, I340T FI was injected at 250nM with inactive WT FI and WT FH1-4 (both at 125nM).

Haemolytic sheep red blood cells (SRBC) cofactor assay

Haemolysis assays were performed as per those described in Tortajada et al. (29) with some modification. FI variants were titrated 1:2 8 times in a 96-well plate in complement fixation diluent (CFD) [supplemented with 2µg/mL FH (CompTech)] before incubation with C3b-coated SRBC for 10 mins at 37°C.

Washing and incubation with FB (20μg/mL) and FD (2μg/mL) followed by further washing and incubation with 2% Guinea pig serum in 10mM EDTA resulted in lysis of the cells dependent on FH1-4 concentration. A 0% lysis control with no FD/FB incubation was used to normalise and give % protection plotted. Data is representative of 3 experimental repeats performed in duplicate.

Statistical analysis

All statistical analysis presented herein was performed using GraphPad Prism V8 (GraphPad Software, La Jolla, CA, USA). For fluid phase CA assays, data were expressed as means +/- SD and standard t-tests were used to identify any differences in activity between variants and the WT protein. For haemolytic SRBC assays mean +/- SD for individual points is plotted by bars and IC50s with 95% confidence intervals were calculated using the 'normalised response (4 parameter fit)' non-linear model.

Results

Generation of fully processed factor I

Fully processed FI with no evidence of unprocessed pro-I on SDS-PAGE (Figures 2A–C) was generated using an IRES vector containing *Furin* and *CFI* genes (Figure 2D). The recombinant FI generated using the *Furin-IRES-CFI* vector demonstrated equivalent activity to FI purified from human serum (Figure 2E and Supplemental Figure 1). Using this template an inactive FI variant was generated for use in real-time AP TMC regulatory complex analysis. Mutation of the proteolytic serine residue S525 to an alanine (S525A FI) prevented proteolysis of C3b (25) (Figures 3A, B; Supplemental Figure 2).

Variant selection and protein preparation

Rare variants in *CFI* and *CFH* associated with AMD (Supplemental Tables 3, 4) [FI: I340T (13, 20, 30–32), R406H

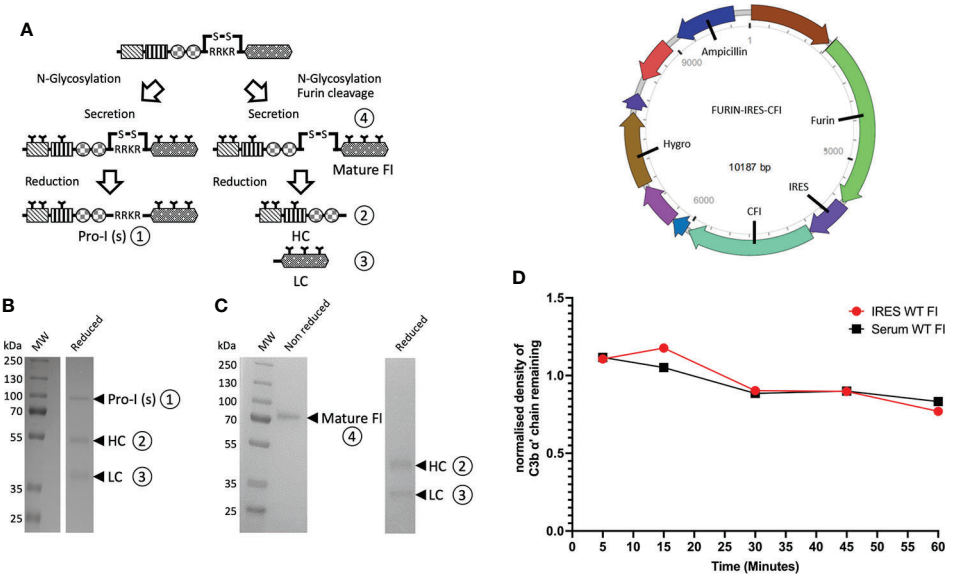

FIGURE 2
Utilisation of an IRES vector to produce fully processed FI in mammalian cells. **(A)** FI is synthesized as a single polypeptide chain precursor [pro-I]-81 kDa. Upon translocation to the endoplasmic reticulum, and prior to secretion, pro-I undergoes post-translational processing involving cleavage at its linking peptide (RRKR) and N-glycosylation of both chains. In mammalian cells transfected with a vector containing only the *CFI* gene, not all of the pro-I undergoes cleavage of the RRKR linker peptide. This results in secretion of an N-glycosylated pro-I [pro-I(s)] ① of 88 kDa and a mature disulphide-linked FI ④ consisting of a 50 kDa heavy chain (HC) ② and a 38 kDa light chain (LC) ③. The incomplete cleavage of the pro-I form is thought to be due to the high expression of the protein that saturates the cleaving ability of the cells. **(B)** Reduced SDS-PAGE of historic generation of recombinant FI demonstrating a mixture of uncleaved inactive Pro-I (s) ① and the HC② and chain ③ of fully processed mature FI. **(C)** Reduced and non-reduced SDS-PAGE gel of recombinant FI using our optimised *Furin-IRES-CFI* vector demonstrating only mature FI ④ with no Pro-I(s) on the reduced gel. **(D)** A map of the *Furin-IRES-CFI* vector by VectorBuilder: https://en.vectorbuilder.com/vector/VB171219-1127wqz.html. **(E)** C3b α' chain degradation analysis of the fluid-phase activity of IRES WT FI compared to serum purified FI, over time. Plotted is the density of C3b α' chain remaining (y-axis) after incubation with recombinant or serum purified FI with C3b and FH across a range of timepoints (5 – 60 minutes) at 37°C during a fluid-phase cofactor assay. The density of the α' chain band was normalised to the density of the β chain band, before the resultant Figure was normalised to a negative control containing no FI, giving a proportion of α' chain remaining compared to the no FI control.

10.3389/fimmu.2022.1028760

(13, 16, 30, 31), K441R (13, 16, 30, 31), P553S (13, 16, 30, 31) and FH CCP 1-4: P26S (33), T91S (33), R166W (33), R232Q (33)] were modelled within the context of the AP regulatory TMC (25) (Figure 1). FH variants were generated in the framework of the N-terminal domains of FH, CCPs 1–4, as previously described (34) (Supplemental Figure 3A). FI variants were produced using the *Furin-IRES-CFI* vector (Supplemental Figures 3B, C). Additionally, we generated R83S *CFH*, which is a highly deleterious C3 glomerulopathy (C3G)-associated non-functional variant that was used a positive control for dysfunction (27) and H380R *CFI*, which was identified in a patient with clinical *CFI* deficiency (35) and was predicted to be inactive due to mutation of the FI active site (36).

Rare AMD -linked *CFH* Variant characterisation

CCP1-4 FH variants were characterised by standard assays prior to analysis of TMC formation. Fluid phase cofactor activity (CA) assays with FI and C3b revealed observable (Figure 4A) and statistically significant (Figure 4B) reductions in C3b α' chain degradation by R83S (P = 0.0006), R166W (P = 0.0075) and R232Q (P = 0.0082) (64%, 58% and 41% reduced compared to WT, respectively). Meanwhile, P26S and T91S had similar fluid phase CA to the WT protein (4% and 3% reduced compared to WT, respectively).

Variants were further analysed by measurement of affinity (K_D) to C3b using surface plasmon resonance (SPR). Assays were performed twice, once in HBST and once in PBST (PBST shown). The WT showed similar C3b binding affinity to FH CCP1-4 to previous publications, with an approximate K_D of 10μM (26, 27, 37). P26S and T91S bound C3b with similar affinity to WT (K_D ~11.5 and ~9.4 μM, respectively) whilst R166W showed reduced affinity (~16.7μM). R83S and R232Q were broadly abrogated in C3b binding even at high (20μM) concentrations and as such their C3b affinities were designated as not calculable (NC) (Figure 4C).

Furthermore, measurement of decay accelerating activity (DAA) by SPR consistently revealed that R83S and R232Q had a near total loss of DAA of the AP C3 convertase consistent with their lack of binding to C3b. Meanwhile, R166W, P26S and T91S had only minor reductions in function in the DAA assay (Figure 5). Strikingly, R166W showed disproportionately reduced CA compared to DAA.

Real-time analysis of FH variants in formation of the AP regulatory tri-molecular complex

Assessment of the formation of the AP regulatory tri-molecular complex using SPR is complicated by cleavage of the substrate C3b by active FI protein (Supplemental Figure 4). To overcome the issue of substrate cleavage, the inactive (S525A) FI variant was used in the formation of the AP regulatory TMC

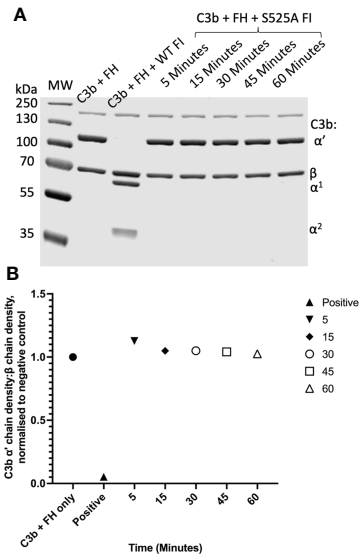

FIGURE 3
Fluid phase analysis of inactive (S525A) FI. **(A)** SDS-PAGE demonstrates a lack of proteolytic activity of IRES S525A FI across a range of timepoints (5 – 60 minutes). Activity was assessed by the ability of factor I in combination with its cofactor, FH, to cleave C3b to its inactive form, iC3b. C3b cleavage was indicated by the generation of the α1 (68kDa) and the two α2 (46kDa, 43kDa) bands as demonstrated by the WT FI (positive) control. **(B)** Lack of activity of S525A FI – densitometry analysis. Licor ImageStudio Lite with median background subtraction was utilised to perform densitometry analysis on the SDS-PAGE gels revealing no activity of the S525A FI. The density of the α'-chain was given as a ratio of the β-chain density before being normalised to a negative control (with no FI) to give a relative density of the α'-chain remaining for each reaction.

to facilitate real-time analysis of the effect of FH variants on TMC formation as measured by SPR (Figure 6). Injections of WT FH CCP1-4 with inactive FI onto a C3b thiol coupled surface revealed the formation of synergistic complexes; these were larger and long lasting compared to the bi-molecular complexes formed by C3b and FH1-4 (Supplemental Figure 5). The results were consistent with the earlier standard CA assays with 59nM injections of R166W (7RU), R232Q (6RU) and R83S (5RU) displaying minimal TMC formation compared to WT, whilst P26S (29RU) and T91S (30RU) generated peak RUs of approximately 75% that of WT (40RU) TMC.

Comparison of FH variant TMC formation efficacy was equivalent when C3b was tethered by amine coupling (Supplemental Figure 6) or covalently bound through nucleophilic attack on the internal thioester of nascent C3b. Although responses were higher and the orientation physiological in the thiol-coupled method, C3b bound to the chip *via* targeting of its thioester bond is hydrolysed in a time-dependent manner. Therefore, the AP convertase, C3bBb, was generated at the start and end of each experiment as a measurement of surface stability showing ~12% loss of surface

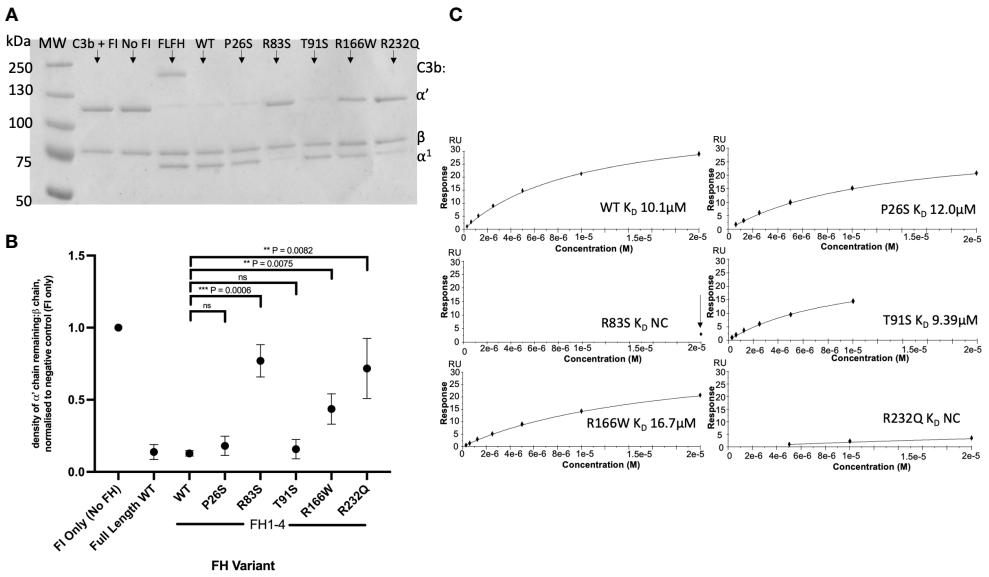

FIGURE 4
Characterisation of AMD –linked FH CCP 1-4 Variants. **(A)** Fluid phase cofactor assays for FH1-4 variants. Separation of FI -cleaved C3b products by SDS-PAGE followed by Coomassie staining was used to reveal the α′, β and α1 chains of C3b. **(B)** Densitometry analysis of C3b breakdown by each FH1-4 variant. The mean (+/- SD) density of the normalised α′-chain present in the products of 3 fluid phase reactions is plotted for each FH 1-4 variant. The density of the α′-chain was given as a ratio of the β-chain density before being normalised to a negative control (with no FH CCP 1-4) to give a relative density of the α′-chain remaining for each reaction. Higher (closer to 1) α′-chain remaining suggests reduced cofactor activity of the FH CCP 1-4 variants. A standard t test was used to compare mean normalised α′-chain remaining values for each variant vs the WT. **P < 0.01; ***P < 0.001. ns = non-significant. **(C)** 20μM (and 6 subsequent 1:2 serially diluted concentrations) of each FH CCP 1-4 variant and WT was injected onto a C3b –coupled CM5 chip (800-1000RU) to give an estimated K_D binding affinity of each variant to C3b after analysis by SPR using a BIAcore S200. SPR Figures are representative of at least 2 repeats.

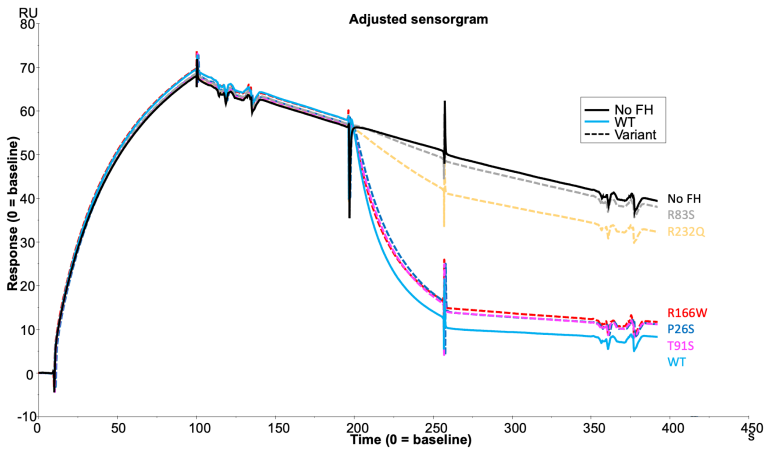

FIGURE 5
DAA Assay for AMD -linked FH CCP1-4 Variants. C) Each FH CCP 1-4 variant and WT was injected at 250nM onto a C3b -coupled CM5 chip (800RU) after building of the AP C3 convertase to reveal the DAA of each variant compared to WT and a no FH1-4 injection as measured by SPR using a BIAcore S200. SPR Figures are representative of at least 2 repeats.

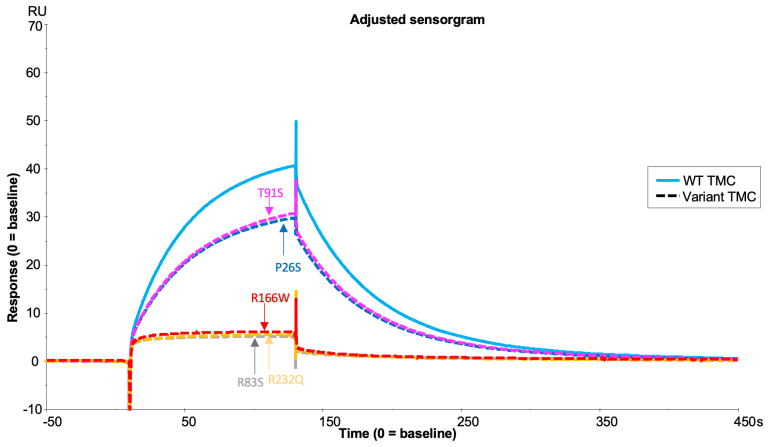

FIGURE 6
TMC building SPR assay for FH1-4 variant analysis. Each FH CCP 1-4 variant was injected at 59nM with 118nM of S525A FI onto a C3b (1000RU) thiol –coupled CM5 chip surface and analysis by SPR revealed real-time binding of the AP regulatory TMC for each variant and the WT. SPR Figures are representative of at least 2 repeats.

activity (Supplemental Figure 7A). The amine coupled surface, however, exhibited no loss of C3b between the first convertase injection and the last during an otherwise identical experiment (Supplemental Figure 7B).

Rare AMD-linked *CFI* Variant Characterisation

Fully processed FI variants (with no pro-I) were first characterised using fluid phase CA assays measuring proteolytic cleavage of the C3b α' chain. These fluid phase assays revealed similar levels of activity for R406H (5.5% reduced) and K441R (9% reduced) compared to WT, whilst P553S (14.4% reduced vs WT, P = 0.046) had significantly reduced C3b cleavage with full length FH as the cofactor (Figures 7A, B). The fluid phase CA assay data were corroborated by a haemolytic C3b cofactor assay on sheep erythrocytes, demonstrating that WT, K441R, R406H and P553S had similar ability to protect C3b-coated sheep RBC from complement AP mediated lysis, albeit that R406H and P553S exhibited minor non-significant reductions in efficacy (Figure 7C).

Real-time analysis of FI variants in formation of the AP regulatory trimolecular complex

Analysis of the TMC is hindered by the FI variants possessing C3b-cleaving activity (e.g. R406H, K441R, P553S) as the complex rapidly dissociates following cleavage. To circumvent this, we generated the FI variants on an inactive (S525A) FI variant backbone (e.g. double mutant proteins: R406H/S525A; K441R/S525A; P553S/S525A). This facilitated real-time visualisation of TMC formation for each FI variant versus the inactive WT (e.g. WT/S525A) (Figure 8). When the TMC was assembled on a C3b thioester-coupled surface, inactive P553S formed substantially less TMC compared to the inactive WT FI protein as measured by SPR after injection at 62.5nM (62.9 RU, 65% of WT). Inactive R406H showed a minor reduction in efficacy in this assay (74.6 RU, 77% of WT), akin to the effects of P26S and T91S in the FH1-4 variant analysis. Meanwhile, K441R TMC building activity was almost identical to the WT inactive protein (91.2 RU, 94% of WT). These findings agreed with fluid phase and haemolytic assay data and the trend was also replicated when building TMCs on an amine C3b -coupled surface (Supplemental Figure 8).

Dominant Negative effect of *CFI* Variants in fluid phase cofactor assays

Real-time SPR analysis demonstrated that inactive FI (S525A) formed stable, long lasting C3b:FH:FI complexes compared to active FI (Figure 9 and Supplemental Figure 9). This implied that secreted inactive variants in *CFI* may cause a competitive inhibitory effect on the WT FI protein. To test this hypothesis, increasing concentrations of S525A were added to WT FI in a fluid phase CA assay demonstrating a concentration-dependent inhibition of WT activity. Cleavage was reduced by 15% at equimolar concentrations, and by 20% at 2-fold molar concentrations. (Figures 10A, B).

Although S525A is not a reported mutation in patients, a review of patient associated mutations revealed several variants that would be predicted to have a similar effect: I340T [AMD

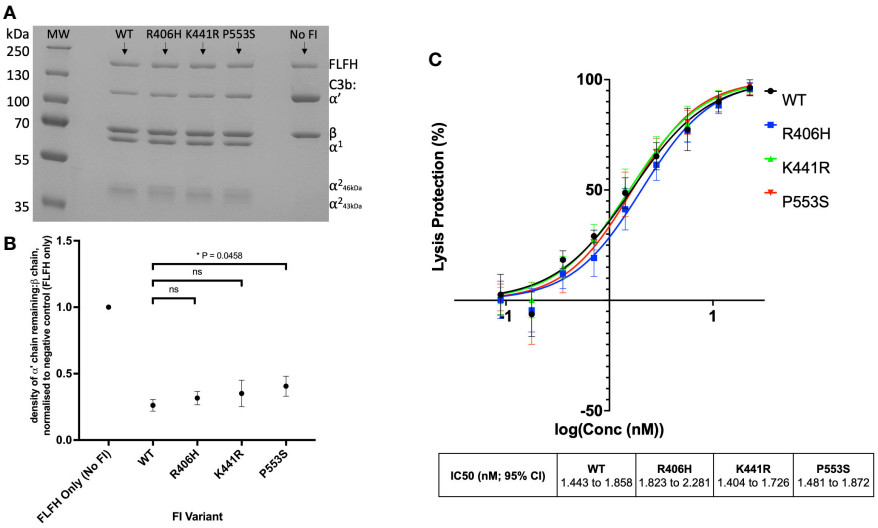

IC50 (nM; 95% CI)	WT	R406H	K441R	P553S
	1.443 to 1.858	1.823 to 2.281	1.404 to 1.726	1.481 to 1.872

FIGURE 7
Characterisation of AMD –linked CFI Variants. **(A)** Fluid phase cofactor assays for FI variants. Separation of C3b products by SDS-PAGE followed by Coomassie staining was used to reveal the α′, β and α1 chains of C3b. **(B)** Densitometry analysis of C3b breakdown by each FI variant. The mean (+/- SD) density of the normalised α′-chain present in the products of 3 fluid phase reactions is plotted for each FI variant. The density of the α′-chain was given as a ratio of the β-chain density before being normalised to a negative control (with no FI) to give a relative density of the α′-chain remaining for each reaction. Higher (closer to 1) α′–chain remaining suggests reduced cofactor activity of the FI variants. Fluid phase assays were repeated 3 times and a standard t test was used to compare mean normalised α′-chain remaining values for each variant vs the WT FLFH = full-lenght factor H. *P < 0.05. ns = non-significant. **(C)** Haemoltyic assays of CA for FI variants. Fi variants were titrated through C3b-coated SRBCs before the AP C3 convertase was built on any C3b remaining on the cell surfaces. Cells were lysed with Guinea pig serum in an FI concentration dependent manner with a readout of OD at 412nm. The efficacy of each FI variant was calculated using a non-linear 4-parameter fit curve after normalization to no FI (100%) and 0% (buffer only) lysis controls and IC50s are given with 95% CIs. Each plotted point is % protection from lysis compared to the 0% lysis control and bars represent SD for each point calculated from 3 experimental repeats run in duplicate.

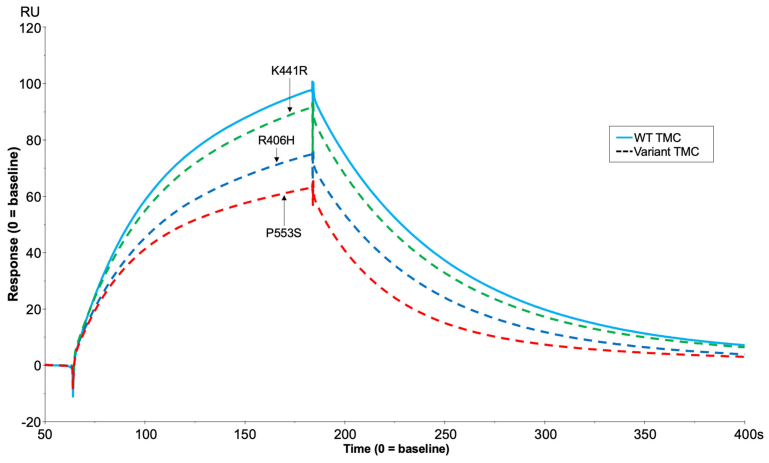

FIGURE 8
TMC building SPR assay for FH1-4 variant analysis. Each inactive FI variant (S525A+R406H/K441R/P553S/WT) was injected at 62.5nM with 118nM of FH CCP1-4 onto a C3b (1000RU) thiol -coupled CM5 chip surface and analysis by SPR revealed real-time binding of the AP regulatory TMC for each variant and the WT. SPR Figures are representative of at least 2 repeats.

10.3389/fimmu.2022.1028760

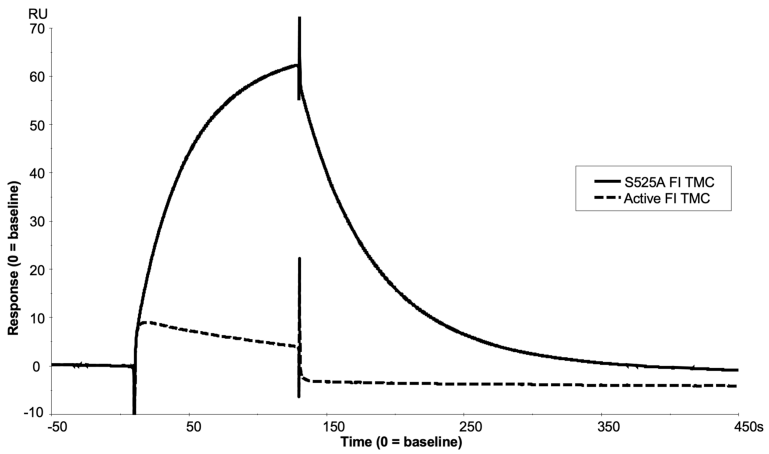

FIGURE 9
SPR analysis of the inactive FI variant vs active FI. Injection of 118nM of active FI with 118nM of FH1-4 onto a C3b thiol coupled (1000RU) CM5 chip resulted in near immediate loss of C3b on the chip surface as shown by a downward trend in RU vs time (dashed line) upon injection, exhibiting loss of FH1-4 binding affinity to iC3b vs C3b. Meanwhile, injection of 118nM of inactive FI and 118nM of FH1-4 onto the same surface resulted in the building of a comparably large AP regulatory TMC (of ~60RU) (solid line) which did not immediately dissociate when the injection finished at 120 seconds.

(31), atypical haemolytic uraemic syndrome (aHUS) (20)] and H380R [functional FI deficiency (35)], D519N and D524 [aHUS (20)]. Two variants, I340T and H380R, were taken forward for further analysis due to their existence in AMD and topology within the FI active site, respectively.

Neither I340T nor H380R demonstrated any enzymatic activity in fluid phase CA assays, as shown in "C1" lanes in Figure 11A and Supplemental Figure 10A, respectively. When increasing concentrations of I340T or H380R were added to WT FI in a fluid phase CA assay, competitive inhibition was demonstrated. I340T was shown to inhibit the activity of the WT protein by ~25% at equimolar concentrations, and by 30% at 2-fold molar concentrations (Figure 11B). H380R was shown to inhibit the activity of the WT protein by ~20% at equimolar and 35% at 2-fold molar concentrations (Supplemental Figure 10B). An additional test for non-specific protein interference in fluid phase kinetics was performed using human serum albumin (HSA); and no concentration-dependent blocking effect was demonstrated with this serum-abundant protein (Supplemental Figure 11). These data provide evidence that the inactive FI dominant negative effect is a specific effect of FI interaction with C3b and/or FH that does not result in cleavage of C3b but does competitively inhibit the activity of WT FI.

Real-time analysis of TMC formation in the presence of disease-linked inactive FI variants

To further assess the biological impact of the inactive FI variants, SPR was undertaken with single mutants. As with the mutant S525A, the patient associated mutation, H380R, could bind to C3b:FH complexes without cleavage of the surface bound substrate, explaining its competitive inhibition of WT active FI (Supplemental Figures12). However, unlike with H380R and S525A FI, when I340T was injected with FH1-4 there was no evidence of a TMC being formed (Figure 12), yet when I340T FI alone was injected at higher concentrations (350nM) onto a C3b coupled surface, some direct interaction with C3b was observed (Supplemental Figure 13). Further, addition of I340T at 2-fold molar concentration [vs S525A FI (125nM)] during formation of WT inactive (S525A) TMC resulted in ~25% lower maximum RU in keeping with the CA assays and confirming the competitive effect (Figure 13).

Wider applicability of the TMC building assay

AP regulatory TMCs were also assembled on the SPR chip with FH-like protein 1 (FHL-1), soluble complement receptor 1 (sCR1, CD35) (TP10) and membrane cofactor protein (MCP, CD46) (Supplemental Figures 14, 15). This opens the possibility to interrogate the functional impact of variants in these other cofactors which will be important in other complement mediated diseases such as paroxysmal nocturnal haemoglobinuria (38), aHUS (39) and C3G (40).

Discussion

The ability to produce recombinant fully processed FI is a significant methodological advance which underpins this study.

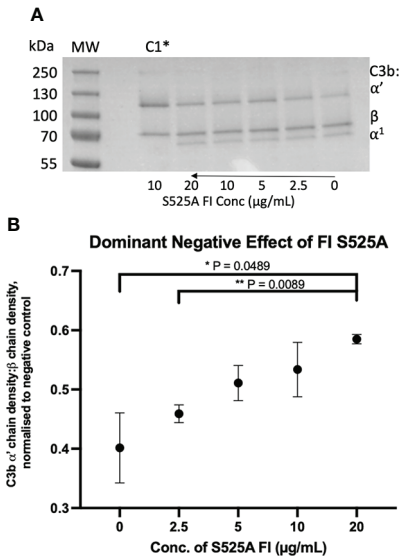

FIGURE 10
Identification and characterisation of a dominant negative effect in a model inactive FI variant. **(A)** Fluid phase assay revealed a dominant negative effect of inactive (S525A) FI on active FI. Addition of 5μL of 0, 2.5, 5, 10 and 20 μg/mL inactive FI to a standard FI cofactor assay before incubation resulted in an inhibitory effect as shown by lower levels of breakdown of the C3b α′-chain when 20μg/mL inactive FI was spiked compared to a 0μg/mL control lane. *C1 = Control 1 (negative control including C3b, FH1-4, S525A and no WT FI. **(B)** S525A dominant negative effect – densitometry analysis. Licor ImageStudio Lite with median background subtraction was utilised to perform densitometry analysis on the SDS-PAGE gels resulting from 2 individual repeats of the S525A dominant negative fluid phase assay described. Graphpad prism V8 was utilised to test for differences between tests and mean +/- SD is plotted. *P < 0.05; **P < 0.01. C1 = control 1 [C3b, FH1-4 and S525A FI only (no WT FI)].

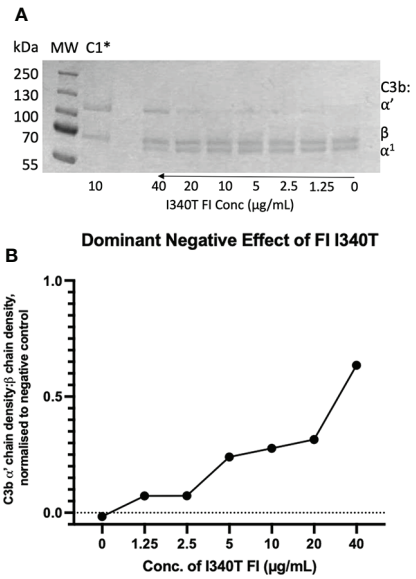

FIGURE 11
Identification and characterisation of a dominant negative effect in an AMD -linked FI variant. **(A)** Fluid phase assay revealed a dominant negative effect of I340T FI upon active WT FI. Addition of 5μL of 0, 1.25, 2.5, 5, 10, 20 and 40 μg/mL I340T FI to a standard FI cofactor assay before incubation resulted in an inhibitory effect as shown by lower levels of breakdown of the C3b α′-chain when 40 μg/mL inactive FI was spiked compared to a 0 μg/mL control lane. *C1 = Control 1 (negative control including C3b, FH1-4, I340T and no WT FI. **(B)** I340T dominant negative effect – densitometry analysis. Licor ImageStudio™ Lite with median background subtraction was utilised to perform densitometry analysis on the SDS-PAGE gel resulting from the I340T dominant negative fluid phase assay described. Plotted are densities of C3b α′ -chain remaining normalised to the beta chain for each test and normalised to the negative control (C1) value. Graph produced using GraphPad Prism V8. C1 = control 1 [C3b, FH1-4 and I340T FI only (no WT FI)].

Recombinant FI production has historically yielded a mixture of active FI and inactive pro-I (20, 41) with co-transfection of cells with furin and FI vectors ineffective (41) and ex-vitro cleavage of pro-I inefficient (42).

In AMD, where the manifestation of disease may take decades, the effects of rare genetic variants may be small. Variations in the amount of inactive pro-I contaminating protein preparations may therefore mask small defects in activity. The *Furin-IRES-CFI* vector circumvented these problems, yielding completely processed FI with equivalent activity to serum-purified protein. Additionally, the ability to make fully processed FI allowed us to produce an inactive, fully processed variant to generate a real-time analysis of the AP regulatory TMC to view the activity of variants in FH and FI. The use of SPR to visualise the AP regulatory TMC represents huge potential for analysis of functional effects of AP protein variants.

In analysis of AMD-linked *CFH* variants (summarised in Supplemental Table 5), marked dysfunction in AP regulation was observed in 2 variants: one in CCP 3 (R166W) and another in CCP 4 (R232Q) (25, 43, 44). R232Q resides in CCP 4 and forms part of a contact region with macroglobulin (MG) 1 and thioester (TED) domains of C3b. It is highly deleterious, abrogating both CA and DAA due to impaired C3b binding and consequently a failure to form the regulatory TMC. R232Q replicates the effects seen in the C3G-associated R83S variant which likewise perturbs a contact patch between C3b and the terminal region of FH CCP 1 and the CCP 1-2 linker to the α′ N-terminal region and MG7 domain in C3b.

In contrast to R232Q, R166W sits in the third contact site with the CUB domain of C3b but also at the interface with the SP domain of FI (25, 43, 44). Its affinity for C3b was affected mildly (16-20μM vs 10μM in the WT protein) with a minor decrease in DAA. In comparison, CA activity was markedly reduced and TMC formation was profoundly affected with the slightly higher RU compared to R83S and R232Q reflecting the maintained ability of R166W to bind C3b.

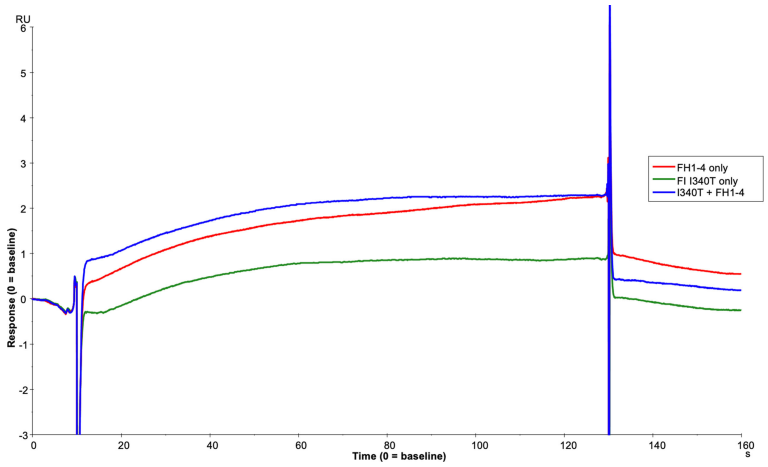

FIGURE 12
I340T does not form a TMC with C3b and FH CCP1-4. Using the BIAcore S200, FH1-4 (red line) and I340T FI (green line) were injected at 125nM individually and in combination (blue line) onto a 1000RU C3b coupled CM5 chip surface. I340T FI did not display synergy with FH1-4 indicating no or minimal formation of the AP regulatory TMC.

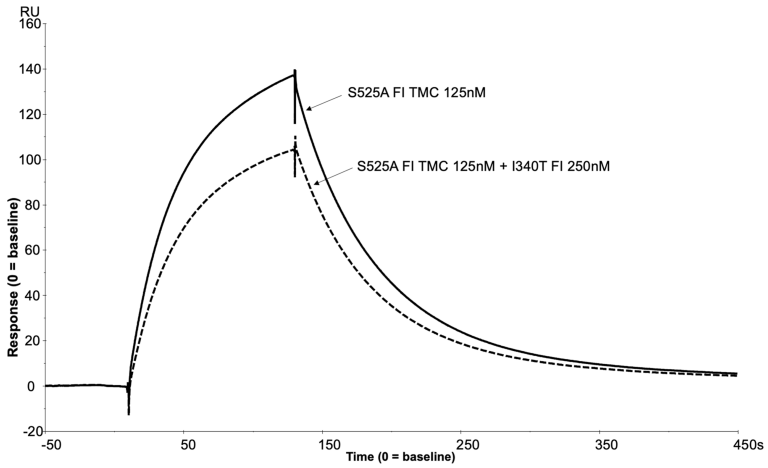

FIGURE 13
SPR reveals I340T FI inhibits formation of the AP regulatory TMC. To build an AP regulatory TMC 125nM of inactive WT FI and 125nM of FH CCP 1-4 was injected onto a C3b thiol coupled (1000RU) CM5 chip (solid line). A further TMC was built by injection of 125nM of Inactive WT FI, 250nM of I340T FI and 125nM of FH CCP 1-4 onto the same thiol coupled chip (dotted line). Addition of the I340T FI protein resulted in an ~25% lower maximum RU compared to inactive WT FI only as measured by SPR on the Biacore S200. SPR assays are representative of at least 2 independent experiments.

The remaining 2 variants, P26S and T91S, displayed only minor differences in CA, DAA and TMC building, exhibiting levels of defect similar to the common I62V risk SNP for AMD (26, 29). As both P26S and T91S are solvent exposed and not predicted to interact directly with either FH or FI, any effect is likely due to minor steric alteration introduced by the variants (25, 43, 44).

Three analysed AMD associated FI variants (R406H, K441R and P553S) demonstrated the ability to cleave C3b (as summarised in Supplemental Table 5). Fluid phase CA assays demonstrated non-significant reductions in C3b cleavage efficacy by R406H and K441R, while P553S demonstrated a significant, albeit small, reduction compared to WT FI. Our real-time assessment of these variants on an inactive FI backbone correlated closely with the CA assay results. P553S demonstrated the largest reduction in TMC formation and R406H and K441R demonstrated less marked defects. Despite the impaired binding and activity, P553S does not interface with either C3b or FH and

is distinct from the catalytic triad (25, 45). P553S resides in a disordered loop in free FI which is stabilized upon formation of the TMC, a process that may be perturbed by the variant impacting substrate binding. The R406H variant is also in an unstructured loop in free FI and when complexed, is at an interface between FH and FI interacting with E123 in CCP 2 of FH suggesting a stabilizing role of this interaction (25, 45). The K441R variant has the least impact of any of the variants analysed, despite a predicted interaction with N136 in CCP 2 of FH (25, 45). The K441R variant does not result in a substantial alteration in charge or size of the side chain at position 441, which may explain this lack of impact.

Previous functional analysis of P553S, R406H and K441R using serum assays and recombinant protein has been contradictory (20–22, 46) likely due to an inability to adequately quantitate mutant vs wild type proteins and/or the level of contamination with Pro-I (20, 21). The real-time TMC binding assay described herein demonstrates that minor alterations in CA at the surface or in the fluid phase can be deciphered by SPR. These data suggest this new method is highly sensitive to changes in the binding efficacies of FI variants to C3b:FH complexes. That predisposing polymorphism in C3, FB and FH have small additive effects (47) reinforces the requirement for accurate analysis of variants.

Additionally, this TMC formation assay has allowed us for the first time to demonstrate dominant negative effects (48) of FI mutants described in AMD, aHUS and functional FI immunodeficiency.

The H380R FI variant was detected in a patient with a clinical complement deficiency (35). H380 along with D429 and S525 form the catalytic triad of FI. With the catalytic site mutated, H380R FI could not cleave C3b and was completely inactive. This allowed the variant to be used in TMC building experiments (without mutating onto an S525A backbone) demonstrating formation of the regulatory complex. Because the SPR analysis shows a slow on, slow off binding pattern, the inactive complexes may exist for considerably longer than active complexes, which appear to cleave C3b instantaneously and destabilise the complex (Figure 9 and Supplemental Figure 9). The fact that H380R FI could readily bind C3b:FH complexes without cleaving C3b, suggested competitive inhibition of WT FI was possible, and this was demonstrated using a CA assay (Supplemental Figure 10). This dominant negative effect would have no consequence in the homozygous proband presenting with immunodeficiency but would be predicted to impair WT function in heterozygous relatives.

The I340T FI variant, which has been identified in aHUS (20) and AMD cohorts (16) also demonstrated a dominant negative effect in fluid phase CA assays. Unlike H380R however, I340T showed little evidence of TMC formation but it did bind C3b and displayed the ability to inhibit WT FI in TMC formation. This is due to loss of the isoleucine that stabilises an oxyanion hole at a catalytic triad interaction site on C3b. Thus, we demonstrated that secreted variants distinct from the catalytic triad which have impaired CA activity but retain the ability to interact with C3b and/or FH, have the capability to competitively inhibit WT FI.

There are further rare *CFI* variants described in aHUS and AMD [D519N, S524V (20)] that result in FI protein with a complete or near complete lack of function which may display a dominant negative effect. In addition to inactive FI variants, FH variants such as R166W may also exhibit a dominant negative effect as a result of almost normal binding to C3b but with an impaired ability to form a TMC impacting C3b cleavage by FI.

The dominant negative effect of inactive FI proteins may have clinical implications since supplementation of FI by sub-retinal gene therapy currently being trialled for the treatment of dry AMD (Gyroscope therapeutics; NCT04566445, NCT04437368) (49) may be less effective in patients with variants like I340T. In these instances, excess FI may need to be added to the eye to counteract the dominant negative effect. It may also be predicted that dominant negative effects in FH variants (e.g. R166W) may similarly impair FH supplementation studies.

In summary, the ability to produce recombinant fully processed FI is a significant technological advance, generating recombinant FI for accurate functional analysis, with the potential for efficient large scale industrial production for use as a biologic, or for incorporation into gene therapy in clinical use.

The method described herein for the building of the complement AP regulatory TMC on a carboxymethyl chip surface and analysis by SPR has the potential to add significant sensitivity and granularity in genetic variant and/or complement drug characterisation for use in clinical trial stratification, diagnostics, drug development and personalised treatment of AMD or other complement -mediated diseases. The dominant negative effect of an inactive FI variant that is secreted could also have implications for therapeutic application and should be taken into consideration when treating patients with AMD and rare *CFI* variants with supplementation therapy.

Data availability statement

The raw data supporting the conclusions of this article will be made available by the authors, without undue reservation.

Author contributions

TH & DK wrote the manuscript. DK, KM and AL, conceived and directed the study. TH, TC, KS-J, VB, AB, EW, VS, DS, NT, and CH, generated & purified proteins, undertook complement functional assays, undertook surface plasmon resonance assays and analysed relevant data. All authors contributed to the article and approved the submitted version.

Funding

The research presented herein was supported/funded by NIHR Newcastle Biomedical Research Centre at Newcastle upon Tyne Hospitals NHS Foundation Trust. DK was funded by Fight for Sight, the Wellcome Trust, the Medical Research Council, Kidney Research UK, and Complement UK. CLH was funded by a grant from Newcastle University. EKSW was funded by Northern Counties Kidney Research Fund and was an MRC clinical research fellow and an NIHR Academic Clinical Lecturer. TMH was funded by Alexion Pharmaceuticals *via* Complement UK. The funder had no involvement in the study design, data collection and analysis, decision to publish, or preparation of the manuscript. VB is a Medical Research Council/Kidney Research UK Clinical Research Training Fellow (MR/R000913/1). KSJ is a Medical Research Council (MRC) clinical research fellow (MR/R001359/1). KJM was funded by the Northern Counties Kidney Research Fund, the Newcastle Healthcare Charities, and a Kidney Research UK project grant (RP7/2015). TEC and AJB.

Conflict of interest

TH has received employment income and equity from Gyroscope Therapeutics, Novartis. EW has received consultancy income from Alexion Pharmaceuticals, Biocryst and Novartis. AL has received consultancy income and equity from Gyroscope Therapeutics and consultancy income from Novartis and Alexion Pharmaceuticals. DS has received consultancy income or funding from Alcon, Bayer Pharmaceuticals, Boehringer Ingelheim, BVI Medical, the Dutch Ophthalmic Research Centre, Gyroscope Therapeutics, Roche, and Alcon. KM has received consultancy income from Freeline Therapeutics and MPM Capital as well as grant income from Gemini Therapeutics and Catalyst Biosciences. CH has recently consulted for Roche, Gyroscope Therapeutics, Q32 Bio, Freeline Therapeutics, Biocryst and Chinook Therapeutics; all income was donated to Newcastle University. CH has received grant income from Ra Pharmaceuticals, and employment income and equity from Gyroscope Therapeutics. DK has received consultancy income and equity from Gyroscope Therapeutics, and consultancy income from Alexion Pharmaceuticals, Novartis, Apellis and Sarepta. DK, KM, CH, TH and TC are authors of patent applications referencing recombinant complement factor I production or formation of the C3b/FH/FI trimolecular complex. TH and CH are employees of Gyroscope Therapeutics, a Novartis company; their contributions to this work were solely at Newcastle University, the opinions are entirely their own and not necessarily those of Gyroscope Therapeutics nor Novartis.

The remaining authors declare that the research was conducted in the absence of any commercial or financial relationships that could be constructed as a potential conflict of interest.

Publisher's note

All claims expressed in this article are solely those of the authors and do not necessarily represent those of their affiliated organizations, or those of the publisher, the editors and the reviewers. Any product that may be evaluated in this article, or claim that may be made by its manufacturer, is not guaranteed or endorsed by the publisher.

Supplementary material

The Supplementary Material for this article can be found online at: https://www.frontiersin.org/articles/10.3389/fimmu.2022.1028760/full#supplementary-material

References

1. Wong WL, Su X, Li X, Cheung CM, Klein R, Cheng CY, et al. Global prevalence of age-related macular degeneration and disease burden projection for 2020 and 2040: A systematic review and meta-analysis. *Lancet Glob Health* (2014) 2:e106–16. doi: 10.1016/S2214-109X(13)70145-1

2. Fritsche LG, Igl W, Bailey JN, Grassmann F, Sengupta S, Bragg-Gresham JL, et al. A large genome-wide association study of age-related macular degeneration highlights contributions of rare and common variants. *Nat Genet* (2016) 48:134–43. doi: 10.1038/ng.3448

3. Fagerness JA, Maller JB, Neale BM, Reynolds RC, Daly MJ, Seddon JM. Variation near complement factor I is associated with risk of advanced AMD. *Eur J Hum Genet* (2009) 17:100–4. doi: 10.1038/ejhg.2008.140

4. Yates JR, Sepp T, Matharu BK, Khan JC, Thurlby DA, Shahid H, et al. Complement C3 variant and the risk of age-related macular degeneration. *N Engl J Med* (2007) 357:553–61. doi: 10.1056/NEJMoa072618

5. Gold B, Merriam JE, Zernant J, Hancox LS, Taiber AJ, Gehrs K, et al. Variation in factor b (BF) and complement component 2 (C2) genes is associated with age-related macular degeneration. *Nat Genet* (2006) 38:458–62. doi: 10.1038/ng1750

6. Hageman GS, Anderson DH, Johnson LV, Hancox LS, Taiber AJ, Hardisty LI, et al. A common haplotype in the complement regulatory gene factor h (HF1/CFH) predisposes individuals to age-related macular degeneration. *Proc Natl Acad Sci USA* (2005) 102:7227–32. doi: 10.1073/pnas.0501536102

7. Edwards AO, Ritter R3rd, KJ A, Manning A, Panhuysen C, Farrer LA. Complement factor h polymorphism and age-related macular degeneration. *Science* (2005) 308:421–4. doi: 10.1126/science.1110189

8. Haines JL, Hauser MA, Schmidt S, Scott WK, Olson LM, Gallins P, et al. Complement factor h variant increases the risk of age-related macular degeneration. *Science* (2005) 308:419–21. doi: 10.1126/science.1110359

9. Klein RJ, Zeiss C, Chew EY, Tsai JY, Sackler RS, Haynes C, et al. Complement factor h polymorphism in age-related macular degeneration. *Science* (2005) 308:385–9. doi: 10.1126/science.1109557

10. Beguier F, Housset M, Roubeix C, Augustin S, Zagar Y, Nous C, et al. The 10q26 risk haplotype of age-related macular degeneration aggravates subretinal inflammation by impairing monocyte elimination. *Immunity* (2020) 53:429–41.e8. doi: 10.1016/j.immuni.2020.07.021

11. Richards A, Kavanagh D, Atkinson JP. Inherited complement regulatory protein deficiency predisposes to human disease in acute injury and chronic inflammatory statesthe examples of vascular damage in atypical hemolytic uremic syndrome and debris accumulation in age-related macular degeneration. *Adv Immunol* (2007) 96:141–77. doi: 10.1016/S0065-2776(07)96004-6

12. Harboe M, Ulvund G, Vien L, Fung M, Mollnes TE. The quantitative role of alternative pathway amplification in classical pathway induced terminal complement activation. *Clin Exp Immunol* (2004) 138:439–46. doi: 10.1111/j.1365-2249.2004.02627.x

13. Seddon JM, Yu Y, Miller EC, Reynolds R, Tan PL, Gowrisankar S, et al. Rare variants in CFI, C3 and C9 are associated with high risk of advanced age-related macular degeneration. *Nat Genet* (2013) 45:1366–70. doi: 10.1038/ng.2741

14. van de Ven JP, Nilsson SC, Tan PL, Buitendijk GH, Ristau T, Mohlin FC, et al. A functional variant in the CFI gene confers a high risk of age-related macular degeneration. *Nat Genet* (2013) 45:813–7. doi: 10.1038/ng.2640ng.2640

15. Maller J, George S, Purcell S, Fagerness J, Altshuler D, Daly MJ, et al. Common variation in three genes, including a noncoding variant in CFH, strongly influences risk of age-related macular degeneration. *Nat Genet* (2006) 38:1055–9. doi: 10.1038/ng1873

16. Kavanagh D, Yu Y, Schramm EC, Triebwasser M, Wagner EK, Raychaudhuri S, et al. Rare genetic variants in the CFI gene are associated with advanced age-related macular degeneration and commonly result in reduced serum factor I levels. *Hum Mol Genet* (2015) 24:3861–70. doi: 10.1093/hmg/ddv091

17. Tzoumas N, Kavanagh D, Cordell HJ, Lotery AJ, Patel PJ, Steel DH. Rare complement factor I variants associated with reduced macular thickness and age-related macular degeneration in the UK biobank. *Hum Mol Genet* (2022) 31 (16):2678-92. doi: 10.1093/hmg/ddac060

18. Jones AV, MacGregor S, Han X, Francis J, Harris C, Kavanagh D, et al. Evaluating a causal relationship between complement factor I protein level and advanced age-related macular degeneration using mendelian randomisation. *Opthalmol Sci* (2022) 2(2):100146. doi: 10.1016/j.xops.2022.100146

19. Dobo J, Kocsis A, Dani R, Gal P. Proprotein convertases and the complement system. *Front Immunol* (2022) 13:958121. doi: 10.3389/fimmu.2022.958121

20. Kavanagh D, Richards A, Noris M, Hauhart R, Liszewski MK, Karpman D, et al. Characterization of mutations in complement factor I (CFI) associated with hemolytic uremic syndrome. *Mol Immunol* (2008) 45:95–105. doi: 10.1016/j.molimm.2007.05.004

21. Java A, Baciu P, Widjajahakim R, Sung YJ, Yang J, Kavanagh D, et al. Functional analysis of rare genetic variants in complement factor I (CFI) using a serum-based assay in advanced age-related macular degeneration. *Transl Vis Sci Technol* (2020) 9:37. doi: 10.1167/tvst.9.9.37

22. Java A, Pozzi N, Love-Gregory LD, Heusel JW, Sung YJ, Hu Z, et al. A multimodality approach to assessing factor I genetic variants in atypical hemolytic uremic syndrome. *Kidney Int Rep* (2019) 4:1007–17. doi: 10.1016/j.ekir.2019.04.003

23. Nilsson SC, Kalchishkova N, Trouw LA, Fremeaux-Bacchi V, Villoutreix BO, Blom AM. Mutations in complement factor I as found in atypical hemolytic uremic syndrome lead to either altered secretion or altered function of factor I. *Eur J Immunol* (2010) 40:172–85. doi: 10.1002/eji.200939280

24. Tan PL, Garrett ME, Willer JR, Campochiaro PA, Campochiaro B, Zack DJ, et al. Systematic functional testing of rare variants: Contributions of CFI to age-related macular degeneration. *Invest Ophthalmol Vis Sci* (2017) 58:1570–76. doi: 10.1167/iovs.16-20867

25. Xue X, Wu J, Ricklin D, Forneris F, Di Crescenzio P, Schmidt CQ, et al. Regulator-dependent mechanisms of C3b processing by factor I allow differentiation of immune responses. *Nat Struct Mol Biol* (2017) 24:643–51. doi: 10.1038/nsmb.3427

26. Pechtl IC, Kavanagh D, McIntosh N, Harris CL, Barlow PN. Disease-associated n-terminal complement factor h mutations perturb cofactor and decay-accelerating activities. *J Biol Chem* (2011) 286:11082–90. doi: 10.1074/jbc.M110.211839

27. Wong EK, Anderson HE, Herbert AP, Challis RC, Brown P, Reis GS, et al. Characterization of a factor h mutation that perturbs the alternative pathway of complement in a family with membranoproliferative GN. *J Am Soc Nephrol* (2014) 25:2425–33. doi: 10.1681/ASN.2013070732

28. Harris CL, Abbott RJ, Smith RA, Morgan BP, Lea SM. Molecular dissection of interactions between components of the alternative pathway of complement and decay accelerating factor (CD55). *J Biol Chem* (2005) 280:2569–78. doi: 10.1074/jbc.M410179200

29. Tortajada A, Montes T, Martinez-Barricarte R, Morgan BP, Harris CL, de Cordoba SR. The disease-protective complement factor h allotypic variant Ile62 shows increased binding affinity for C3b and enhanced cofactor activity. *Hum Mol Genet* (2009) 18:3452–61. doi: 10.1093/hmg/ddp289

30. Geerlings MJ, de Jong EK, den Hollander AI. The complement system in age-related macular degeneration: A review of rare genetic variants and implications for personalized treatment. *Mol Immunol* (2017) 84:65–76. doi: 10.1016/j.molimm.2016.11.016

31. Hallam TM, Marchbank KJ, Harris CL, Osmond C, Shuttleworth VG, Griffiths H, et al. Rare genetic variants in complement factor I lead to low FI plasma levels resulting in increased risk of age-related macular degeneration. *Invest Ophthalmol Vis Sci* (2020) 61:18. doi: 10.1167/iovs.61.6.18

32. de Jong S, de Breuk A, Bakker B, Katti S, Hoyng CB, Nilsson SC, et al. Functional analysis of variants in complement factor I identified in age-related macular degeneration and atypical hemolytic uremic syndrome. *Front Immunol* (2022) 12:789897. doi: 10.3389/fimmu.2021.789897

33. Triebwasser MP, Roberson ED, Yu Y, Schramm EC, Wagner EK, Raychaudhuri S, et al. Rare variants in the functional domains of complement factor h are associated with age-related macular degeneration. *Invest Ophthalmol Vis Sci* (2015) 56:6873–8. doi: 10.1167/iovs.15-17432

34. Wong EKS, Hallam TM, Brocklebank V, Walsh PR, Smith-Jackson K, Shuttleworth VG, et al. Functional characterization of rare genetic variants in the n-terminus of complement factor h in aHUS, C3G, and AMD. *Front Immunol* (2020) 11:602284. doi: 10.3389/fimmu.2020.602284

35. Franco-Jarava C, Alvarez de la Campa E, Solanich X, Morandeira-Rego F, Mas-Bosch V, Garcia-Prat M, et al. Early versus late diagnosis of complement factor I deficiency: Clinical consequences illustrated in two families with novel homozygous CFI mutations. *J Clin Immunol* (2017) 37:781–89. doi: 10.1007/s10875-017-0447-x

36. Fremeaux-Bacchi V, Miller EC, Liszewski MK, Strain L, Blouin J, Brown AL, et al. Mutations in complement C3 predispose to development of atypical hemolytic uremic syndrome. *Blood* (2008) 112:4948–52. doi: 10.1182/blood-2008-01-133702

37. Schmidt CQ, Herbert AP, Kavanagh D, Gandy C, Fenton CJ, Blaum BS, et al. A new map of glycosaminoglycan and C3b binding sites on factor h. *J Immunol* (2008) 181:2610–9. doi: 10.4049/jimmunol.181.4.2610

38. Wong EKS, Kavanagh D. Diseases of complement dysregulation-an overview. *Semin Immunopathol* (2018) 40:49–64. doi: 10.1007/s00281-017-0663-8

39. Brocklebank V, Wood KM, Kavanagh D. Thrombotic microangiopathy and the kidney. *Clin J Am Soc Nephrol* (2018) 13:300–17. doi: 10.2215/CJN.00620117

40. Smith RJH, Appel GB, Blom AM, Cook HT, D'Agati VD, Fakhouri F, et al. C3 glomerulopathy - understanding a rare complement-driven renal disease. *Nat Rev Nephrol* (2019) 15:129–43. doi: 10.1038/s41581-018-0107-2

41. Wong MJ, Goldberger G, Isenman DE, Minta JO. Processing of human factor I in COS-1 cells co-transfected with factor I and paired basic amino acid cleaving enzyme (PACE) cDNA. *Mol Immunol* (1995) 32:379–87. doi: 10.1016/0161-5890(94)00151-p

42. Kavanagh D, Marchbank K. Recombinant mature complement factor i, patent application GB2018320.8. (2020). Available at: https://patentscope.wipo.int/search/en/detail.jsf?docId=WO2018170152.

43. Wu J, Wu YQ, Ricklin D, Janssen BJ, Lambris JD, Gros P. Structure of complement fragment C3b-factor h and implications for host protection by complement regulators. *Nat Immunol* (2009) 10:728–33. doi: 10.1038/ni.1755

44. Morgan HP, Schmidt CQ, Guariento M, Blaum BS, Gillespie D, Herbert AP, et al. Structural basis for engagement by complement factor h of C3b on a self surface. *Nat Struct Mol Biol* (2011) 18:463–70. doi: 10.1038/nsmb.2018

45. Roversi P, Johnson S, Caesar JJ, McLean F, Leath KJ, Tsiftsoglou SA, et al. Structural basis for complement factor I control and its disease-associated sequence polymorphisms. *Proc Natl Acad Sci U.S.A.* (2011) 108:12839–44. doi: 10.1073/pnas.1102167108

46. Geerlings MJ, Kremlitzka M, Bakker B, Nilsson SC, Saksens NT, Lechanteur YT, et al. The functional effect of rare variants in complement genes on C3b degradation in patients with age-related macular degeneration. *JAMA Ophthalmol* (2017) 135:39–46. doi: 10.1001/jamaophthalmol.2016.4604

47. Heurich M, Martínez-Barricarte R, Francis NJ, Roberts DL, Rodríguez de Córdoba S, Morgan BP, et al. Common polymorphisms in C3, factor b, and factor h collaborate to determine systemic complement activity and disease risk. *Proc Natl Acad Sci USA* (2011) 108:8761–66. doi: 10.1073/pnas.1019338108

48. Herskowitz I. Functional inactivation of genes by dominant negative mutations. *Nature* (1987) 329:219–22. doi: 10.1038/329219a0

49. Dreismann AK, McClements ME, Barnard AR, Orhan E, Hughes JP, Lachmann PJ, et al. Functional expression of complement factor I following AAV-mediated gene delivery in the retina of mice and human cells. *Gene Ther* (2021) 28:265–76. doi: 10.1038/s41434-021-00239-9

Frontiers in Immunology

Explores novel approaches and diagnoses to treat immune disorders.

The official journal of the International Union of Immunological Societies (IUIS) and the most cited in its field, leading the way for research across basic, translational and clinical immunology.

Discover the latest Research Topics

See more →

Frontiers

Avenue du Tribunal-Fédéral 34
1005 Lausanne, Switzerland
frontiersin.org

Contact us

+41 (0)21 510 17 00
frontiersin.org/about/contact